

UNCLASSIFIED

AD NUMBER

AD879198

LIMITATION CHANGES

TO:

Approved for public release; distribution is unlimited.

FROM:

**Distribution authorized to U.S. Gov't. agencies and their contractors;
Administrative/Operational Use; NOV 1970. Other requests shall be referred to Air Force Flight Dynamics Lab., Wright-Patterson AFB, OH 45433.**

AUTHORITY

AFFDL ltr 12 Nov 1971

THIS PAGE IS UNCLASSIFIED

AD879198

AFFDL-TR-70-10

Volume I, Part II

(DD)

LOW ALTITUDE ATMOSPHERIC TURBULENCE *SG*

LO-LOCAT PHASE III

Volume I, Part II

Data Analysis

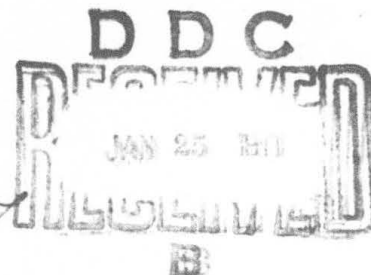
J. W. JONES, R. H. MIELKE, G. W. JONES, et al

THE BOEING COMPANY

AD No.
DDC FILE COPY
DDC PUBLICATIONS

TECHNICAL REPORT AFFDL-TR-70-10, VOLUME I, PART II

NOVEMBER 1970



This document is subject to special export controls and each transmittal to foreign governments or foreign nationals may be made only with prior approval of the Air Force Flight Dynamics Laboratory (FBE), Wright-Patterson Air Force Base, Ohio 45433.

AIR FORCE FLIGHT DYNAMICS LABORATORY
AIR FORCE SYSTEMS COMMAND
WRIGHT-PATTERSON AIR FORCE BASE, OHIO

**Best
Available
Copy**

NOTICE

When Government drawings, specifications, or other data are used for any purpose other than in connection with a definitely related Government procurement operation, the United States Government thereby incurs no responsibility nor any obligation whatsoever; and the fact that the Government may have formulated, furnished, or in any way supplied the said drawings, specifications, or other data, is not to be regarded by implication or otherwise as in any manner licensing the holder or any other person or corporation, or conveying any rights or permission to manufacture, use, or sell any patented invention that may in any way be related thereto.

This document is subject to special export controls and each transmittal to foreign governments or foreign nationals may be made only with prior approval of the Air Force Flight Dynamics Laboratory (FBE), Wright-Patterson Air Force Base, Ohio, 45433.

The distribution of this report is limited because it contains information that would significantly diminish the technological lead time of the United States and friendly foreign nations by revealing formulas, processes, or techniques having a potential strategic or economic value not generally known throughout the world.

SESSION NO.	
ESTD	WHITE SECTION <input type="checkbox"/>
DC	BUFF SECTION <input checked="" type="checkbox"/>
AMENDED	<input type="checkbox"/>
SUBMISSION	<input type="checkbox"/>
.....	
.....	
DISTRIBUTION/AVAILABILITY CODES	
DIST.	AVAIL. AND/OR SPECIAL
P2	

Copies of this report should not be returned unless return is required by security considerations, contractual obligations, or notice on a specific document.

LOW ALTITUDE ATMOSPHERIC TURBULENCE

LO-LOCAT PHASE III

Volume II, Part II

Data Analysis

J. W. JONES, R. H. MIELKE, G. W. JONES, et al

This document is subject to special export controls and each transmittal to foreign governments or foreign nationals may be made only with prior approval of the Air Force Flight Dynamics Laboratory (FBE), Wright-Patterson Air Force Base, Ohio, 45433.

FOREWORD

This is the final report on the Low-Low Altitude CAT research work conducted under Contract Number F33615-68-C-1468 (LO-LOCAT Phase III). The report was prepared by The Boeing Company, Wichita Division, for the Air Force Flight Dynamics Laboratory, Wright-Patterson Air Force Base, Ohio.

The LO-LOCAT Phase III project was part of Advanced Development Program 682E (ALLCAT) and was under the direction of ADP 682E Program Director, Mr. E. Brazier, and the Technical Coordinator, Mr. Neal V. Loving. Mr. Jan Garrison, FBE, was the Air Force Project Engineer.

The research effort was conducted under the Boeing supervision of Mr. F. K. Atnip, Program Manager. Mr. C. F. Peterson was the Project Pilot. Mr. D. B. Marshall was in charge of instrumentation, Mr. H. H. Depew directed the data processing effort, Mr. J. D. Gault was in charge of data analysis, and Mr. W. B. Moreland (Boeing-Seattle) directed the meteorological forecasts and analysis. Airplane maintenance and inspection were the responsibility of Mr. J. Strain and Mr. J. Bonawitz, respectively.

Mr. Gerald A. Comstock piloted the observer airplane over the Peterson Field, Colorado, high mountain route and was also backup pilot for this program. While acting in this latter capacity during a data gathering flight over the Griffiss AFB, New York route, Mr. Comstock was fatally injured in a forced landing following an engine flameout.

Authors of this report, other than those shown on the cover, were Messrs D. E. Gunter and K. R. Monson.

The report was submitted by the authors 17 August 1970. It was reviewed by Mr. Jan Garrison and Dr. T. Swaney (Boeing) who made many constructive comments and suggestions.

This technical report has been reviewed and is approved.


GORDON R. NEGAARD, Major, USAF
Chief, Design Criteria Branch
Structures Division
Air Force Flight Dynamics Laboratory

ABSTRACT

This report presents procedures, analysis methods, and final results pertaining to the LO-LOCAT Phase III program. Approximately 150 hours of low altitude (100 - 1000 feet) turbulence and associated meteorological data were recorded from 16 August 1968 through 30 June 1969. The original program was curtailed by approximately six weeks due to the crash of the T-33 research airplane. A model of the turbulence environment at low-level is presented in terms of gust velocity primary peaks, level crossings, amplitude samples, rms values, and gust maxima, as well as derived equivalent gusts, turbulence scale lengths and power spectra. Mathematical expressions for turbulence spectra, scale length and primary peak statistics are shown. Correlations between atmospheric gust velocities and meteorological and geophysical phenomena are evaluated. It was found that gust velocity magnitude at low altitude is most affected by atmospheric stability and terrain. Gust velocity rms values above 1.5 fps may be approximated by truncated Gaussian distributions. For wavelengths less than 15,000 feet, turbulence spectra are best represented by the von Karman mathematical expressions. The turbulence, sampled for 4-1/2 minute intervals over a distance of approximately 32 miles at absolute altitudes below 1,000 feet, was found to be basically stationary, isotropic, and homogeneous. A high percentage of Phase III data were recorded over high mountains since very little high mountain data were recorded under contour flight conditions at low level during Phases I and II. Phase III data are compared with data from Phases I and II and with data from other low altitude programs.

This report consists of two volumes with each volume divided into two parts. Parts I and II of Volume I give the techniques and results of data analysis. Part I of Volume II provides the details pertaining to data acquisition, instrumentation, calibrations and checks, data processing, and data quality. Data tabulations and plots, and a log of pertinent information concerning the program are also presented in Volume II Part I. Part II of Volume II contains the power spectral density and other frequency data plots.

(Distribution of this abstract is unlimited.)

TABLE OF CONTENTS

VOLUME I DATA ANALYSIS

PART I

		<u>PAGE NO.</u>
SECTION I	INTRODUCTION	1
1. Instrumentation	3	
2. Data Categorization Technique	4	
3. Data Analysis	5	
4. Data Gaps in the Turbulence Model	7	
SECTION II	SUMMARY	12
SECTION III	GUST VELOCITY TIME FUNCTION	17
5. Run Test for Stationarity	17	
6. Ensemble Averaging	19	
7. Gaussian Distribution Check	30	
8. Primary Peak Count	32	
9. Amplitude Count	50	
10. Level Crossings Count	56	
11. Comparison of Counting Techniques	62	
12. Correlation of Peak Distributions with Geophysical Category	87	
SECTION IV	GUST VELOCITY INTENSITY	104
13. Gust Velocity RMS Statistical Analysis	104	
14. Gust Velocity RMS versus Inflight Measured Wind Velocity	149	
15. Maximum Derived Equivalent Gust Velocities	183	
16. Maximum Gust Velocity During Each Sample	189	
17. Severe and Extreme Turbulence Samples	190	
18. Gust Velocity Magnitude versus Temperature Correlations	263	
SECTION V	GUST VELOCITY SPECTRA	272
19. Instrumentation Anomalies, Low Intensity Turbulence Levels	272	
20. Statistical Confidence and Independency	275	
21. Homogeneity	280	
22. Isotropy	288	
23. Normalized Spectra	296	
24. Cross Spectra	317	
25. Truncated Standard Deviations	332	

TABLE OF CONTENTS

		<u>PAGE NO.</u>
SECTION V	GUST VELOCITY SPECTRA (Contd.)	
26.	Gust Velocity Distance History Power Spectra	336
27.	Spectra During High Speed Flight	342
28.	Experimental/Mathematical Spectra Comparison	347
29.	Recommended Spectra Shape	354
30.	Turbulence Scale Length	356
31.	Turbulence Microscales	399
REFERENCES	VOLUME I	408

VOLUME I DATA ANALYSIS

PART II

SECTION VI	> GEOPHYSICAL CHARACTERISTICS	1
32.	Terrain Profiles	1
33.	Wind Speed	22
34.	Viscous Dissipation Rate	53
SECTION VII	> TURBULENCE FORECASTING	60
35.	Meteorological Data Sampling	60
36.	Forecast Evaluations	67
37.	Case Studies - Phases I and II	76
38.	Case Studies - Phase III	111
39.	Richardson Number	143
40.	Stability Ratio	152
SECTION VIII	> BREN TOWER, THUNDERSTORM, AND WAKE TURBULENCE INVESTIGATIONS	160
41.	BREN Tower Flyby	160
42.	Thunderstorm Turbulence	173
43.	Wake Turbulence	192
SECTION IX	> COMPARISON OF LO-LOCAT PHASES I AND II WITH PHASE III DATA	249
44.	Gust Velocity RMS Values	249
45.	Peak Count	268
46.	Power Spectra	282
47.	Scale Lengths	287
48.	Relationships Between Turbulence and Meteorological Data	294

TABLE OF CONTENTS

	<u>PAGE NO.</u>	
SECTION X	COMPARISON OF LO-LOCAT (PHASES I, II, AND III) WITH OTHER LOW ALTITUDE TURBULENCE DATA	313
49. Peak Count	313	
50. Power Spectra Comparison	320	
SECTION XI	ADDITIONAL RESEARCH	349
51. Gust Acceleration	352	
52. Wind Spectra	394	
53. High Intensity Gust Program Re-Evaluation	413	
SECTION XII	CONCLUSIONS	450
REFERENCES	VOLUME I	453

VOLUME II DATA ACQUISITION AND PROCESSING, DATA PLOTS, AND TABULATIONS

PART I

APPENDIX I	AIRPLANE MODIFICATION AND INSTRUMENTATION DETAILS	1
I.1	Airplane Modification	1
I.2	Gust Boom and Probe Design	2
I.3	Airplane Instrumentation	3
I.4	Mobile Ground Station	14
APPENDIX II	CALIBRATIONS AND CHECKS	25
II.1	Calibrations in the Laboratory and at the Airplane	25
II.2	Wind Tunnel Static Calibration of the Gust Probe	25
II.3	Wind Tunnel Dynamic Calibration of the Gust Probe	27
II.4	Dynamic Calibration of the Gust Probe Installed on the Airplane	28
II.5	Inflight Calibration of Angles of Attack and Sideslip Differential Pressures	29
II.6	Inflight Calibration of the Gust Probe and Airplane Airspeed Systems	31
II.7	Gust Probe and Boom Natural Frequency Determination	32
II.8	Outside Air Temperature Calibration	33
II.9	Radiometer (Ground Surface Temperature) Calibration	34

TABLE OF CONTENTS

	<u>PAGE NO.</u>
APPENDIX II CALIBRATIONS AND CHECKS (Contd.)	
II.10 Radar Altimeter Check	37
II.11 Ground Speed Calibration Verification	37
APPENDIX III DATA QUALITY	53
III.1 Evaluation of Transducer Inaccuracies	53
III.2 Bias Error Corrections	54
III.3 Frequency Response Compensation	55
III.4 Instrumentation Noise Removal	56
III.5 Evaluation of Instrumentation Noise Not Removed	57
III.6 Drift Analysis	59
III.7 Evaluation of Interchangeable Variables	63
III.8 Probe Motion Removal Evaluation	65
III.9 Overall Quality of Gust Velocity Calculations	66
III.10 Digital Filtering Application and Evaluation	67
APPENDIX IV DATA ACQUISITION OPERATION	103
IV.1 Operations	103
IV.2 Flight Operations	104
IV.3 Ground Operations	105
APPENDIX V DATA PROCESSING	113
V.1 Ground Station Data Processing	113
V.2 Computer Programs	116
V.3 Multiple Regression	135
APPENDIX VI TEST LOG	143
APPENDIX VII GUST VELOCITY PEAK, AMPLITUDE, AND LEVEL CROSSINGS COUNT DATA	182
APPENDIX VIII DATA TABULATIONS	268
REFERENCES VOLUME II	338

VOLUME II FREQUENCY DATA PLOTS

PART II

APPENDIX IX GUST VELOCITY POWER SPECTRA AND ASSOCIATED DATA	1-457
---	-------

LIST OF ILLUSTRATIONS

VOLUME I, PART II

<u>FIGURE NO.</u>	<u>TITLE</u>	<u>PAGE NO.</u>
32.1	McConnell Route Terrain Profile Distance History	8
32.2	Edwards Route Terrain Profile Distance History	9
32.3	Peterson Route Terrain Profile Distance History	10
32.4	Griffiss Route Terrain Profile Distance History	11
32.5	McConnell Route Terrain Profile Power Spectra	12
32.6	McConnell Route Terrain Profile Power Spectra	13
32.7	Edwards Route Terrain Profile Power Spectra	14
32.8	Edwards Route Terrain Profile Power Spectra	15
32.9	Peterson Route Terrain Profile Power Spectra	16
32.10	Peterson Route Terrain Profile Power Spectra	17
32.11	Griffiss Route Terrain Profile Power Spectra	18
32.12	Griffiss Route Terrain Profile Power Spectra	19
32.13	Average Radar Altitude per Leg - Target Altitude versus Terrain Roughness	20
32.14	Average Radar Altitude per Leg - Target Altitude versus Terrain Roughness	21
33.1	Wind Speed Cumulative Probability Associated with Type of Terrain	26
33.2	Wind Speed Cumulative Probability Associated with Absolute Altitude	27
33.3	Wind Speed Cumulative Probability Associated with Atmospheric Stability	28
33.4	Wind Speed Cumulative Probability Associated with Time of Day	29
33.5	Wind Speed Cumulative Probability Associated with Geographic Location	30

LIST OF ILLUSTRATIONS

VOLUME I, PART II

<u>FIGURE NO.</u>	<u>TITLE</u>	<u>PAGE NO.</u>
33.6	Effects of Season on Wind Speed Cumulative Probability at Peterson	31
33.7	Effects of Absolute Altitude on Wind Speed Cumulative Probability over High Mountains	32
33.8	Effects of Absolute Altitude on Wind Speed Cumulative Probability over Low Mountains	33
33.9	Effects of Absolute Altitude on Wind Speed Cumulative Probability over Desert	34
33.10	Effects of Absolute Altitude on Wind Speed Cumulative Probability over Plains	35
33.11	Effects of Terrain Type on Wind Speed Cumulative Probability at 250 Feet	36
33.12	Effects of Terrain Type on Wind Speed Cumulative Probability at 750 Feet	37
33.13	Effects of Geographic Location on Wind Speed Cumulative Probability over High Mountains	38
33.14	Effects of Geographic Location on Wind Speed Cumulative Probability over Low Mountains	39
33.15	Effects of Geographic Location on Wind Speed Cumulative Probability over Plains	40
33.16	Effects of Atmospheric Stability on Wind Speed Cumulative Probability at Edwards	41
33.17	Effects of Atmospheric Stability on Wind Speed Cumulative Probability at Griffiss	42
33.18	Effects of Atmospheric Stability on Wind Speed Cumulative Probability at Peterson	43
33.19	Effects of Atmospheric Stability on Wind Speed Cumulative Probability at McConneli	44
33.20	Effects of Time of Day on Wind Speed Cumulative Probability at Edwards	45

LIST OF ILLUSTRATIONS

VOLUME I, PART II

<u>FIGURE NO.</u>	<u>TITLE</u>	<u>PAGE NO.</u>
33.21	Effects of Time of Day on Wind Speed Cumulative Probability at Griffiss	46
33.22	Effects of Time of Day on Wind Speed Cumulative Probability at Peterson	47
33.23	Effects of Time of Day on Wind Speed Cumulative Probability at McConnell	48
33.24	Comparison of Wind Speed Cumulative Probabilities for the Different Program Phases at Edwards	49
33.25	Comparison of Wind Speed Cumulative Probabilities for the Different Program Phases at Griffiss	50
33.26	Comparison of Wind Speed Cumulative Probabilities for the different Program Phases at Peterson	51
33.27	Comparison of Wind Speed Cumulative Probabilities for the different Program Phases at McConnell	52
34.1	Variation of Viscous Dissipation Rate for Time of Day	54
34.2	Variation of Viscous Dissipation Rate for Altitude and Atmospheric Stability	55
34.3	Variation of Viscous Dissipation Rate for High Mountains and Plains Terrain	56
34.4	Variation of Viscous Dissipation Rate for High Mountain and Plains Terrain, Phases I and II	57
34.5	LO-LOCAT Viscous Dissipation Rates Compared to Those from Other Studies	58
34.6	Variation of Dissipation Rate for Stability Categories	59
35.1	Comparison of Averaged Observed Meteorological Conditions with Normal Conditions	63
35.2	McConnell Route	64
35.3	Edwards Route	65

LIST OF ILLUSTRATIONS

VOLUME I, PART II

<u>FIGURE NO.</u>	<u>TITLE</u>	<u>PAGE NO.</u>
35.4	Peterson Route	66
37.1	November 7, 1966 Surface Analysis, McConnell Route	82
37.2	November 7, 1966 850 MB Analysis, McConnell Route	83
37.3	April 5, 1967 Surface Analysis, Peterson Route	84
37.4	April 5, 1967 Surface Analysis, Peterson Route	85
37.5	April 5, 1967 700 MB Analysis, Peterson Route	86
37.6	April 28, 1967 Surface Analysis, Peterson Route	87
37.7	April 28, 1967 Surface Analysis, Peterson Route	88
37.8	April 28, 1967 700 MB Analysis, Peterson Route	89
37.9	May 12, 1967 Surface Analysis, Edwards Route	90
37.10	May 12, 1967 Surface Analysis, Edwards Route	91
37.11	May 12, 1967 850 MB Analysis, Edwards Route	92
37.12	May 26, 1967 Surface Analysis, Griffiss Route	93
37.13	May 26, 1967 850 MB Analysis, Griffiss Route	94
37.14	August 21, 1967 Surface Analysis, Peterson Route	95
37.15	September 20, 1967 Surface Analysis, Edwards Route	96
37.16	September 20, 1967 850 MB Analysis, Edwards Route	97
37.17	December 13, 1967 Surface Analysis, Edwards Route	98
37.18	December 13, 1967 Surface Analysis, Edwards Route	99
37.19	December 13, 1967 850 MB Analysis, Edwards Route	100

LIST OF ILLUSTRATIONS

VOLUME I, PART II

<u>FIGURE NO.</u>	<u>TITLE</u>	<u>PAGE NO.</u>
37.20	December 13, 1967 850 MB Analysis, Edwards Route	101
37.21	November 4, 1966 Surface Analysis, McConnell Route	102
37.22	November 4, 1966 850 MB Analysis, McConnell Route	103
37.23	December 5, 1966 Surface Analysis, Peterson Route	104
37.24	December 5, 1966 700 MB Analysis, Peterson Route	105
37.25	November 16, 1967 Surface Analysis, Griffiss Route	106
37.26	November 16, 1967 Surface Analysis, Griffiss Route	107
37.27	November 16, 1967 850 MB Analysis, Griffiss Route	108
37.28	December 6, 1967 Surface Analysis, Edwards Route	109
37.29	December 6, 1967 850 MB Analysis, Edwards Route	110
38.1	November 7, 1968 Surface Analysis, Edwards Route	116
38.2	November 7, 1968 850 MB Analysis, Edwards Route	117
38.3	November 7, 1968 Surface Analysis, Edwards Route	118
38.4	November 13, 1968 Surface Analysis, Edwards Route	119
38.5	November 13, 1968 850 MB Analysis, Edwards Route	120

LIST OF ILLUSTRATIONS

VOLUME I, PART II

<u>FIGURE NO.</u>	<u>TITLE</u>	<u>PAGE NO.</u>
38.6	November 13, 1968 850 MB Analysis, Edwards Route	121
38.7	November 13, 1968 Surface Analysis, Edwards Route	122
38.8	November 13, 1968 Surface Analysis, Edwards Route	123
38.9	December 2, 1968 Surface Analysis, Edwards Route	124
38.10	December 2, 1968 850 MB Analysis, Edwards Route	125
38.11	December 2, 1968 850 MB Analysis, Edwards Route	126
38.12	December 2, 1968 Surface Analysis, Edwards Route	127
38.13	February 25, 1969 Surface Analysis, Peterson Route	128
38.14	February 25, 1969 700 MB Analysis, Peterson Route	129
38.15	February 25, 1969 Surface Analysis, Peterson Route	130
38.16	February 25, 1969 Surface Analysis, Peterson Route	131
38.17	February 25, 1969 Surface Analysis, Peterson Route	132
38.18	February 26, 1969 Surface Analysis, Peterson Route	133
38.19	February 26, 1969 700 MB Analysis, Peterson Route	134
38.20	February 26, 1969 Surface Analysis, Peterson Route	135

LIST OF ILLUSTRATIONS

VOLUME I, PART II

<u>FIGURE NO.</u>	<u>TITLE</u>	<u>PAGE NO.</u>
38.21	February 26, 1969 Surface Analysis, Peterson Route	136
38.22	February 26, 1969 Surface Analysis, Peterson Route	137
38.23	March 19, 1969 Surface Analysis, Peterson Route	138
38.24	March 19, 1969 700 MB Analysis, Peterson Route	139
38.25	March 19, 1969 Surface Analysis, Peterson Route	140
38.26	March 19, 1969 Surface Analysis, Peterson Route	141
38.27	March 19, 1969 Surface Analysis, Peterson Route	142
39.1	Gust Velocity RMS Probabilities Associated with High Mountain Terrain for Richardson Number Bands	144
39.2	Gust Velocity RMS Probabilities Associated with Low Mountain Terrain for Richardson Number Bands	145
39.3	Gust Velocity RMS Probabilities Associated with Plains Terrain for Richardson Number Bands	146
39.4	Gust Velocity RMS Probabilities Associated with 250 Foot Altitude for Richardson Number Bands	147
39.5	Gust Velocity RMS Probabilities Associated with 750 Foot Altitude for Richardson Number Bands	148
39.6	Gust Velocity RMS Probabilities Associated with Dawn for Richardson Number Bands	149
39.7	Gust Velocity RMS Probabilities Associated with Mid-Morning for Richardson Number Bands	150
39.8	Gust Velocity RMS Probabilities Associated with Mid-Afternoon for Richardson Number Bands	151
40.1	Gust Velocity Probabilities Associated with Dawn for Stability Ratio Bands	153
40.2	Gust Velocity Probabilities Associated with Mid-Morning for Stability Ratio Bands	154

LIST OF ILLUSTRATIONS

VOLUME I, PART II

<u>FIGURE NO.</u>	<u>TITLE</u>	<u>PAGE NO.</u>
40.3	Gust Velocity Probabilities Associated with Mid- Afternoon for Stability Ratio Bands	155
40.4	Gust Velocity Probabilities Associated with High Mountains for Stability Ratio Bands	156
40.5	Gust Velocity Probabilities Associated with Plains for Stability Ratio Bands	157
40.6	Gust Velocity Probabilities Associated with 250- Foot Altitude for Stability Ratio Bands	158
40.7	Gust Velocity Probabilities Associated with 750- Foot Altitude for Stability Ratio Bands	159
41.1	BREN Tower Location	163
41.2	Gust Velocity Time History for BREN Tower Fly-by No. 1	164
41.3	Gust Velocity Time History for BREN Tower Fly-by No. 7	165
41.4	Turbulence Spectra Data for BREN Tower Fly-by No. 1	166
41.5	Turbulence Spectra Data for BREN Tower Fly-by No. 7	167
41.6	Surface Synoptic Analysis, 8 January 1969, 2000 GMT	168
41.7	Comparison of Longitudinal Spectra from T-33 Airplane to BREN Tower - Fly-by No. 7	169
41.8	Comparison of Lateral Spectra from T-33 Air- plane to BREN Tower - Fly-by No. 7	170
41.9	Comparison of Vertical Spectra from T-33 Air- plane to BREN Tower - Fly-by No. 7	171
41.10	Comparison of Vertical Spectra from BREN Tower to that Reported by Kaimal	172

LIST OF ILLUSTRATIONS

VOLUME I, PART II

<u>FIGURE NO.</u>	<u>TITLE</u>	<u>PAGE NO.</u>
42.1	Principle Flight Area of Operation Rough Rider	178
42.2	Gust Velocity, Normal Acceleration, and Total Temperature Time Histories for Test 270, Sample No. 15	179
42.3	Gust Velocity, Normal Acceleration, and Total Temperature Time Histories for Test 270, Sample No. 18	180
42.4	Gust Velocity, Normal Acceleration, and Total Temperature Time Histories for Test 273, Sample No. 3	181
42.5	Gust Velocity, Normal Acceleration, and Total Temperature Time Histories for Test 273, Sample No. 12	182
42.6	Gust Velocity, Normal Acceleration, and Total Temperature Time Histories for Test 273, Sample No. 15	183
42.7	Gust Velocity, Normal Acceleration, and Total Temperature Time Histories for Test 273, Sample No. 3	184
42.8	Gust Velocity, Normal Acceleration, and Total Temperature Time Histories for Test 275, Sample No. 9	185
42.9	Gust Velocity, Normal Acceleration, and Total Temperature Time Histories for Test 275, Sample No. 12	186
42.10	Gust Velocity, Normal Acceleration, and Total Temperature Time Histories for Test 275, Sample No. 21	187
42.11	Gust Velocity, Normal Acceleration, and Total Temperature Time Histories for Test 275, Sample No. 24	188
42.12	Gust Velocity, Normal Acceleration, and Total Temperature Time Histories for Test 275, Sample No. 27	189

LIST OF ILLUSTRATIONS

VOLUME I, PART II

<u>FIGURE NO.</u>	<u>TITLE</u>	<u>PAGE NO.</u>
42.13	Gust Velocity, Normal Acceleration, and Total Temperature Time Histories for Test 275, Sample No. 30	190
42.14	Turbulence Spectra for Tests 274 and 275	191
43.1	Racetrack Pattern - Wake Turbulence Investigation	199
43.2	Element Longitudinal Spacing During Enroute Portion of Pattern	200
43.3	C-141 Element Formations in Drop Zone	201
43.4	C-141 Element Formations in Drop Zone	202
43.5	Gust Velocity Time Histories - Test 0284, Sample No. 5	203
43.6	Gust Velocity Time Histories - Test 0284, Sample No. 7	204
43.7	Gust Velocity Time Histories - Test 0284, Sample No. 8	205
43.8	Gust Velocity Time Histories - Test 0284, Sample No. 9	206
43.9	Gust Velocity Time Histories - Test 0284, Sample No. 16	207
43.10	Gust Velocity Time Histories - Test 0284, Sample No. 17	208
43.11	Gust Velocity Time Histories - Test 0284, Sample No. 18	209
43.12	Gust Velocity Time Histories - Test 0284, Sample No. 19	210
43.13	Gust Velocity Time Histories - Test 0284, Sample No. 20	211
43.14	Gust Velocity Time Histories - Test 0284, Sample No. 21	212

LIST OF ILLUSTRATIONS

VOLUME I, PART II

<u>FIGURE NO.</u>	<u>TITLE</u>	<u>PAGE NO.</u>
43.15	Gust Velocity Time Histories - Test 0284, Sample No. 25	213
43.16	Gust Velocity Time Histories - Test 0284, Sample No. 26	214
43.17	Gust Velocity Time Histories - Test 0284, Sample No. 27	215
43.18	Gust Velocity Time Histories - Test 0284, Sample No. 29	216
43.19	Gust Velocity Time Histories - Test 0284, Sample No. 36	217
43.20	Gust Velocity Time Histories - Test 0284, Sample No. 38	218
43.21	Gust Velocity Time Histories - Test 0284, Sample No. 39	219
43.22	Gust Velocity Time Histories - Test 0285, Sample No. 3	220
43.23	Gust Velocity Time Histories - Test 0285, Sample No. 4	221
43.24	Gust Velocity Time Histories - Test 0285, Sample No. 6	222
43.25	Gust Velocity Time Histories - Test 0285, Sample No. 7	223
43.26	Gust Velocity Time Histories - Test 0285, Sample No. 7 (Continued)	224
43.27	Gust Velocity Time Histories - Test 0285, Sample No. 8	225
43.28	Gust Velocity Time Histories - Test 0285, Sample No. 8 (Continued)	226
43.29	Gust Velocity Time Histories - Test 0285, Sample No. 9	227

LIST OF ILLUSTRATIONS

VOLUME I, PART II

<u>FIGURE NO.</u>	<u>TITLE</u>	<u>PAGE NO.</u>
43.30	Gust Velocity Time Histories - Test 0285, Sample No. 10	228
43.31	Gust Velocity Time Histories - Test 0285, Sample No. 10 (Continued)	229
43.32	Gust Velocity Time Histories - Test 0285, Sample No. 11	230
43.33	Gust Velocity Time Histories - Test 0285, Sample No. 12	231
43.34	Gust Velocity Time Histories - Test 0285, Sample No. 17	232
43.35	Gust Velocity Time Histories - Test 0285, Sample No. 18	233
43.36	Gust Velocity Time Histories - Test 0285, Sample No. 18 (Continued)	234
43.37	Gust Velocity Time Histories - Test 0285, Sample No. 19	235
43.38	Gust Velocity Time Histories - Test 0285, Sample No. 20	236
43.39	Gust Velocity Time Histories - Test 0285, Sample No. 21	237
43.40	Gust Velocity Time Histories - Test 0285, Sample No. 22	238
43.41	Fluid Velocity Distribution Within the Effects of Theoretical Vortex Flow	239
43.42	Gust Velocity Time History - Wake Turbulence Vortex Size and Shape Investigation	240
43.43	Gust Velocity Time History - Wake Turbulence Vortex Size and Shape Investigation	241
43.44	Gust Velocity Time History - Wake Turbulence Vortex Size and Shape Investigation	242

LIST OF ILLUSTRATIONS

VOLUME I, PART II

<u>FIGURE NO.</u>	<u>TITLE</u>	<u>PAGE NO.</u>
43.45	Gust Velocity Time History - Wake Turbulence Vortex Size and Shape Investigation	243
43.46	Gust Velocity Time History - Wake Turbulence Vortex Size and Shape Investigation	244
43.47	Gust Velocity Time History - Wake Turbulence Vortex Size and Shape Investigation	245
43.48	Gust Velocity Time History - Wake Turbulence Vortex Size and Shape Investigation	246
43.49	Gust Velocity Time History - Wake Turbulence Vortex Size and Shape Investigation	247
43.50	Gust Velocity Time History - Wake Turbulence Vortex Size and Shape Investigation	248
44.1	Comparison of Gust Velocity RMS Values from Phases I and II with Those from Phase III for Data Recorded over High Mountains at Edwards	255
44.2	Comparison of Gust Velocity RMS Values from Phases I and II with Those from Phase III for Data Recorded over High Mountains at Edwards and Griffiss	256
44.3	Comparison of Gust Velocity RMS Values from Phases I and II with Those from Phase III for Data Recorded over Desert at Edwards	257
44.4	Comparison of Gust Velocity RMS Values from Phases I and II with Those from Phase III for Data Recorded over Plains at McConnell, Peterson, and Griffiss	258
44.5	Comparison of Phases I and II and Phase III Mean Gust Velocity RMS Values as a Function of Terrain	259
44.6	Comparison of Phases I and II and Phase III Mean Gust Velocity RMS Values as a Function of Absolute Altitude	260
44.7	Comparison of Phases I and II and Phase III Mean Gust Velocity RMS Values as a Function of Atmospheric Stability	261

LIST OF ILLUSTRATIONS

VOLUME I, PART II

<u>FIGURE NO.</u>	<u>TITLE</u>	<u>PAGE NO.</u>
44.8	Extrapolated Longitudinal Gust Velocity RMS Cumulative Probability	262
44.9	Extrapolated Lateral Gust Velocity RMS Cumulative Probability	263
44.10	Extrapolated Vertical Gust Velocity RMS Cumulative Probability	264
44.11	Comparison of Standardized Longitudinal Gust Velocity RMS Cumulative Probability Distribution from Phases I and II with that from Phase III	265
44.12	Comparison of Standardized Lateral Gust Velocity RMS Cumulative Probability Distribution from Phases I and II with that from Phase III	266
44.13	Comparison of Standardized Vertical Gust Velocity RMS Cumulative Probability Distribution from Phases I and II with that from Phase III	267
45.1	Terrain Effects on Longitudinal Gust Velocity Peaks - LO-LOCAT Phases I and II and Phase III	270
45.2	Terrain Effects on Lateral Gust Velocity Peaks - LO-LOCAT Phases I and II and Phase III	271
45.3	Terrain Effects on Vertical Gust Velocity Peaks - LO-LOCAT Phases I and II and Phase III	272
45.4	Altitude Effects on Longitudinal Gust Velocity Peaks - LO-LOCAT Phases I and II	273
45.5	Altitude Effects on Lateral Gust Velocity Peaks - LO-LOCAT Phases I and II	274
45.6	Altitude Effects on Vertical Gust Velocity Peaks - LO-LOCAT Phases I and II	275
45.7	Stability Effects on Longitudinal Gust Velocity Peaks - LO-LOCAT Phases I and II	276
45.8	Stability Effects on Lateral Gust Velocity Peaks - LO-LOCAT Phases I and II	277

LIST OF ILLUSTRATIONS

VOLUME I, PART II

<u>FIGURE NO.</u>	<u>TITLE</u>	<u>PAGE NO.</u>
45.9	Stability Effects on Vertical Gust Velocity Peaks - LO-LOCAT Phases I and II	278
45.10	Time of Day Effects on Longitudinal Gust Velocity Peaks - LO-LOCAT Phases I and II	279
45.11	Time of Day Effects on Lateral Gust Velocity Peaks - LO-LOCAT Phases I and II	280
45.12	Time of Day Effects on Vertical Gust Velocity Peaks - LO-LOCAT Phases I and II	281
46.1	Longitudinal Gust Velocity Power Spectra Comparison	283
46.2	Lateral Gust Velocity Power Spectra Comparison	284
46.3	Vertical Gust Velocity Power Spectra Comparison	285
46.4	Phases I, II, and III Turbulence Spectra Model	286
47.1	Comparison of σ_t and σ_T as Determined from Phases I and II and Phase III - Edwards, High Mountains, Fall	290
47.2	Comparison of Longitudinal Scale Length Cumulative Probabilities from Phases I and II with Those from Phase III for Data Obtained Over High Mountains at Edwards	291
47.3	Comparison of Longitudinal Scale Length Cumulative Probabilities from Phases I and II with Those from Phase III for Data Obtained Over Plains at McConnell	292
47.4	Comparison of Longitudinal Scale Length Cumulative Probabilities from Phases I and II with Those from Phase III for Data Obtained Over Plains at Peterson	293
49.1	Comparison of Longitudinal Gust Velocity Distribution for Different Test Programs	316
49.2	Comparison of Lateral Gust Velocity Distribution for Different Test Programs	317
49.3	Comparison of Vertical Gust Velocity Distribution for Different Test Programs	318

LIST OF ILLUSTRATIONS

VOLUME I, PART II

<u>FIGURE NO.</u>	<u>TITLE</u>	<u>PAGE NO.</u>
49.4	Variation of Characteristic Frequency with True Airspeed	319
50.1	Reference X.1 (F-106) Lateral Gust Velocity Normalized Spectra	333
50.2	Reference X.1 (F-106) Vertical Gust Velocity Normalized Spectra	334
50.3	Reference X.1 (F-106) and von Karman Spectra Comparison	335
50.4	Reference X.2 (F-106) Lateral Gust Velocity Normalized Spectra	336
50.5	Reference X.2 (F-106) Vertical Gust Velocity Normalized Spectra	337
50.6	Reference X.2 (F-106) and von Karman Spectra Comparison	338
50.7	Reference X.3 (T-38) Lateral Gust Velocity Normalized Spectra	339
50.8	Reference X.3 (T-38) Vertical Gust Velocity Normalized Spectra	340
50.9	Reference X.3 (T-38) and von Karman Spectra Comparison	341
50.10	Reference X.4 (B-52E) Lateral Gust Velocity Normalized Spectra	342
50.11	Reference X.4 (B-52E) Vertical Gust Velocity Normalized Spectra	343
50.12	Reference X.5 (B-52H) Lateral Gust Velocity Normalized Spectra	344
50.13	Reference X.5 (B-52H) Vertical Gust Velocity Normalized Spectra	345
50.14	Reference X.4 (B-52E) and von Karman Spectra Comparison	346

LIST OF ILLUSTRATIONS

VOLUME I, PART II

<u>FIGURE NO.</u>	<u>TITLE</u>	<u>PAGE NO.</u>
50.15	Reference X.5 (B-52H) and von Karman Spectra Comparison	347
50.16	Reference X.7 (B-58) Gust Velocity Power Spectrum with $\gamma = .015$ (No Prewhitening)	348
51.1	Effect of Small Angle Assumption on Gust Velocity Time Series	368
51.2	Effect of Small Angle Assumption on Gust Velocity Spectra	369
51.3	Comparisons of Gust Spectra	370
51.4	Drift in Gust Velocities Obtained from Gust Accelerations Without High-Pass Filtering	371
51.5	Effects of Data Extension on Gust Acceleration Spectra	372
51.6	Comparison of Gust Velocity Spectra Obtained Using 0.046 cps Time and Frequency Domain Filters	373
51.7	Average of Thirty Longitudinal Spectra	374
51.8	Average of Thirty Lateral Spectra	375
51.9	Average of Thirty Vertical Spectra	376
51.10	Comparison of Gust Velocity Standard Deviations Obtained from the Gust Velocity and Acceleration Techniques	377
51.11	Comparison of Turbulence Scale Lengths Obtained from the Gust Velocity and Acceleration Techniques	378
51.12	Comparison of Gust Velocity σ_1 and Gust Acceleration σ	379
51.13	Difference Between Gust Velocity Spectrum Estimates and Unfiltered Gust Acceleration and Filtered Gust Velocity	380
51.14	Modified High-Pass Filter Transfer Function	381

LIST OF ILLUSTRATIONS

VOLUME I, PART II

<u>FIGURE NO.</u>	<u>TITLE</u>	<u>PAGE NO.</u>
51.15	Average of Ten Longitudinal Spectra	382
51.16	Average of Ten Lateral Spectra	383
51.17	Average of Ten Vertical Spectra	384
51.18	Comparison of Spectra Obtained Using 0.026 cps Frequency and 0.023 cps Time Domain Filters	385
51.19	Gust Velocity and Gust Acceleration Probability Distributions	386
51.20	Gust Velocity Standard Deviations versus Maximum Gust Encountered	387
51.21	Normalized Gust Velocity/Gust Acceleration Level Crossings	388
51.22	Comparison of Gust Velocity Level Crossing Cumulative Probability Distributions	389
51.23	Gust Acceleration Probability Distributions for Thirty Combined Samples	390
51.24	Comparison of Gust Velocity and Acceleration Level Crossing Probability Density Functions	391
51.25	Gust Velocity and Gust Acceleration Level Crossing Distributions Compared to Rice's Equation	392
51.26	Actual Gust Velocity Level Crossing Probabilities Compared to Equations from Gust Acceleration Data	393
52.1	Ormsby Low-Pass Digital Filter Used to Filter Winds Data	399
52.2	Ormsby Low-Pass Digital Filter Used as First Pass in the Two Pass Procedure for High-Pass Filtering Winds Data	400
52.3	Ormsby High-Pass Digital Filter Used as Second Pass in the Two Pass Procedure for High-Pass Filtering Winds Data	401
52.4	Time Histories of Filtered and Unfiltered Wind Velocities	402

LIST OF ILLUSTRATIONS

VOLUME I, PART II

<u>FIGURE NO.</u>	<u>TITLE</u>	<u>PAGE NO.</u>
52.5 thru 52.8	Wind Velocity Normalized Spectra	403
52.9 thru 52.12	Wind Velocity Normalized Spectra	404
52.13 thru 52.16	Wind Velocity Normalized Spectra	405
52.17 thru 52.20	Wind Velocity Normalized Spectra	406
52.21 thru 52.24	Wind Velocity Normalized Spectra	407
52.25 thru 52.28	Wind Velocity Normalized Spectra	408
52.29 thru 52.32	Wind Velocity Normalized Spectra	409
52.33 and 52.34	Wind Velocity Normalized Spectra	410
52.35	Average Longitudinal Wind and Gust Spectra for 30 Selected Data Samples	411
52.36	Average Lateral Wind and Gust Spectra for 30 Selected Data Samples	412
53.1	Ground Station Low-Pass Analog Filters	421
53.2	Effects of Accelerometer Location Correction on Lateral Gust Velocity Power Spectral Density	422
53.3	Effects of Accelerometer Location Correction on Vertical Gust Velocity Power Spectral Density	423
53.4	Comparison of Vertical Gust Velocity Time History Before and After High-Pass Filtering	424
53.5	Comparison of Original and Re-Processed Extreme Values of Longitudinal Gust Velocity	425
53.6	Comparison of Original and Re-Processed Extreme Values of Lateral Gust Velocity	426

LIST OF ILLUSTRATIONS

VOLUME I, PART II

<u>FIGURE NO.</u>	<u>TITLE</u>	<u>PAGE NO.</u>
53.7	Comparison of Original and Re-Processed Extreme Values of Vertical Gust Velocity	427
53.8	Comparison of Original and Re-Processed RMS Gust Velocities	428
53.9	Gust Velocity Peak Count Distribution for an Individual Sample	429
53.10	Gust Velocity Amplitude Count Distribution for an Individual Sample	430
53.11	Gust Velocity Level Crossing Distribution for an Individual Sample	431
53.12	Comparison of Original and Re-Processed Peak Count Distributions	432
53.13	Gust Velocity Peak Distribution for Re-Processed High Intensity Gust Samples	433
53.14	Comparison of Lateral Gust Velocity Peak Count from High Intensity Gust Investigation and LO-LOCAT Phase III	434
53.15	Comparison of Vertical Gust Velocity Peak Count from High Intensity Gust Investigation and LO-LOCAT Phase III	435
53.16	Gust Velocity Peak Count Probability Distribution for Re-Processed High Intensity Gust Samples	436
53.17	Gust Velocity Level Crossing Probability Distribution for Re-Processed High Intensity Gust Samples	437
53.18	Gust Velocity Amplitude Count Probability Distribution for Re-Processed High Intensity Gust Samples	438
53.19	Chi-Square Test for Statistical Normality	439
53.20	Longitudinal Gust Velocity Power Spectra of an Individual Turbulence Sample	440
53.21	Lateral Gust Velocity Power Spectra of an Individual Turbulence Sample	441

LIST OF ILLUSTRATIONS

VOLUME I, PART II

<u>FIGURE NO.</u>	<u>TITLE</u>	<u>PAGE NO.</u>
53.22	Vertical Gust Velocity Power Spectra of an Individual Turbulence Sample	442
53.23	Comparison of Average Longitudinal Re-Processed High Intensity Gust Spectra with LO-LOCAT Phase III Spectra	443
53.24	Comparison of Average Lateral Re-Processed High Intensity Gust Spectra with LO-LOCAT Phase III Spectra	444
53.25	Comparison of Average Vertical Re-Processed High Intensity Gust Spectra with LO-LOCAT Phase III Spectra	445
53.26	Average Experimental to von Karman Spectrum Ratio	446
53.27	Average Experimental to Lumley-Panofsky and Busch-Panofsky Spectrum Ratios	447
53.28	Average Homogeneity for Re-Processed High Intensity Gust Data	448
53.29	Average Coherency and Isotropy Characteristics	449

LIST OF TABLES
VOLUME I, PART II

<u>TABLE NO.</u>	<u>TITLE</u>	<u>PAGE NO.</u>
32.1	McConnell Route Characteristics	4
32.2	Edwards Route Characteristics	5
32.3	Peterson Route Characteristics	6
32.4	Griffiss Route Characteristics	7
36.1	Verification of GWC Forecasts (Phase III)	72
36.2	Verification of Showalter Index (Phase III)	73
36.3	Verification of Richardson Numbers (Phase III)	74
36.4	Turbulence Forecasts versus Turbulence Observed	75
41.1	BREN Tower Fly-By Data	161
41.2	Temperature ($^{\circ}$ C) History from BREN Tower During T-33 Fly-By	161
42.1	Test Log of Valid Data Recorded for Operation Rough Rider (1969) by the LO-LUCAT T-33A Airplane	175
42.2	Meteorological Data and Gust Velocity Standard Deviations	176
43.1	Wake Turbulence Test Information	193
43.2	Minimum and Maximum Gust Velocities	196
43.3	Calculated Vortex Sizes	197
44.1	Percentage of Gust Velocity Data Obtained During Contour Flight over Various Terrains	249
44.2	Comparison of Phase III High Mountain Data by Location	250
44.3	Comparison of Gust Velocity RMS Values - All Data	250
44.4	Comparison of Gust Velocity RMS Mean Values	251
44.5	Relative Amount of Data from Various Locations	252

LIST OF TABLES
VOLUME I, PART II

<u>TABLE NO.</u>	<u>TITLE</u>	<u>PAGE NO.</u>
44.6	Comparison of Gust Velocity RMS Values over Low Mountain Terrain	252
44.7	Estimated Distribution of Gust Velocity RMS Values	254
47.1	Average Scale Lengths and Standard Deviations for Phases I and II and Phase III	287
47.2	Average Scale Lengths and Standard Deviations - Edwards High Mountain Terrain, Fall Season - Phases I and II and Phase III	288
49.1	Pertinent Information for Low Altitude Turbulence Programs	315
50.1	Reference X.1 (F-106) Turbulence Data	321
50.2	Reference X.2 (F-106) Turbulence Data	323
50.3	Reference X.3 (T-38) Turbulence Data	326
50.4	Reference X.4 (B-52E) Turbulence Data	327
50.5	Reference X.5 (B-52H) Turbulence Data	328
50.6	Reference X.6 (B-66) Turbulence Data - Group A	329
50.7	Reference X.6 (B-66) Turbulence Data - Group B	330
50.8	Reference X.6 (B-66) Turbulence Data - Group C	331
XI.1	LO-LOCAT Phase III Samples Selected for Additional Research	350
XI.2	High Intensity Gust (F-106) Samples Selected for Additional Research	351
51.1	Comparison of Gust Acceleration Standard Deviations	353
51.2	Comparison of Gust Acceleration Standard Deviations	354
51.3	Effects of Rate Measurements in Gust Acceleration Calculations	355
51.4	Mean Values	355

LIST OF TABLES
VOLUME I, PART II

<u>TABLE NO.</u>	<u>TITLE</u>	<u>PAGE NO.</u>
51.5	Effects of Differentiated Airspeed and Attitude Means	356
51.6	Comparisons of Gust Velocity Standard Deviations	357
51.7	Comparison of Standard Deviations and Scale Lengths Calculated from Filtered and Unfiltered Gust Acceleration Data (Test 159, Sample 15)	357
51.8	Comparison of Gust Velocity Standard Deviations with Two Different High-Pass Filters	361
51.9	Filter Effect on Scale Length	361
51.10	Primary Peak, Amplitude, and Level Crossing Standard Deviations for Category 122000	365
52.1	Average Scale Lengths Calculated During the LO-LOCAT Program	398
53.1	Extreme Values of $\dot{\theta}$ and $\dot{\psi}$	414
53.2	Comparison of Characteristic Frequencies	416
53.3	Average Standard Deviations for the Re-Processed High Intensity Gust Investigation Samples	417
53.4	Comparison of High Intensity Gust Investigation Scale Lengths with Those Obtained During LO-LOCAT Phase III	420

SYMBOLS

Infrequently used symbols are defined after the equation in which they are used.

Symbols and Abbreviations:

A	Regression coefficient.
A thru H, J, K	Angle of attack equation coefficients.
A' thru H', J', K'	Angle of sideslip equation coefficients.
A(n)	Complex finite transform.
$\tilde{A}(n)$	Complex conjugate of A(n).
a	"Universal Constant" in the longitudinal gust velocity component spectrum expression; shape parameter used in spectra mathematical expressions; constant in gust velocity rms distribution equation.
B	Air stability ratio.
b	Constant in gust velocity rms distribution equation.
b_1, b_2	Constants in the analytical expressions of the peak count probability distributions.
C	Constant in the Lumley-Panofsky equation.
CC	Cloud cover (percent).
CDT	Central Daylight Time.
C_L	Airplane lift curve slope (radians) ¹ .
C_v	Constant in the Busch-Panofsky equations.
c	Length of mean aerodynamic chord (feet).
c.g.	Airplane center of gravity.
cpf	Cycles/foot.
cps	Cycles/second.
DOY	Day of year.
d	Degrees of freedom; distance traveled (statute miles); differential.

SYMBOLS

Symbols and Abbreviations:

E_1	Normalized standard error of a regression coefficient.
E_α	Total crossings of the level α .
e	Base of natural logarithms (2.71828).
F	F-ratio or F-test of significance in regression analysis.
$F(x)$	Cumulative probability distribution function.
f	Frequency (cycles/second); function.
$f(r)$	Longitudinal correlation function.
f_b	Frequency of occurrence in band b.
f_c	Cutoff frequency of a low-pass filter (cycles/second).
f_N	Nyquist or folding frequency (cycles/second).
f_s	Sampling frequency (samples/second).
GMT	Greenwich Mean Time.
G_s	Ground speed (feet/second).
g	Earth's gravitational constant at sea level (32.174 feet/second) 2 .
$g(r)$	Lateral or vertical correlation function.
H	Altitude above the earth's surface (feet); true altitude (feet).
H_e	Calibrated pressure altitude (feet).
$H(f)$	Filter transfer function.
Hg	Symbol for the element mercury.
H_I ,	Indicated reading of tower altimeter (feet).
H_I, H_1	Indicated pressure altitude (feet).
$\overline{H}_N(f)$	Constrained filter transfer function.

SYMBOLS

Symbols and Abbreviations:

H_p	Pressure altitude (feet).
H_t	Terrain elevation (feet).
h	True heading (degrees).
h_m	Magnetic heading (degrees).
h_n	Filter weights at time $t \pm n \Delta t$.
\bar{h}_n	Constrained filter weights.
$h(t, \tau)$	Time domain weighting function.
h_0	Constant in empirical scale length equation.
i	Counter; time series sample.
IAS	Indicated airspeed.
IRIG	Inter-range Instrumentation Group.
j	Square root of minus one.
$K_{a,b}$	Constants.
KIAS	Knots indicated airspeed.
K_g	Gust alleviation factor.
K_t	Ram recovery factor for QAT probe.
k	Spatial frequency (cycles/foot); order of the derivative of the transfer function $H(f)$; indicates number of records.
L	Turbulence scale length (feet).
L_h	Constant in empirical scale length equation.
M	True Mach number.
m	Maximum lag ($f_N/\Delta f$); slope of a line; number of functions of the input variables; and meters.
mb	Millibar.
mm	Millimeter.

SYMBOLS

Symbols and Abbreviations:

N	Total number of conditions, data points, samples, peaks, bands, or filter weights.
NBFM	Narrow band frequency modulation.
N ₀	Characteristic frequency from power spectral density (cycles/foot).
N _{OL}	Number of zero level crossings.
N _p	Total number of peaks per mile obtained using extrapolation technique (characteristic frequency).
N _{pe}	Total number of peaks obtained using extrapolation technique.
N _{α}	Crossings per mile of the level α .
n	Acceleration in g units; counter; number of data points; shape parameter in spectra mathematical expressions.
OAT	Outside air temperature (degrees Fahrenheit).
O _n	Run test observation of the mean.
O' _n	Run test observation of the mean square.
PSD	Power spectral density.
PST	Pacific Standard Time.
P _s	Static pressure (inches of mercury).
P _{s₁}	Indicated static pressure (inches of mercury).
P ₀	Standard atmospheric pressure at sea level (29.921 inches of mercury).
P ₁ , P ₂	Intercepts of the exponential curves for the analytical expressions of the peak count probability distributions.
Q	Number of independent variables in the regression equation.
q _c	Calibrated impact pressure (inches of mercury).

SYMBOLS

Symbols and Abbreviations:

q_I	Indicated impact pressure (inches of mercury).
R_A	Radar altitude (feet).
R	Richardson number.
$[R]$	Rotation matrix used to transform measurements from the airplane reference axes to the earth reference axes.
R_1	Value of rms gust velocity at a given wind speed as read from least square line (feet/second).
$R(i)$	Autocorrelation function.
$R_{xy}(i)$	Cross correlation function.
rms	Root mean square.
$R(\tau)$	Gust velocity covariance function.
$R(\tau)/R(0)$	Gust velocity autocorrelation function where $\tau = 0 \dots \tau_L$.
r	Distance (feet).
r_c	Value of r at which the autocorrelation function crosses zero.
S	Airplane planform wing area (feet^2); horizontal distance - miles.
S_{SE}	Sine of solar elevation.
T_a	Ambient air temperature (degrees Rankine).
$T_{\text{filt.}}$	Time width of filter weight function.
T_G	Ground surface temperature (degrees Fahrenheit).
T_I	Calibrated outside air temperature (degrees Rankins).
T_0	Temperature at sea level under standard conditions (518.69 degrees Rankine).
T_s	Air temperature at the surface (degrees centigrade).

SYMBOLS

Symbols and Abbreviations:

T _{A1}	Temperature at 250 feet (degrees Fahrenheit).
T _{A2}	Temperature at 750 feet (degrees Fahrenheit).
T _{A3}	Temperature at 1000 feet (degrees Fahrenheit).
T _{A4}	Temperature at flight altitude plus 1000 feet (degrees Fahrenheit).
T _{A7}	Temperature at flight altitude (degrees Fahrenheit).
T _{D2}	Dew point at 750 feet (degrees Fahrenheit).
T _{D3}	Dew point at 1000 feet (degrees Fahrenheit).
T _{D4}	Dew point at flight altitude plus 1000 feet (degrees Fahrenheit).
T _{D5}	Dew point at 850mb (degrees centigrade).
TOD	Time of day.
t	Time (seconds); standardized variable.
U _{de}	Derived equivalent gust velocity (feet/second).
u	Longitudinal gust velocity (feet/second); positive-aft.
v	True airspeed or ground speed (feet/second).
V _e	Equivalent airspeed (feet/second).
V _T	True airspeed (feet/second).
{v}	Represents the matrix of true airspeed components corrected for pitch and yaw.
v	Lateral gust velocity (feet/second), positive to the right.
W	Airplane weight (pounds); wind speed (feet/second).
WA	Angle between airplane ground track and wind vector (degrees) positive - wind vector from the left, zero degrees - direct tail wind.
W _{A4}	Wind direction at flight altitude plus 1000 feet (degrees azimuth).

SYMBOLS

Symbols and Abbreviations:

W_D	Wind direction (degrees azimuth).
\bar{W}_E	Average easterly winds (feet/second).
\bar{W}_N	Average northerly winds (feet/second).
W_S	Wind speed at the surface (knots).
W_6	Wind speed at 700mb (knots).
w	Vertical gust velocity (feet/second), positive - upward.
x	Amplitude.
x_b	Mid-band value.
x_i	i^{th} value of x ; predictors; coefficient of simple linear correlation; value of gust velocity rms at a given wind speed (feet/second).
x_a	Level of gust velocity (feet/second).
$x_k(t_1)$	k^{th} record included in the ensemble averaging scheme.
$x(t)$	Sampled value of time series.
Y	Dependent variable; regression function.
α	Angle of attack (degrees), positive - nose above relative wind; levels of gust velocity used in level crossing procedures; confidence limit.
β	Angle of sideslip (degrees), positive - nose left of relative wind.
Γ	Standard lapse rate (0.00356 degrees Fahrenheit/foot), positive - temperature decrease with increasing altitude.
Γ_d	Dry adiabatic lapse rate (0.0055 degrees Fahrenheit/foot).
γ	Ratio of specific heats for air (1.40).
$\gamma^2(k)$	Coherency function.

SYMBOLS

Symbols and Abbreviations:

Δ	Incremental or difference.
Δf	Change in frequency (cycles/second); frequency range spanned by filter roll-off; frequency interval between adjacent PSD data points.
ΔH	Distance above or below reference point (feet); difference in terrain elevation (feet).
Δh	Static pressure error (feet).
ΔN_{ZCG}	Incremental load factor (acceleration units).
ΔP_s	Static pressure position error (inches of mercury).
$\Delta P_s/q_I$	Pressure coefficient (dimensionless).
ΔP_a	Angle of attack differential pressure (inches of mercury).
ΔP_θ	Angle of sideslip differential pressure (inches of mercury).
ΔT_{u_z}	Vertical temperature gradient (degrees Fahrenheit/foot).
ΔT_H	Horizontal temperature gradient (degrees Fahrenheit/mile).
ΔT_s	Atmospheric stability (degrees Fahrenheit/1000 feet), positive - temperature increase with increasing altitude.
Δt	Time interval between data samples (seconds).
ΔW_{D_z}	Vertical wind direction gradient (degrees/foot).
ΔW_H	Horizontal wind gradient (feet/second/mile).
ΔW_{HEW}	Horizontal east-west wind gradient (feet/second/mile).
ΔW_z	Vertical wind velocity gradient (feet/second/foot).

SYMBOLS

Symbols and Abbreviations:

δ	Drift angle (degrees), positive to the right.
ϵ	Viscous dissipation rate (feet ² /second ³); emissivity factor; filter empirical error bounds (percent).
η	Kolmogorov microscale (feet).
θ	Pitch angle (degrees), positive - nose up.
$\dot{\theta}$	Rate of pitch (degrees/second), positive - nose moving up.
λ	Taylor turbulence microscale length (feet); characteristic wavelength (feet); terrain wavelength (feet).
μ	Air viscosity (pound second/feet ²); mean value; airplane mass ratio.
μ_2, μ_3	Constant in gust velocity rms distribution equation.
$\mu_x(t)$	Ensemble average time function.
ν	Kinematic viscosity (feet ² /second); degrees of freedom.
π	3.1416. . . .
ρ	Air density (slugs/foot ³).
ρ_0	Standard air density at sea level (0.002378 slugs/foot ³).
σ	Standard deviation of a statistical sample; standard deviation (fps) from gust velocity spectra between 0.0416 and 10 cps; Stefan-Boltzman constant.
σ_D	Standard deviation about a least square line.
σ_L	Standard deviation of level crossing distribution.
σ_N	Standard deviation of noise.
σ_{pe}	Standard deviation of primary peaks obtained using extrapolated value of N_{pe} .
σ_R	Standard deviation of recorded data.
σ_T	Standard deviation obtained from the truncated gust velocity spectra (feet/second).

SYMBOLS

Symbols and Abbreviations:

σ_t	Standard deviation of the gust velocity time series (feet/second).
σ_{tr}	Standard deviation of terrain roughness (feet).
σ_a	Standard deviation of angle of attack differential pressure (inches of mercury).
σ_s	Standard deviation of sideslip differential pressure (inches of mercury).
σ_v	Standard deviation (dispersion of the distribution) of gust velocity rms (feet/second).
σ_1	Standard deviation of the derivative of the time function divided by $2\pi V$ (cps for gust velocity).
σ_2, σ_3	Constant used in rms gust velocity distribution equation.
τ	Lag time for the weighting operation convolution (seconds).
Φ	One-dimensional gust velocity power spectral density.
$\Phi(k)$	Power spectral estimates.
$\Phi(n)$	Raw estimate of power spectral density.
$\Phi'(n)$	Averaged estimate of power spectral density.
$\Phi_{xy}(n)$	Estimate of cross power spectral density.
Φ_{90}	Power spectra 90 per cent confidence interval.
ϕ	Roll angle (degrees), positive - right wind down.
$\dot{\phi}$	Rate of roll (degrees/second), positive - right wing moving down.
χ	Chi statistic.
ψ	Yaw angle (degrees), positive - nose right.
$\dot{\psi}$	Rate of yaw (degrees/second), positive - airplane nose moving right.
ω	Frequency (radians/second).

SYMBOLS

Subscripts and Superscripts:

b	Band number.
D	Based on the Dryden equation.
e	Extrapolated value.
filt.	Filtered value.
H	Horizontal.
i	Sample number.
N	Noise.
n	Counter.
K	Based on the von Karman equation.
max	Indicates maximum value.
min	Indicates minimum value.
P	Peak count; based on the Lumley-Panofsky equation.
T	Truncated; obtained from tower.
t	From the gust velocity time series.
u	From the longitudinal gust velocity component.
v	From the lateral gust velocity component.
w	From the vertical gust velocity component.
x	Longitudinal.
y	Lateral.
z	Vertical.
o	Initial value.
I	Pertaining to quadrant 1; indicates LO-LOCAT Phases I and II.
II	Pertaining to quadrant 2.
III	Pertaining to quadrant 3; indicates LO-LOCAT Phase III.

SYMBOLS

Subscripts and Superscripts:

IV Pertaining to quadrant 4.

Related to level crossing count.

Primes indicate Hanned estimates unless otherwise noted.

Overbars depict time means.

2 Refers to starting point of leg.

3 Refers to ending point of leg.

32 Refers to difference between start and end.

Weather Chart Symbols

Surface Charts:

— 1018 Sea level pressure (millibars)

----- 50 Temperature (° F.)

Cloud Cover:

○ Clear

⊕ 6/10

⊖ 1/10

● 7/10 or 8/10

⊖ 2/10 or 3/10

● 9/10

⊖ 4/10

● Overcast

⊖ 5/10

⊗ Sky obscured

Wind:

○ Calm

—○ 10 Knots

—○ ≤ 2 Knots

—○ 15 Knots

—○ 5 Knots

—○ 50 Knots

Tail points in the direction from which the wind is blowing.

SYMBOLS

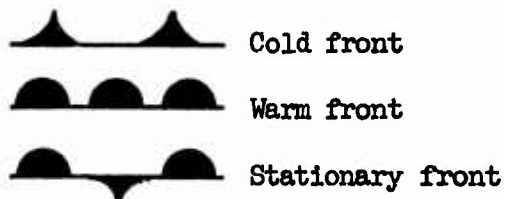
Weather Chart Symbols (Contd.)

Surface Charts (Contd.):

Precipitation:

- | | |
|------------|-----------------|
| .. Rain | ▽ Rain shower |
| ** Snow | † Snow shower |
| ,, Drizzle | ✖ Freezing rain |
| ≡ Fog | TC Thunderstorm |

Fronts:



Upper Air Charts

- 1540 Height of pressure surface (meters)
- - - 1530 Intermediate height values (meters)

SECTION VI
GEOPHYSICAL CHARACTERISTICS

32. TERRAIN PROFILES

The primary purpose of the LO-LOCAT Program was to describe the probability distribution of the gust velocity rms values over a wide variety of meteorological and topographical conditions. Flight routes were established in California (Edwards route), Colorado (Peterson route), Kansas (McConnell route), and New York (Griffiss route) to achieve those objectives.

It was found that several factors must be considered in the design of routes of this type. Predominant landmarks are desirable at the beginning of each leg. Heading of the airplane relative to the sun is an important safety consideration for early and late flights. From an operational standpoint, the amount of time each leg cannot be flown due to adverse weather must be taken into account. Features of the terrain surrounding a route leg may influence results as well as the terrain coincident with the leg. This factor must be considered along with orientation of legs with respect to mountain ridge lines and prevailing winds.

Characteristics of each route were determined by defining the terrain profile and calculating terrain roughness values and characteristic wavelengths. The terrain profile was determined by subtracting airplane radar altitude from pressure altitude. Linear trends in the profiles were removed to reduce the effects of Gibbs' phenomenon when calculating the spectra. Altitude versus distance plots of terrain profiles are presented in Figures 32.1 through 32.4.

Power spectral densities, standard deviations, and characteristic wavelengths of the terrain profiles were calculated. Power spectra of terrain profiles for each route are presented in Figures 32.5 through 32.12.

Terrain roughness rms values were calculated by:

$$\sigma_{tr} = \left[\frac{1}{N} \sum_{i=1}^N (x_i - \bar{x})^2 \right]^{1/2} \quad (32.1)$$

where x_i is the i th value of the terrain profile in feet, $i = 1$ to N , and \bar{x} is the arithmetic mean.

Characteristic wavelengths (λ) in feet were obtained by:

$$\lambda = \frac{\sigma}{\sigma_1} \quad (32.2)$$

where:

$$\sigma = \left[\int_0^a \Phi(k) dk \right]^{1/2} \quad (\text{feet}) \quad (32.3)$$

$$\sigma_1 = \left[\int_0^a k^2 \Phi(k) dk \right]^{1/2} \quad (\text{cycle}) \quad (32.4)$$

and: $\Phi(k)$ is the power spectral density of the terrain profile.

Comparison of the McConnell route terrain spectra for Phases I and II with the Phase III terrain spectra shows that the Phase III spectra approach a constant power level at a lower frequency (longer wavelength) than does the Phases I and II data. The Phase III spectra were truncated at lower frequencies because of the high sensitivity of the σ_1 calculation to high frequency noise. Truncating the spectra at lower frequencies had very little effect on σ . The σ_1 and hence λ values were affected considerably by the lack of valid high frequency information. The reduction in the valid frequency range of the terrain spectra is due to the increased speed of the airplane during Phase III and the response time of the altitude recording system, (Reference Appendix II).

The accuracy of the terrain height measurement is also affected by the terrain roughness. That is, the radar altimeter is more accurate in measuring a ramp type rather than a step type altitude change. This is evidenced by the comparison of the Phase III McConnell plains, and Edwards high mountain data. The high mountain terrain spectra approaches the constant power level at a lower frequency than does the plains terrain spectra. Therefore, the upper limit of integration (a) in Equations 32.3 and 32.4 was varied from route to route but was generally $1.2/V$ cpf for the rough terrain data and $2.5/V$ cpf for the plains or smooth terrain data where V is ground speed in feet/second. As a result, wavelengths are defined to approximately 500 feet for mountainous terrain and 250 feet for the plains.

The terrain roughness (σ_{tr}), wavelength (λ), and terrain classification, along with a general description of each route, are presented in Tables 32.1 through 32.4.

The category altitudes of 250 and 750 feet are nominal absolute target altitudes at which the pilot was to fly the airplane. The actual flight altitude did not always correspond with the nominal target altitudes. For the greater part, this occurred for flight over the rougher terrains where small crevices and canyons into which the airplane could not maneuver to maintain absolute contour flight increased the average radar altitude. Tables 32.1 through 32.4 also present the average radar altitude for each test altitude for each leg. Figures 32.13 and 32.14 pictorially illustrate the data in Tables 32.1 through 32.4. As can be seen, the rougher the terrain the greater the deviation from the test altitude.

The data obtained over Leg No. 6 of the Edwards route were categorized as both high mountain and low mountain data. This is the result of changing the category after analysis of the terrain profile and roughness. A total of 31 samples of data obtained from 24 October to 14 November 1968 were analyzed as high mountain data. Fifty-five samples obtained from 14 November 1968 to 8 January 1969 were analyzed as low mountain data.

TABLE 32.1
MCCONNELL ROUTE CHARACTERISTICS

Leg	Classification	Terrain		Target Altitude (Feet)	Average Radar Altitude (Feet)
		σ_{tr} (ft)	λ (ft)		
1	Plains	44	4960	250	276
				750	749
2	Plains	59	5100	250	269
				750	757
3	Plains	45	4400	250	267
				750	750
4	Plains	59	4890	250	284
				750	761
5	Plains	62	4730	250	281
				750	753
6	Plains	62	4310	250	276
				750	746
7	Plains	54	4030	250	264
				750	741
8	Plains	111	6330	250	269
				750	756
General geophysical features: Scattered to numerous trees, small lakes, and paved and unpaved roads.					

TABLE 32.2

EDWARDS ROUTE CHARACTERISTICS

Leg	Classification	Terrain		Target Altitude (Feet)	Average Radar Altitude (Feet)
		σ_{tr} (ft)	λ (ft)		
1	Low Mountain	402	10980	250	294
				750	695
2	Desert	186	9760	250	257
				750	738
3	High Mountain	667	8720	250	474
				750	820
4	Water	11	6560	250	245
				750	769
5	High Mountain	948	10660	250	536
				750	843
6	*	305	11080	250	292
				750	747
7	Desert	475	9670	250	287
				750	711
8	Low Mountain	667	8070	250	350
				750	721

General Geophysical Features: Mountainous areas consisted of Joshua trees, large rocks, paved and unpaved roads, and flat sand. Desert areas consisted of brush cover, scattered trees, flat sand, and paved and unpaved roads. The water leg was located over the Pacific Ocean.

* Classified as high mountain for turbulence samples obtained from 24 October 1968 through 14 November 1968 and low mountain from 15 November 1968 through 8 January 1969.

TABLE 32.3

PETERSON ROUTE CHARACTERISTICS

Leg	Terrain			Target Altitude (Feet)	Average Radar Altitude (Feet)
	Classification	σ_{tr} (ft)	λ (ft)		
1	High Mountain	542	9520	250	362
				750	637
2	High Mountain	922	13030	250	363
				750	653
3	High Mountain	503	13630	250	274
				750	673
4	High Mountain	806	11130	250	324
				750	635
5	High Mountain	662	9640	250	406
				750	666
6	High Mountain	518	10170	250	332
				750	578
7	High Mountain	569	9950	250	357
				750	726
8	Plains	90	7360	250	254
				750	710

General Geophysical Features: Mountainous areas consisted of grass land, numerous trees, large rocks, and paved and unpaved roads. Plains area was generally flat grass land, flat sandy soil, and paved and unpaved roads.

TABLE 32.4

GRIFFISS ROUTE CHARACTERISTICS

Leg	Terrain			Target Altitude (Feet)	Average Radar Altitude (Feet)
	Classification	σ_{tr} (ft)	λ (ft)		
1	Plains	113	5100	250	265
				750	717
2	Low Mountain	214	5345	250	244
				750	681
3	Low Mountain	222	6990	250	300
				750	689
4	Low Mountain	323	11500	250	297
				750	701
5	Low Mountain	275	9200	250	358
				750	673
6	Low Mountain	382	12650	250	364
				750	686
7	Plains	161	5820	250	239
				750	675
8	Plains	98	4400	250	237
				750	706
General Geophysical Features: Numerous coniferous and deciduous trees, numerous scattered lakes, and small rocks.					

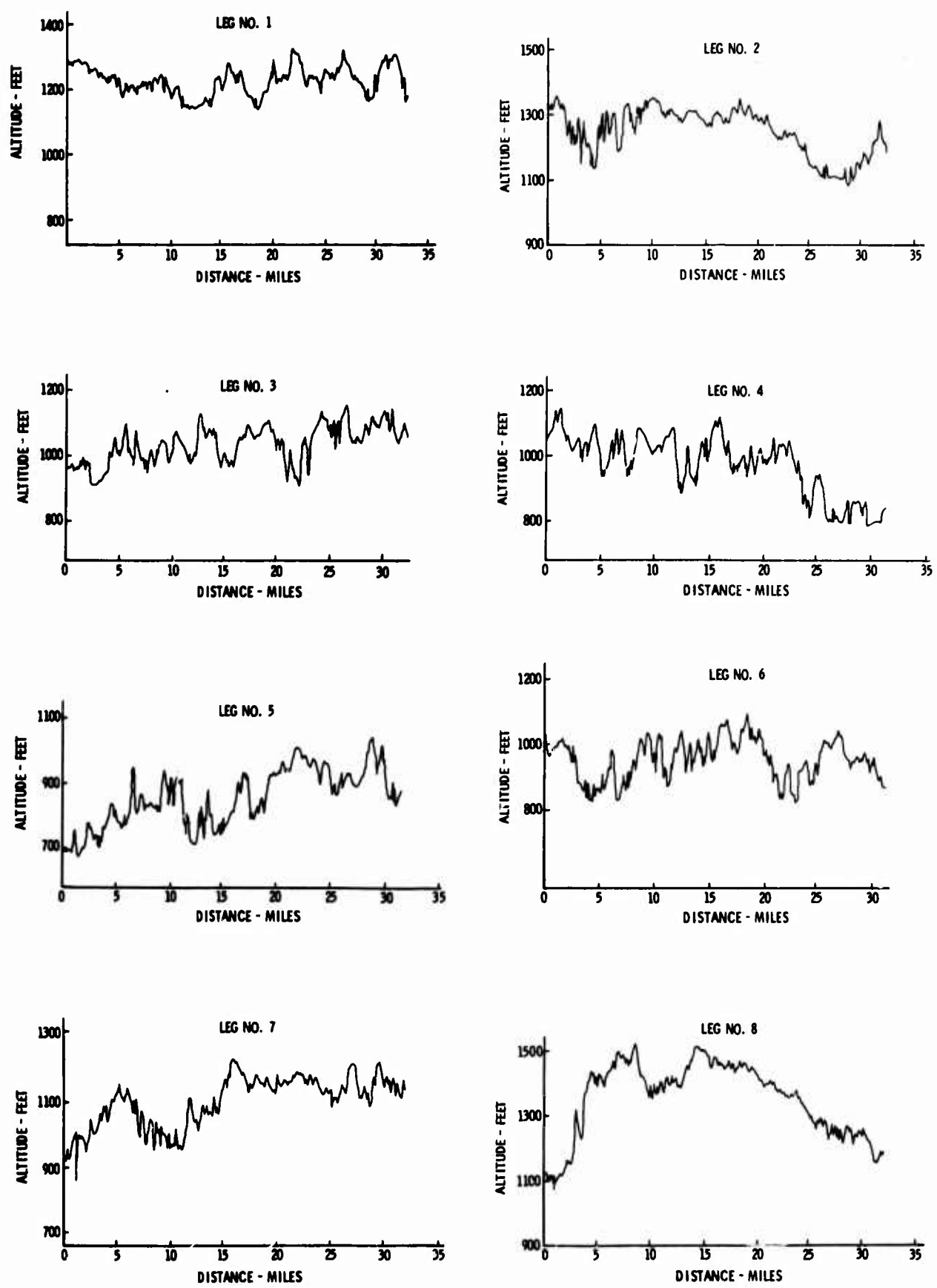


Figure 32.1 McConnell Route Terrain Profile Distance History

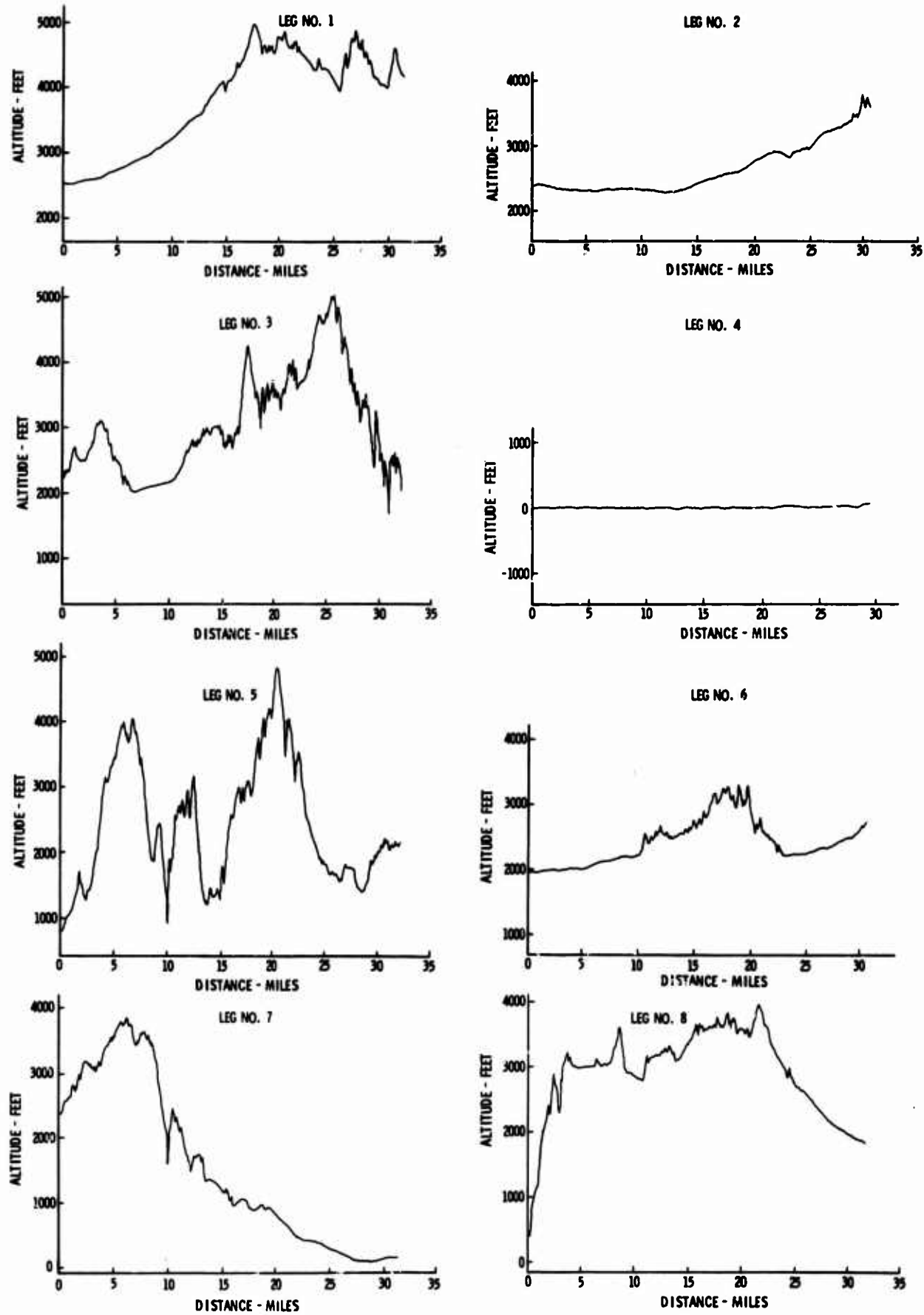


Figure 32.2 Edwards Route Terrain Profile Distance History

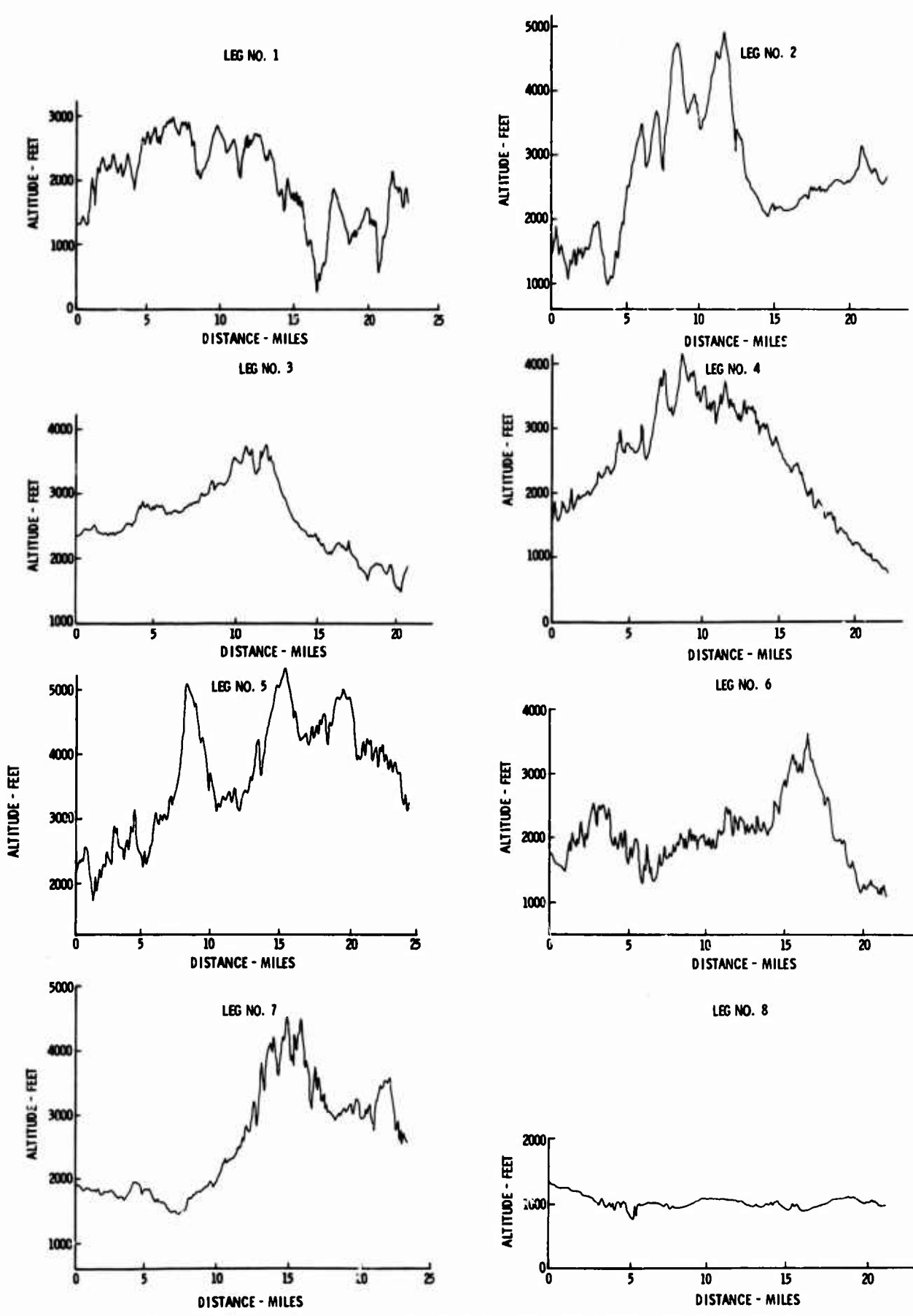


Figure 32.3 Peterson Route Terrain Profile Distance History

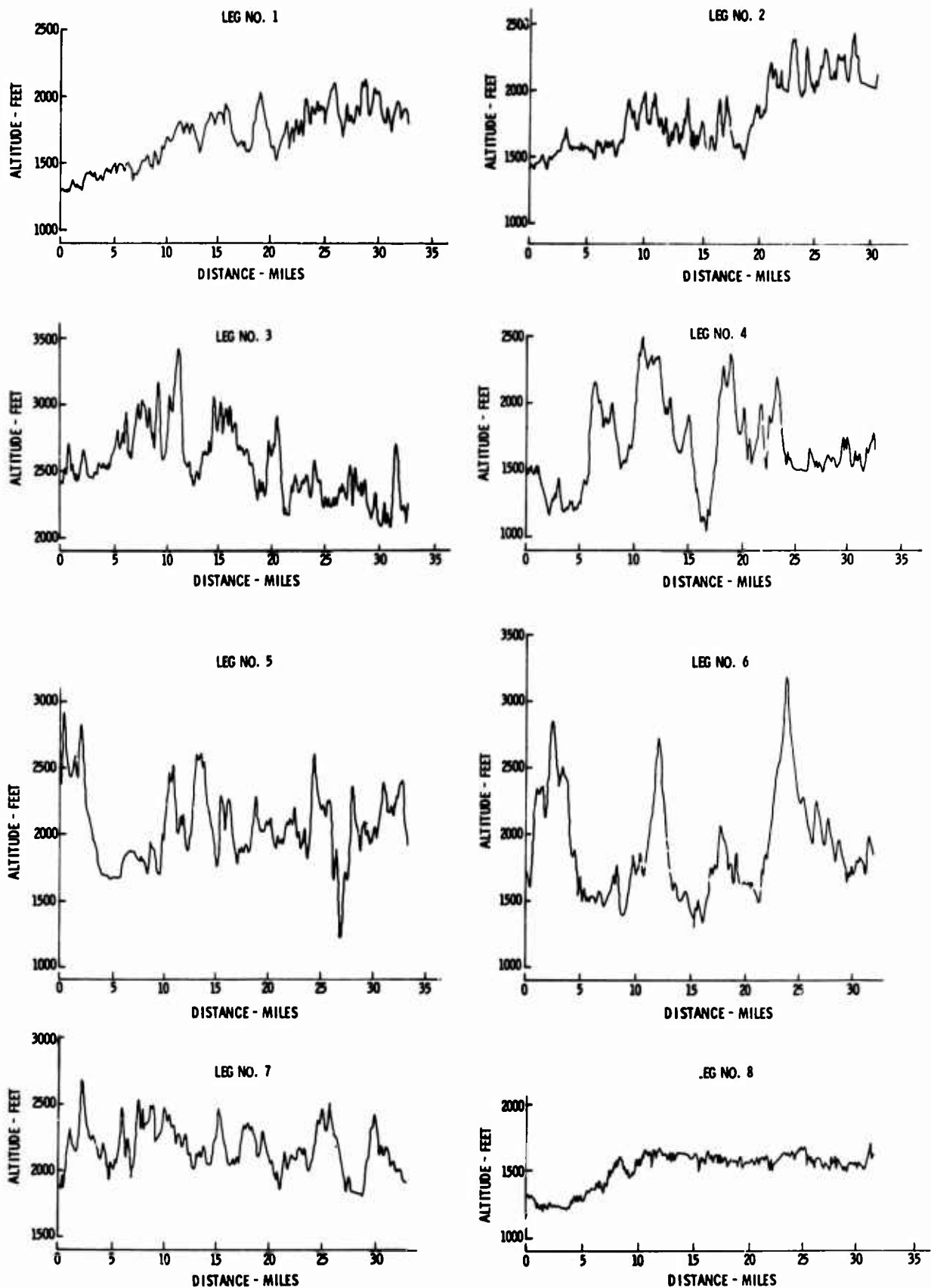


Figure 32.4 Griffiss Route Terrain Profile Distance History

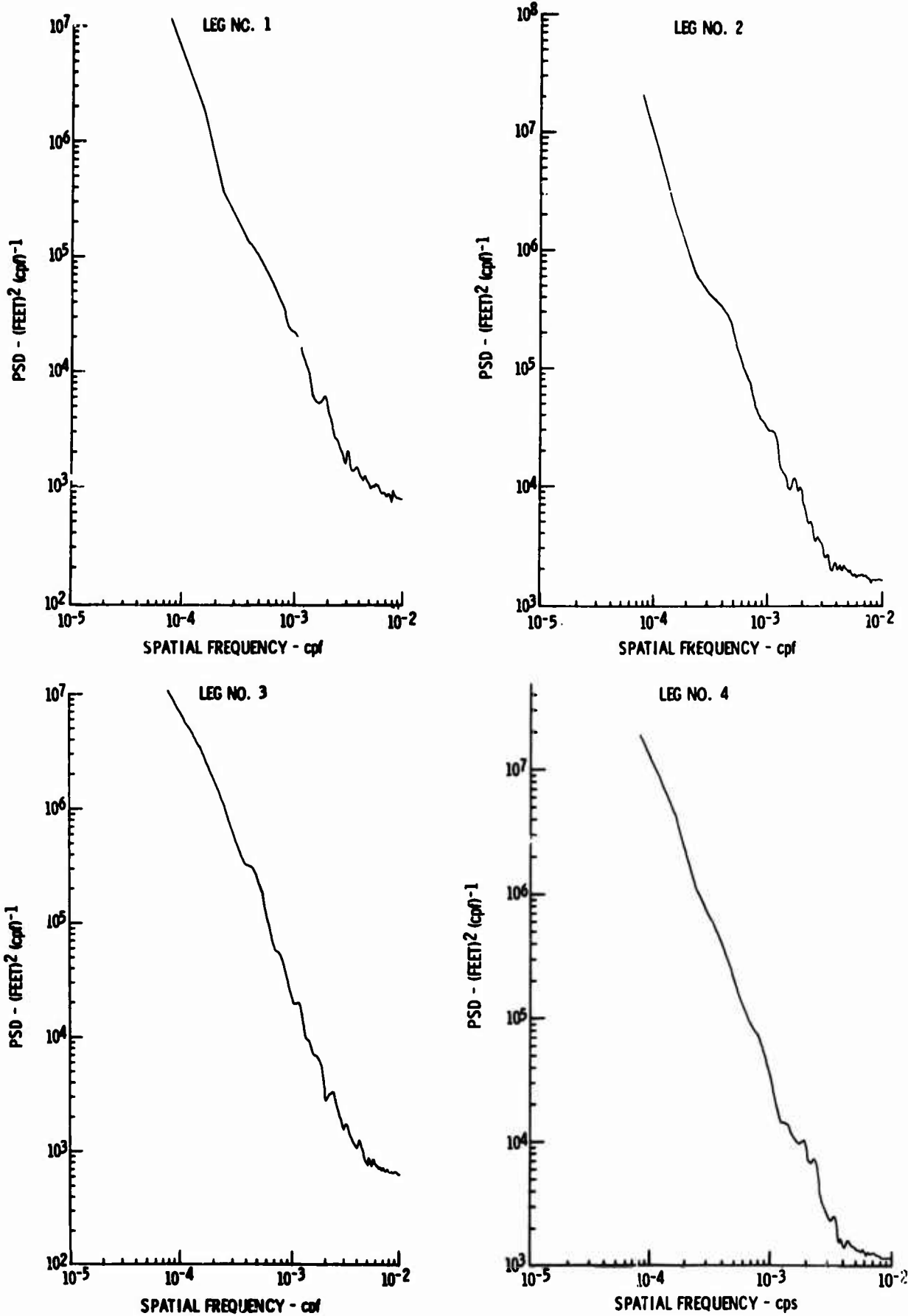


Figure 32.5 McConnell Route Terrain Profile Power Spectra

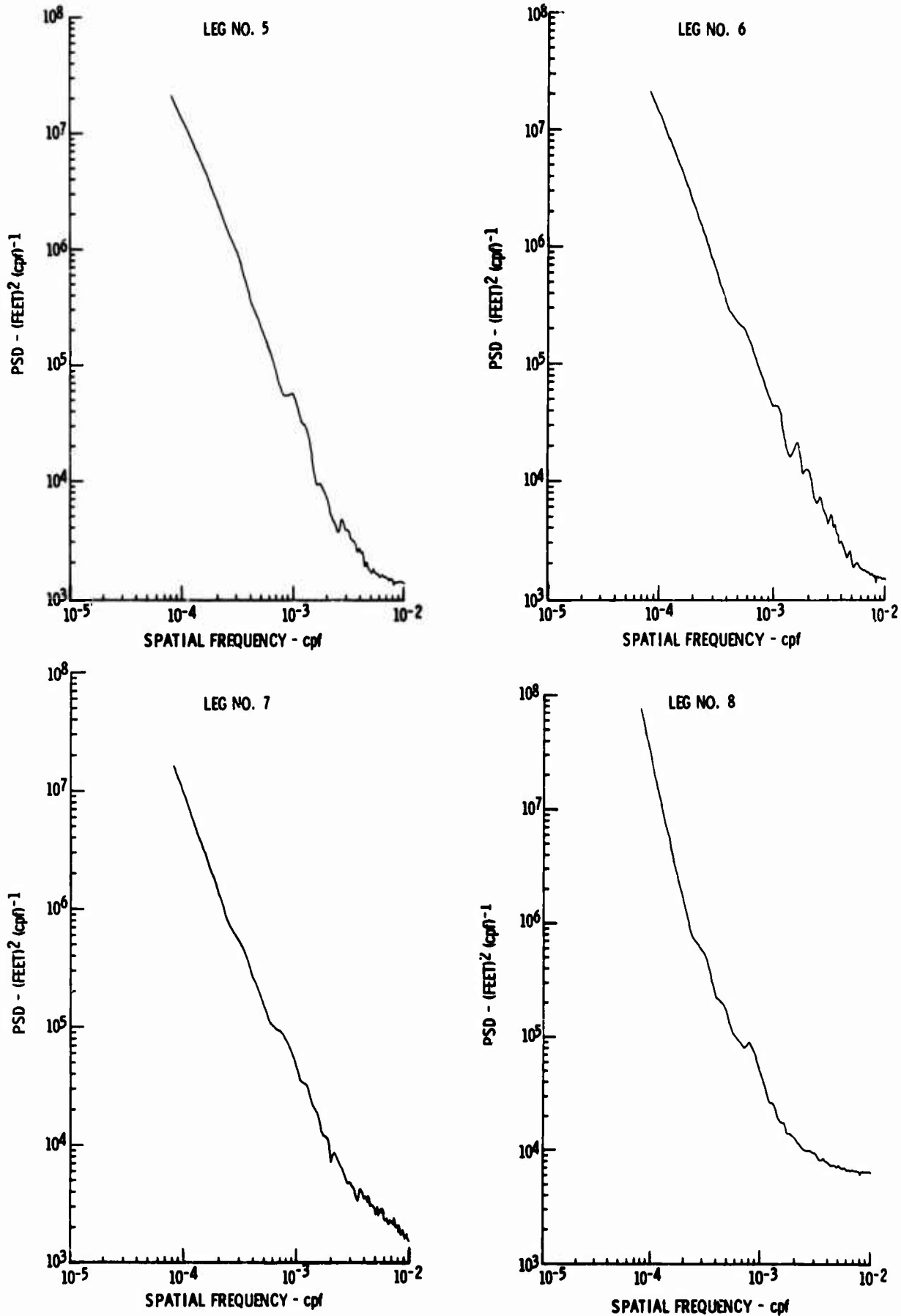


Figure 32.6 McConnell Route Terrain Profile Power Spectra

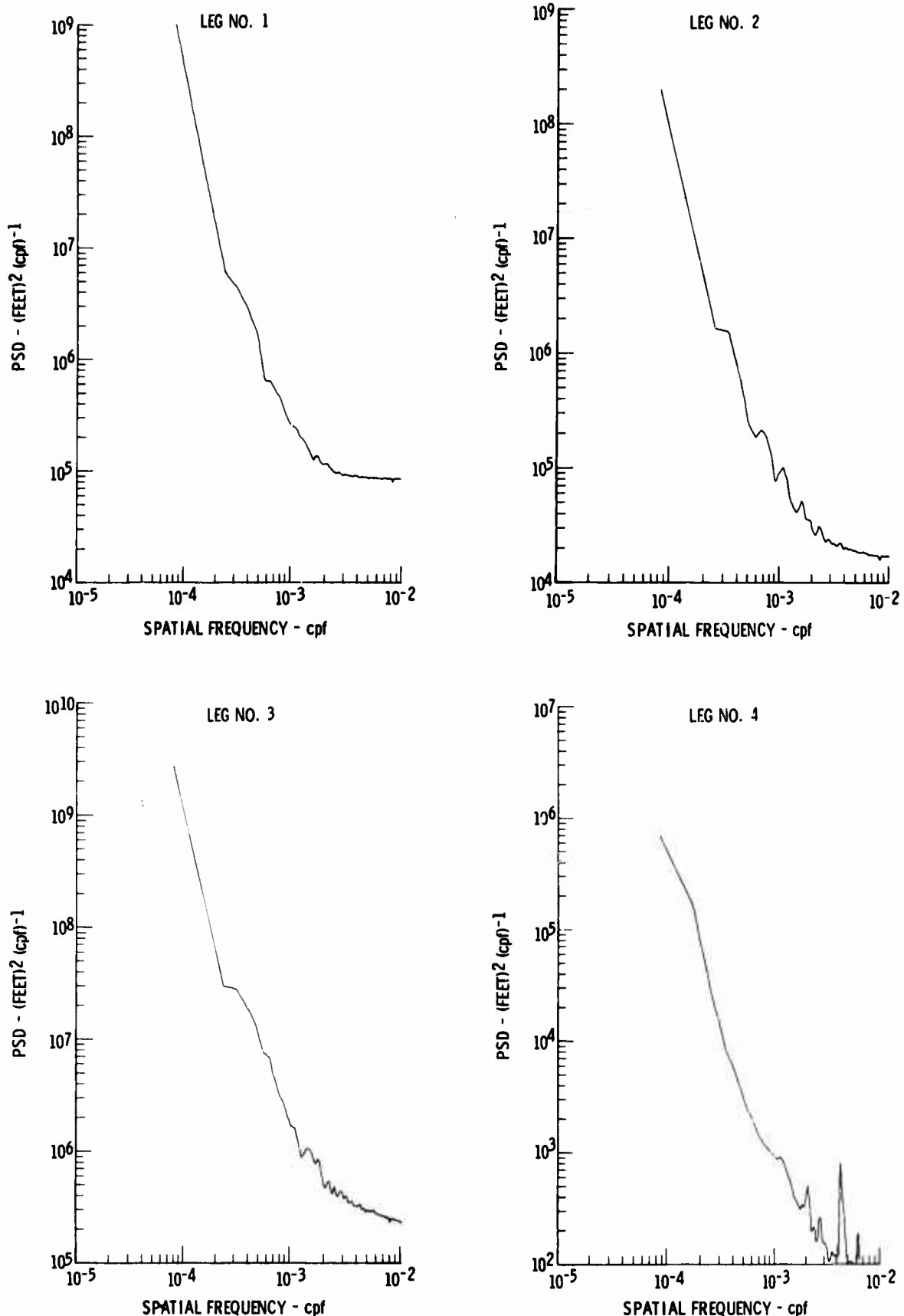


Figure 32.7 Edwards Route Terrain Profile Power Spectra

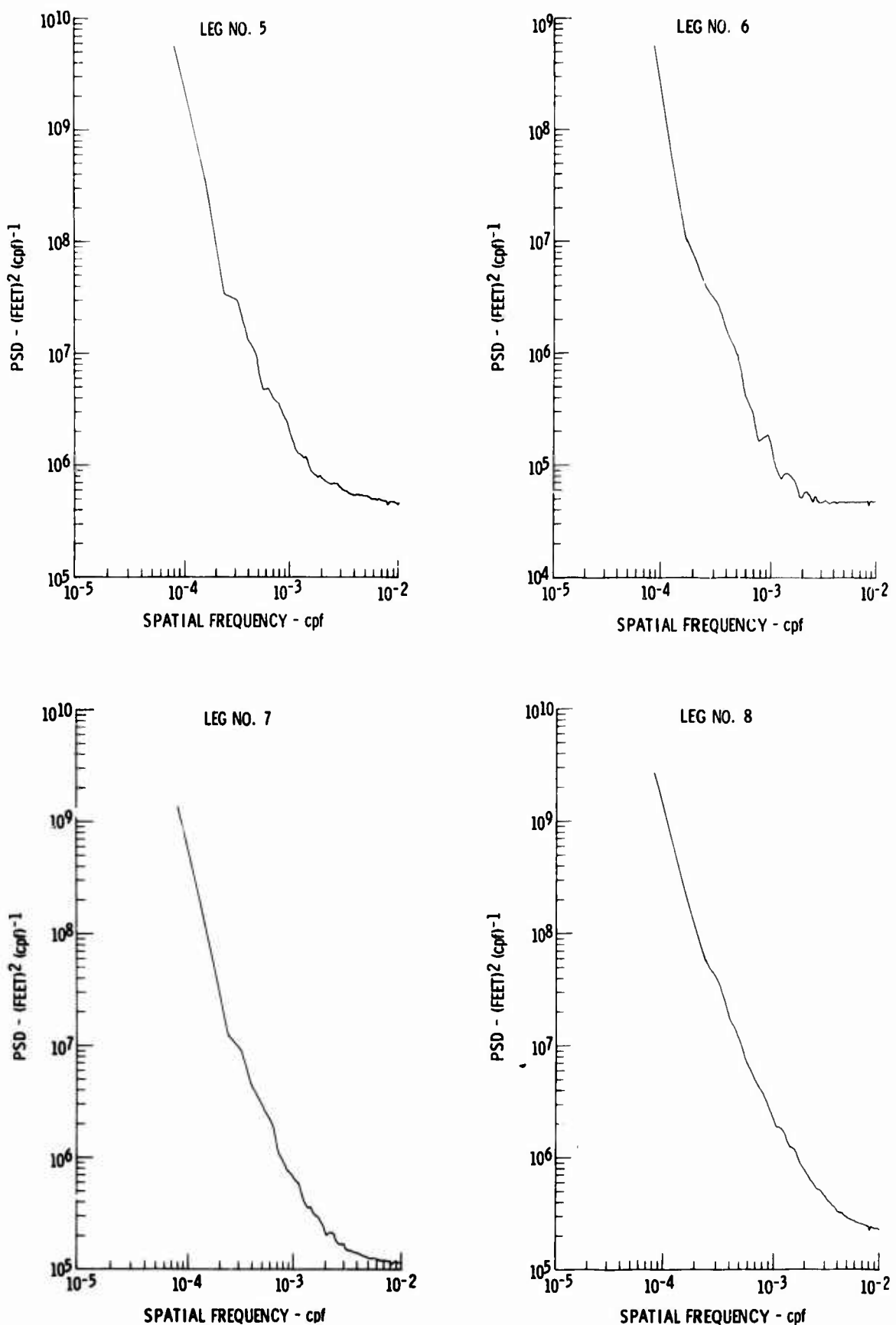


Figure 32.8 Edwards Route Terrain Profile Power Spectra

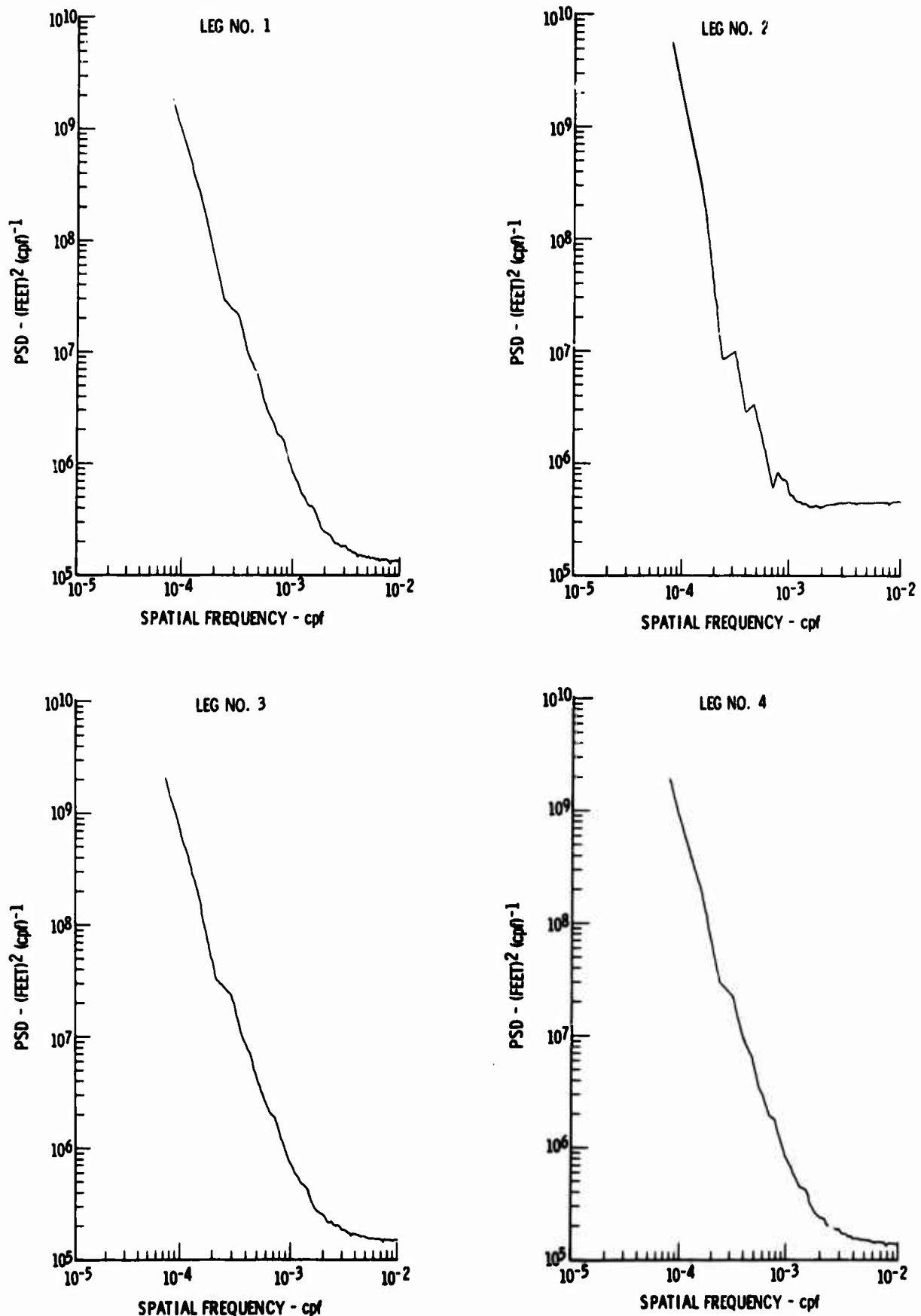


Figure 32.9 Peterson Route Terrain Profile Power Spectra

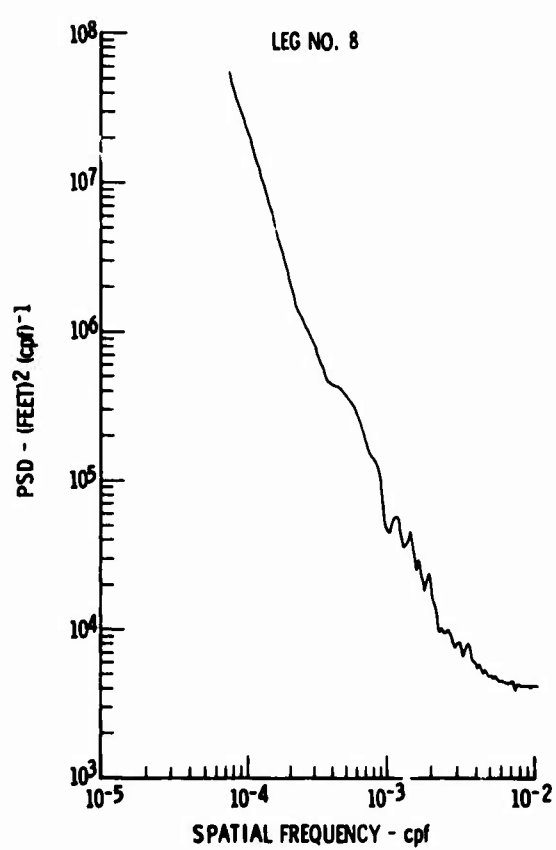
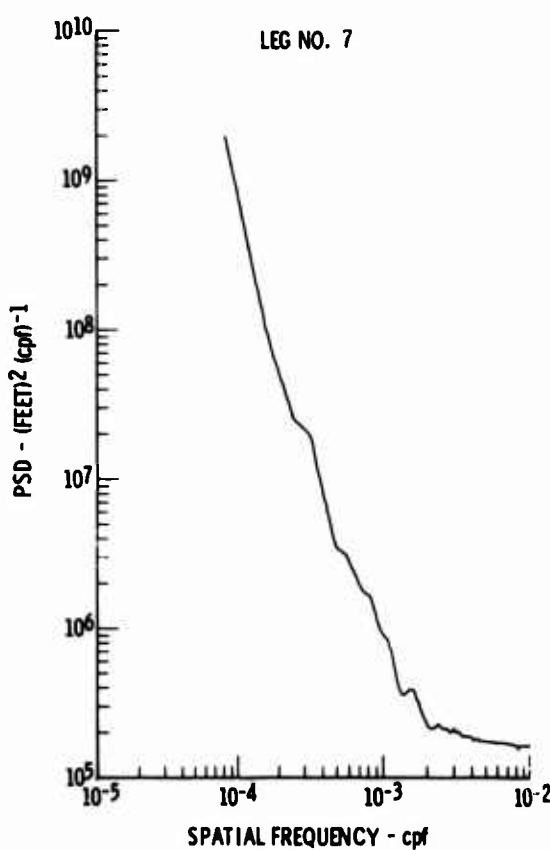
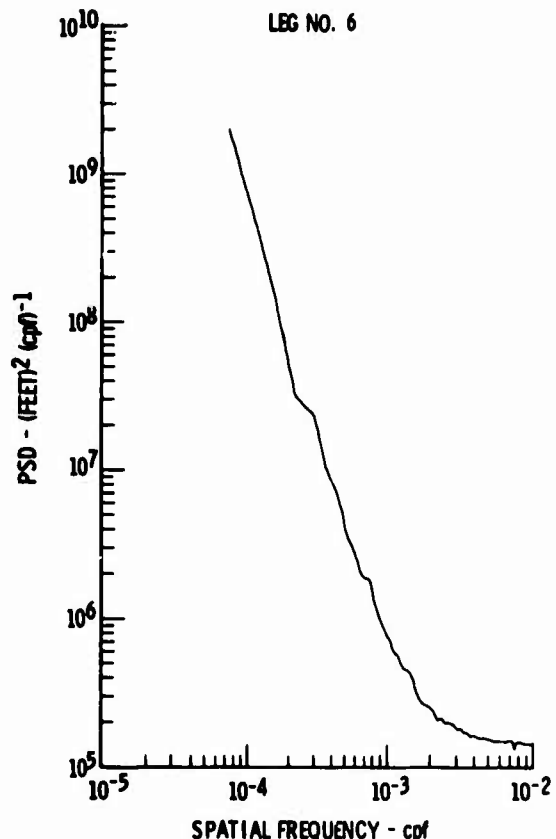
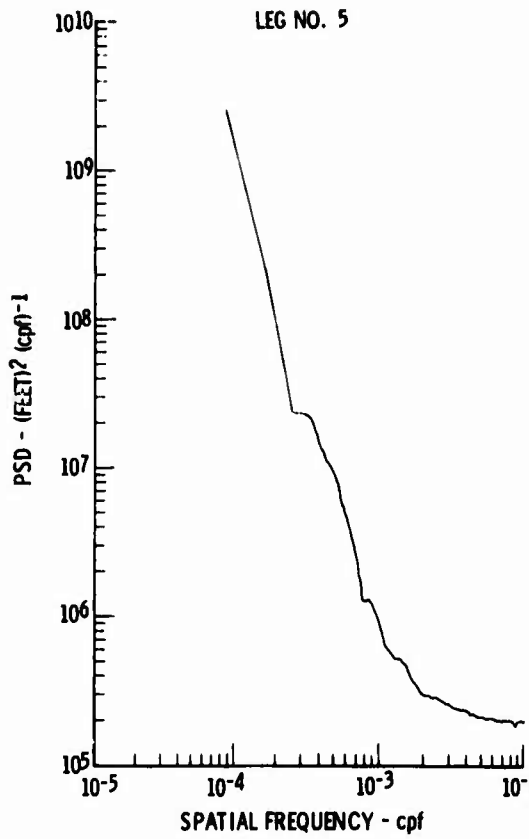


Figure 32.10 Peterson Route Terrain Profile Power Spectra

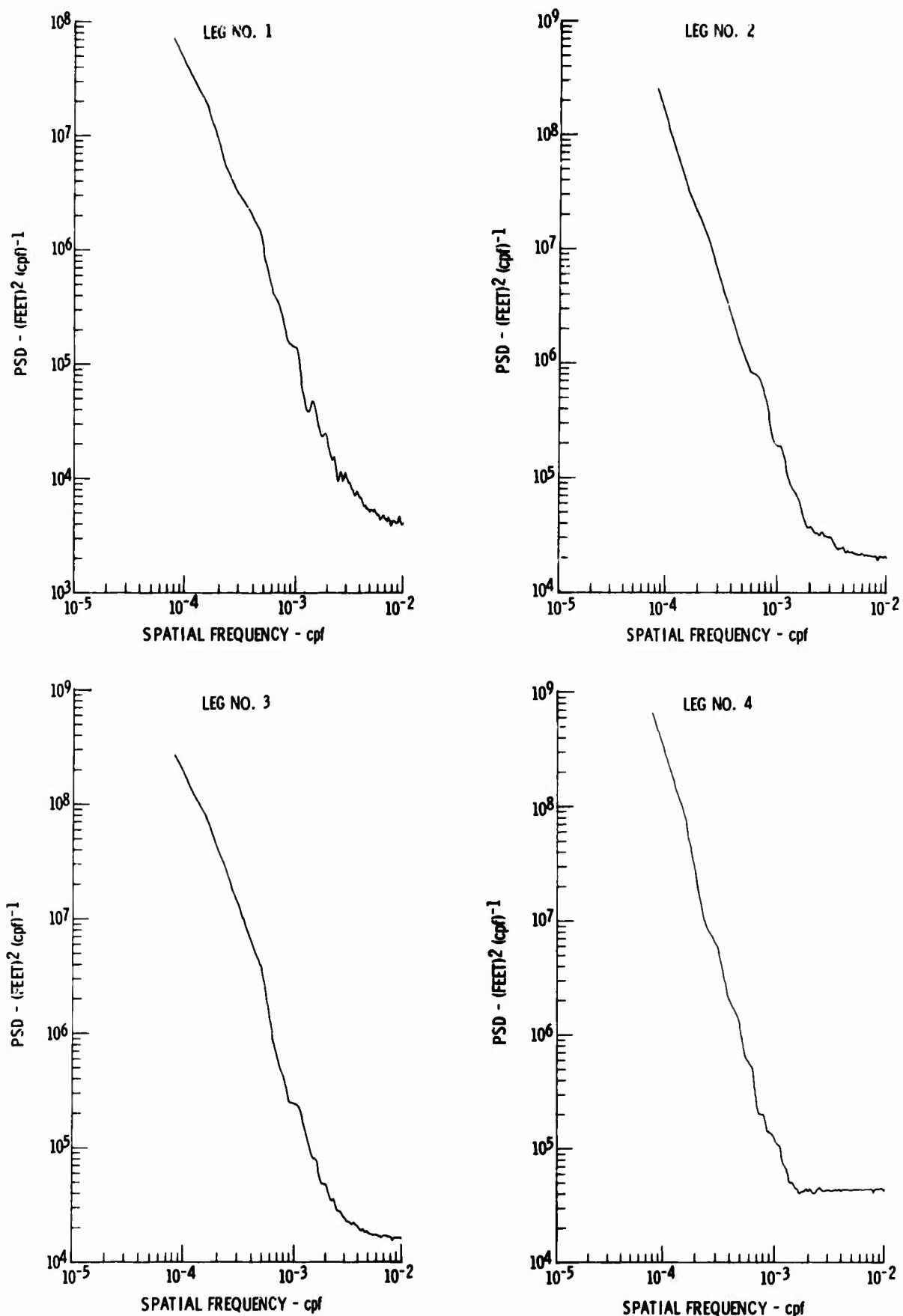


Figure 32.11 Griffiss Route Terrain Profile Power Spectra

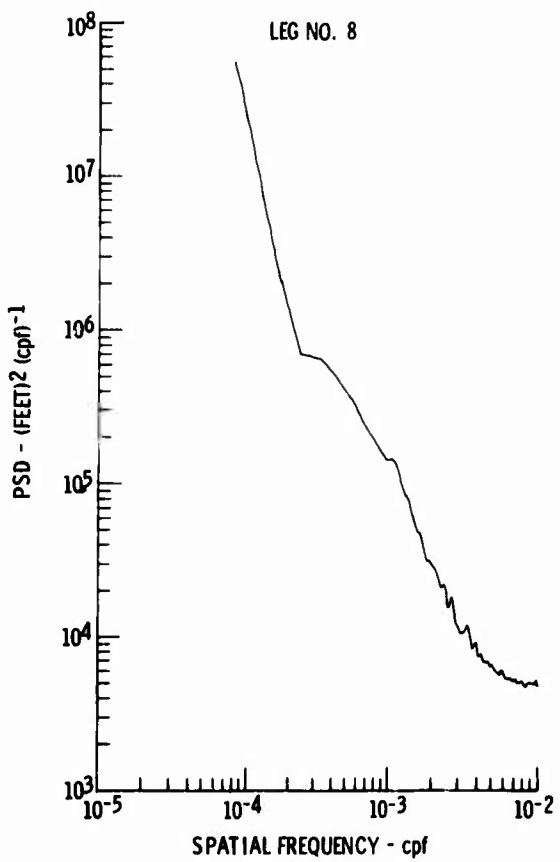
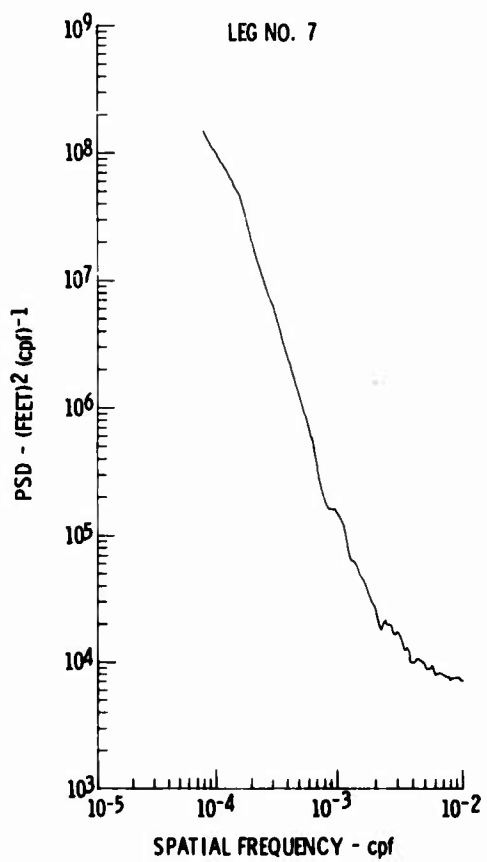
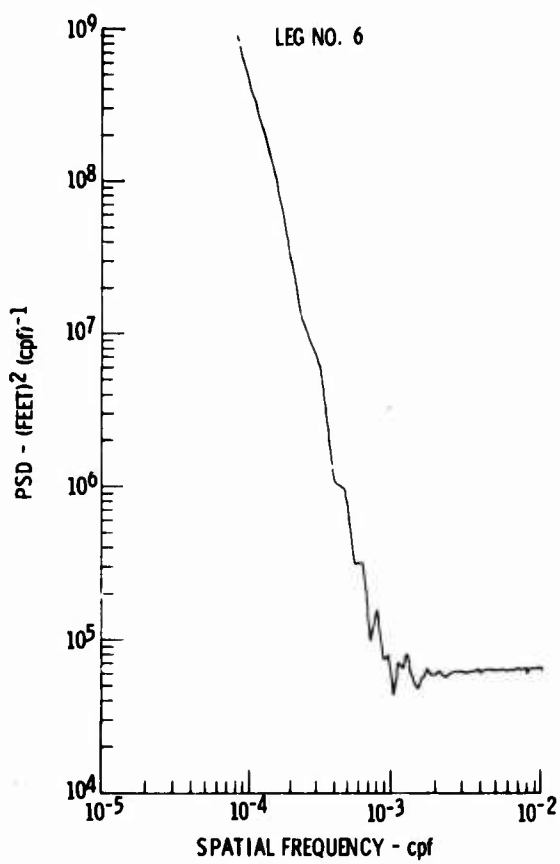
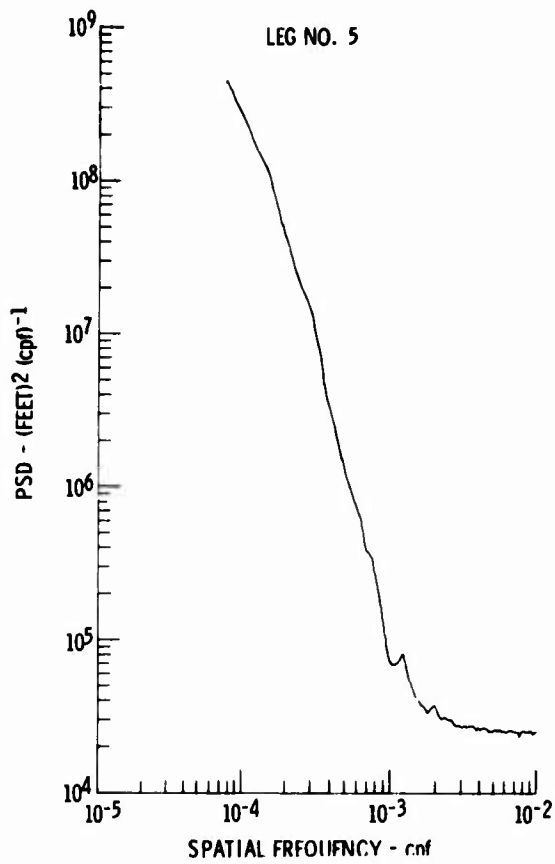


Figure 32.12 Griffiss Route Terrain Profile Power Spectra

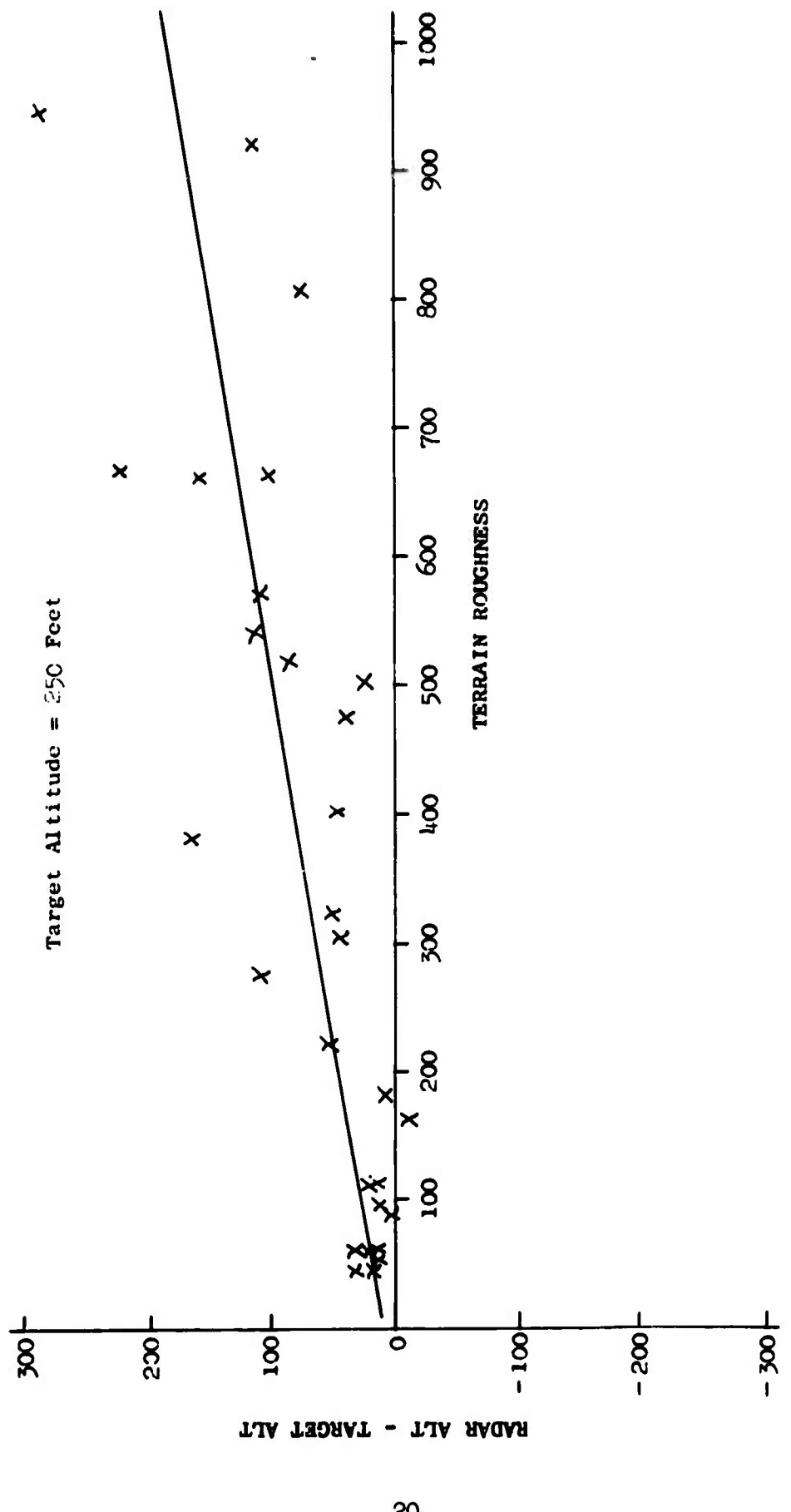


Figure 32.13 Average Radar Altitude per LCG - Target Altitude versus Terrain Roughness

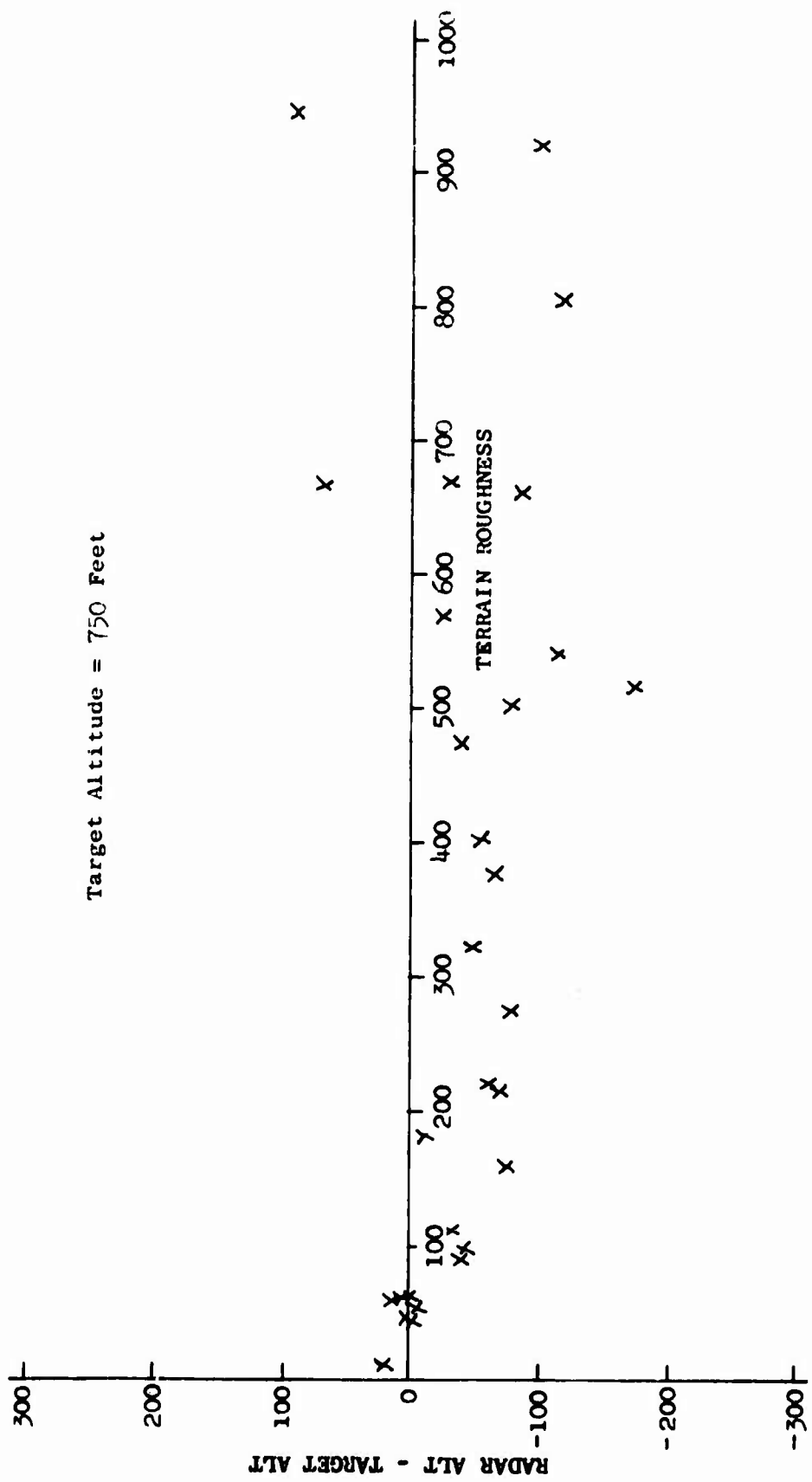


Figure 32.14 Average Radar Altitude per Leg - Target Altitude versus Terrain Roughness

33. WIND SPEED

Wind speeds were computed at the rate of 100 data samples per second using data recorded by airplane instrumentation during each four and one-half minute turbulence sample. These data were then averaged for each turbulence sample. The equations used for these calculations are shown in Appendix V.

The wind speed data were analyzed statistically. The data within a category were grouped into 5 fps wide bands of wind speed. The cumulative probabilities of these data were calculated and plotted versus the lower limit of the respective band. For each category presented, a minimum of 30 wind samples were used to establish a cumulative probability curve having adequate reliability. Because of the need for a representative number of samples in each category, various combinations of geophysical situations could not be analyzed. However, the data presented indicate the variation of wind speed trends with respect to the most pertinent individual category components.

Variations of wind speed with each of the five major category components (terrain, altitude, stability, time of day, and location) were investigated. The results are shown in Figures 33.1 through 33.5. It should be kept in mind that these data were not obtained during all seasons at any of the test locations.

Figure 33.1 shows the wind speed variation with the different types of terrain. Winds were highest over the plains, followed by high mountains, low mountains, and desert. The data obtained over the water did not contain a sufficient number of samples to be analyzed in this manner.

Figure 33.2 indicates that, with respect to altitude, greater wind speeds were generally recorded at 750 feet. Only at the largest wind speed values is the probability greater of encountering a given wind speed at 250 feet than at 750 feet.

The variations of wind speed with atmospheric stability are shown in Figure 33.3. These data show that the cumulative probability for a given wind speed was lower for the very stable atmospheric conditions than for a stable, neutral, or unstable condition.

The effects of time of day on wind speed cumulative probabilities are shown in Figure 33.4. No significant trend is noted in these data.

A large variation of wind speed as a function of geographic location is shown in Figure 33.5. The winds recorded at the McConnell and Peterson locations were significantly greater than those recorded at Edwards and Griffiss.

The season of the year category was not analyzed separately. For the Phase III data, an analysis by both season and location was not made because of the way the data were obtained. At McConnell Air Force Base, Kansas, approximately 90 per cent of the data were obtained during the summer and only 10 per cent during the fall. At Edwards Air Force Base, California, data obtained during the fall accounted for approximately

80 per cent of the total. Approximately 20 per cent of the Edwards data were obtained during the winter. At Griffiss, only four per cent of the data were recorded during the summer with the rest being recorded in the spring. Peterson was the only location where a significant amount of data were obtained during more than one season of the year. Approximately 48 and 52 per cent were obtained during the winter and spring seasons, respectively, at Peterson. The wind speed cumulative probabilities for the data recorded at Peterson are shown as a function of those two seasons in Figure 33.6. The cumulative probability was significantly larger for a given wind speed during the winter.

Because of the disturbance of atmospheric flow caused by the surrounding terrain, wind speed was analyzed to determine the combined effects of terrain and altitude. The wind speed cumulative probability plots for these categories are shown in Figures 33.7 through 33.10. The figures show approximately the same effects of altitude with respect to data obtained over high mountains, low mountains, and plains; i.e., greater wind speeds at the higher altitude. The data obtained over the desert show very little variation with altitude, with the wind speeds being slightly greater at 250 feet. The relationships of wind speed cumulative probabilities to terrain type appear to be approximately the same, regardless of altitude (Figures 33.11 and 33.12).

In Figures 33.1 through 33.5, each of the five primary category components are varied. The most significant variations in wind speed cumulative probability seem to occur with terrain type and location. Actually, these two category components are tied together. For example, all of the legs at McConnell were over plains; seven of the eight legs at Peterson were over high mountains; and the only desert leg was at Edwards. Therefore, it would be expected that these categories might show similar effects. Since there was such a significant variation of wind speed with these category components, geographic location was held constant while the other category components were varied. In this manner, the effects of the other category components could be more readily seen.

A comparison of the same types of terrain at different locations is shown in Figures 33.13 through 33.15. Winds were substantially greater over the high mountain legs at Peterson than over the Edwards high mountain terrain (Figure 33.13). Winds over the low mountain legs, however, were approximately the same at Edwards and at Griffiss (Figure 33.14). As shown in Figure 33.15, the winds over these legs at McConnell and Peterson were approximately the same and somewhat greater in magnitude than the winds over the Griffiss plains.

The wind cumulative probabilities of Figures 33.16 through 33.19 show the effects of atmospheric stability at each geographic location. The general trend is for the winds to increase as the atmosphere becomes more unstable. The only exception occurs for the McConnell data. At that location, there does not appear to be any significant wind change trends with atmospheric stability.

Variation of wind speed cumulative probability with time of day is shown for data obtained at the various geographic locations in Figures 33.20

through 33.23. The wind speeds at Edwards and Griffiss show a tendency to increase somewhat as the day progressed. The dawn data at Griffiss are not shown because of the small amount recorded. Wind speeds at Peterson appear to be fairly consistent, irrespective of time of day (Figure 33.22). Wind speeds at McConnell showed a different relationship with time of day than did the data at the other locations in that the cumulative probability for a given wind speed is significantly greater at dawn than at either mid-moring or mid-afternoon (Figure 33.23).

Wind speed characteristics during Phases I and II were also compared to those encountered during Phase III.

As was the case for Phases I and II, the Phase III wind data were found to vary with category (see Reference I.2). Location and season produced the greatest effects on these data. A comparison of these data from the various phases is shown in Figures 33.24 through 33.27. The Phases I and II data shown pertain only to the season corresponding to the Phase III data at a given location. These comparisons show that the Phase III wind speed cumulative probabilities were smaller for the data recorded at Edwards and Griffiss, but greater for the McConnell and Peterson data. The Phases I and II wind speed data at Peterson are for the plains terrain only since the high mountain wind data at Peterson were not analyzed because those legs were not contour flown.

The effects of altitude, atmospheric stability, and time of day on wind speed cumulative probabilities were approximately the same for all phases. During Phases I and II, the winds were highest at dawn for the Peterson route data, however, as mentioned previously, these data included only plains legs at that location.

There was only one plains leg at Peterson for the Phase III Program, and so there were not enough data, based on 30 samples as a minimum, to compare time of day effects on wind speed cumulative probability. However, the mean value for this plains leg was greater at dawn than at either of the other two times of day.

A summary of the more significant findings of this analysis is as follows:

- The most significant changes in wind speed cumulative probability occur with changes in location. Changes in season were also found to be significant through analysis of the Phases I and II data.
- Wind speed cumulative probability tends to be slightly greater at 750 feet than at 250 feet.
- Wind speed cumulative probability increases slightly as atmospheric stability decreases.
- Wind speeds tend to be greater at dawn over the McConnell and Peterson plains than at the other times of day. At the Griffiss and Edwards locations, the cumulative probability for a given wind speed increases as the day progresses. Winds over the Peterson high mountains are fairly consistent, regardless of time of day.

- Trends in wind speed statistics, as affected by geophysical variations, were consistent during all phases of the LO-LOCAT Program.
- With regard to season, wind speed cumulative probabilities were greater at McConnell and Peterson, and smaller at Edwards and Griffiss during Phase III than during Phases I and II.
- For the seasons of the year within which the data were recorded, wind speeds were significantly greater at McConnell and Peterson than at the other two locations.

Wind speed and direction are listed in Appendix VI for each gust velocity sample. The corresponding geophysical category for each sample is also listed. An analysis of wind spectra is presented in Section 52.

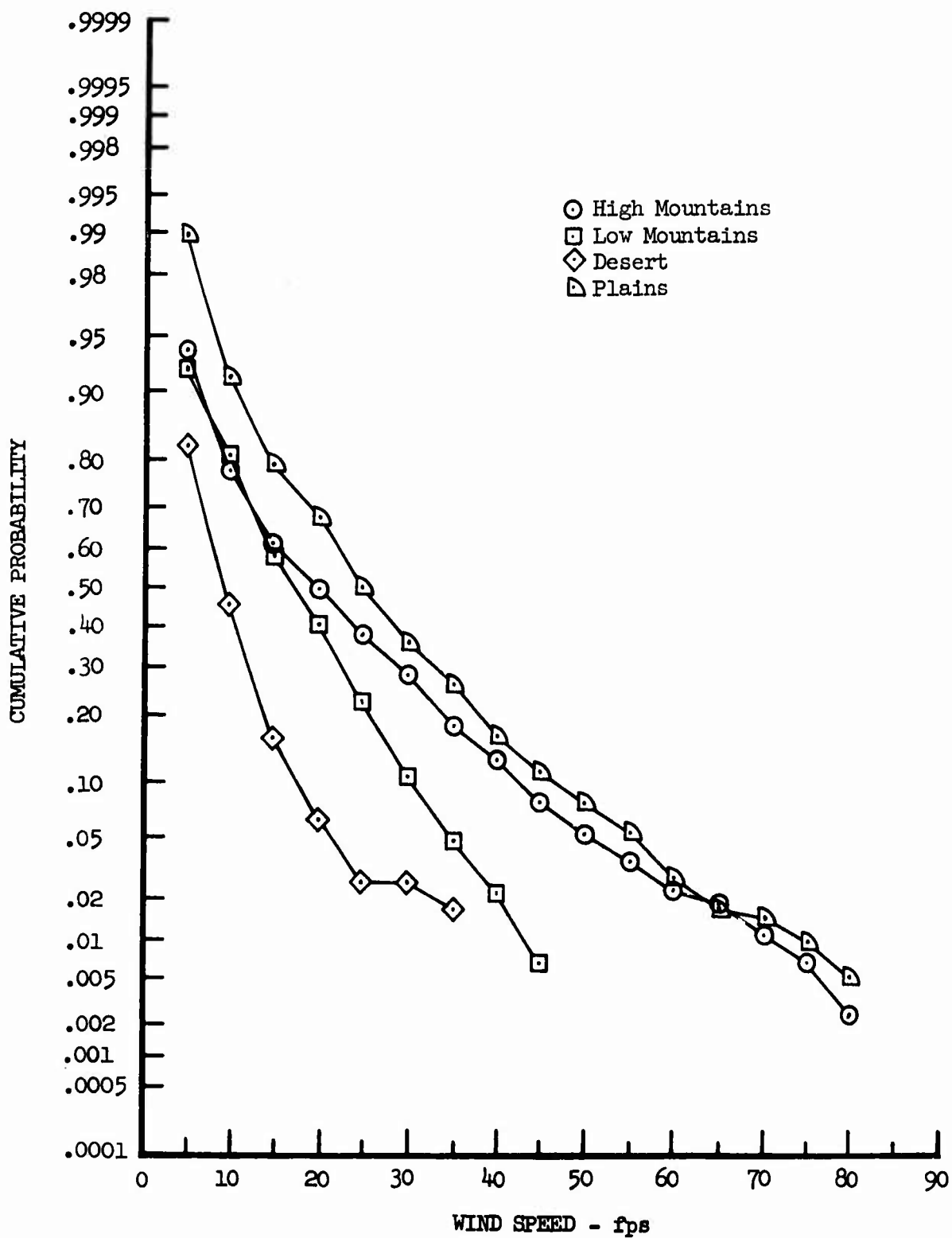


Figure 33.1 Wind Speed Cumulative Probability Associated with Type of Terrain

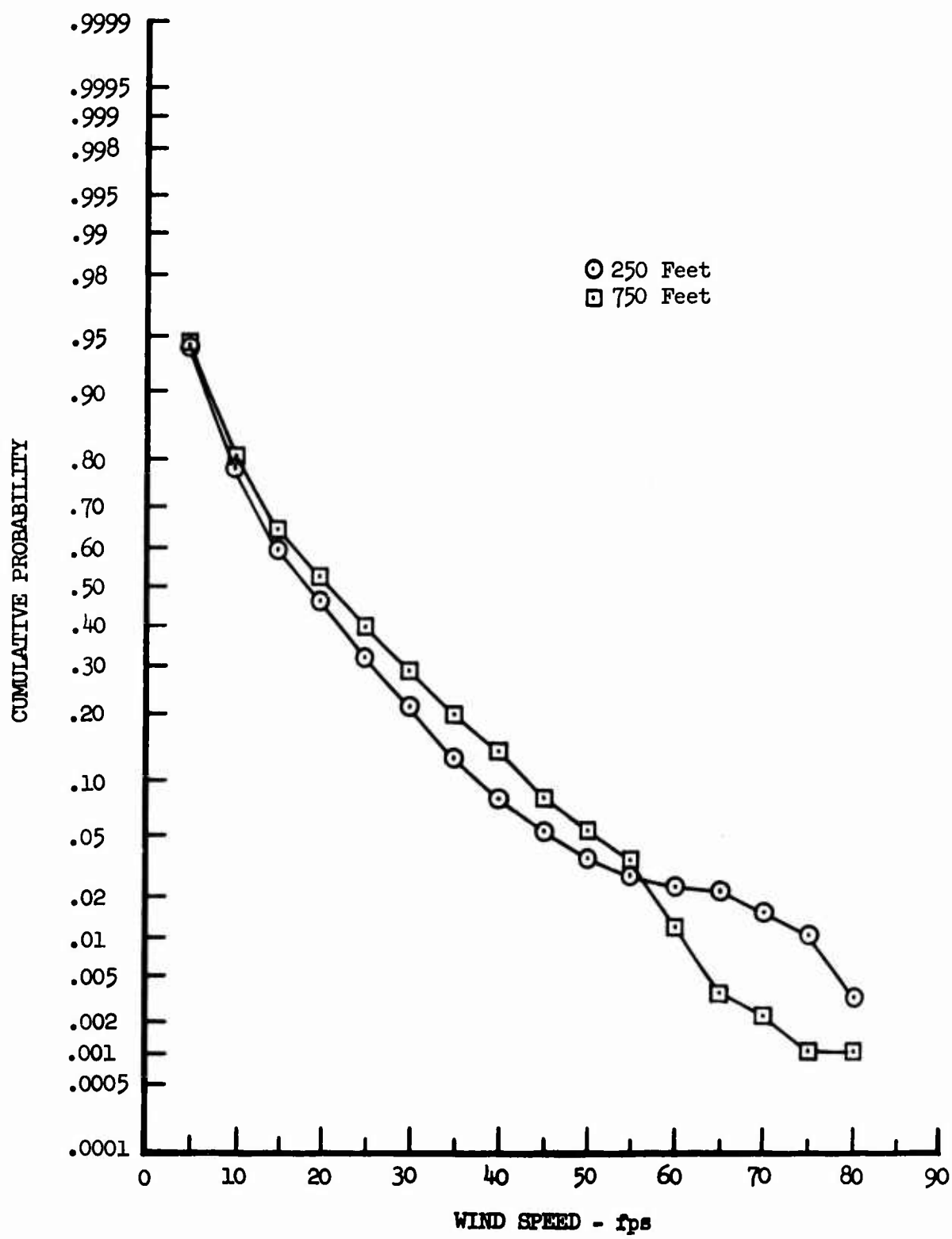


Figure 33.2 Wind Speed Cumulative Probability Associated with Absolute Altitude

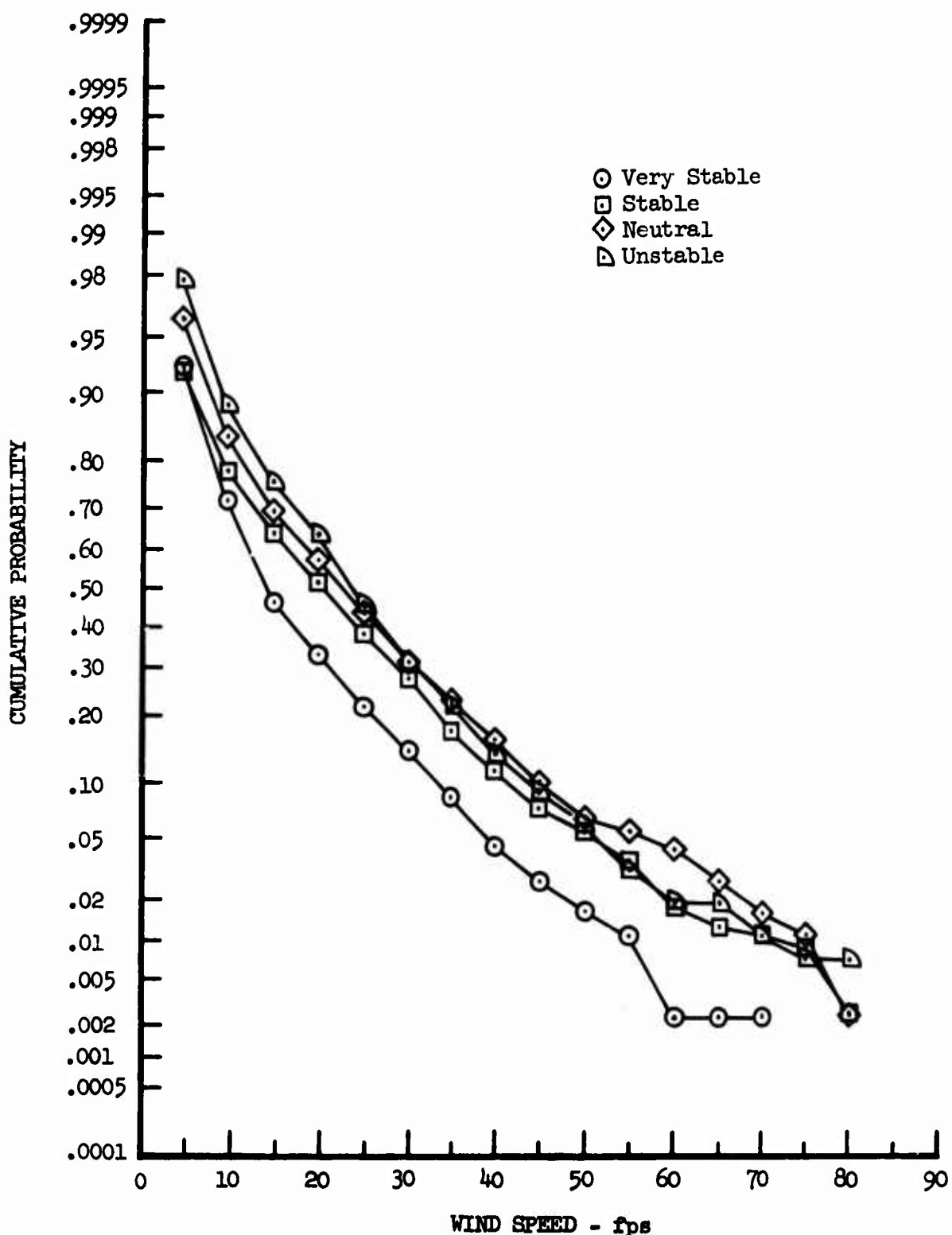


Figure 33.3 Wind Speed Cumulative Probability Associated with Atmospheric Stability

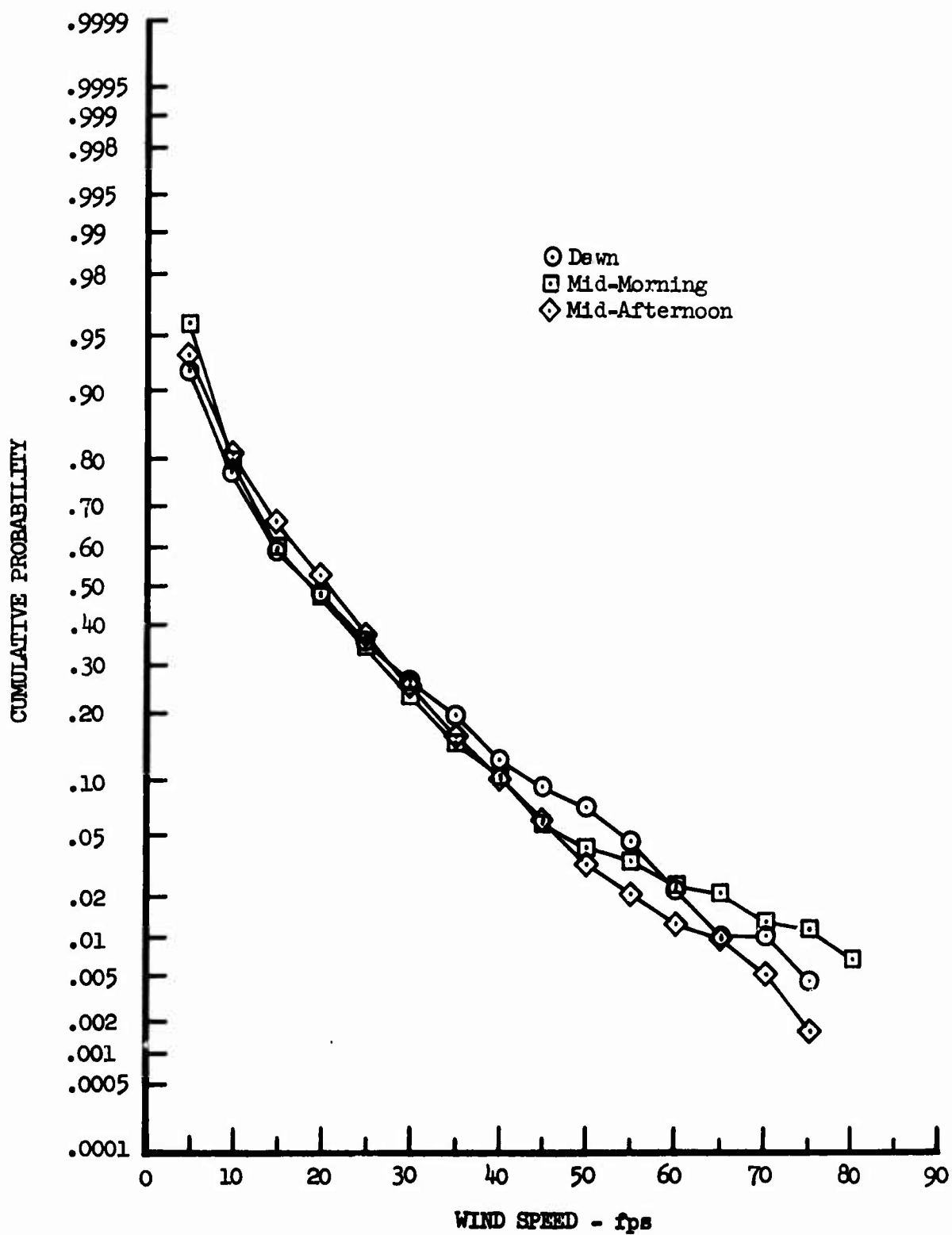


Figure 33.4 Wind Speed Cumulative Probability Associated with Time of Day

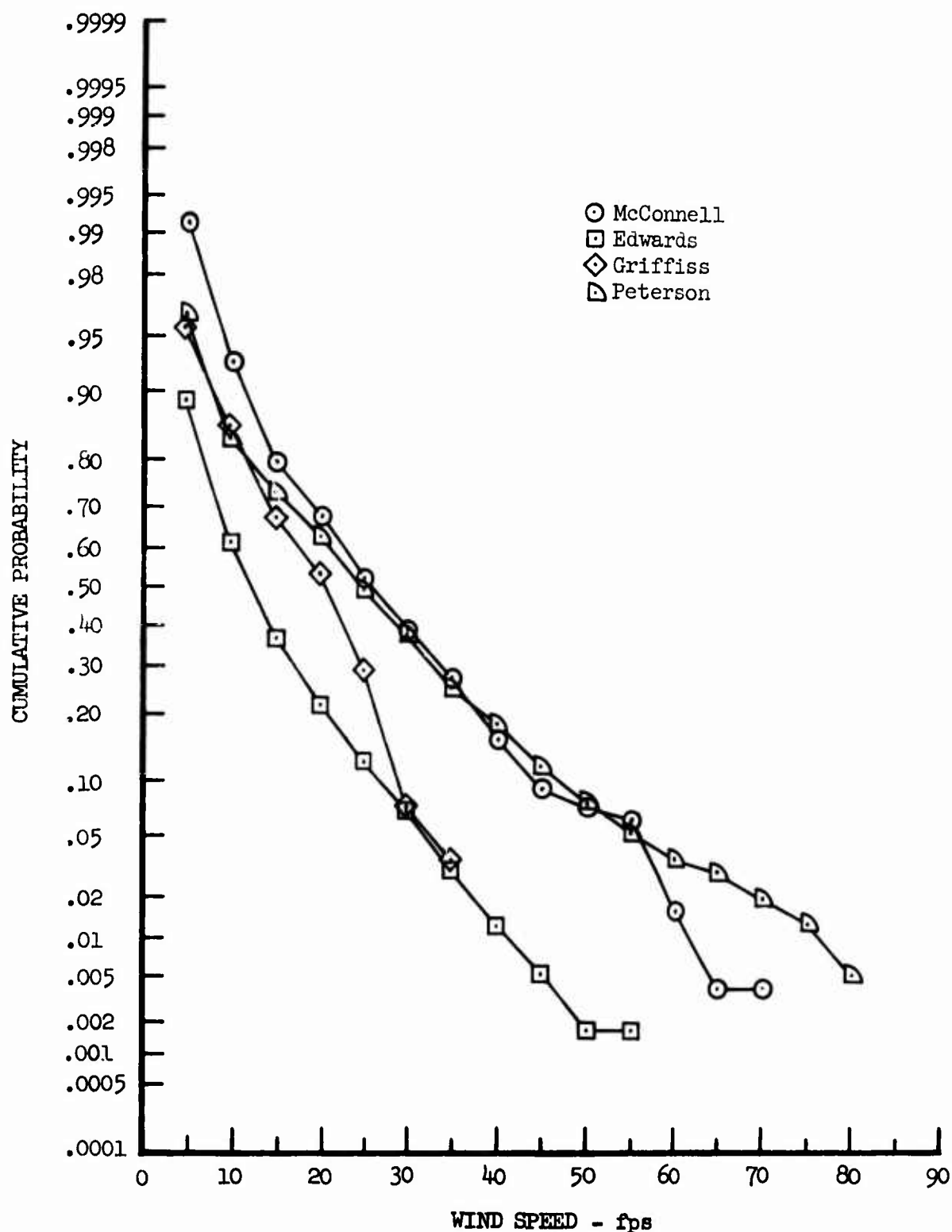


Figure 33.5 Wind Speed Cumulative Probability Associated with Geographic Location

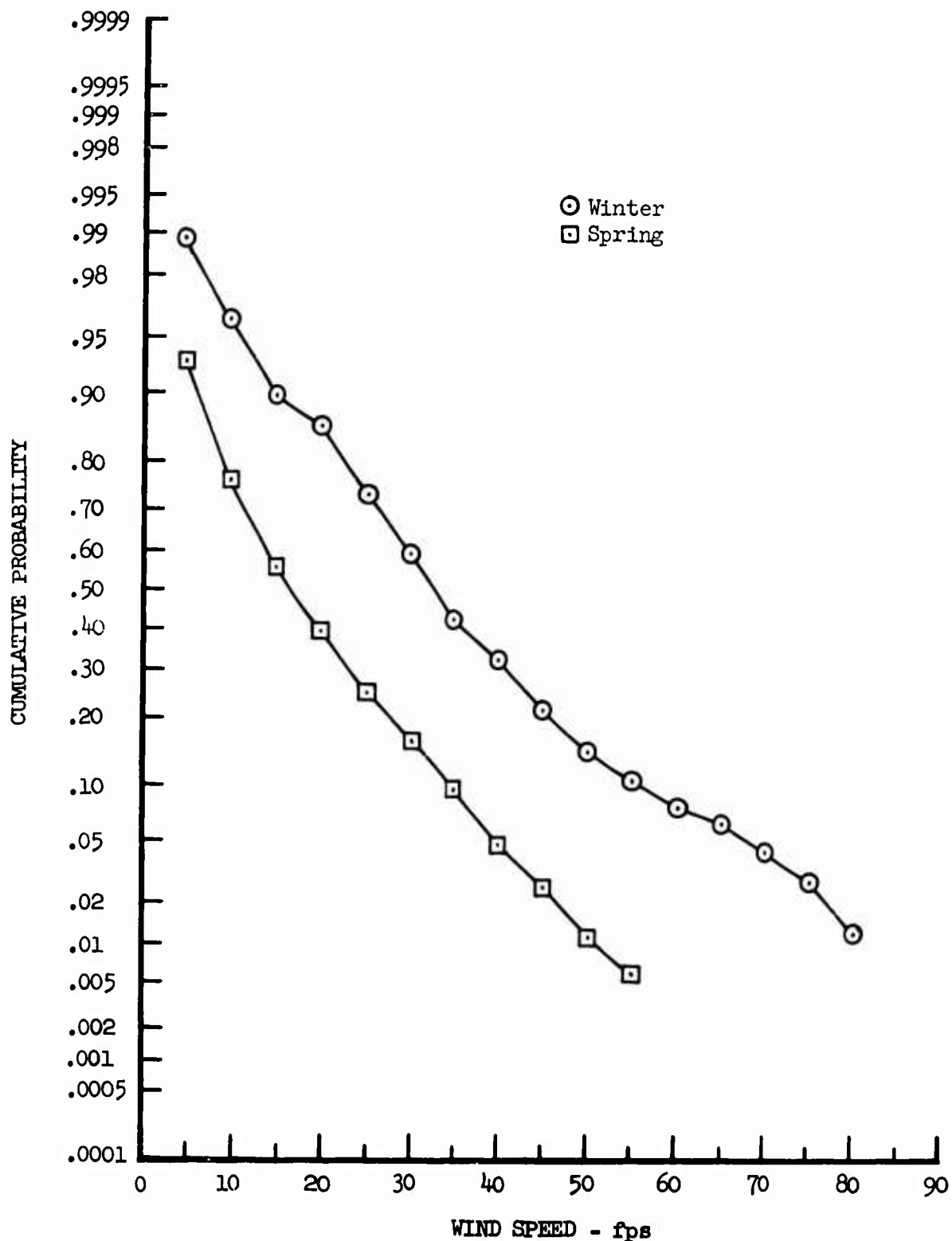


Figure 33.6 Effects of Season on Wind Speed Cumulative Probability at Peterson

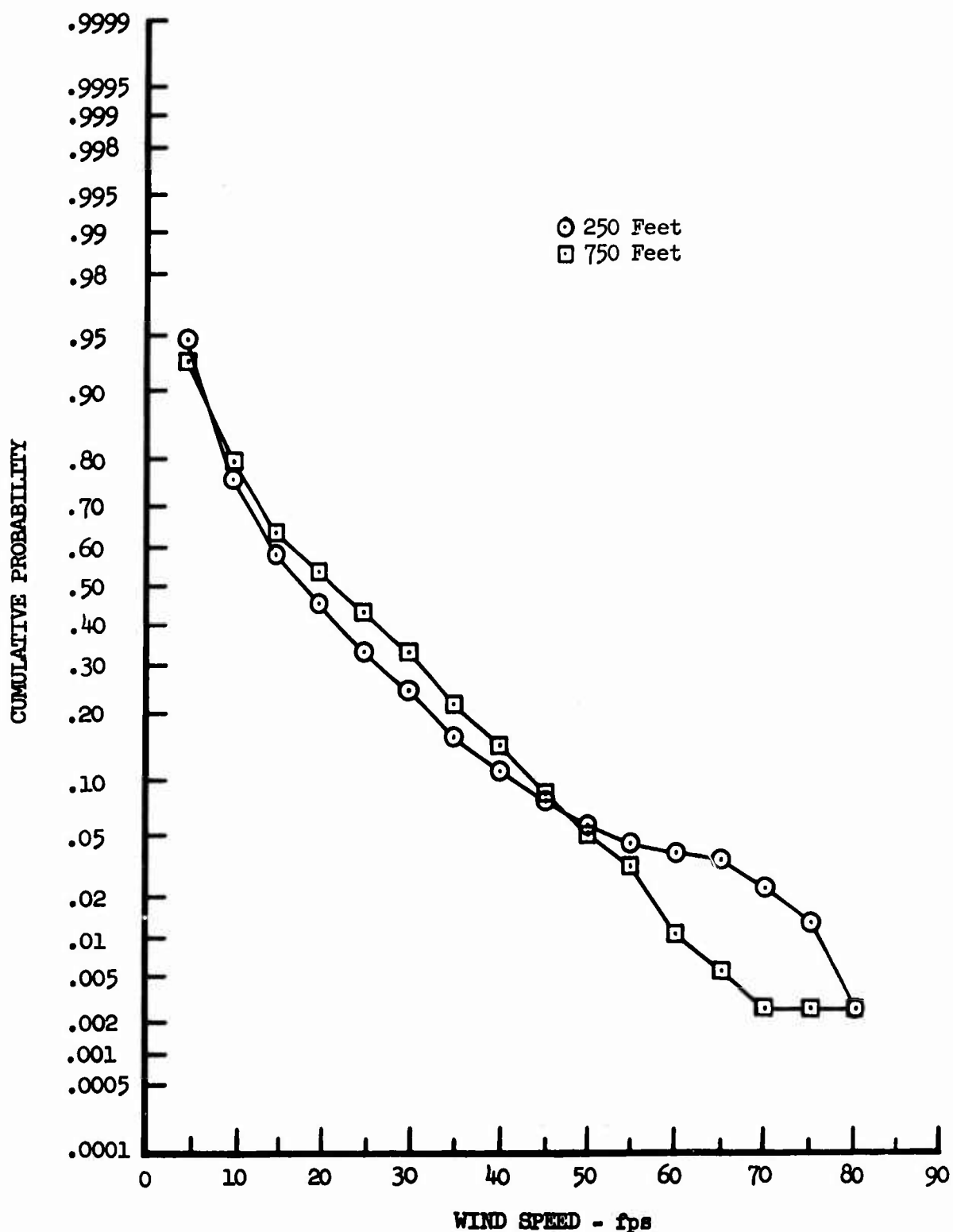


Figure 33.7 Effects of Absolute Altitude on Wind Speed Cumulative Probability over High Mountains

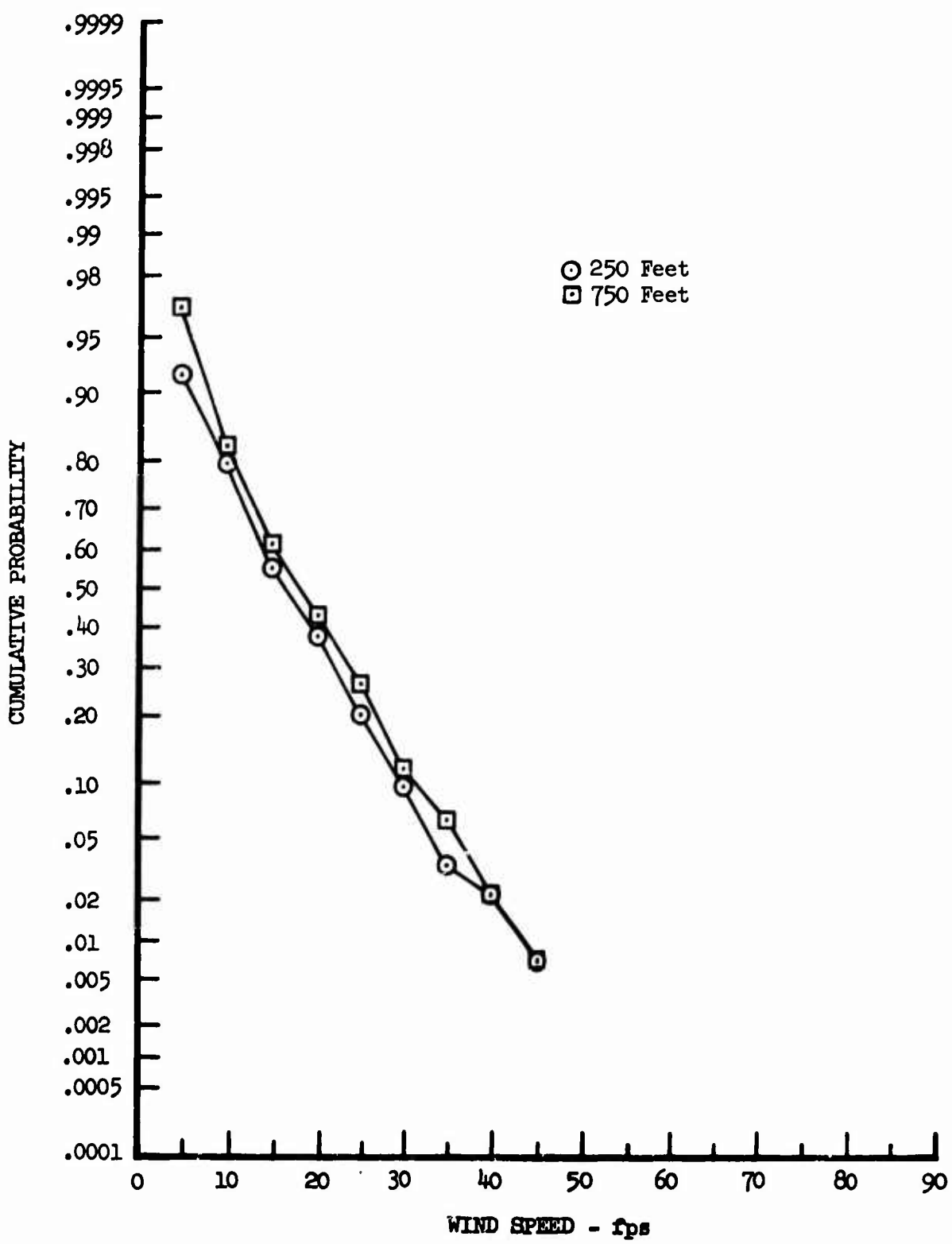


Figure 33.8 Effects of Absolute Altitude on Wind Speed Cumulative Probability over Low Mountains

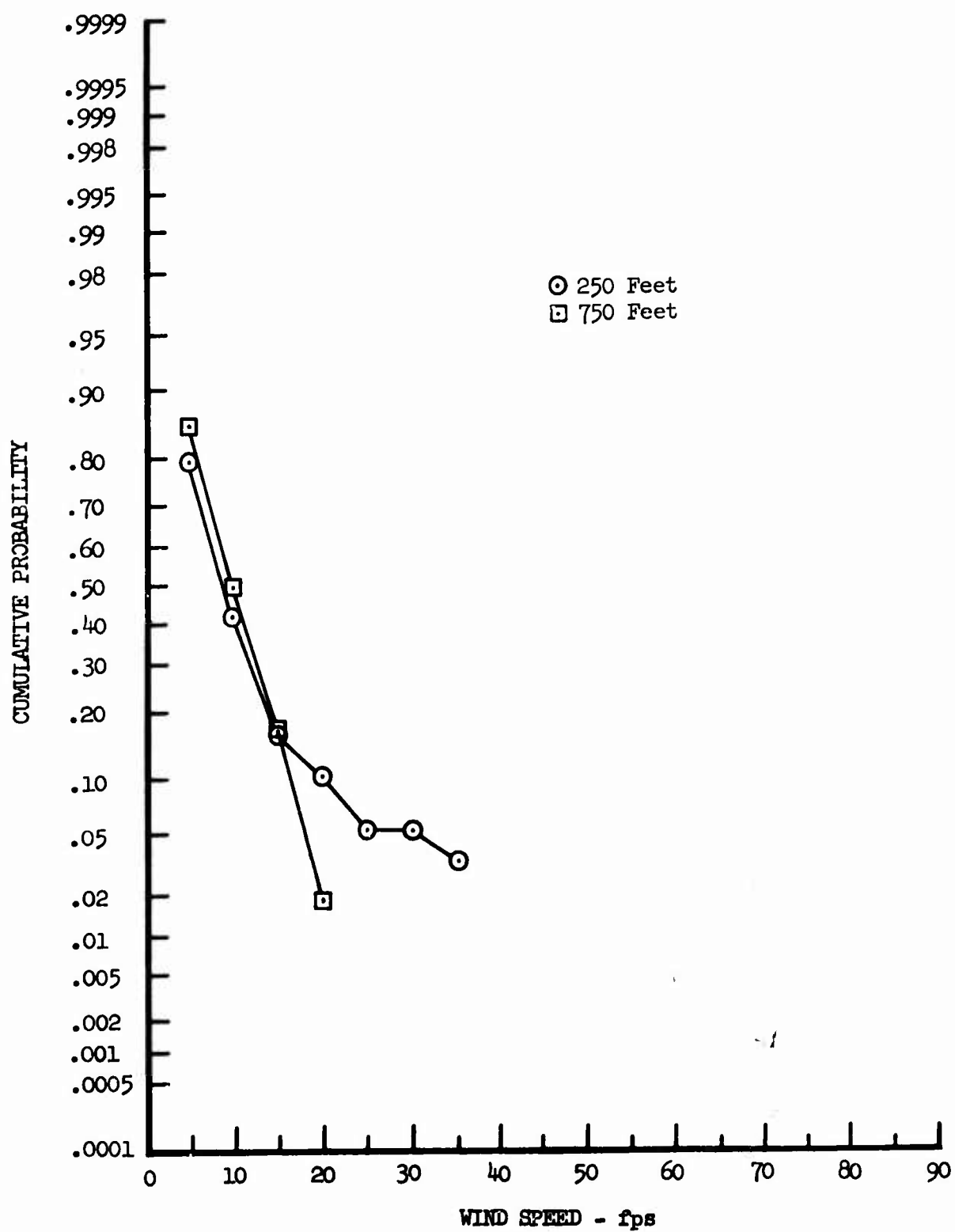


Figure 33.9 Effects of Absolute Altitude on Wind Speed Cumulative Probability over Desert

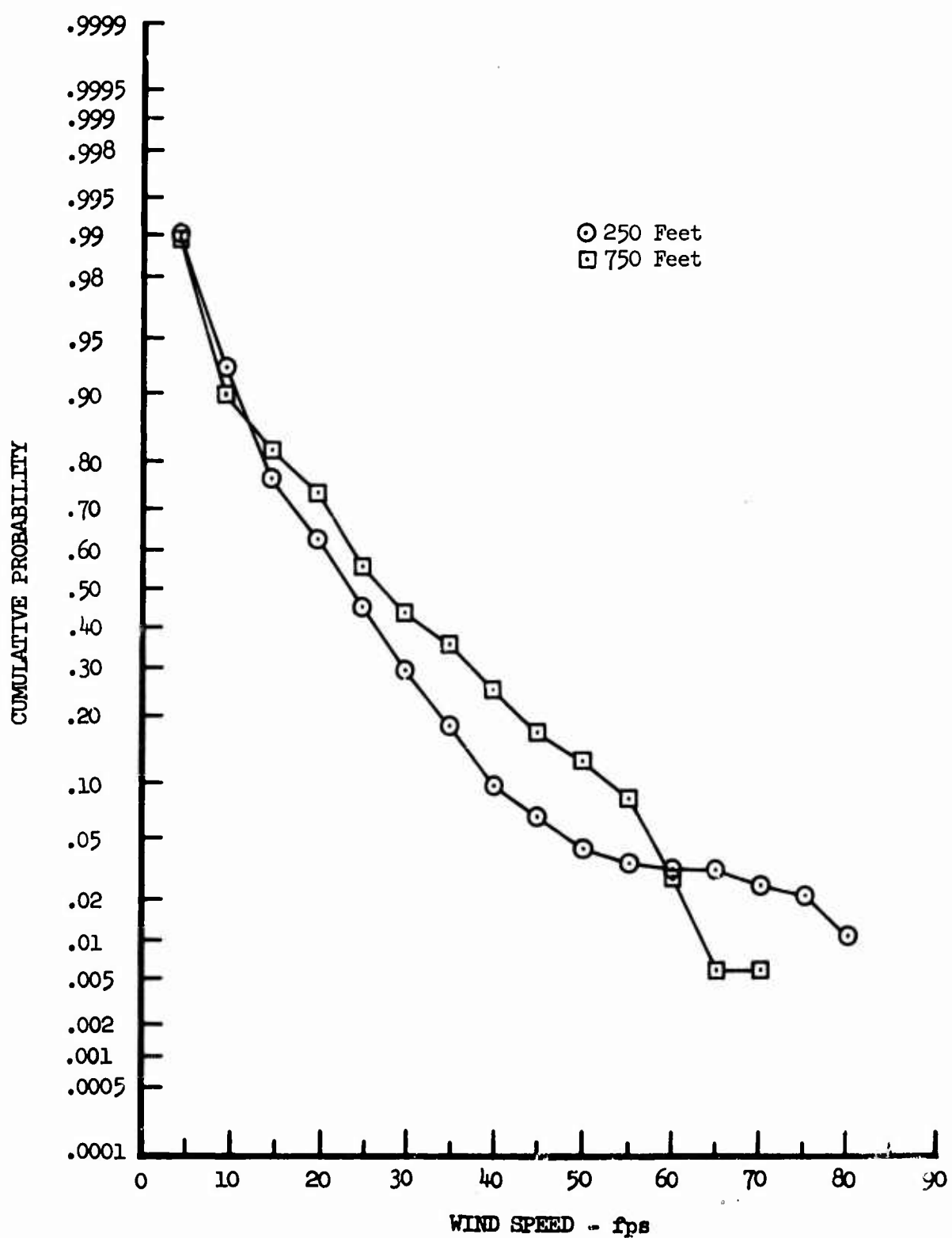


Figure 33.10 Effects of Absolute Altitude on Wind Speed Cumulative Probability over Plains

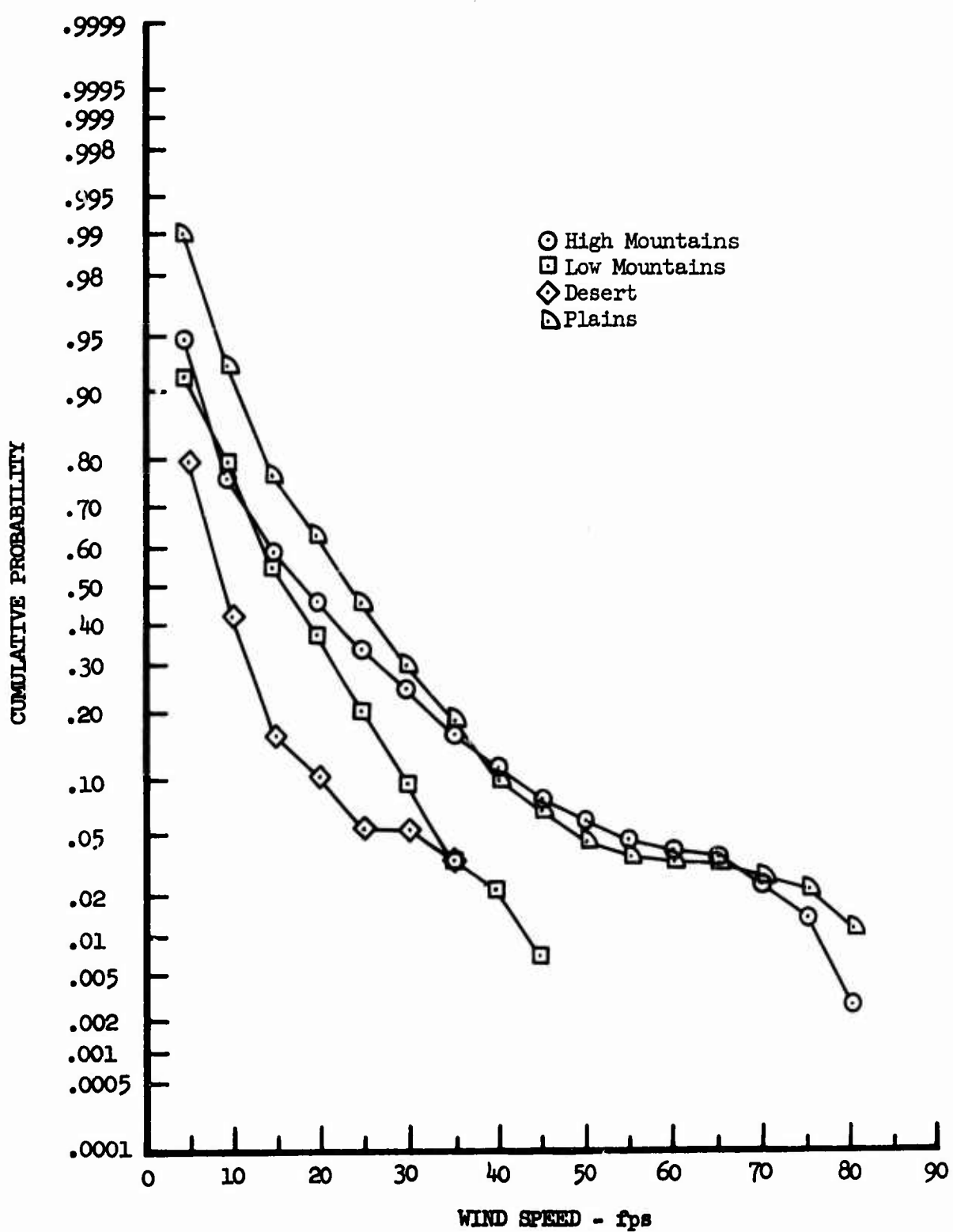


Figure 33.11 Effects of Terrain Type on Wind Speed Cumulative Probability at 250 Feet

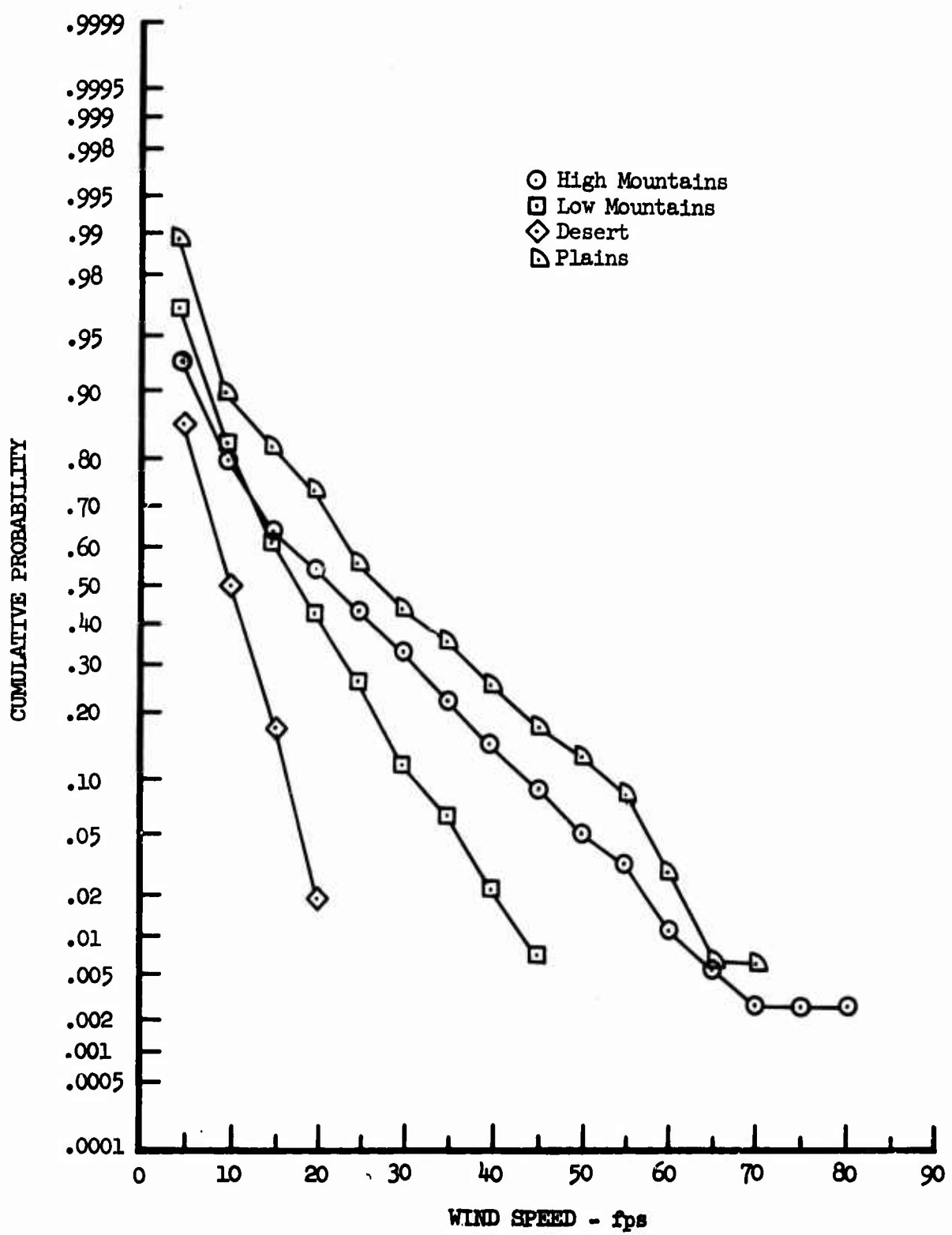


Figure 33.12 Effects of Terrain Type on Wind Speed Cumulative Probability at 750 Feet

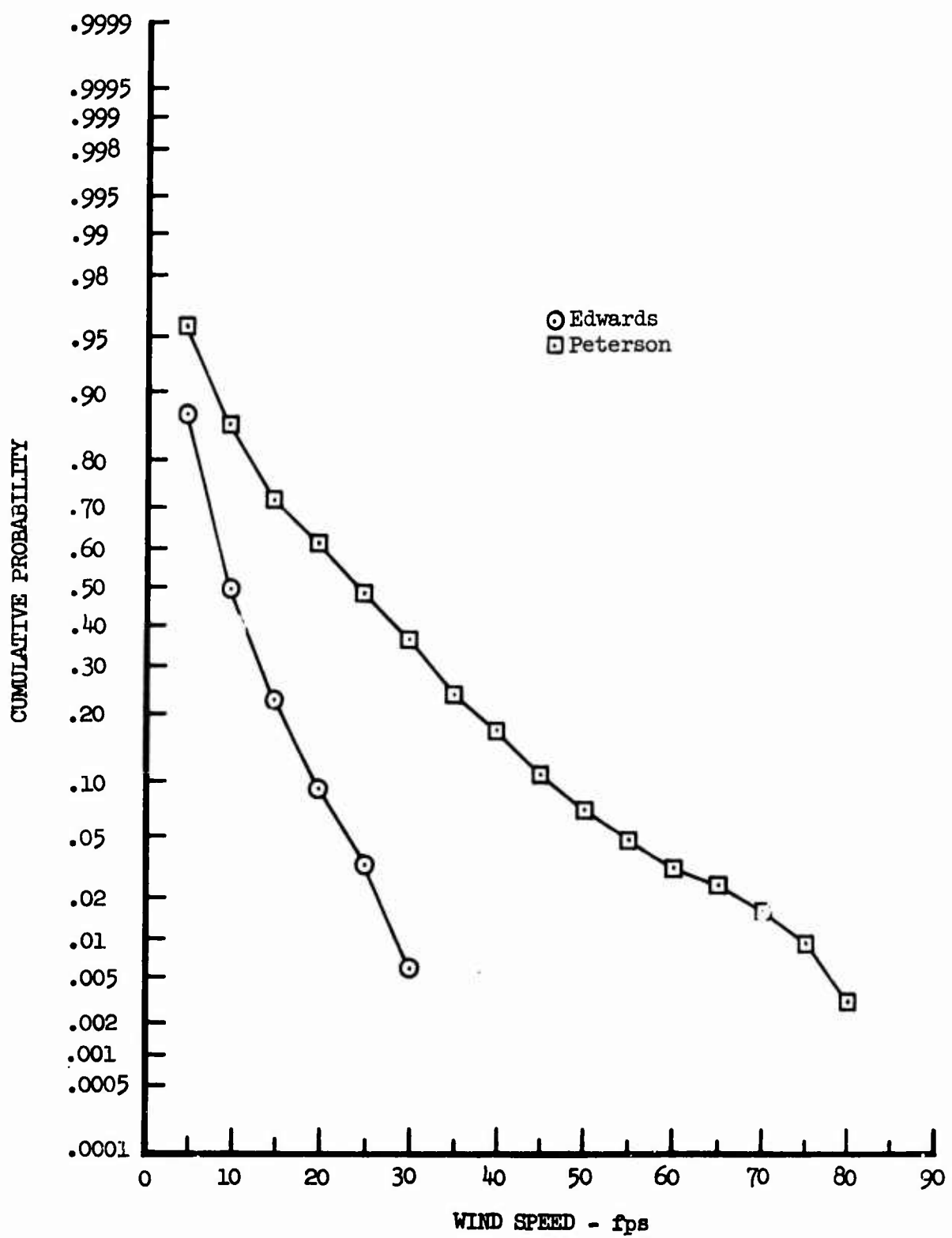


Figure 33.13 Effects of Geographic Location on Wind Speed Cumulative Probability over High Mountains

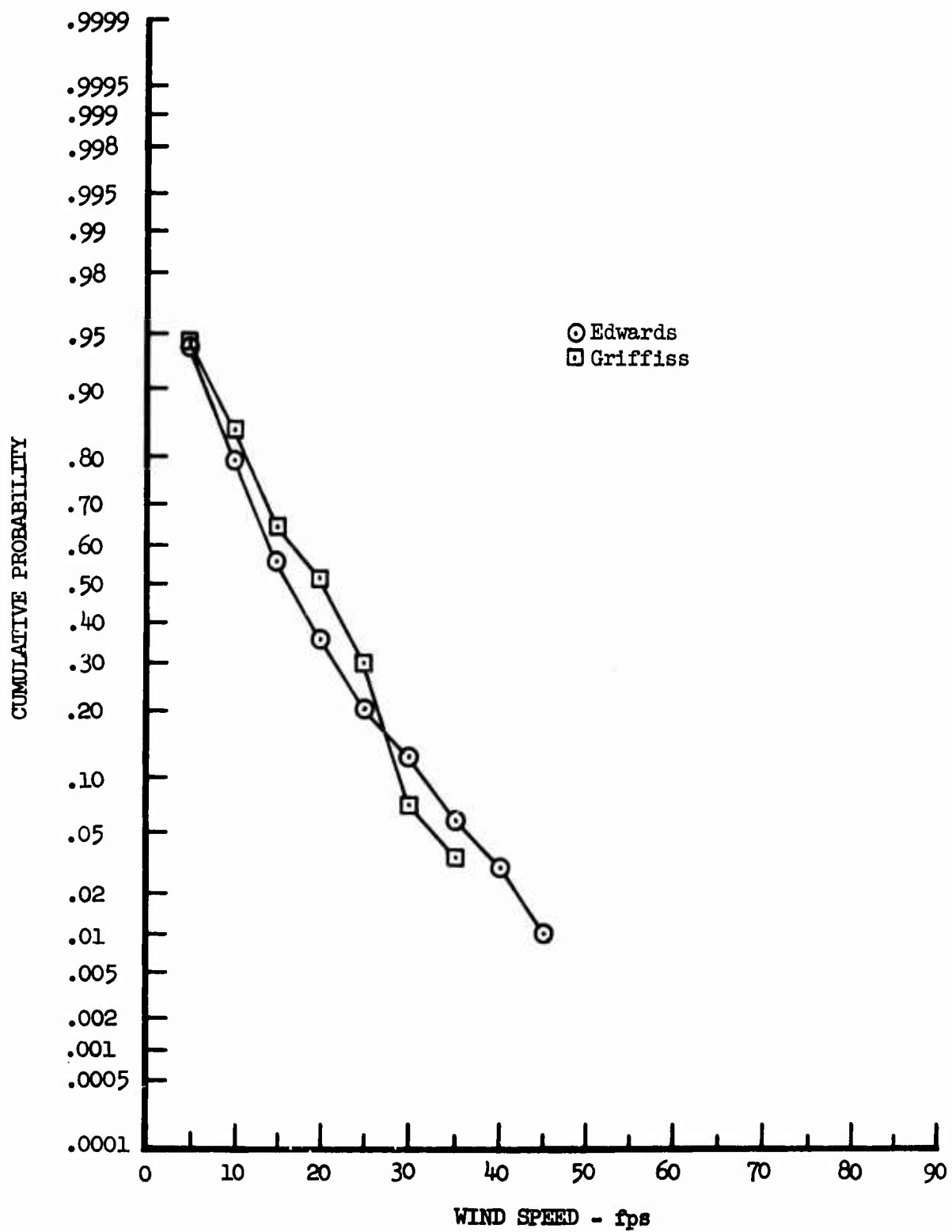


Figure 33.14 Effects of Geographic Location on Wind Speed Cumulative Probability over Low Mountains

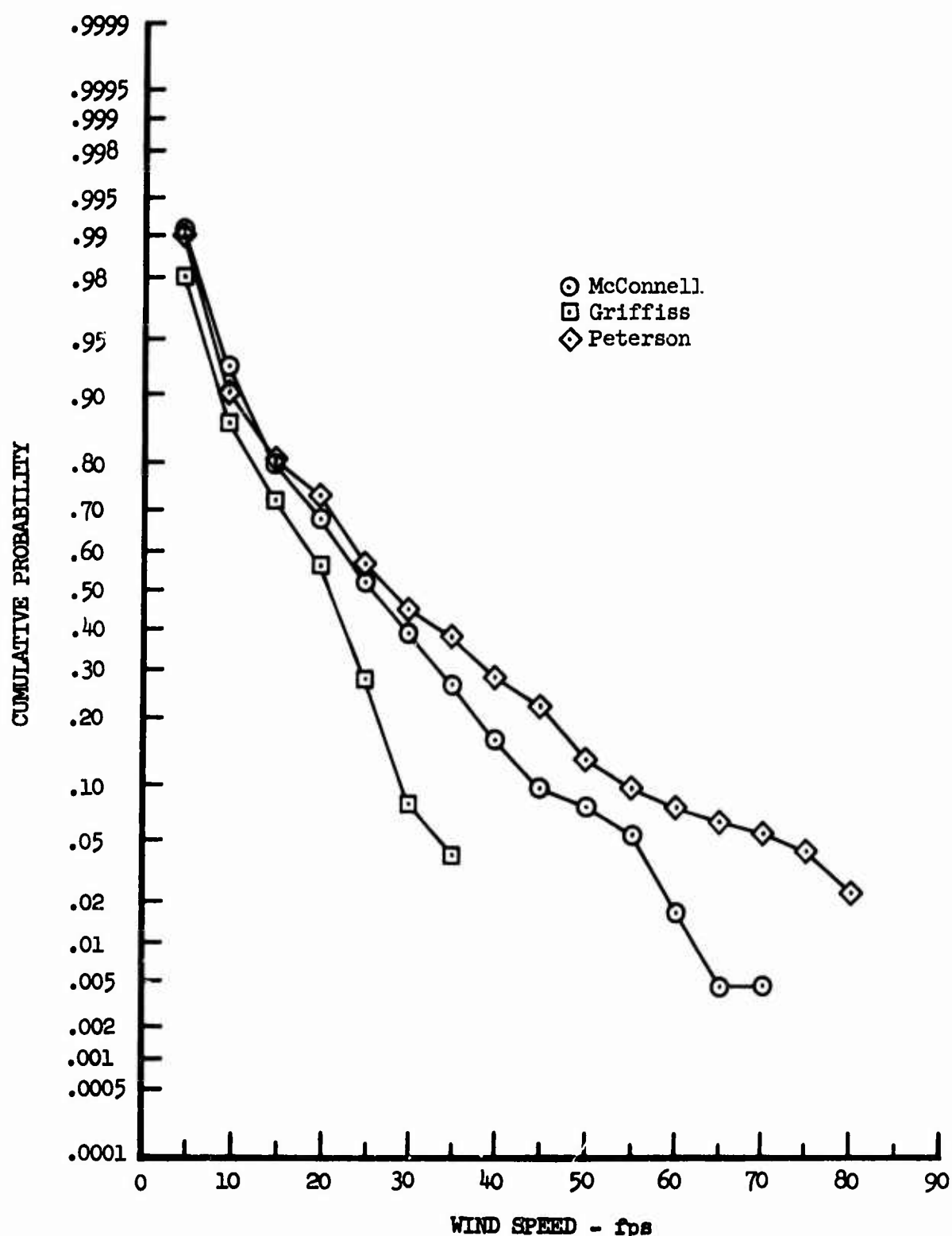


Figure 33.15 Effects of Geographic Location on Wind Speed Cumulative Probability over Plains

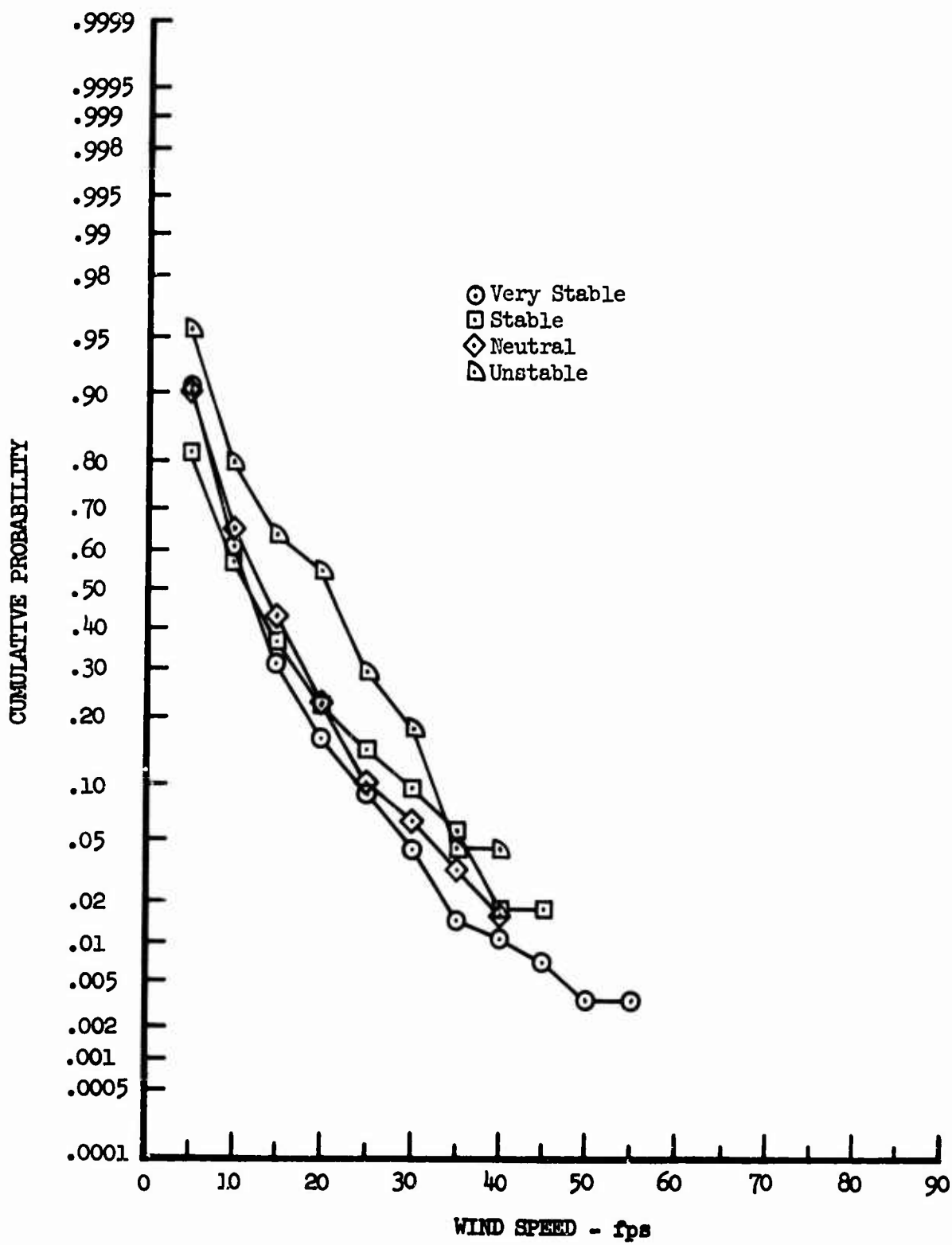


Figure 33.16 Effects of Atmospheric Stability on Wind Speed Cumulative Probability at Edwards

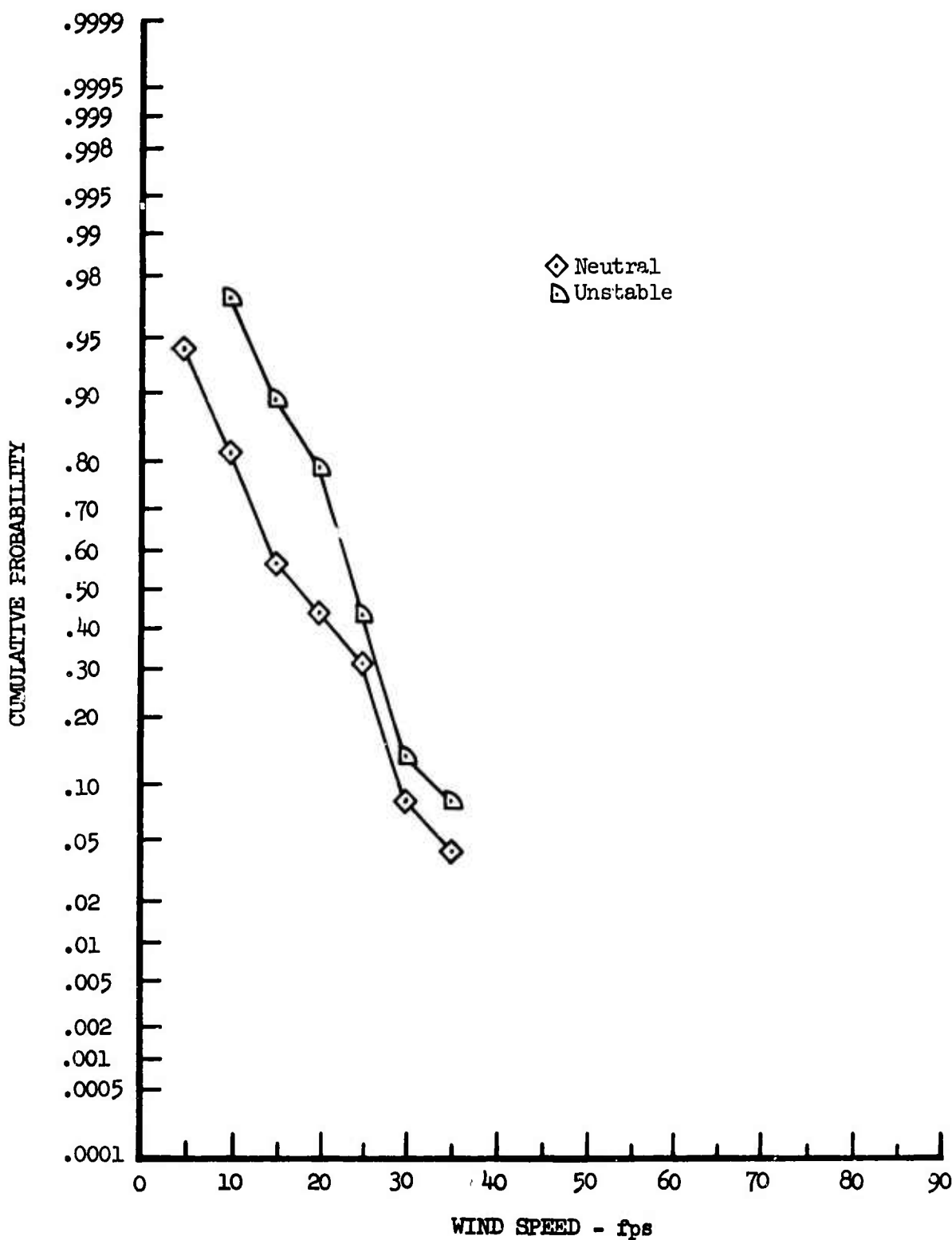


Figure 33.17 Effects of Atmospheric Stability on Wind Speed Cumulative Probability at Griffiss

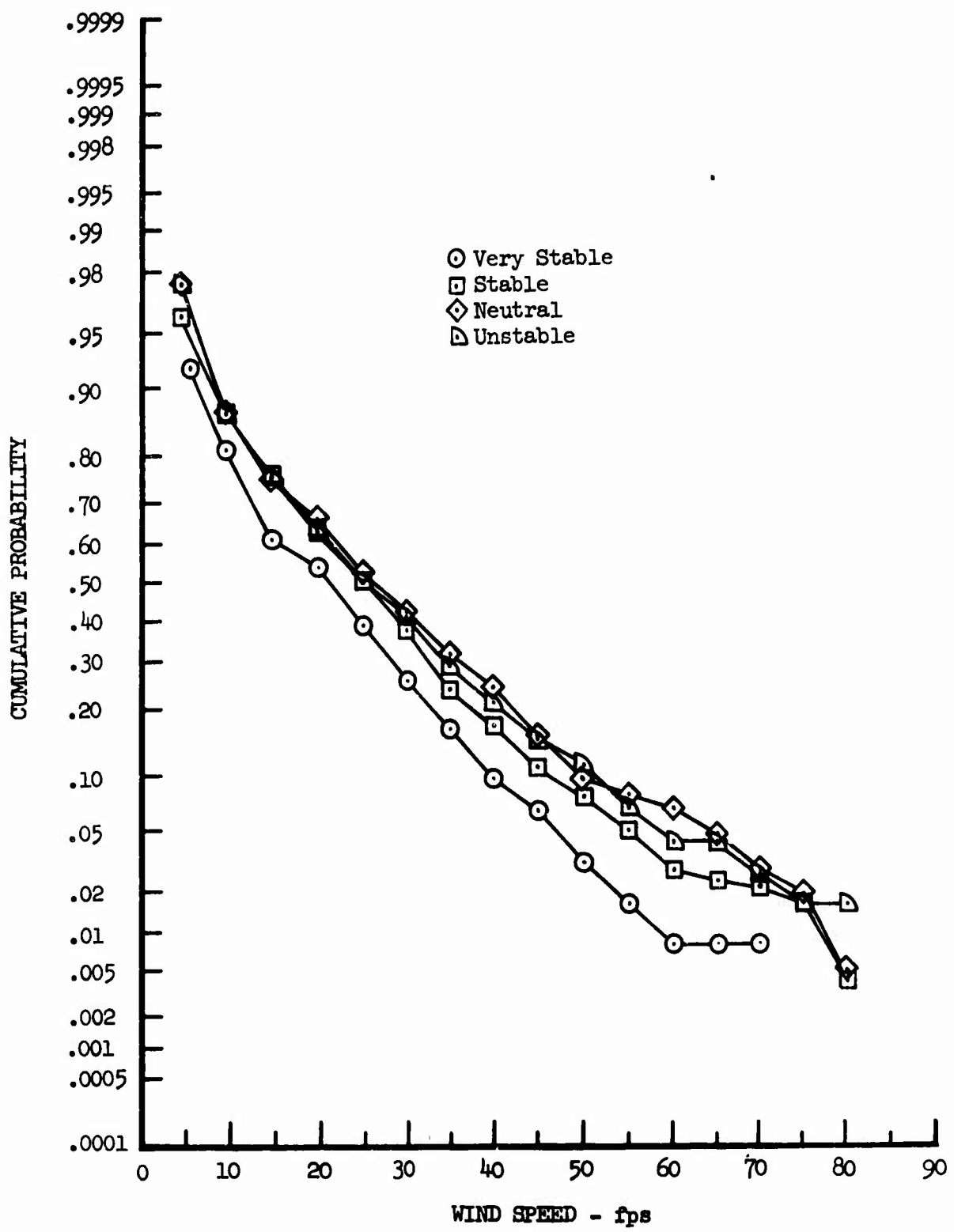


Figure 33.18 Effects of Atmospheric Stability on Wind Speed Cumulative Probability at Peterson

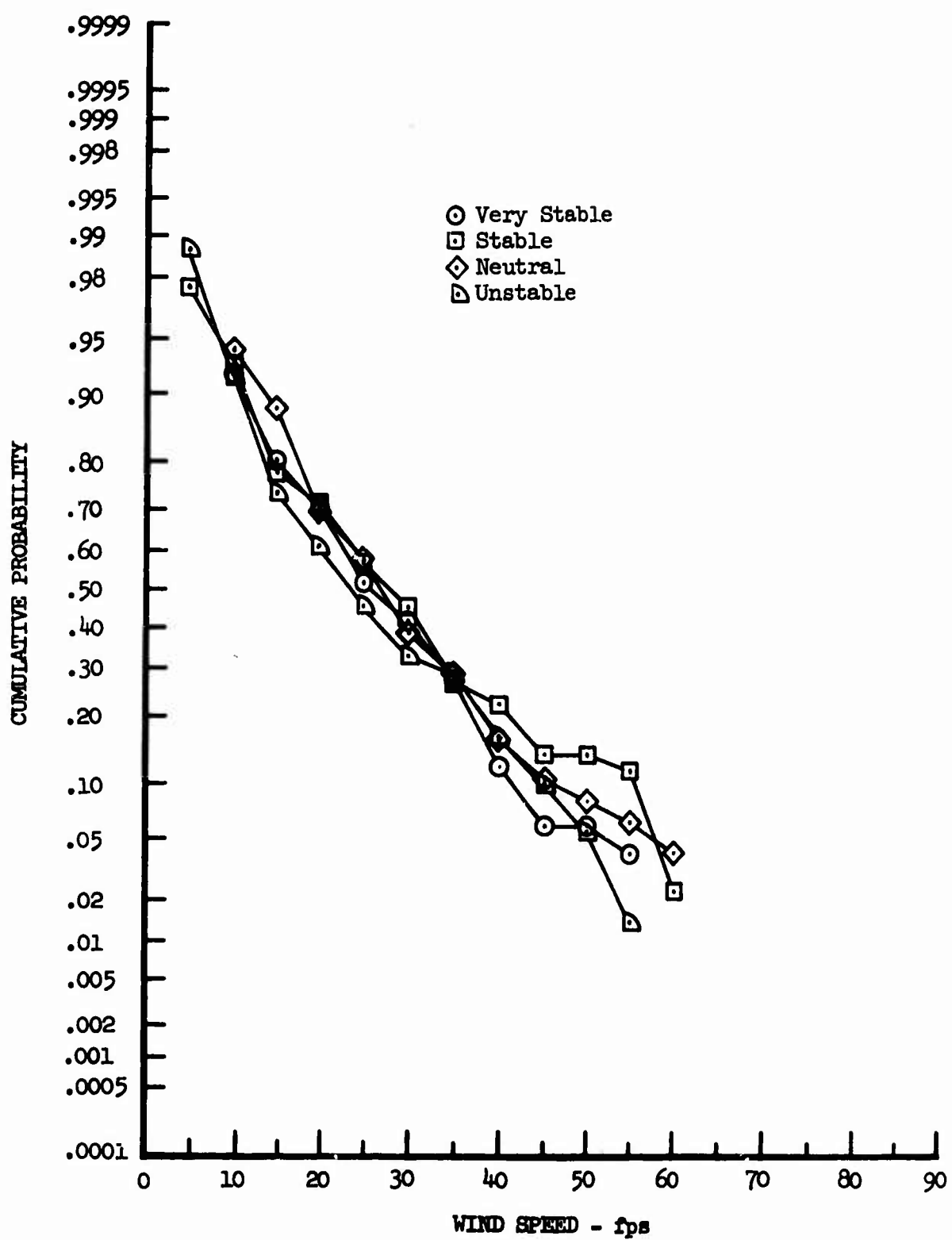


Figure 33.19 Effects of Atmospheric Stability on Wind Speed Cumulative Probability at McConnell

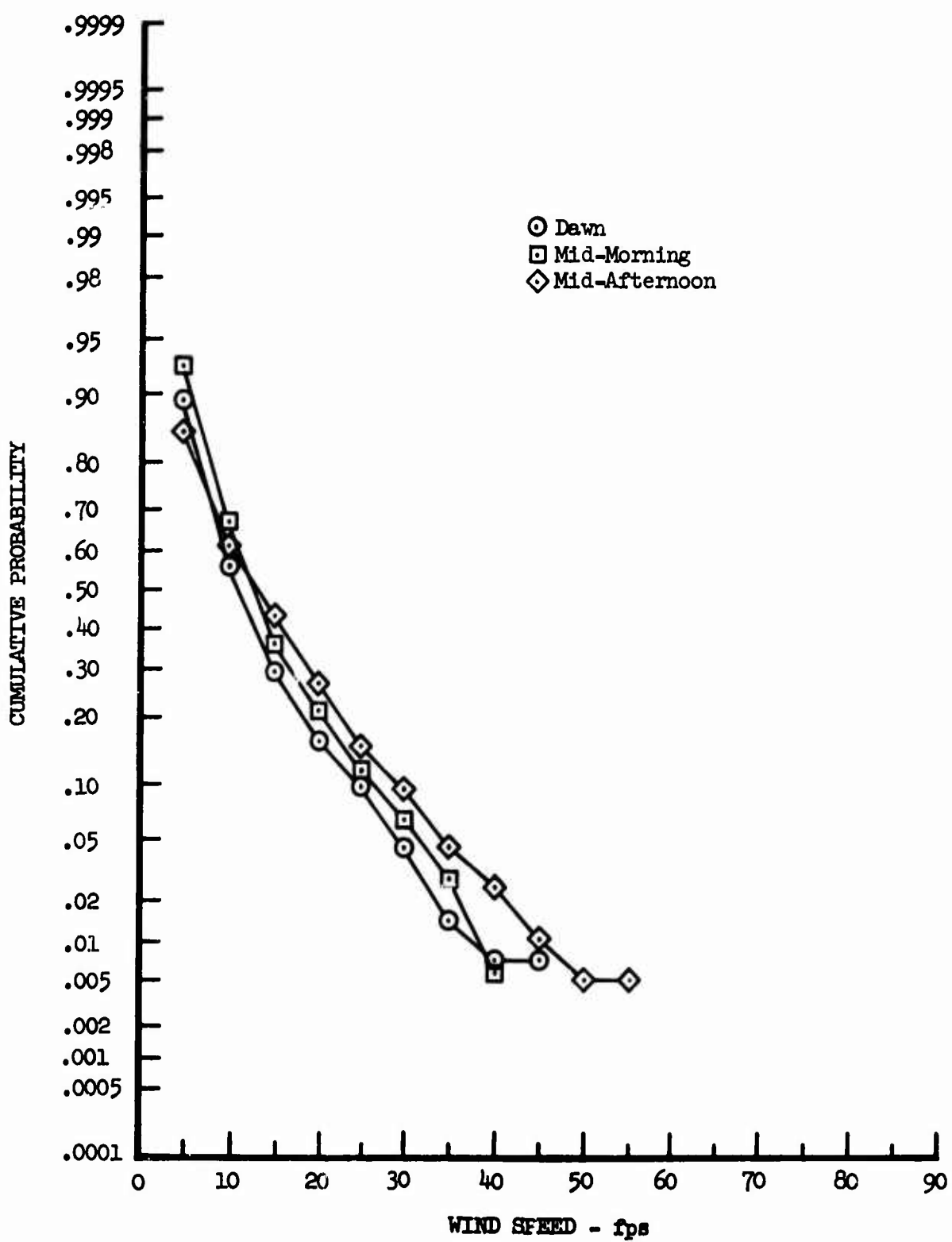


Figure 33.20 Effects of Time of Day on Wind Speed Cumulative Probability at Edwards

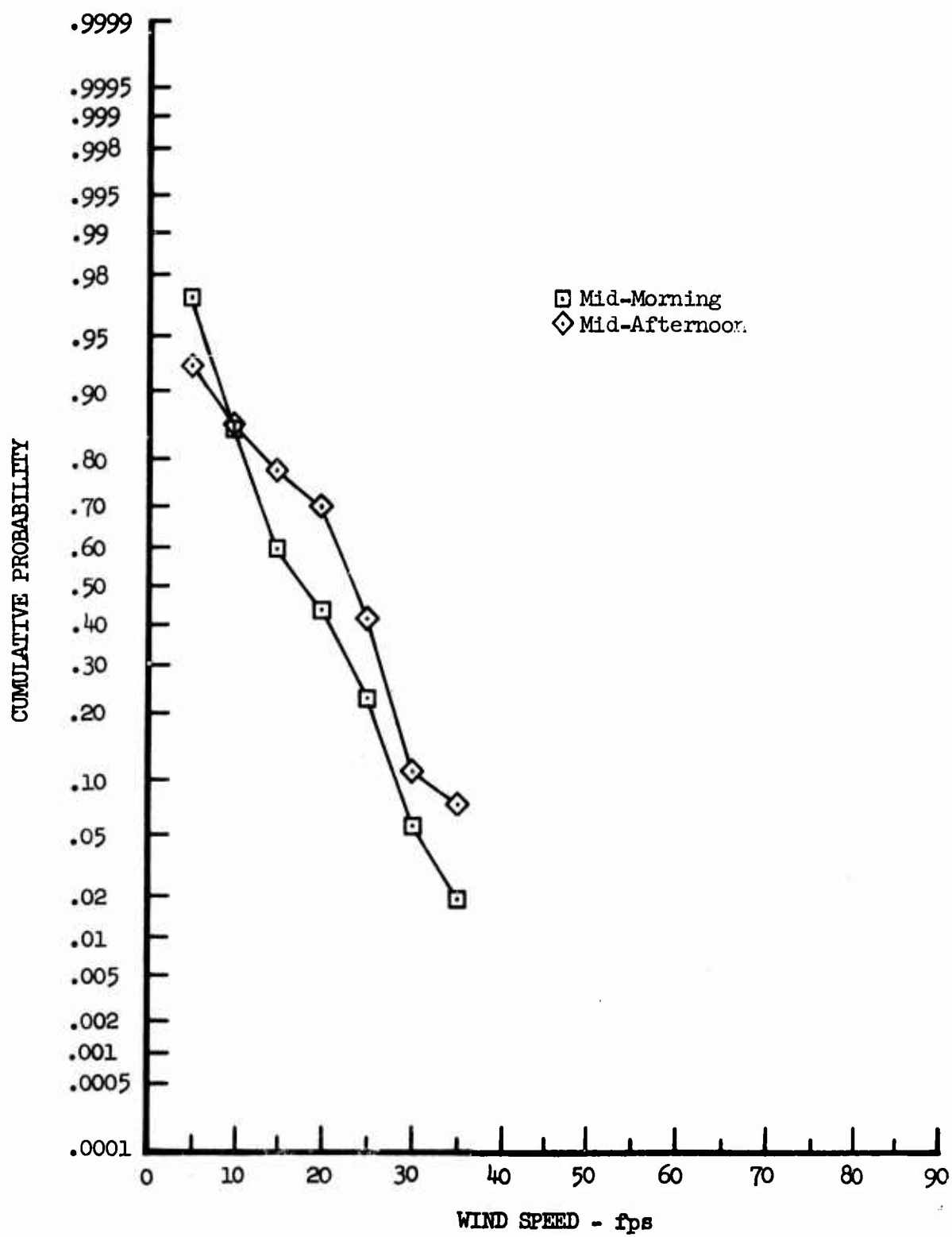


Figure 33.21 Effects of Time of Day on Wind Speed Cumulative Probability at Griffiss

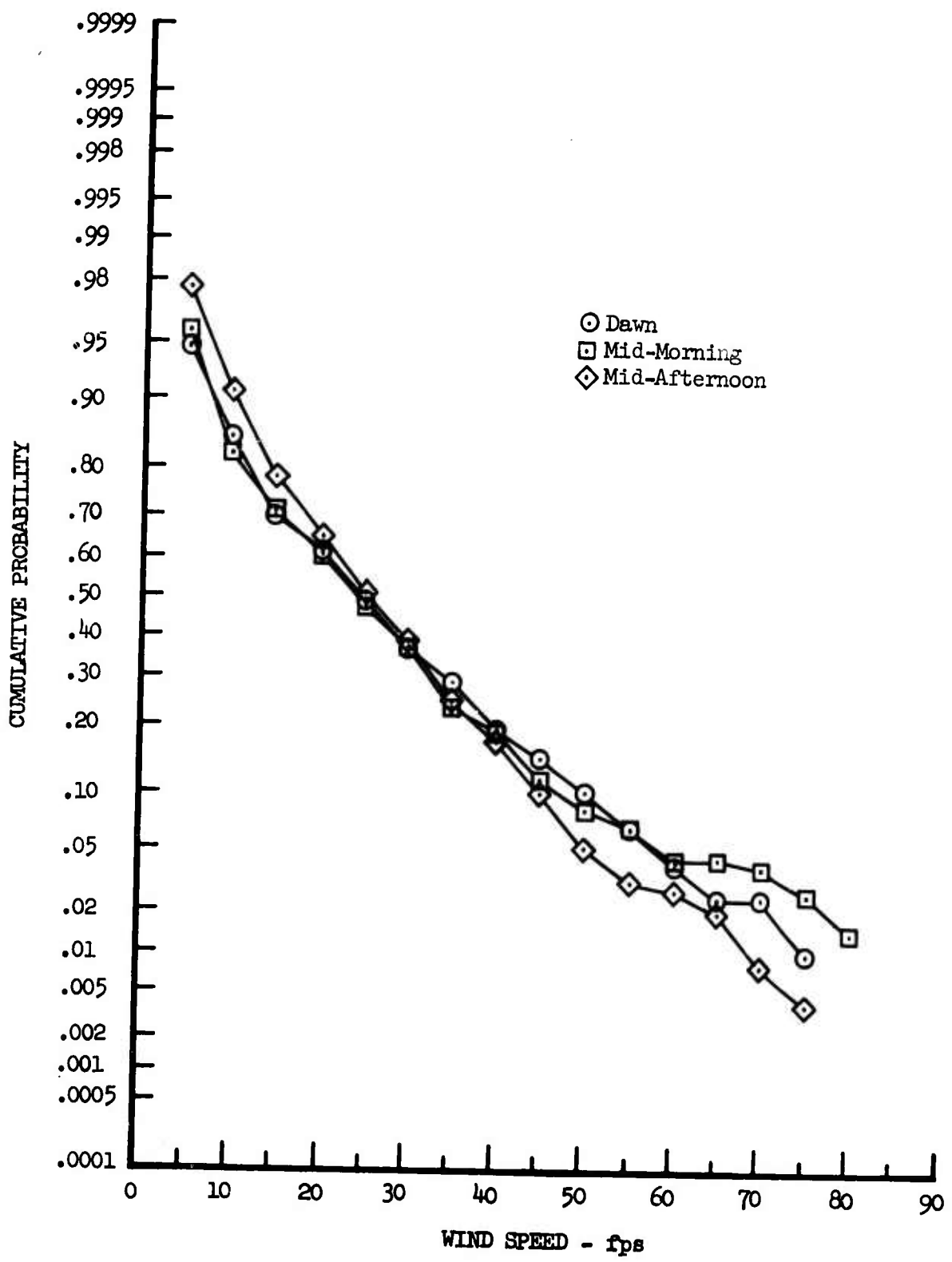


Figure 33.22 Effects of Time of Day on Wind Speed Cumulative Probability at Peterson

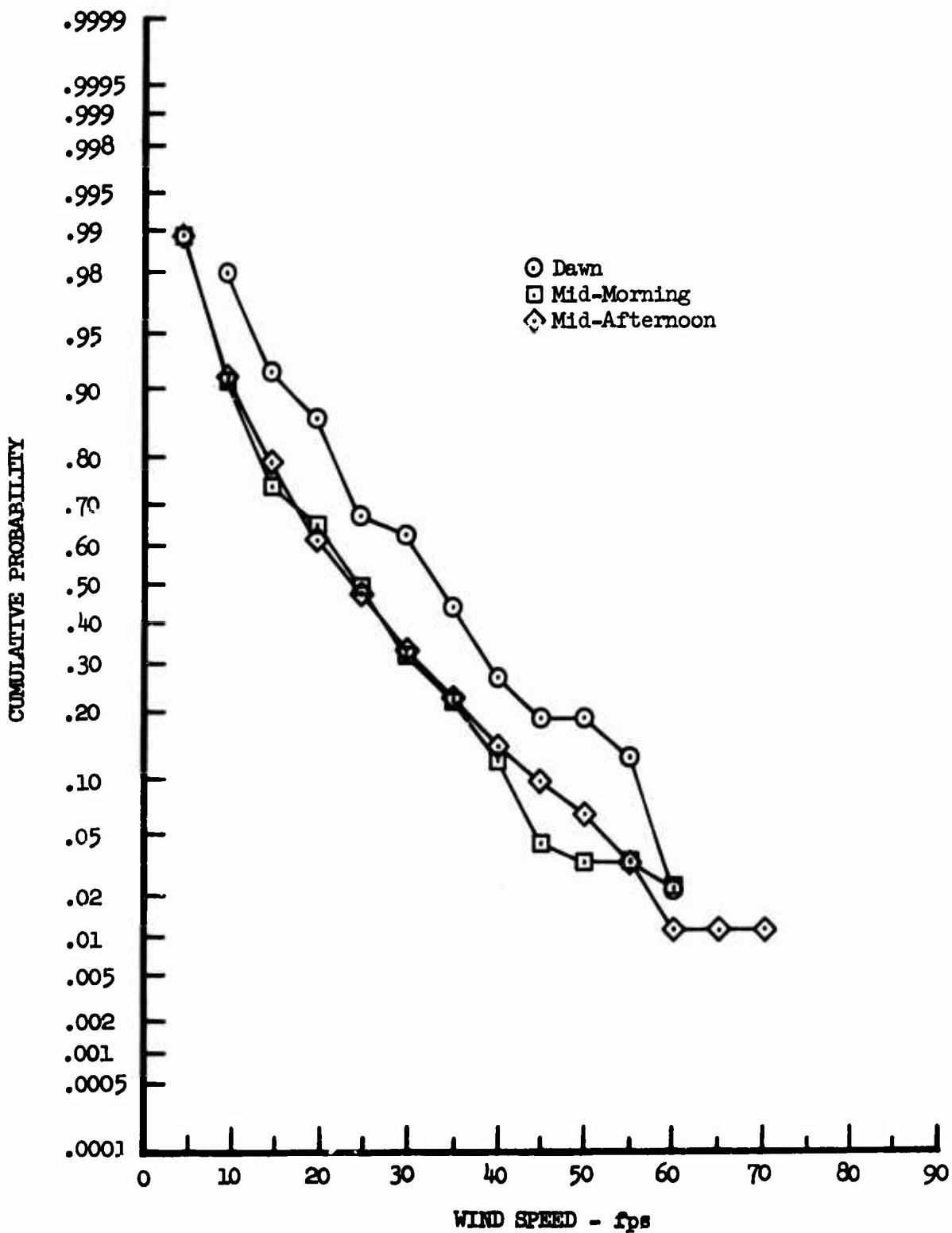


Figure 33.23 Effects of Time of Day on Wind Speed Cumulative Probability at McConnell

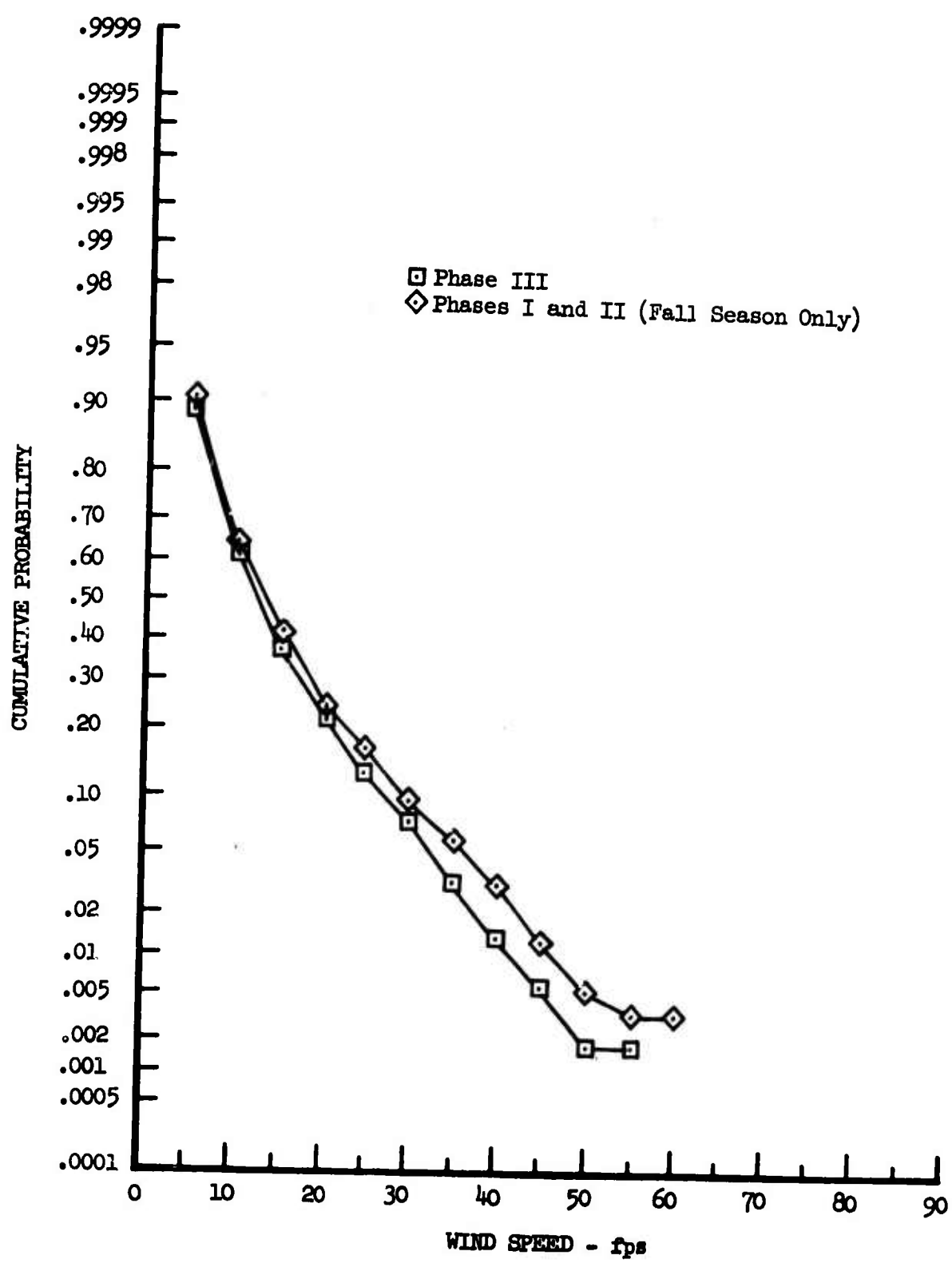


Figure 33.24 Comparison of Wind Speed Cumulative Probabilities for the Different Program Phases at Edwards

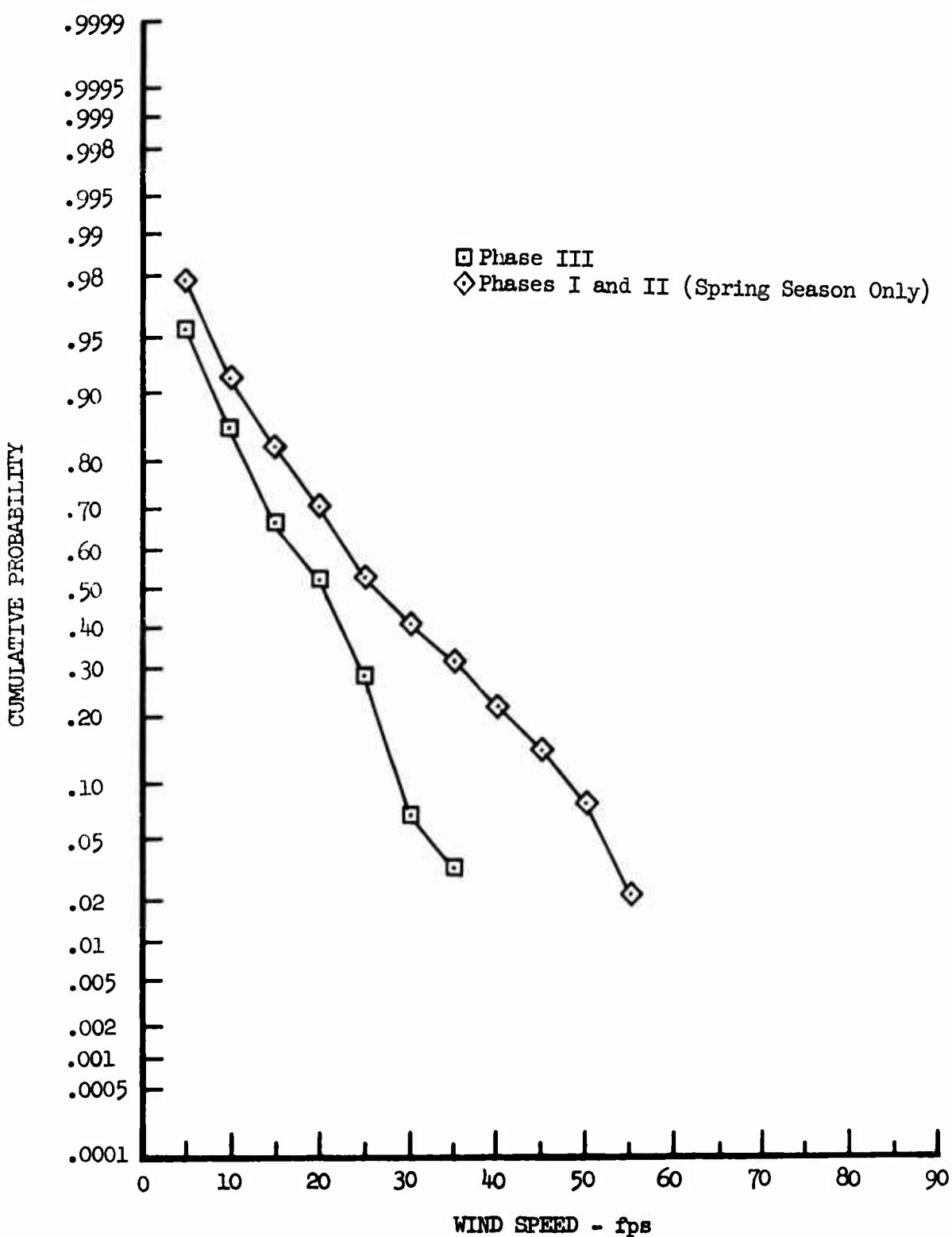


Figure 33.25 Comparison of Wind Speed Cumulative Probabilities for the Different Program Phases at Griffiss

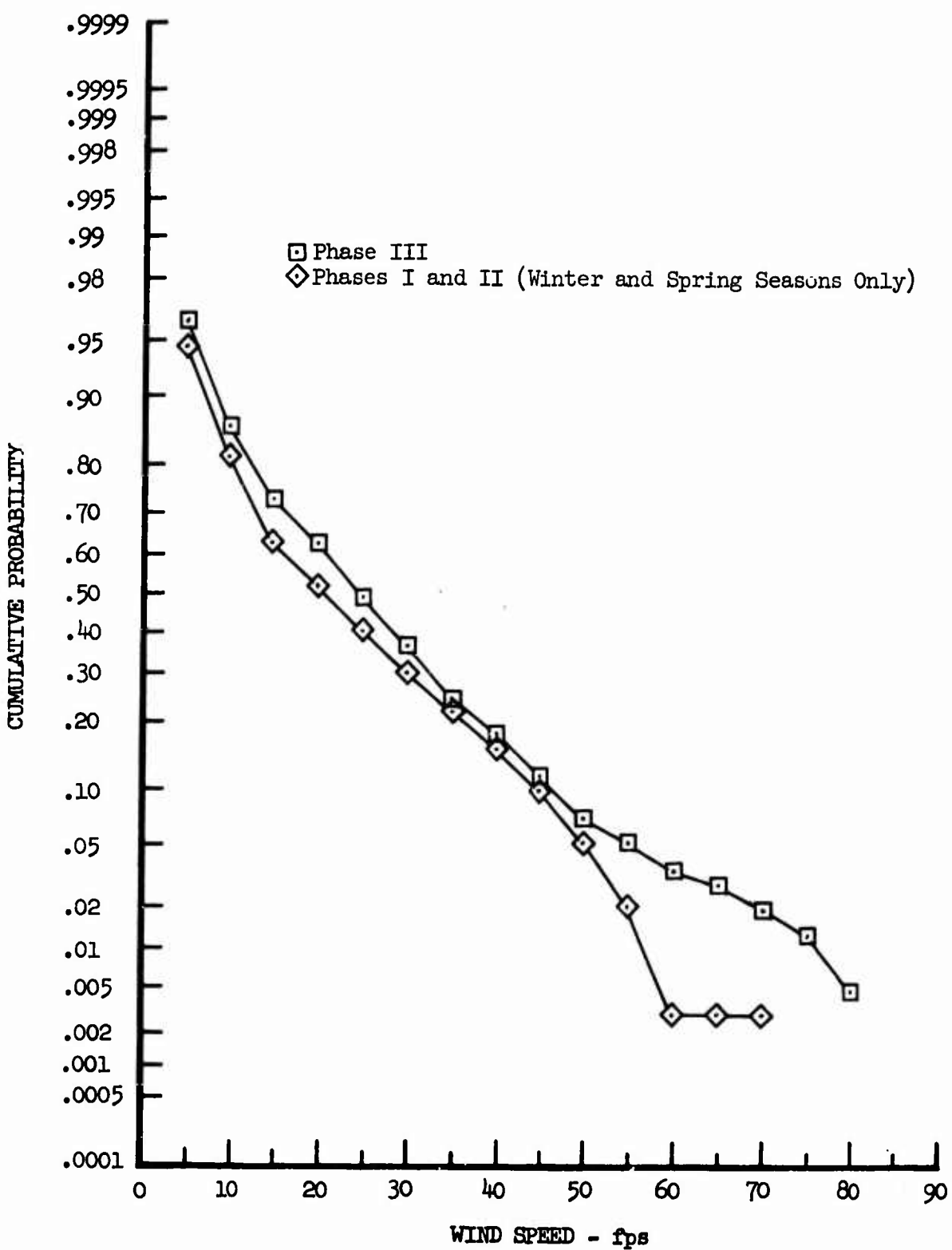


Figure 33.26 Comparison of Wind Speed Cumulative Probabilities for the Different Program Phases at Peterson

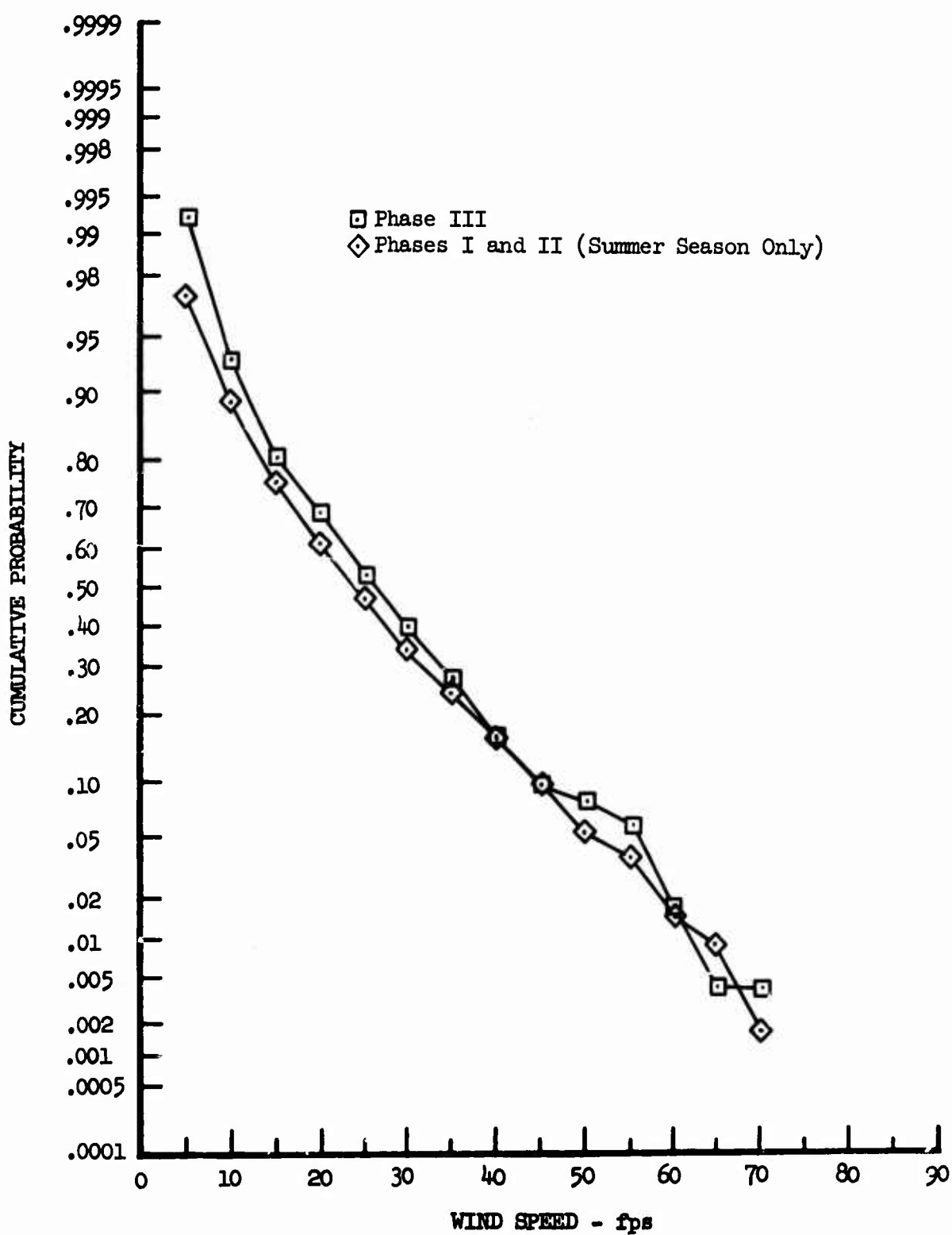


Figure 33.27 Comparison of Wind Speed Cumulative Probabilities for the Different Phases at McConnell

34. VISCOUS DISSIPATION RATE

Dissipation of kinetic energy into heat by viscous forces at the smallest eddy sizes is a significant factor in the atmospheric energy balance, especially in the lower atmosphere. Dissipation rates were calculated using the following equation (see Reference I.2 for the derivation):

$$\epsilon = 0.764 \sigma_{t_u}^3 / L_K u \quad (34.1)$$

The cumulative probabilities of encountering given dissipation rates were determined for variations in time of day and altitude. Figure 34.1 shows the comparisons of these probabilities for the three times of day. The effect of stability at each altitude is shown in Figure 34.2. These data are clearly a function of stability but do vary some with altitude. Figure 34.3 shows the variations with terrain. This shows that for rough (high mountain) terrain, the dissipation rate is much higher than for flat (plains) terrain. This is because turbulence data were recorded over the high mountains primarily during the most severe season. A more reasonable indication of terrain effects is probably indicated by the Phases I and II data shown in Figure 34.4.

The viscous dissipation rate has been estimated in lower layers (Reference 34.1) to range from $1 \text{ cm}^2/\text{sec}^3$ ($1.08 \times 10^{-3} \text{ ft}^2/\text{sec}^3$) at 500 m (1520 ft.) to $10^5 \text{ cm}^2/\text{sec}^3$ ($108 \text{ ft}^2/\text{sec}^3$) at the surface. The data presented in Figure 34.5 show a considerable amount of scatter when the scale magnitudes are closely inspected. The LO-LOCAT data lend support to these values. It can be seen (Figure 34.6) that a reduction of the scatter is made by separation of the data into stability categories. This indicates that as the stability becomes more unstable, the dissipation rate increases.

It is concluded that the dissipation rate decreases with altitude due to the primary influence of atmospheric stability which has a major influence on σ_{t_u} . The average values for each stability range determined for the LO-LOCAT data are considered representative of the altitudes flown.

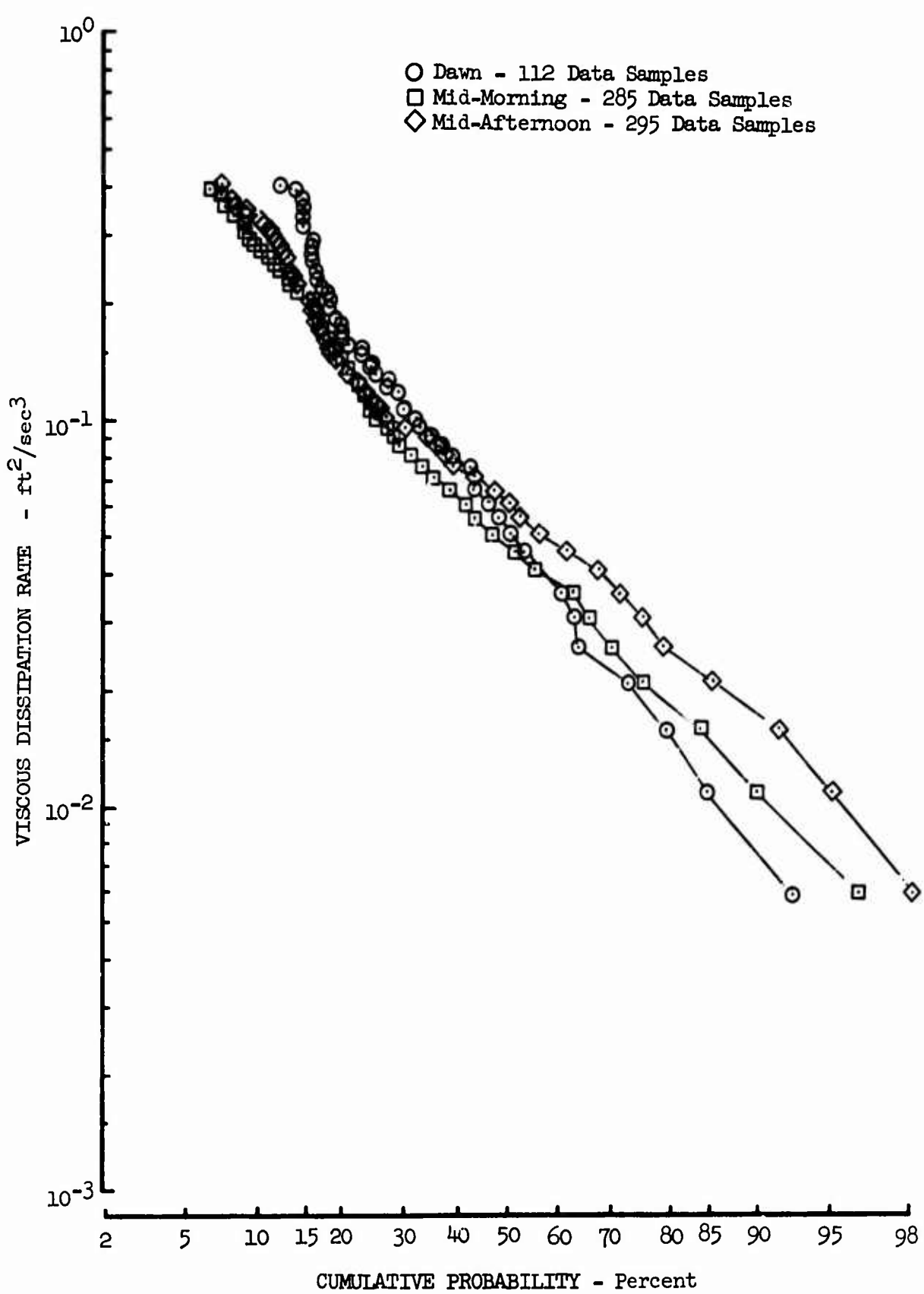


Figure 34.1 Variation of Viscous Dissipation Rate for Time of Day

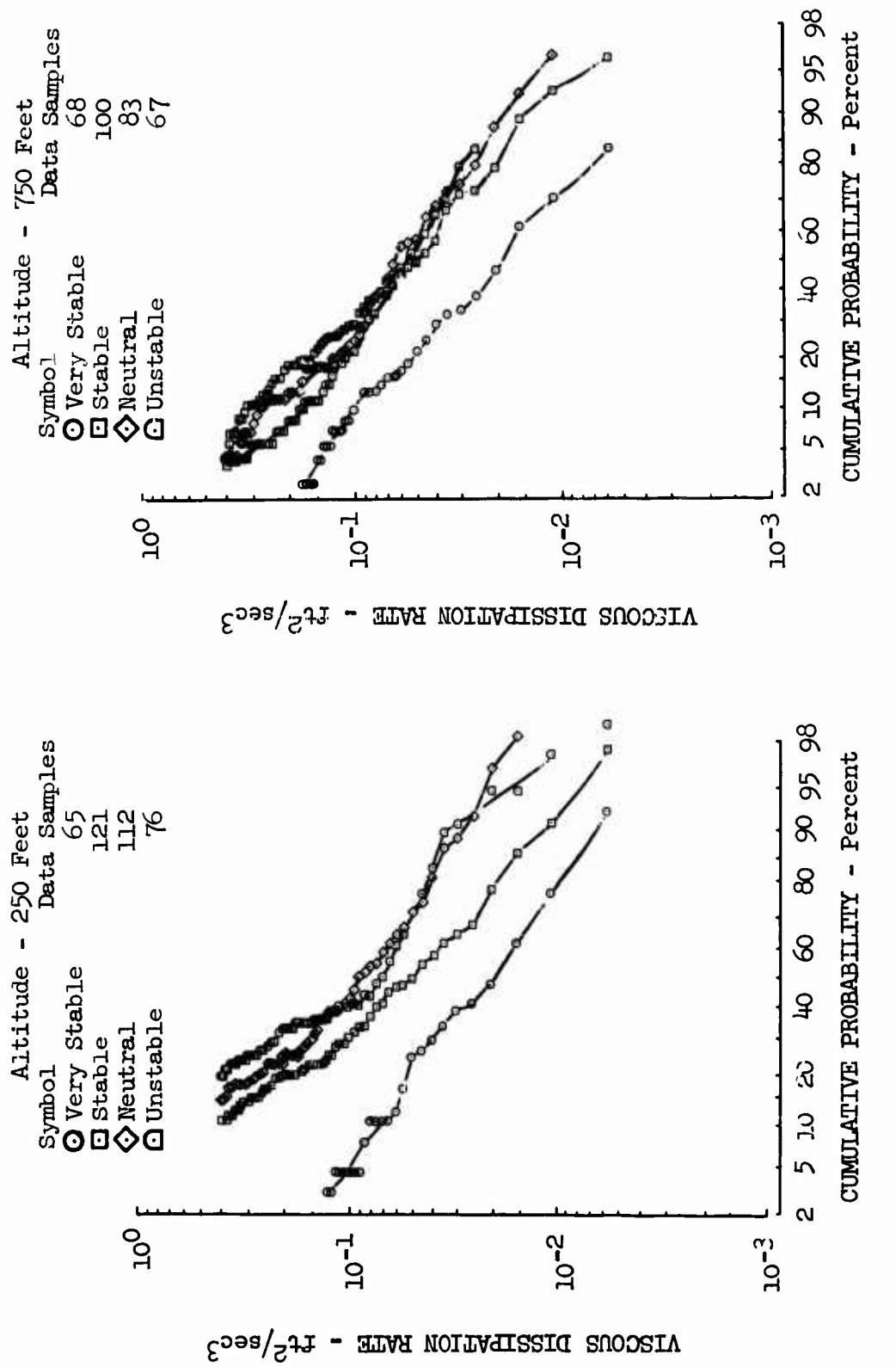


Figure 34.2 Variation of Viscous Dissipation Rate for Altitude and Atmospheric Stability

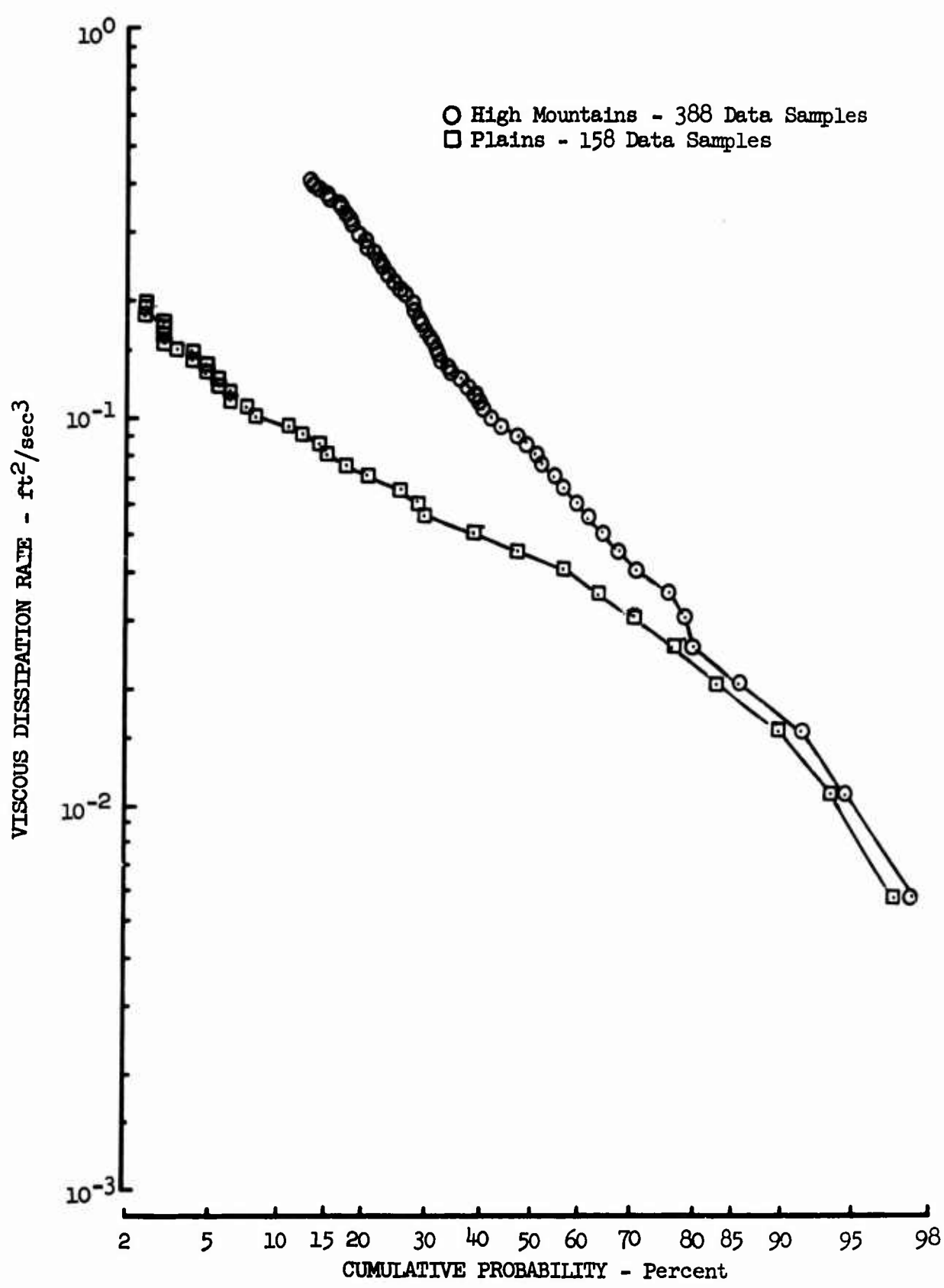


Figure 34.3 Variation of Viscous Dissipation Rate for High Mountains and Plains Terrain

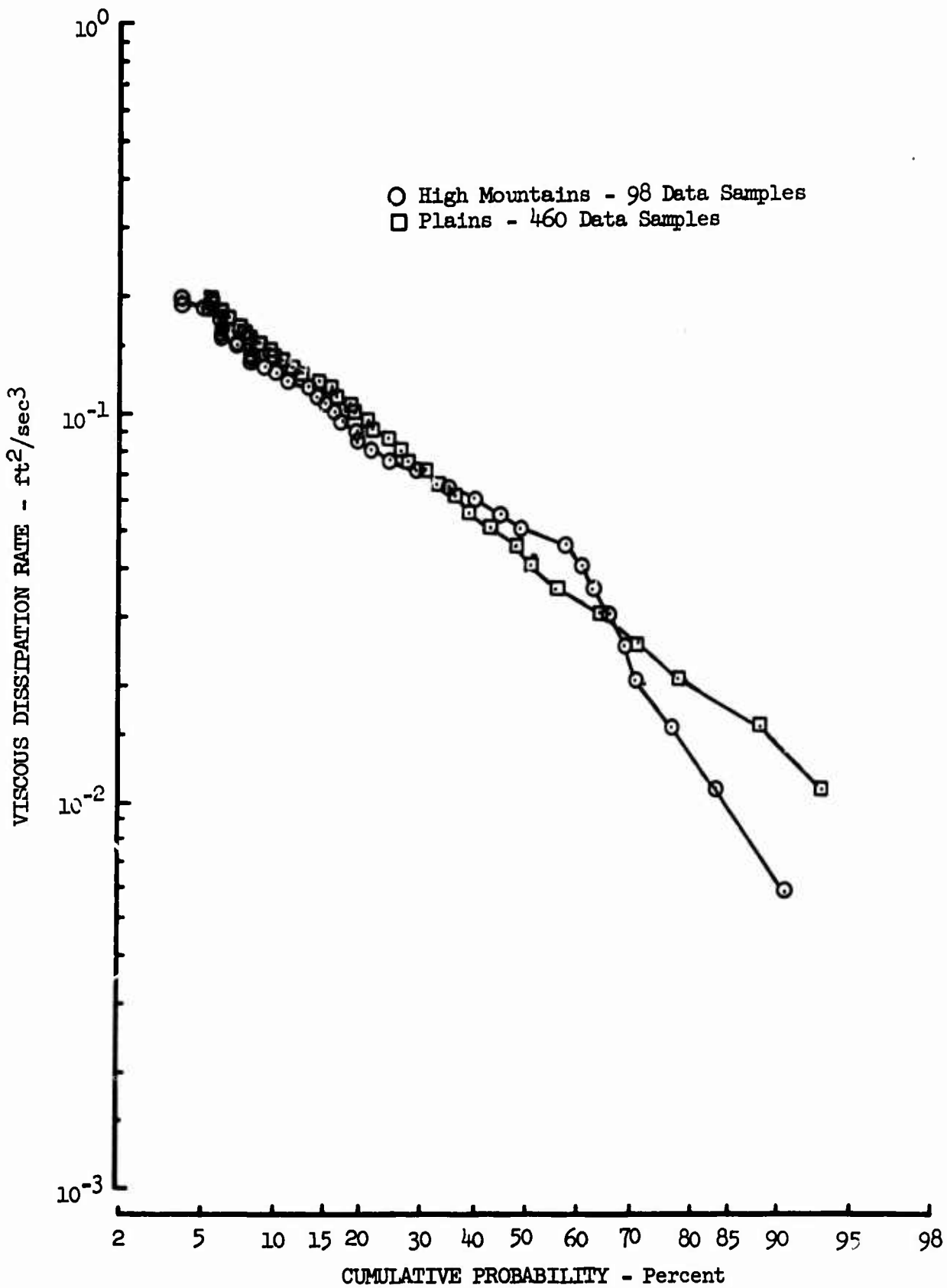


Figure 34.4 Variation of Viscous Dissipation Rate for High Mountain and Plains Terrain, Phases I and II

<u>LO-LO CAT Phases I and II Mean Values</u>	<u>NSSL Flights Operation</u>	<u>Reference 31.1 Values</u>
• All Stabilities	Rough Rider	○ Taylor --- Wilkins
◊ Very Stable	□ Unstable	△ Lettau —— Priestley
◇ Stable	BREN Tower Flyby	+ Deacon × MacCready
△ Neutral	△ - Neutral	(A) Kellogg
▽ Unstable	■ - Stable	(B) Charnock
<u>LO-LO CAT Phase III Value Range</u>		(C) Seneca
		(D) Frenkiel and Katz
		(E) Tank
		(F) Wilkins

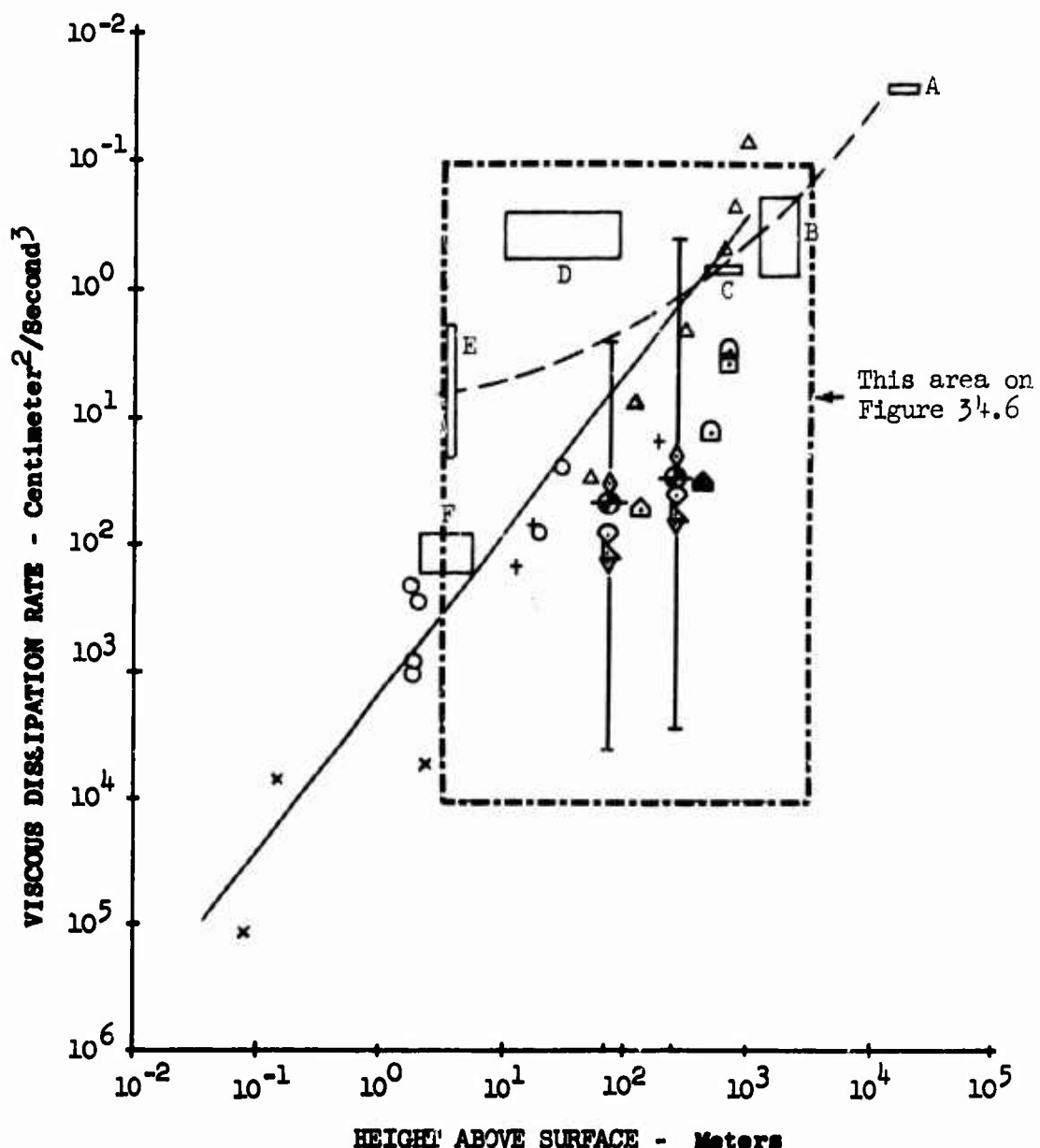


Figure 34.5 LO-LOCAT Viscous Dissipation Rates Compared to Those from Other Studies

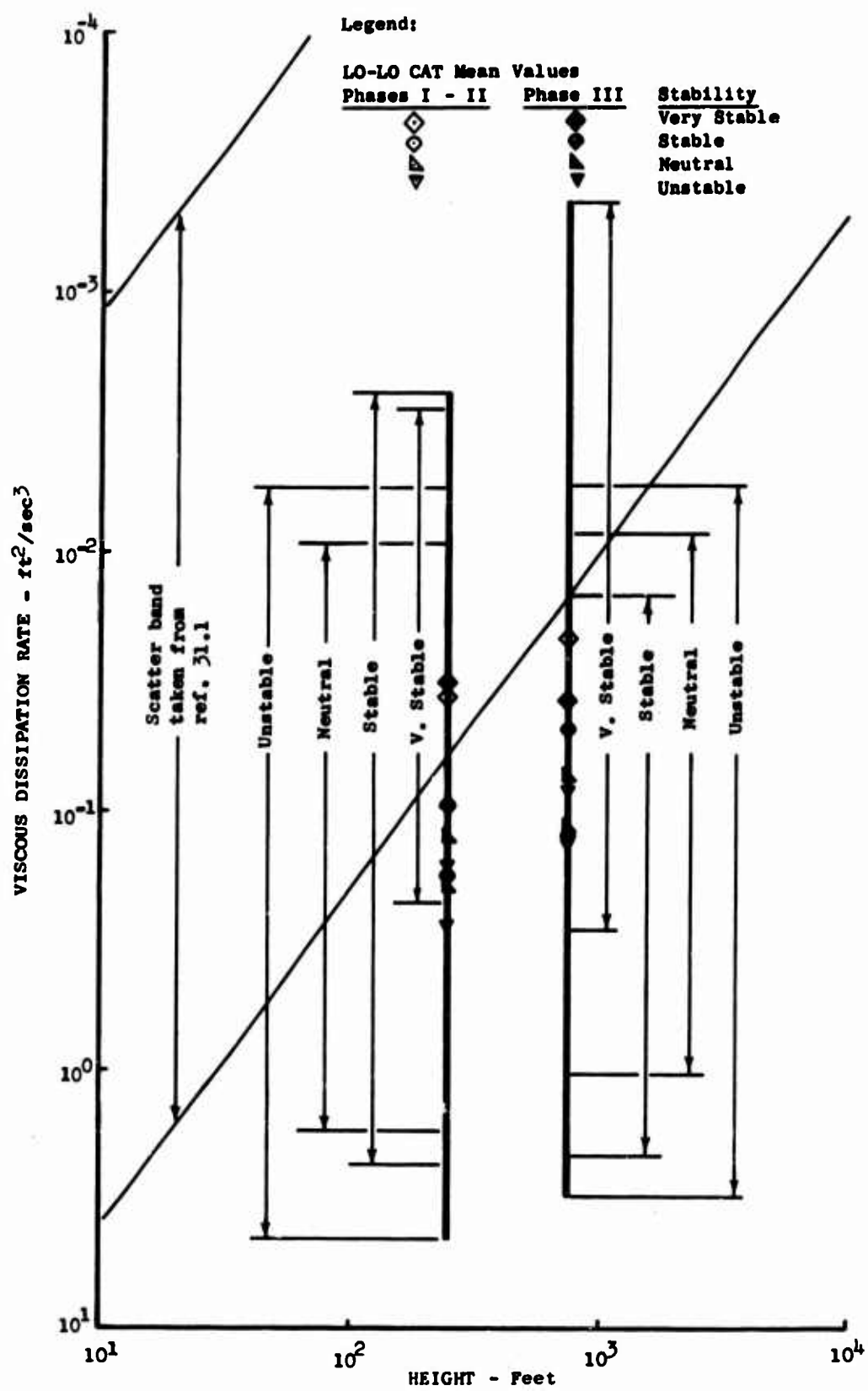


Figure 34.6 Variation of Dissipation Rate for Stability Categories

SECTION VII

TURBULENCE FORECASTING

During the LO-LOCAT Phase III Program, a concentrated effort was directed toward meteorological observation and turbulence forecasting. Improved techniques in forecasting turbulence intensity were developed through multiple regression analysis using the recorded gust velocity rms values and meteorological data. Subjective forecasting techniques employed for individual flights were varied at the particular site of each route, and was essentially dependent on the local synoptic situation. Primary emphasis in the forecast centered on wind speed and direction, cloud forms, and terrain type. The forecast methods are evaluated in this section showing the degree of success achieved for each location.

Generally, the subjective and objective forecasts used for this program can be employed to increase the current turbulence forecasting skill. The one most consistent indication of low level turbulence was vertical wind shear and lapse rate. This is shown in the Richardson number as well as the diurnal trend for plains type terrain. Mountainous terrain required a more specific knowledge of geographic geometry and greater details concerning wind velocity in order to predict the occurrence of mechanical turbulence.

35. METEOROLOGICAL DATA SAMPLING

Three main types of meteorological data were recorded during this program: that recorded in flight, that recorded by rawinsonde, and that derived from surface observations. The meteorological data recorded in flight were primarily obtained during the surveys performed prior to the recording of each 4.5-minute turbulence sample. During these surveys; air temperature, ground surface temperature, wind speed and direction, absolute and pressure altitude, airplane speed and heading, and pilot comments concerning the state of the atmosphere were recorded. Vertical gradients were determined to define lapse rate, wind shear, and atmospheric stability parameters. Standard Weather Bureau and Air Force rawinsonde observations were utilized whenever applicable; however, the greatest reliance was placed on the special observations provided at each base by the USAF 6th Weather Squadron (Mobile). A Boeing meteorologist at each base of operations provided weather and turbulence forecasts and recorded pertinent data for subsequent analysis. Flight weather conditions were forecasted in cooperation with the Air Force base weather personnel. Hourly surface observations were received by teletype from adjacent first order weather stations and special surface observations were provided by cooperative observers. Meteorological information derived from pilot debriefing was also recorded.

Selected meteorological data recorded by the airplane instrumentation are listed in the Test Log, Appendix VI.

A summary of the climatological record comparing the average observed conditions during each flight period to the past or normal record is given in Figure 35.1. Records from the nearest U.S. Weather Bureau station were used for this comparison. These stations are located at the Wichita, Kansas, Municipal Airport for the McConnell route; the Kern County Air Terminal, Bakersfield, California, for the Edwards route; and Peterson Field, Colorado Springs, Colorado, for the Peterson route. Because of the short flight period (26 days) at Griffiss, this comparison was not made for that area.

Cooperative Observers

Cooperative observers in the vicinity of each route were asked to provide observations at times coincident to that of each flight. They were provided with sling psychrometers, thermometers, hand-held anemometers, observation guide-lines, and special recording forms. It was suggested that they provide wet and dry-bulb temperatures, surface winds, and make visual observations with respect to precipitation, type, and per cent of cloud cover.

With the exception of Edwards AFB, an adequate number of observers were recruited (6 at McConnell, 7 at Griffiss, and 8 at Peterson). The regional Weather Bureau Headquarters at Salt Lake City provided four observers for the Edwards route. Three of these could not be profitably utilized due to their location in relationship to the route.

Most of the observers were untrained and the quality of their observations was uncertain. Cloud cover, visibility, and cloud type were the most difficult for them to determine. Wind speed measurements were limited in accuracy by the instrumentation, and in some cases by unrepresentative locations. Wind direction was estimated. In some cases, observation times deviated as much as three hours from the actual flight times.

Rawinsonde Observations

Special rawinsonde observations were provided by a detachment of the USAF 6th Weather Squadron for each flight. Data were recorded from the surface to 500 mb (400 mb at McConnell). Pressure, temperature, dew point, and wind velocity at levels of 250, 750, and 1,000 feet above the ground were recorded. The sounding balloon was inflated so as to rise at the rate of 500 feet per minute. Whenever available, standard rawinsonde observations from nearby fixed installations were also obtained. One of the limitations of the special rawinsonde observations was caused by the fact that the detachment had to be billeted at an Air Force Base to avoid extra expenses. This limitation was particularly severe at Edwards AFB where the detachment was stationed at Oxnard AFB, which was a considerable distance from most of the flight legs. It also had a different climatic regime from all but one of the flight legs. The topography of the Edwards route was complex and no single rawinsonde site could be found that would give observations representative of all the legs.

Sampling Sites

McConnell Air Force Base, Kansas - 16 August 1968 to 25 September 1968

The mobile rawinsonde for the McConnell route was located at Cedar Vale, Kansas, which is approximately equidistant from all the flight legs. Since the entire flight route was over plains, one sounding was considered representative of a given flight. Hourly surface observations were obtained from Wichita, Chanute, and McConnell AFB in Kansas, and from Ponca City in Oklahoma. Weather radar reports were available continuously from McConnell AFB and hourly from the Wichita Weather Bureau. Aperiodic observations were received from Bartlesville, Oklahoma. Six cooperative weather observers were located as shown in Figure 35.2. Surface wind data were available from TITAN II Missile sites located near Legs 1, 2, 7, and 8.

Edwards Air Force Base, California - 8 October 1968 to 8 January 1969

The mobile rawinsonde site was located about six miles north of Oxnard AFB, California, until 22 October 1968 when it was moved to Oxnard AFB. Edwards AFB also provided special rawinsonde observations for each flight (prior to 23 October 1968, only wiresonde observations were provided). In addition to these special observations, rawinsonde data obtained at 0400, 1000, and 1600 PST were routinely provided from Vandenberg AFB, California. These data were analyzed to assist in characterizing the upper air situation. The terrain in the overall route was complex and would have required several mobile rawinsonde locations to obtain representative soundings for each flight leg. Hourly surface observations were obtained from the first order weather station shown on Figure 35.3. Only one cooperative observer (located at Juncal Dam) participated in the program.

Peterson Field, Colorado - 20 January 1969 to 2 May 1969

The USAF Base Weather Station at Peterson Field was a 24-hour forecasting station having a storm detection radar. The U.S. Weather Bureau maintained a 24-hour observing station at the field and the Air Weather Service provided observers to augment the observation section.

The Weather Bureau Regional Headquarters at Kansas City provided the names and addresses of all cooperative weather observers in the vicinity of the Peterson Field route. All observers contacted volunteered to assist with the program, their locations are shown on Figure 35.4.

The meteorological observational network in the vicinity of the flight legs provided hourly surface observations from Buckley Air National Guard Base, Denver, Fraser, Eagle, Aspen, Leadville, Gunnison, Salida, Pueblo, Alamosa, Trinidad, and Colorado Springs and limited surface observations from Castle Rock, Eleven Mile Dam, Antero Reservoir, Woodland Park, Cannon City, Mule Shoe Lodge, Walsenburg, and Westcliffe.

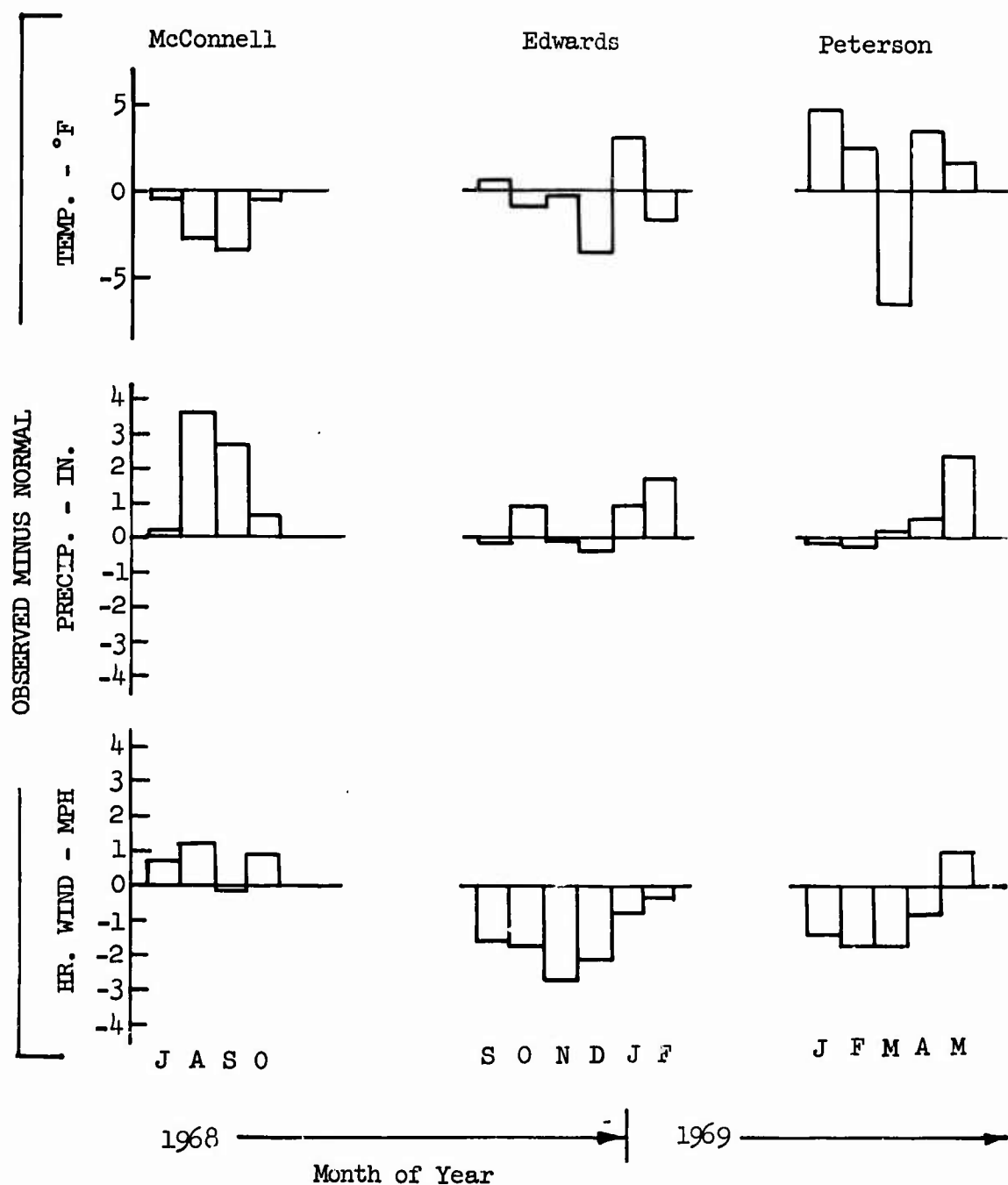


Figure 35.1 Comparison of Averaged Observed Meteorological Conditions with Normal Conditions

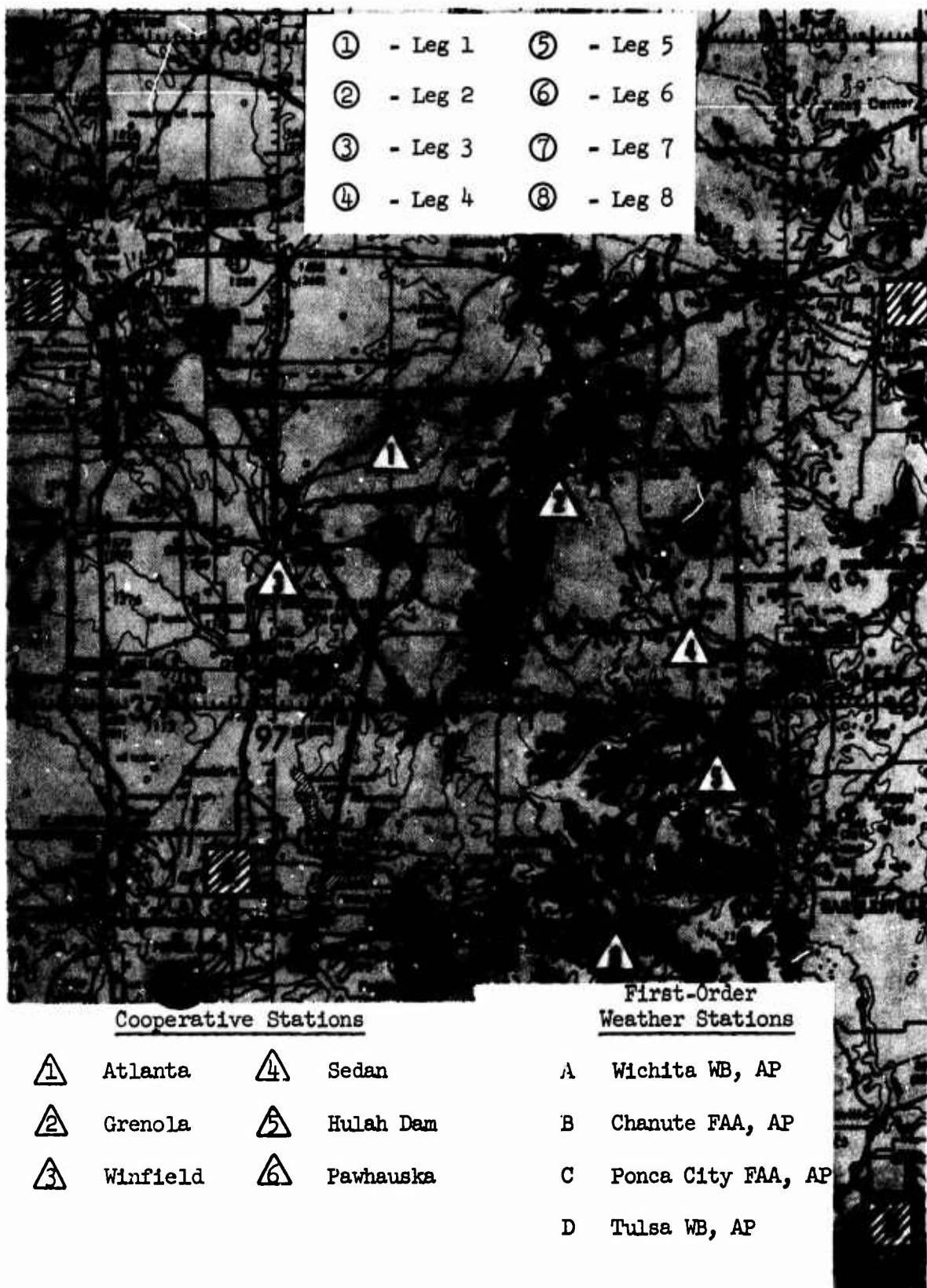
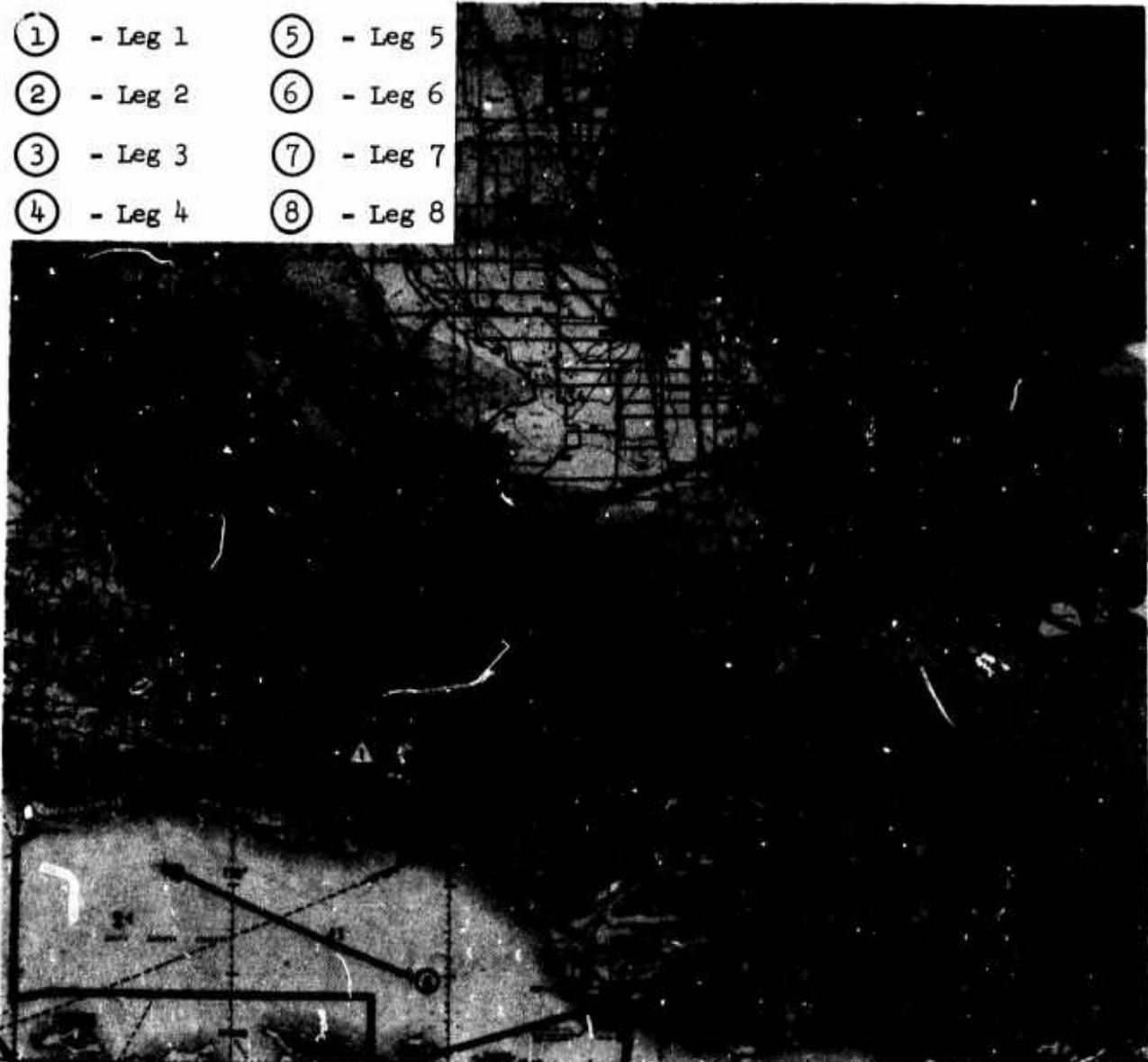


Figure 35.2 McConnell Route



First-Order Weather Stations

- | | |
|-------------------|----------------|
| A. Vandenberg AFB | F. Bakersfield |
| B. Santa Maria | G. Sandberg |
| C. Santa Barbara | H. Palmdale |
| D. Point Magu NAS | I. Edwards AFB |
| E. Oxnard AFB | |

Cooperative Station

- ▲ Juncal Dam

Figure 35.3 Edwards Route

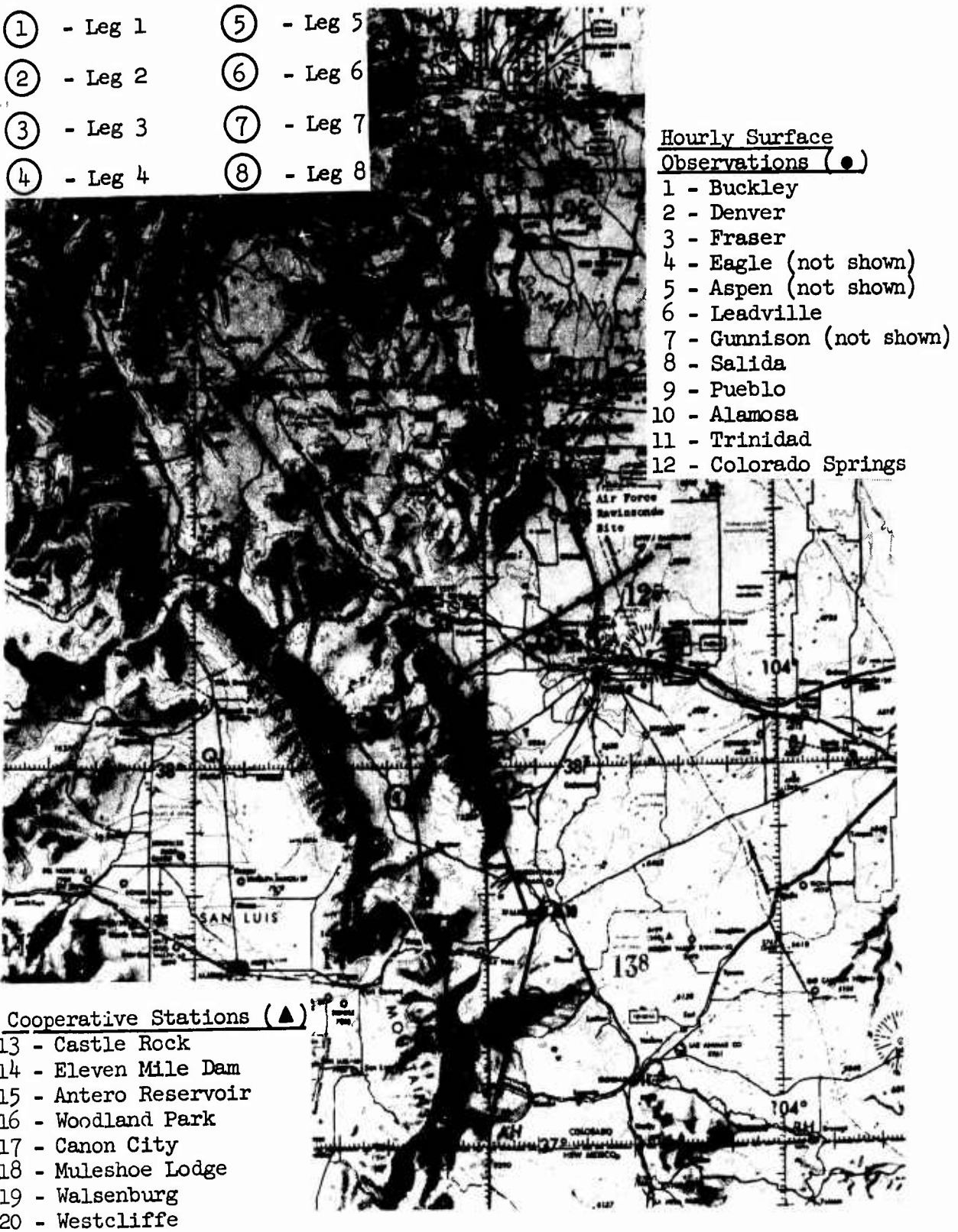


Figure 35.4 Peterson Route

36. FORECAST EVALUATIONS

Subjective Forecasting Techniques

The Second Weather Squadron at Offutt Air Force Base, Nebraska, Global Weather Center (GWC), provided special low-level turbulence forecasts for the Phase III LO-LOCAT flights. These forecasts were based on forecast values of the vertical wind shears, wind speeds from the surface to 1,000 feet, pressure changes, and a value for terrain type. Forecasts were prepared for each type of terrain and specifically for the dawn, mid-morning, and mid-afternoon flights. The forecast consisted of a nondimensional number corresponding to a specific degree of turbulence as follows:

<u>GWC Numerical Forecast</u>	<u>Expected Turbulence</u>
Less than 80	No Turbulence
80 to 119	Light Turbulence
Greater than or equal to 120	Moderate Turbulence

An evaluation of the GWC turbulence forecast was performed by computing the correlation of GWC numbers to observed gust velocity rms values. The correlation was computed for the general case (all values) by using regression analysis with inputs of either linear or squared terms. The resulting correlation coefficients are listed in Table 36.1; a value of zero indicating no correlation and a value of 1.0 perfect correlation. The mean error between the actual gust velocity rms and that predicted from the regression equation is listed in Table 36.1. Also listed are the errors for regression equations of rms values greater than a selected threshold value. This is of interest in defining how well the forecast predicted only the higher rms values. The best forecasts are shown to have been made for the plains terrain with errors of as much as 47 per cent in some other categories.

Another forecasting tool, the Showalter stability index, was compiled for each flight and the same type of regression analysis was performed as for the GWC forecasts. This index is an indication of either a stable or unstable atmospheric condition between the 850 to 500 mb level. The results shown in Table 36.2 indicate that the Showalter stability index is poorly correlated with the gust velocity rms values.

For comparison, Table 36.3 lists the results of regression analysis equations to evaluate Richardson number as a forecast tool. The errors are quite large and the correlation coefficients are near zero. A more practicable result is given from the analysis in Section 39.

The evaluations represented by Tables 36.1 through 36.3 emphasize the difficulty experienced in forecasting low altitude turbulence. These results indicate a need for improved methods in forecasting low altitude turbulence and in evaluating forecasting techniques.

McConnell Air Force Base, Kansas

Turbulence forecasting at McConnell AFB was accomplished using guidelines of the Air Weather Service Manual 55-8, Volume 1. The forecasts were primarily based upon the intensity of the surface winds, the vertical wind shear from the surface to 1,000 feet above the ground, and the type of convective clouds observed or forecast for the period of a given flight. For wind shears of 3 to 5 knots per 1,000 feet, light turbulence was forecast; 6 to 9, moderate; and 10 or higher, severe. For surface winds greater than 15 knots but less than 25, light turbulence was forecast if the air was neutrally stable or unstable. Similarly, moderate turbulence was forecast for winds greater than 25 knots. When cumuliform clouds were forecast, the following degrees of turbulence were forecast in their vicinity: fairweather cumulus, light turbulence; thunderstorms or towering cumulus, moderate; mature or rapidly growing thunderstorms, severe; and severe thunderstorms, extreme turbulence.

Edwards Air Force Base, California

Turbulence varied considerably from leg to leg for a given flight. During the period from 8 October 1968 to 8 January 1969, atmospheric conditions in the area were generally characterized as stable. Brief post frontal instabilities did occur but showers and low clouds over the mountains usually prevented flights during these times.

The most useful subjective forecasting aid for turbulence over the flight legs was wind direction and speed in relation to the terrain covered by each leg. Upper-air soundings from Vandenberg AFB, Oxnard AFB, and Edwards AFB, and surface observations from Sandberg, California were particularly useful in determining low-level wind conditions from the surface to about 2,000 feet above the terrain. Sandberg was the only observing station in the mountains which reported wind velocities.

Turbulence appeared to be highly correlated with terrain. The pilot observed that the most severe encounters occurred near the higher peaks of Legs 3 and 5. For this reason, the subjective techniques are categorized by flight leg:

- Legs 1 and 8: The pilot reported that any low altitude wind speed over 10 knots normally produced at least light turbulence over these legs. A low-altitude wind direction from west-southwest through north-northwest or from east-northeast through south-southeast with speeds in excess of 25 knots resulted in moderate or greater turbulence. On several occasions, turbulence was encountered over the desert to the southeast of the mountains in an apparent lee wave effect.
- Legs 2 and 7: Turbulence was reported during only a few flights over these legs. The low altitude flight path above the valley floor was apparently somewhat sheltered, even from possible effects of strong northerly winds.

- Legs 3 and 5: The most severe turbulence was encountered on these legs. From a forecast standpoint, any low altitude wind speed over 10 knots resulted in reports of at least light turbulence by the pilot over one of the legs. A low altitude wind direction from northwest through northeast or from southwest through southeast, accompanied by speeds in excess of 25 knots, resulted in moderate or greater turbulence. An interesting feature is that the reported turbulence occurred in a different position relative to the terrain, depending on the wind direction. The highest turbulence intensity was generally encountered on the lee side of a major terrain feature.
- Leg 6: Turbulence was reported by the pilot on this leg less often than on Legs 3 and 5. In general, low altitude wind speeds of 20 knots or more produced at least light turbulence on this leg.
- Leg 4: Turbulence was rarely reported on this leg over the coastal water. Light turbulence reported over this leg was most often associated with a strong offshore pressure gradient and a strong Santa Ana wind channeled down the Santa Clara River Valley.

Major emphasis was placed on the low altitude wind from the surface to about 2,000 feet above the surface, since this appeared to be a key factor related to reports of turbulence. Both the direction and speed of the low altitude wind must be forecasted over the flight area from available soundings and observations prior to the turbulence forecast. Given an accurate low altitude wind velocity forecast for the seasonal period of Phase III LO-LOCAT flights, one can, through terrain considerations, prepare a subjective low altitude turbulence forecast.

Peterson Field, Colorado

A method was devised to forecast turbulence for this flight route by making use of the rawinsonde soundings taken at Peterson Field close to the time of each flight. The parameters used were the wind speed and direction at 16,000 feet above sea level. The ruggedness of the terrain and the orientation of ridge lines with respect to the wind direction was a principle factor in forecasting the turbulence intensity for each leg of the route.

- Legs 1, 2, and 4: For wind directions between 256 and 285 degrees, moderate turbulence was forecast for speeds through 30 knots and severe was forecast for greater speeds. For all other directions, light turbulence was forecast for speeds 20 knots or less and moderate for greater speeds.
- Leg 3: For wind directions between 256 and 285 degrees, light turbulence was forecast up through 25 knots and moderate for greater speeds. For all other directions, a forecast of light turbulence was made up through 35 knots while moderate was reserved for speeds greater than 35 knots.

- Legs 5, 6, and 7: For the range of directions between 256 and 285 degrees, moderate turbulence was forecast for all speeds up to 25 knots, severe for speeds between 26 and 40 knots, and extreme for speeds greater than 40 knots. For the two 15-degree sectors between 241 and 255 degrees and 286 and 300 degrees, light turbulence was forecast for 10 knots or less, moderate for 11 through 25 knots, and severe for speeds greater than 25 knots. For all other directions, the forecast was light up through 10 knots and moderate for speeds greater than 10 knots.
- Leg 8: This was a plains leg and east of the mountain ranges. Forecasts for this leg were much like those over the McConnell route.

Objective Forecasts

The objective forecast models developed were based on multiple regression analysis (Appendix V). Because most models developed use the gust velocity rms as the dependent variable, an analysis of maximum gust velocities was conducted to determine if a turbulence index based on maximum gust velocity could prove more significant. It was found that the maximum gust velocities occurred frequently over the same legs of a particular course. This indicates that some local terrain feature or combination of terrain feature and wind pattern was responsible for the maximum gusts. For instance, Legs 7 and 8 at Edwards AFB (Phases I and II routes) were subject to highly localized lee wave turbulence under certain stability and wind conditions, whereas the remaining legs would have light or no turbulence. Therefore, only the gust velocity rms values were evaluated to develop forecast models. In a case study of twelve of the highest rms values for each base, Section 38, it was found that variables such as vertical wind shear and Richardson number proved to be better indications of the turbulence level than when all of the data were used in this regression analysis. It was decided to eliminate the lower gust velocity rms values from the Phases I and II data. Analysis indicated that 2.40 fps was a suitable cutoff point for all but the water leg. The small number of samples precluded the possibility of eliminating the lower gust velocity rms for this leg. Similarly, all the Phase III data was retained since there were fewer samples than in the case of Phases I and II. The regression equations derived for the LO-LOCAT Program are presented in Section 48 of this report.

Forecasting Skill

The correct and incorrect number of turbulence intensity forecasts made for the McConnell, Edwards, and Peterson routes are listed in Table 36.4. Turbulence intensities are expressed: no turbulence, N; light turbulence, L; moderate turbulence, M; severe turbulence, S; and extreme turbulence, E. Also listed in Table 36.4 are the percentage of times various intensities were observed when a particular intensity was forecasted and the percentages of time various intensities were forecasted when a particular intensity was observed. For example, consider light intensity turbulence for the McConnell route. Light turbulence was forecasted a total of nine times, and, of this number no turbulence was observed 4/9 (44.4%) of the time, light turbulence

was observed 4/9 (44.4%) of the time, moderate turbulence was observed 1/9 (11.1%) of the time and neither severe nor extreme turbulence were observed. On the other hand, light turbulence was observed a total of 26 times, and, of this number, no turbulence was forecasted 12/26 (46.2%) of the time, light turbulence was forecasted 4/26 (15.4%) of the time, moderate turbulence was forecasted 6/26 (23.1%) of the time, severe turbulence was forecasted 3/26 (11.5%) of the time, and extreme turbulence was not forecasted. It will be observed that the principal, negative slope diagonals of the table represent the correct forecasts.

A further evaluation of the forecasts was made by calculating the Heidke skill score as described in AWSM 105-40 (REV), 1955:

$$\text{Skill Score} = \frac{F-D}{T-D}$$

where: $F = a + d$

$$T = a + b + c + d$$

$$D = \frac{(a+c)(a+b) + (b+d)(c+d)}{a+b+c+d} = \text{the number that can be expected to be correct based on the sample.}$$

and a , b , c , and d were determined from the following:

		Observed		
		Yes	No	Total
Forecast	Yes	a	c	a + c
	No	b	d	b + d
	Total	a + b	c + d	a + b + c + d

This skill score can vary from -1.0 to 1.0. A score of 0.0 should occur when the total number of correct forecasts just equals the number expected to occur by chance.

The turbulence intensity at McConnell was forecast correctly only 11.11 per cent of the time; however, if only the occurrence of turbulence is considered, the percentage rises to 31.48. The skill scores are -0.1212 for the occurrence of turbulence and -0.2000 for the turbulence intensity for McConnell AFB.

The forecasts were consistently better for Edwards AFB. The turbulence intensity was correctly forecast 77.35 per cent of the time and the prediction for the occurrence of turbulence was 80.58 per cent correct. The

skill scores for Edwards AFB are 0.4769 for predicting the intensity of turbulence and 0.5298 for its occurrence.

The intensity of turbulence at Peterson Field was correctly forecast 49.8 per cent of the time and the occurrence of turbulence 97.8 per cent of the time. Skill scores for Peterson Field are 0.1986 for predicting the intensity of turbulence and zero for the occurrence of turbulence. The zero skill score results from the fact that the forecasting scheme never forecasts "no turbulence."

TABLE 36.1
VERIFICATION OF GWC FORECASTS (PHASE III)

Vertical Gust rms Values					
Terrain	Linear(L) or Square(S)	Overall Mean Error (Per Cent)	Error Above Threshold (Per Cent)	Threshold (fps)	Correlation Coefficients
High Mountains (Edwards)	L	40.00	34.18	4.5	-0.0505
High Mountains (Peterson)	S	31.78	19.20	4.5	0.2176
Low Mountains	S	40.82	46.36	4.0	0.1981
Desert	L	47.36	47.36	2.5	0.3039
Plains	L	31.00	20.00	4.0	0.6285
Lateral Gust rms Values					
Terrain	Linear(L) or Square(S)	Overall Mean Error (Per Cent)	Error Above Threshold (Per Cent)	Threshold (fps)	Correlation Coefficients
High Mountains (Edwards)	S	30.21	19.07	4.5	0.0447
High Mountains (Peterson)	S	42.38	21.64	4.5	0.1574
Low Mountains	L	30.63	16.91	4.0	0.2974
Desert	L	30.13	29.79	2.5	0.4581
Plains	L	27.26	14.77	4.0	0.6087

TABLE 36.2
VERIFICATION OF SHOWALTER INDEX (PHASE III)

Vertical Gust rms Values					
Terrain	Linear(L) or Square(S)	Overall Mean Error (Per Cent)	Error Above Threshold (Per Cent)	Threshold (fps)	Correlation Coefficients
High Mountains (Edwards)	S	39.80	35.14	4.5	-0.0865
High Mountains (Peterson)	S	33.02	19.16	4.5	-0.0649
Low Mountains	L	43.92	45.27	4.0	0.1372
Desert	L	57.93	57.93	2.5	-0.0428
Plains	S	41.06	32.43	4.0	-0.2964

Lateral Gust rms Values					
Terrain	Linear(L) or Square(S)	Overall Mean Error (Per Cent)	Error Above Threshold (Per Cent)	Threshold (fps)	Correlation Coefficients
High Mountains (Edwards)	S	30.11	35.14	4.5	-0.0657
High Mountains (Peterson)	S	43.16	21.83	4.5	-0.0610
Low Mountains	L	31.02	49.15	4.0	0.2023
Desert	L	31.98	31.98	2.5	-0.0663
Plains	S	34.33	36.27	4.0	-0.3384

TABLE 36.3
VERIFICATION OF RICHARDSON NUMBERS (PHASE III)

Vertical Gust rms Values					
Terrain	Linear(L) or Square(S)	Overall Mean Error (Per Cent)	Error Above Threshold (Per Cent)	Threshold (fps)	Correlation Coefficients
High Mountains (Edwards)	L	33.73	44.25	4.5	-0.1790
High Mountains (Peterson)	L	32.57	18.87	4.5	-0.0529
Low Mountains	L	44.08	46.02	4.0	-0.0540
Desert	L	56.97	34.29	2.5	-0.1508
Plains	S	44.59	36.06	4.0	-0.3344

Lateral Gust rms Values					
Terrain	Linear(L) or Square(S)	Overall Mean Error (Per Cent)	Error Above Threshold (Per Cent)	Threshold (fps)	Correlation Coefficients
High Mountains (Edwards)	L	26.39	34.62	4.5	-0.1683
High Mountains (Peterson)	L	42.99	21.73	4.5	-0.0764
Low Mountains	L	31.38	37.96	4.0	-0.0726
Desert	L	31.89	31.39	2.5	-0.1206
Plains	L	36.49	34.81	4.0	-0.3292

TABLE 36.4

TURBULENCE FORECASTS VERSUS TURBULENCE OBSERVED

Observed										Peterson			
McConnell				Edwards									
N	L	M	S	N	L	M	S	N	L	M	S		
N	1	12	13	0	398	70	10	0	0	0	0	0	0
L	4	4	1	0	46	93	11	0	6	82	63	3	0
M	5	6	1	0	0	8	9	0	6	90	165	43	8
S	3	4	0	0	0	2	0	2	0	4	38	29	13
E	*	*	*	*	*	*	*	*	0	0	4	4	4
Number of Forecast				Number of Forecast				Number of Forecast					
N	3.8	46.2	50.0	0	83.3	14.6	2.1	0	0	0	0	0	0
L	44.4	44.4	11.1	0	30.7	62.0	7.3	0	3.9	53.2	41.0	1.9	0
M	41.7	50.0	8.3	0	0	47.1	52.9	0	1.9	28.8	53.0	13.7	2.6
S	42.8	57.1	0	0	50.0	0	50.0	0	4.8	45.2	34.5	15.5	
E	*	*	*	*	*	*	*	*	0	0	33.3	33.3	33.4
Forecast				Forecast				Forecast					
N	7.7	46.2	86.7	0	89.6	40.5	33.3	0	0	0	0	0	0
L	30.8	15.4	6.7	0	10.4	53.8	36.7	0	50.0	46.6	23.4	3.8	0
M	38.5	23.1	6.7	-	0	4.6	30.0	0	50.0	51.1	61.1	54.4	32.0
S	23.1	15.4	0	0	1.2	0	100	0	2.3	14.0	36.7	52.0	
E	*	*	*	*	*	*	*	*	0	0	1.5	5.1	16.0

* No forecasts for this turbulence level.
 N, L, M, S, and E refer to turbulence intensity, i.e.: no turbulence, light, moderate, severe, and extreme.

37. CASE STUDIES - PHASES I AND II

Twelve flight days, characterized by having recorded the highest vertical gust velocity rms values, were selected from each of the four locations for case studies. Although the gust velocity rms values had limited range, the maximum vertical gust velocities ranged from about 16 to 50 fps, with an average of about 27 fps. A short summary of the weather associated with each flight is given. This summary was derived from the three-hourly surface maps, the 700 millibar charts, and the data recorded by the airplane. No consistent synoptic pattern was discerned.

The most consistent feature of the turbulence of these flights was the high vertical wind shears. The average wind shear over the low mountains was 3.29 knots per 100 feet; for high mountains and plains, the values were 1.94 and 1.53 knots per 100 feet, respectively.

The next most consistent feature was the low value of the Richardson numbers. For the low mountain legs the Richardson number (R) never exceeded 0.015. R over the high mountain legs were small negative values, with the exception of one case where it was plus 0.49. Over the plains there was less consistency: there was a high value of 2.42, three values between one and two, one value between one-half and one, and seventeen values less than one-half.

Higher average vertical gust velocity rms values were encountered over mountain legs than over the plains legs (high mountains 6.59 fps; low mountains 6.55 fps; plains 4.94 fps). The lowest gust velocity rms values over the mountains was also higher than the average for the plains. Likewise the highest gust velocity rms value for the plains was less than the average for the mountains. These same relationships also held true for the maximum vertical gust velocities averages: high mountains 33.49 fps; low mountains 32.31 fps; plains 21.81 fps. There was some tendency for these extremes to occur during the spring season. This was true for 16 out of 26 cases over the plains and for 6 out of 14 cases over the low mountains.

A diurnal increase in turbulence intensity appeared only for the plains legs: mid-morning and afternoon flights accounted for 24 out of the 26 cases. The sine of the solar elevation being greater than 0.65 for these 24 cases suggested that this might be due to convective activity. However, the high wind shears and the fact that unstable lapse rates were in the minority indicate that convective activity was not directly responsible for the diurnal increase in those cases.

Large rms Cases

Eight of the forty-eight case studies characterized by large vertical gust velocity rms values are presented below. Selected gust velocity data and meteorological parameters are given for each case. Surface and upper-air charts associated with each flight accompany the analyses.

McConnell Air Force Base (November 7, 1966)

General Synoptic Situation

An area of low pressure was centered over the Kansas-Nebraska region and a diffuse cold front lay across central Kansas (Figures 37.1 and 37.2). Moist, stable air with clear skies covered the flight route. The winds at the surface were from the south at about 15 knots and at 850 mb they were from the southwest at 35 knots. The flight area is indicated by the dotted outline.

Dawn Flight

Although the gust velocity rms values for this flight are among the larger values observed at this base (vertical and lateral were 4.4 fps over leg 7), the maximum vertical gust was still quite small (16 fps). The Richardson number was large and positive over leg 7; the meteorological conditions clearly were not conducive to any significantly large amounts of turbulence.

Peterson Field (April 5, 1967)

General Synoptic Situation

A trough of low pressure extended from Idaho east-southeastward to Kansas. A cold front was in this trough and two more cold fronts extended southward on the east and west sides of Colorado. The data in Figures 37.3 through 37.5 are for winds from the west at 15 knots prevailing at the surface, while at 700 mb, winds were west-southwest at 40 knots. Scattered cumulus clouds and stable air predominated.

Mid-Morning Flight

Observed gust velocities were not large (maximum vertical gust over leg 8 was 22 fps). The wind direction was essentially normal to the mountain range immediately upwind from leg 8 and appeared to be the main turbulence producing element in the synoptic picture. The Richardson number was small and positive and the wind at flight altitude was 8 knots.

Peterson Field (April 28, 1967)

General Synoptic Situation

As seen in Figures 37.6 and 37.7, a trough of low pressure was over eastern Colorado. Winds in the flight area were generally from the south at 5 to 10 knots. Dry, unstable air with scattered clouds prevailed. At 1500 GMT, a diffuse cold front was just east of the flight area, but was no longer discernible at 1800 GMT. At 700 mb (Figure 37.8), winds were southwesterly at 20 to 25 knots.

Mid-Morning Flight

A large negative Richardson number ($R = -2.55$), for leg 7, resulted from an unstable lapse rate together with a small value for vertical wind shear.

The observed turbulence (maximum vertical gust of 18 fps on leg 7) was primarily attributed to thermal convection.

Edwards Air Force Base (May 12, 1967)

General Synoptic Situation

A high pressure area off the west coast extended across California (see Figures 37.9 through 37.11). Winds over the test area were generally from the north at 5 to 15 knots. Scattered to broken clouds were present.

Mid-Afternoon Flight

The wind direction at 850 mb was essentially perpendicular to the range of mountains over which leg 4 passed. The wind speeds at 850 mb were 10 to 20 knots and most likely were not sufficient to produce well-developed mountain waves. Nevertheless, the moderately strong wind shear (2.1 knots per 100 feet) together with the roughness of the terrain were undoubtedly adequate to produce the high gust velocity rms values which were encountered (6.4 fps in the vertical).

Griffiss Air Force Base (May 26, 1967)

General Synoptic Situation

An intense low pressure system was situated just off the New England coast (see Figures 37.12 and 37.13). A high pressure area was extending down over the eastern Great Lakes region. Moist, stable air with scattered clouds prevailed. Winds at flight level were northerly at 30 to 35 knots while at 850 mb they were from the northeast at 45 knots.

Dawn Flight

The lateral component, for leg 8, showed a maximum gust of 33 fps and the gust velocity rms value was 8.5 fps. Due to the winds from the northeast at 850 mb, the airplane was flying on the lee side mountains which rose to 1500 feet above the lowlands. A possible lee-wave situation may have been present, thus causing large gust velocities over relatively smooth terrain during stable conditions.

Peterson Field (August 21, 1967)

General Synoptic Situation

A weak high pressure system was situated over central Colorado with a slight trough of lower pressure over the eastern portion of the state (Figure 37.14). Surface winds were about 10 knots from the southeast over the flight area. Broken clouds with some cumulonimbus were present. At 700 mb, the pressure gradient was nearly flat.

Mid-Afternoon Flight

The observed gust velocity rms values for this case were the smallest of the selected cases of large gust velocities. The maximum longitudinal gust

for leg 7 was 12 fps and the corresponding gust velocity rms value was 3.5 fps. Most likely the turbulence encountered here was thermal in nature. The wind was not in such a direction as to induce turbulence, and the high surface temperatures were indicative of convection. Wind at flight altitude was only 3 knots and the vertical wind shear was 0.6 knots per 100 feet.

Edwards Air Force Base (September 20, 1967)

General Synoptic Situation

Figures 37.15 and 37.16 show that low pressure was situated directly off the California coast and a small, weak surface high pressure cell was located just north of the Mexican border. Surface winds were very light and skies mostly clear in the vicinity of the flight route. At 850 mb, winds were from the east at 20 knots or less.

Mid-Morning Flight

A maximum vertical gust of 36 fps and a vertical gust velocity rms value of 7.4 fps were observed for leg 4. Unstable conditions with strong vertical wind shear (2.7 knots per 100 feet) combined to give the large gust velocities. A Richardson number of -0.03 was calculated from data obtained over this flight leg.

Edwards Air Force Base (December 13, 1967)

General Synoptic Situation

An extensive and intense high pressure area was centered over British Columbia with a ridge line extending southward into California. A low pressure area was located south of the flight route and is shown in the surface analysis for 1500 GMT in Figure 37.17. This synoptic pattern is frequently associated with Santa Ana winds, which are relatively strong, warm and dry off-shore winds observed along the southern California coast. A fast-moving cold front had passed through the area the previous night, bringing very dry air. The front became stationary for several hours near the Mexican border (Figure 37.17). Throughout the flight area the surface pressure gradient gradually increased and the winds were forecast to increase. The surface winds, which varied in direction from northwest to northeast, were influenced by the terrain. Figure 37.18 shows the surface conditions at 1800 GMT.

The synoptic pattern at 850 mb is shown in Figures 37.19 and 37.20 where the pressure-height gradient was not unusual. The air flow as represented from vertical soundings was from the northeast in contrast to the more easterly flow suggested by the pressure gradient. At this height (about 2500 feet above lowest ground), the effects of terrain were still present. Low pressure indicated at both the 850 and 700 mb levels was centered over San Diego.

Dawn Flight

Turbulence was encountered over legs 6, 7, and 8, with maximum vertical gusts of 50 fps over legs 7 and 8. Neutrally stable air and scattered clouds were observed over the route. Winds at flight altitude were 20 knots over leg 6 and 28 knots over leg 7. Legs 6 and 7 run through the Santa Clara River valley directly in the lee of the coastal mountains. A rawinsonde sounding was not available and therefore it was not known whether lee waves were present in the valley. However, the wind at 850 mb, which corresponds approximately to the heights of the mountains, was about 35 knots. This was more than adequate for the generation of lee waves if a stable layer was present at higher levels. This could explain the difference of 20 fps in the maximum gust velocity over legs 6 and 7. Leg 8 lies partly in the same valley so that lee waves could also be experienced there. Leg 8 also crosses part of the mountain range increasing the possibility of lee effects from some of the high isolated peaks. The wind shears were 1.4 knots per 100 feet over leg 6 and 1.3 over leg 7. The Richardson numbers were small and negative.

Mid-Morning Flight

Turbulence was encountered over legs 7 and 8, with maximum vertical gusts of 50 fps on leg 7. Unstable lapse rates were recorded. Winds at flight altitude were 22 knots over leg 7 and 28 knots over leg 8. Wind shears were 2.6 knots per 100 feet over leg 7 and 2.3 over leg 8. The Richardson numbers were small and negative.

Low rms Cases

A total of four case studies were made on situations characterized by low gust velocity rms values. The purpose of this was to see if there were any outstanding differences in the overall synoptic patterns as compared to the high gust velocity rms cases. One case from each of the four locations was selected.

McConnell Air Force Base (November 4, 1966)

General Synoptic Situation

The flight area was located in the region ahead of a warm front which extended eastward from a low pressure trough over west Texas (see Figures 37.21 and 37.22). Winds at the surface and at 850 mb were approximately 25 knots from the east. Skies were mostly overcast with some rain occurring north of the flight area.

Mid-Afternoon Flight

The maximum gust, for the vertical component over leg 8, was 7 fps with a corresponding gust velocity rms value of 1.6 fps. A large positive Richardson number was calculated, indicating stable conditions with little wind shear. Low gust velocity encounters would normally be expected.

Peterson Field (December 5, 1966)

General Synoptic Situation

A stationary front was located across south central New Mexico and the Texas panhandle. At the surface, a trough was located from north to south through eastern Colorado (Figure 37.23). Winds in the flight area were light and variable at the surface and were from the southwest at around 25 knots at 700 mb (Figure 37.24). Broken to overcast skies predominated.

Dawn Flight

A maximum vertical gust of 12 fps and a vertical gust velocity rms value of 1.5 fps were recorded over leg 1. The small values for the gust velocities were undoubtedly related to the fairly small vertical wind shear (1.1 knots per 100 feet) and the very stable lapse rate.

Griffiss Air Force Base (November 16, 1967)

General Synoptic Situation

A ridge of high pressure extended northward over Pennsylvania and New York from a high pressure system centered over North Carolina. (See Figures 37.25 and 37.26). Winds in the flight area were from the west at around 10 knots. Scattered to broken clouds with a few isolated snow showers were present. At 850 mb (Figure 37.27), winds were from the west at 25 knots.

Mid-Afternoon Flight

Stable conditions together with a wind trajectory coming over Lake Ontario combined to give low gust velocities for leg 7. Leg 7 lies mostly over flat land on the western edge of the mountains. The vertical gust velocity rms value was 1.7 fps.

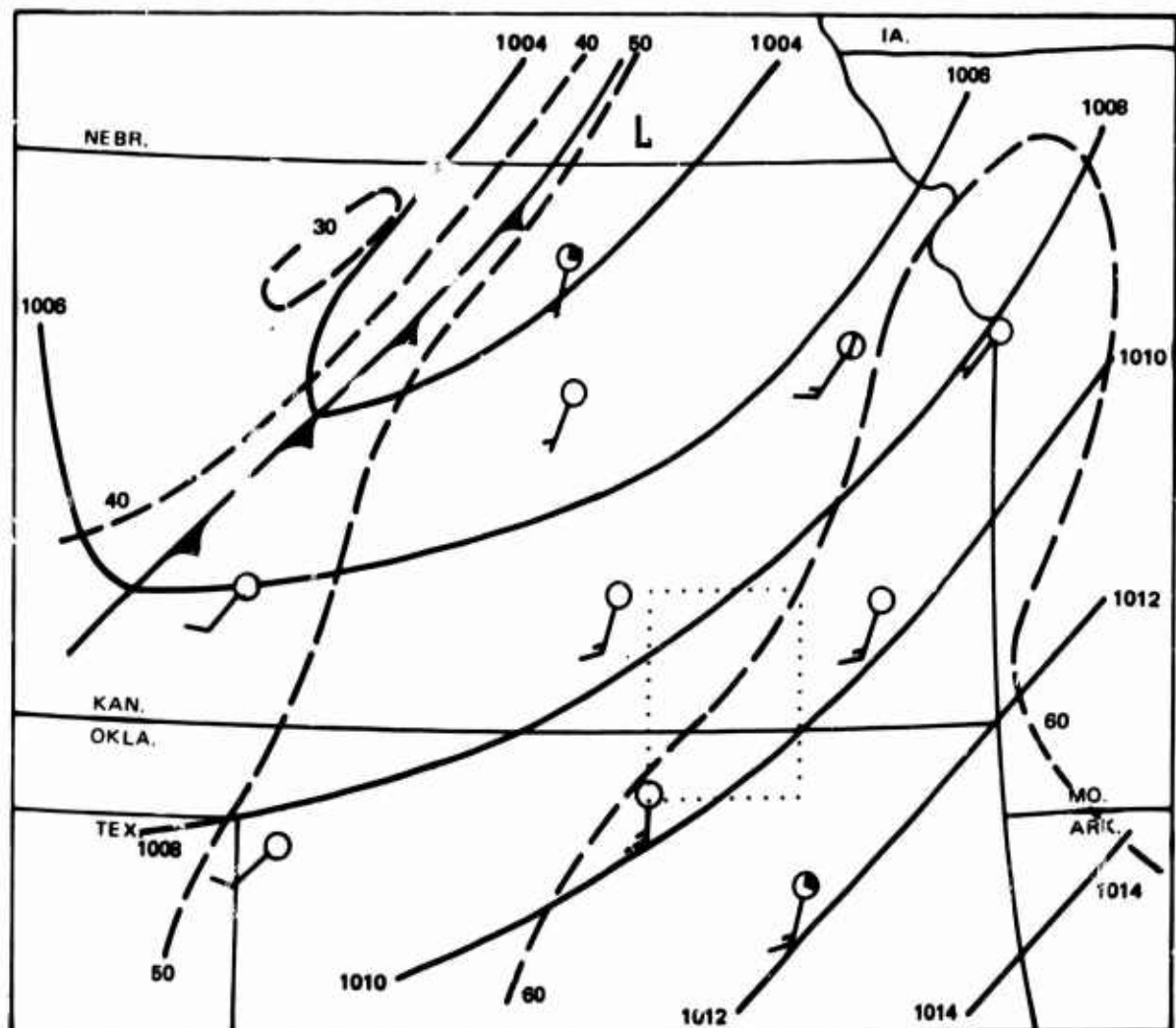
Edwards Air Force Base (December 6, 1967)

General Synoptic Situation

An intense low pressure system was over the Gulf of Alaska and an accompanying frontal system was located off the west coast. High pressure covered Nevada and northern California (Figure 37.28). Winds at the surface were light and variable. At 850 mb (Figure 37.29), the surface high pressure was replaced by a trough of low pressure with winds still remaining fairly light at 5 to 10 knots.

Mid-Morning Flight

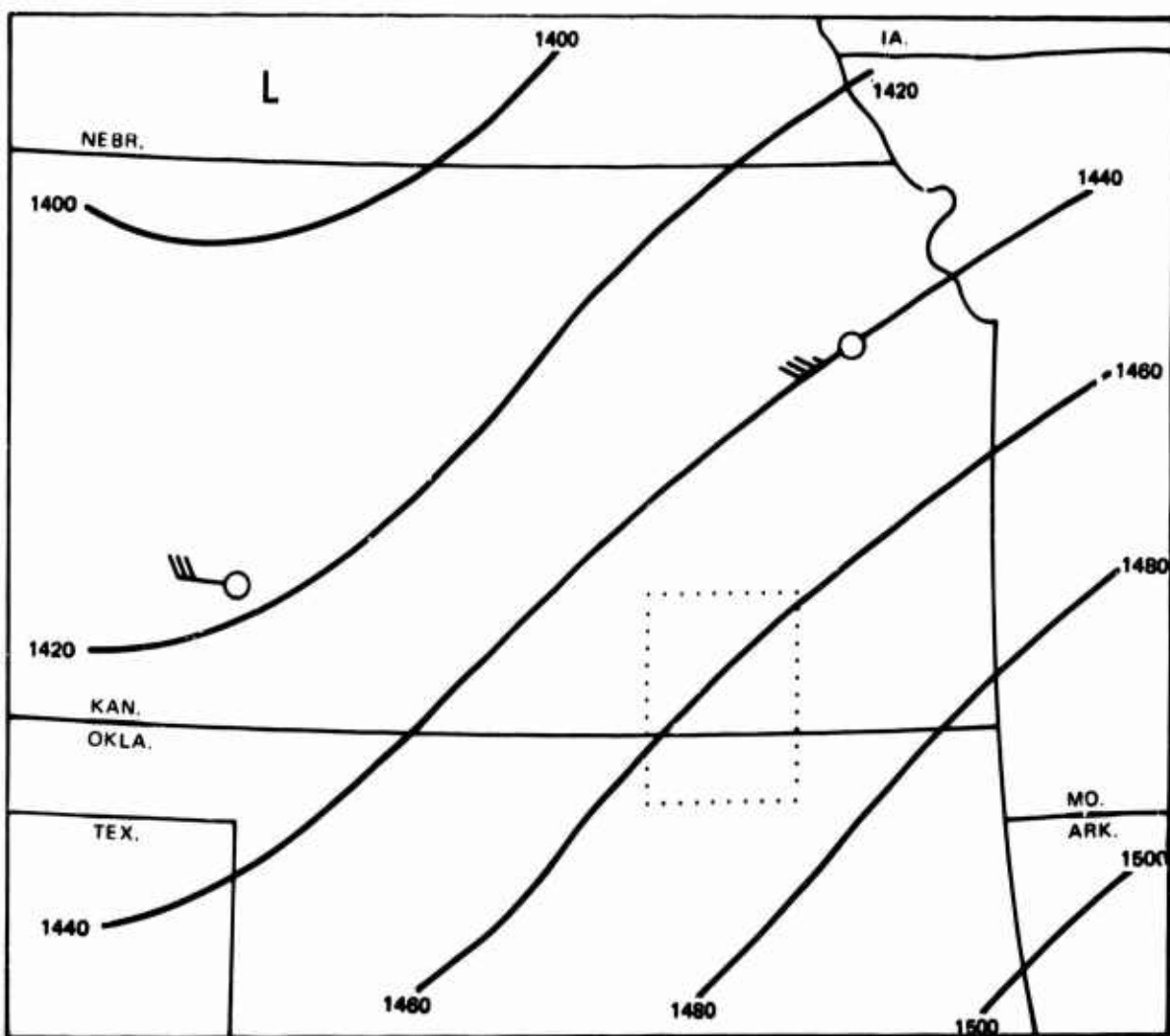
A maximum vertical gust velocity of 10 fps occurred over leg 4 and the corresponding gust velocity rms value was 1.6 fps. The lapse rate was stable and the vertical wind shear was 1.6 knots per 100 feet. The wind at flight altitude was roughly parallel to the mountain range which is crossed by the flight track. This accounted for the small gust velocities.



McCONNELL AFB
DATE — 7 NOVEMBER 1966
TIME — 1200 GMT

SURFACE ANALYSIS

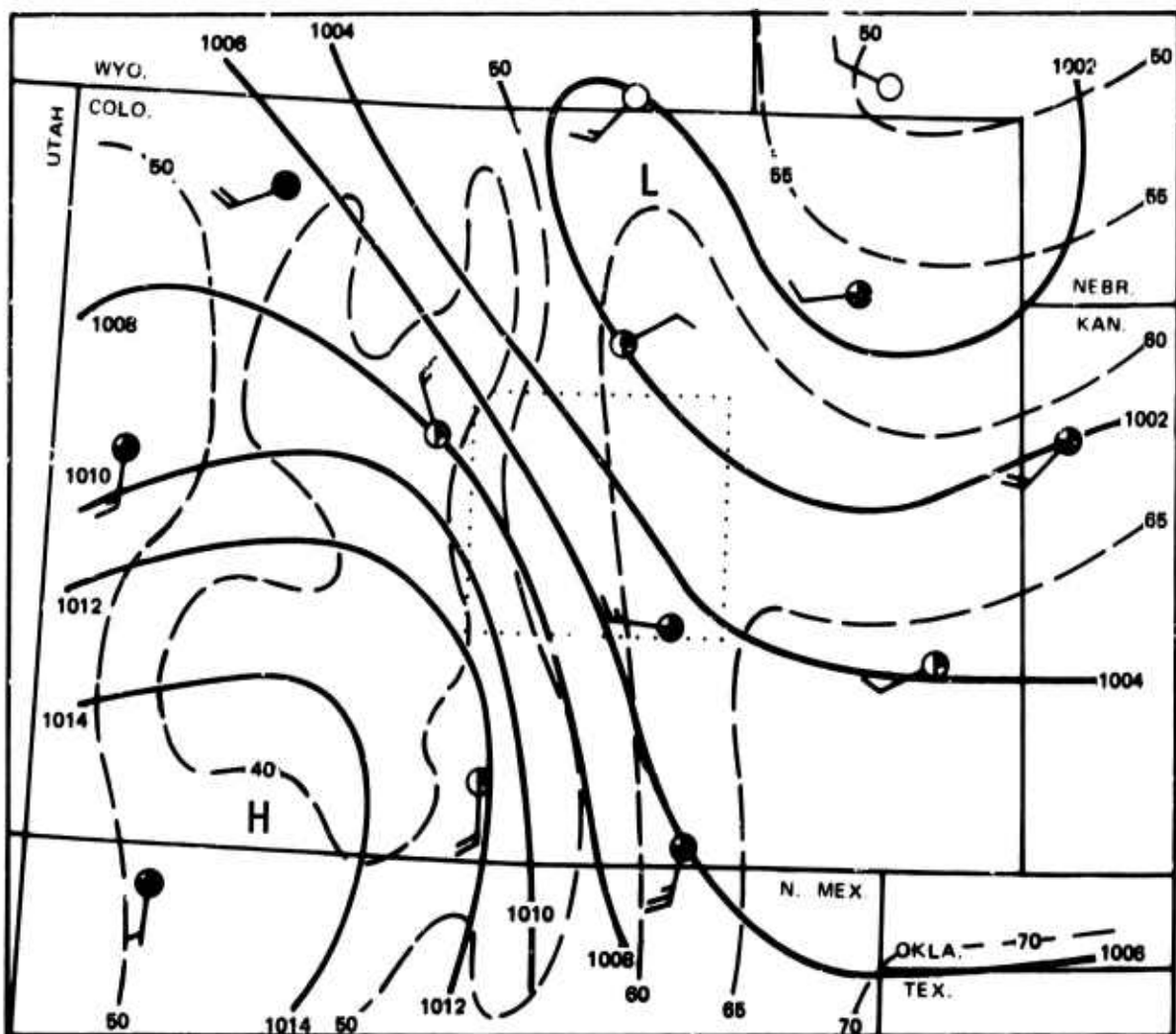
Figure 37.1 November 7, 1966 Surface Analysis, McConnell Route



McCONNELL AFB
DATE - 7 NOVEMBER 1966
TIME - 1200 GMT

850 MB ANALYSIS

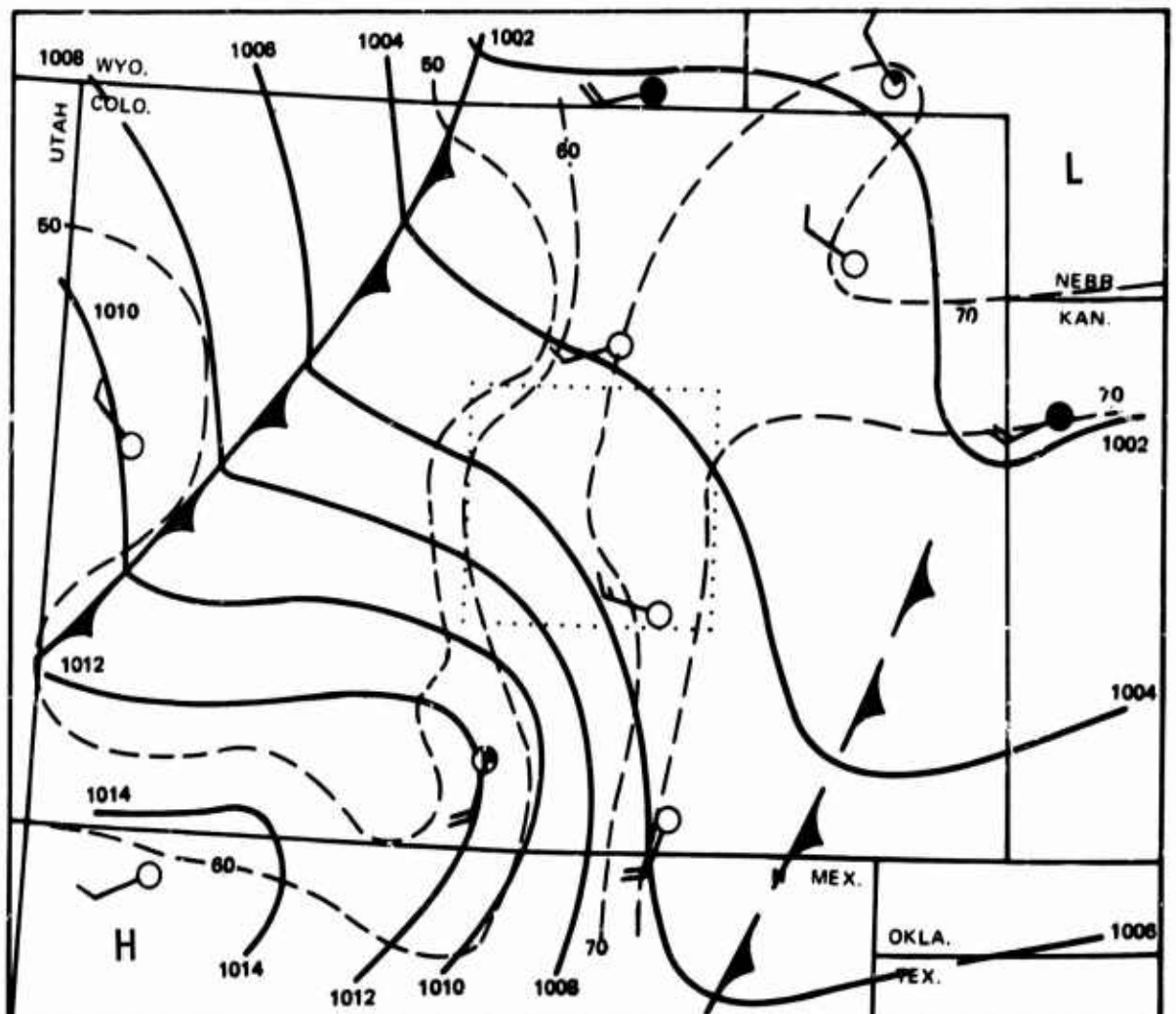
Figure 37.2 November 7, 1966 850 MB Analysis, McConnell Route



PETERSON FLD
DATE - 5 APRIL 1967
TIME -- 1500 GMT

SURFACE ANALYSIS

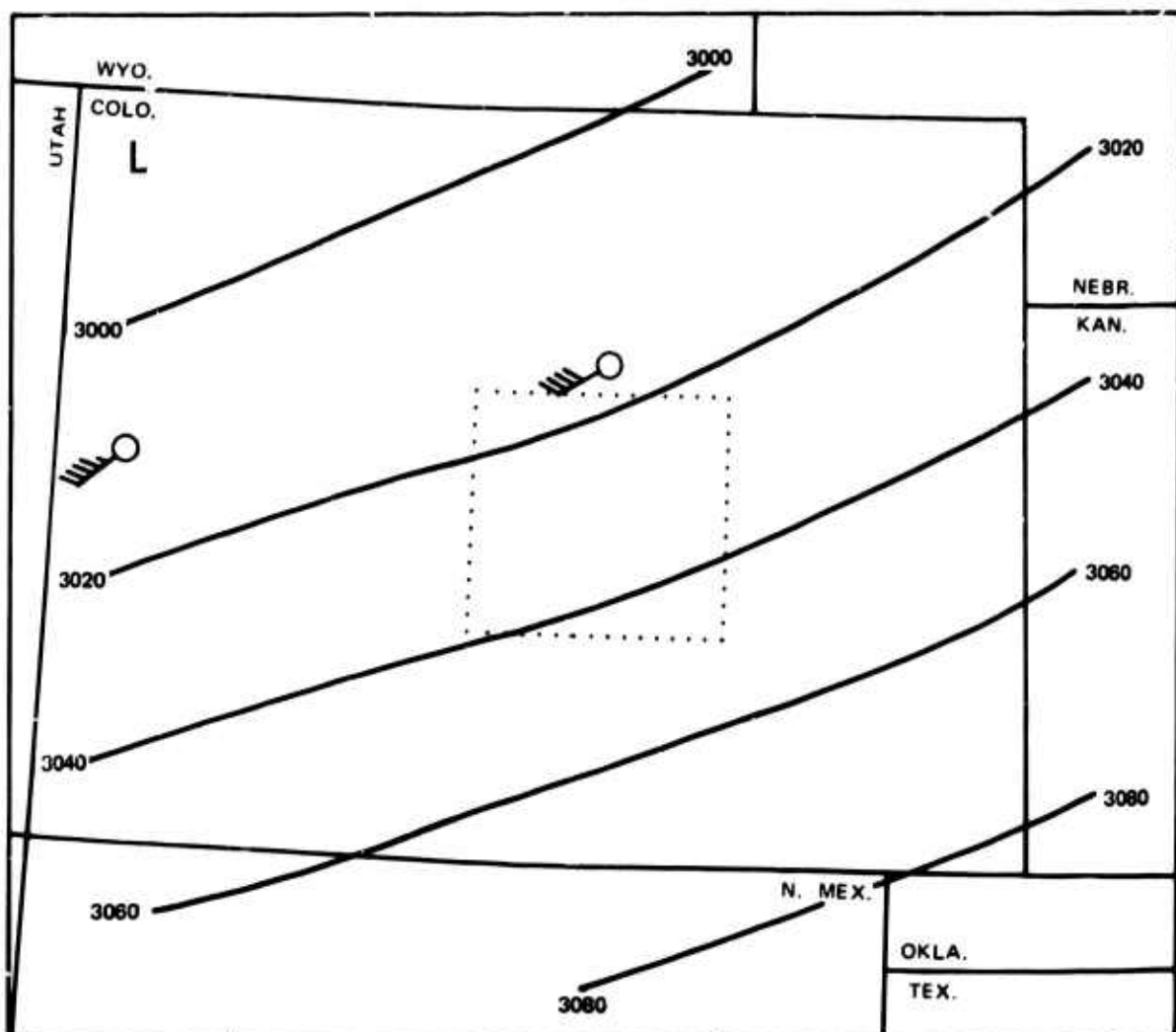
Figure 37.3 April 5, 1967 Surface Analysis, Peterson Route



PETTERSON FLD
DATE - 5 APRIL 1967
TIME - 1800 GMT

SURFACE ANALYSIS

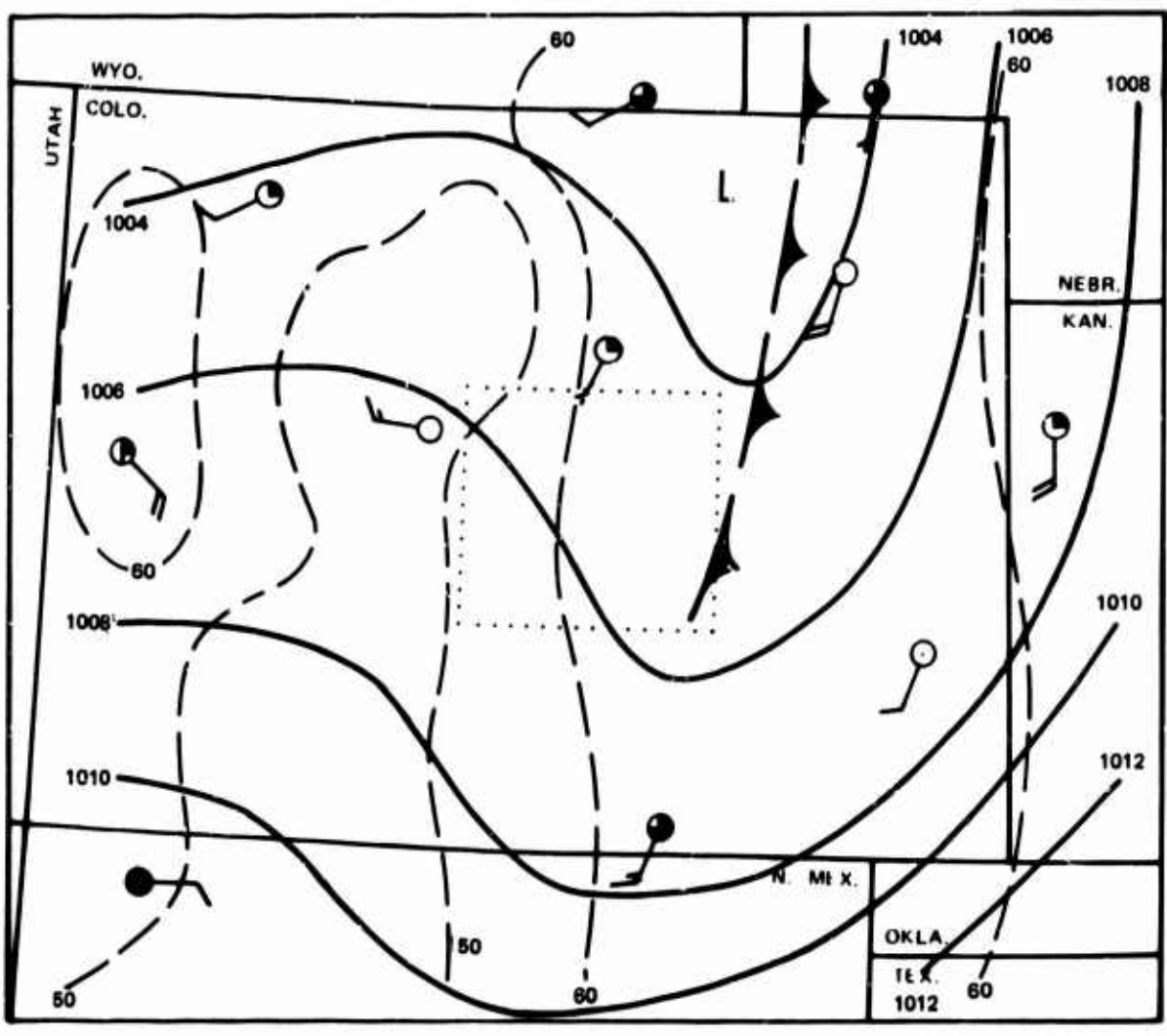
Figure 37.4 April 5, 1967 Surface Analysis, Peterson Route



PETERSON FLD
DATE — 5 APRIL 1967
TIME — 1200 GMT

700 MB ANALYSIS

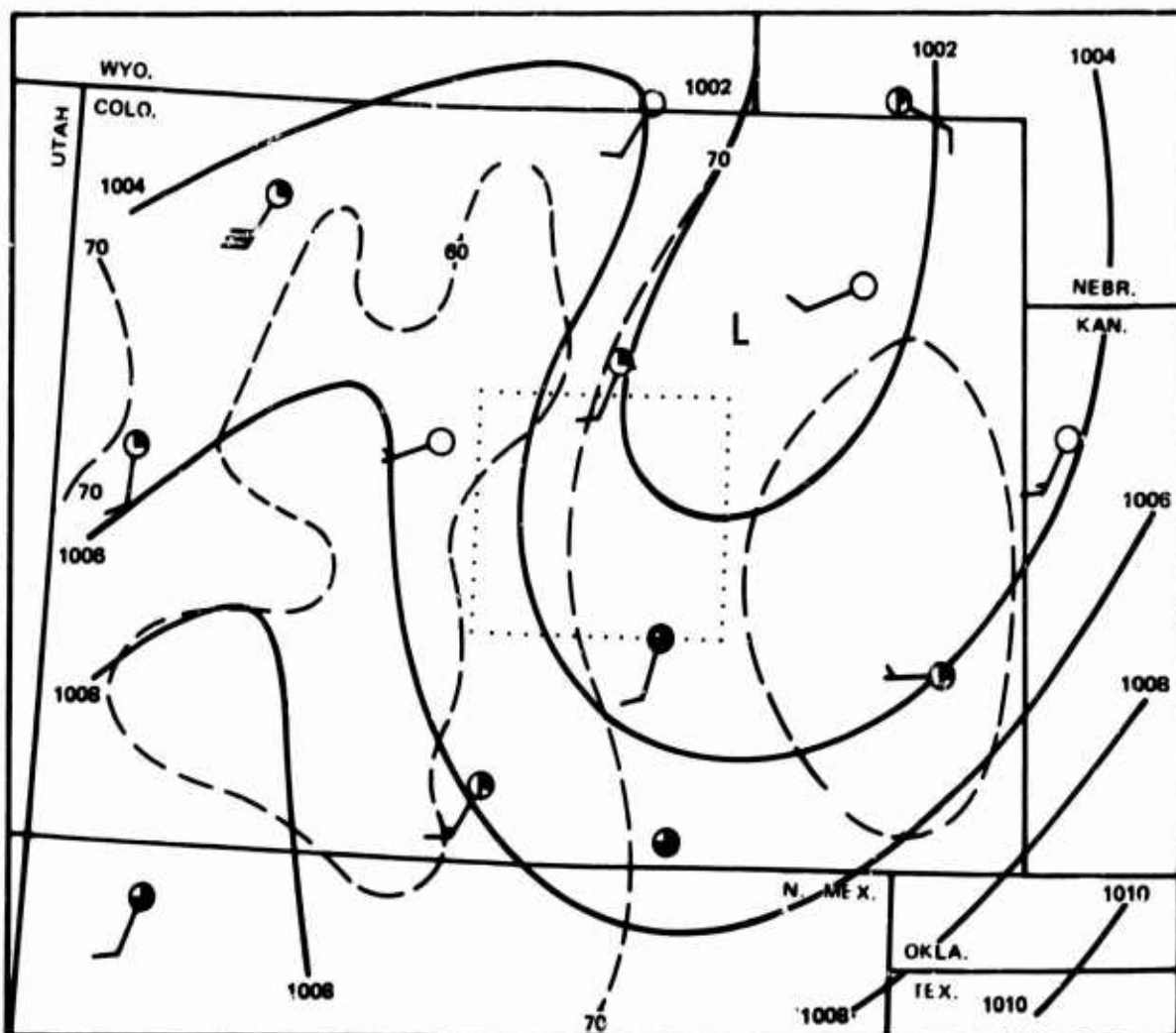
Figure 37.5 April 5, 1967 700 MB Analysis, Peterson Route



PETERSON FLD
DATE - 28 APRIL 1967
TIME - 1500 GMT

SURFACE ANALYSIS

Figure 37.6 April 28, 1967 Surface Analysis, Peterson Route



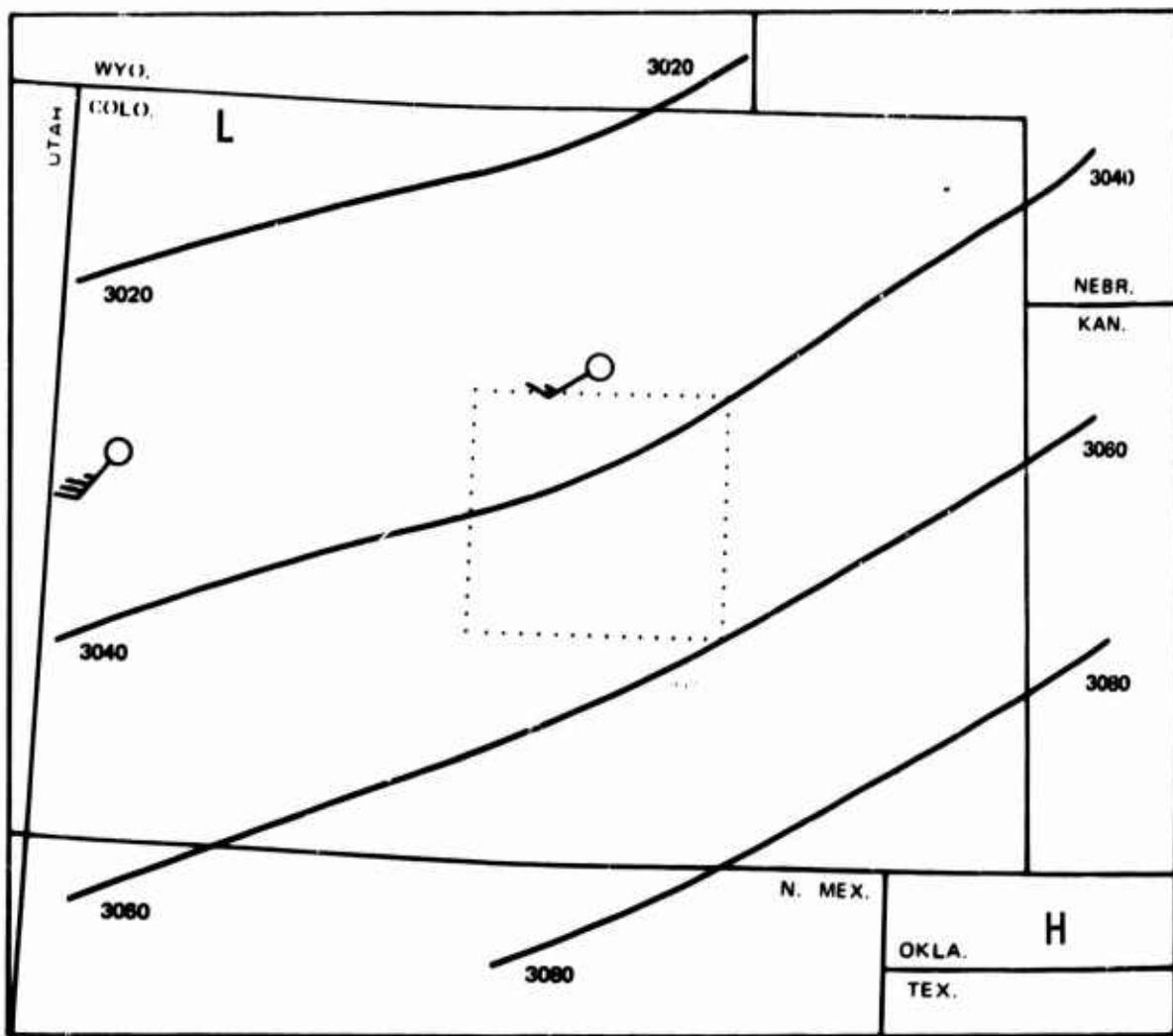
PETERSON FLD.

DATE — 28 APRIL 1967

TIME — 1800 GMT

SURFACE ANALYSIS

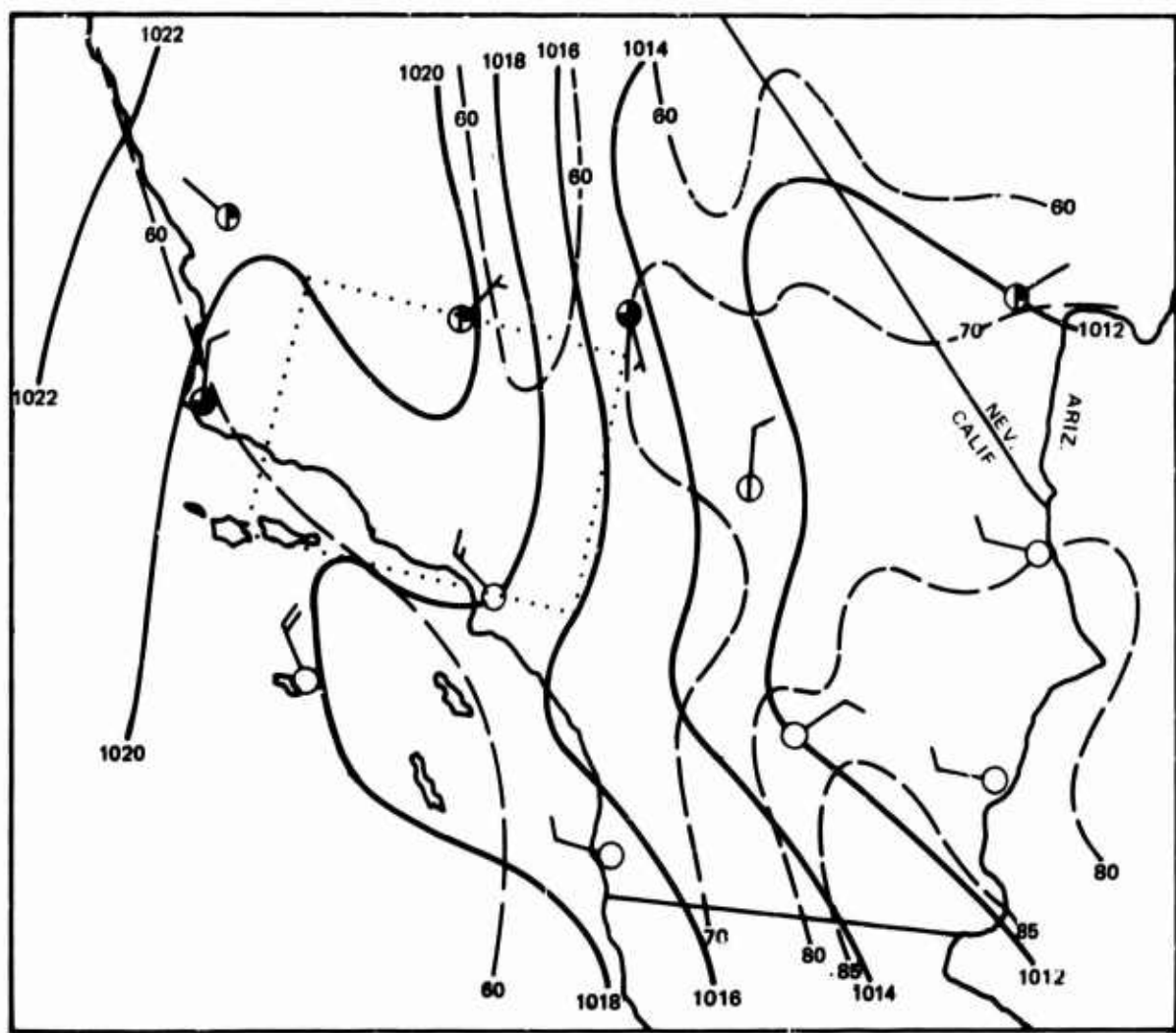
Figure 37.7 April 28, 1967 Surface Analysis, Peterson Route



PETERSON FLD
DATE - 28 APRIL 1967
TIME - 1200 GMT

700 MB ANALYSIS

Figure 37.8 April 28, 1967 700 MB Analysis, Peterson Route



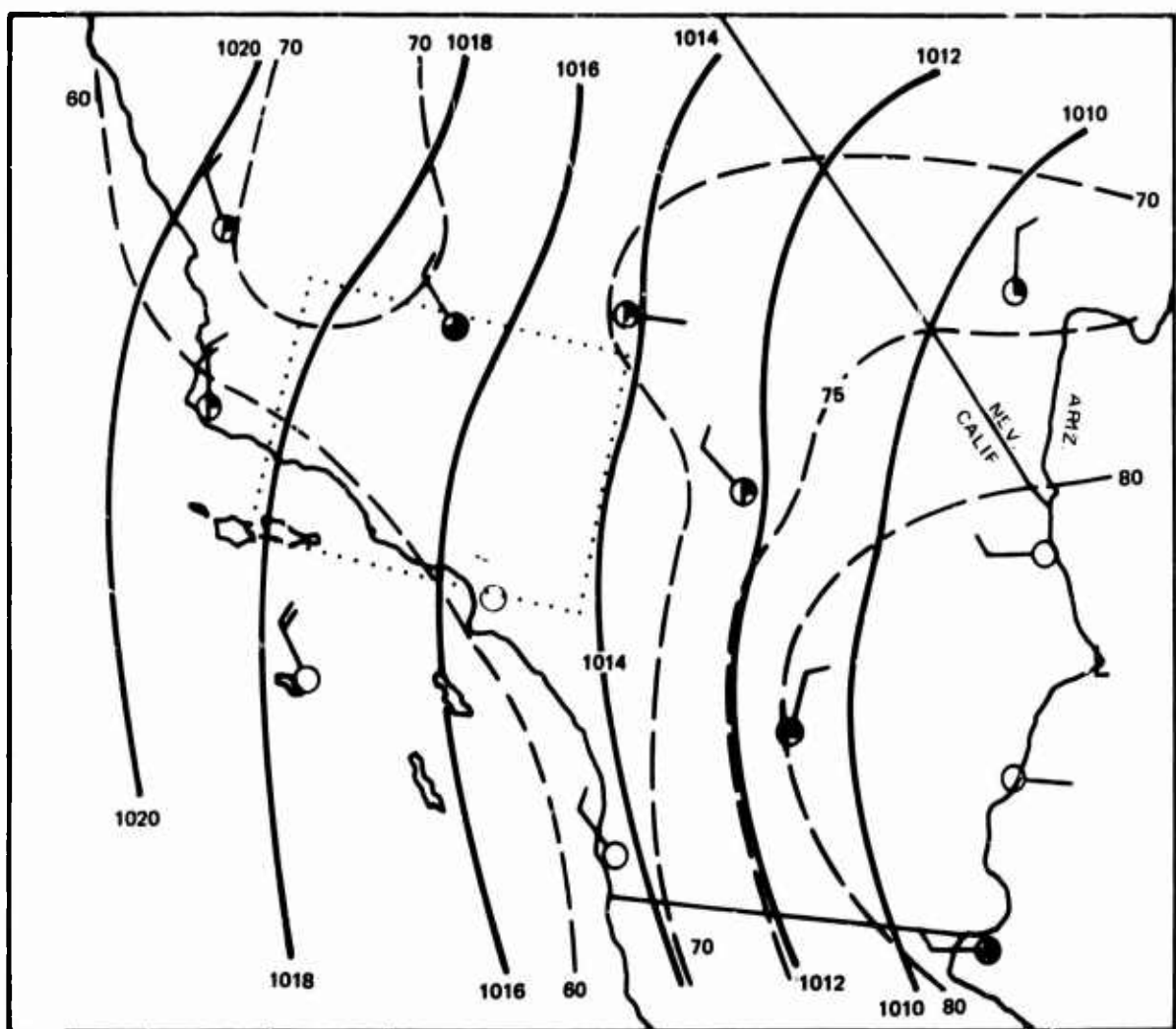
EDWARDS AFB

DATE - 12 MAY 1967

TIME - 2100 GMT

SURFACE ANALYSIS

Figure 37.9 May 12, 1967 Surface Analysis, Edwards Route
90



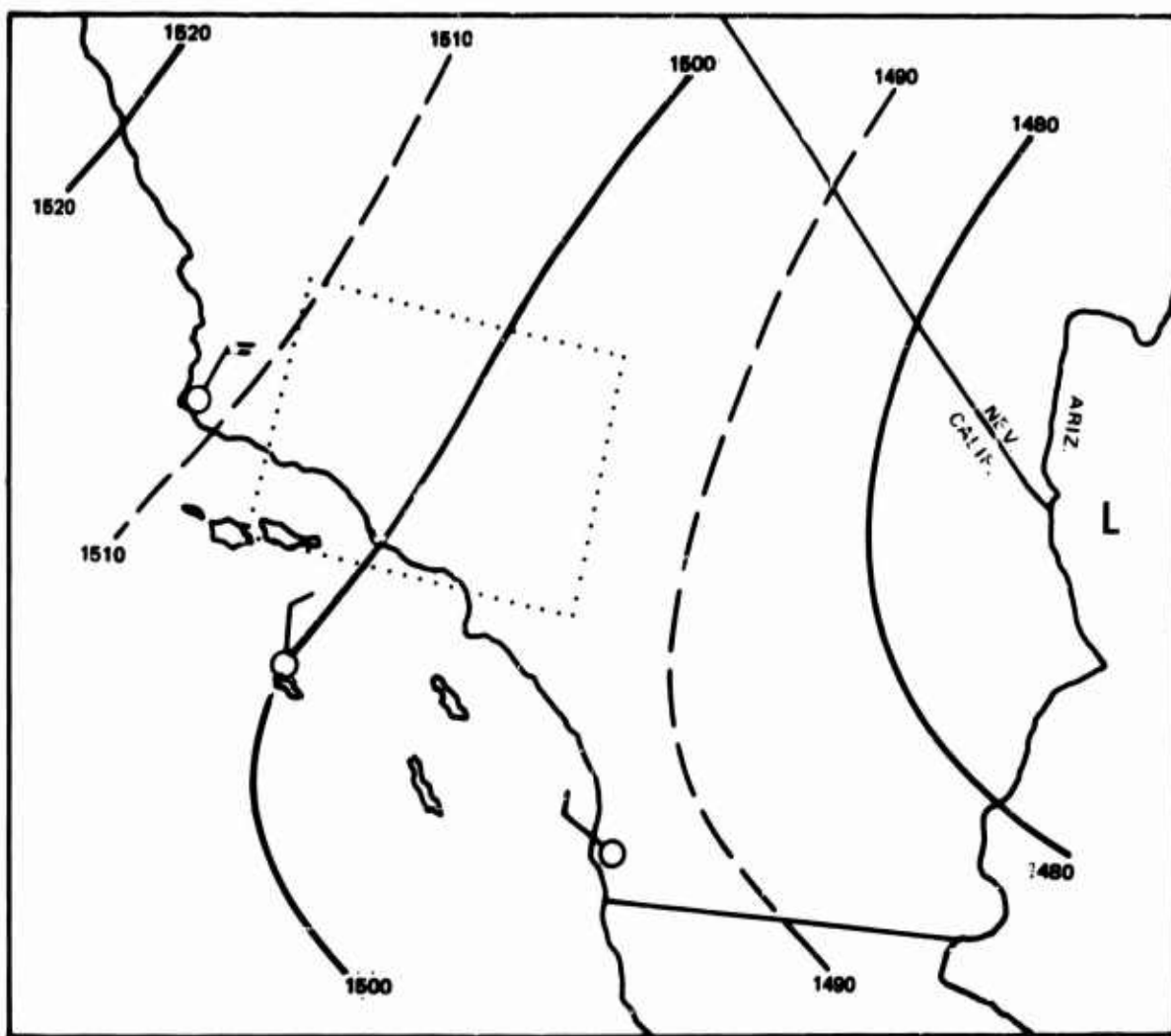
EDWARDS AFB

DATE -- 13 MAY 1967

TIME -- 0000 GMT

SURFACE ANALYSIS

Figure 37.10 May 12, 1967 Surface Analysis, Edwards Route
91



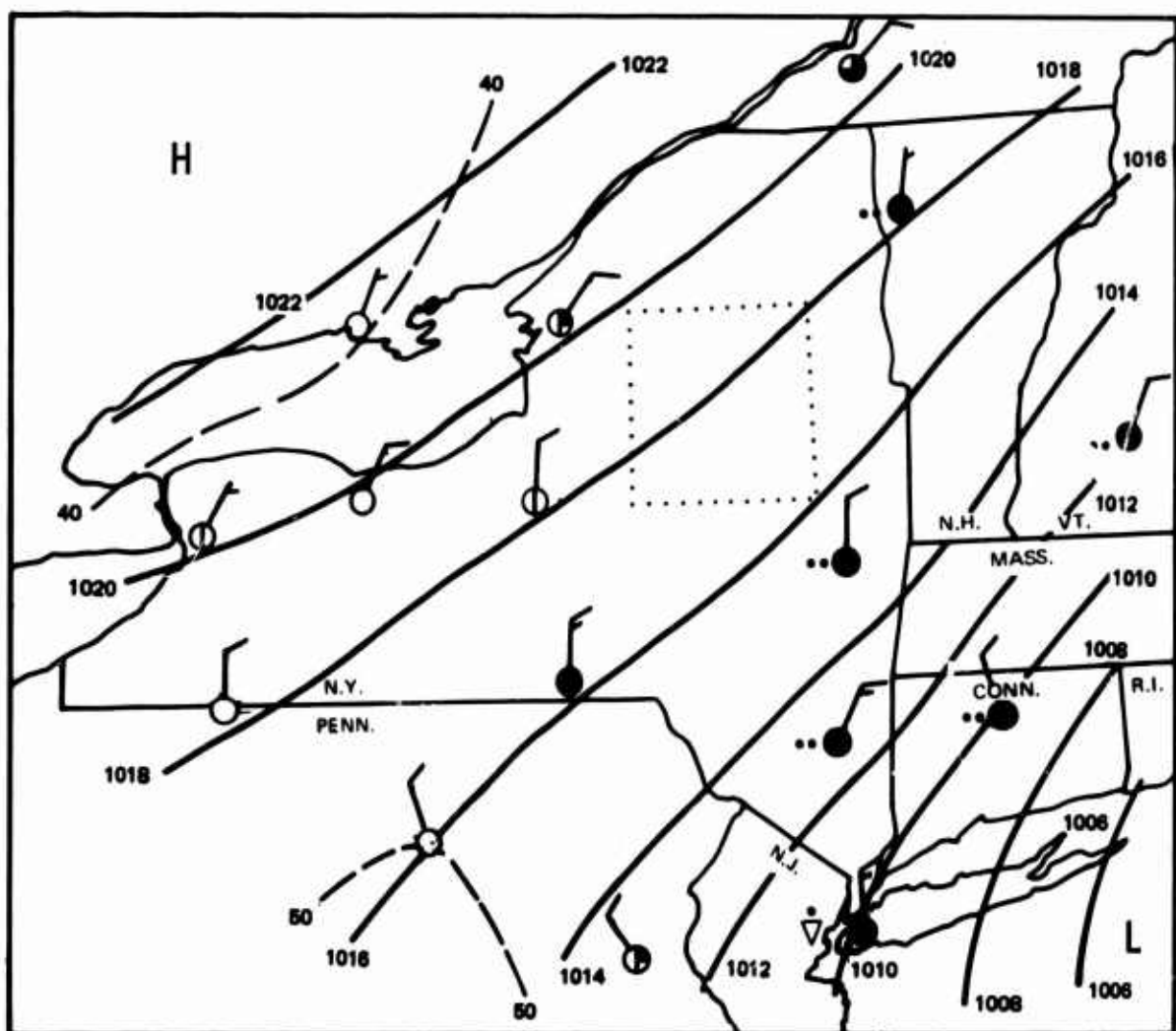
EDWARDS AFB

DATE - 13 MAY 1967

TIME - 0000 GMT

850 MB ANALYSIS

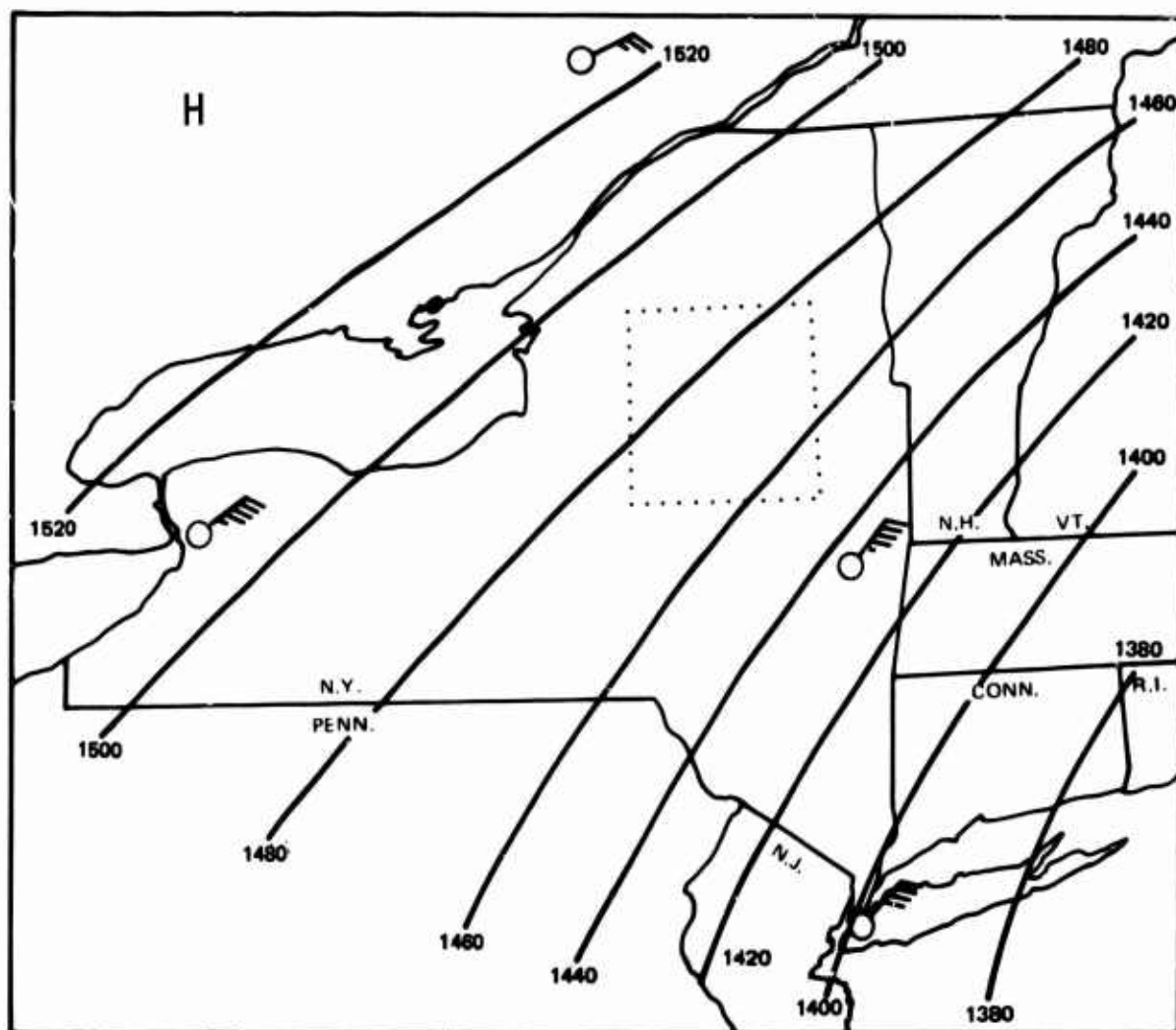
Figure 37.11 May 12, 1967 850 MB Analysis, Edwards Route



GRIFFISS AFB
DATE - 26 MAY 1967
TIME - 0900 GMT

SURFACE ANALYSIS

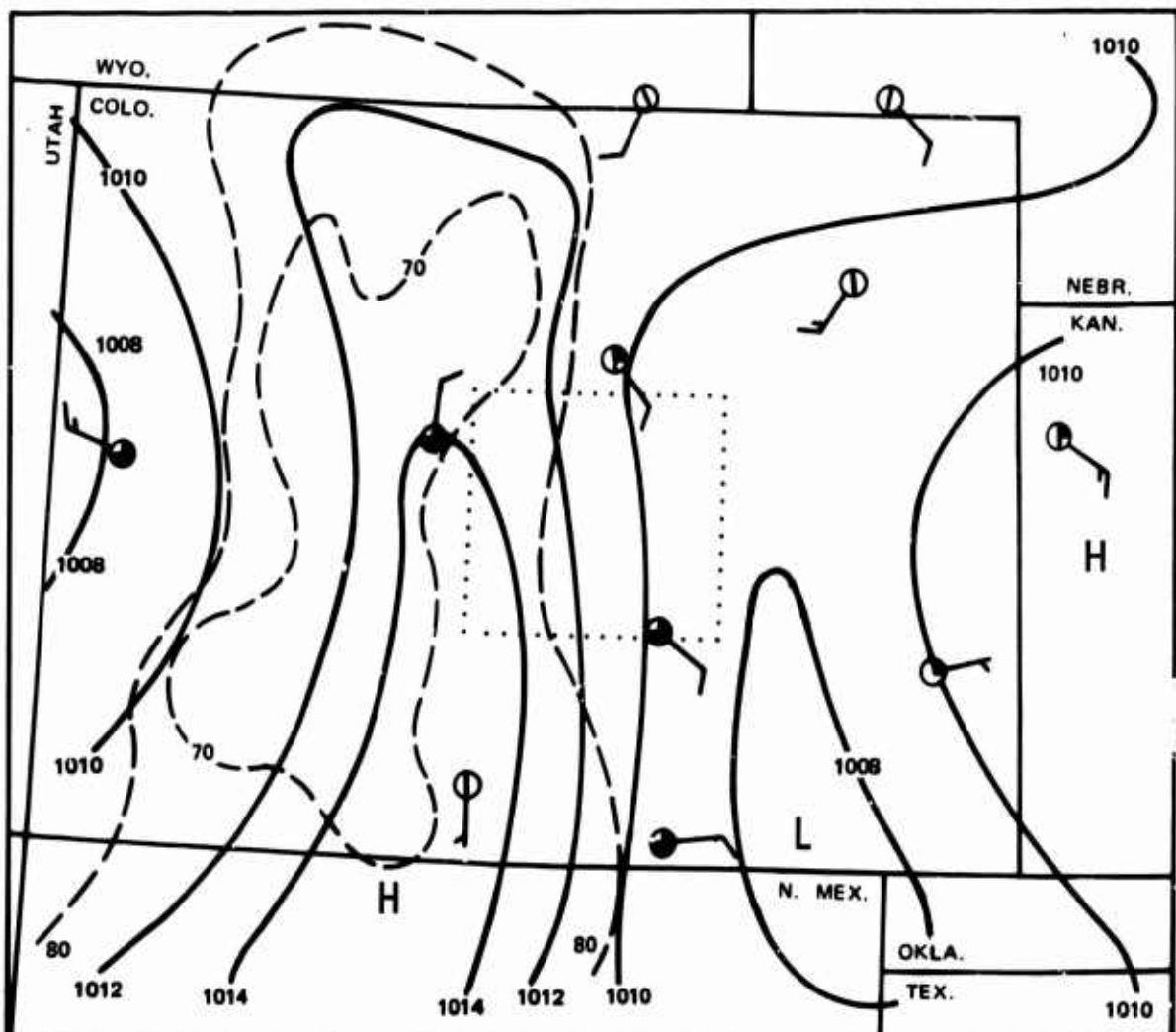
Figure 37.12 May 26, 1967 Surface Analysis, Griffiss Route



GRIFFISS AFB
DATE — 26 MAY 1967
TIME — 1200 GMT

850 MB ANALYSIS

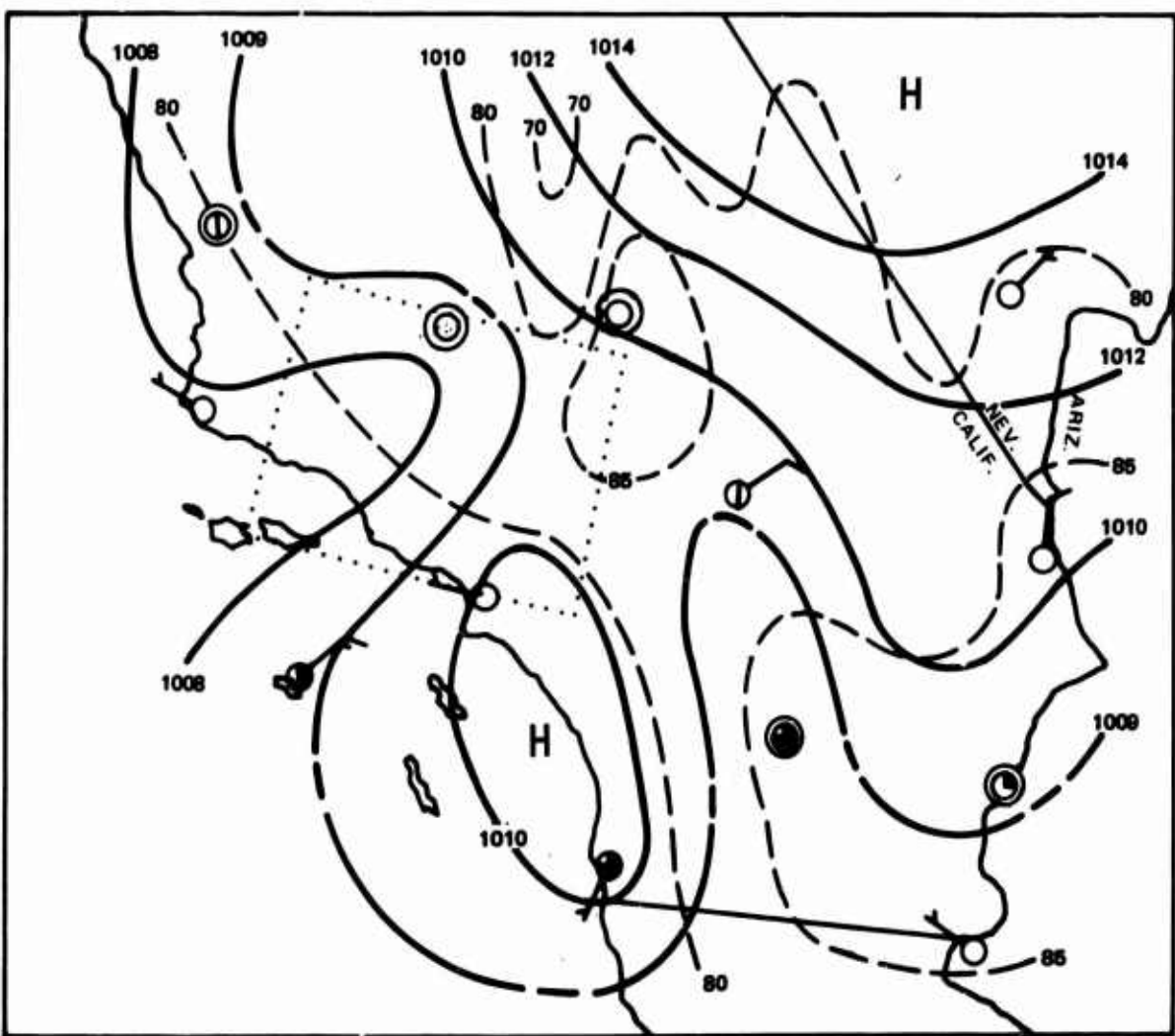
Figure 37.13 May 26, 1967 850 MB Analysis, Griffiss Route



PETERSON FLD
DATE - 21 AUGUST 1967
TIME - 2100 GMT

SURFACE ANALYSIS

Figure 37.14 August 21, 1967 Surface Analysis, Peterson Route



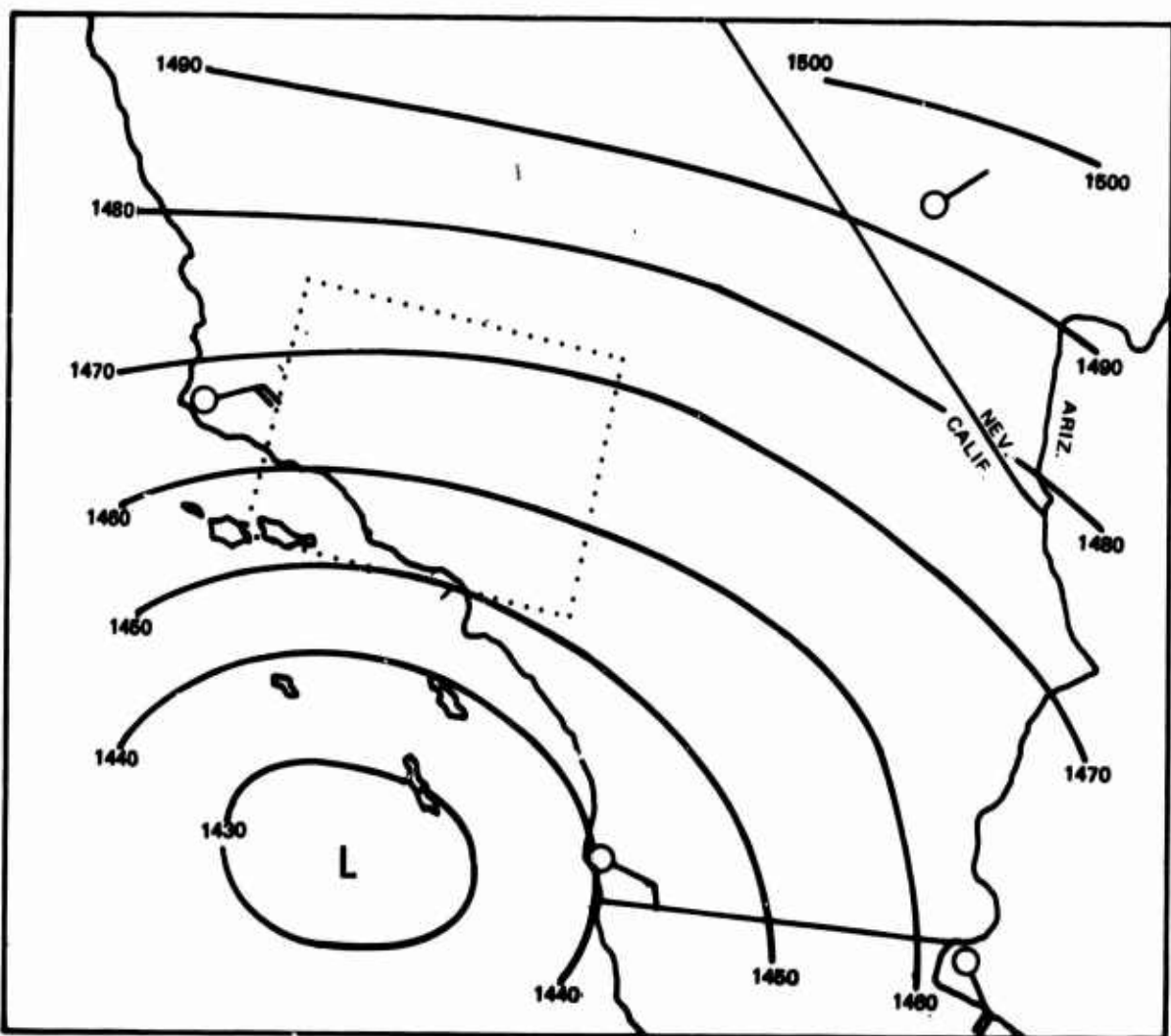
EDWARDS AFB

DATE - 20 SEPT 1967

TIME - 1800 GMT

SURFACE ANALYSIS

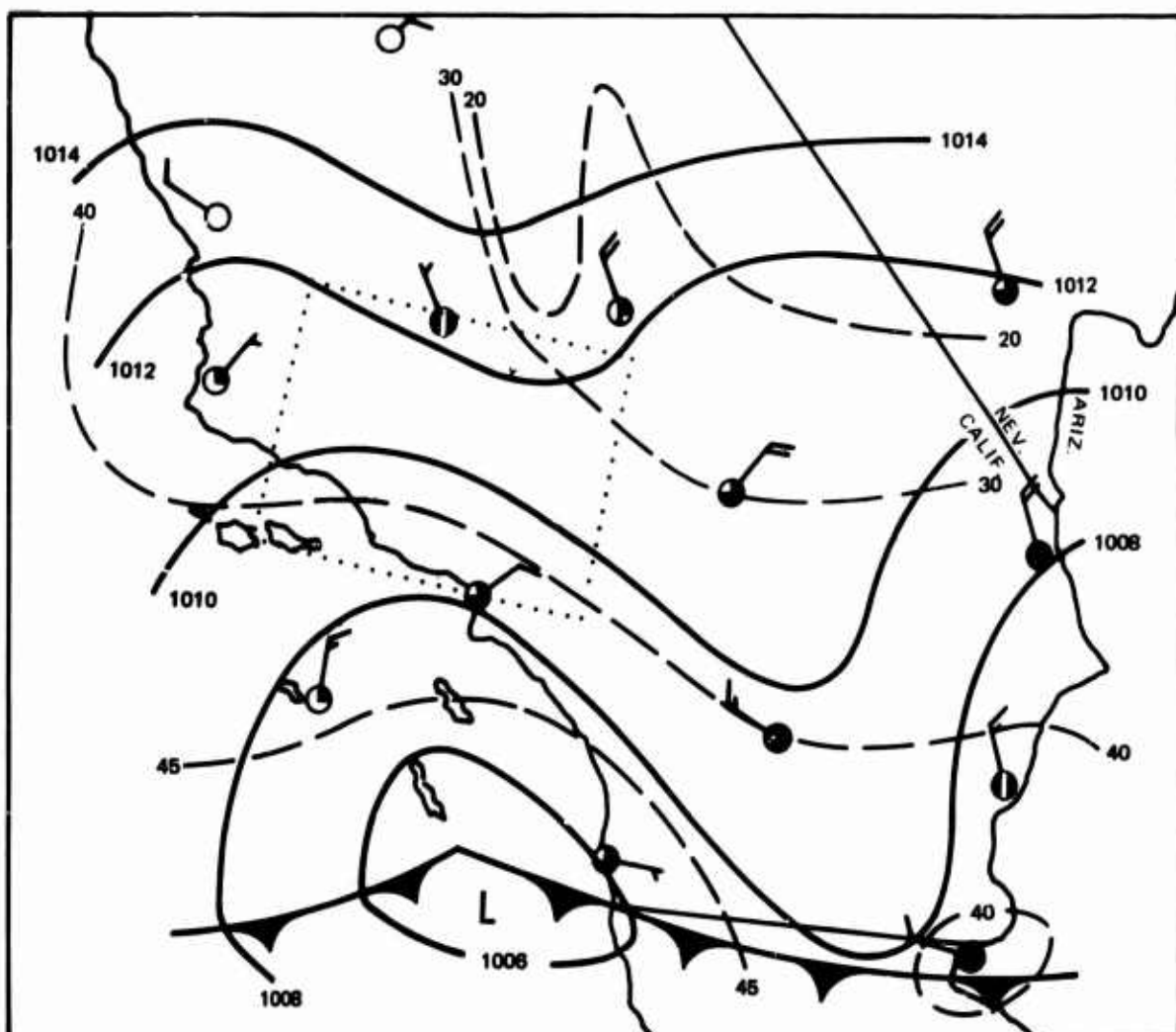
Figure 37.15 September 20, 1967 Surface Analysis, Edwards Route



EDWARDS AFB
DATE - 20 SEPT 1967
TIME - 1200 GMT

850 MB ANALYSIS

Figure 37.16 September 20, 1967 850 MB Analysis, Edwards Route



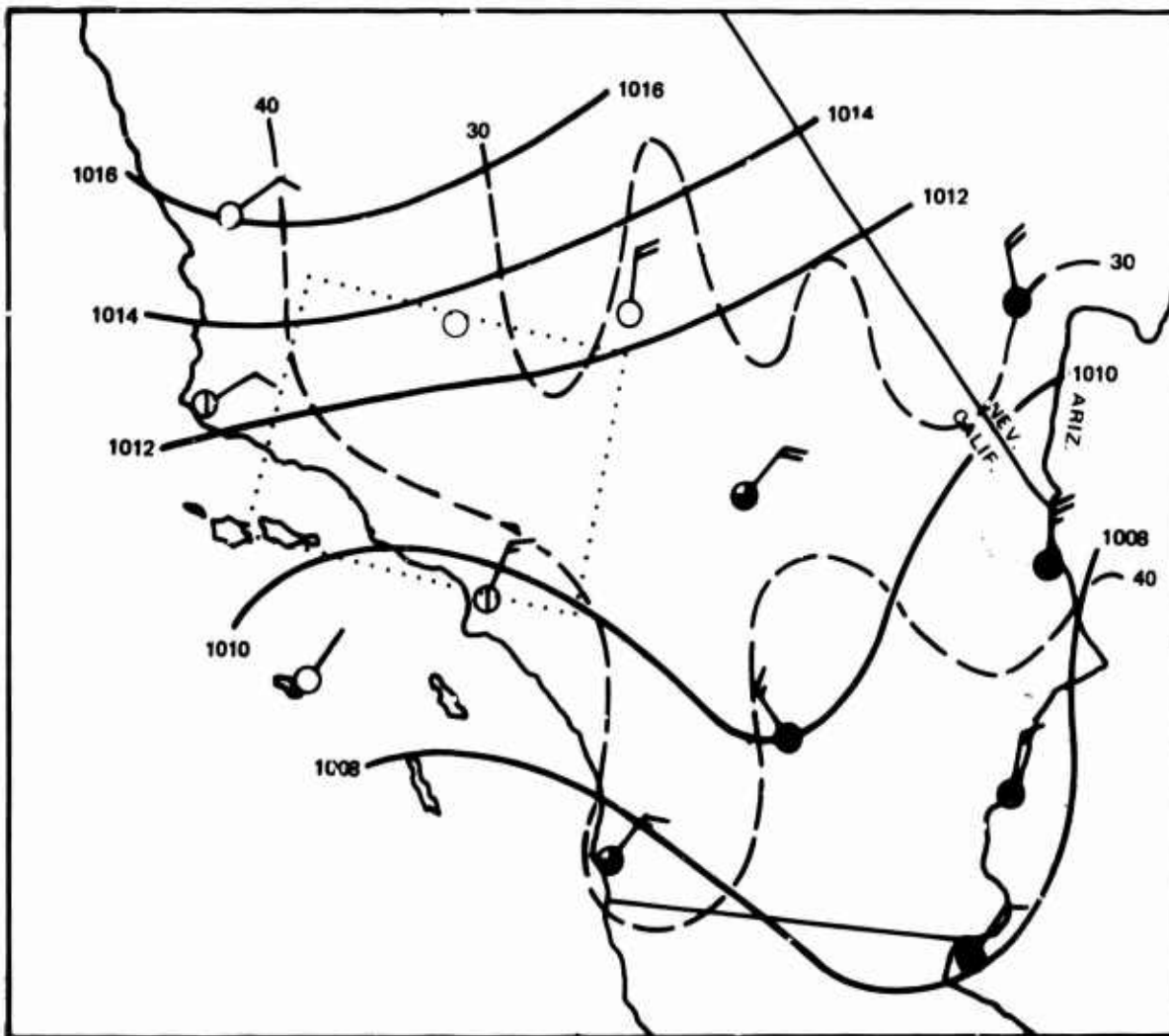
EDWARDS AFB

DATE -- 13 DEC 1967

TIME -- 1500 GMT

SURFACE ANALYSIS

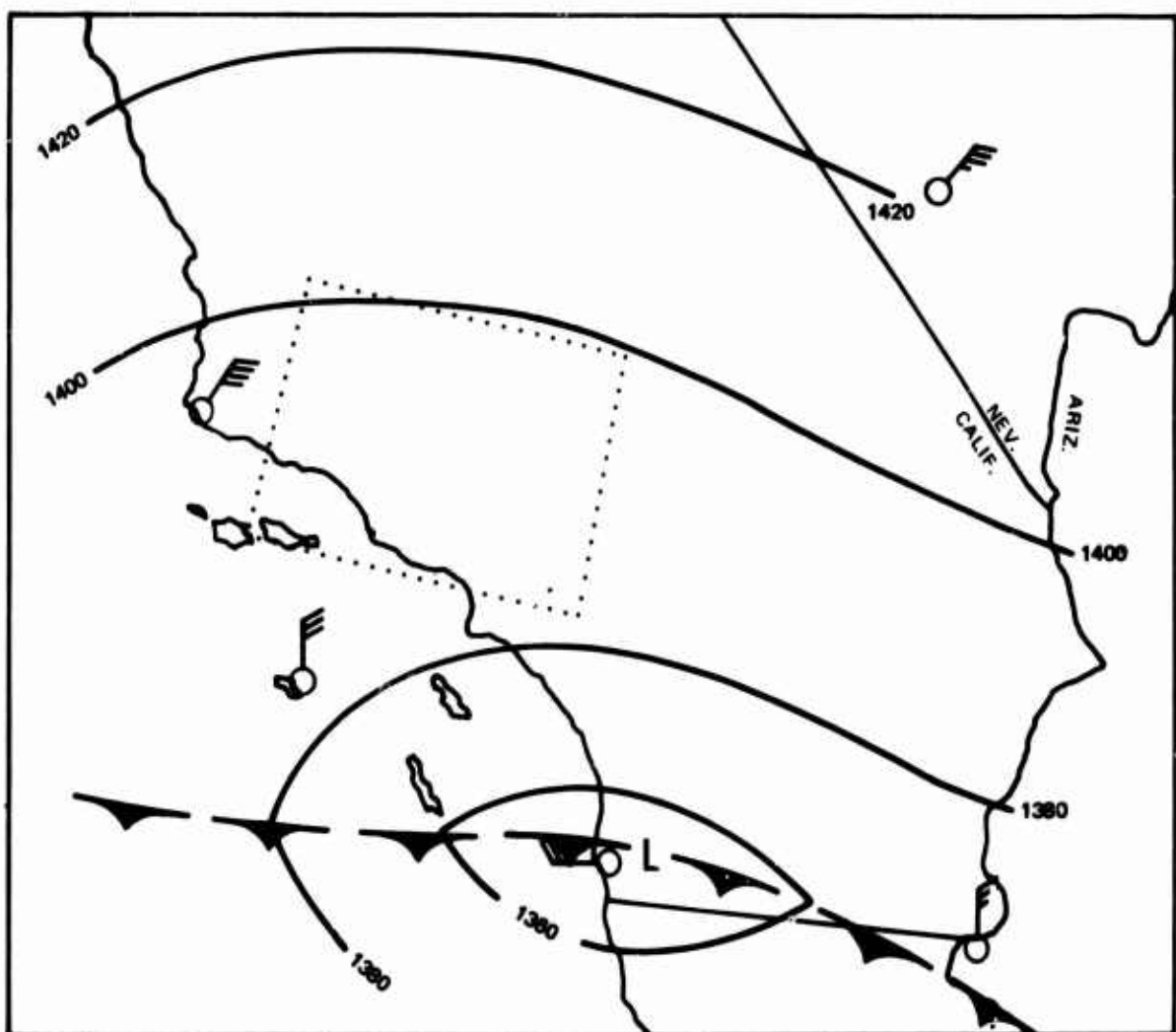
Figure 37.17 December 13, 1967 Surface Analysis, Edwards Route



EDWARDS AFB
DATE - 13 DEC 1967
TIME - 1800 GMT

SURFACE ANALYSIS

Figure 37.18 December 13, 1967 Surface Analysis, Edwards Route
99



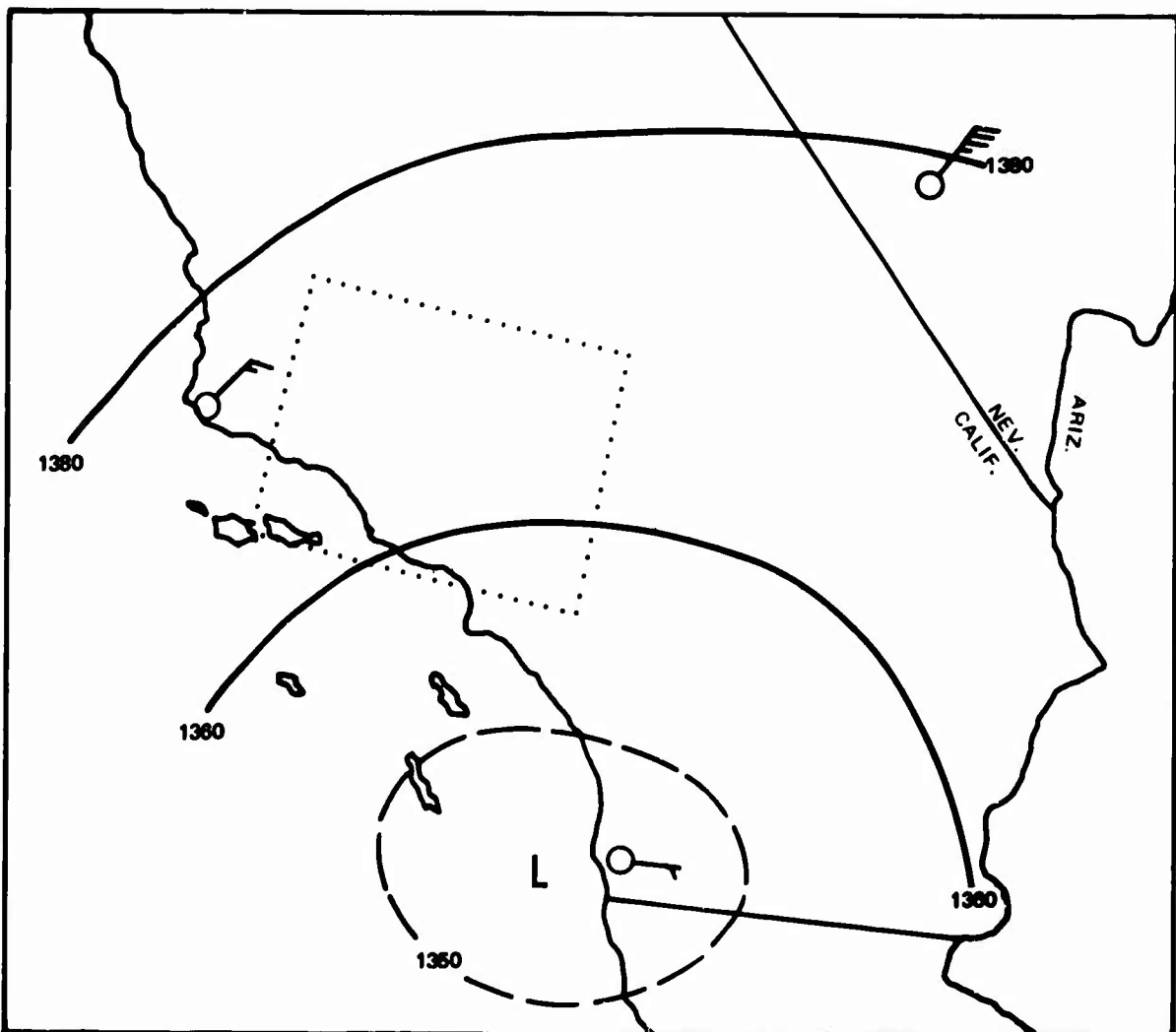
EDWARDS AFB

DATE - 13 DEC 1967

TIME - 1200 GMT

850 MB ANALYSIS

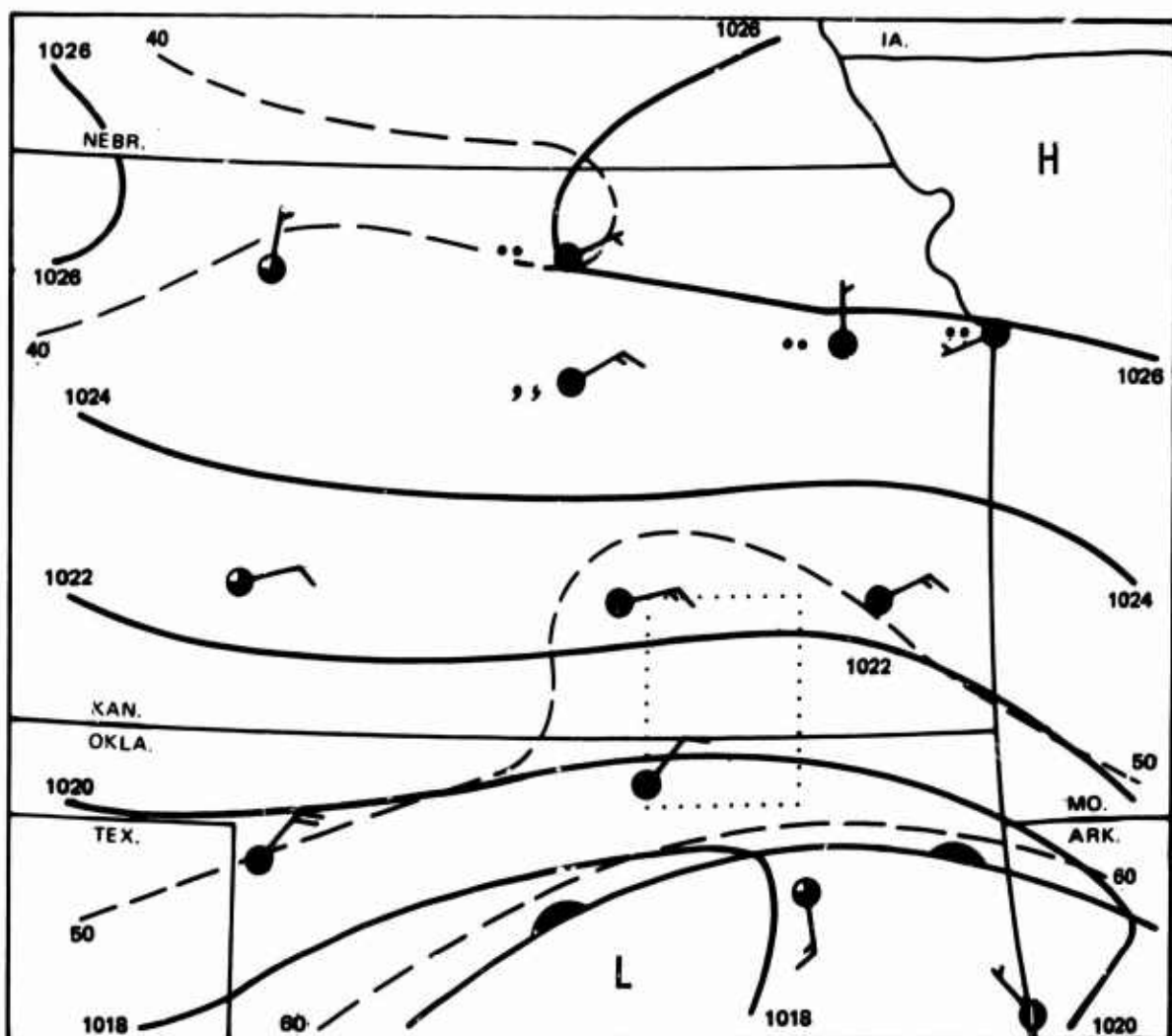
Figure 37.19 December 13, 1967 850 MB Analysis, Edwards Route



EDWARDS AFB
DATE — 14 DEC 1967
TIME — 0000 GMT

850 MB ANALYSIS

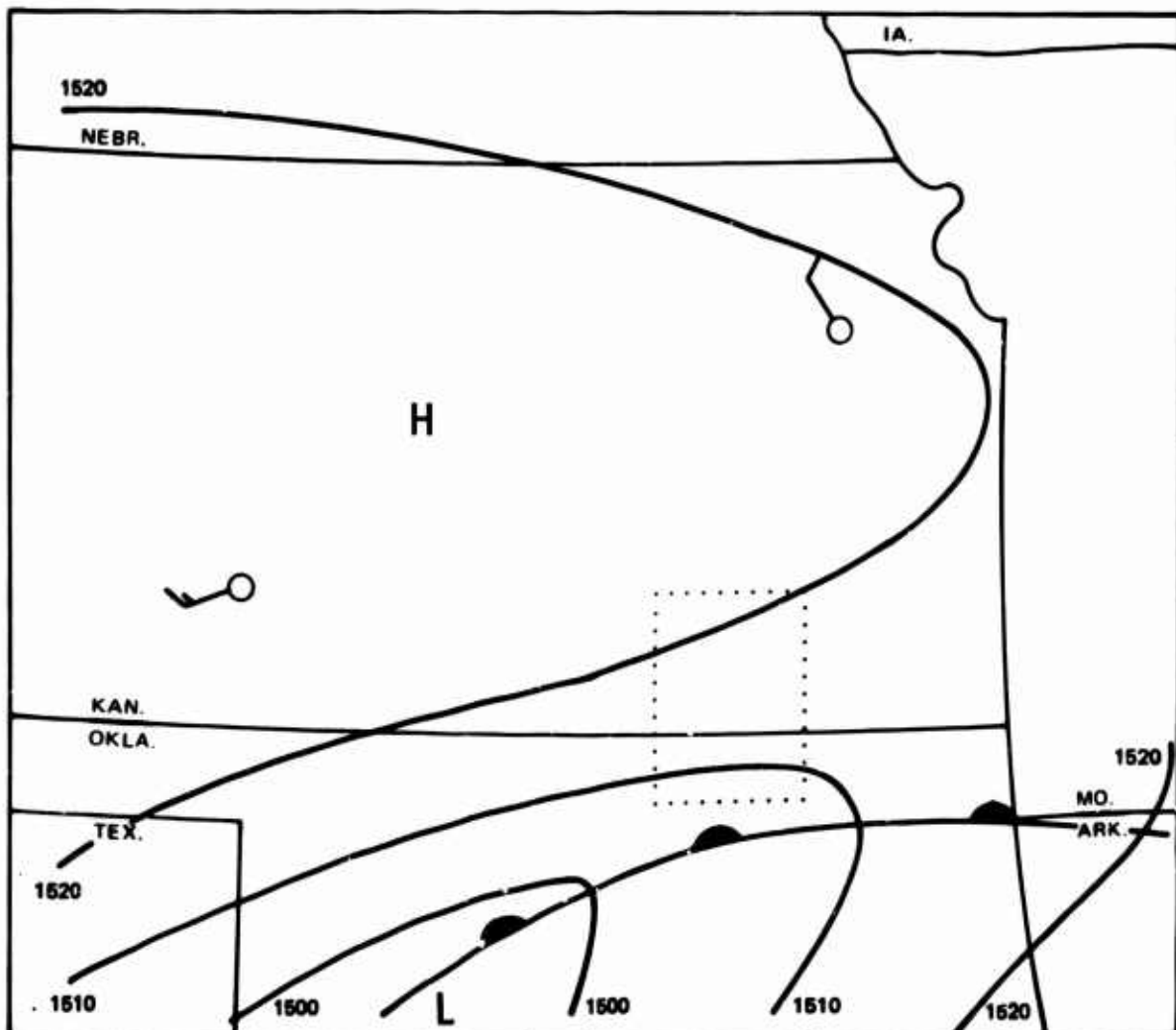
Figure 37.20 December 13, 1967 850 MB Analysis, Edwards Route
101



McCONNELL AFB
DATE - 4 NOVEMBER 1966
TIME - 2100 GMT

SURFACE ANALYSIS

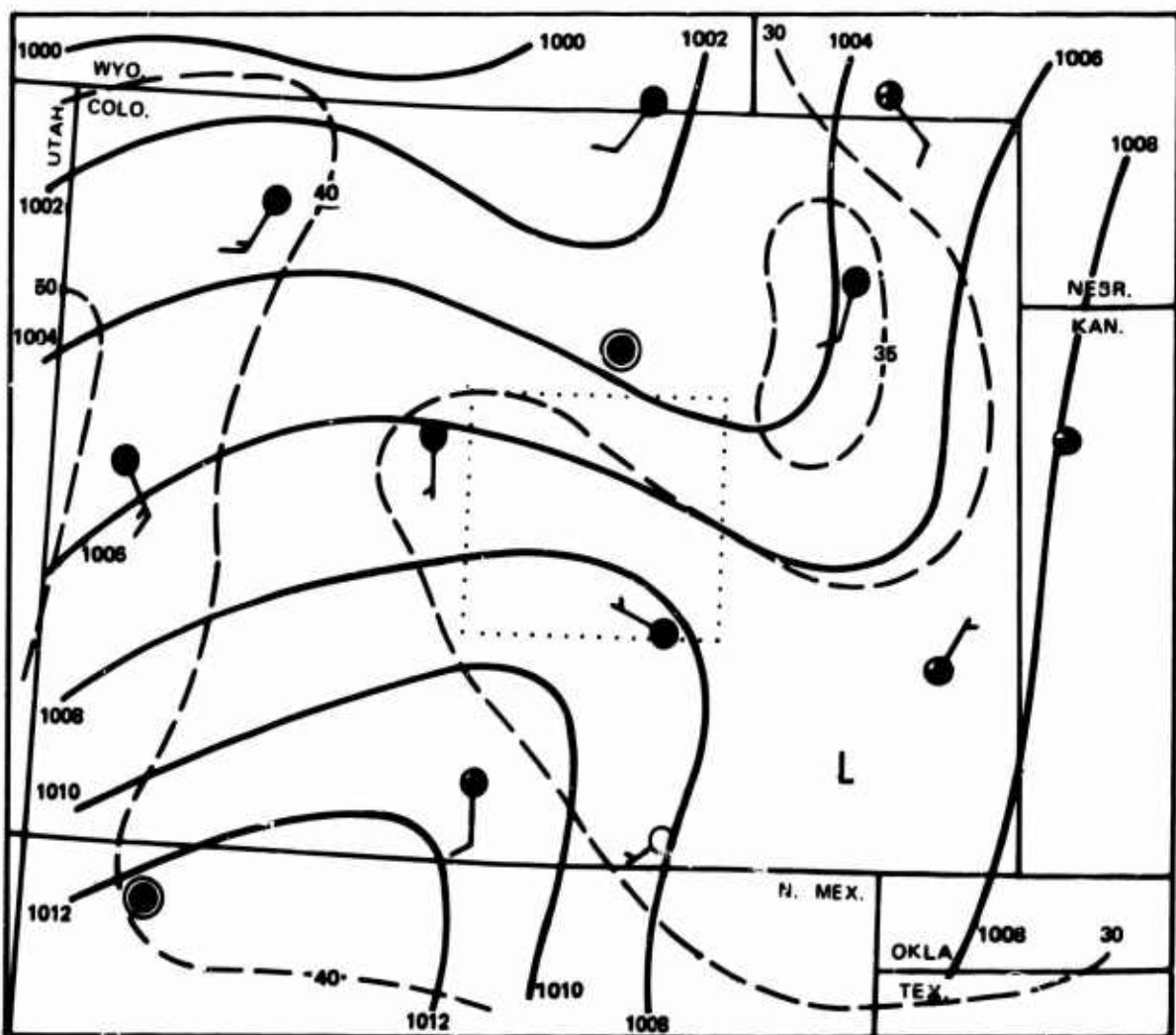
Figure 37.21 November 4, 1966 Surface Analysis, McConnell Route
102



McCONNELL AFB
DATE - 5 NOVEMBER 1966
TIME - 0000 GMT

850 MB ANALYSIS

Figure 37.22 November 4, 1966 850 MB Analysis, McConnell Route
103



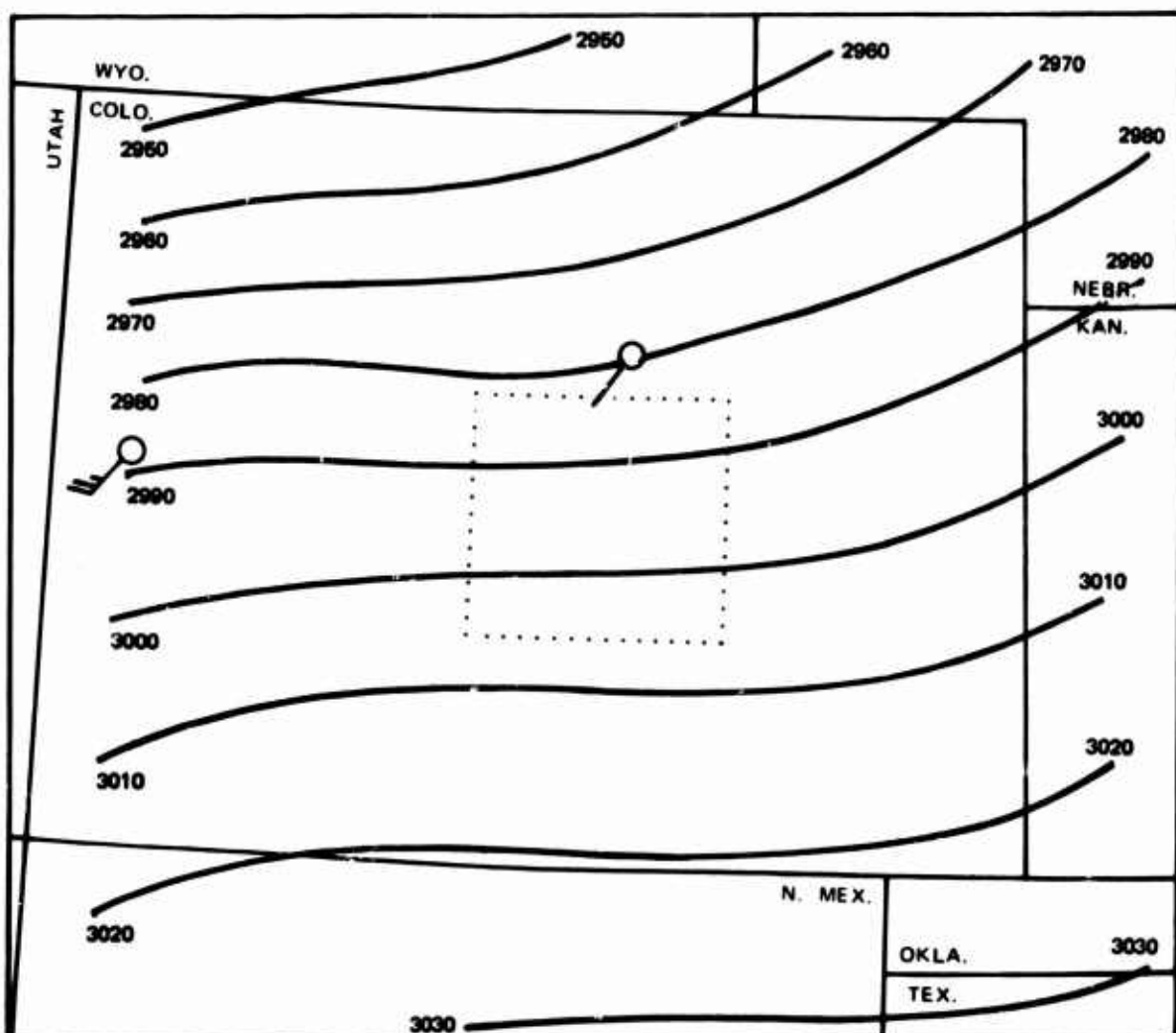
PETERSON FLD

DATE - 5 DECEMBER 1966

TIME - 1500 GMT

SURFACE ANALYSIS

Figure 37.23 December 5, 1966 Surface Analysis, Peterson Route



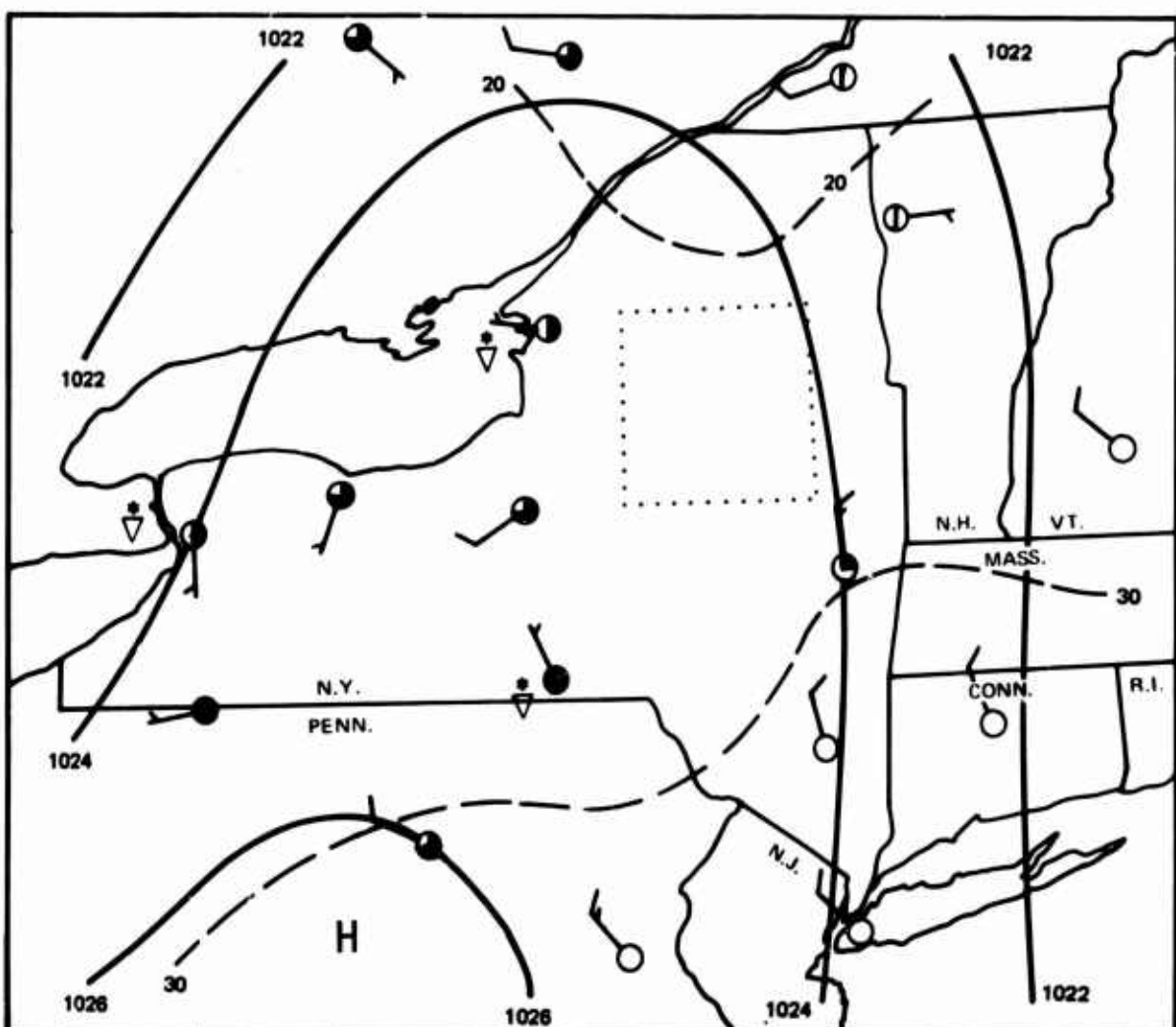
PETERSON FLD

DATE - 5 DECEMBER 1966

TIME - 1200 GMT

700 MB ANALYSIS

Figure 37.24 December 5, 1966 700 MB Analysis, Peterscn Route



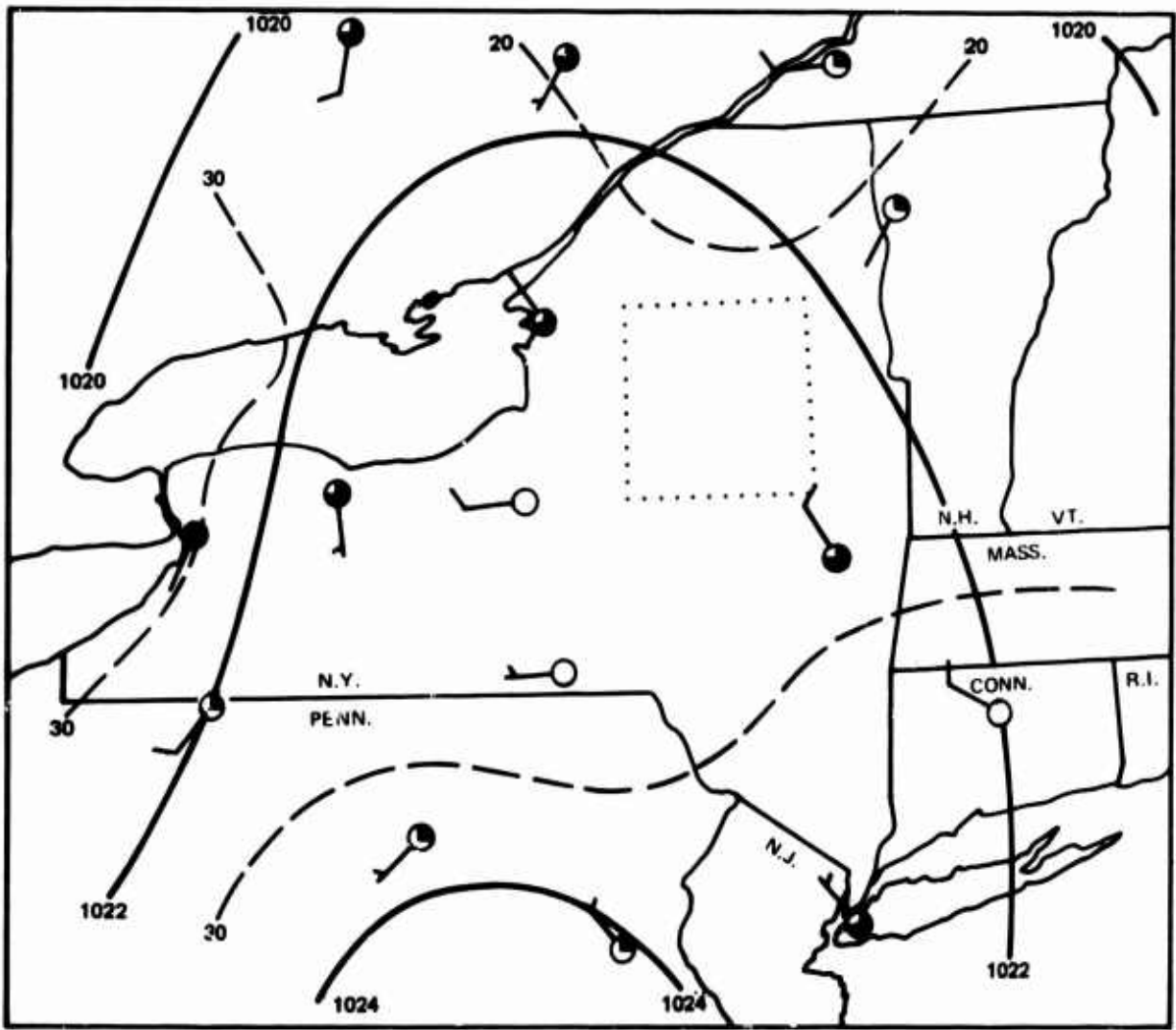
GRIFFISS AFB

DATE - 16 NOVEMBER 1967

TIME - 1000 GMT

SURFACE ANALYSIS

Figure 37.25 November 16, 1967 Surface Analysis, Griffiss Route



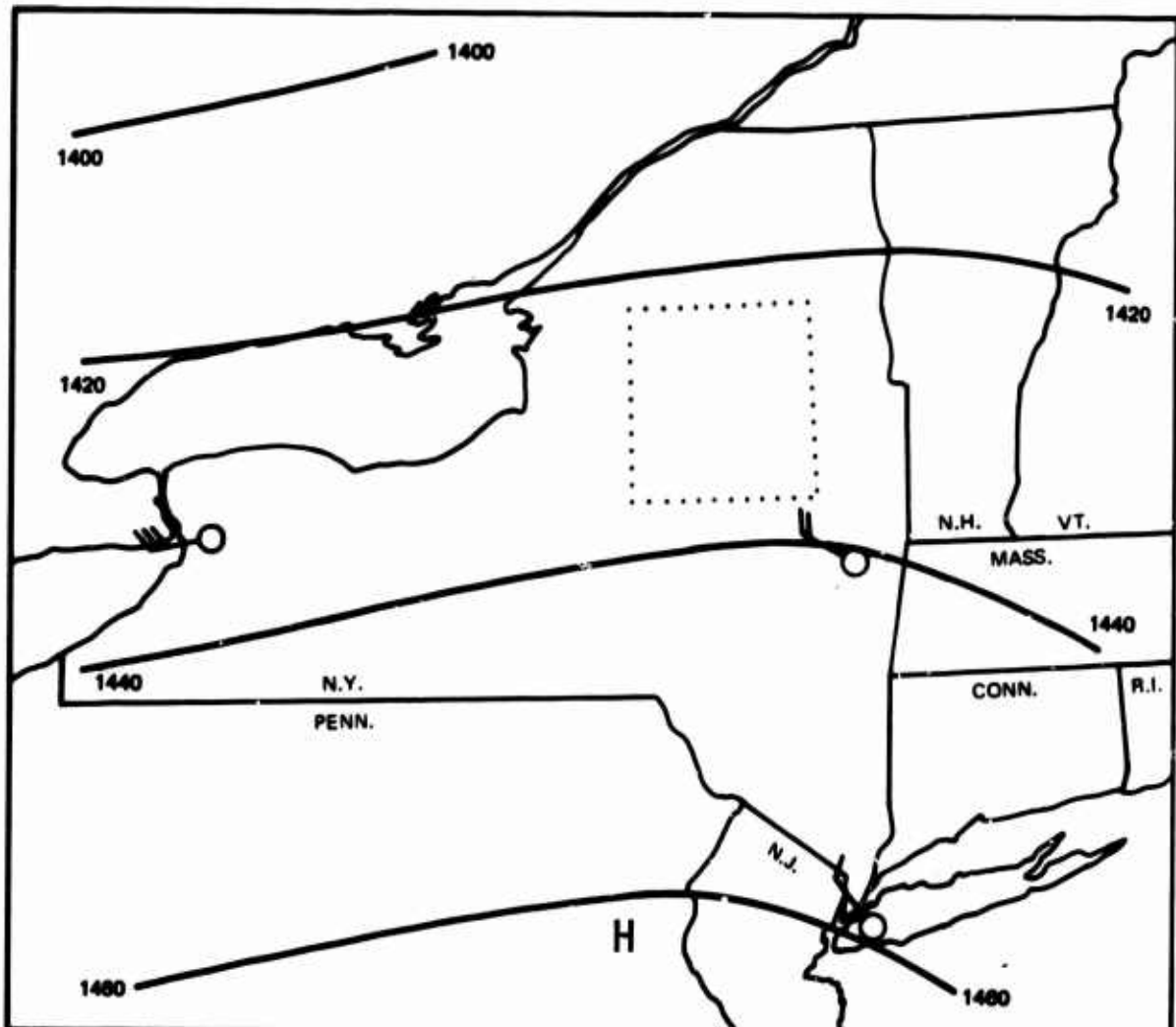
GRIFFISS AFB

DATE — 16 NOVEMBER 1967

TIME — 2100 GMT

SURFACE ANALYSIS

Figure 37.26 November 16, 1967 Surface Analysis, Griffiss Route



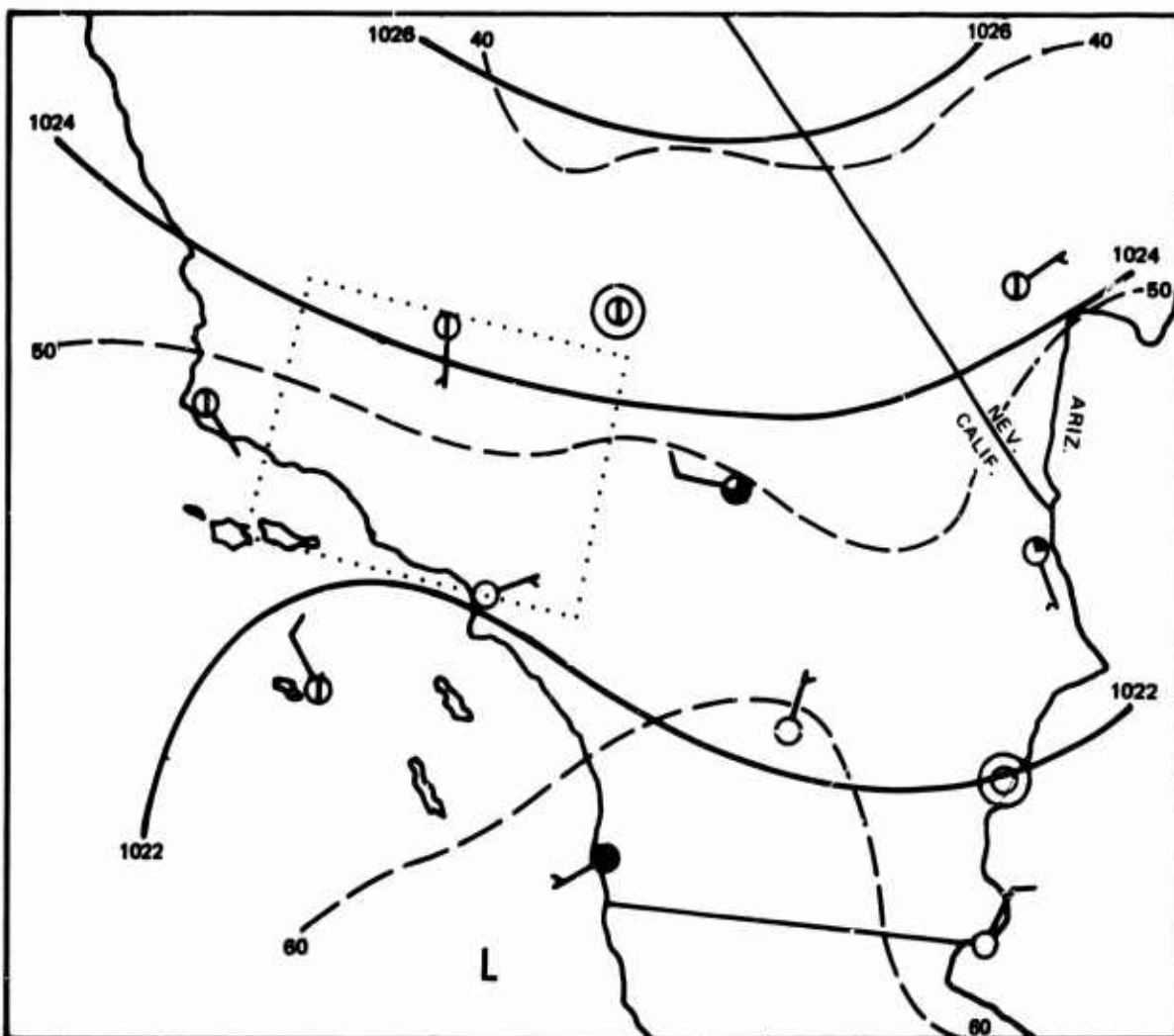
GRIFFISS AFB

DATE - 17 NOVEMBER 1967

TIME - 0000 GMT

850 MB ANALYSIS

Figure 37.27 November 16, 1967 850 MB Analysis, Griffiss Route



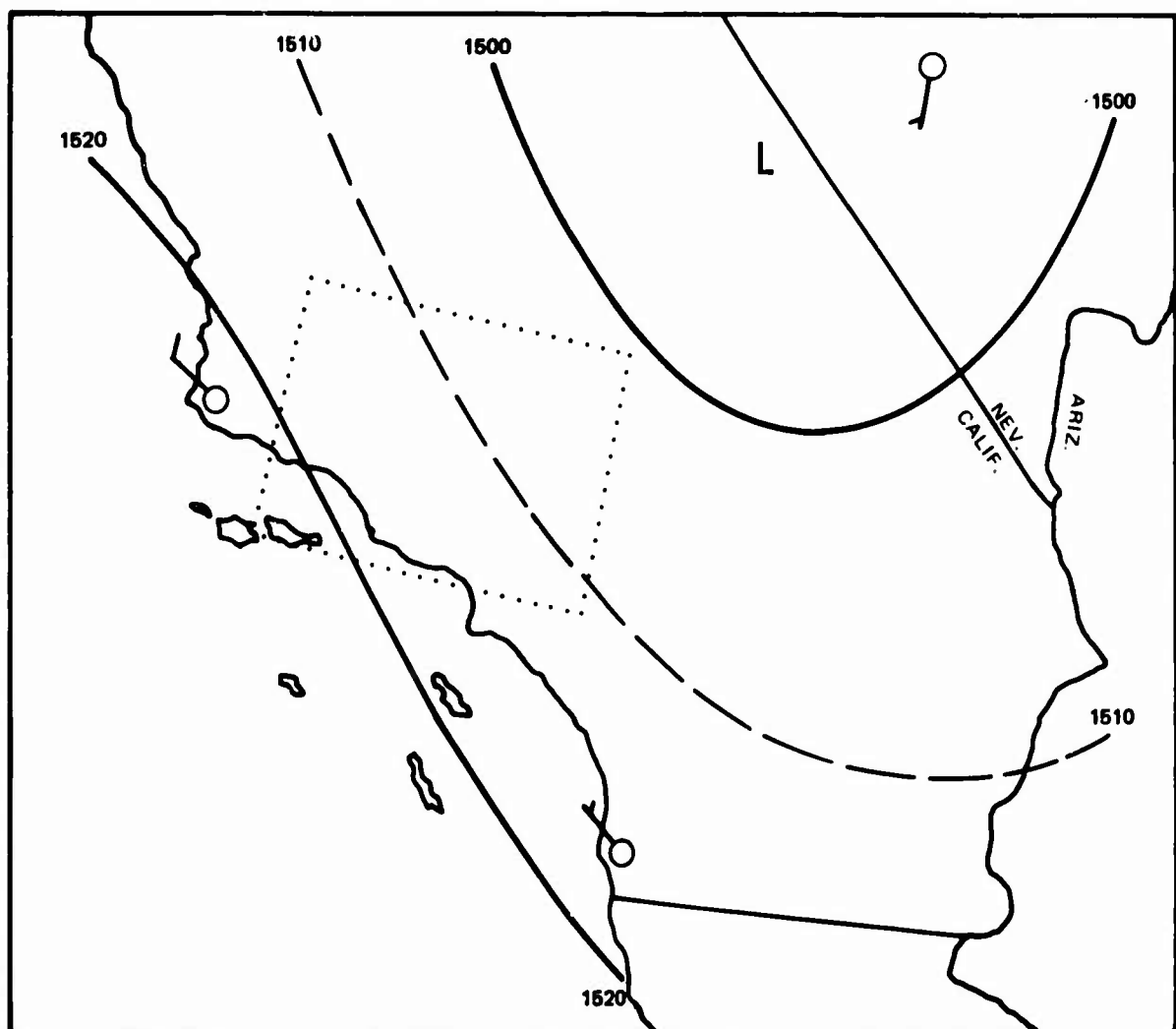
EDWARDS AFB

DATE - 6 DEC 1967

TIME - 1800 GMT

SURFACE ANALYSIS

Figure 37.28 December 6, 1967 Surface Analysis, Edwards Route



EDWARDS AFB
DATE - 7 DEC 1967
TIME - 0000 GMT

850 MB ANALYSIS

Figure 37.29 December 6, 1967 850 MB Analysis, Edwards Route

38. CASE STUDIES - PHASE III

Maximum gust velocity, as well as gust velocity rms values, were significantly greater during Phase III than during Phases I and II. Case studies were made for six different flight days which were characterized by particularly turbulent conditions. The predominant feature at both the Edwards and Peterson routes was the relationship between wind velocity and terrain. The greatest degree of turbulence was encountered when winds of 20 or 25 knots or greater were oriented across the major mountain ranges at angles close to the perpendicular. Evidence of well-developed mountain waves was present in some of the cases and lacking in others. Large gust velocities were generally accompanied by a large vertical wind shear value.

Edwards Air Force Base (7 November 1968)

General Synoptic Situation

High pressure was located over the central United States and southern Canada. A secondary ridge of this high pressure region extended southward into central California. An intense low pressure system was approaching the western North America coast. Figure 38.1 shows the synoptic situation as it appeared at 2100 GMT. At 500 mb, a ridge oriented north-south along the coast intensified during the day. Wind at 850 mb was generally from the north at 20 to 30 knots (Figure 38.2).

Mid-Afternoon Flight

Figure 38.3 is a more detailed analysis of the flight area. At the surface, winds of approximately 10 knots from the north were oriented perpendicular to the coastal mountains due to the fairly strong offshore pressure gradient. It will be seen that this pressure and wind pattern was present for most of the cases during which significant turbulence was observed. In the lee of the mountains along the coastal low lands, winds were generally parallel to the mountain range or oriented significantly towards the mountains, producing possible convergence. Moderate turbulence was observed over legs 3 and 5, both of which pass at right angles over major ridges. Maximum vertical gusts encountered for these legs were 34 and 37 fps, respectively. Atmospheric stability was characterized as stable over leg 3 and neutral over leg 5. The corresponding Richardson numbers were 5.17 and -0.001. The remaining legs show substantially lower maximum gusts and gust velocity rms values. Turbulence was not reported by the pilot. Clearly, the nature of the terrain and the orientation of the wind were the primary factors in producing the observed turbulence for this flight.

Edwards Air Force Base (13 November 1968)

General Synoptic Situation

Figure 38.4 shows the surface synoptic analysis for 1800 GMT. A large high pressure system was centered over the eastern Pacific Ocean at 37° N and 135° W from which a broad ridge extended eastward into Oregon and towards Colorado. A minor ridge was observed to pass through central California

and south towards Yuma, Arizona. This ridge caused a generally high pressure gradient through the flight area. Winds through this area were mostly from the north to east at about 10 to 15 knots. The temperature pattern shown by the dashed isotherms was generally influenced by the topographical variation in surface heights.

A low pressure center occurred over the southern California border at 850 mb for 0000 and 1200 GMT as indicated in Figures 38.5 and 38.6. This was associated with a surface low pressure cell and frontal system which extended through Arizona. Winds at 850 mb through the flight area were north to northeast. Little change was observed in the pattern of pressure-heights in the flight area during the 12-hour period. At 500 mb, a broad trough having a north-south axis along the coastal states intensified during the 12-hour period examined. Such development generally causes a slow-down of movement of surface systems.

Mid-Morning Flight

Stable and relatively dry atmospheric conditions prevailed over the route legs during this flight. A detailed analysis of the flight area is shown in Figure 38.7. The pilot reported moderate to severe turbulence over legs 3 and 5 with the largest gust velocities occurring to the lee of major terrain features. The north winds, in some local cases exceeding 25 knots at flight altitudes, crossed the coastal mountains. Considerable variation was observed between the wind directions and speeds observed over individual legs, and it was concluded that this variation was closely correlated with the resulting turbulence. The large wind speed components for legs 3 and 5 combined with the cross-ridge effects resulted in gust velocity rms values of 12.0 and 8.5 fps, respectively. Gust velocity rms values less than 3.5 fps were noted for the other legs of this flight. Flight along leg 4 resulted in the lowest gust velocity rms value of this flight (1.2 fps). This leg is essentially parallel to and in the lee of the coastal ridge but over the Pacific Ocean. It was concluded that the terrain effects on the winds did not extend far downwind because of the synoptic pattern.

Mid-Afternoon Flight

Figure 38.8 shows that the synoptic situation was still essentially the same as during the mid-morning flight. Coastal stations showed more of a tendency toward onshore winds than earlier in the day. The pilot reported turbulence as moderate on legs 3 and 5 and the vertical gust velocity rms values for these legs were 6.2 and 6.6 fps, respectively. Stable atmospheric conditions were prevalent over both of these legs.

Edwards Air Force Base (2 December 1968)

General Synoptic Situation

A region of high pressure was centered 600 miles off the California coast with a ridge extending eastward over northern California and Nevada. During the day, this ridge appeared to intensify. A secondary ridge line lay roughly along the Sierra Nevada range as is seen in the 1800 GMT analysis in Figure 38.9. Winds aloft were generally from the north. At 850 mb,

the high pressure ridge over California extended eastward and the winds tended to shift more to the east. (Figures 38.10 and 38.11).

Mid-Morning Flight

A strong offshore pressure gradient prevailed over the flight area with winds at the surface from the north or northeast at 15 to 25 knots (Figure 38.12). Maximum vertical gusts of 44 and 37 fps were observed over legs 3 and 5; the pilot reported light and moderate turbulence, respectively. The pattern was essentially identical with the previous cases and consisted of strong northerly winds oriented across the coastal ranges with significant turbulence over legs 3 and 5. Neutral stability prevailed on both legs. Vertical gust velocity rms values were less than 3.5 for the remaining legs.

Peterson Field (25 February 1969)

General Synoptic Situation

At the surface, a region of low pressure was centered roughly over Wyoming with a trough extending towards the southeast over eastern Colorado (Figure 38.13). The upper air charts indicated a ridge line running north to south and passing over Kansas. The winds at 700 mb over the flight area were from the southwest at 20 to 30 knots as seen in Figure 38.14. Stationary fronts were located to the north and west of Colorado but did not directly influence the flight region.

Dawn Flight

Figure 38.15 shows the synoptic pattern for this flight. The pilot reported moderate turbulence on leg 4 and extreme turbulence on leg 5. The vertical gust velocity rms value recorded for leg 5 was 12.2 fps, and the vertical wind shear was 3.1 knots per 100 feet. Leg 5 passes along a ridge of peaks at the southern end of the Sangre de Cristo range. The 36-knot wind from the southwest recorded by the airplane strongly indicated that a mountain wave type of disturbance was responsible for the extreme turbulence. The sounding made concurrently with this flight indicated a stable layer between 14,000 and 17,000 feet which would tend to increase the mountain wave effect.

Mid-Morning Flight

Figure 38.16 indicates there was little change in the synoptic pattern between the dawn and mid-morning flights. The low pressure trough had moved eastward, but the winds were still from the southwest over the major mountain ridges. Severe turbulence was encountered over leg 5 where the wind velocity was almost 40 knots and the vertical wind shear approximated 3 knots per 100 feet.

Mid-Afternoon Flight

Figure 38.17 indicates that the surface low pressure trough had moved further east. Severe turbulence was encountered on legs 5 and 7. The stable

layer, noted just above the level of the peaks on the dawn sounding, had become less pronounced. Vertical wind shear over legs 5 and 7 were unusually high, being 5.7 and 5.2 knots per 100 feet, respectively.

Peterson Field (26 February 1969)

General Synoptic Situation

A low pressure center was located over eastern Colorado and moved slowly eastward. A cold front trailed southwestward from this system and a stationary front extended eastward over Kansas. Figure 38.18 shows the synoptic situation as it appeared at 1800 GMT. An upper level low pressure trough moved across the state during the day. Its position at 0000 GMT can be seen in Figure 38.19. Winds over the flight area at 700 mb were generally from the west at 25 to 30 knots.

Dawn Flight

The pilot reported severe to extreme turbulence on leg 5. This was accompanied by a vertical gust velocity rms value of 11.7 fps. Figure 38.20 indicates winds at the surface were variable at 10 knots or less. The sounding taken concurrently with this flight indicated that winds increased from 3 to 28 knots between the 10,000 and 12,000-foot levels. A shallow stable layer at approximately 14,000 feet dissipated later in the day. Standing lenticular clouds were present during this flight as well as the mid-morning flight. This evidence clearly points to mountain waves as being the primary cause of the observed turbulence.

Mid-Morning Flight

Figure 38.21 shows that the surface winds had increased in speed by mid-morning and were generally from the west. On this flight, the pilot reported extreme turbulence on leg 5 and severe turbulence on leg 6. The gust velocity rms values for these legs were 11.7 and 7.8 fps, respectively. Neutral stability was recorded for leg 5 and stable for leg 6.

Mid-Afternoon Flight

Surface conditions, Figure 38.22, were essentially the same as on the previous flight. Extreme turbulence with a vertical gust velocity rms value of 15.0 fps was recorded over leg 5. The atmospheric conditions were consistent with other instances of observed high intensity turbulence: an unstable lapse rate, a negative Richardson number, and a large vertical wind shear of 5 knots per 100 feet.

Peterson Field (19 March 1969)

General Synoptic Situation

At dawn, a low pressure system was located over western Kansas with its accompanying cold front extending across southern Colorado. During the day, this system moved east and cool air pushed into the state from the northwest. A high pressure area centered over eastern Oregon dominated

the northwest coast. Figure 38.23 shows the situation as it appeared at 1800 GMT. The upper level trough associated with this system moved across Colorado during the day. Winds at 700 mb were generally from the west at 30 to 35 knots as shown in Figure 38.24.

Dawn Flight

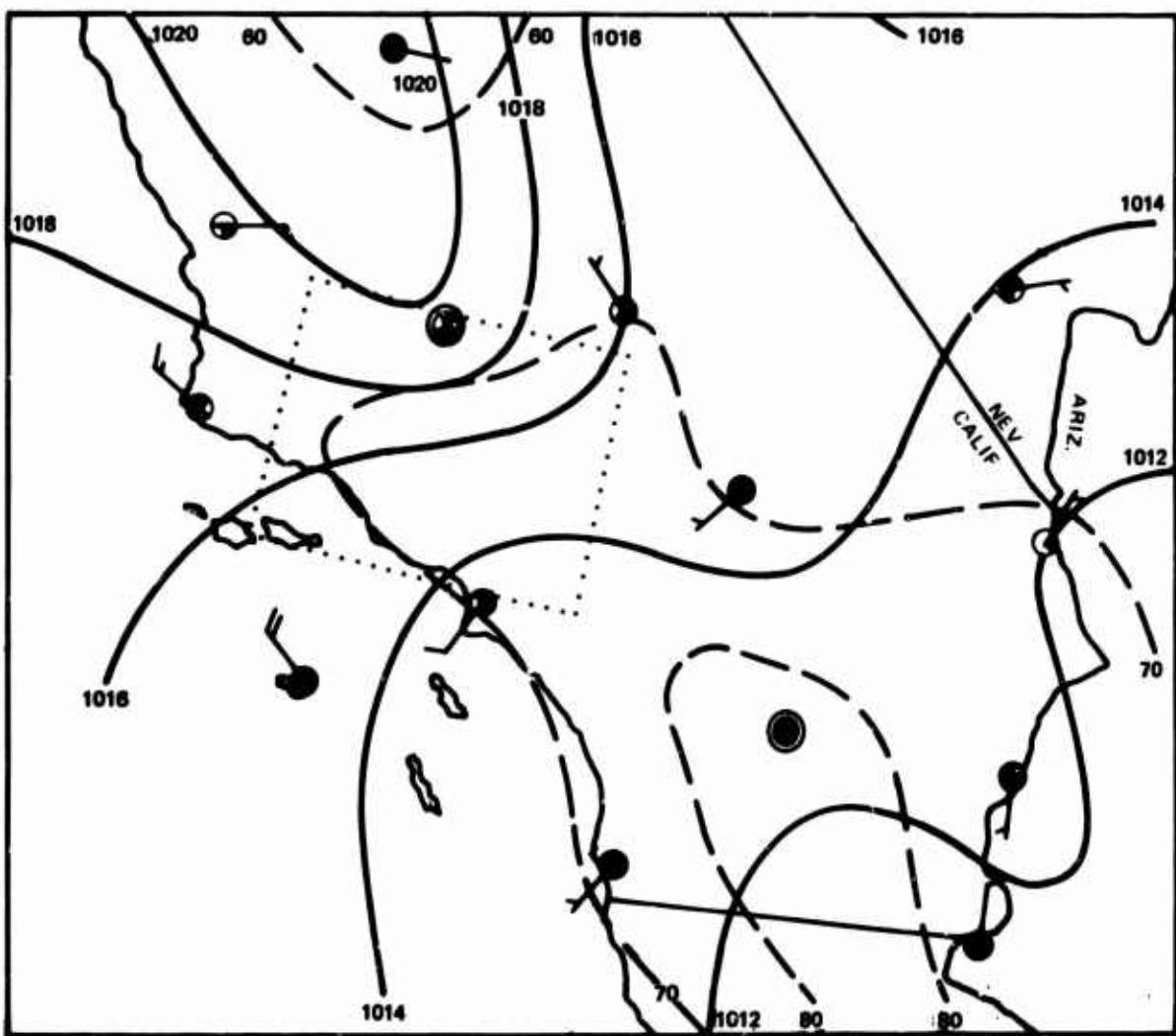
The pilot reported severe turbulence for legs 5, 6, and 7. Vertical gust velocity rms values for legs 5 and 6 were slightly more than 10 fps. The vertical gust velocity rms value for leg 7 was only 5.9 fps. Longitudinal and lateral gust velocity rms values were also lower for leg 7. A wind speed of 45 knots was observed on leg 6. Vertical wind shears for legs 5 and 6 were nearly 5 knots per 100 feet. Figure 38.25 shows that the winds were predominantly from the west and were oriented nearly perpendicular to the major ridges. Although the sounding before this flight did not indicate a pronounced stable layer just above the level of the peaks, there was probably a fairly strong mountain wave type of disturbance present. The lapse rate was generally stable above 600 mb.

Mid-Morning Flight

Vertical gust velocity rms values in excess of 8 fps were encountered over legs 1, 5, 6, and 7. Wind shears and wind velocities approximated those observed during the dawn flight. Wind speeds at the surface had increased somewhat as seen in Figure 38.26. Speeds of 25 to 30 knots were not uncommon at the time of the mid-morning flight. The Richardson numbers for legs 3, 4, 5, 6, and 8 were slightly negative. The turbulence encountered on leg 6 was judged extreme by the pilot.

Mid-Afternoon Flight

Although the gust velocity rms values and the pilot's estimates indicated a lesser degree of turbulence, the atmospheric parameters remained roughly unchanged from those of the mid-morning flight. A sharp inversion appeared between 16,500 and 18,500 feet on the sounding associated with this flight. It was accompanied by a strong increase of wind speed with height. This feature was possibly associated with a lee-wave effect which was present locally in the area of the balloon ascent. Absence of the inversion earlier in the day led to the conclusion that it was not a major influencing feature of the observed turbulence.



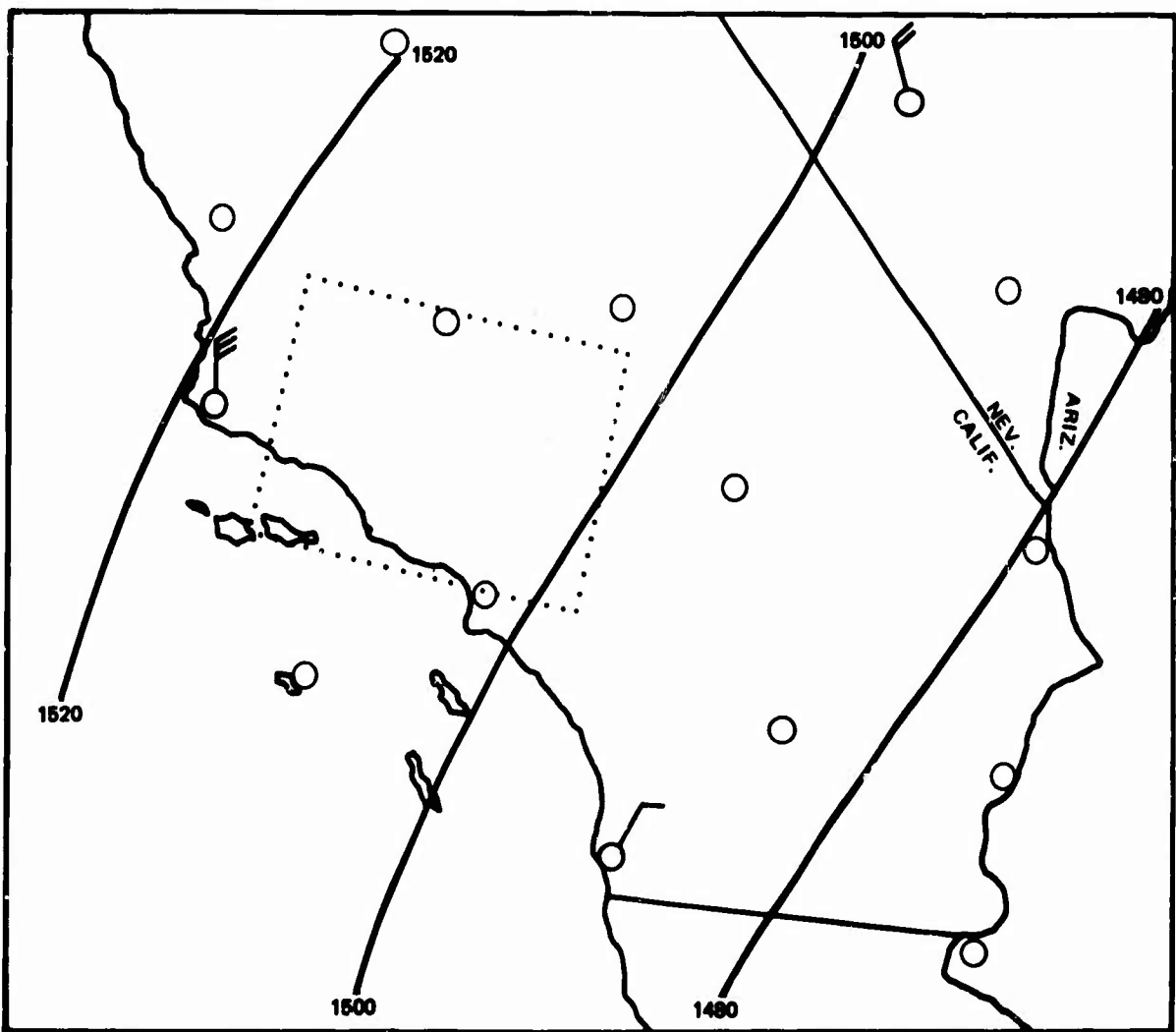
EDWARDS AFB

DATE - 7 NOV 1968

TIME - 2100 GMT

SURFACE ANALYSIS

Figure 38.1 November 7, 1968 Surface Analysis, Edwards Route



EDWARDS AFB
DATE - 8 NOV 1968
TIME - 0000 GMT

850 MB ANALYSIS

Figure 38.2 November 7, 1968 850 MB Analysis, Edwards Route

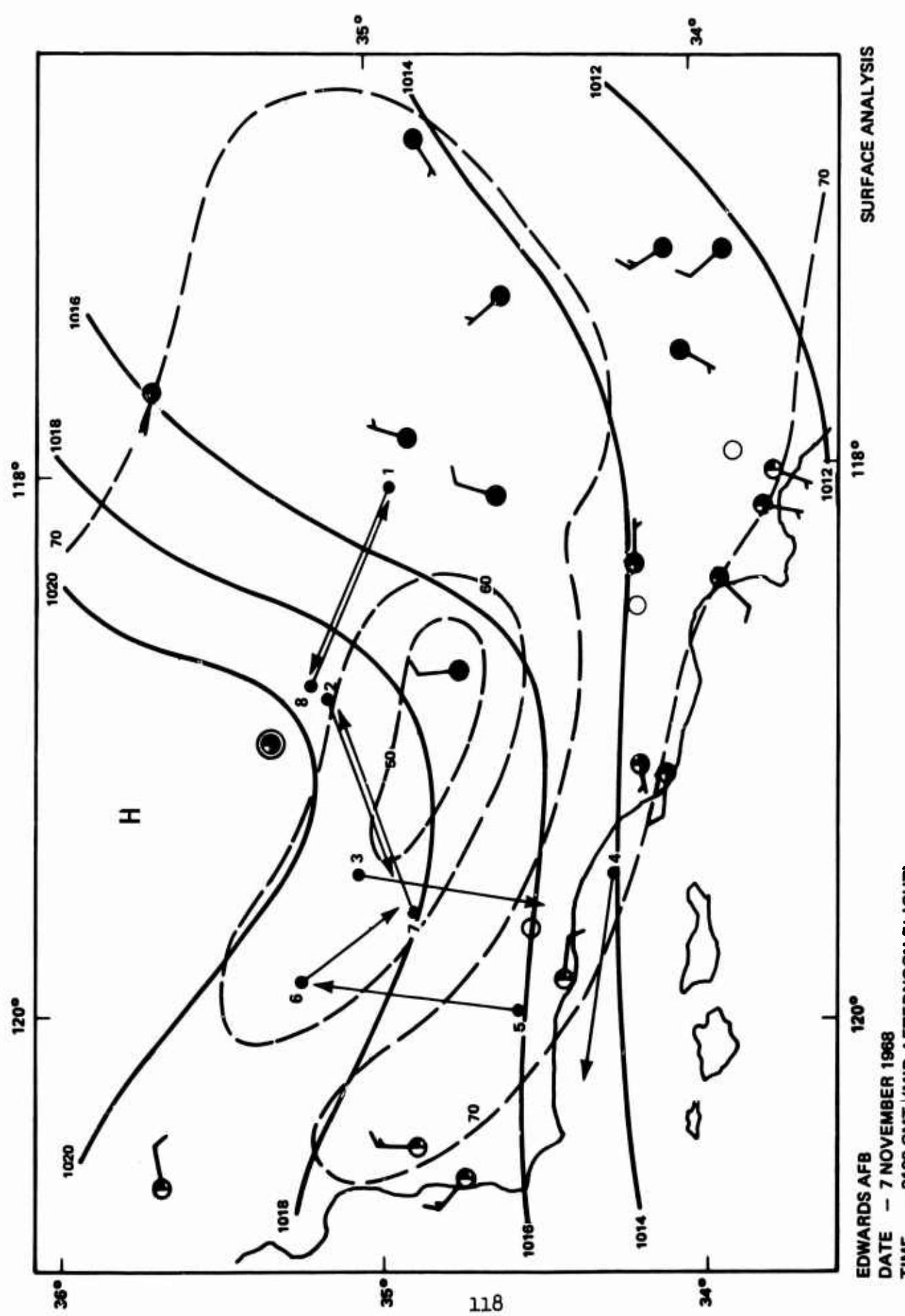
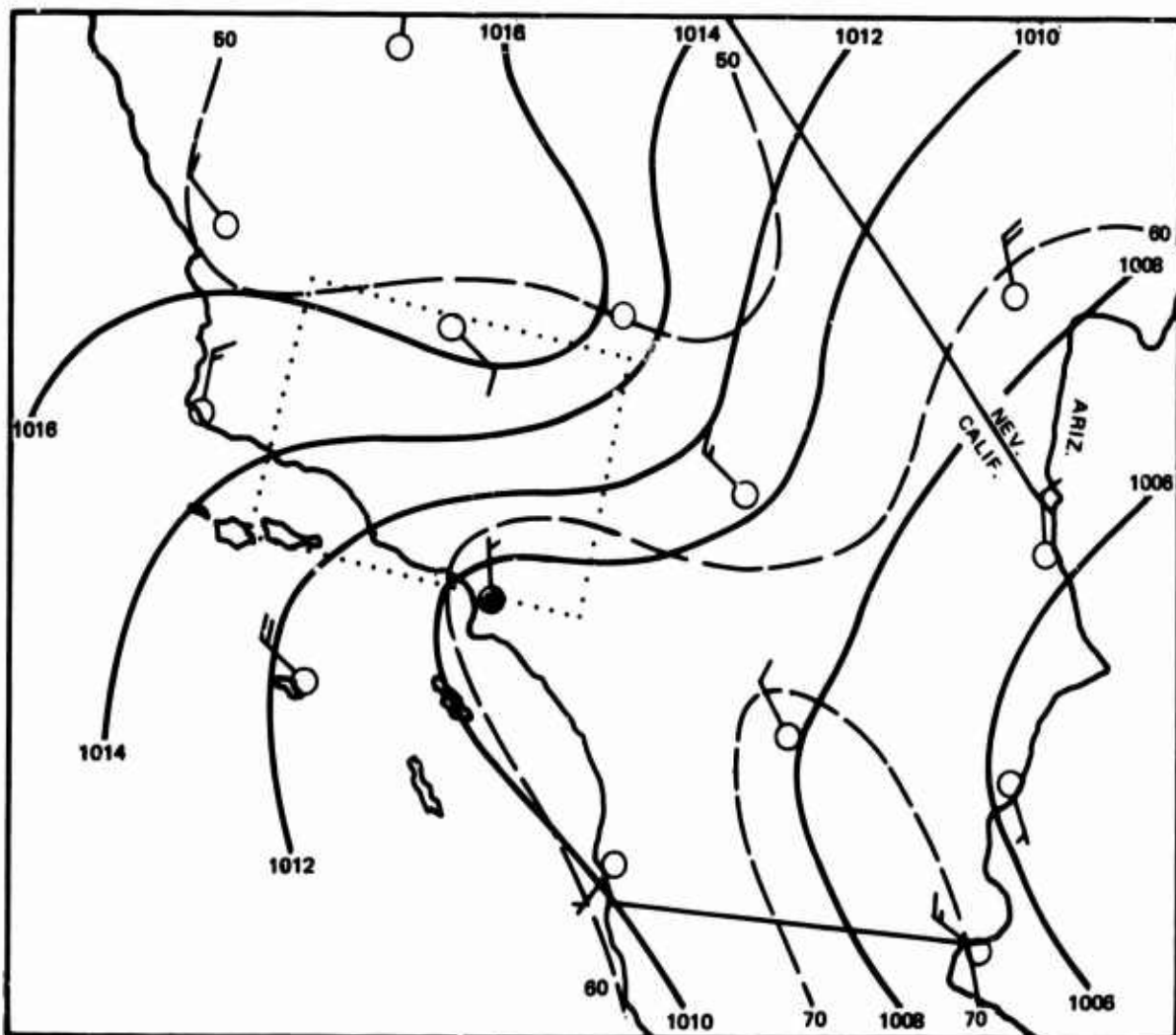


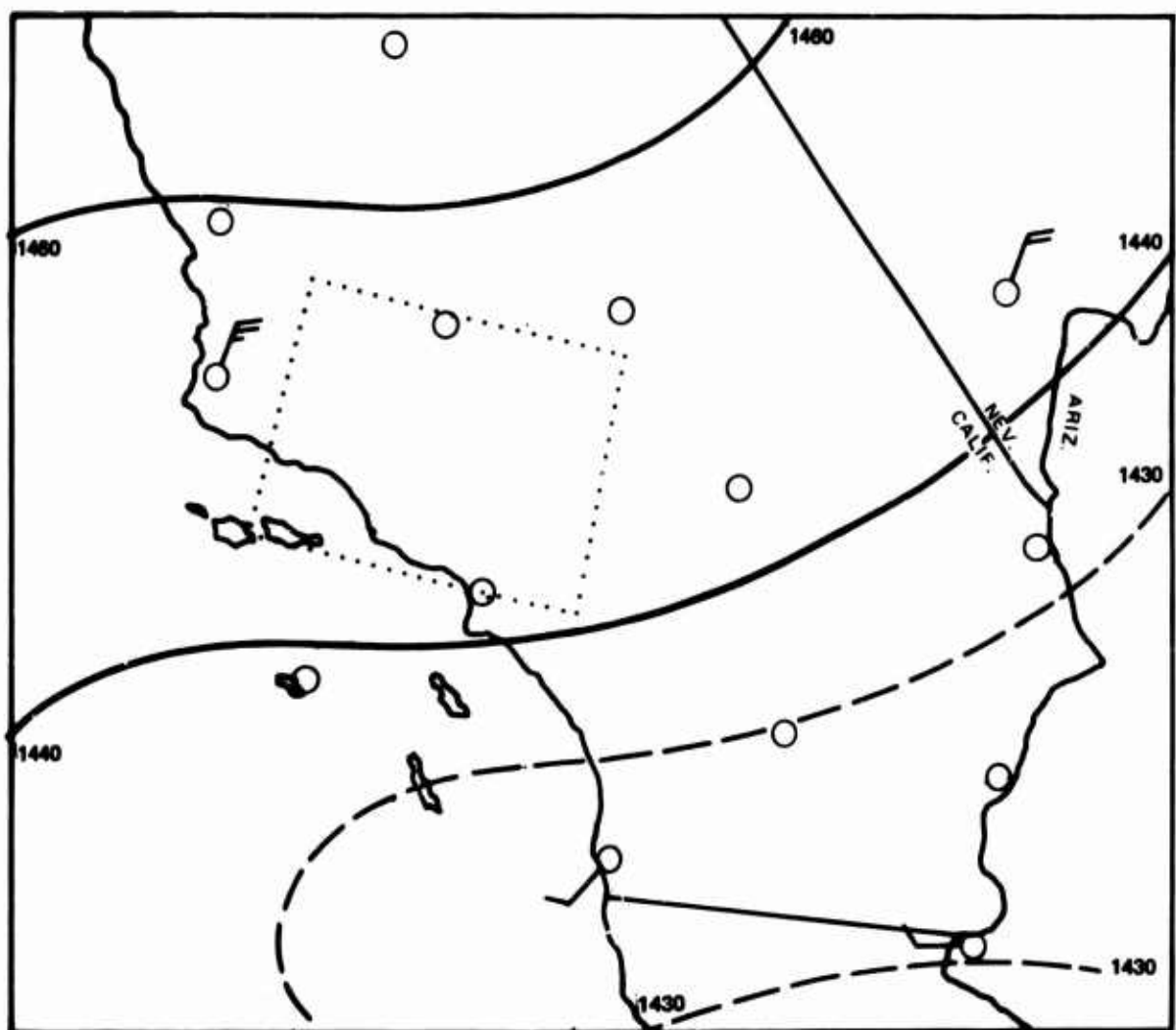
Figure 38.3 November 7, 1968 Surface Analysis, Edwards Route



EDWARDS AFB
DATE - 13 NOV 1968
TIME - 1800 GMT

SURFACE ANALYSIS

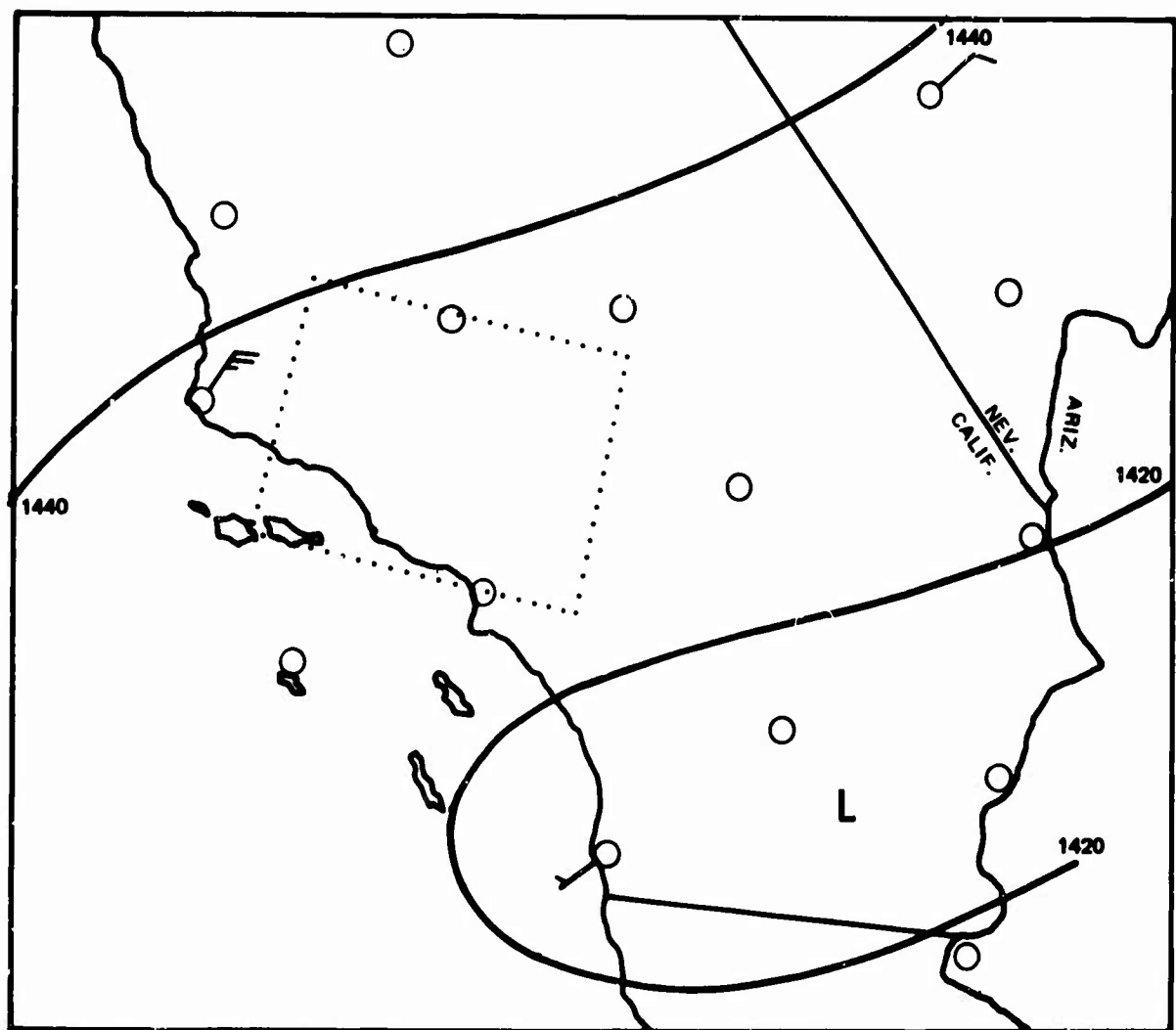
Figure 38.4 November 13, 1968 Surface Analysis, Edwards Route



EDWARDS AFB
DATE — 13 NOV 1968
TIME — 1200 GMT

850 MB ANALYSIS

Figure 38.5 November 13, 1968 850 MB Analysis, Edwards Route



EDWARDS AFB
DATE - 14 NOV 1968
TIME - 0000 GMT

850 MB ANALYSIS

Figure 38.6 November 13, 1968 850 MB Analysis, Edwards Route

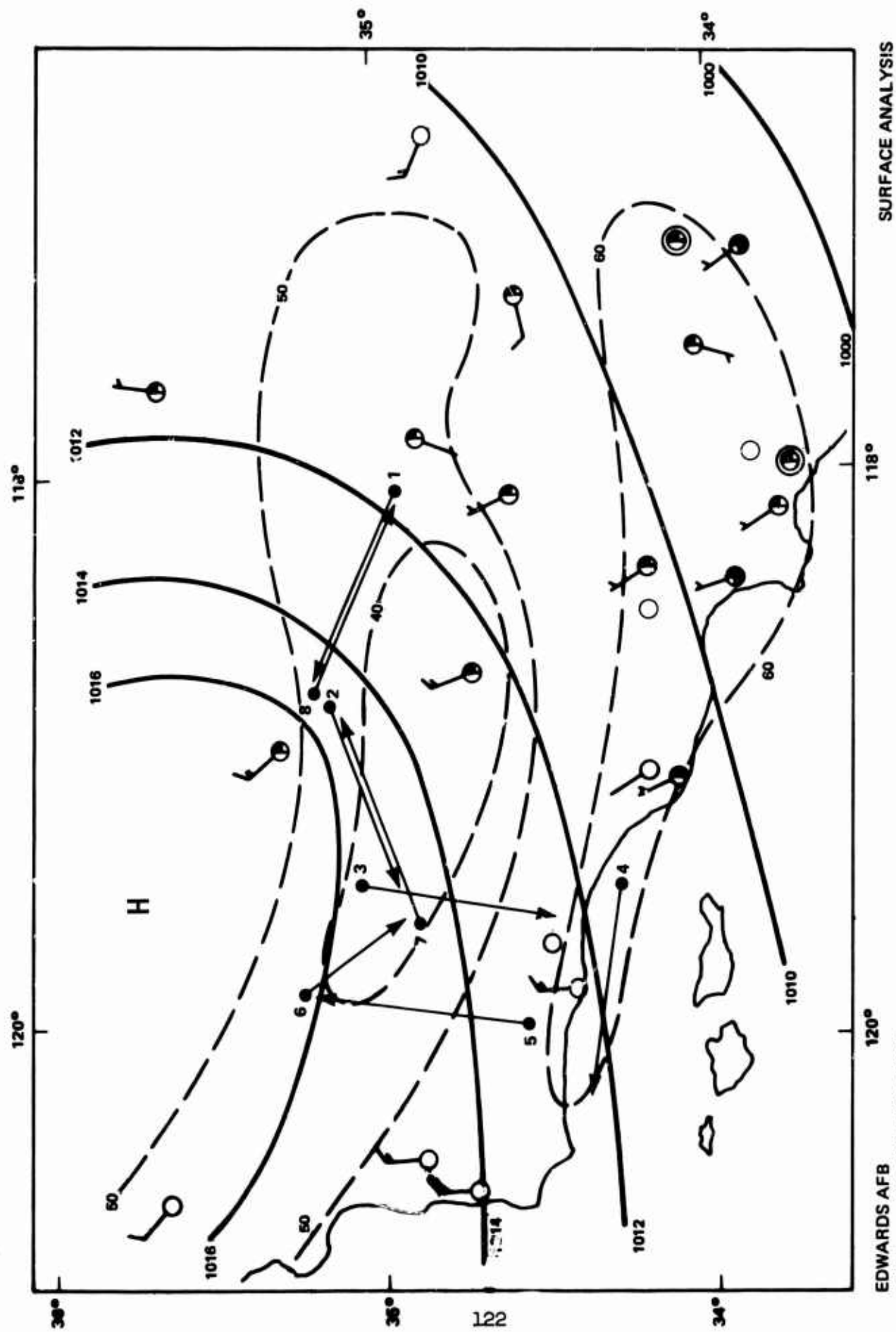


Figure 38.7 November 13, 1968 Surface Analysis, Edwards Route

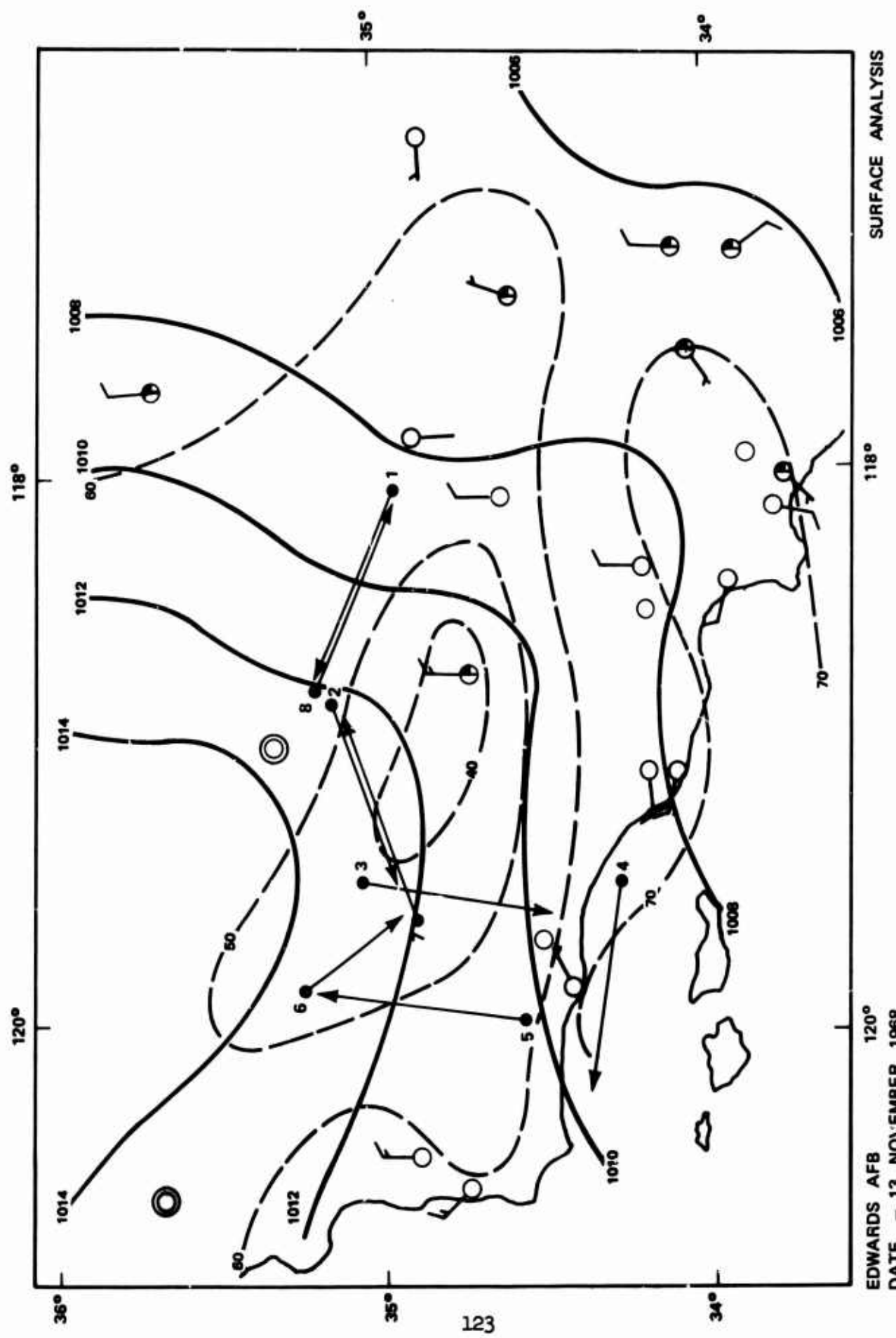
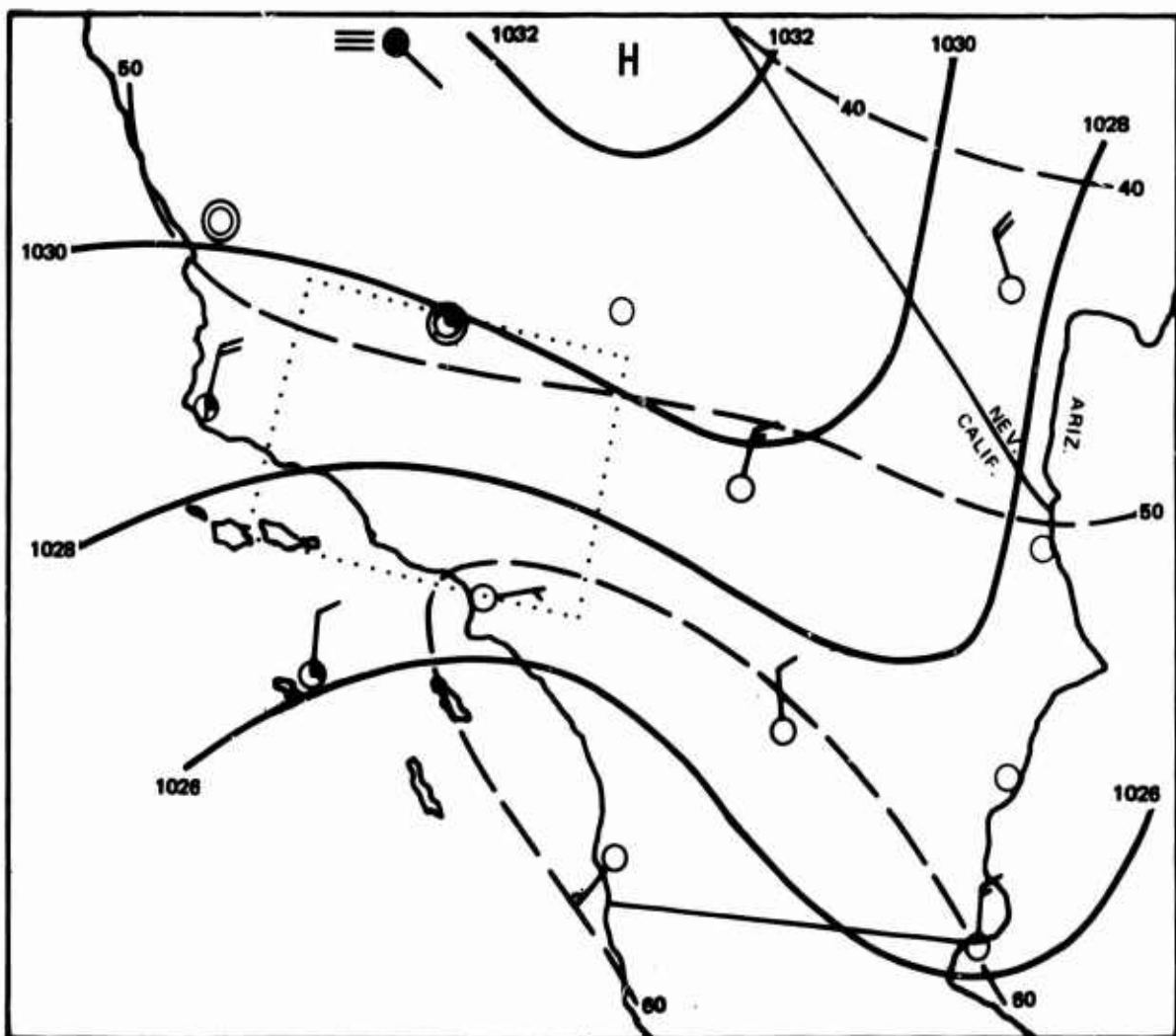


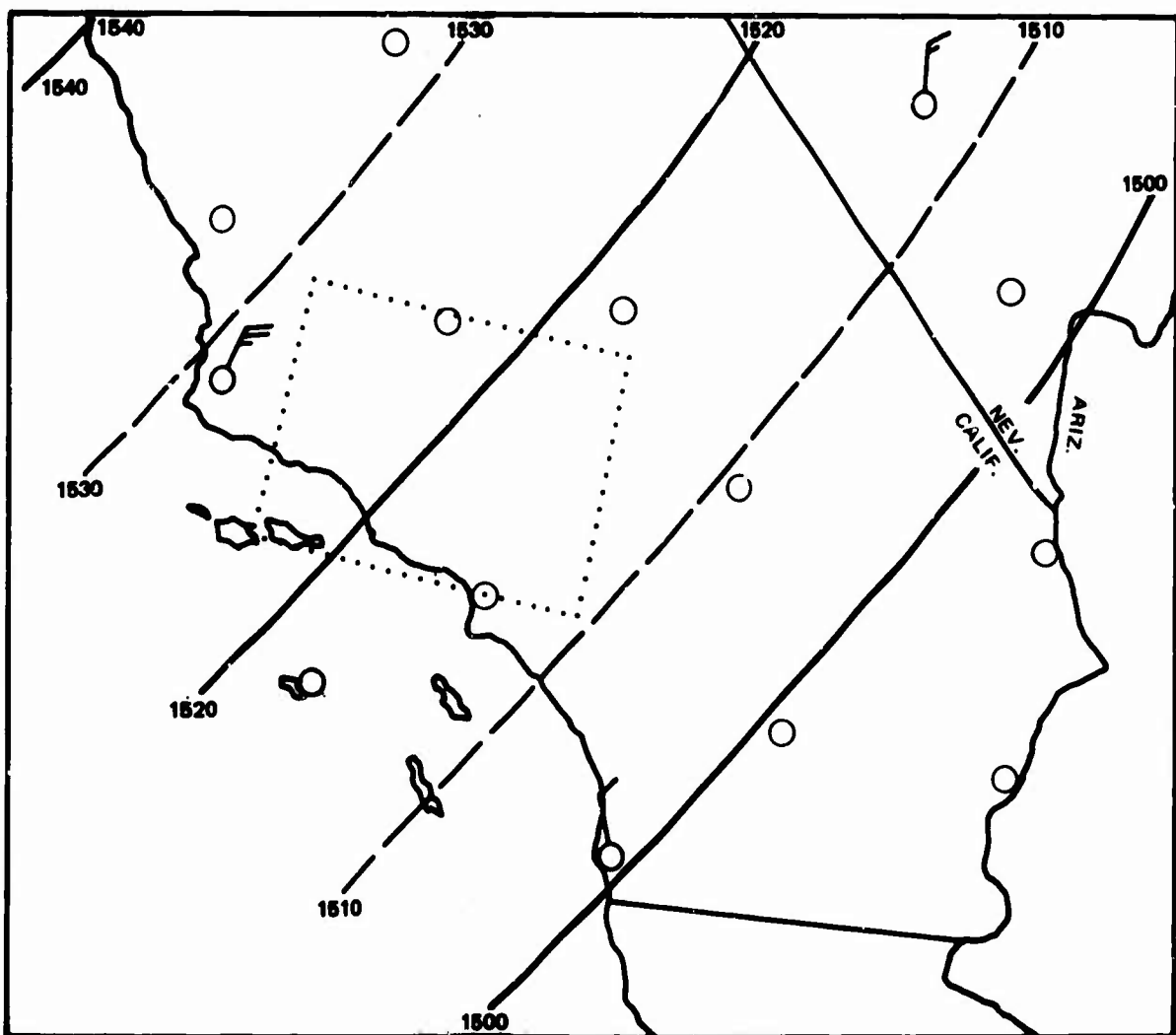
Figure 38.8 November 13, 1968 Surface Analysis, Edwards Route



EDWARDS AFB
DATE — 2 DEC 1968
TIME — 1800 GMT

SURFACE ANALYSIS

Figure 38.9 December 2, 1968 Surface Analysis, Edwards Route



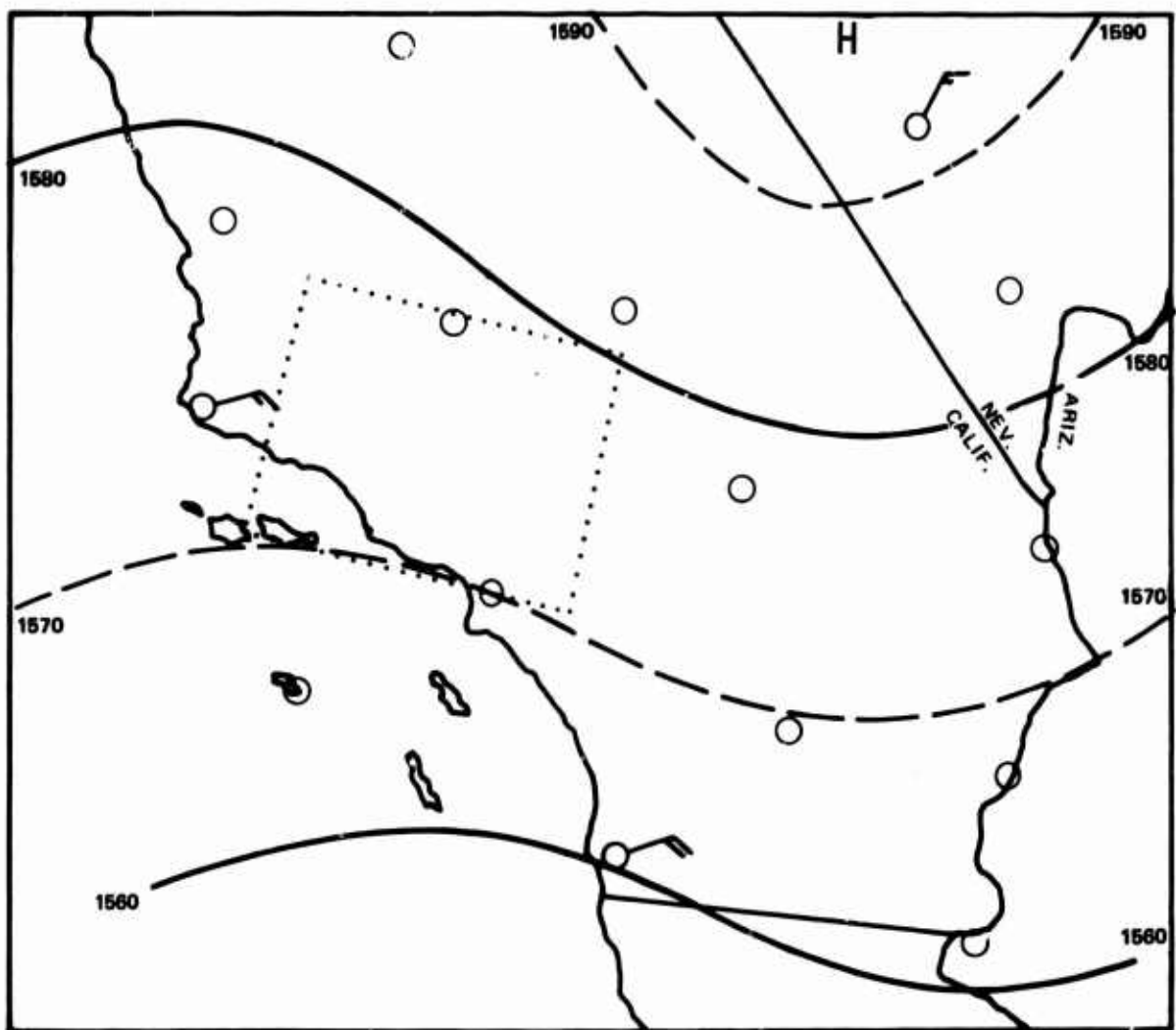
EDWARDS AFB

DATE — 2 DEC 1968

TIME — 1200 GMT

850 MB ANALYSIS

Figure 38.10 December 2, 1968 850 MB Analysis, Edwards Route



EDWARDS AFB
DATE - 3 DEC 1968
TIME - 0000 GMT

850 MB ANALYSIS

Figure 38.11 December 2, 1968 850 MB Analysis, Edwards Route
126

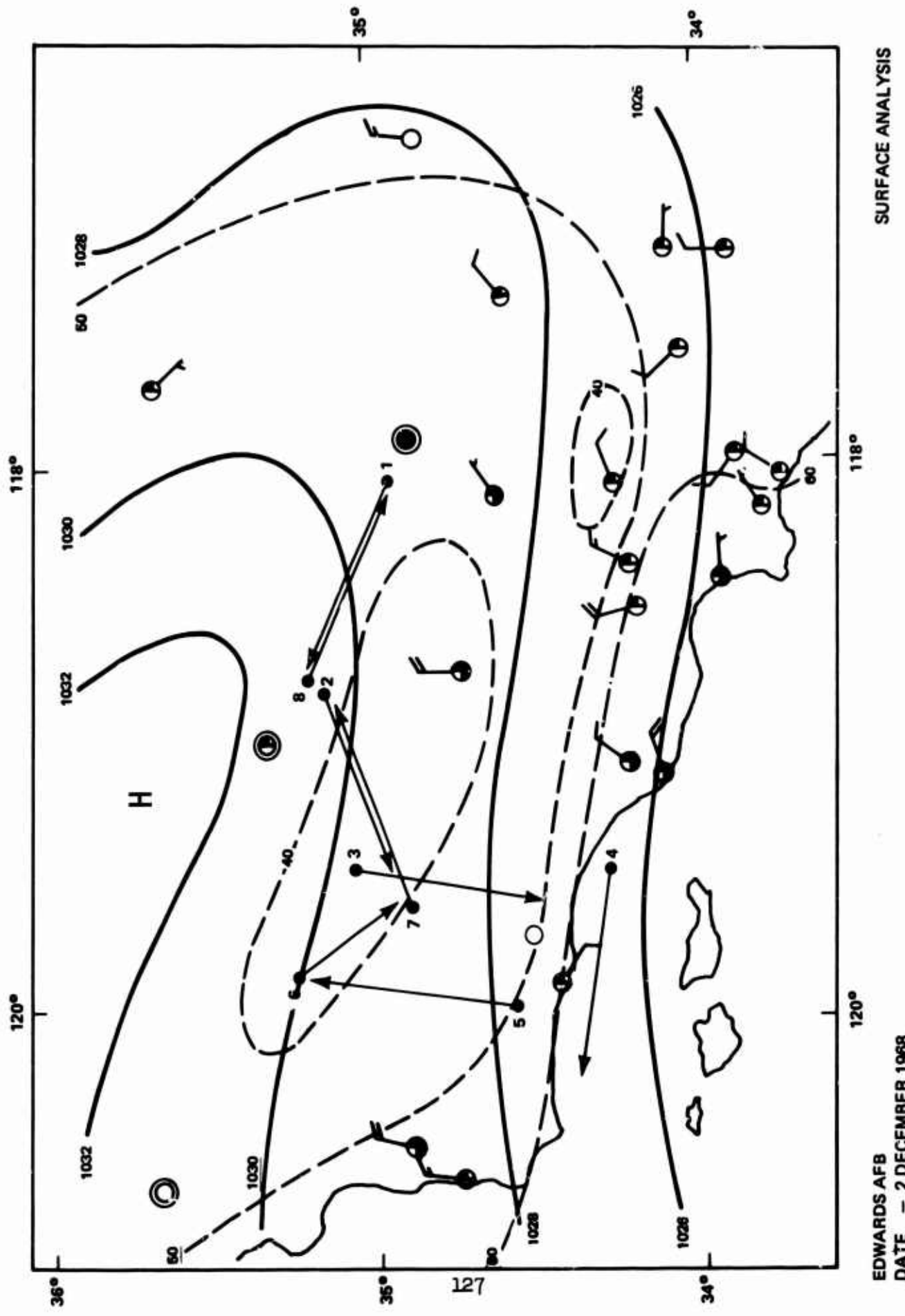
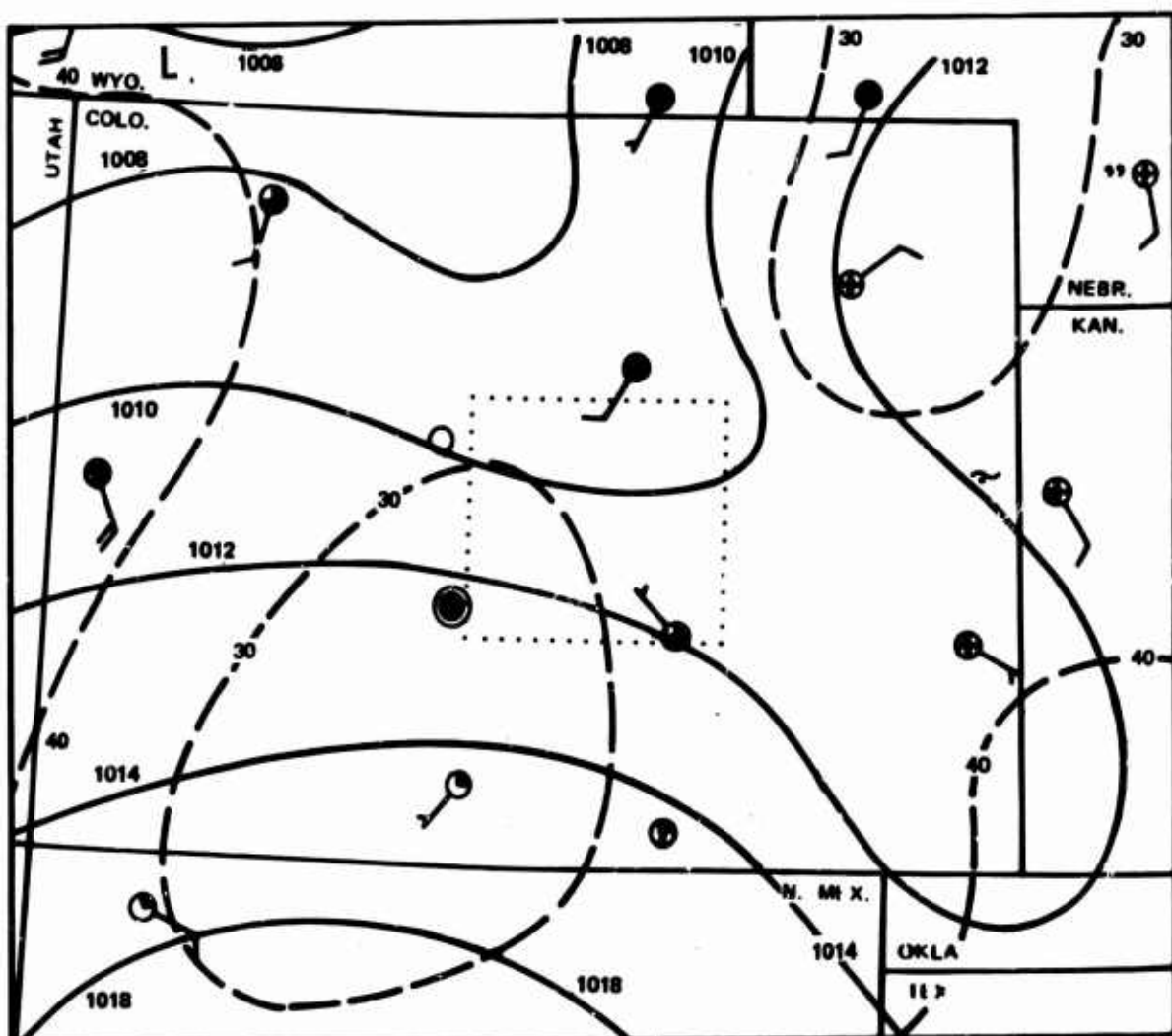


Figure 38.12 December 2, 1968 Surface Analysis, Edwards Route



PETERSON FLD
DATE - 25 FEBRUARY 1969
TIME - 1500 GMT

SURFACE ANALYSIS

Figure 38.13 February 25, 1969 Surface Analysis, Peterson Route
128

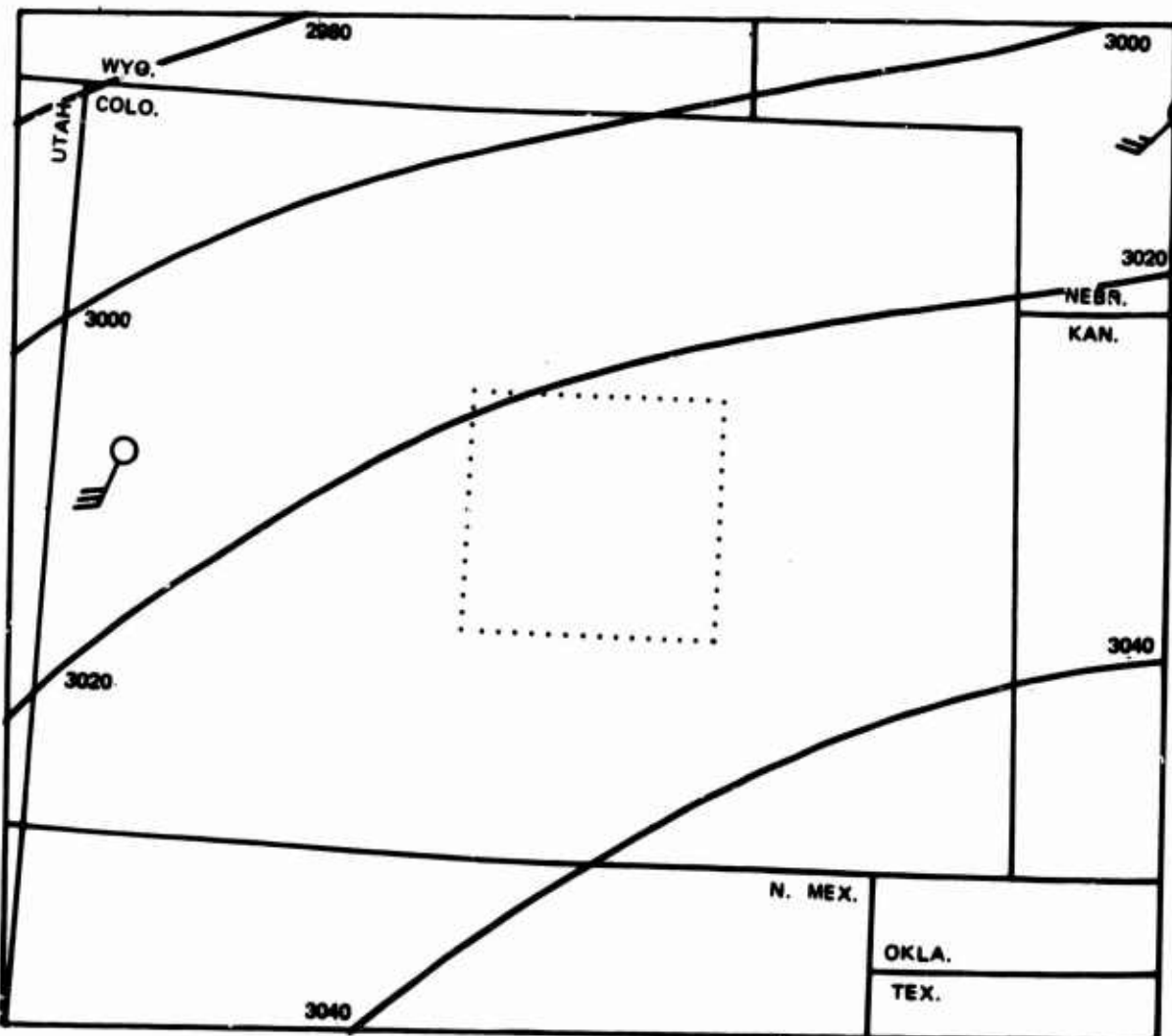


Figure 38.14 February 25, 1969 700 MB Analysis, Peterson Route

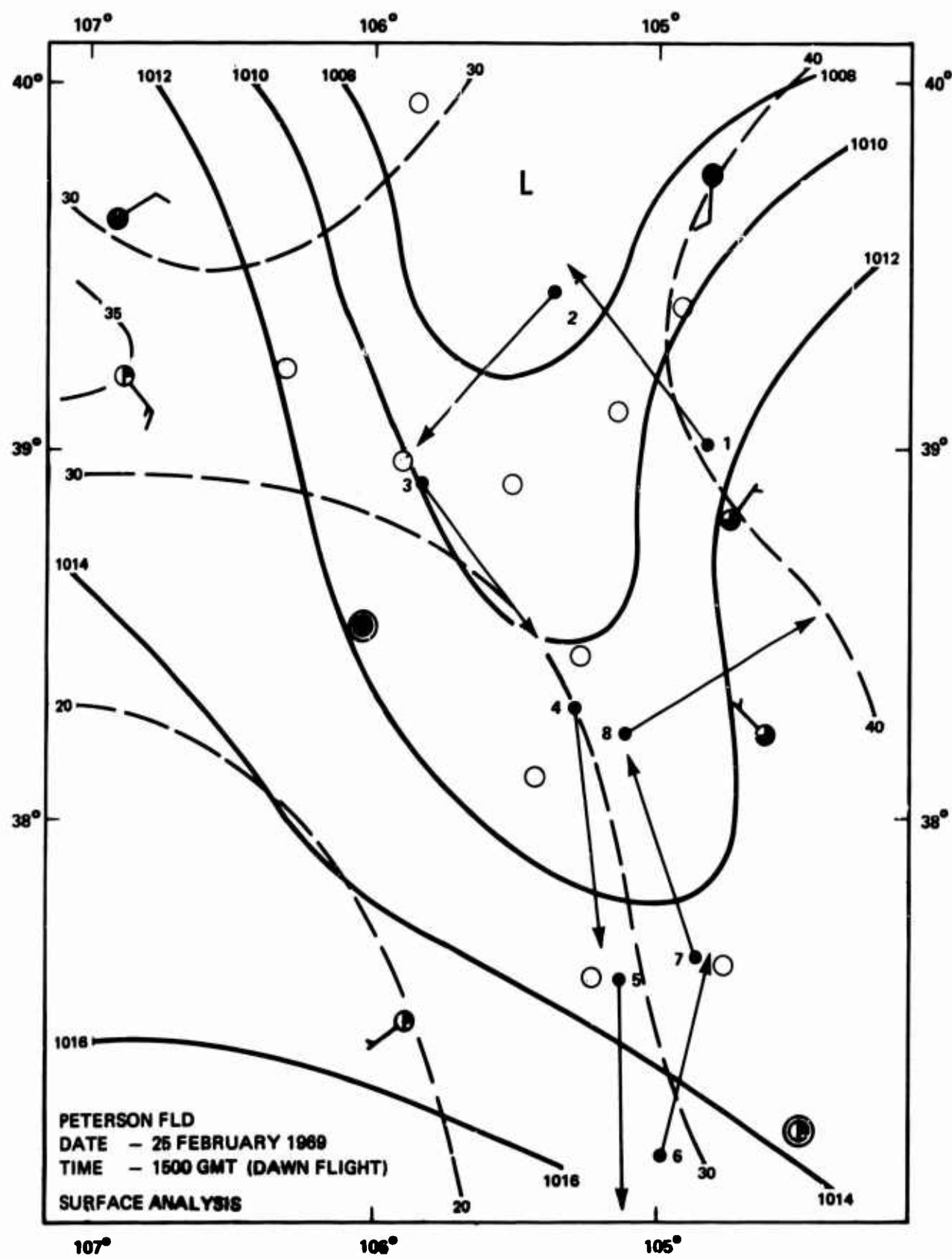
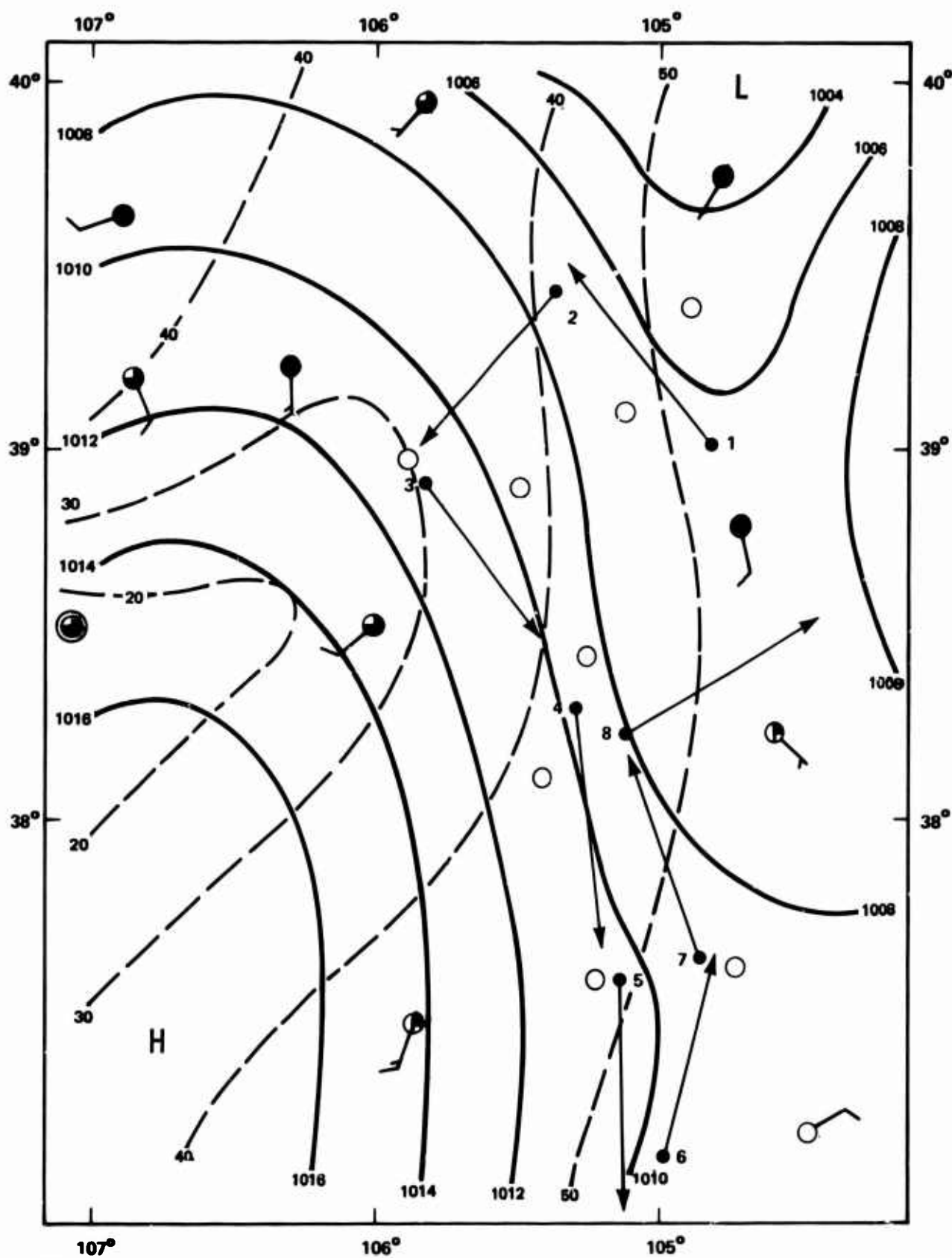


Figure 38.15 February 25, 1969 Surface Analysis, Peterson Route



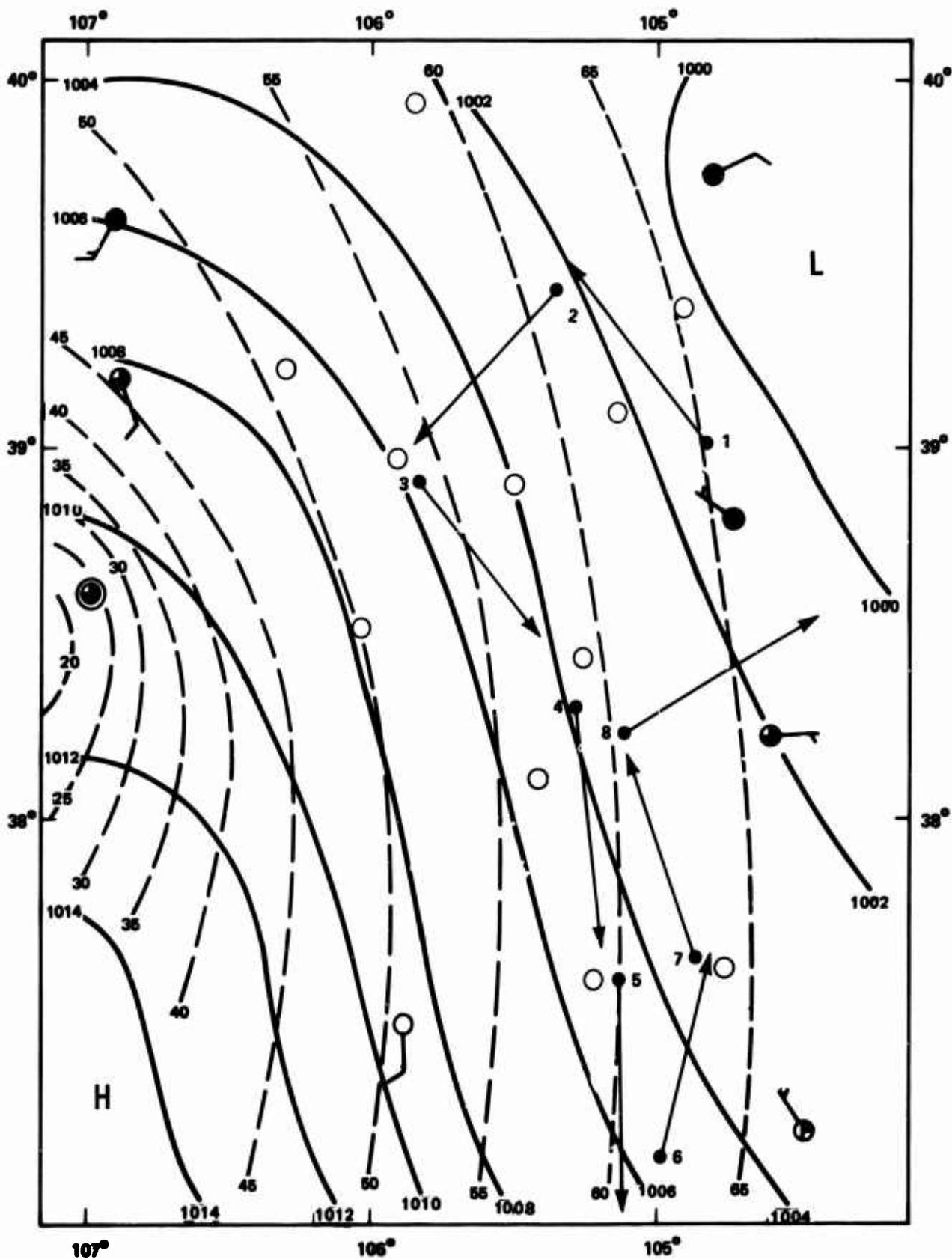
PETERSON FLD

DATE - 25 FEBRUARY 1969

TIME - 1800 GMT (MID-MORNING FLIGHT)

SURFACE ANALYSIS

Figure 38.16 February 25, 1969 Surface Analysis, Peterson Route



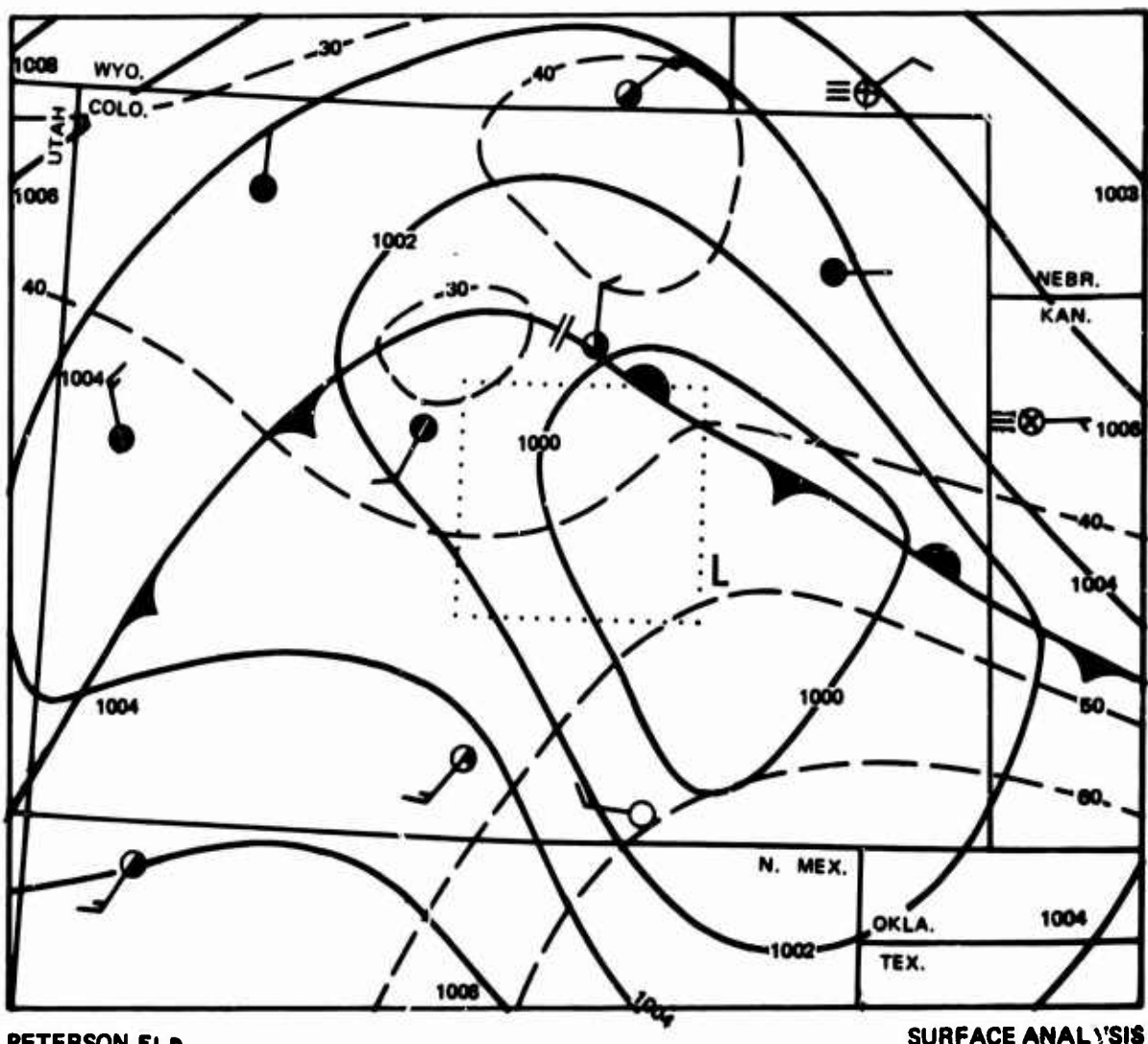
PETERSON FLD

DATE - 25 FEBRUARY 1969

TIME - 2100 GMT (MID-AFTERNOON FLIGHT)

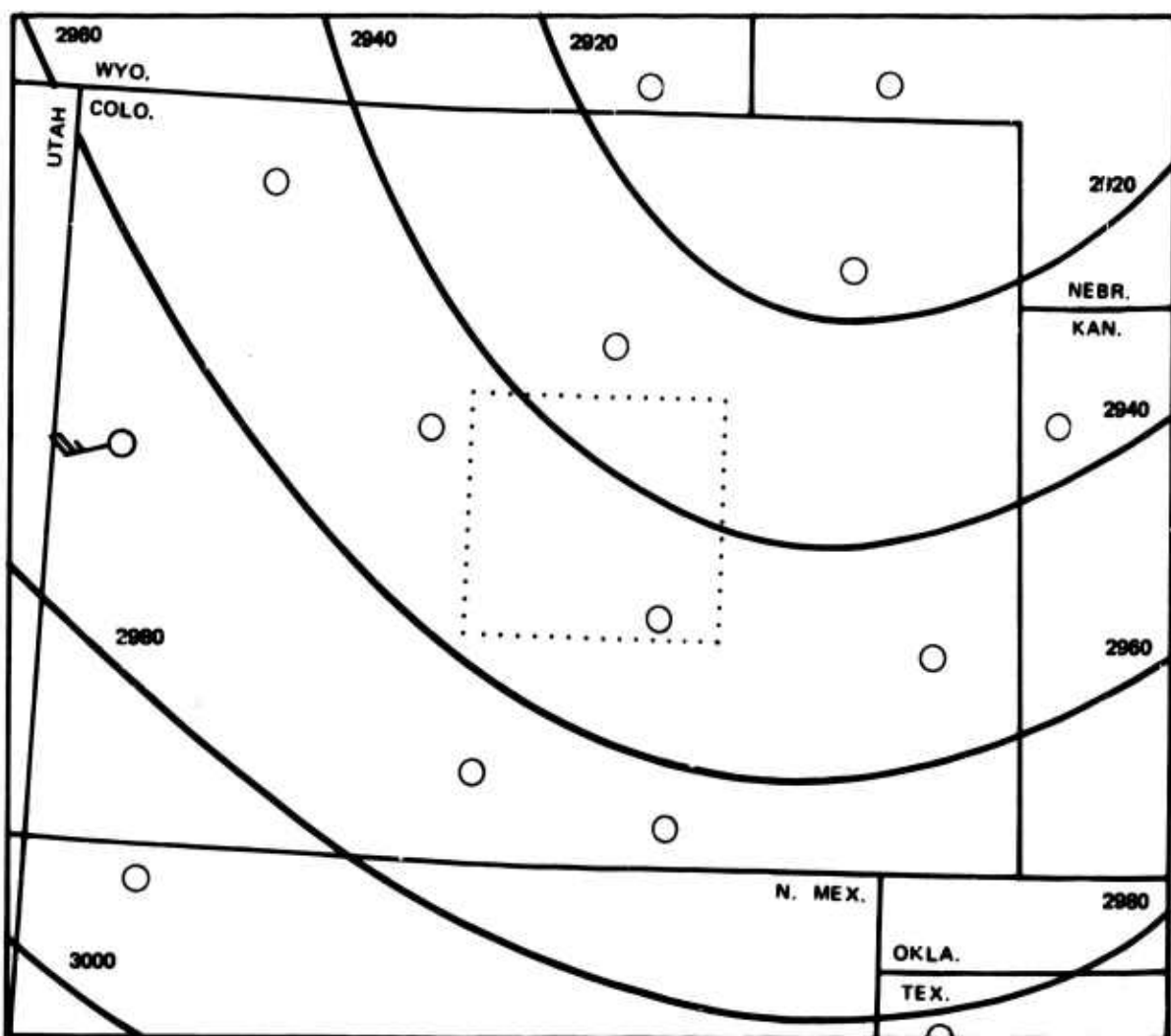
SURFACE ANALYSIS

Figure 38.17 February 25, 1969 Surface Analysis, Peterson Route



PETTERSON FLD
 DATE - 26 FEBRUARY 1969
 TIME - 1800 GMT

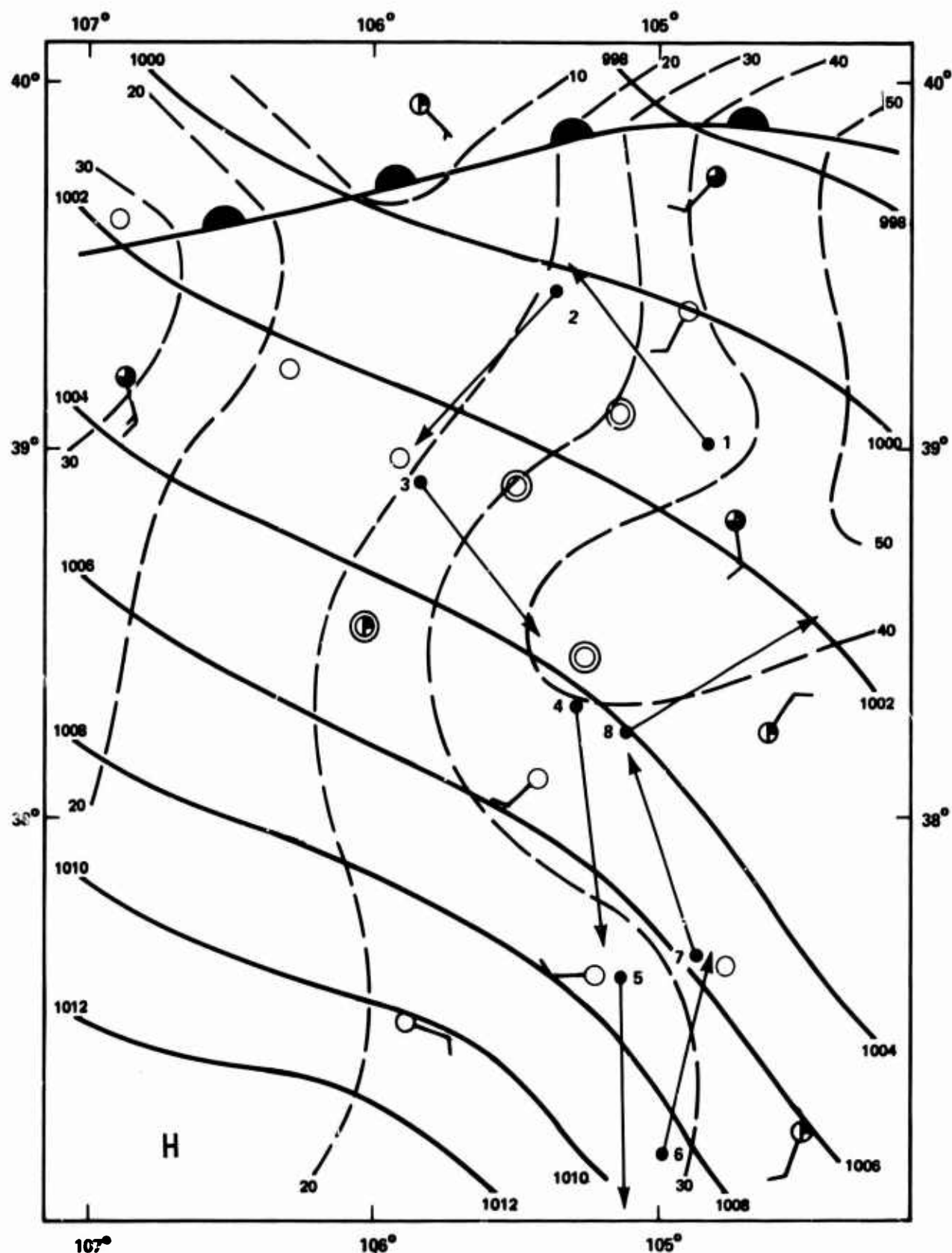
Figure 38.18 February 26, 1969 Surface Analysis, Peterson Route



PETERSON FLD
DATE - 27 FEBRUARY 1969
TIME - 0000 GMT

700 MB ANALYSIS

Figure 38.19 February 26, 1969 700 MB Analysis, Peterson Route



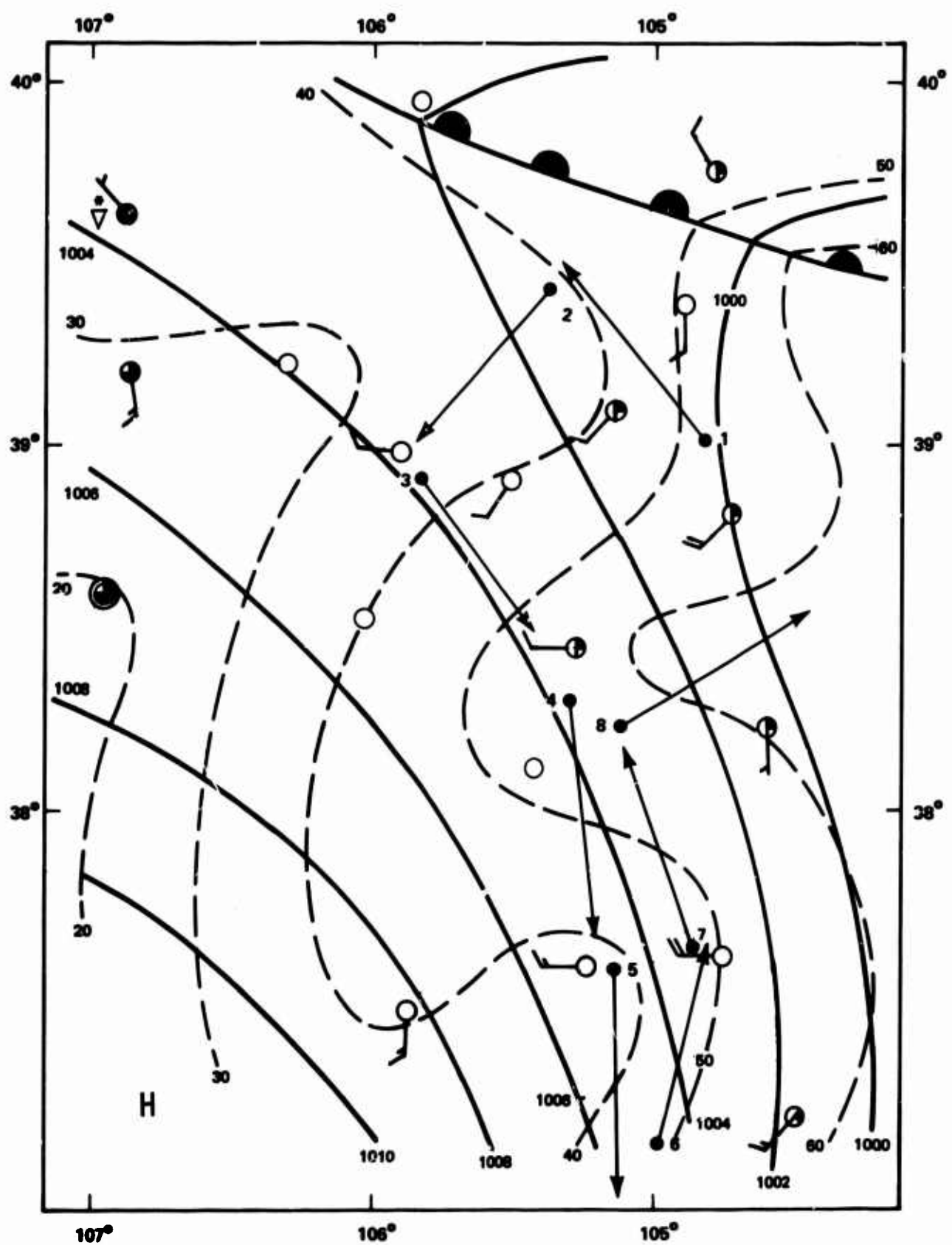
PETERSON FLD

DATE - 26 FEBRUARY 1969

TIME - 1500 GMT (DAWN FLIGHT)

SURFACE ANALYSIS

Figure 38.20 February 26, 1969 Surface Analysis, Peterson Route



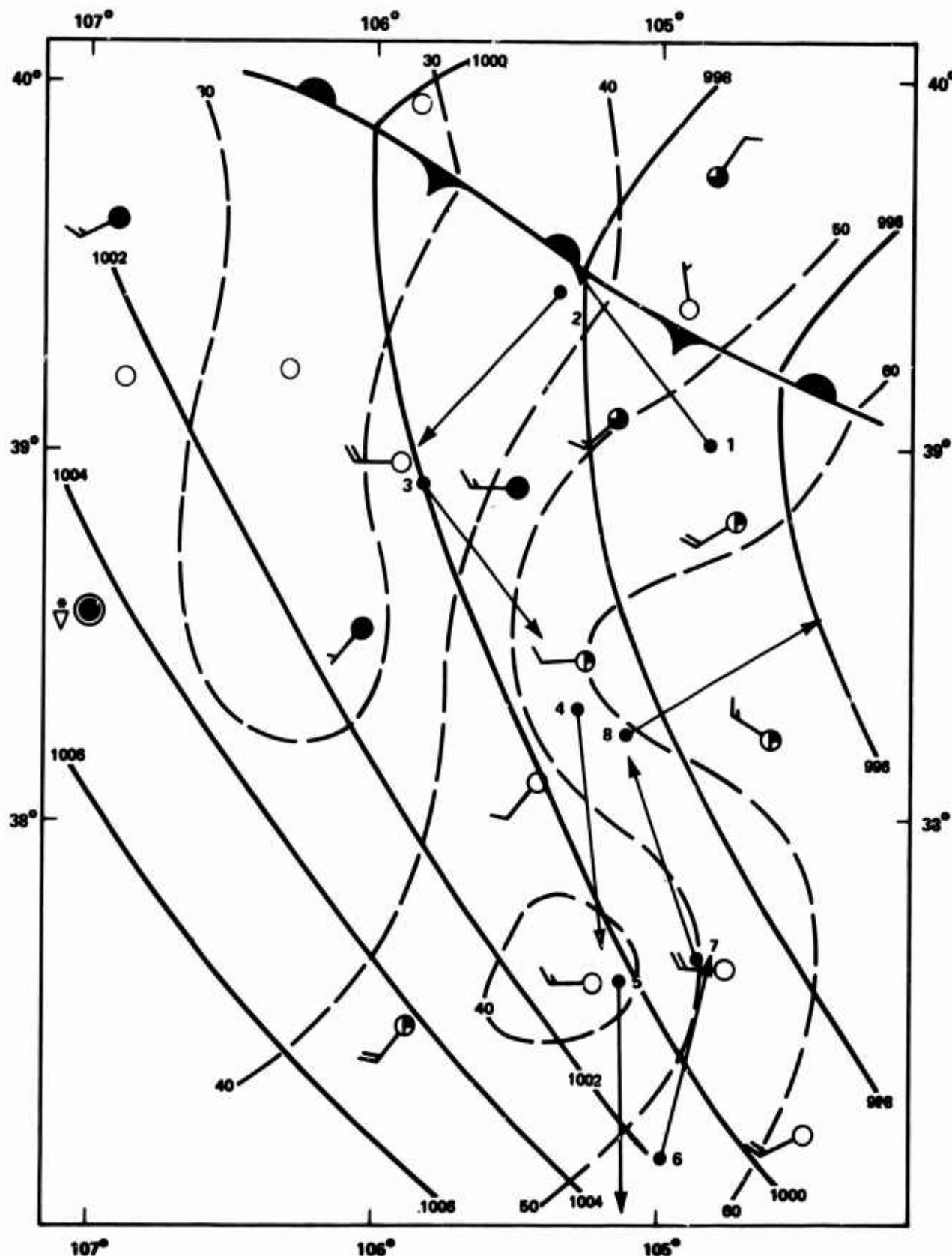
PETERSON FLD

DATE - 26 FEBRUARY 1969

TIME - 1700 GMT (MID-MORNING FLIGHT)

SURFACE ANALYSIS

Figure 38.21 February 26, 1969 Surface Analysis, Peterson Route



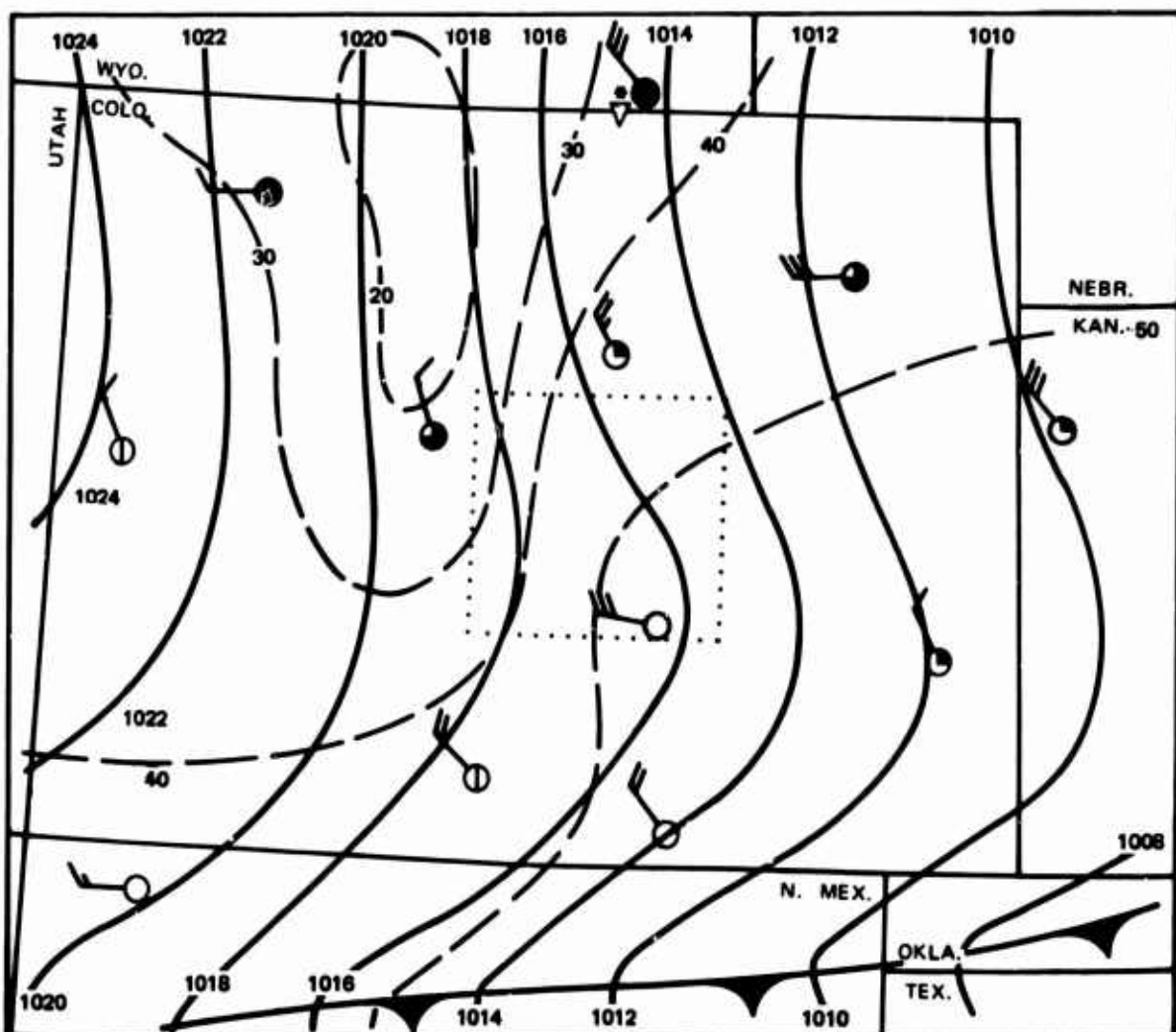
PETERSON FLD

DATE - 26 FEBRUARY 1969

TIME - 2100 GMT (MID-AFTERNOON FLIGHT)

SURFACE ANALYSIS

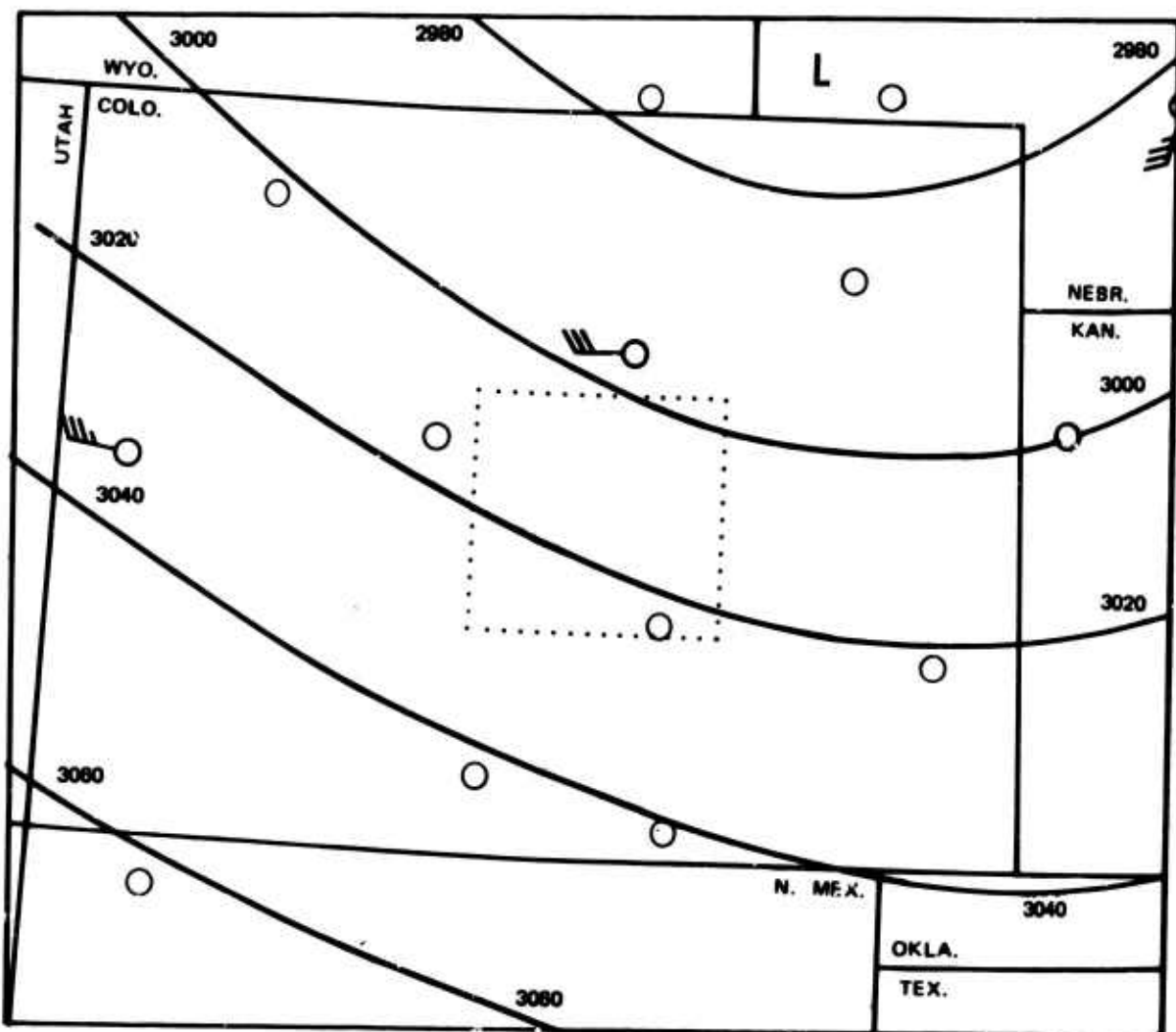
Figure 38.22 February 26, 1969 Surface Analysis, Peterson Route



PETERSON PLO
DATE - 19 MARCH 1969
TIME - 1800 GMT

SURFACE ANALYSIS

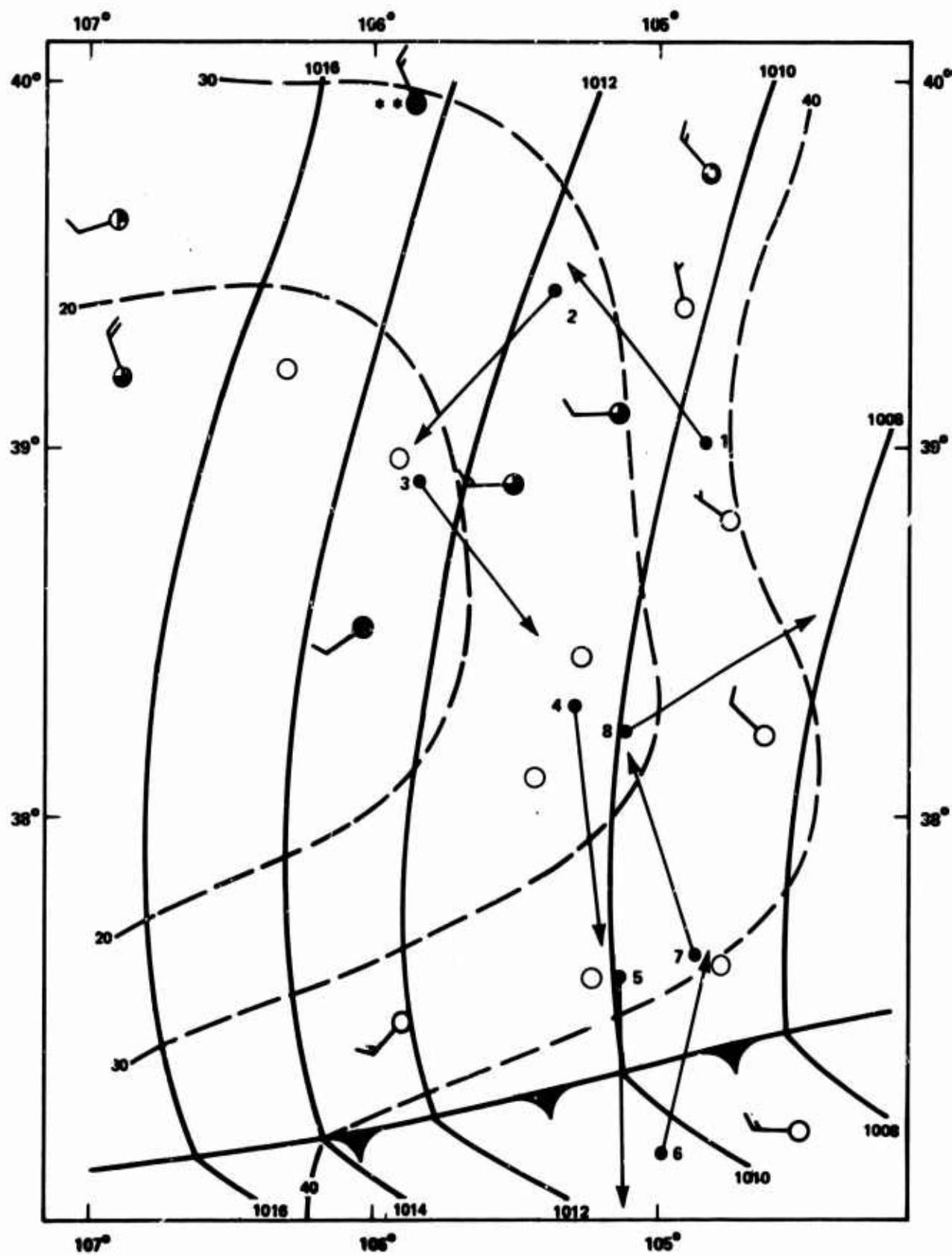
Figure 38.23 March 19, 1969 Surface Analysis, Peterson Route



PETERSON FLD
DATE - 19 MARCH 1969
TIME - 1200 GMT

700 MB ANALYSIS

Figure 38.24 March 19, 1969 700 MB Analysis, Peterson Route
139



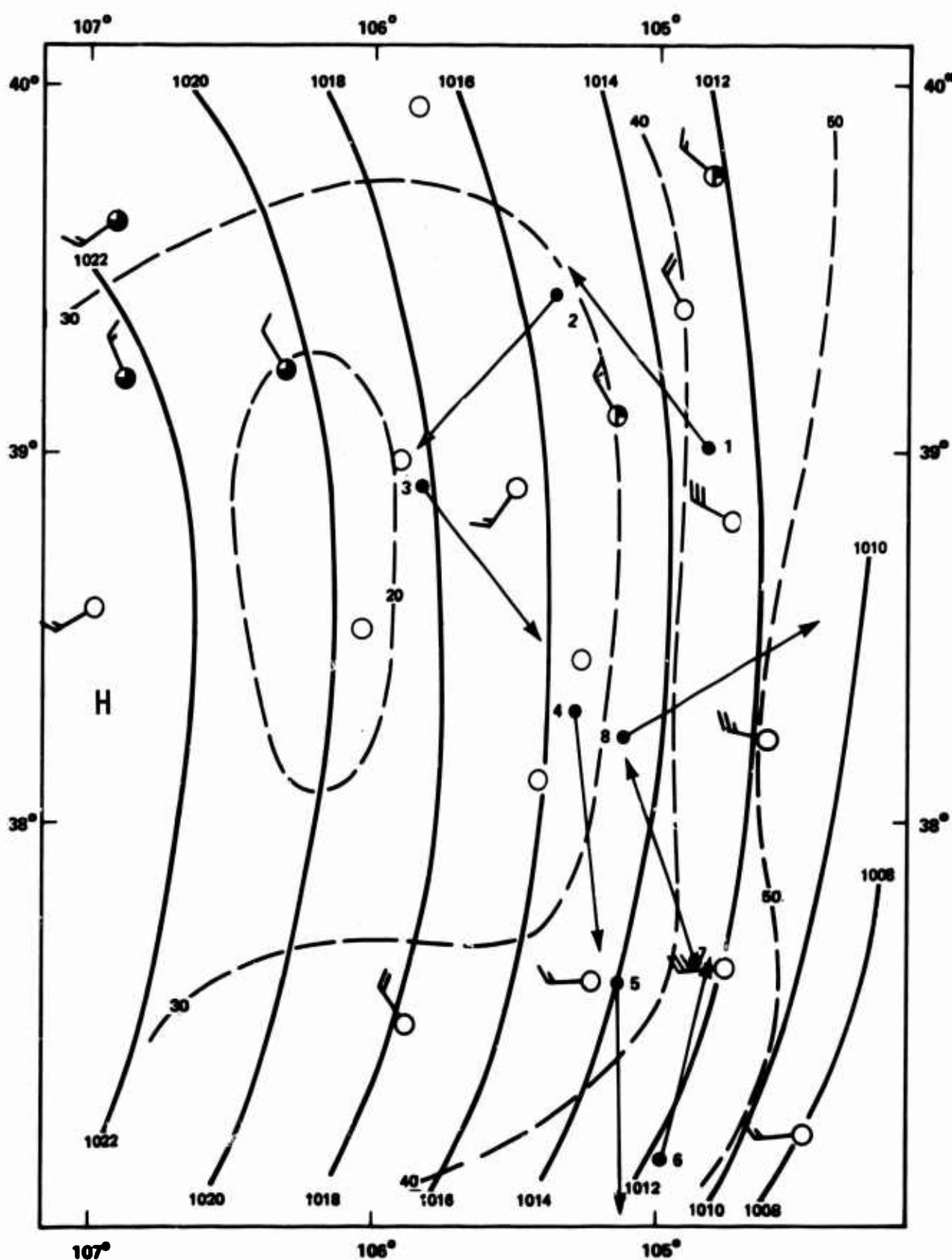
PETERSON FLD

DATE - 19 MARCH 1969

TIME - 1400 GMT (DAWN FLIGHT)

SURFACE ANALYSIS

Figure 38.25 March 19, 1969 Surface Analysis, Peterson Route



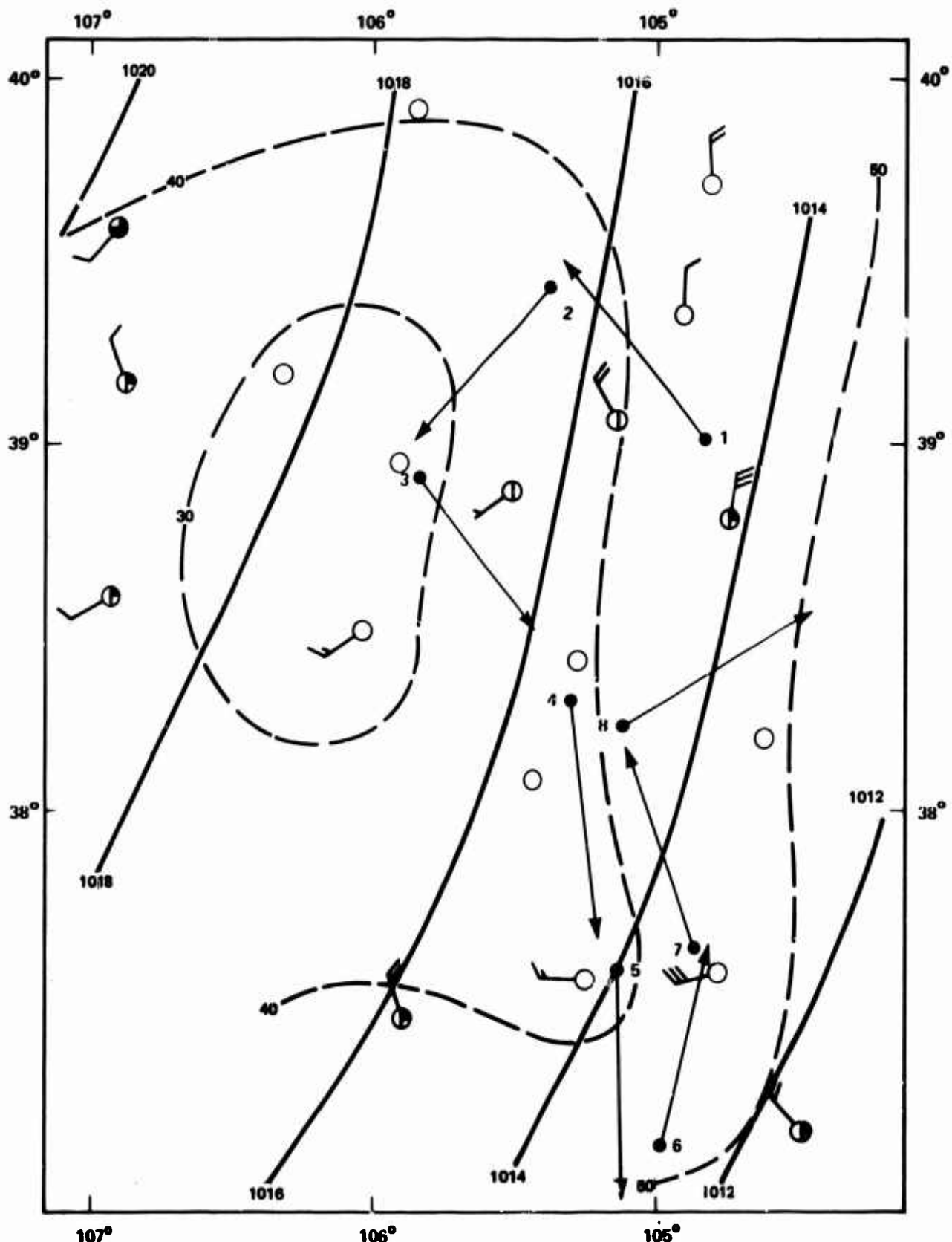
PETERSON FLD

DATE - 19 MARCH 1969

TIME - 1700 GMT (MID-MORNING FLIGHT)

SURFACE ANALYSIS

Figure 38.26 March 19, 1969 Surface Analysis, Peterson Route



PETERSON FIELD

DATE - 19 MARCH 1969

TIME - 2100 GMT (MID-AFTERNOON FLIGHT)

SURFACE ANALYSIS

Figure 38.27 March 19, 1969 Surface Analysis, Peterson Route

39. RICHARDSON NUMBER

The relationship of Richardson number to the intensity of atmospheric turbulence has been the subject of many investigations. In many of these investigations, either the turbulence and/or the meteorological data were approximated or there was a large time lapse between the meteorological and the turbulence recordings. The sample size was seldom large.

During the LO-LOCAT Program, more than 10,000 Richardson number samples were calculated and compared to the corresponding turbulence intensity. Richardson numbers were calculated using the following equation:

$$R = \frac{g}{T_a} \frac{(\Gamma_d - \Delta T_{az})}{(\Delta W_z)^2} \quad (39.1)$$

The terms of equation 39.1 were calculated as shown in Appendix V. Variable bands of Richardson number values were chosen such that the largest number of samples possible would appear in each band while using the largest possible number of bands. The distributions of gust velocity rms values for each of the bands of Richardson number were computed. The cumulative probability of encountering rms values equal to or greater than the given values for the various bands are shown in Figures 39.1 through 39.8 for the terrain, altitude, and time of day categories.

The terrain categories of high mountains, low mountains, and plains (desert and water categories contained less than the minimal number of samples) are shown in Figures 39.1 through 39.3. It can be seen in these figures that the probability of occurrence for equivalent magnitudes of gust velocity rms values is much greater for high mountains than for the other terrain categories. For instance, if Richardson number was less than -0.2 for high mountain terrain, the probability was 80 per cent that the gust velocity rms value would equal or exceed 4.0 fps. The probability was 15 per cent for the same rms value occurring over plains terrain.

The altitude categories of 250 and 750 feet are shown in Figures 39.4 and 39.5. These figures indicate that the probability of encountering a gust velocity rms value of any magnitude for all Richardson numbers is slightly greater at 250 feet.

The time of day categories of dawn, mid-morning, and mid-afternoon are shown in Figures 39.6 through 39.8. In general, the probabilities of occurrence of given rms gusts were greater at mid-afternoon than at mid-morning and dawn.

Figures 39.1 through 39.8 graphically portray the fact that there is a significant increase in the probability of encountering any given gust rms value whenever the Richardson number approaches a value of 0.2. This fact, also observed during Phases I and II, was reported in References I.2 and 39.1. According to References 39.2 and 39.3, there are theoretical arguments that the critical Richardson number for the onset of turbulence is less than 0.25.

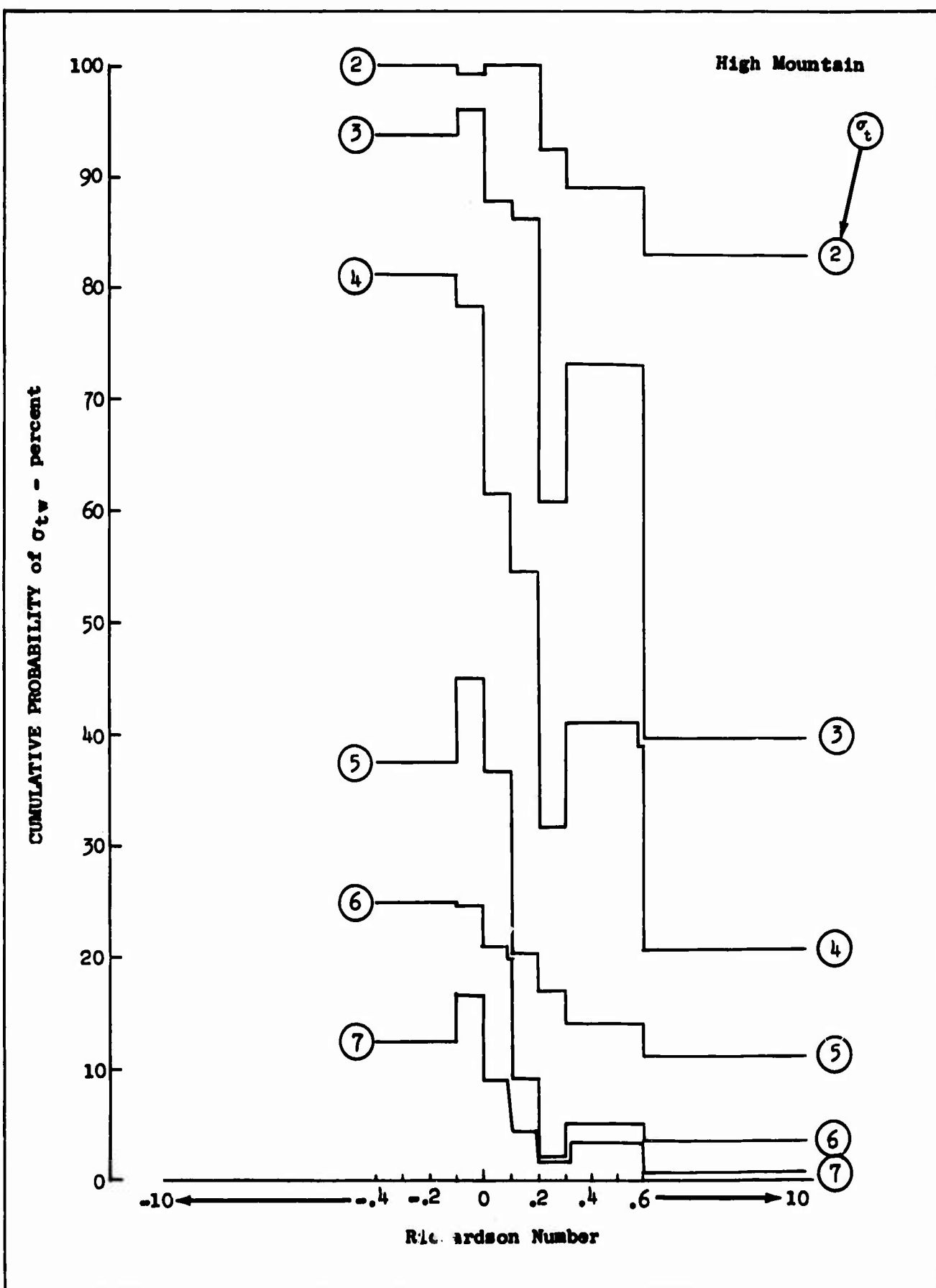


Figure 39.1 Gust Velocity RMS Probabilities Associated with High Mountain Terrain for Richardson Number Bands

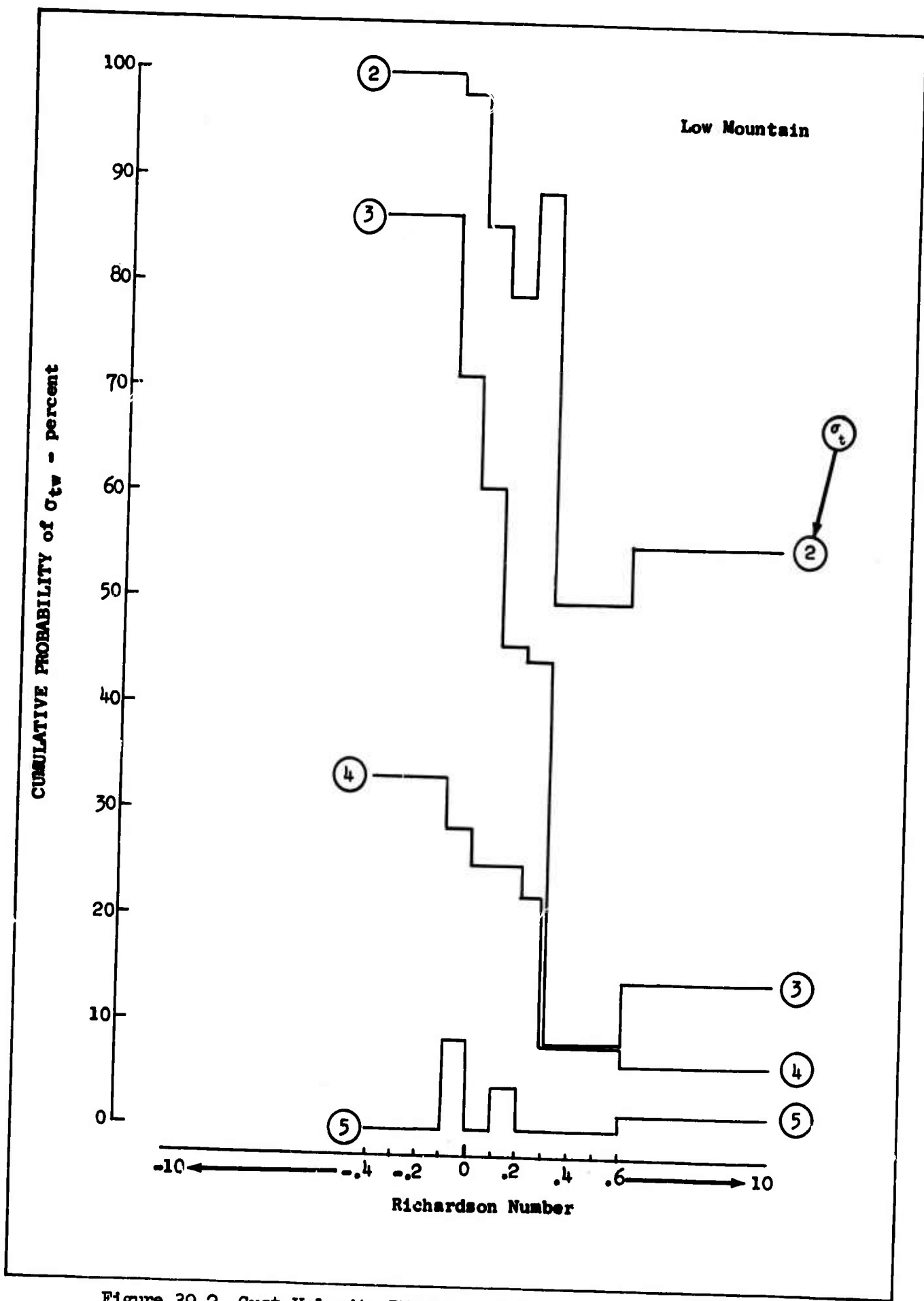


Figure 39.2 Gust Velocity RMS Probabilities Associated with Low Mountain Terrain for Richardson Number Bands

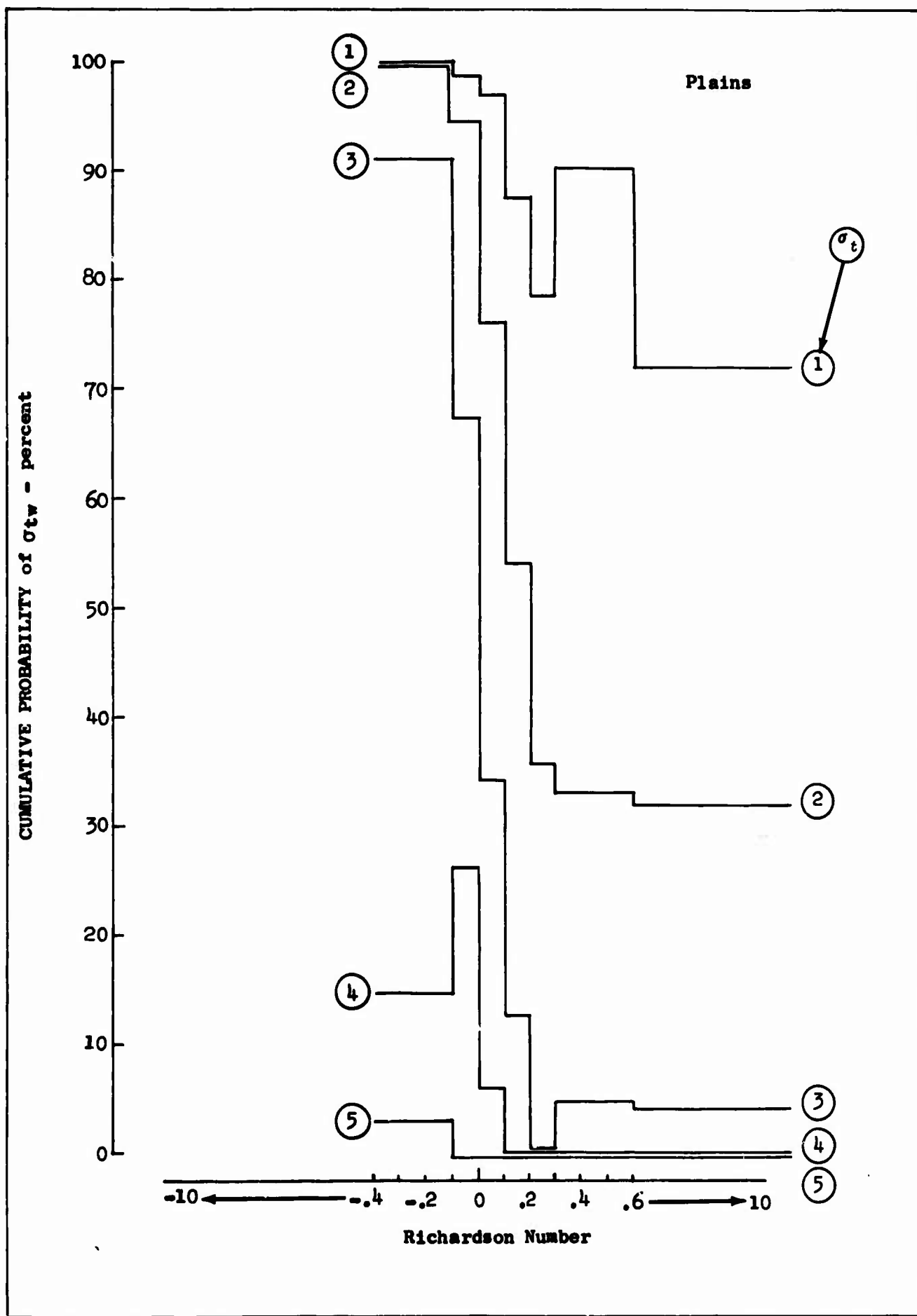


Figure 39.3 Gust Velocity RMS Probabilities Associated with Plains Terrain for Richardson Number Bands

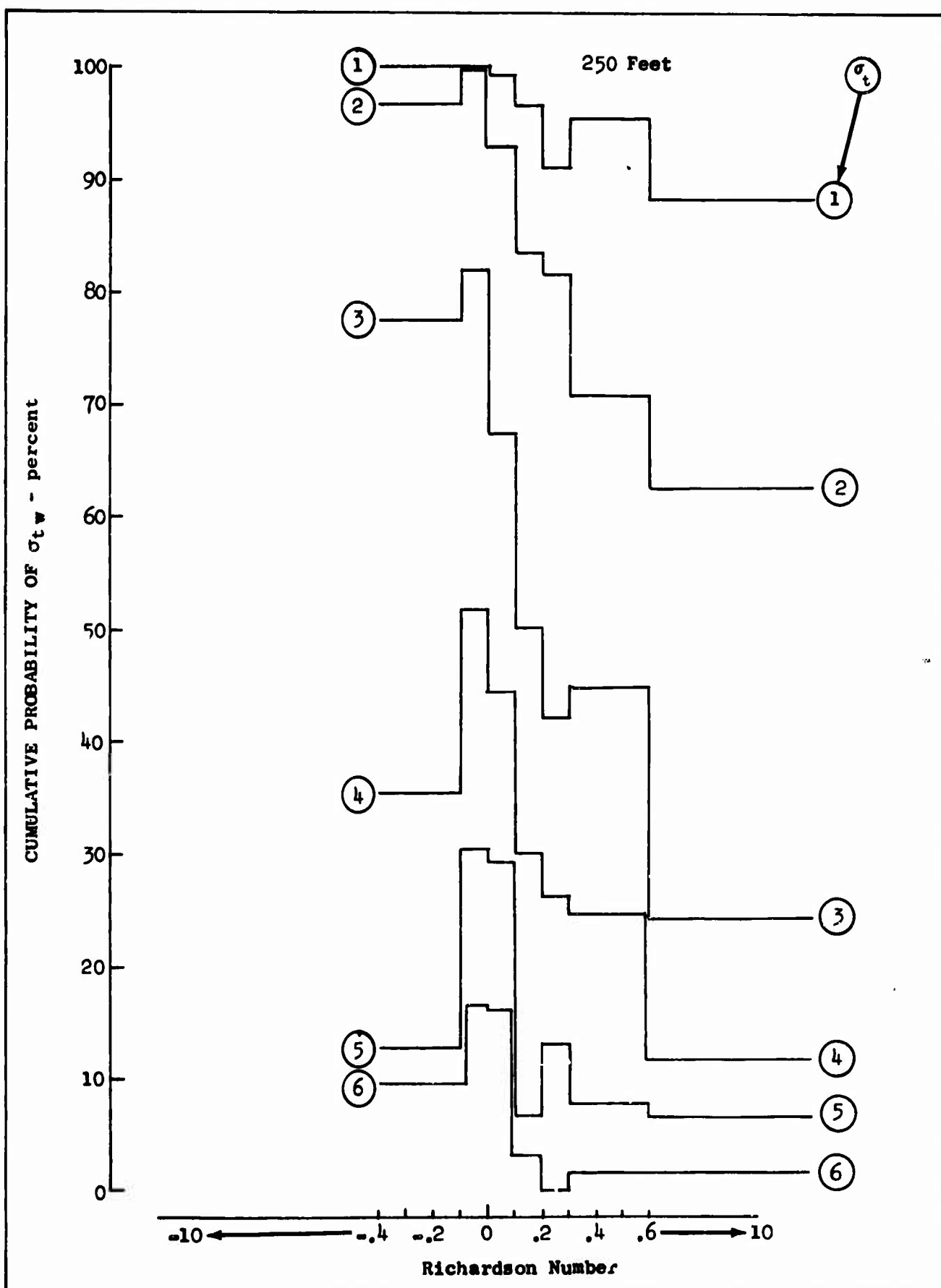


Figure 39.4 Gust Velocity RMS Probabilities Associated with 250 Foot Altitude for Richardson Number Bands

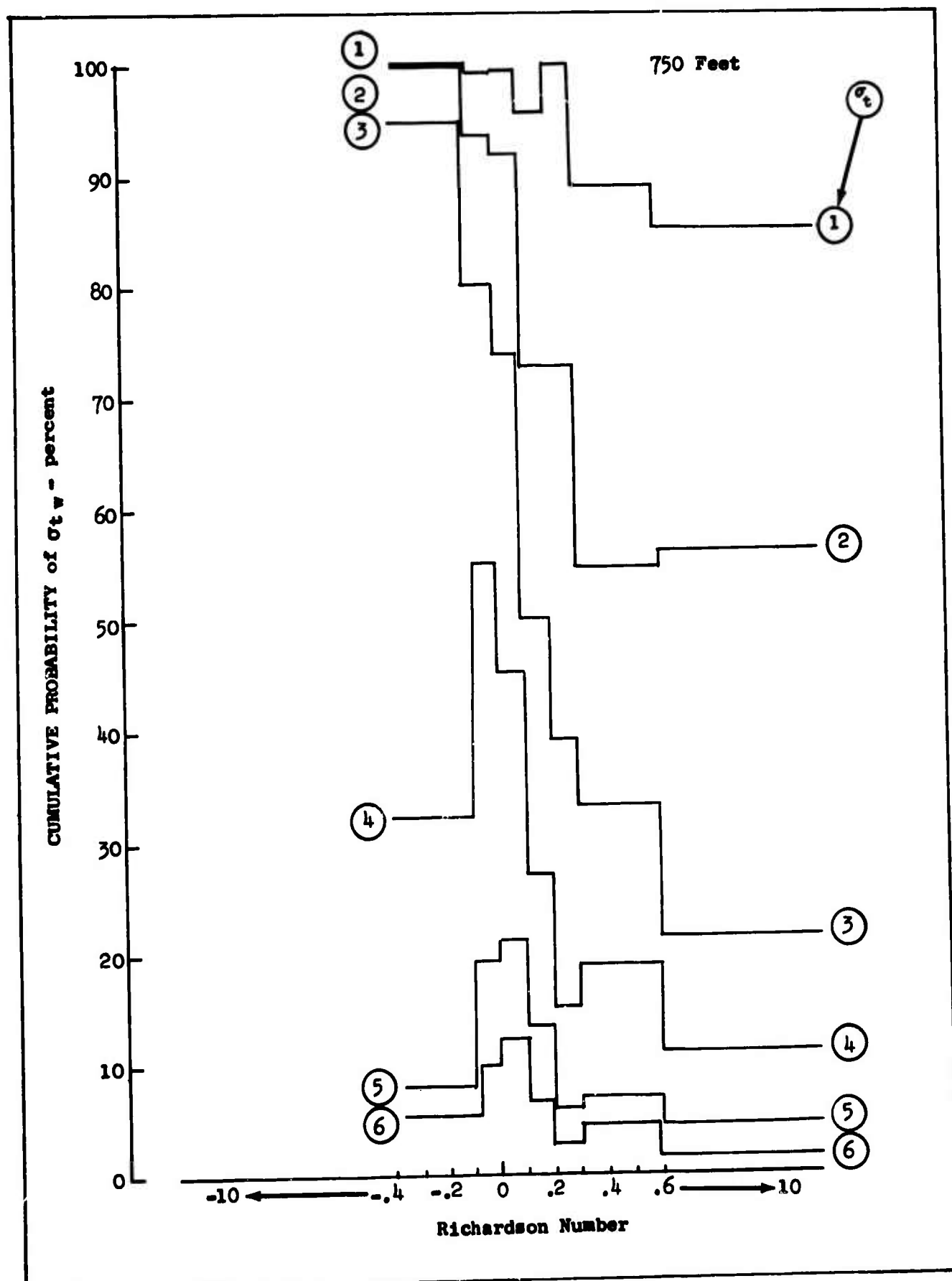


Figure 39.5 Gust Velocity RMS Probabilities Associated with 750 Foot Altitude for Richardson Number Bands

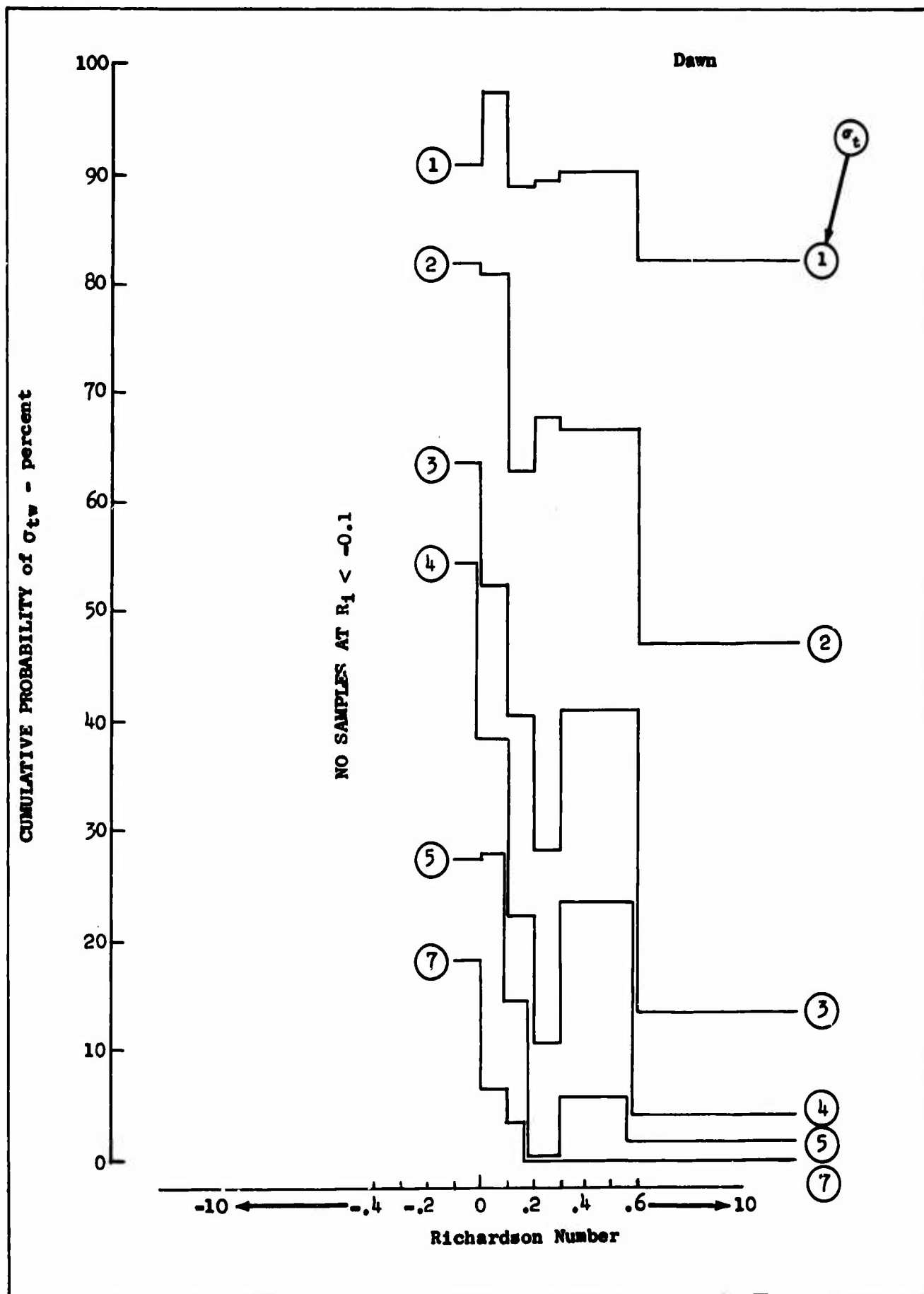


Figure 39.6 Gust Velocity RMS Probabilities Associated with Dawn for Richardson Number Bands

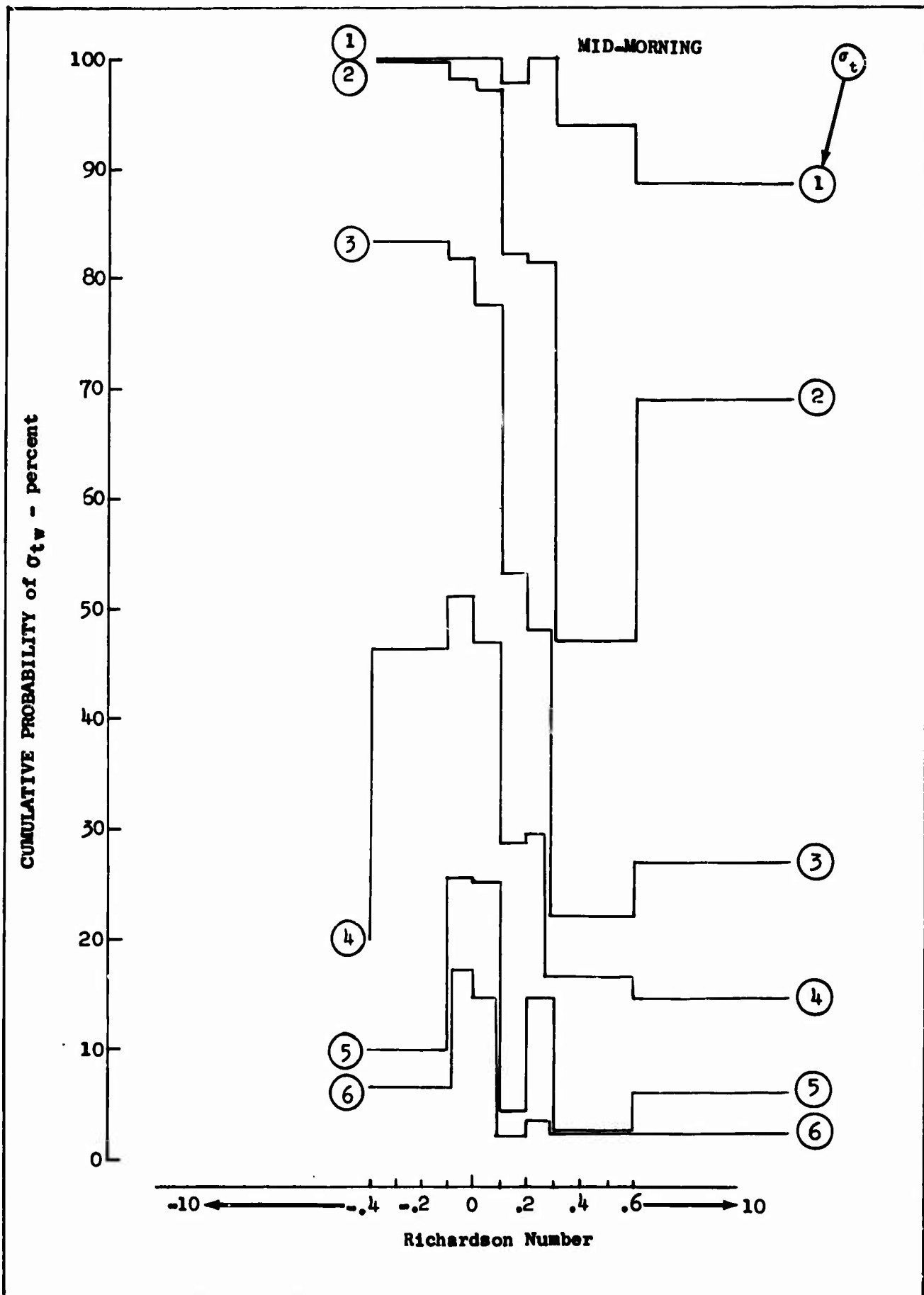


Figure 39.7 Gust Velocity RMS Probabilities Associated with Mid-Morning for Richardson Number Bands

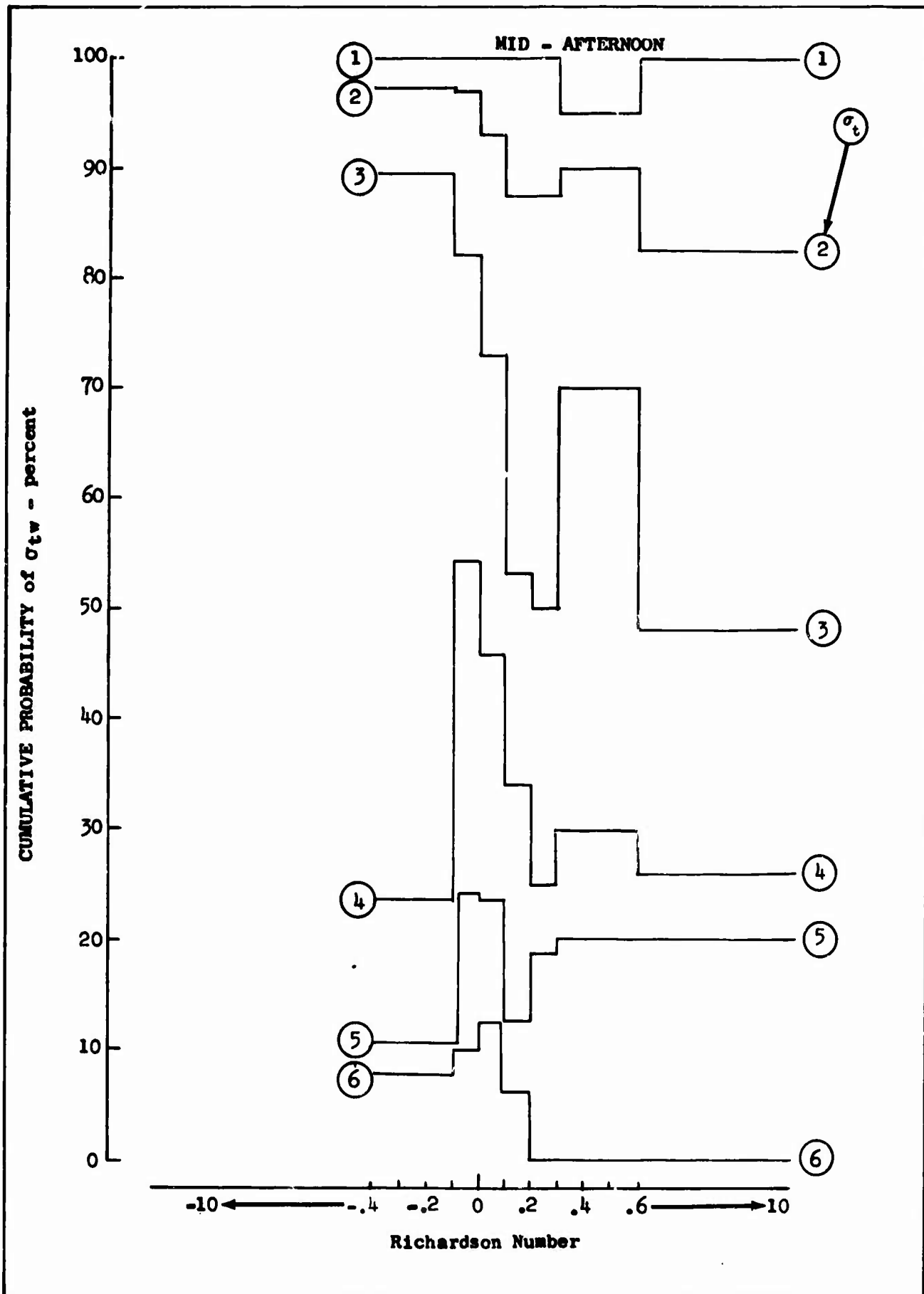


Figure 39.8 Gust Velocity RMS Probabilities Associated with Mid-Afternoon for Richardson Number Bands

40. STABILITY RATIO

A stability ratio was calculated for all turbulence samples recorded during Phase III using the following equation:

$$B = \frac{g}{\tau_a} \left(\frac{\bar{H}}{\bar{W}} \right)^2 \left(\Gamma_d - \Delta T_{az} \right) \quad (40.1)$$

References 40.1 and 40.2 suggest that since B is a function of wind speed rather than wind shear, it is a more suitable parameter than Richardson number to express convective instability. The reason for this, as stated in Reference 40.2, is that wind gradients at the lower levels are usually so small under unstable conditions that Richardson numbers become over sensitive to instrumental inaccuracies in the wind speed measurements. This was not found to be true. The correlations of stability ratio and Richardson number with turbulence intensity were essentially the same as can be seen by comparing the stability ratio in Figures 40.1 through 40.7 with Richardson numbers in Figures 39.1 through 39.8. These curves show that the stability ratio and Richardson numbers produce approximately the same results.

The conclusion regarding stability ratio is that this parameter could be used in place of Richardson number, but it is not necessarily better correlated with turbulence intensity than the Richardson number.

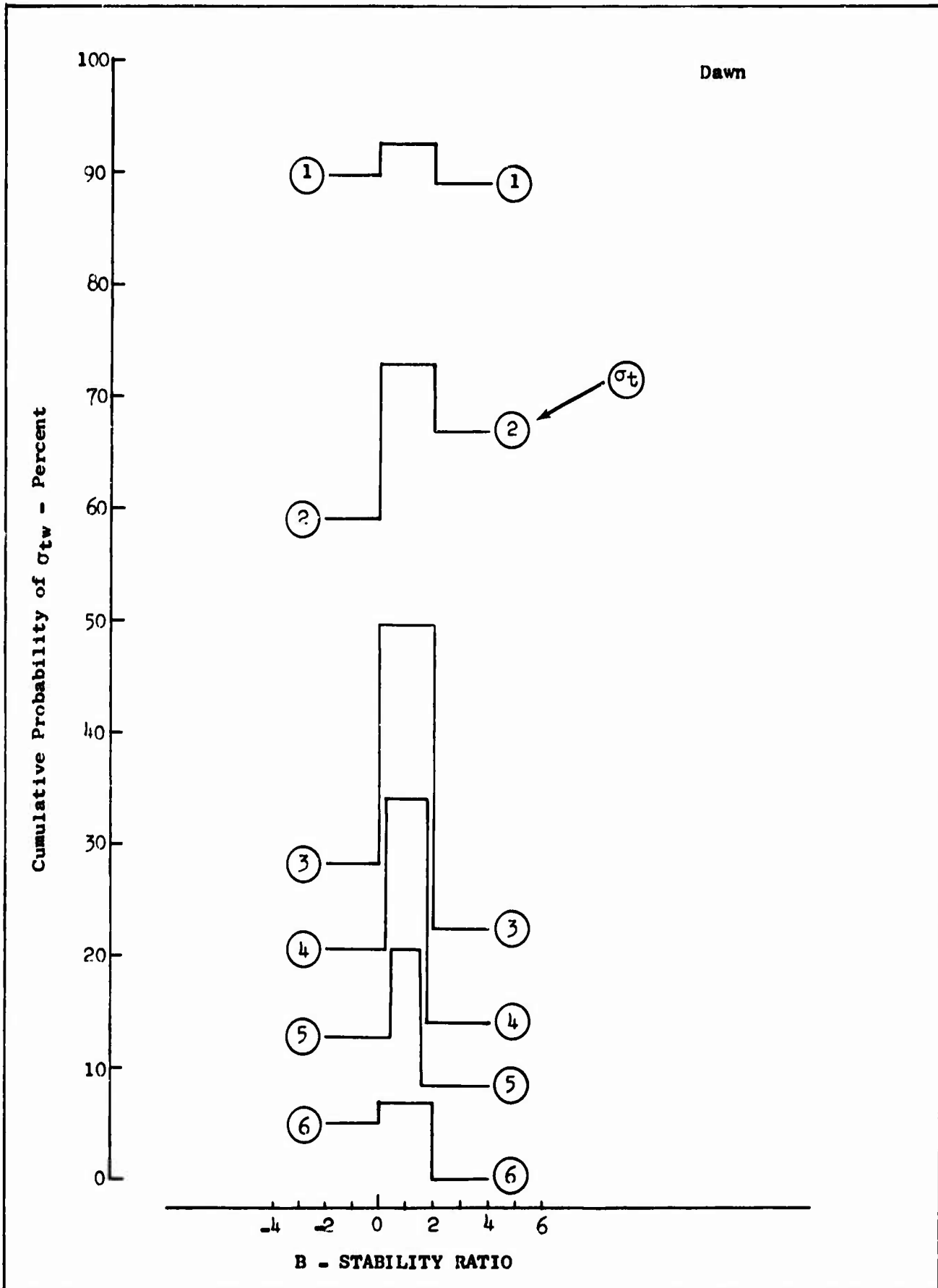


Figure 40.1 Gust Velocity RMS Probabilities Associated with Dawn
for Stability Ratio Bands
153

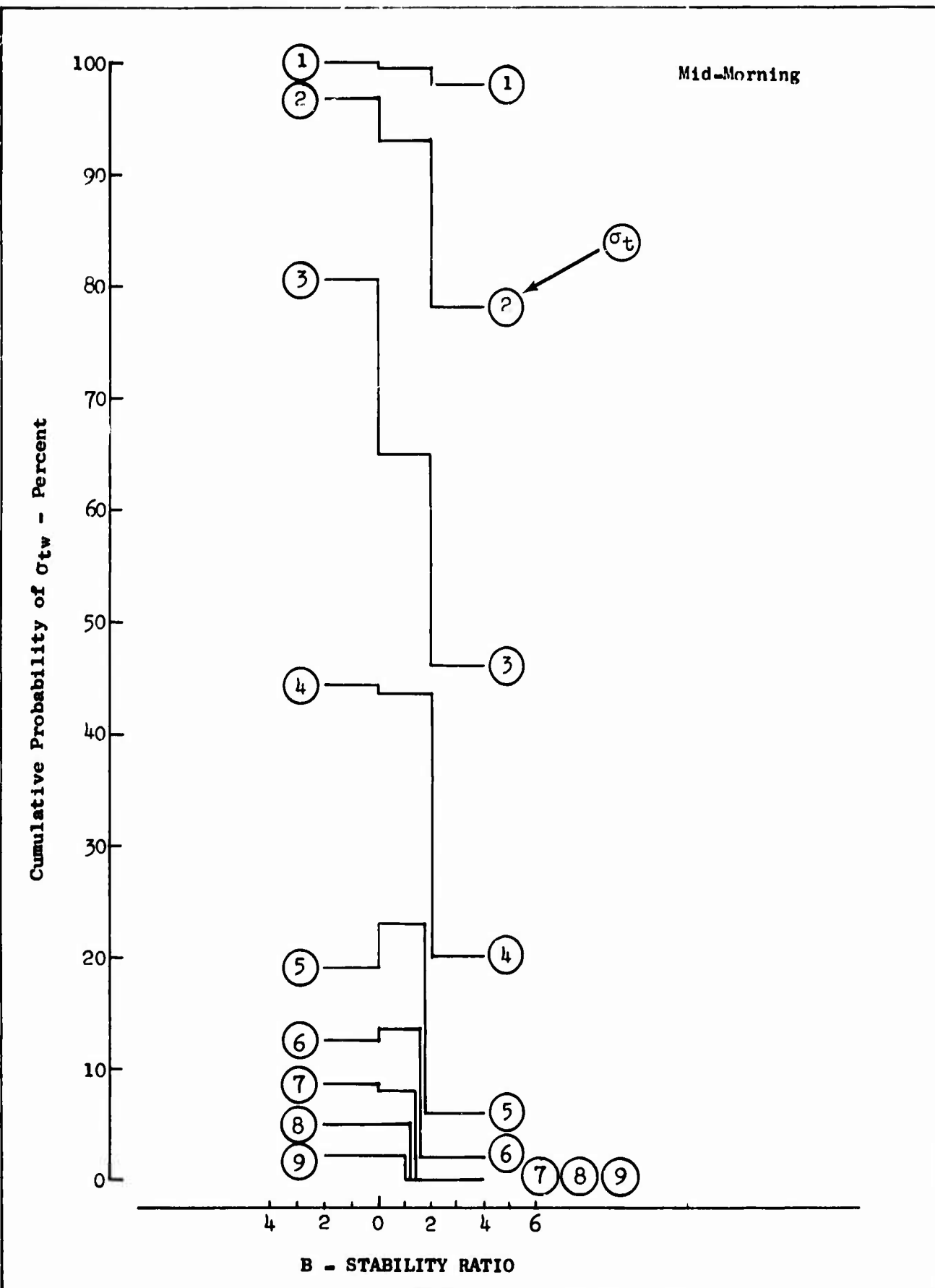


Figure 40.2 Gust Velocity RMS Probabilities Associated with Mid-Morning for Stability Ratio Bands

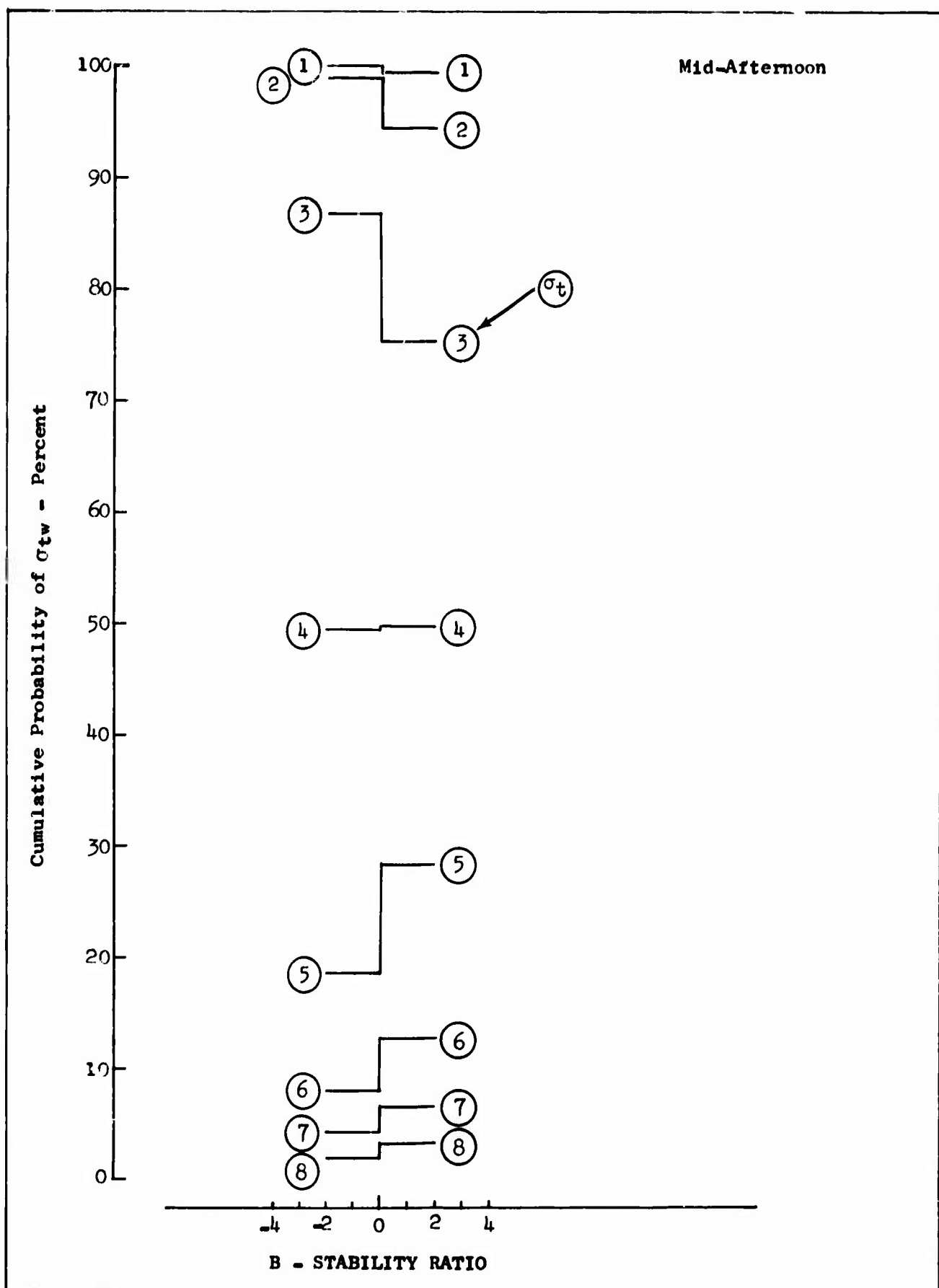


Figure 40.3 Gust Velocity RMS Probabilities Associated with Mid-Afternoon for Stability Ratio Bands

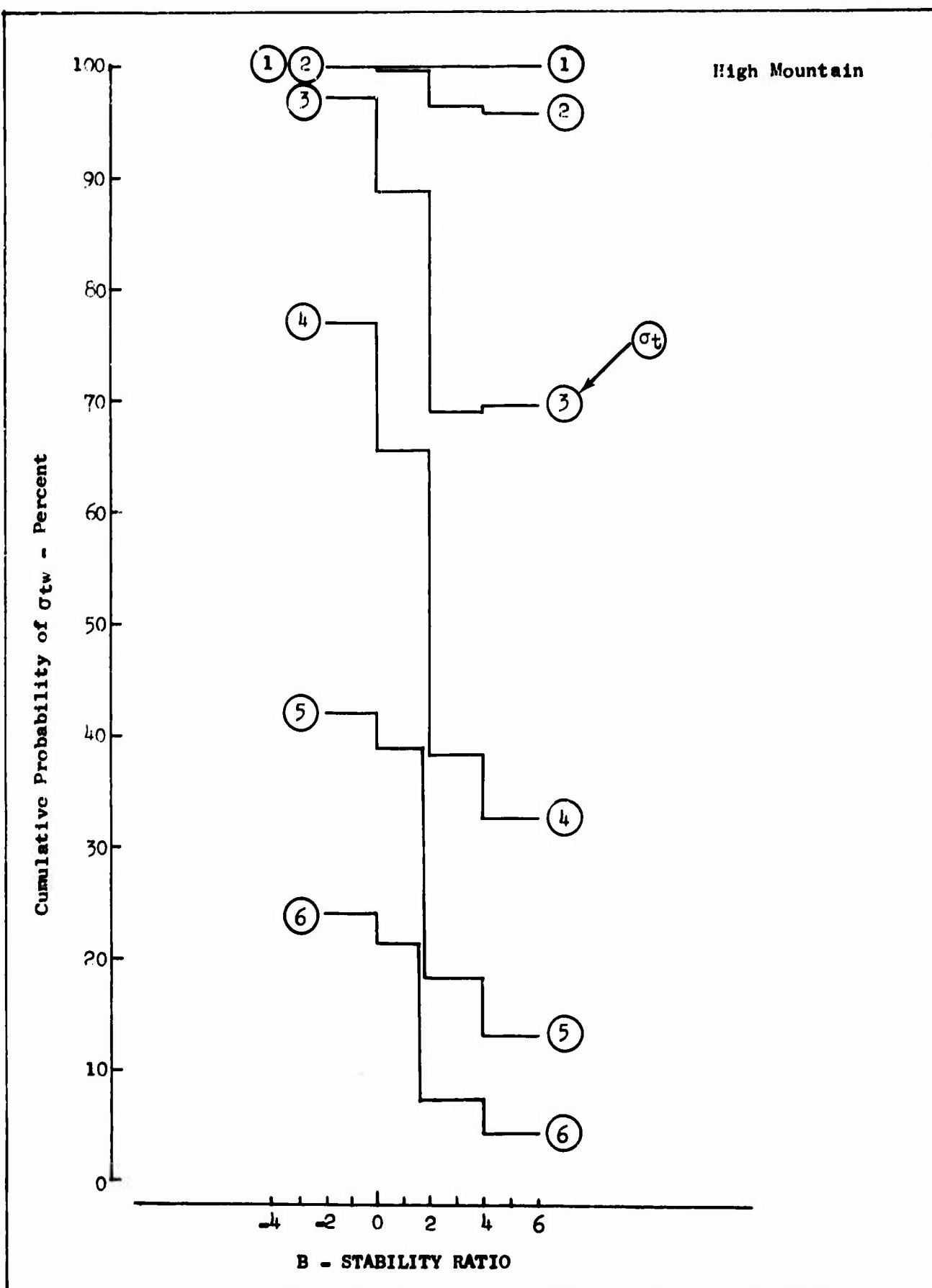


Figure 40.4 Gust Velocity RMS Probabilities Associated with High Mountains for Stability Ratio Bands

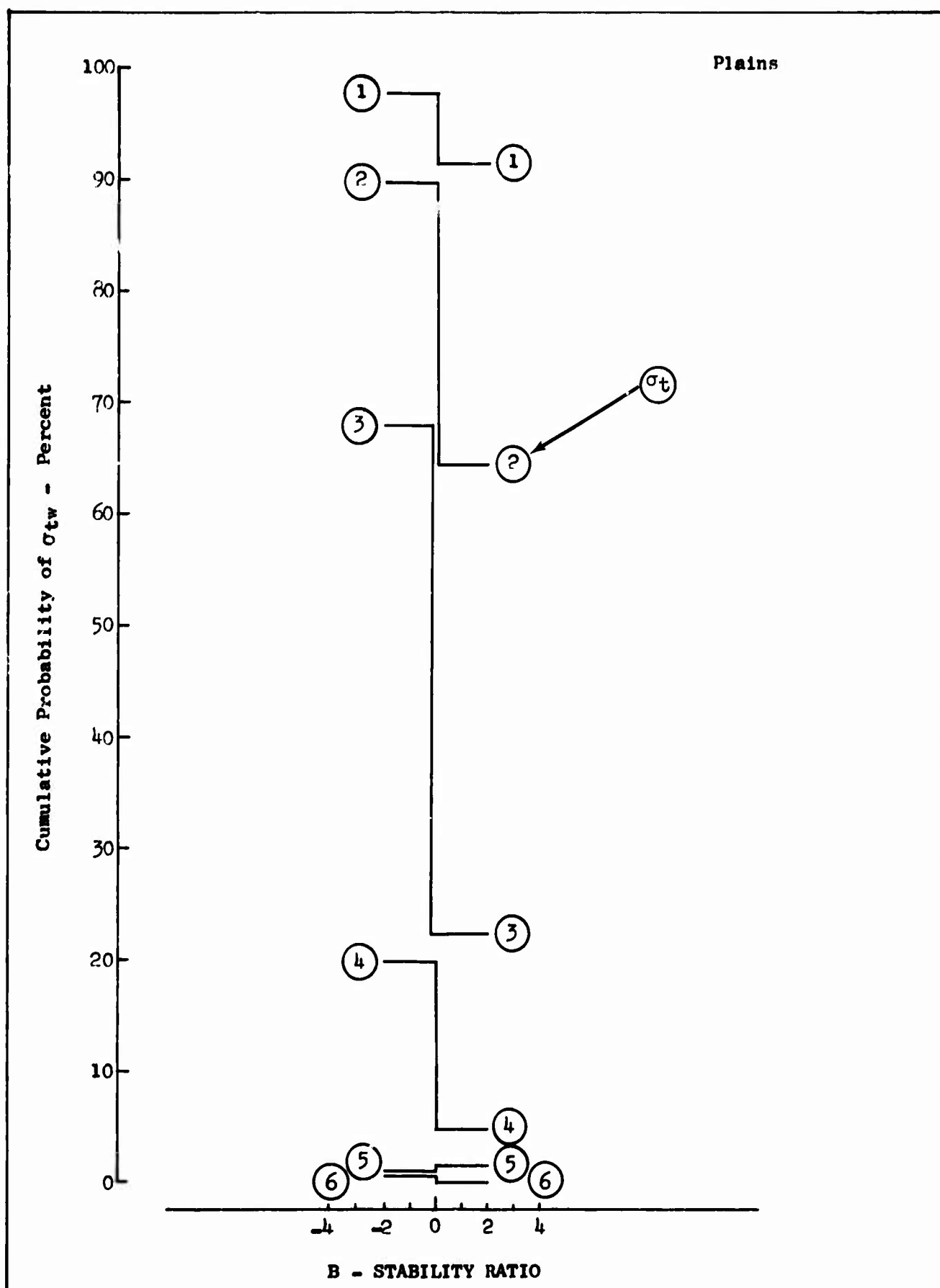


Figure 40.5 Gust Velocity RMS Probabilities Associated with Plains for Stability Ratio Bands

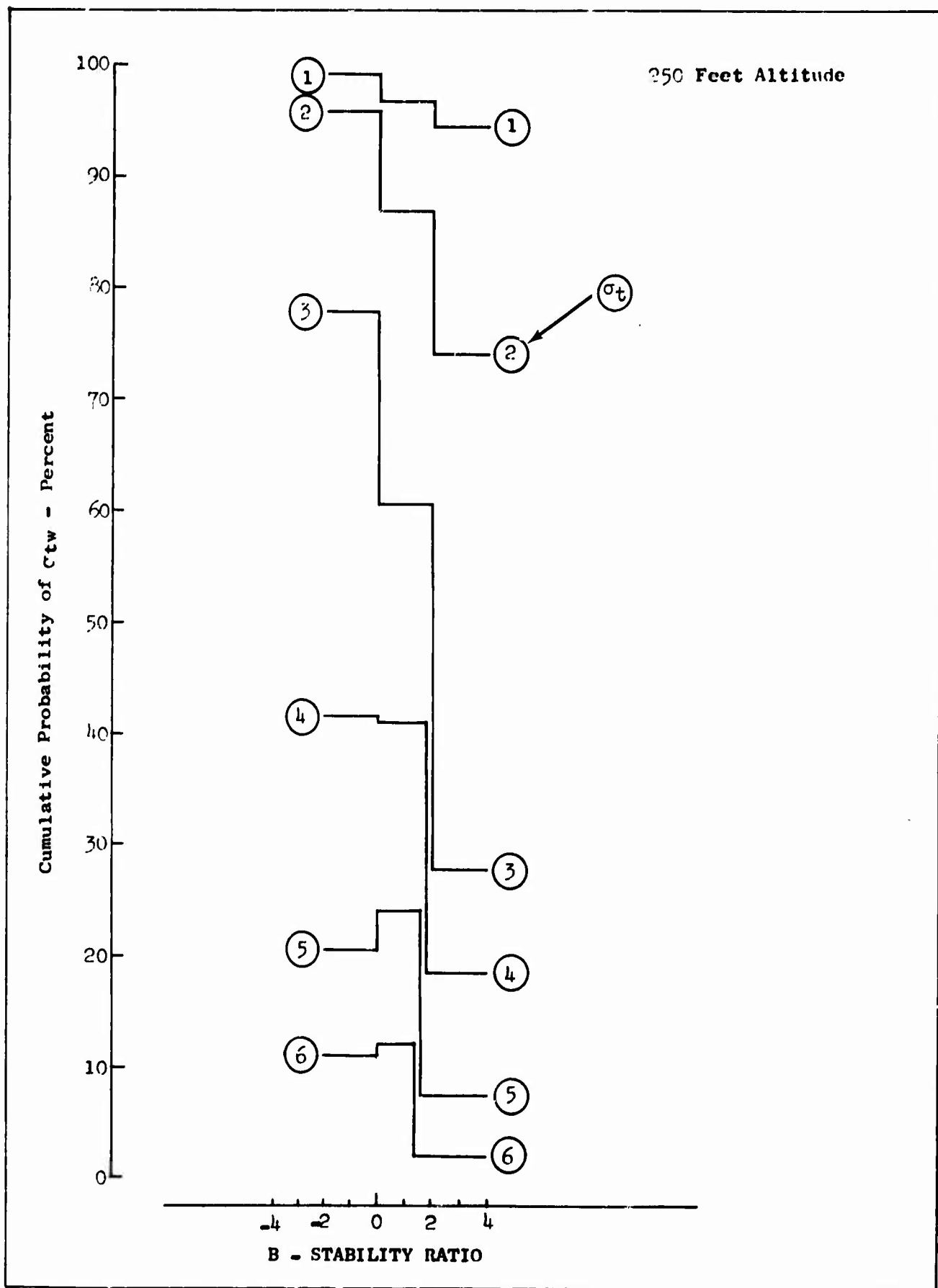


Figure 40.6 Gust Velocity RMS Probabilities Associated with 250-Foot Altitude for Stability Ratio Bands

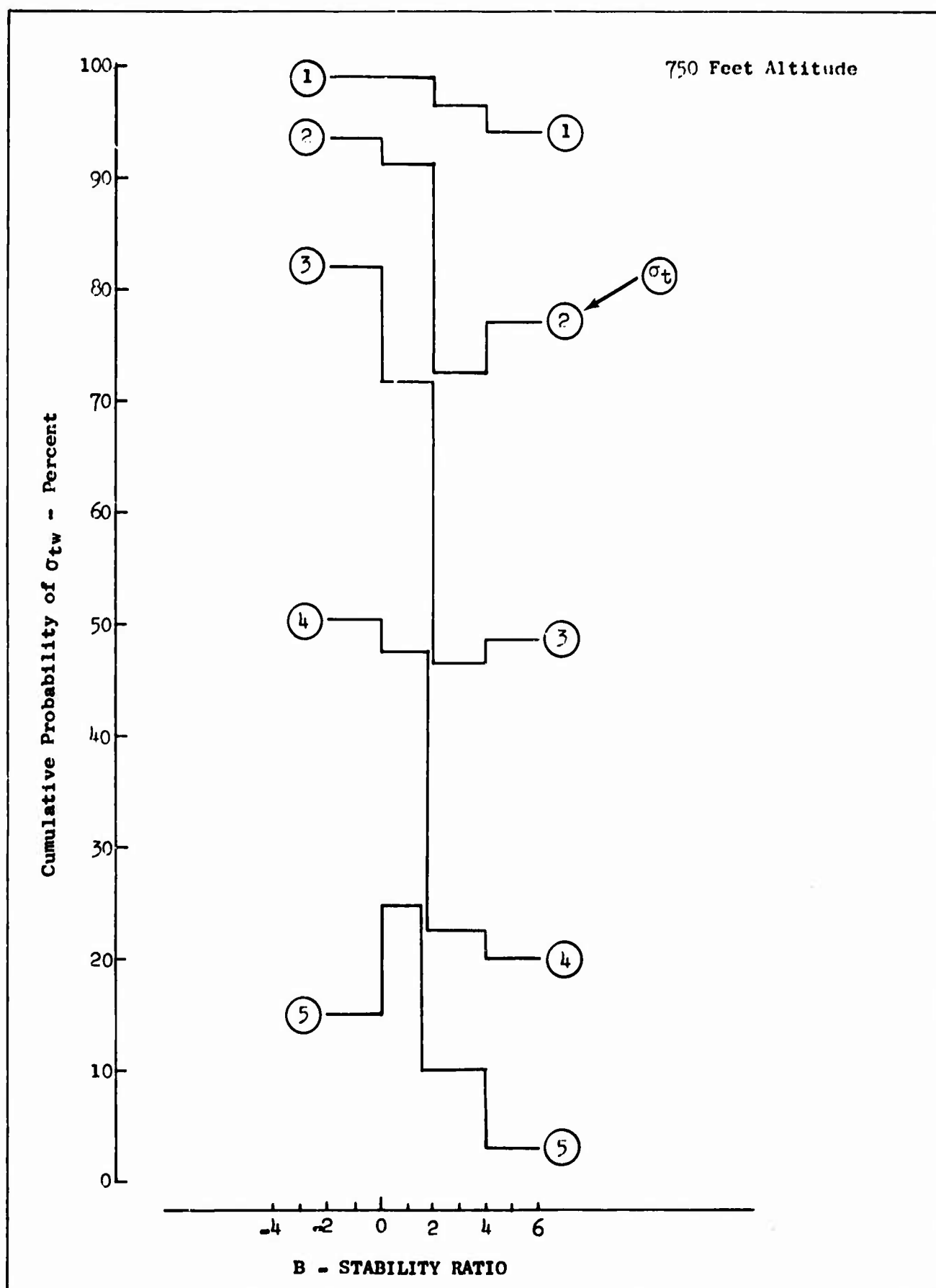


Figure 40.7 Gust Velocity RMS Probabilities Associated with 750-Foot Altitude for Stability Ratio Bands

SECTION VIII

BREN TOWER, THUNDERSTORM, AND WAKE TURBULENCE INVESTIGATIONS

41. BREN TOWER FLYBY

The 1,520-foot BREN Tower is located approximately 74 miles northwest of Las Vegas, Nevada, in restricted area R-4808, as shown in Figure 41.1. Elevation at the base of the tower is 3,640 feet above mean sea level. Terrain in the vicinity is rather mountainous with very little vegetation. The tower is situated on Jackass Flats, which extends to the east-northeast and west-southwest. Terrain elevation increases to a ridge of 5,000 to 7,000 feet within 7 to 12 miles of the northwest and northeast of the tower. Skull Mountain rises to an elevation of 5,500 feet within 3 miles southeast of the tower and Little Skull Mountain rises to 4,500 feet within 4 miles southwest of the tower.

The BREN Tower is instrumented with temperature and wind sensors at the 85, 155, 295, 435, 575, 715, 995, and 1,510-foot levels. Meteorological Research, Inc. Vectorvanes are installed at the 145, 565, and 1,505-foot levels. The MRI Vectorvanes respond to wind velocity, both in the horizontal and vertical planes, from which time histories of the three orthogonal components of velocity can be derived. The response of each vane to fluctuations in azimuth angle, elevation angle, and wind speed was recorded on a strip chart. Only the vanes at the 145 and 565-foot levels were fully operational for this flyby.

The LO-LOCAT T-33 airplane was flown near the tower on 8 January 1969, to obtain concurrent airplane and tower measurements of low altitude turbulence. Eight passes, each approximately nine miles in length, were made on alternate 60-degree and 240-degree magnetic headings.

The first of eight flybys was begun at 1202 PST and the last flyby was completed at 1227 PST. The first four passes were made near the top of the tower and the last four passes were flown near the 565-foot tower level. The wind was reported to be from the north at 27 fps. The pilot reported that the turbulence was light during the passes. Subsequent data processing revealed the maximum gust velocity during the test to be approximately 31 fps. The average of the maximum values for all eight passes was less than 15 fps.

Atmospheric survey data were obtained prior to each flyby flown on the 60-degree heading. The surveys were conducted by flying the airplane over a fixed point at 100 feet and 1000 feet above the terrain. Survey data were used to determine the vertical gradients associated with the flybys made on both the 60 and 240 degree headings.

The first and seventh passes were chosen for spectral analysis because of the good homogeneity and isotropy characteristics of the turbulence. Time histories of the gust velocity components for each of these flybys are shown in Figures 41.2 and 41.3. Variables derived from inflight data are shown in Table 41.1 for each of the two flybys.

TABLE 41.1
BREN TOWER FLYBY DATA

Variable	Pass No. 1	Pass No. 7
σ_{t_u} {fps}	3.36	3.52
σ_{t_v} {fps}	3.52	3.56
σ_{t_w} {fps}	3.31	3.77
W {fps}	26.5	25.8
ΔW_z {fps/ft)	.024	.067
R	.266	-.007
T _G {°F}	80	84
OAT {°F}	44	49
H _p {ft}	5000	4100
V _T {fps}	490	472
d (miles)	8.72	7.96

Power spectral densities from inflight data are shown in Figures 41.4 and 41.5. The von Karman scale lengths were approximately 600 feet. Homogeneity, isotropy, and coherency characteristics are also shown in Figures 41.4 and 41.5.

The surface synoptic analysis for the time of the flybys is shown in Figure 41.6. A cold front moved rapidly through the BREN Tower area about dawn and low-level winds shifted after frontal passage such that they were from the north varying from 15 to 30 knots. The 500 mb synoptic analysis showed a broad trough located west of the Rocky Mountains with moderate flow from the west-northwest over southern Nevada. The sky condition during the flyby consisted of scattered altocumulus below thin broken cirrostratus; visibility was unlimited. Temperature data recorded at five-minute intervals during the flybys are presented in Table 41.2 and indicate that low-level atmospheric conditions were neutral to unstable.

TABLE 41.2
TEMPERATURE (°C) HISTORY FROM BREN TOWER DURING T-33 FLYBY

Tower Level (feet)	Local Time (PST)						
	1200	1205	1210	1215	1220	1225	1230
1510	5.07	5.25	5.56	5.80	5.95	6.03	6.07
995	6.43	6.37	6.90	7.02	7.24	7.47	7.43
715	7.19	7.15	7.71	8.00	8.00	8.22	8.34
575	7.46	7.48	8.00	8.36	8.37	8.47	8.69
435	7.82	7.89	8.36	8.79	8.83	8.86	9.07
295	8.32	8.37	8.88	9.25	9.31	9.29	9.58
155	8.77	8.83	9.33	9.61	9.66	9.73	10.09
85	9.63	9.67	10.03	10.56	10.75	11.03	11.12

Wind velocity data recorded at the tower over the time period from 11:57:52 to 12:31:59 were read from the strip chart to obtain one-second averages. This provided a time history consisting of 2,048 data points. A time history of the fluctuating component was derived by subtracting the mean wind vector for the sample from each one-second average wind vector. The resulting one-second turbulent fluctuation vector was resolved into orthogonal components referenced to the mean wind axis so that in the horizontal plane, the longitudinal component (u) was along the mean wind axis and the lateral component (v) was normal to the mean wind axis. The component in the vertical plane (w) was used as calculated. Time histories of the computed turbulence components showed maximum one-second average wind gusts of 16 to 18 feet per second.

Estimates of power spectral density were computed using the Cooley and Tukey fast Fourier transform algorithm (Reference 41.1). The raw spectral estimates were smoothed using a technique described by Hirsh and Clay (Reference 41.2) and Daniell (Reference 41.3). The technique involved the averaging of adjacent raw spectral estimates to determine a smoothed estimate. Application of this technique provides best results when enough raw estimates are averaged to smooth the spectrum and the averaging is performed over a sufficiently narrow frequency band width so that significant features in the spectrum are not smoothed into adjacent spectral estimates.

When performing spectral analysis on discrete data from a continuous time series, the problem of aliased energy folded about the Nyquist frequency into the sample spectrum must be considered. In this analysis, the undesirable effect of aliasing was suppressed (References 41.4 and 41.5) by taking one-second time averages.

In the comparison of concurrent aircraft and tower measurements of the turbulence spectra, it was assumed that the mean wind speed is sufficiently high such that G. I. Taylor's hypothesis (Reference 18.2) applies. If this hypothesis is valid, space turbulence spectra from the T-33 aircraft measurements should be equivalent to time turbulence spectra from the BREW tower measurements. Also, Lappe (Reference 41.6) reported that changes in the spectrum for varying flight path direction appeared no greater than the changes for identical flight paths.

Turbulence spectra from the aircraft and tower data of the longitudinal, lateral, and vertical components for the 565-foot level are presented in Figures 41.7, 41.8, and 41.9. The spatial frequency plotted on the abscissa was derived from the frequency scale by dividing by the mean horizontal wind speed. The power spectral estimates were multiplied by the mean horizontal wind speed and normalized by dividing by the respective variances.

The spectrum of the vertical gust velocity component obtained from the tower data is compared in Figure 41.10 with spectra published by Kaimal in Reference 41.7. Kaimal's data were obtained during unstable atmospheric conditions using the measurements from sonic anemometers located at several levels on the Cedar Hill Tower in Texas.



Figure 41.1 BREN Tower Location

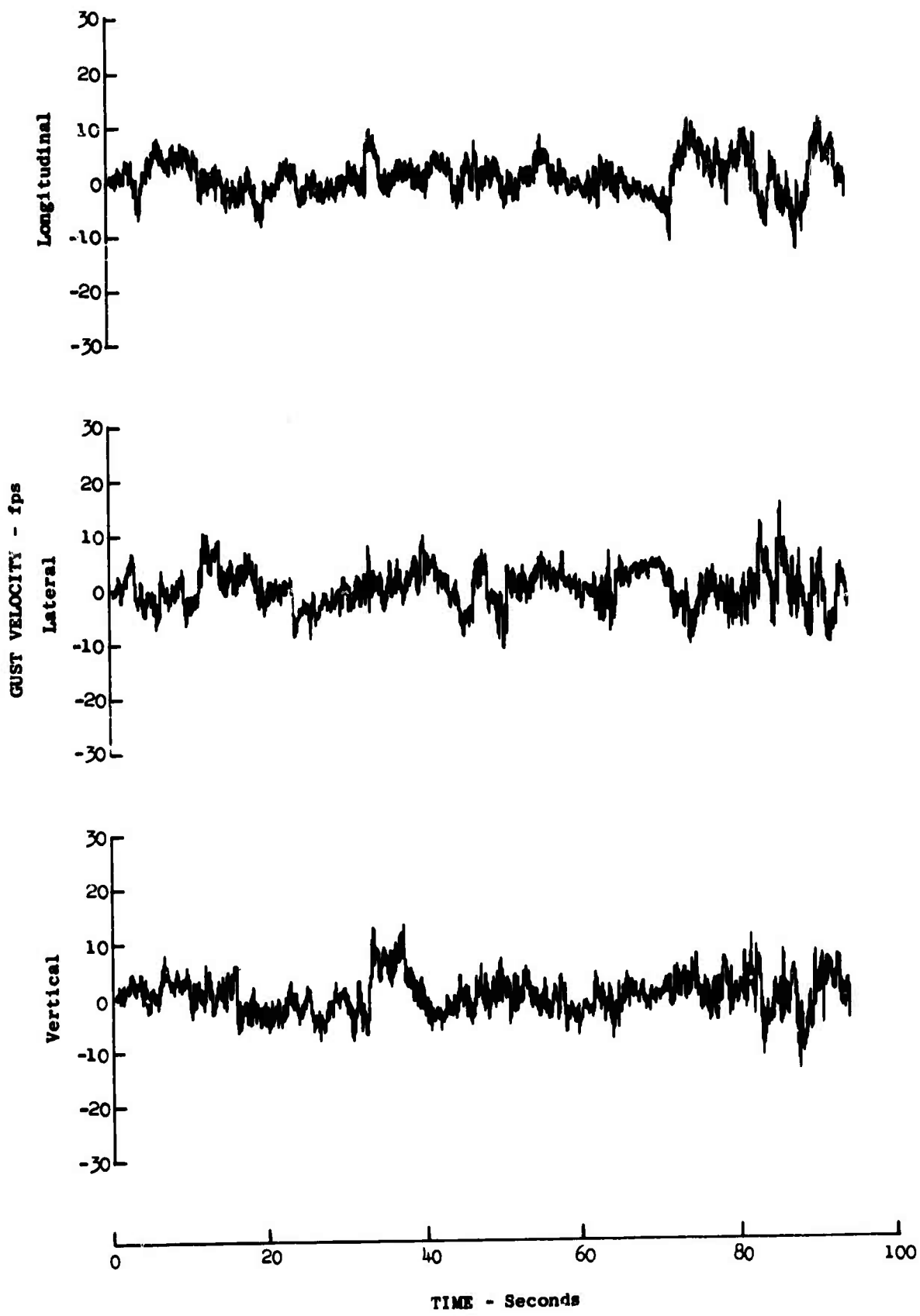


Figure 41.2 Gust Velocity Time History for BREN Tower Fly-by No. 1

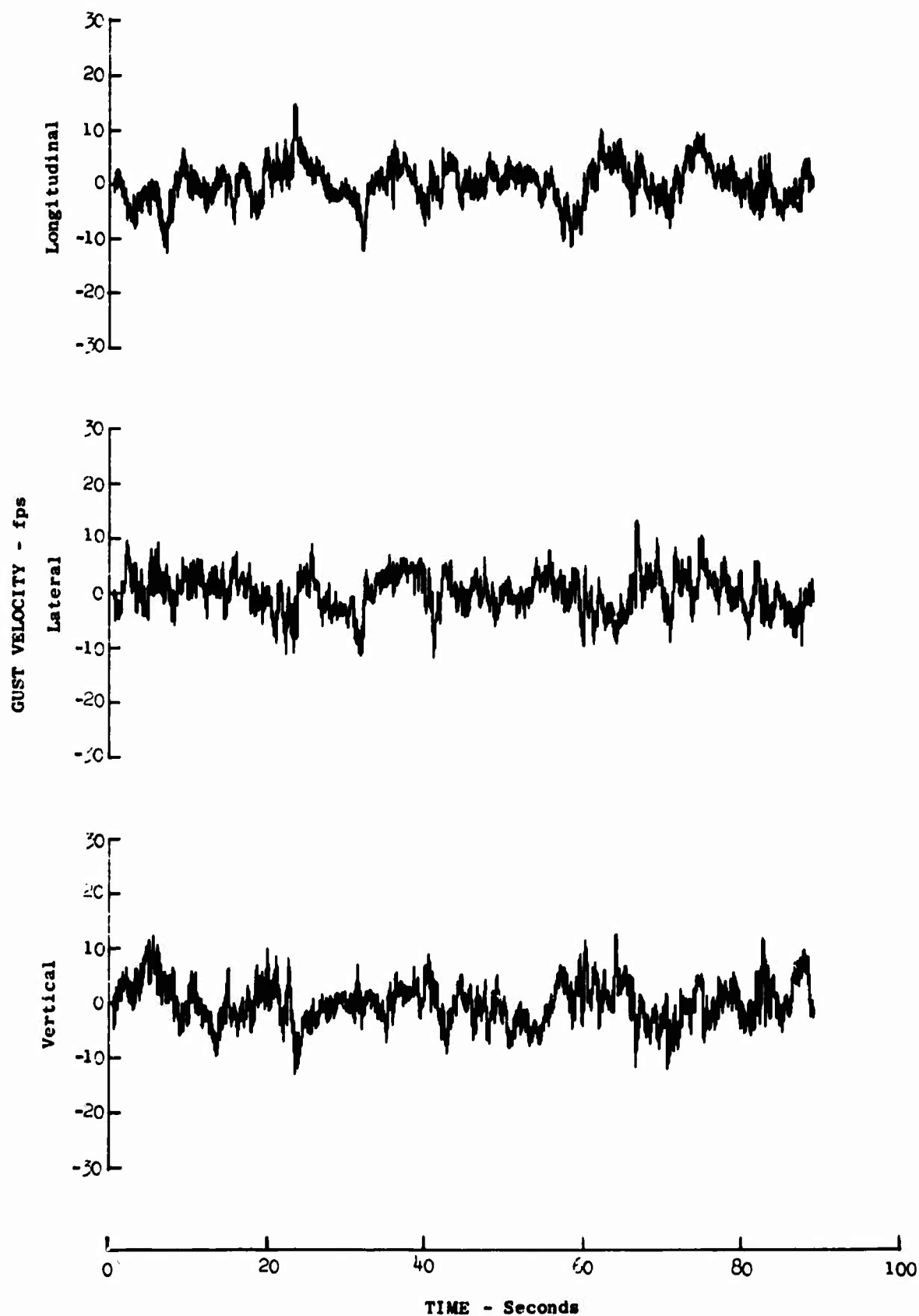


Figure 41.3 Gust Velocity Time History for BREN Tower Fly-by No. 7

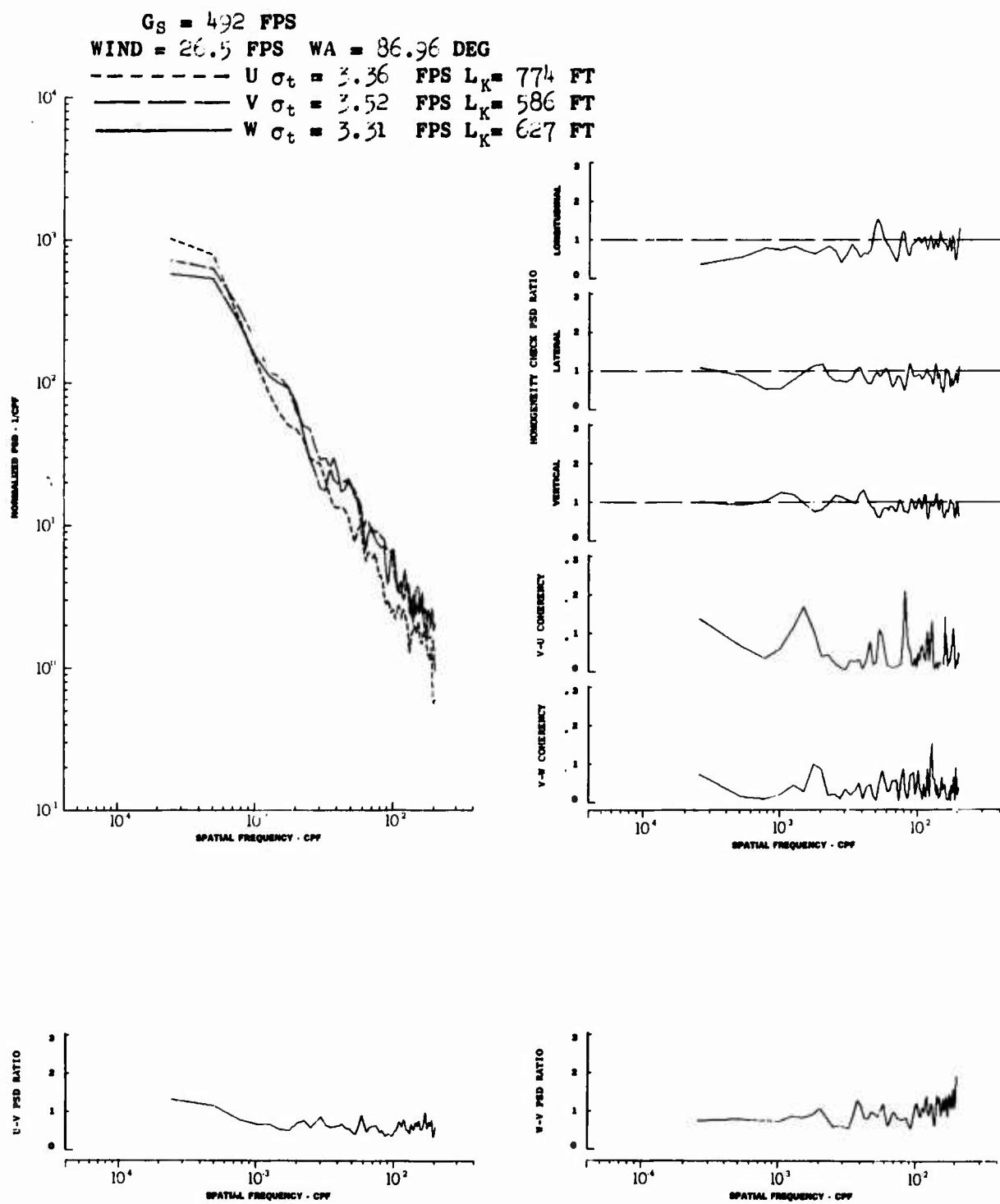


Figure 41.4 Turbulence Spectra Data for BKEN Tower Fly-by No. 1

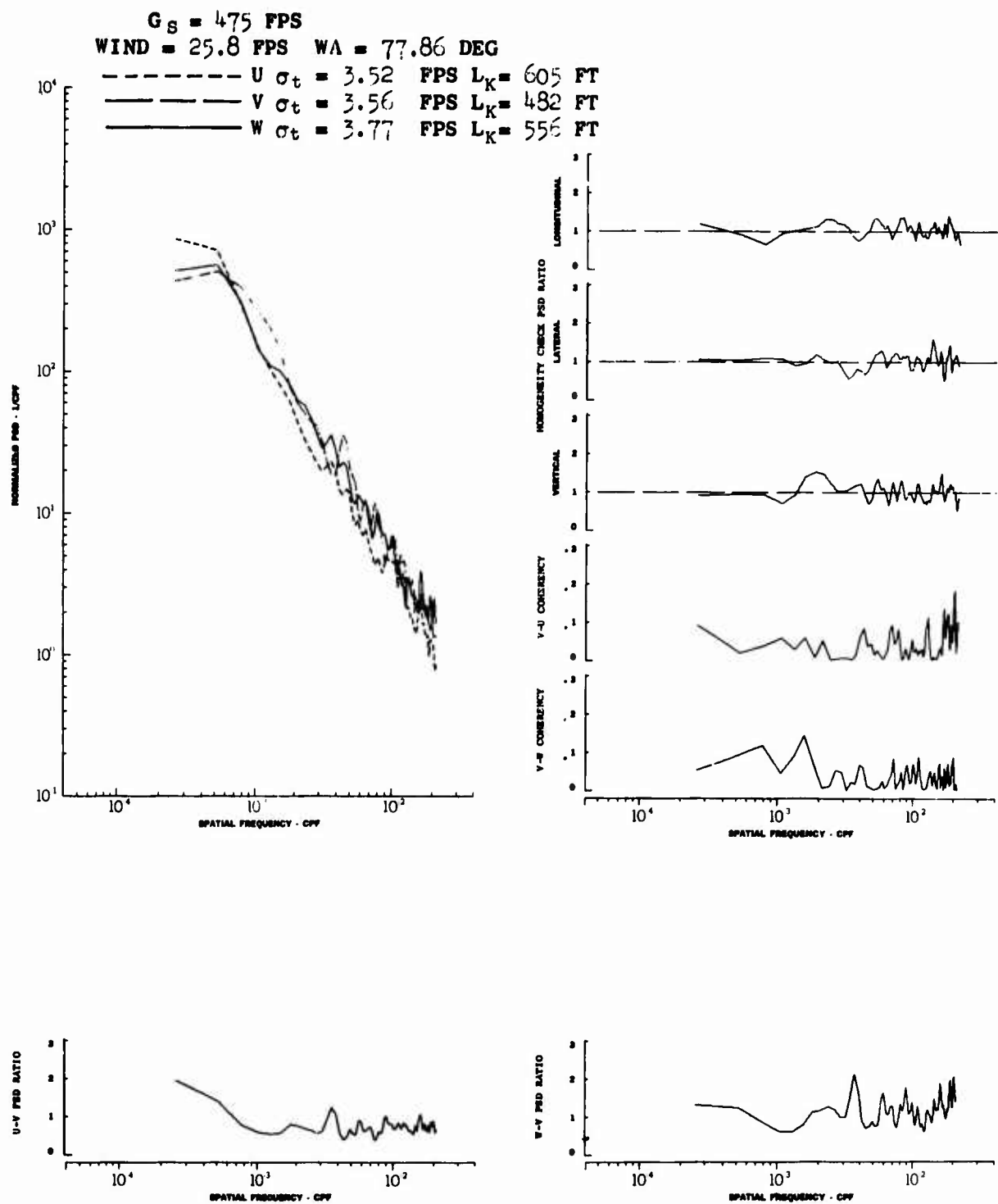


Figure 41.5 Turbulence Spectra Data for BREN Tower Fly-by No. 7

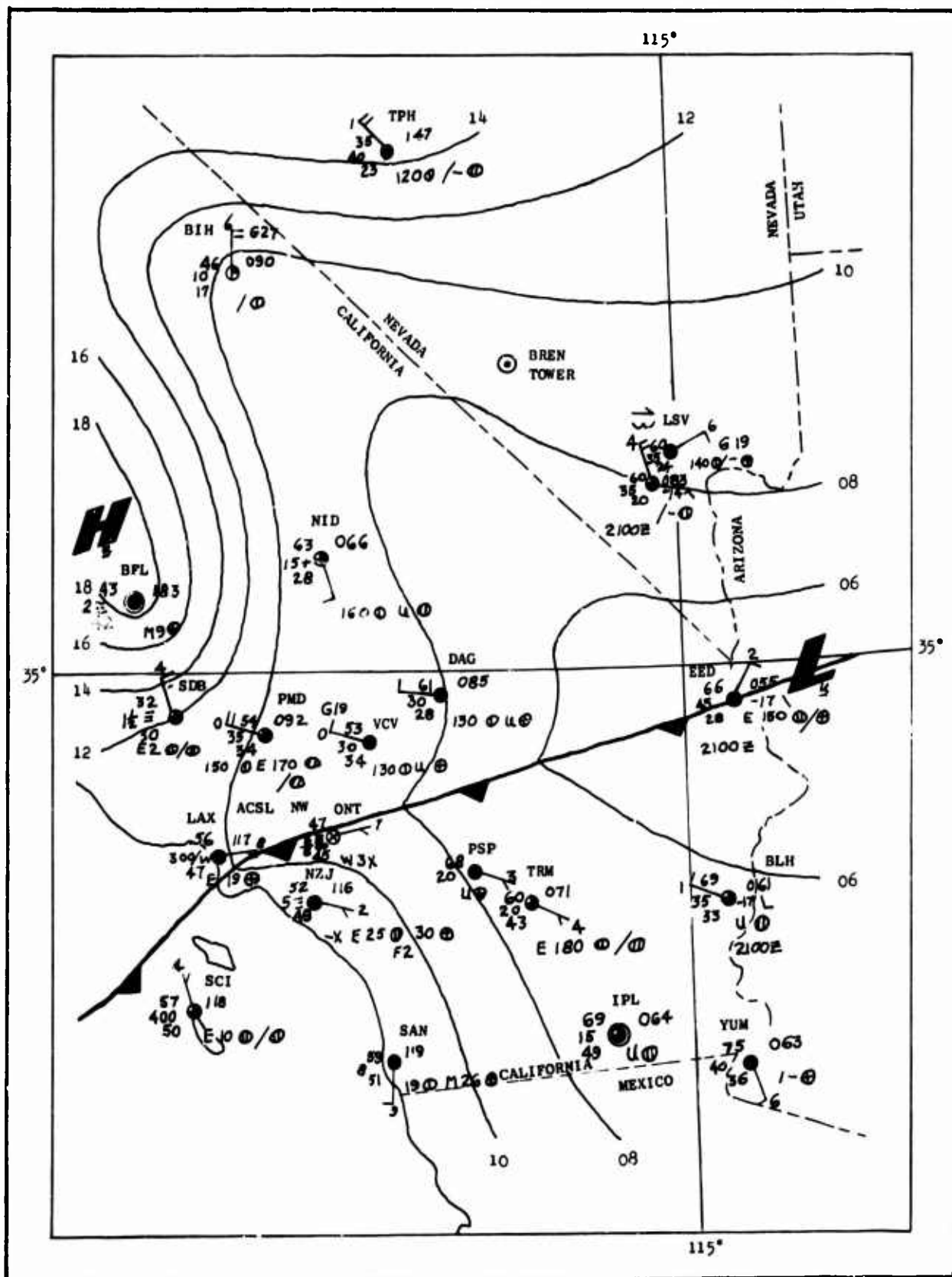


Figure 41.6 Surface Synoptic Analysis, 8 January 1969, 2000 GMT

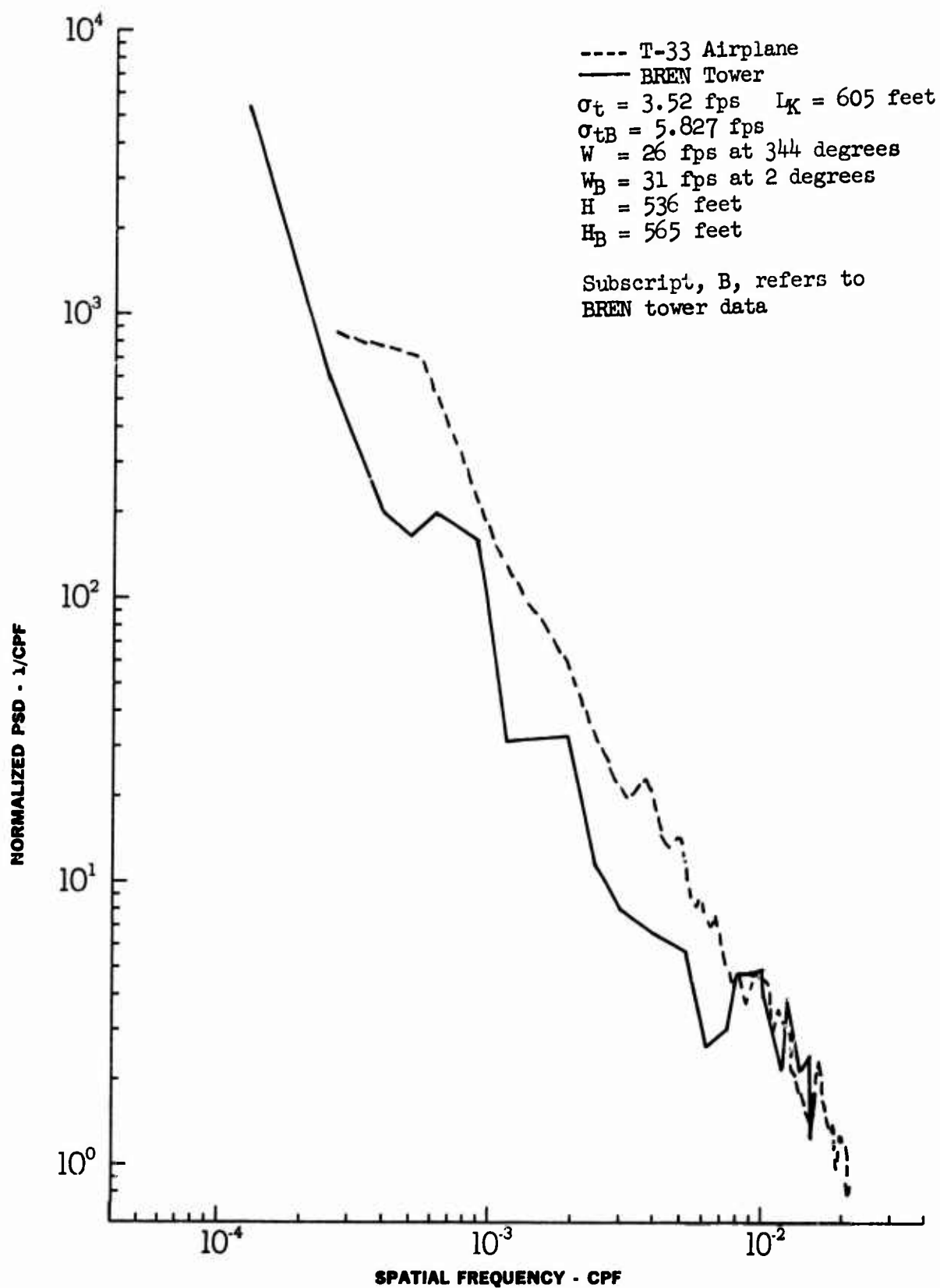


Figure 41.7 Comparison of Longitudinal Spectra from T-33 Airplane to BREN Tower-Fly-by No. 7

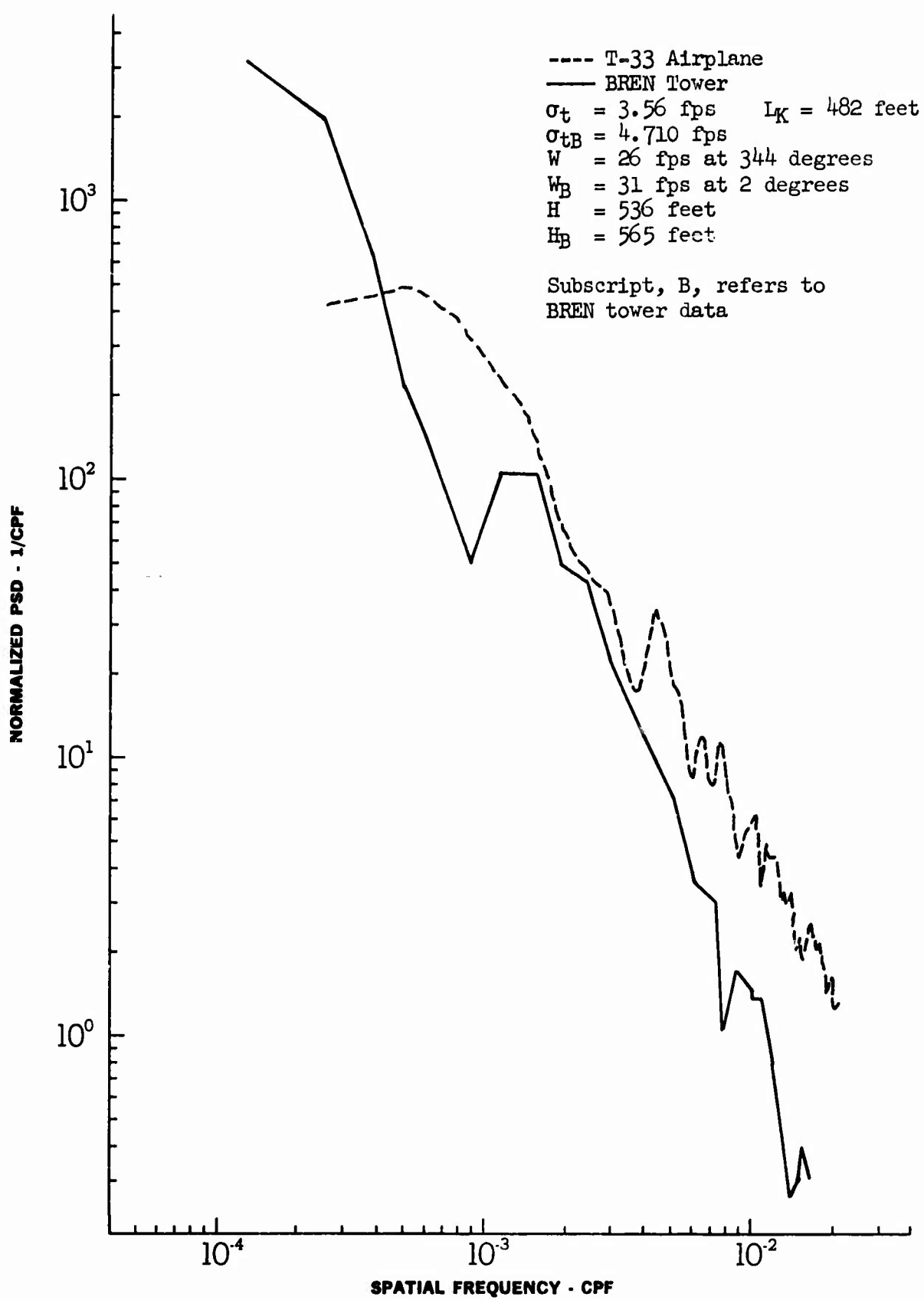


Figure 41.8 Comparison of Lateral Spectra from T-33 Airplane to BREN Tower-Fly-by No. 7

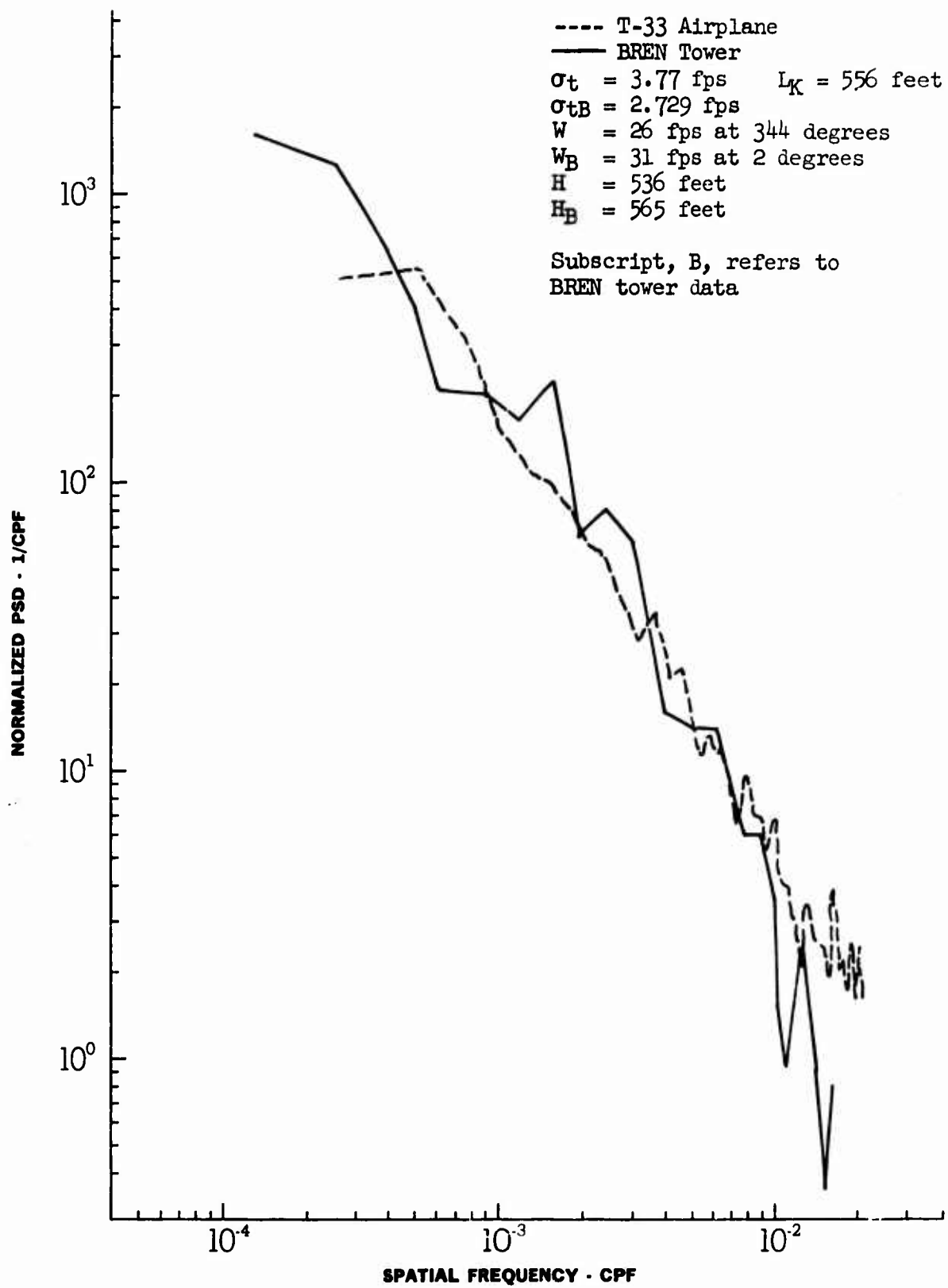


Figure 41.9 Comparison of Vertical Spectra from T-33 Airplane to BREN Tower -Fly-by No. 7

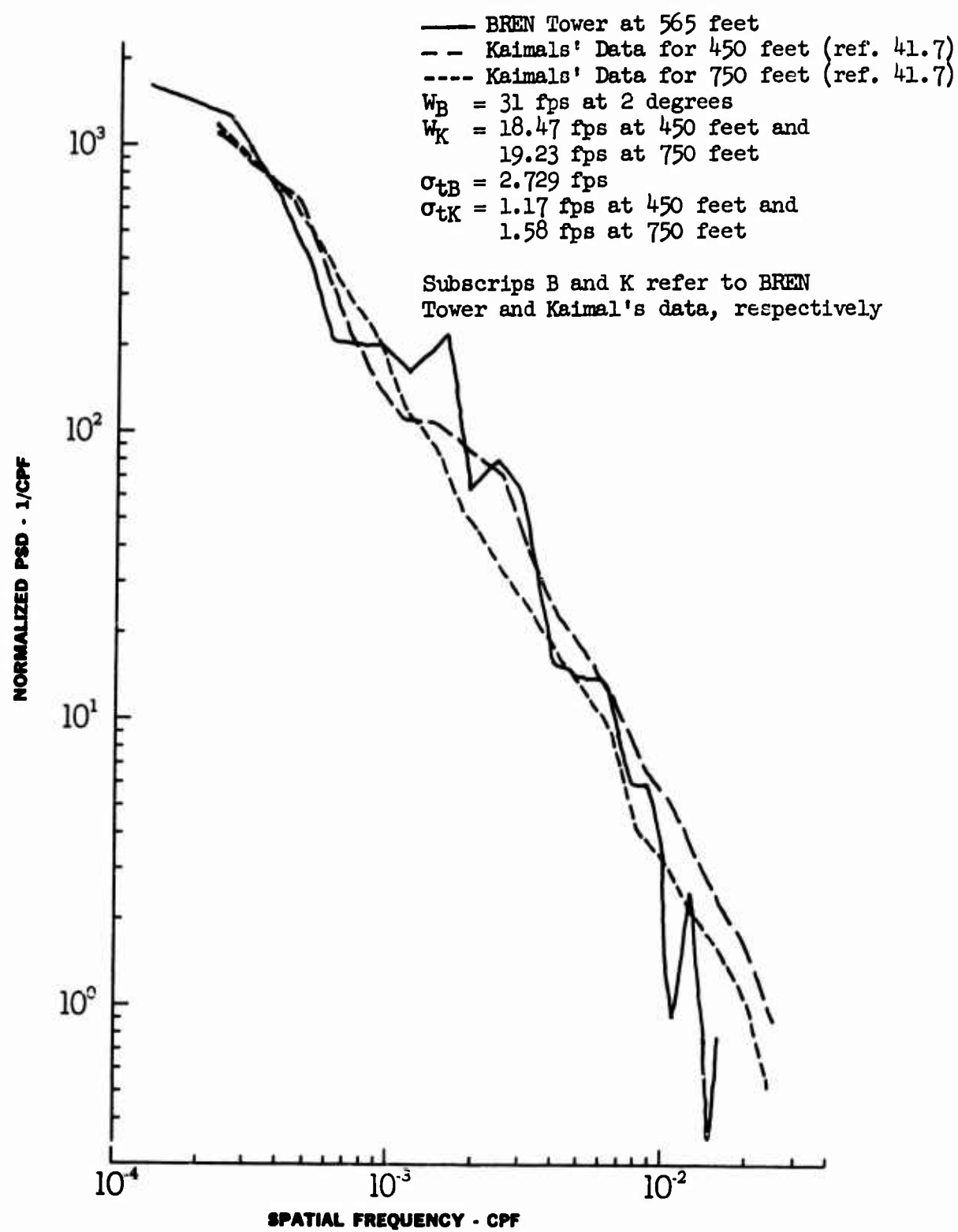


Figure 41.10 Comparison of Vertical Spectra from BREN Tower to that Reported by Kaimal - Fly-by No. 7

42. THUNDERSTORM TURBULENCE

The T-33 airplane was located at Tinker AFB, Oklahoma, from 8 May to 23 May 1969, to support the research activity, Operation Rough Rider, directed by the National Severe Storms Laboratory (NSSL) of Norman, Oklahoma.

Six flights, directed by an NSSL flight coordinator and an FAA controller, were conducted within a 50-mile radius of the NSSL installation to obtain gust velocity and meteorological data near thunderstorms and convective cloud formations. Unfortunately, no severe thunderstorm activity developed in this area during the above time period.

The FAA controller provided air traffic separation and direction while the NSSL flight coordinator maintained surveys of possible unsafe weather situations and notified the pilot of any advisable changes in the flight plan. The 50-mile radius, shown in Figure 42.1, was determined primarily by the limitations in the radars capability to provide detailed weather information. Also, the control radar and voice communication capabilities were marginal beyond 50 miles.

A total of thirty-five samples were recorded near thunderstorm activity and, on one flight, data were recorded during five passes made near the instrumented WKY-TV tower.

Data were obtained as during standard low level flights. The sample lengths were 4-1/2 minutes in duration with exception to the tower flybys which were approximately 2 minutes in duration. Prior to each sample, 5 seconds of data were recorded above and below the sample altitude to provide vertical gradient information. Terrain in the flight area generally resembled the plains-type terrain on the McConnell route. The data samples were examined at various stages in the processing sequence. Only the twelve samples shown in Table 42.1 were considered to be valid in all respects. The primary problem with the other samples was the presence of extraneous noise spikes in the airspeed measurement. These spikes were probably the result of precipitation entering the probes pressure sensing ports.

Time histories of the gust velocity components, normal acceleration at the airplane center of gravity, and total air temperature (ambient plus ram rise) were computed for each of the valid samples and are shown in Figures 42.2 through 42.13. Meteorological data, gust velocity standard deviations, and other pertinent parameters were calculated for each of these samples and are presented in Table 42.2. The maximum derived equivalent gust velocity for each sample was calculated from Equation 42.1:

$$U_{de} = (k) \Delta N_{zcc} \quad (42.1)$$

where: $k = \frac{2W}{C_L \cdot \rho_0 \cdot SV_e \cdot K_g}$ (refer to Section 15)

Values of k , which varied with airspeed and altitude, and maximum equivalent gust velocity are also presented in Table 42.2 for each valid sample.

The gust velocity time histories in Figures 42.2 through 42.13 indicate that increases in turbulence intensity may correspond to the proximity of the clouds. Also, there appears to be a total temperature variation corresponding with the gust velocity variations, however, the degree of variation is inconsistent between samples. Exact correlations between total temperature and gust velocity variations were not accomplished because the temperature measurement was not compensated for frequency response. In addition, this variable was smoothed using a 100 data point moving time averaging technique which decreased its frequency response characteristics. This problem was discussed in Section 18.

Gust velocity power spectra are shown in Figure 42.14 for three selected turbulence samples. These samples were chosen on the basis of exhibiting good homogeneous turbulence characteristics. The turbulence intensity, as indicated by the time series standard deviations, was less than or equal to that encountered during low altitude flight over plains terrain.

Conclusions regarding these data are as follows:

- The turbulence intensity recorded near these convective clouds was low.
- Power spectra of the turbulence indicates that the $-5/3$ logarithmic slope relationship occurs near cumulus clouds.
- Air temperature changes near the cumulus clouds occurred, in some instances, when turbulence was encountered.

A more detailed analysis of these data will be accomplished by NSSL.

TABLE 42.1

TEST LOG OF VALID DATA RECORDED FOR OPERATION
ROUGH RIDER (1969) BY THE LO-LOCAT T-33A AIRPLANE

Date	Test	Sample No.	Descriptive Flight Information
12 May 1969	270	15 18	Flight to West (rear) and South of convective cloud southeast of Norman, Oklahoma
15 May 1969	273	3 12 15	Flight near convective cloud south of Norman (360° and 180° headings) and north of Tinker AFB (251° heading). Build-ups to 20,000 feet.
16 May 1969	274	3*	Flight under convective cloud, 3000 feet, 180° heading.
20 May 1969	275	9 12	Flyby of WKY-TV tower, 500 feet and 1000 feet, respectively, 120° and 300° headings.
		21 24* 27* 30	Cross country to Ponca City and return to Tinker AFB, flying at base of clouds. A frontal line lay between Normal and central Kansas. Only light turbulence was reported.

* Power spectra computed for these conditions.

TABLE 42.2
METEOROLOGICAL DATA AND GUST VELOCITY STANDARD DEVIATIONS

Test	270		273		274		
Date	5/12/69		5/15/69		5/16/69		
Variable	Sample No.	15	18	3	12	15	3
σ_{t_s} (fps)		1.71	3.01	1.61	2.16	2.32	2.57
σ_{t_v} (fps)		2.09	3.34	1.67	2.34	2.47	2.73
σ_{t_w} (fps)		2.43	2.68	1.43	2.62	2.56	2.45
T _G (°F)		87.2	94.5	91.3	99.7	100.7	95.5
T _a (°F)		44.9	44.9	64.8	66.4	66.4	67.0
W (fps)		8.8	20.9	29.1	35.0	31.4	21.8
W _D (deg)		62.5	243.2	195.7	161.4	146.7	152.0
ΔT _s (°F/1000 ft)		-4.00	-3.31	-2.35	-5.50	-5.78	-3.57
Ri		2.21	0.140	5.52	0.000	-0.056	0.316
P _s (in.-Hg)		21.652	21.741	27.760	26.946	26.996	26.852
V _T (fps)		652.1	654.2	549.1	558.1	574.7	563.7
G _S (fps)		654.0	661.1	578.0	592.6	546.8	544.7
ΔW _Z (fps/ft)		0.007	0.032	0.006	0.017	0.018	0.019
ΔW _H (fps/mile)		0.144	0.235	1.173	0.546	0.524	0.197
S (miles)		33.4	33.8	29.6	30.3	28.0	27.9
B		87.81	23.19	2.55	-0.0279	-0.521	8.172
w _{max} (fps)		31	15	8	23	17	14
k (fps)		14.67	14.67	17.29	17.29	17.29	17.04
U _{de max} (fps)		16.6	11.0	6.9	9.5	11.2	7.7

TABLE 42.2 (Contd.)
METEOROLOGICAL DATA AND GUST VELOCITY STANDARD DEVIATIONS

Test Date	Sample No.	275				
		5/20/69				
Variable	9	12	21	24	27	30
σ_{t_u} (fps)	2.42	2.16	1.66	1.80	1.76	2.18
σ_{t_v} (fps)	3.30	2.11	1.86	1.95	1.86	1.87
σ_{t_w} (fps)	2.09	2.21	1.74	1.63	1.62	2.18
T_c ($^{\circ}$ F)	105.4	107.1	99.9	99.4	101.3	101.6
T_a ($^{\circ}$ F)	80.0	77.1	65.8	66.0	66.2	66.8
W (fps)	26.3	22.9	30.1	27.5	27.5	26.2
W_D (deg)	122.5	145.9	124.0	132.1	131.8	140.5
ΔT_s ($^{\circ}$ F/1000 ft)	-4.68	-5.80	-5.48	-5.08	-5.22	-5.19
Ri	0.165	-0.199	0.007	0.432	0.434	0.099
P_s (in.-Hg)	28.341	27.816	25.979	25.978	25.893	25.983
V_T (fps)	476.0	451.4	541.0	544.2	541.6	553.2
G_s (fps)	449.8	472.2	552.2	526.3	523.5	533.9
ΔW_z (fps/ft)	0.017	0.009	0.012	0.008	0.006	0.014
ΔW_H (fps/mile)	0.648	0.846	0.411	0.258	0.223	0.033
S (miles)	7.5	16.2	28.2	26.9	26.8	27.3
B	0.126	-0.247	0.0555	0.0002	0.0002	0.0002
w_{max} (fps)	10	12	11	9	10	15
k (fps)	21.16	21.16	17.60	17.60	17.60	17.60
$U_{de\ max}$ (fps)	12.7	9.5	8.8	9.7	9.7	7.9

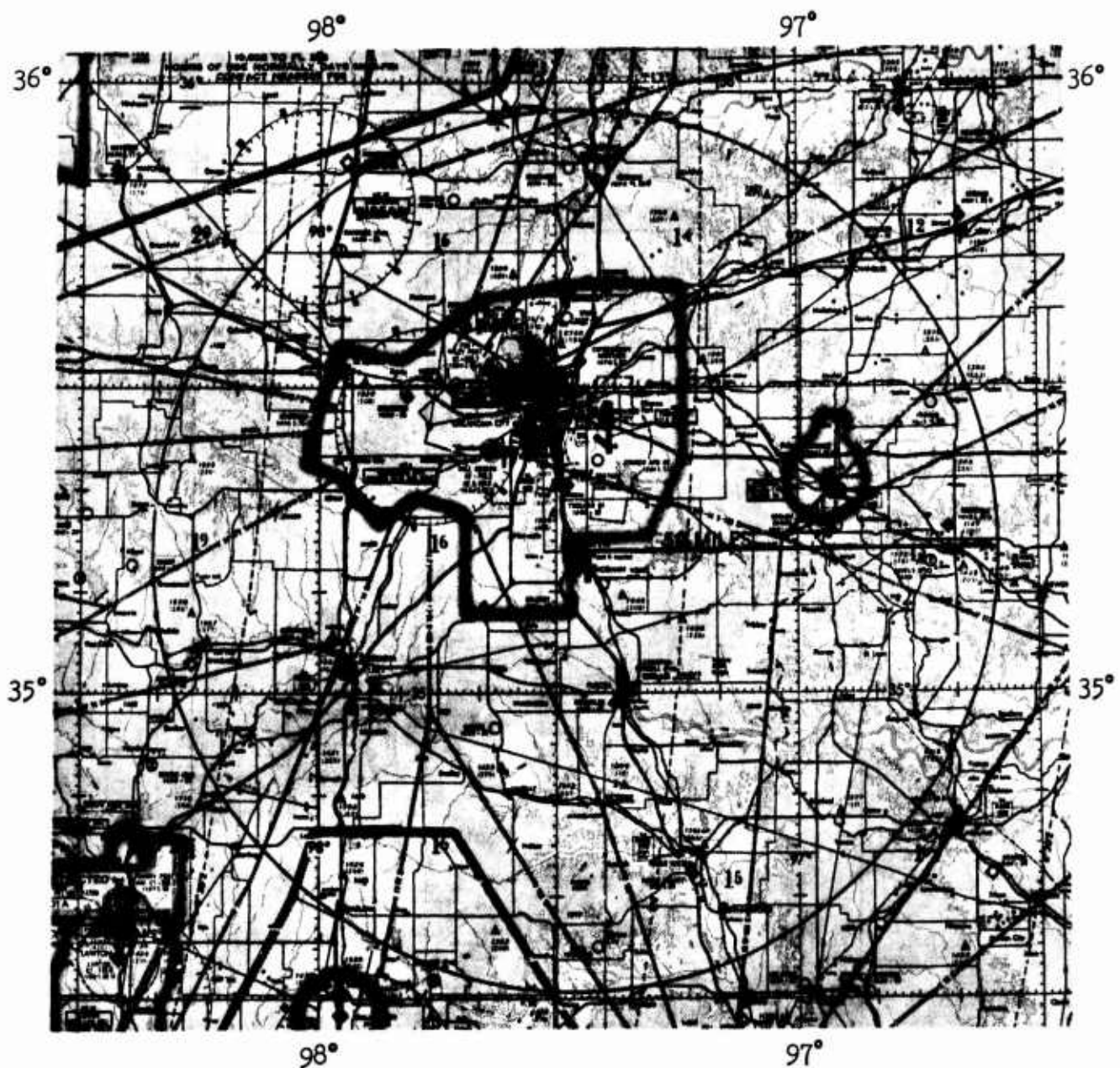


Figure 42.1 Principal Flight Area of Operation Rough Rider

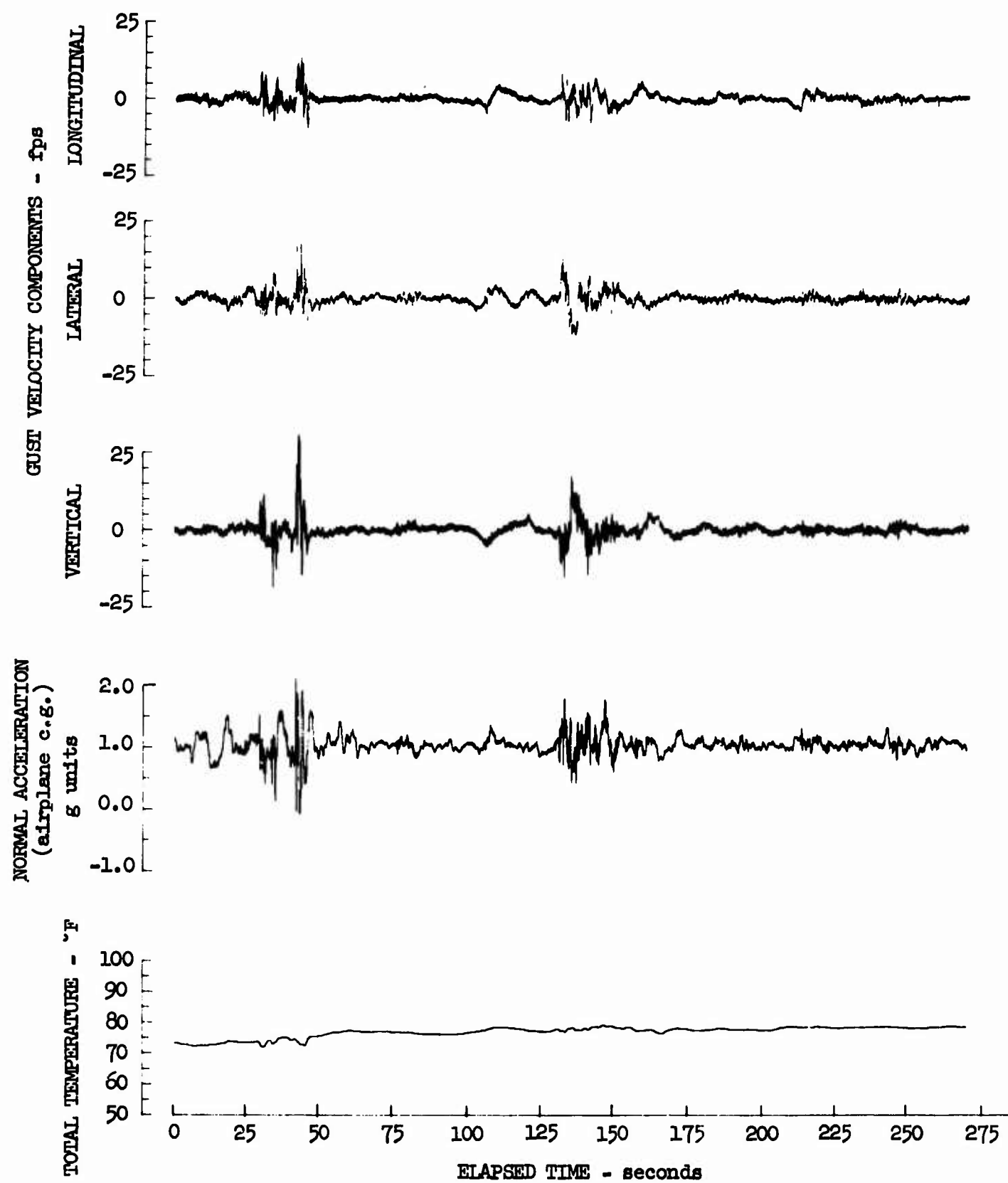


Figure 42.2 Gust Velocity, Normal Acceleration, and Total Temperature Time Histories for Test 270, Sample No. 15

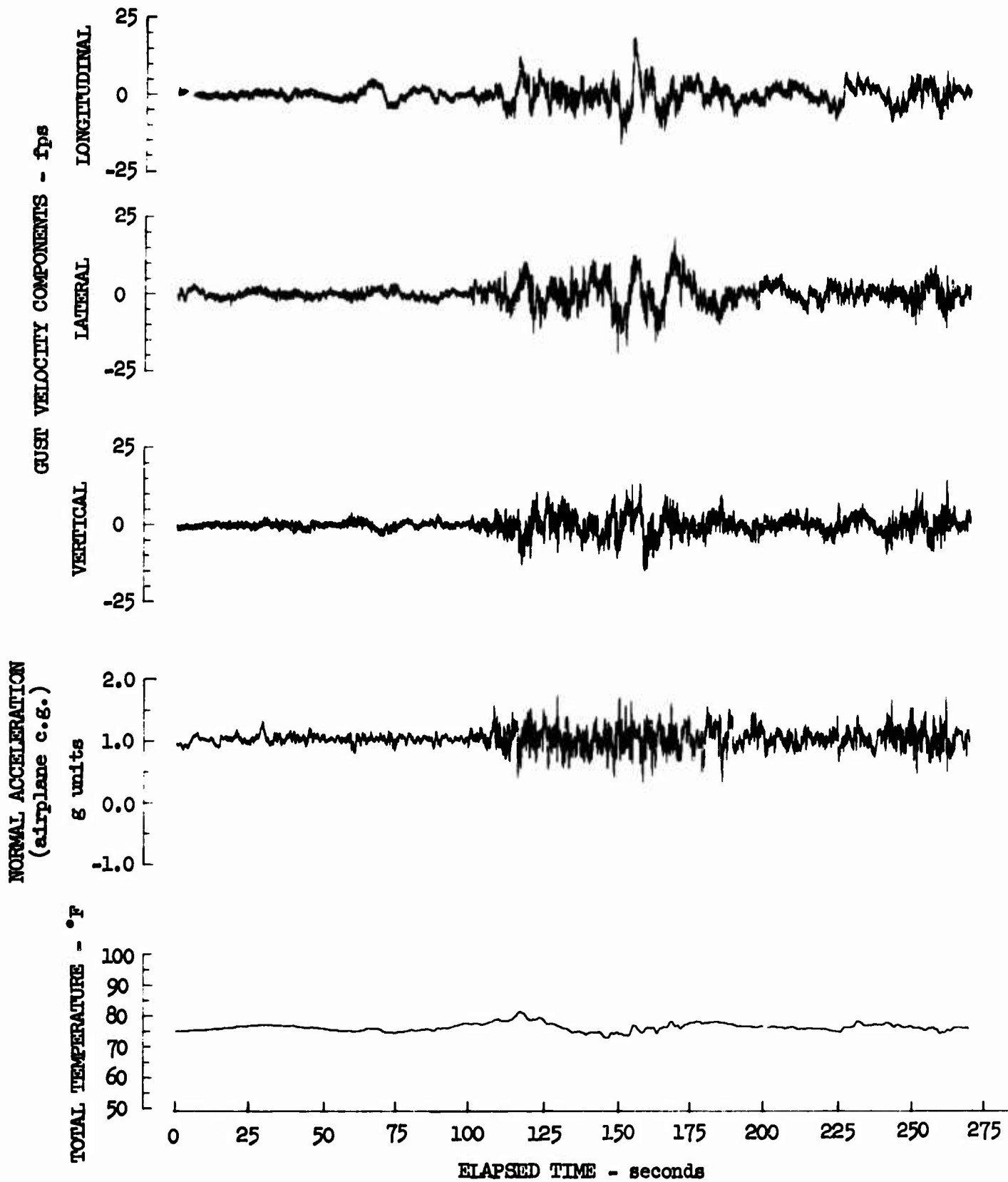


Figure 42.3 Gust Velocity, Normal Acceleration, and Total Temperature Time Histories for Test 270, Sample No. 18

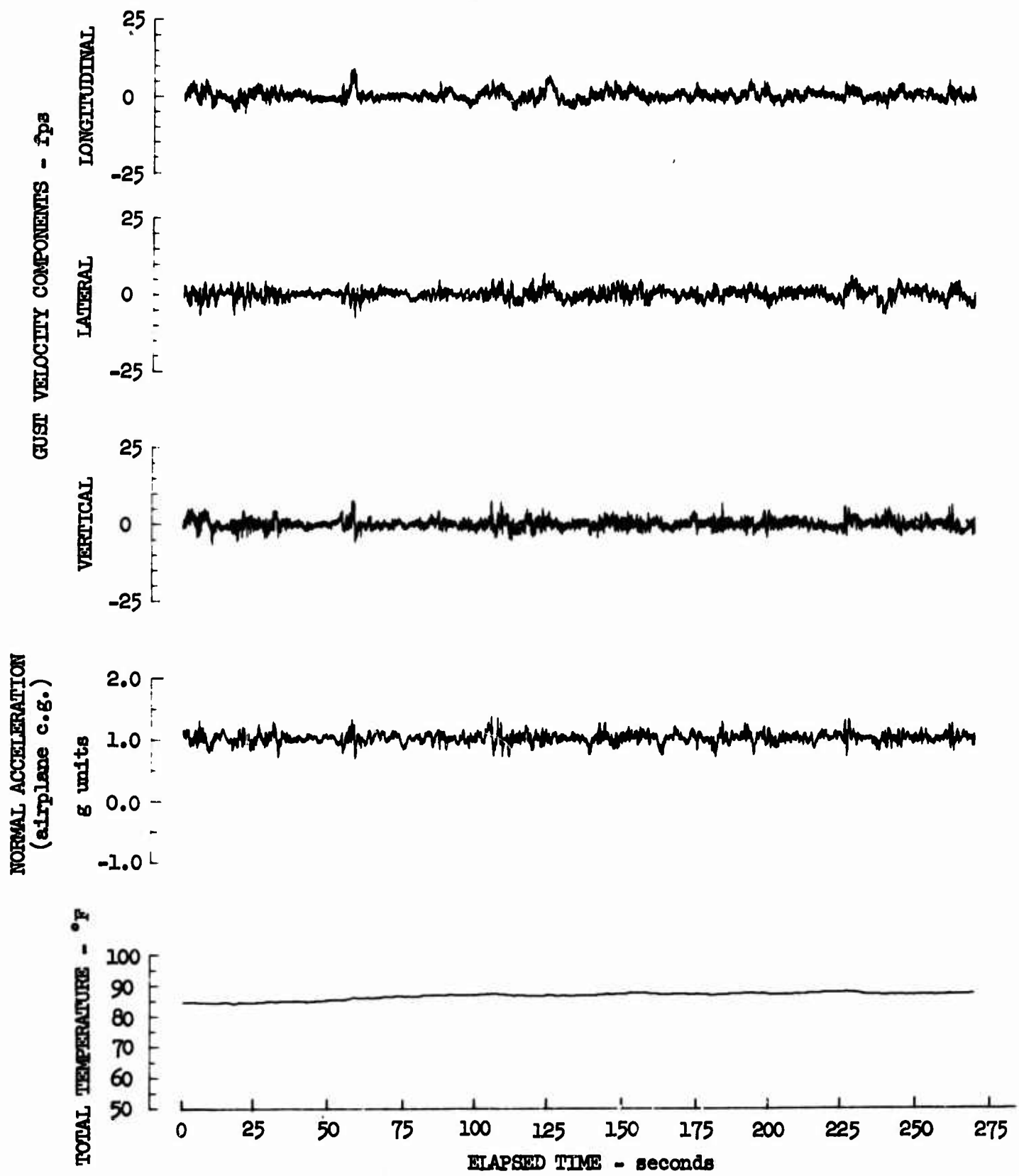


Figure 42.4 Gust Velocity, Normal Acceleration, and Total Temperature Time Histories for Test 273, Sample No. 3

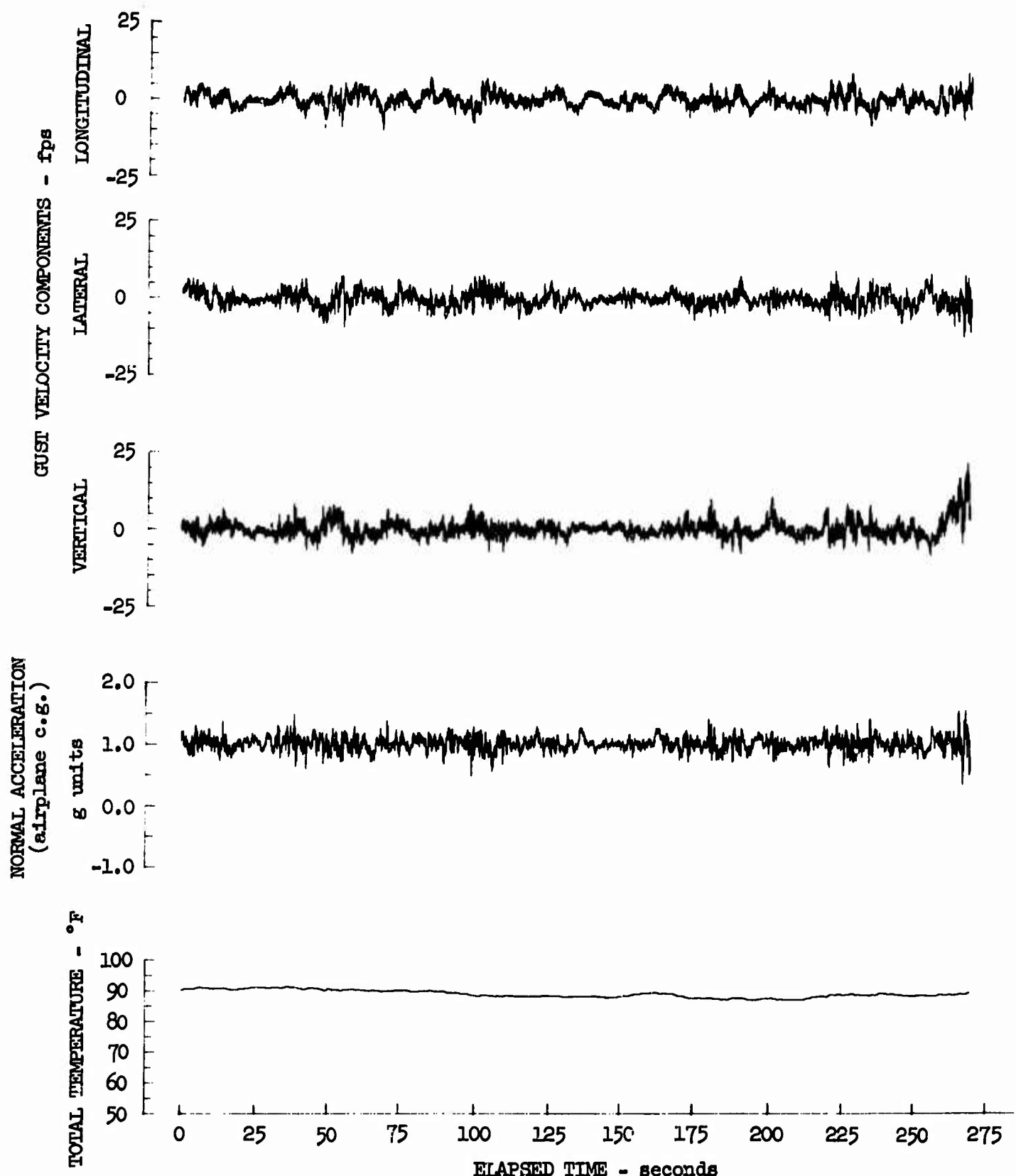


Figure 42.5 Gust Velocity, Normal Acceleration, and Total Temperature Time Histories for Test 2/3, Sample No. 12

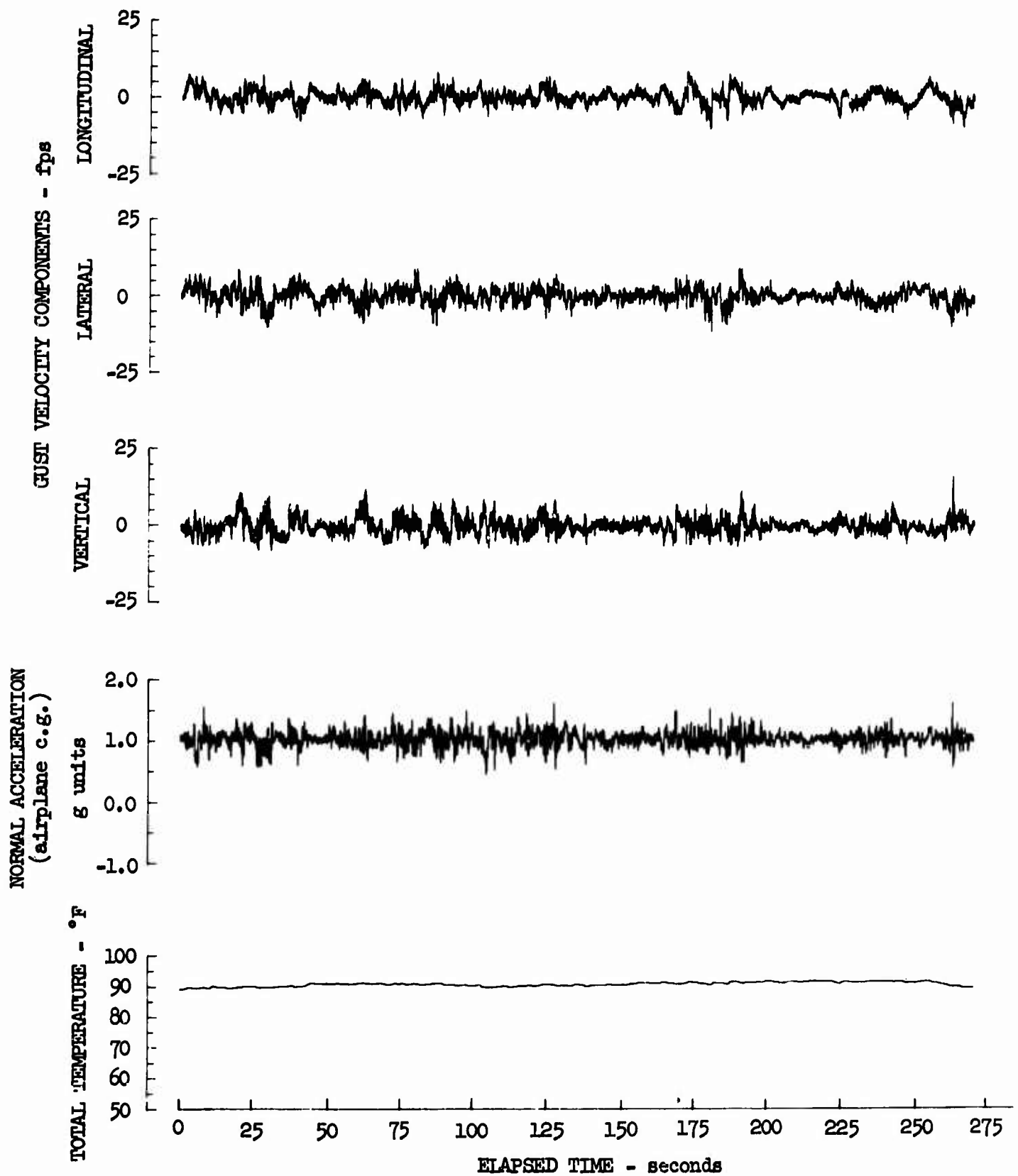


Figure 42.6 Gust Velocity, Normal Acceleration, and Total Temperature Time Histories for Test 273, Sample No. 15

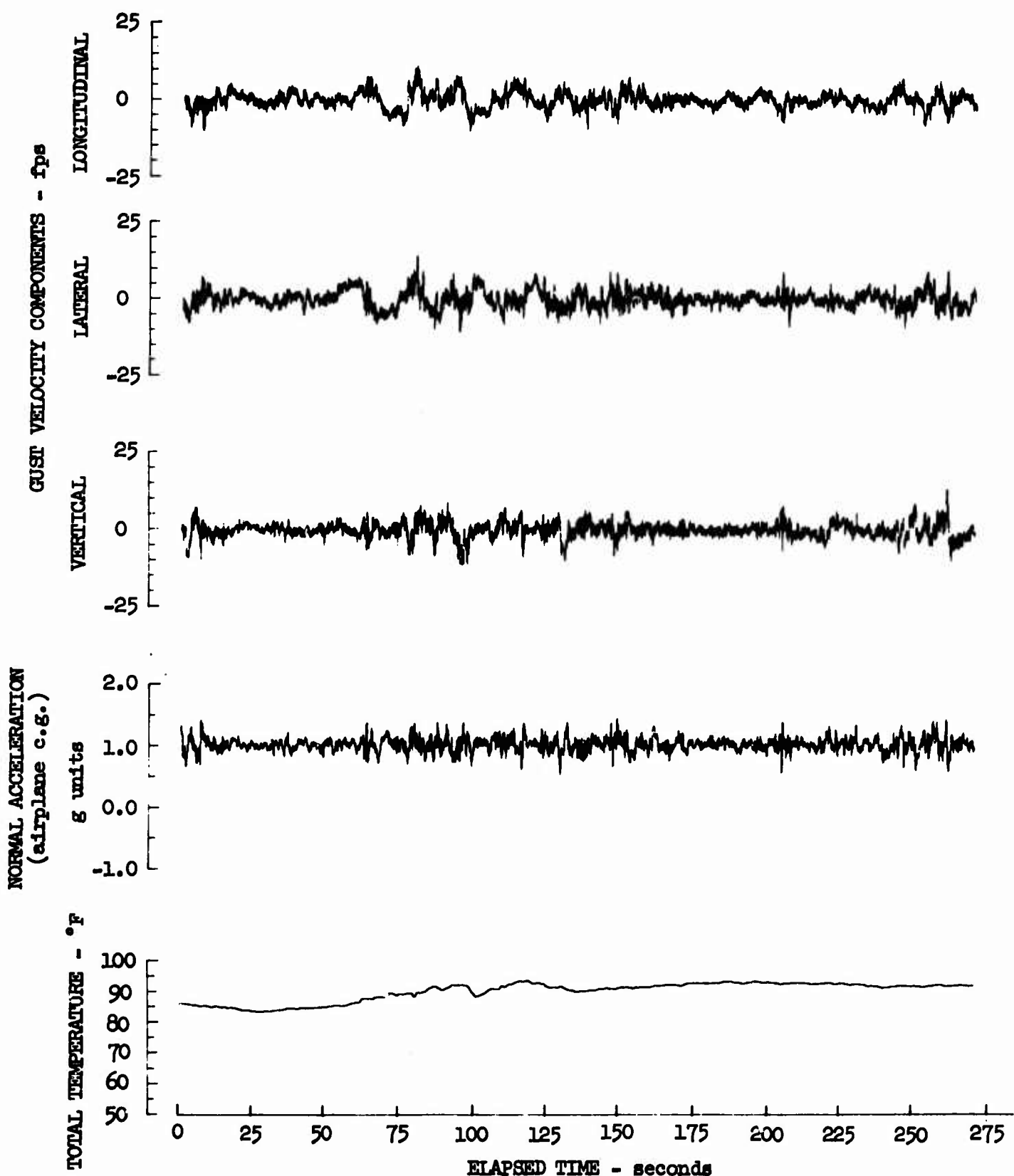


Figure 42.7 Gust Velocity, Normal Acceleration, and Total Temperature Time Histories for Test 274, Sample No. 3

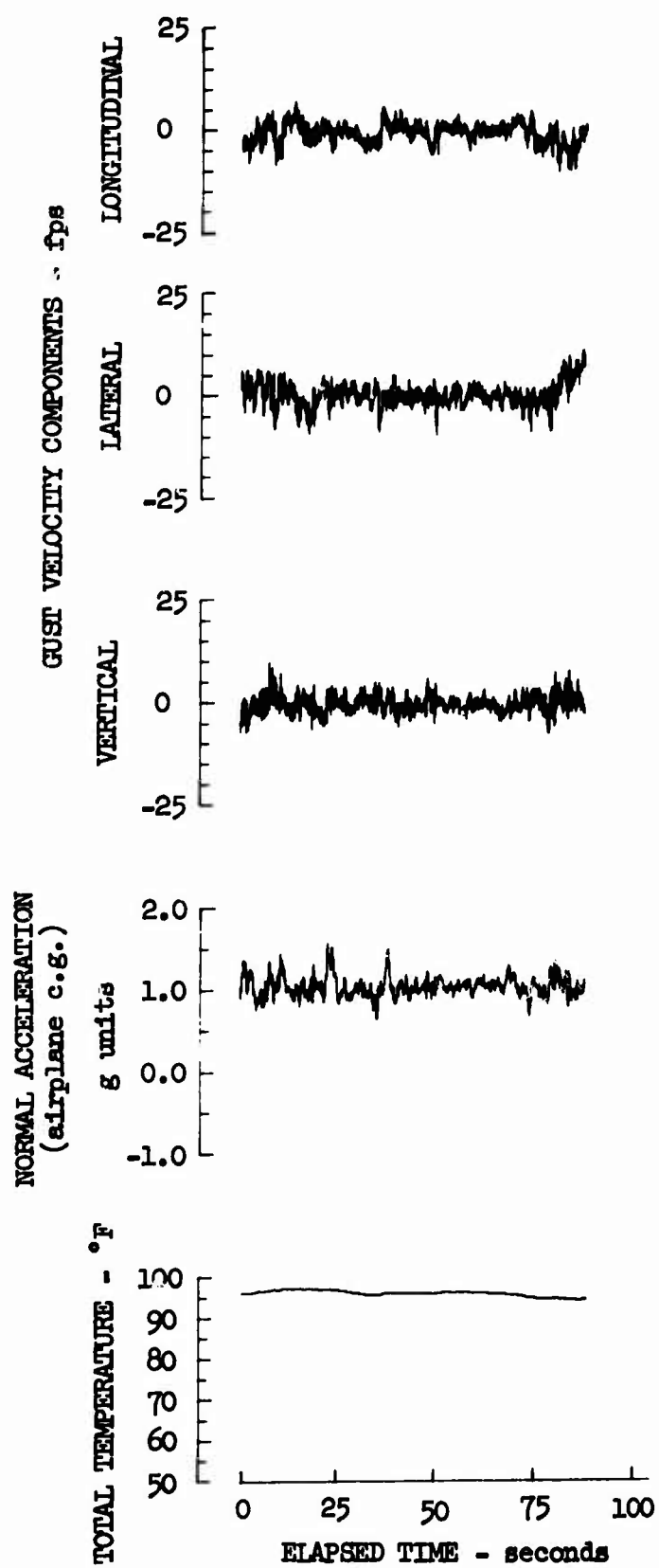


Figure 42.8 Gust Velocity, Normal Acceleration, and Total Temperature Time Histories for Test 275, Sample No. 9

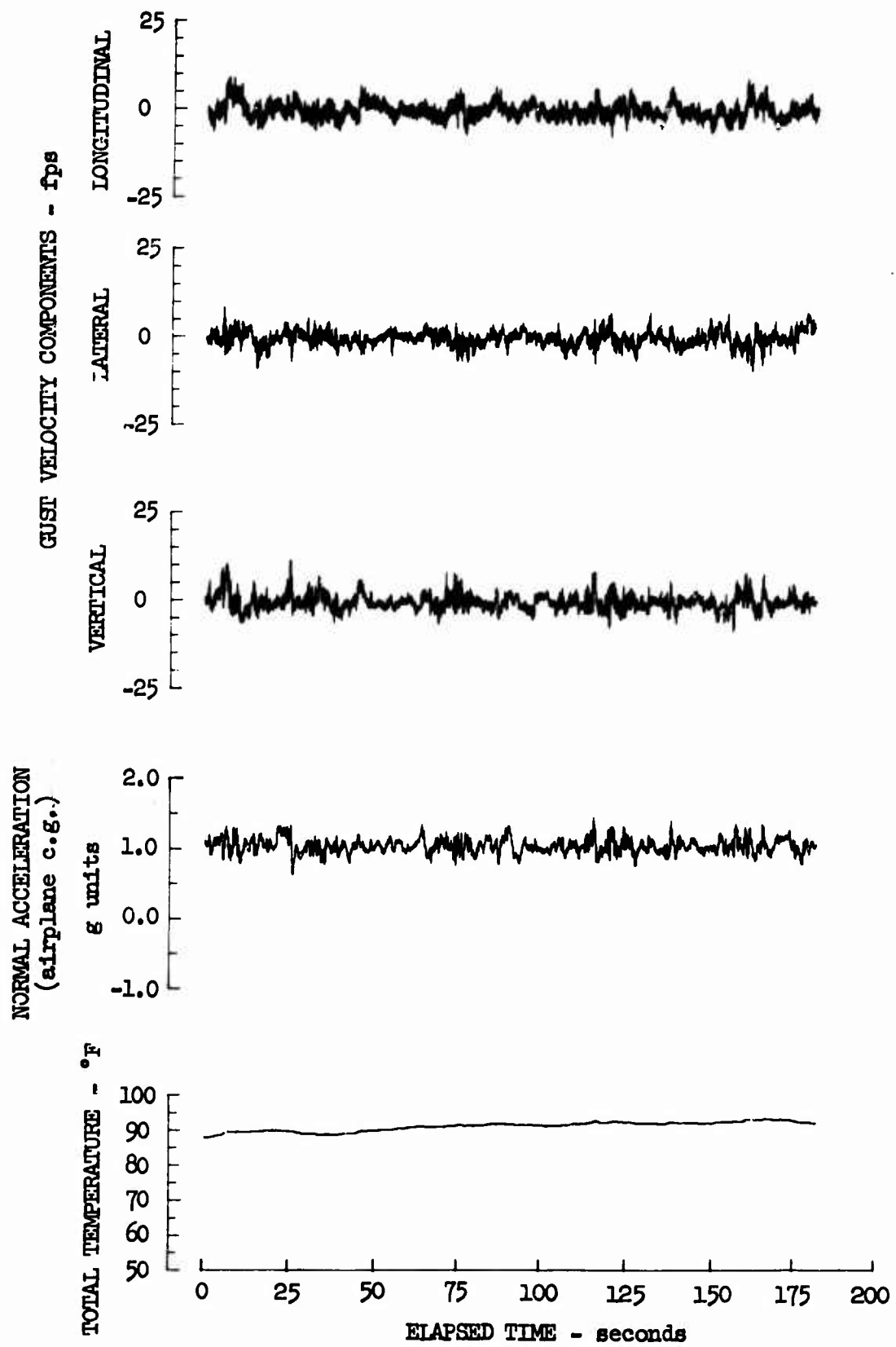


Figure 42.9 Gust Velocity, Normal Acceleration, and Total Temperature Time Histories for Test 275, Sample No. 12

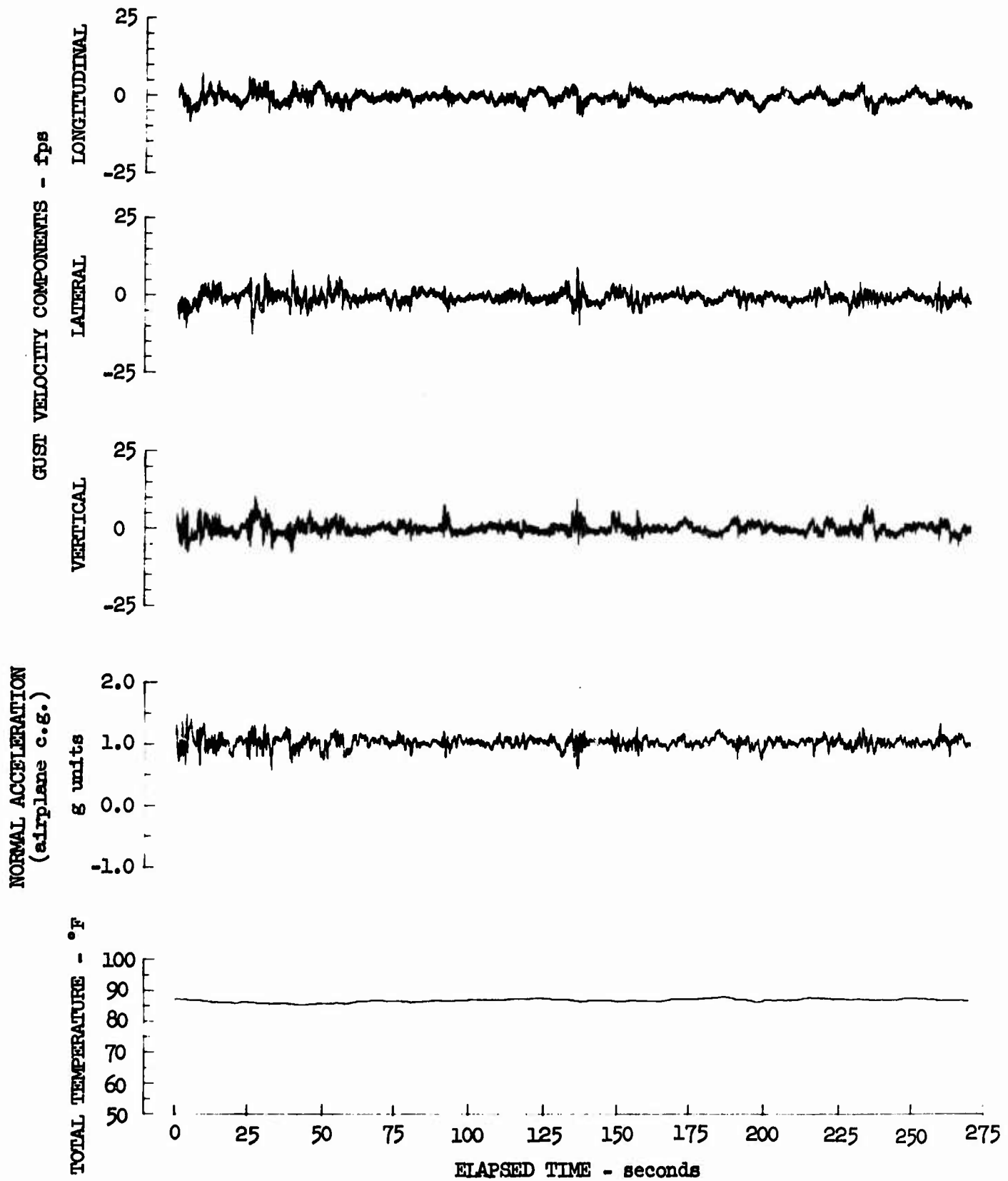


Figure 42.10 Gust Velocity, Normal Acceleration, and Total Temperature Time Histories for Test 275, Sample No. 21

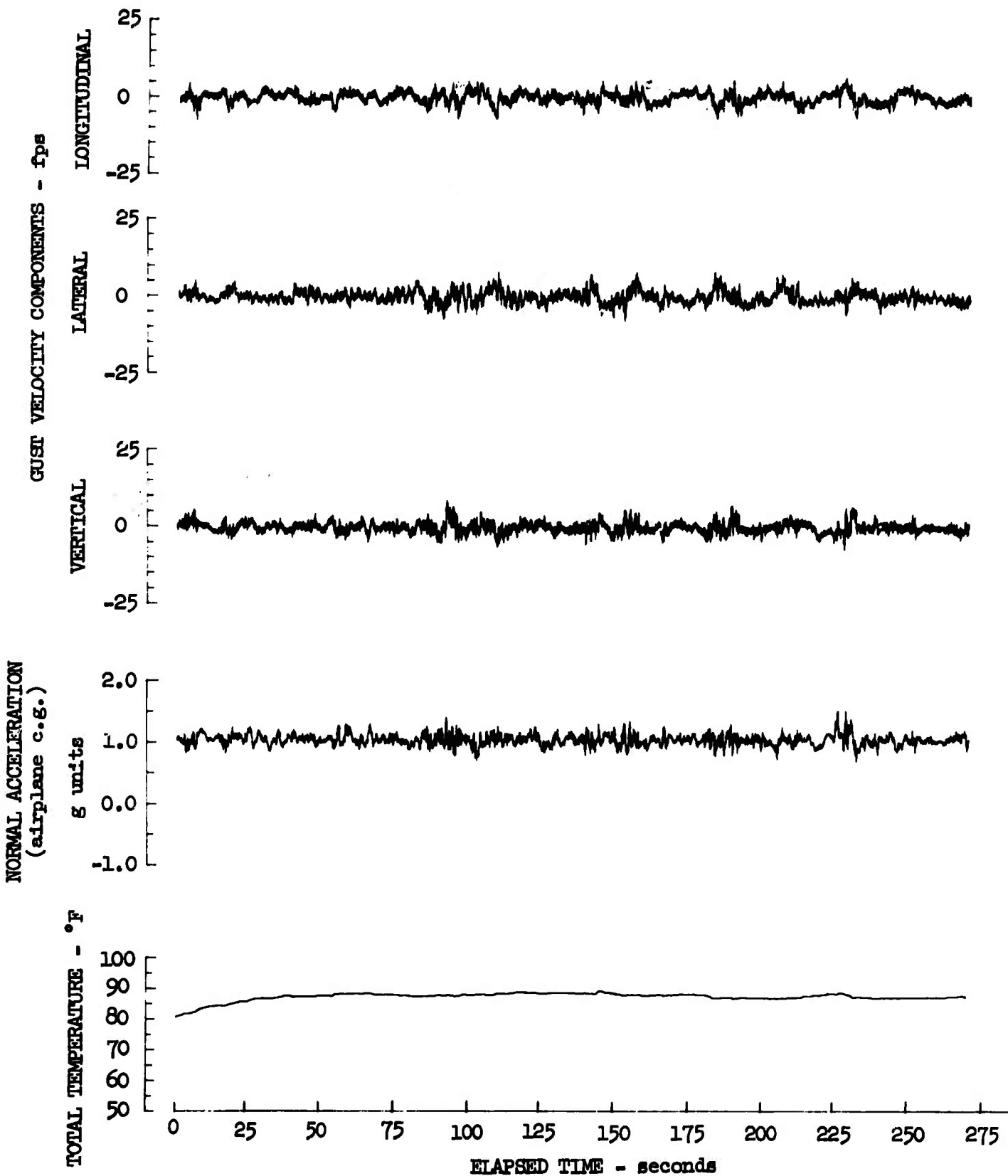


Figure 42.11 Gust Velocity, Normal Acceleration, and Total Temperature Time Histories for Test 275, Sample No. 24

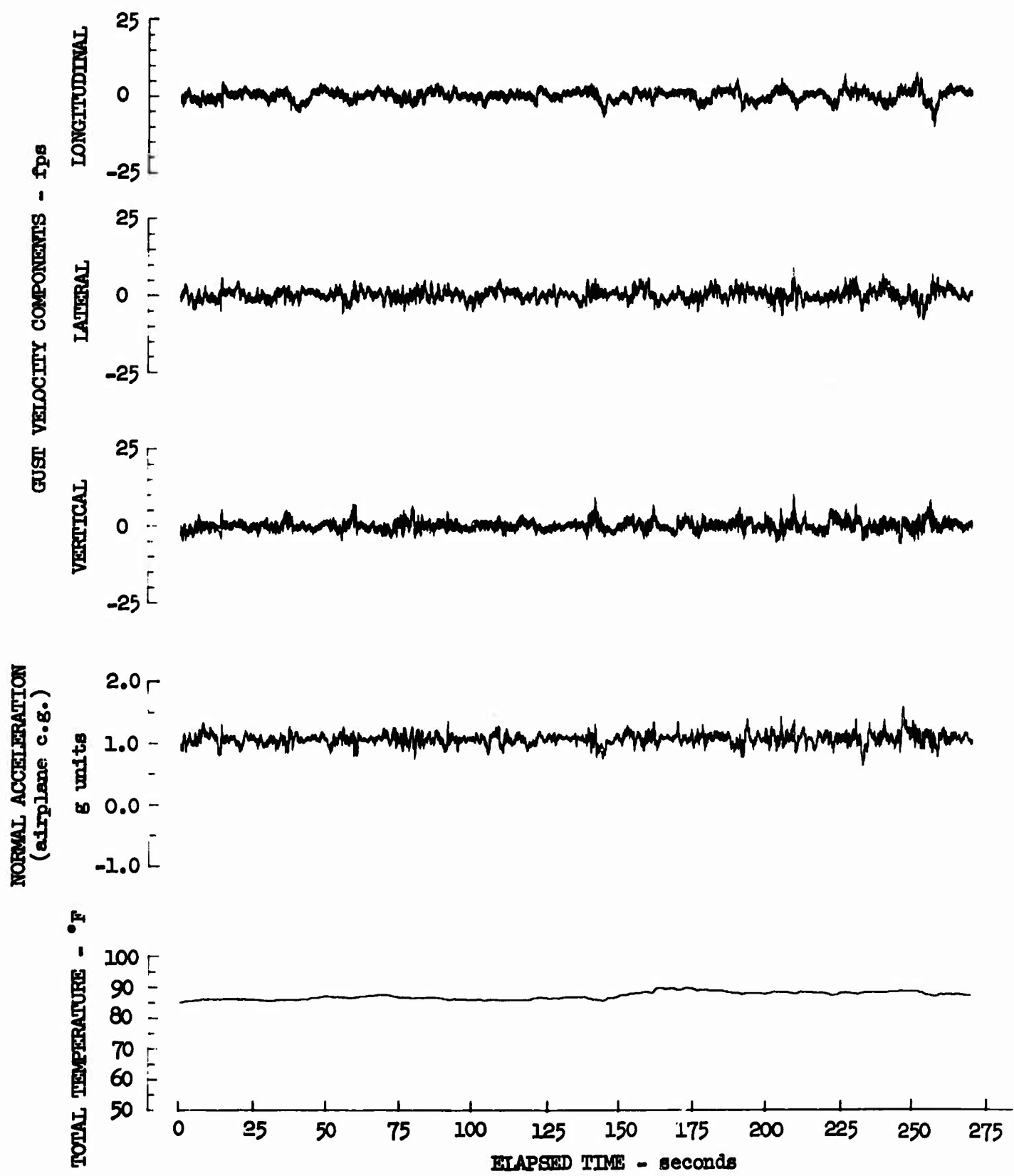


Figure 42.12 Gust Velocity, Normal Acceleration, and Total Temperature Time Histories for Test 275, Sample No. 27

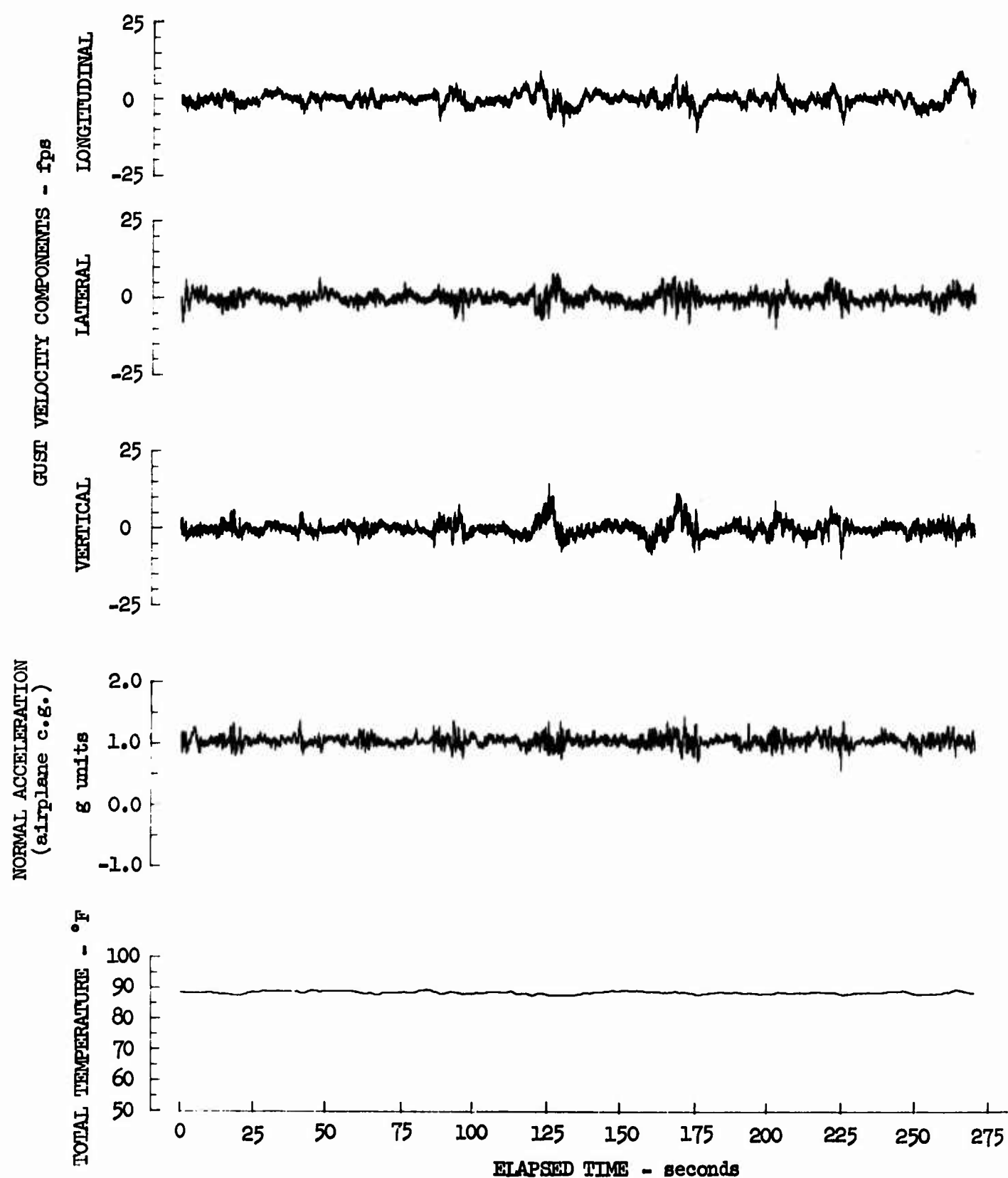


Figure 42.13 Gust Velocity, Normal Acceleration, and Total Temperature Time Histories for Test 275, Sample No. 30

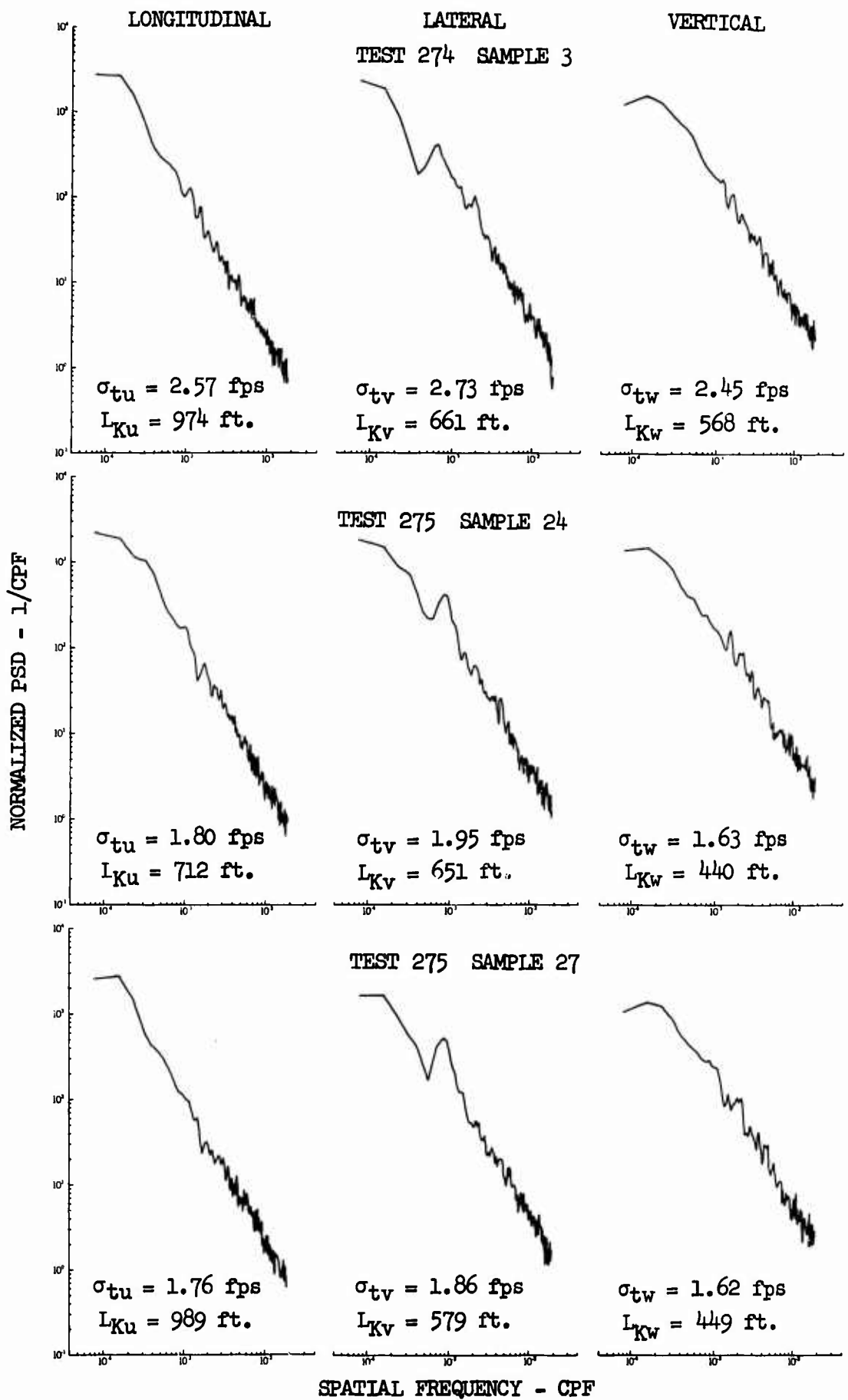


Figure 42.14 Turbulence Spectra for Tests 274 and 275

43. WAKE TURBULENCE

The T-33 airplane was flown behind formations of C-141 airplanes in an effort to qualitatively evaluate the wake turbulence environment generated by these aircraft. This environment is of special interest when associated with paratroop drop tactics. Aircraft-induced turbulence affects the accuracy and efficiency of the drop as well as controllability of the aircraft and, consequently, flight safety.

This testing was done on 10 June 1969, during LO-LOCAT flights 0284 and 0285. Eighteen C-141 aircraft were utilized. Although no troops were dropped during this testing, the procedures used were the same as for an actual drop. The aircraft flew the racetrack pattern shown in Figure 43.1 in a clockwise direction. The pattern was traversed seven times.

The C-141 aircraft were flown in six elements of three aircraft each for the enroute portion of the racetrack pattern (i.e. that portion other than within the drop zone). Two different formations of these elements were employed. The standard VFR in-trail formation concept was used for the first enroute portion. This concept is described in Reference 43.1 and consisted basically of the element spacing shown in Figure 43.2. The elements were flown directly behind one another, and the element wingmen maintained wing tip clearance on both the right and left to avoid jetwash and wing tip vortices. This formation was flown at a terrain clearance altitude of approximately 500 feet and an airspeed of 250 knots.

A modified in-trail concept was used during the other six enroute portions of the racetrack pattern. This concept was the same as the standard concept in that the longitudinal separation between aircraft within an element and between the lead aircraft of the adjacent elements was 2200 feet and 2 miles, respectively. The element wingmen maintained wing tip clearance to the right and left to avoid jetwash and wing tip vortices. However, the differences were as follows:

- The second element lead aircraft maintained a lateral position approximately 500 feet to the right of the number two aircraft in the first element.
- The third element lead maintained a lateral position approximately 500 feet to the left of the number three aircraft in the first element.
- The fourth element followed the same track as element number one but flew at an absolute altitude of 600 feet rather than 500 feet.
- The fifth and sixth elements flew at 600 feet absolute altitude and with the same relative position to element four as elements two and three maintained with respect to element number one.

Figures 43.3 and 43.4 show the four different formations of the elements used during the seven passes over the drop zone portion of the racetrack pattern. Formation number 1 was flown for pass 1, formation number 2 was flown during passes 2 and 3, formation number 3 was flown during passes 4 and 5, and formation number 4 was flown during passes 6 and 7. The longitudinal spacing within all of these formations consisted of 2200 feet between adjacent aircraft, i.e. 6600 feet between element leaders. These formations were assumed at a predetermined slow-down point at the end of the enroute portion of the pattern. At this point, the pilots of the aircraft within an element retarded engines to idle and climbed to an altitude of 1000 feet above the ground. This resulted in an airspeed of approximately 135 knots as the aircraft passed over the drop zone and closed the longitudinal distance between element leaders from 2 miles to 6600 feet. These tactics were designed to increase paratroop concentration in terms of time and space while still maintaining a sufficient distance between aircraft for flight safety. Following the drops, the aircraft descended to 500 feet and accelerated while maneuvering into the modified VFR in-trail concept to repeat the enroute portion.

The lateral separation between adjacent elements (1 and 2, 2 and 3, 3 and 4, 4 and 5, and 5 and 6) in each drop zone formation was determined by the set-up of the ground drop zone points of impact. These approximate distances are shown in Figures 43.3 and 43.4. Additional details of the various C-141 procedures and formations as well as a synopsis of the wake turbulence severity as evaluated by the pilots of these aircraft may be found in Reference 43.2.

The T-33 was flown behind the C-141 aircraft during passes 1, 2, 3, 4, 6, and 7. The airplane was returned to McGuire AFB for refueling during pass 4. A summary of test information is presented in Table 43.1.

TABLE 43.1

WAKE TURBULENCE TEST INFORMATION

Pass No.	Enroute VFR In-Trail Concept	Drop Formation No.	Gust Velocity Data Recorded	LO-LOCAT Test No.
1	Normal	1	Yes	0284
2	Modified	2	Yes	0284
3	Modified	2	Yes	0284
4	Modified	3	No	--
5	Modified	3	Yes	0285
6	Modified	4	Yes	0285
7	Modified	4	Yes	0285

The pilot, during Test 0284, maneuvered the T-33 airplane back and forth across the wake, cutting the C-141 flight paths at approximately 45 degrees. The turbulence reported by the T-33 pilot was from very light to light. During part of Test 0285, the pilot flew the airplane from one mile to approximately 500 feet directly behind the C-141 aircraft and in the same flight path. The pilot flew the T-33 up and down and back and forth across the wake behind the sixth element in order to probe the environment as thoroughly as possible.

Some difficulties were encountered in reducing the data. The LO-LOCAT data processing programs were designed for data samples of a given size whereas the wake turbulence sample size was variable. Likewise, the programs were designed to process only every third sample as gust velocity data, following two atmospheric survey samples at 100 and 1000 feet above the ground. It was impractical to perform the surveys prior to each gust velocity sample during the wake turbulence research. Therefore, because of these irregularities, the data were specially handled during processing.

The shortness of some of the data samples caused a problem with the filtering program. As described in Appendix III, drift was removed from the LO-LOCAT gust velocity data by employing a digital filter to attenuate amplitudes at frequencies below 0.046 cps. However, the procedure used with this filter required a minimum sample length. Some of the gust velocity samples recorded during this testing were not of sufficient length to permit the use of this digital filter.

Because these particular samples were of a short duration, the drift was not excessive and was removed manually by replotting the unfiltered gust velocity time histories about a zero-mean.

Another problem that was handled manually concerned high frequency noise which occurred on the gust velocity traces periodically. The noise was represented by gust velocity excursions ranging from approximately 15 to 25 feet per second. This occurred primarily during periods of flight through relatively calm air during Test 0285 when the T-33 was flown directly behind the C-141 aircraft. This noise occurred at a frequency of approximately 15 cps. After a review of the probe accelerations it was concluded that the gust boom was vibrating at its natural frequency, thus causing the problem. Although turbulence of the necessary wave length to excite the boom may be contained within the wake environment, the recorded magnitude was probably amplified by the vibrating boom. Therefore, the data were manually smoothed in these areas to eliminate the high frequency noise.

The radar altimeter was inoperative during this testing. Also, the Doppler radar, which measured drift angle and ground speed, was inoperative, preventing the calculation of wind speed.

The gust velocity data are presented in the form of time history plots in Figures 43.5 through 43.40. The following items, when available, are included on the time history plots:

- Pertinent T-33 pilot comments recorded in flight.
- Pass number and approximate location on the racetrack pattern (drop zone, leg, or enroute portion).
- Type of C-141 formation.
- Recorded data, including true airspeed, true heading, and pressure altitude.

Not all of the data samples recorded are presented in these figures. A total of 45 samples were recorded during both tests. Thirteen of these samples contained no significant turbulence data and these time history plots are not shown.

As would be expected, most of the turbulence samples shown are quite non-homogeneous. As the T-33 pilot maneuvered through the flight path of the C-141 aircraft, turbulence was encountered only within certain areas. Table 43.2 presents the minimum and maximum gust velocity values recorded for each data sample. The T-33 pilot's comments indicated that very little of the wake turbulence caused any appreciable airplane response. This was probably due to the small size of the vortices and the short duration of time the airplane was within these vortices.

The lack of the T-33 response to the wake turbulence was a hindrance to the pilot in locating the vortex activity. This was the only cue available to the pilot. The mission plan was to have the pilot start the wake surveys at a safe distance behind the C-141 fleet and, with each successive 45° traverse, gradually close the distance from the fleet until the maximum vortex intensity which could be safely traversed was encountered. This plan could not be followed because the pilots motion cues did not indicate any significant vortex intensities. Thus, it is probable that the T-33 never traversed the highest intensity vortices because the data sampling turned out to be fairly random rather than consistent as would be expected from a planned orderly search for maximum vortex intensities.

The velocity distribution of a viscous fluid within a vortex can be represented as shown in Figure 43.41. Viscous effects cause the fluid with diameter d to rotate as a solid body with a given angular velocity, ω , while the angular velocity of the fluid outside diameter d decreases to zero with distance from the center. Several of the gust velocity time histories which best exemplify the shapes and sizes of the wake turbulence vortices encountered during this testing were replotted on expanded time and amplitude scales so that the actual shapes could be more easily seen. These plots are shown in Figures 43.42 through 43.50. In order to estimate the sizes of these vortices, the differential time, Δt , was multiplied by the true airspeed of the T-33 to obtain a distance. The results of these calculations are shown on the figures and are summarized in Table 43.3.

It should be noted that the sampling rate of 100 samples per second may not be high enough to adequately resolve the maximum gust velocities shown in Figures 43.42 through 43.48. Thus, the data presented in these figures may be somewhat less than the maximum vortex intensities actually existing in the

C-141 wake. Also, the smallest Δt is shown to be 0.04 seconds which corresponds to a frequency of approximately 12.5 cps. The amount of attenuation or amplification of data at this frequency was not investigated and is therefore an unknown factor that needs consideration if further evaluation of these data is attempted.

The shapes of the gust velocity traces in Figures 43.49 and 43.50 are not as compatible with the theoretical shape of Figure 43.41 as are the traces in Figures 43.42 through 43.48. Thus, the diameters of the vortices for those two samples have not been calculated. They were plotted on the expanded scales, however, because they represent the highest magnitude gust recorded during this investigation.

TABLE 43.2

MINIMUM AND MAXIMUM GUST VELOCITIES

Test	Sample No.	Minimum Gust Velocity - fps			Maximum Gust Velocity - fps		
		u	v	w	u	v	w
0284	5	- 8	- 7	-10	8	9	8
	7	- 5	-10	-11	4	4	8
	8	-16	-14	-19	5	10	15
	9	- 9	- 6	-12	9	7	5
	16	- 6	- 6	- 9	6	8	8
	17	- 9	-11	-21	18	10	12
	18	-14	-15	-15	13	11	12
	19	- 8	-10	-16	14	10	14
	20	-11	-19	-20	14	18	18
	21	- 7	-31	-23	8	17	31
	25	- 7	- 8	-20	11	14	12
	26	-17	-13	-12	8	12	14
	27	- 6	- 8	-13	12	8	6
	29	-10	-15	-28	22	16	18
	36	-16	-35	-40	14	24	21
	38	-18	- 9	-14	18	13	14
	39	-20	-10	-16	22	12	9
0285	3	-16	-29	-23	19	17	21
	4	-12	-13	-17	11	11	12
	6	-17	-50	-63	10	19	11
	7	- 9	-33	-19	9	39	36
	8	-15	-25	-31	19	35	21
	9	-11	-19	-20	9	23	16
	10	-43	-31	-47	16	43	21
	11	-12	-16	-14	12	17	13
	12	-26	-42	-36	13	24	29
	17	-14	-30	-59	35	49	13
	18	-18	-25	-19	18	20	19
	19	- 7	-16	-13	9	21	16
	20	-18	-24	-20	18	17	18
	21	- 8	-11	-15	9	8	10
	22	-18	-22	-25	38	34	25

The following assumptions were made in calculating vortex diameters:

- The vortices were cylindrical in shape.
- They were penetrated through their centers.
- The penetrations were perpendicular to their axes (actual penetration was approximately 45° to the axis).

Whether or not the gust probe penetrated the exact center of a vortex would be difficult to ascertain. However, an indication of this is the magnitude of the component of gust velocity in the longitudinal direction. If the vortices are cylindrical in shape and spinning around a horizontal axis, then the longitudinal component should theoretically be zero if the vortex were traversed directly through the center. Likewise, if a vortex were penetrated exactly perpendicular to the axis of rotation, then the lateral component of gust velocity would theoretically be zero. Thus, the relative magnitude of the gust velocity components indicate, within the limitations of the assumption mentioned above, the orientation of the vortices with respect to the direction in which they were penetrated. All three components of gust velocity showed some activity for most of the samples recorded. The longitudinal component showed the least activity. Therefore, the diameters calculated should be viewed as being rough indicators of the vortex sizes.

TABLE 43.3

CALCULATED VORTEX SIZES

Test	Sample No.	Gust Velocity Component Used	Calculated Diameter - Feet
0284	20	Vertical	19
0284	20	Vertical	18
0284	20	Vertical	28
0284	20	Vertical	22
0284	21	Lateral	21
0284	21	Vertical	29
0285	3	Vertical	41
0285	3	Vertical	37
0285	7	Vertical	20

The size, velocities, and periods of duration of wake turbulence vortices are probably affected by airplane size, speed, and configuration, as well as meteorological conditions. Unfortunately, the exact location of the T-33 with respect to the C-141 aircraft was not known, although the pilot's comments approximate this information. Therefore, the spatial boundaries of the wake turbulence cannot be closely defined. For future testing of this type, it is recommended that some form of this data, such as radar tracking, be recorded so that the boundaries, and the relative intensity of the vortices within these boundaries, could be investigated. In addition, some type of time correlation between the airplane recording the turbulence environment and the airplanes creating the turbulence would be useful in obtaining more exact affects of the various formations. The formations of the C-141 aircraft, as listed on the gust velocity time history plots, were not correlated with the recorded turbulence data or with the T-33 position. Thus, the type of formation for a given sample were determined by pass number and location on the racetrack pattern. Likewise, pass number and pattern position were estimated by noting heading, altitude, and evaluating ground surface temperature (which was indicative of when the airplane was over water) to determine when the aircraft were in the enroute portion of the pattern over the ocean.

The data indicate larger magnitude gust velocities during Test 0285 than during 0284. However, it should be pointed out that the T-33 was flown closer to, and more directly behind, the C-141 aircraft during Test 0285. In addition, increased convective activity, and therefore, more atmospheric turbulence was reported by the C-141 pilots in Reference 43,2 during the latter test.

In summary, these data should be considered only as a qualitative indication of the C-141 wake environment. The lack of precise position information for the C-141's and the T-33 reduces the possibility of accurately comparing these data to vortex theories. Also, the sampling rate might not have been high enough to adequately resolve the gust velocities at the observed frequencies and the amount of attenuation or amplification of data at observed frequencies above 10.0 cps was not investigated and therefore should be considered as an unknown factor in the analysis of these data. Finally, the lack of T-33 motion cues prevented the pilot from being able to locate the maximum vortices in a systematic manner. It is thus possible that the C-141 wake environment is significantly more severe than indicated by these data.

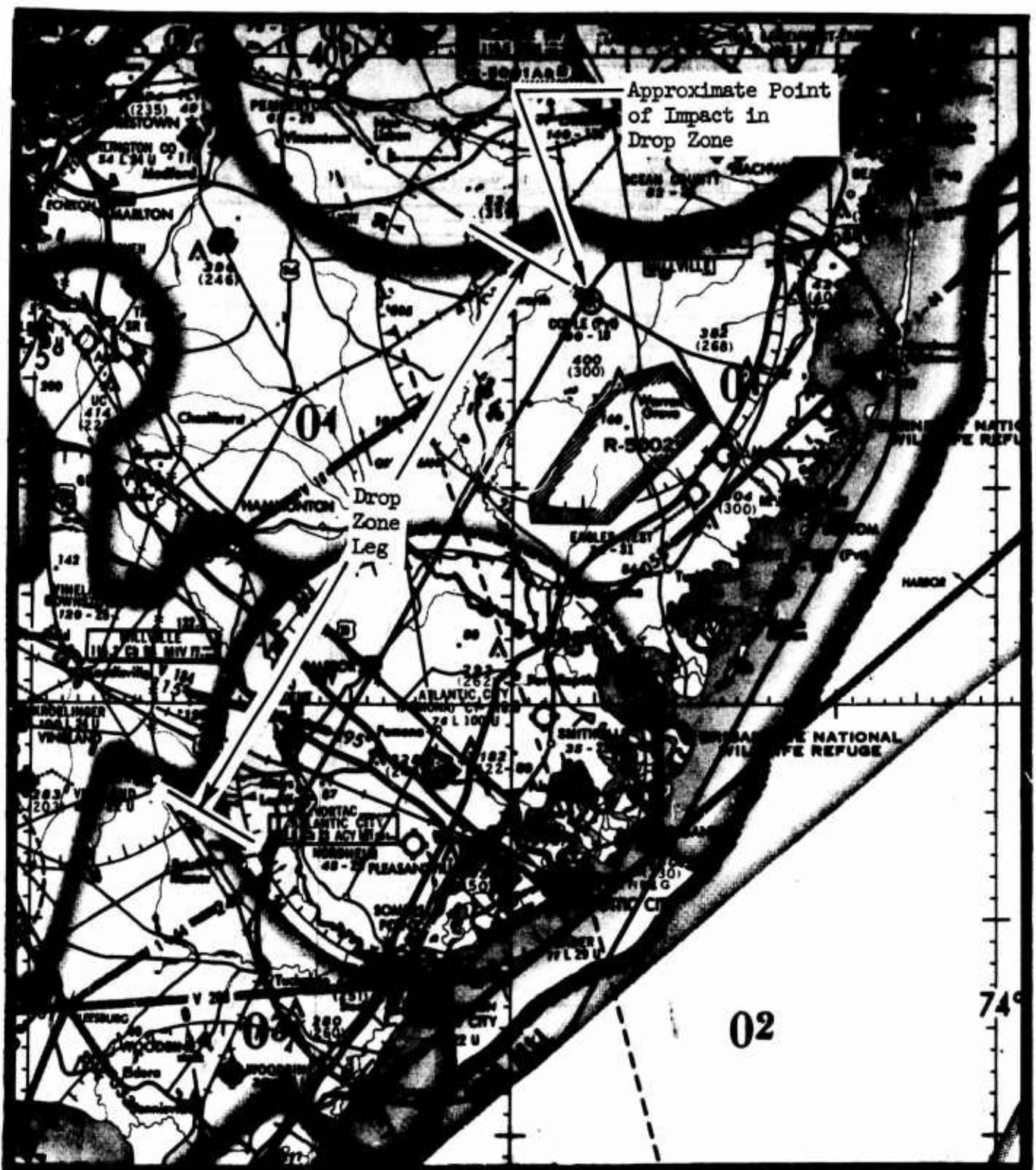


Figure 43.1 Racetrack Pattern - Wake Turbulence Investigation

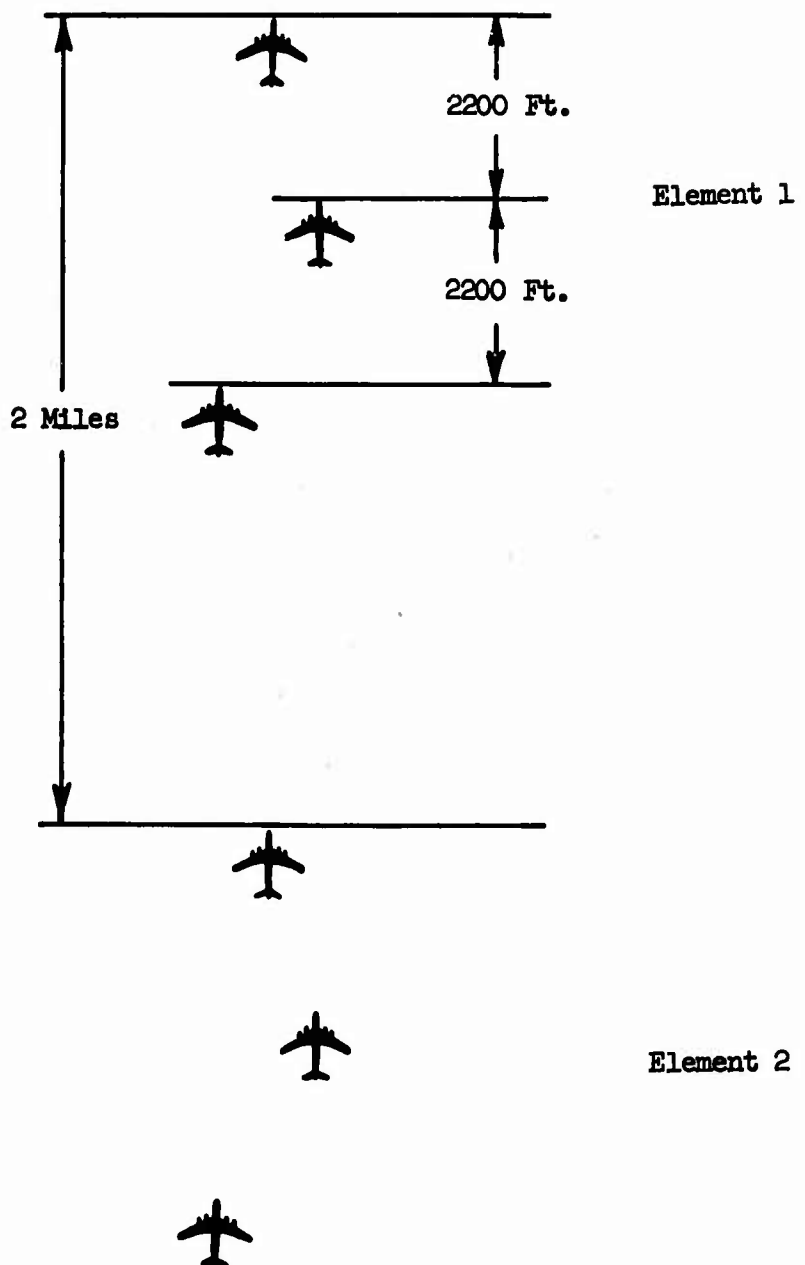


Figure 43.2 Element Longitudinal Spacing During Enroute Portion of Pattern

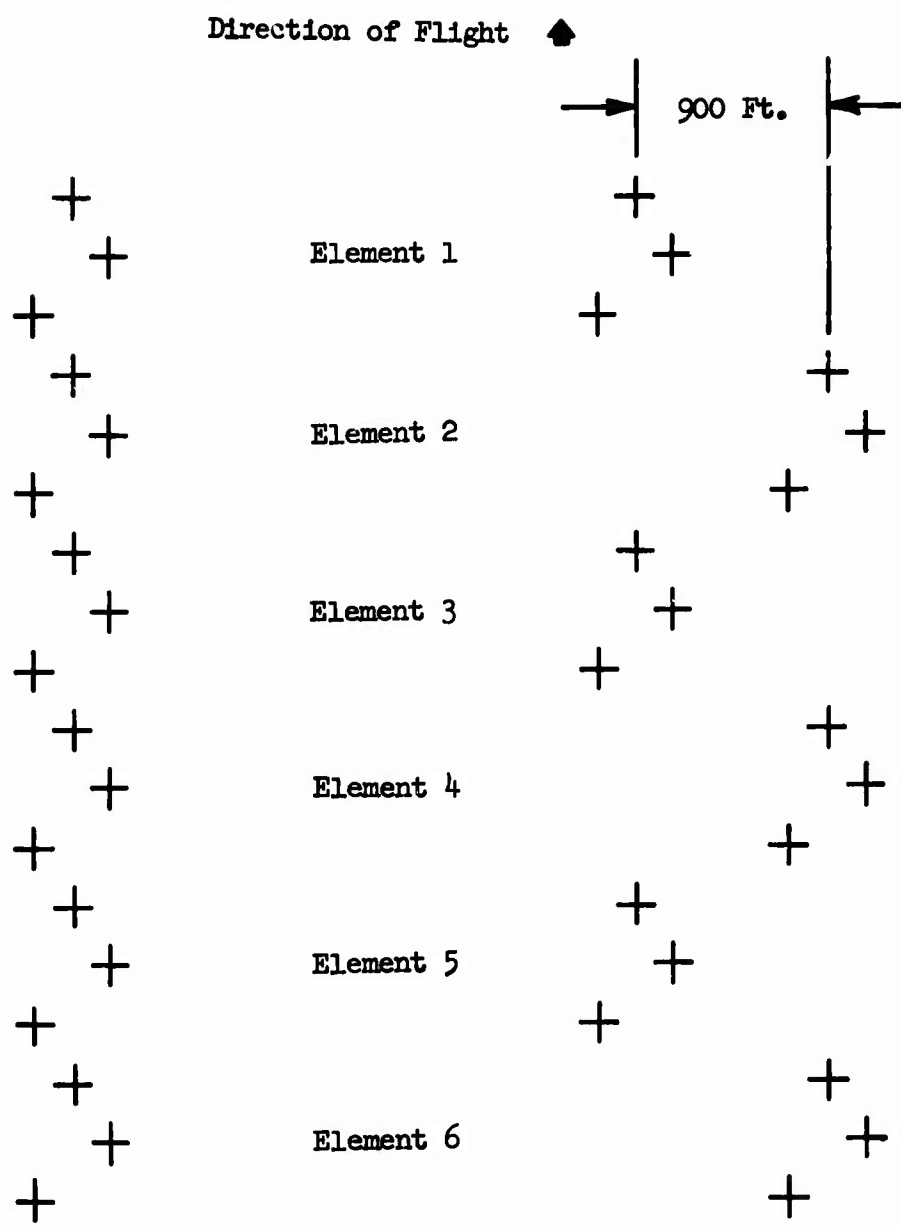


Figure 43.3 C-141 Element Formations in Drop Zone

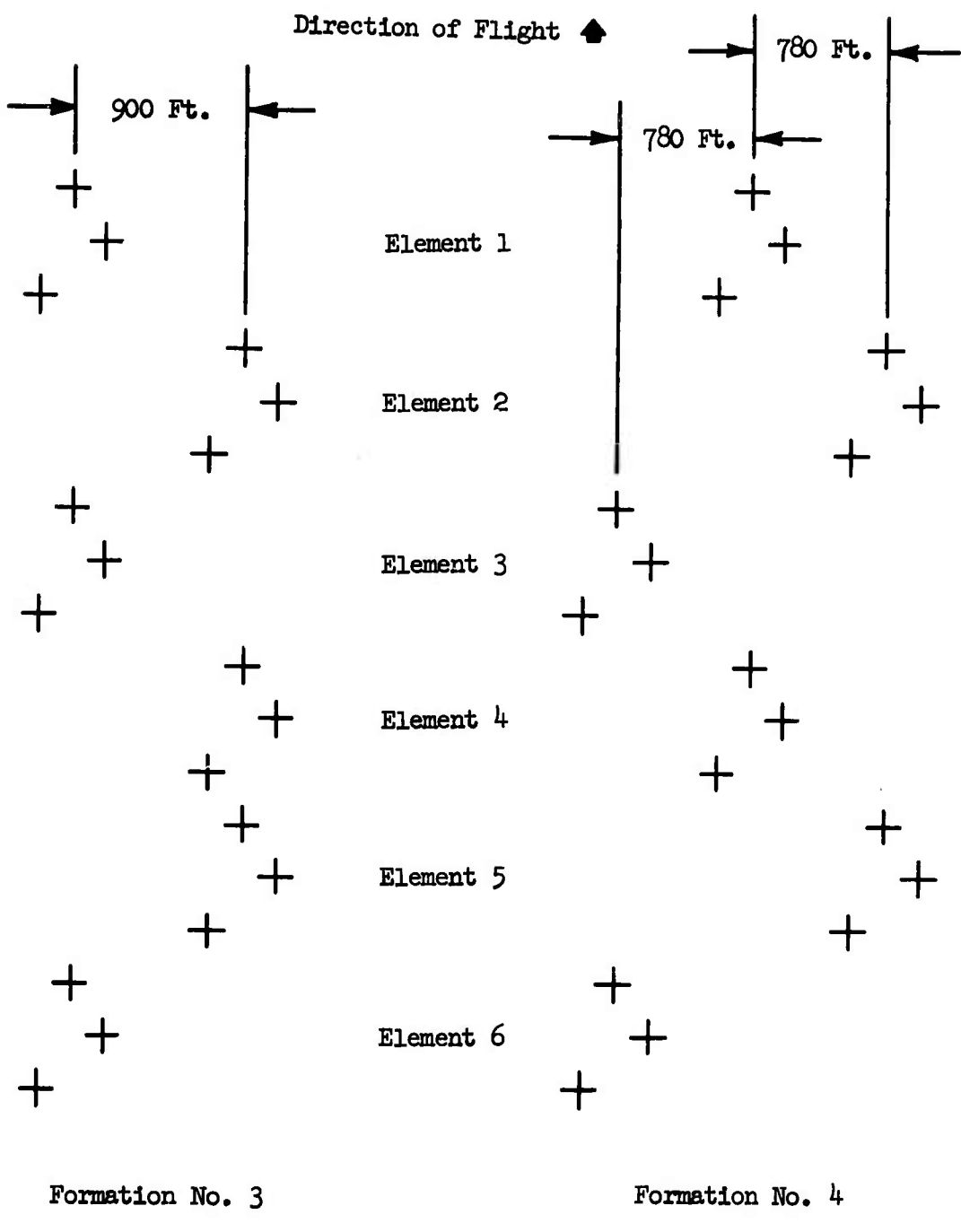


Figure 43.4 C-141 Element Formations in Drop Zone

Location on Racetrack - Drop Zone Leg
Pass No. 1
Type of C-141 Formation - No. 1

No Pilot's Comments

Recorded Data:

$V_T = 299$ knots

$h = \dots$

$H_P = 730$ ft.

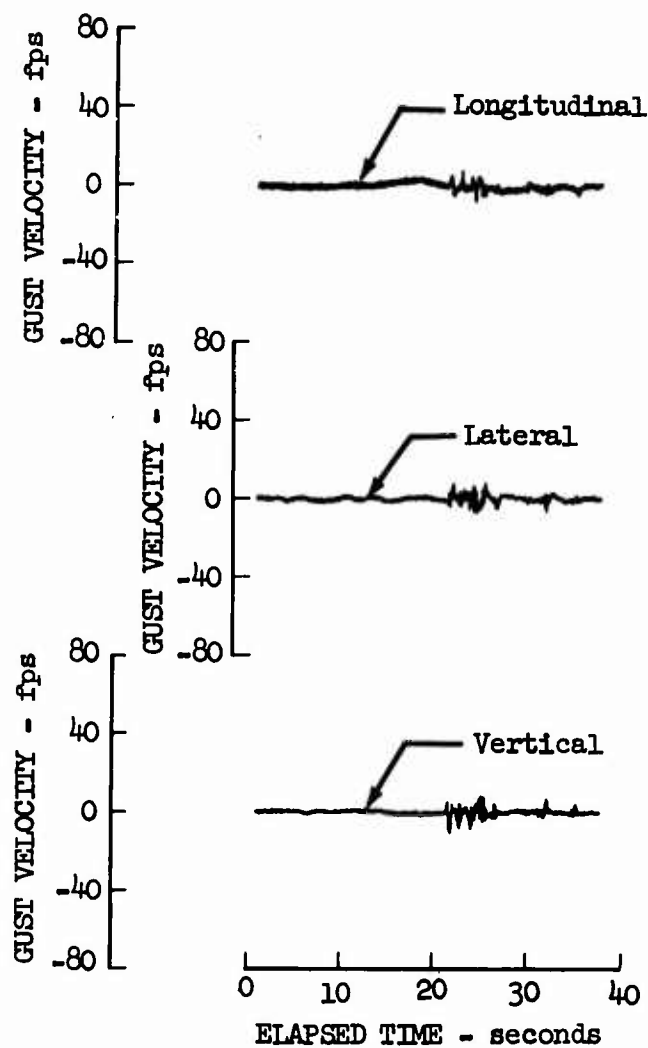


Figure 43.5 Gust Velocity Time Histories - Test 0284,
Sample No. 5

Location on Racetrack - Drop Zone Leg
Pass No. 1
Type of C-141 Formation - No. 1

No Pilot's Comments

Recorded Data:

$V_T = 339$ knots
 $h = \dots$
 $H_P = 950$ ft.

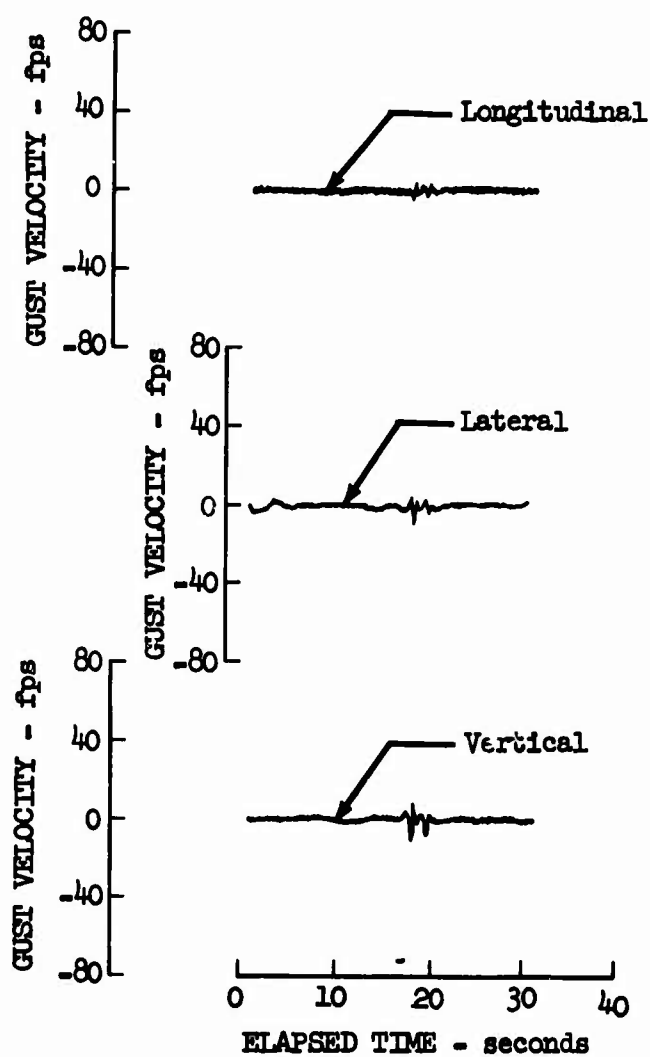


Figure 43.6 Gust Velocity Time Histories - Test 0284,
Sample No. 7

Location on Racetrack - Drop Zone Leg
Pass No. 1
Type of C-141 Formation - No. 1

Recorded Data:

No Pilot's Comments

$V_T = 316$ knots
 $h = 9^\circ$
 $H_P = 1010$ ft.

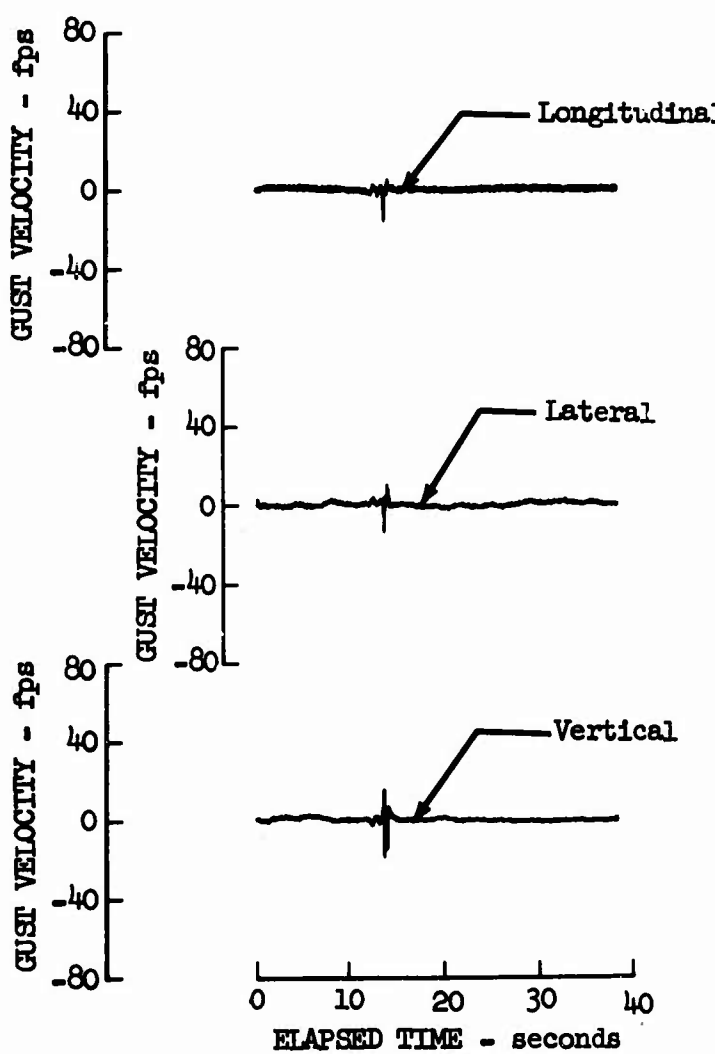


Figure 43.7 Gust Velocity Time Histories - Test 0284,
Sample No. 8

Location on Racetrack - Drop Zone Leg
Pass No. 1
Type of C-141 Formation - No. 1

Recorded Data:

$V_T = 205$ knots

$h = \dots$

$H_P = 1125$ ft.

Pilot's Comments:

Approaching drop zone
 $\frac{3}{4}$ mile behind rear aircraft
Airspeed = 190 knots, altitude 1200 ft.
Very light turbulence through wake

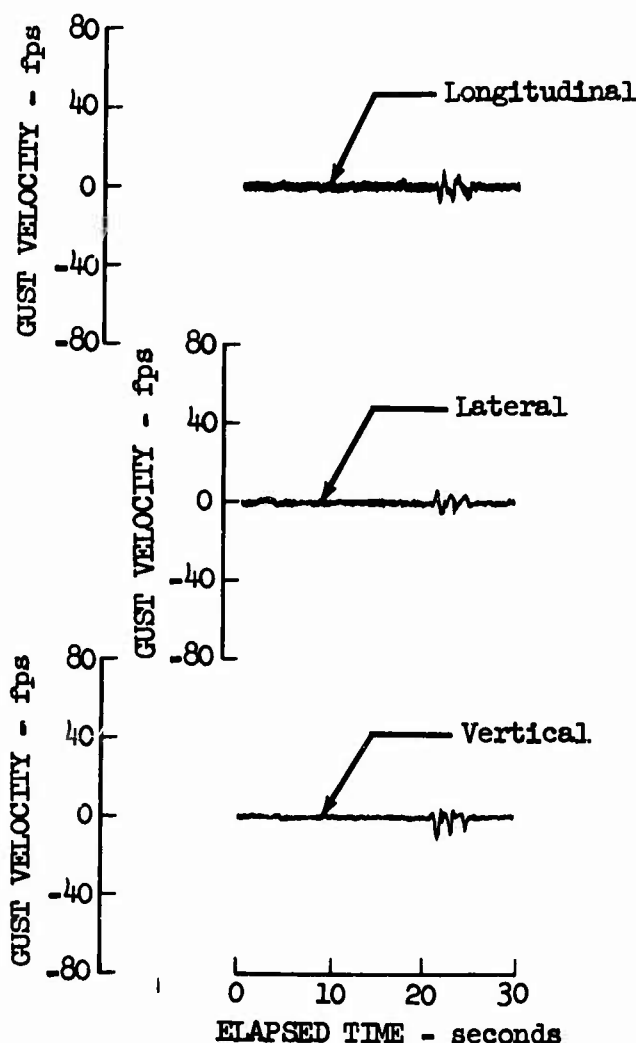


Figure 43.8 Gust Velocity Time Histories - Test 0284,
Sample No. 9

Location on Racetrack - Drop Zone Leg
Pass No. 1
Type of C-141 Formation - No. 1

Recorded Data:

$$V_T = 214 \text{ knots}$$

$$h = 339^\circ$$

$$H_P = 1030 \text{ ft.}$$

Pilot's Comments:

1/2 mile behind rear aircraft
Heading = 335°, altitude = 1000 ft. MSL
Very light wake turbulence

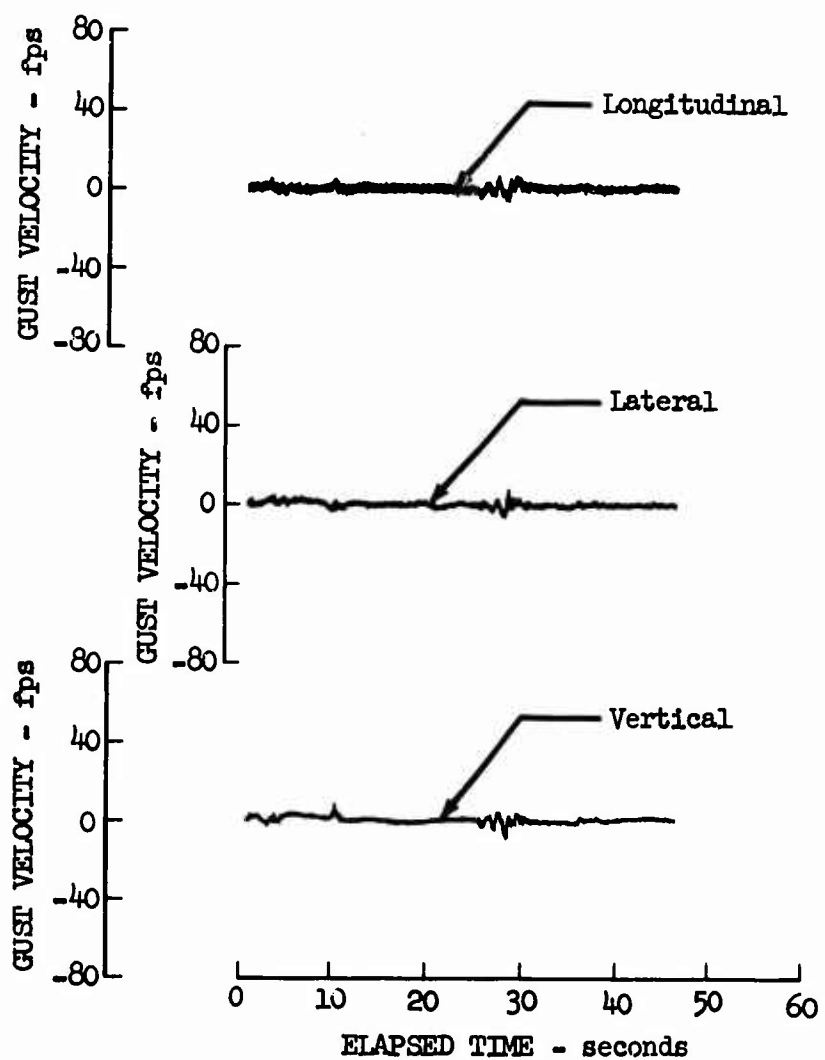


Figure 43.9 Gust Velocity Time Histories - Test 0284,
Sample No. 16

Location on Racetrack - Drop Zone Leg
Pass No. 1
Type of C-141 Formation - No. 1

Recorded Data:

$V_T = 304$ knots
 $h = 119^\circ$
 $H_P = 970$ ft.

Pilot's Comments:

Approaching drop zone
2000 ft. behind rear aircraft
Heading = 85° , altitude = 1000 ft. MSL
Very light turbulence

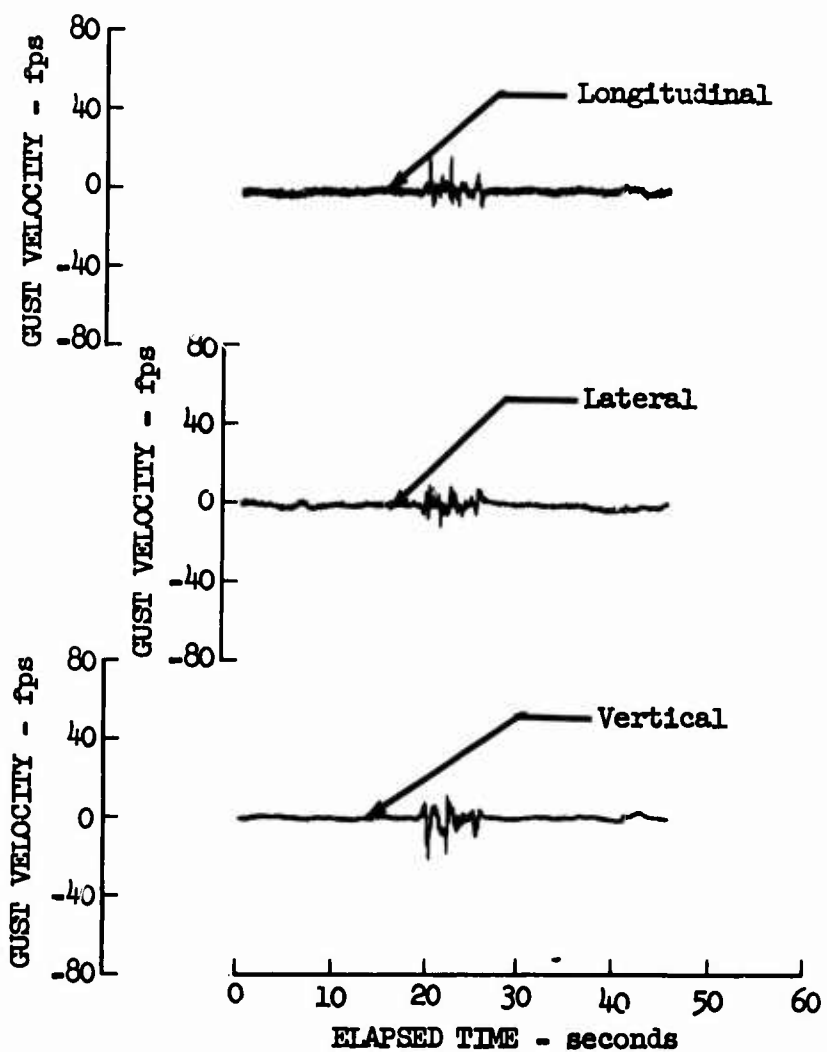


Figure 43.10 Gust Velocity Time Histories - Test 0284,
Sample No. 17

Location on Racetrack - Drop Zone Leg
Pass No. 1
Type of C-141 Formation - No. 1

Recorded Data:

$V_T = 210$ knots
 $h = 343^\circ$
 $H_P = 1100$. ft.

Pilot's Comments:

2000 ft. behind rear aircraft
Heading = 340° , altitude = 1100 ft. MSL
Light turbulence

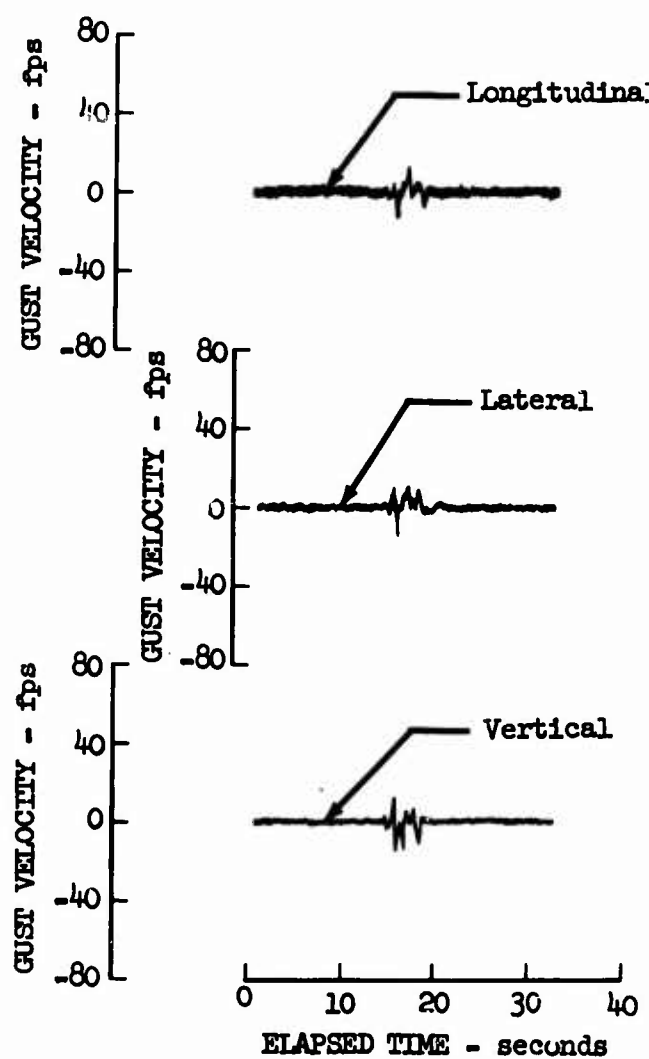


Figure 43.11 Gust Velocity Time Histories - Test 0284,
Sample No. 18

Location on Racetrack - Drop Zone Leg
Pass No. 1
Type of C-141 Formation - No. 1

Recorded Data:

$V_T = 219$ knots

$h = \dots$

$H_P = 1270$ ft.

Pilot's Comments:

1/4 mile behind
Heading = 85° , altitude = 1300 ft.
Airspeed = 210 knots
Very light turbulence

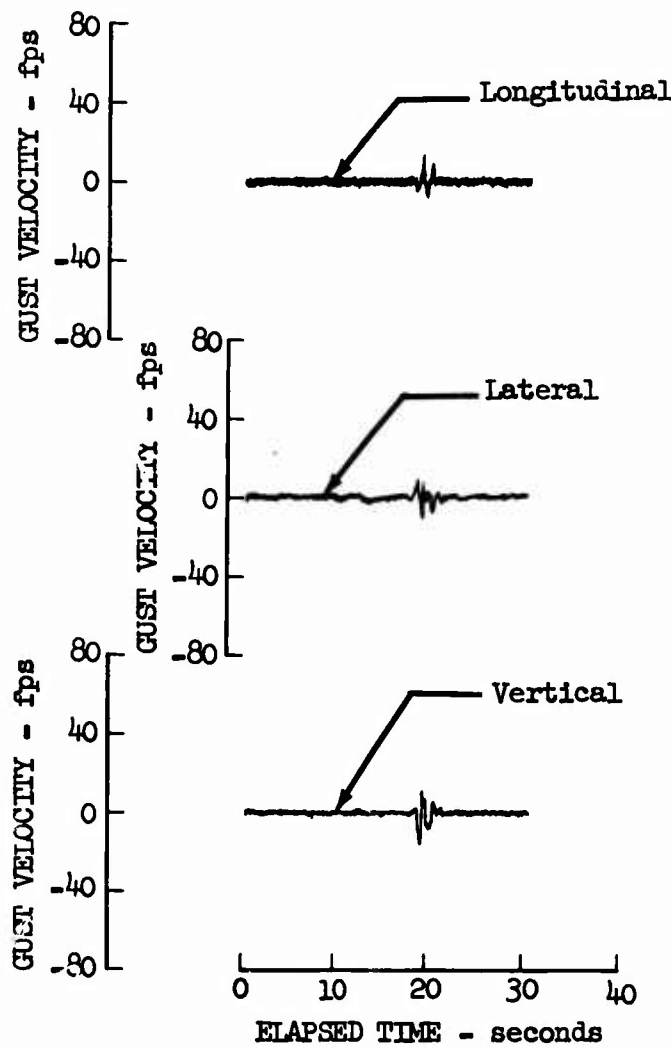


Figure 43.12 Gust Velocity Time Histories - Test 0284,
Sample No. 19

Location on Racetrack - Enroute Portion
Pass No. 2
Type of C-141 Formation - Modified In-Trail Concept

Recorded Data:

$$V_T = 264 \text{ knots}$$

$$h = 162^\circ$$

$$H_P = 580 \text{ ft.}$$

Pilot's Comments:

Descending to 500 ft.
1/2 mile astern
Light, sharp cuts - light turbulence

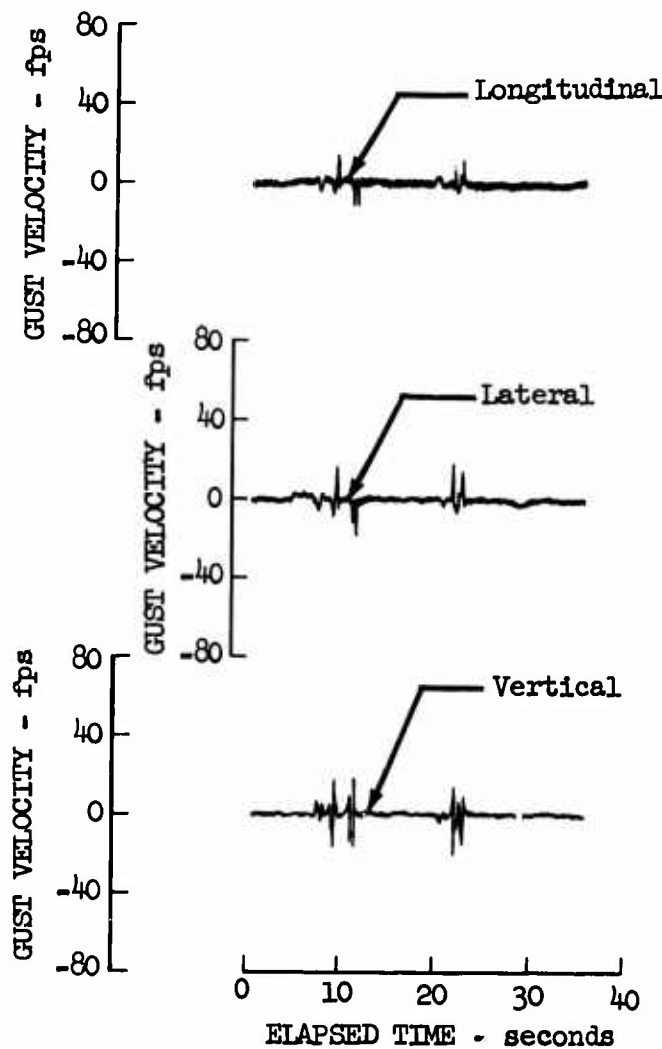


Figure 43.13 Gust Velocity Time Histories - Test 0284,
Sample No. 20

Location on Racetrack - Enroute Portion
Pass No. 2
Type of C-141 Formation - Modified In-Trail Concept

Recorded Data:

$V_T = 250$ knots
 $h = 218^\circ$
 $H_P = 600$ ft.

Pilot's Comments:

1 mile astern, closing to 3/4 mile
Heading = 200°, altitude = 500 ft.
Light turbulence
Slight roll rate at 72 seconds into sample
Cutting wake at approximately 40°

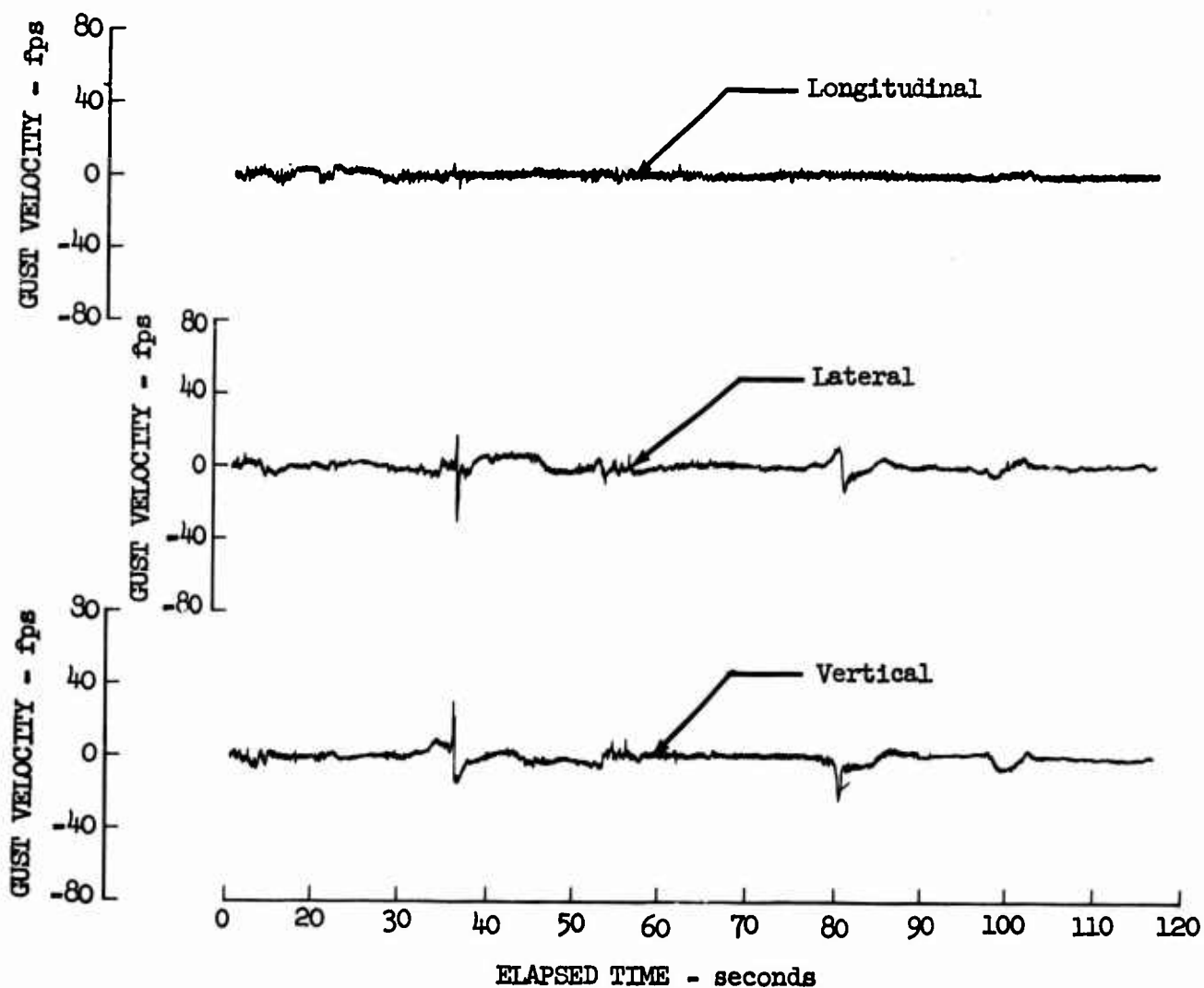


Figure 43.14 Gust Velocity Time Histories - Test 0284,
Sample No. 21

Location on Racetrack - Drop Zone Leg
Pass No. 2
Type of C-141 Formation - No. 2

Recorded Data:

$V_T = 263$ knots
 $h = 86^\circ$
 $H_P = 1820$ ft.

Pilot's Comments:

1 mile to the rear
Heading = 55° , altitude - 2000 ft. MSL
Airspeed = 250 knots
Light turbulence, encountered some roll

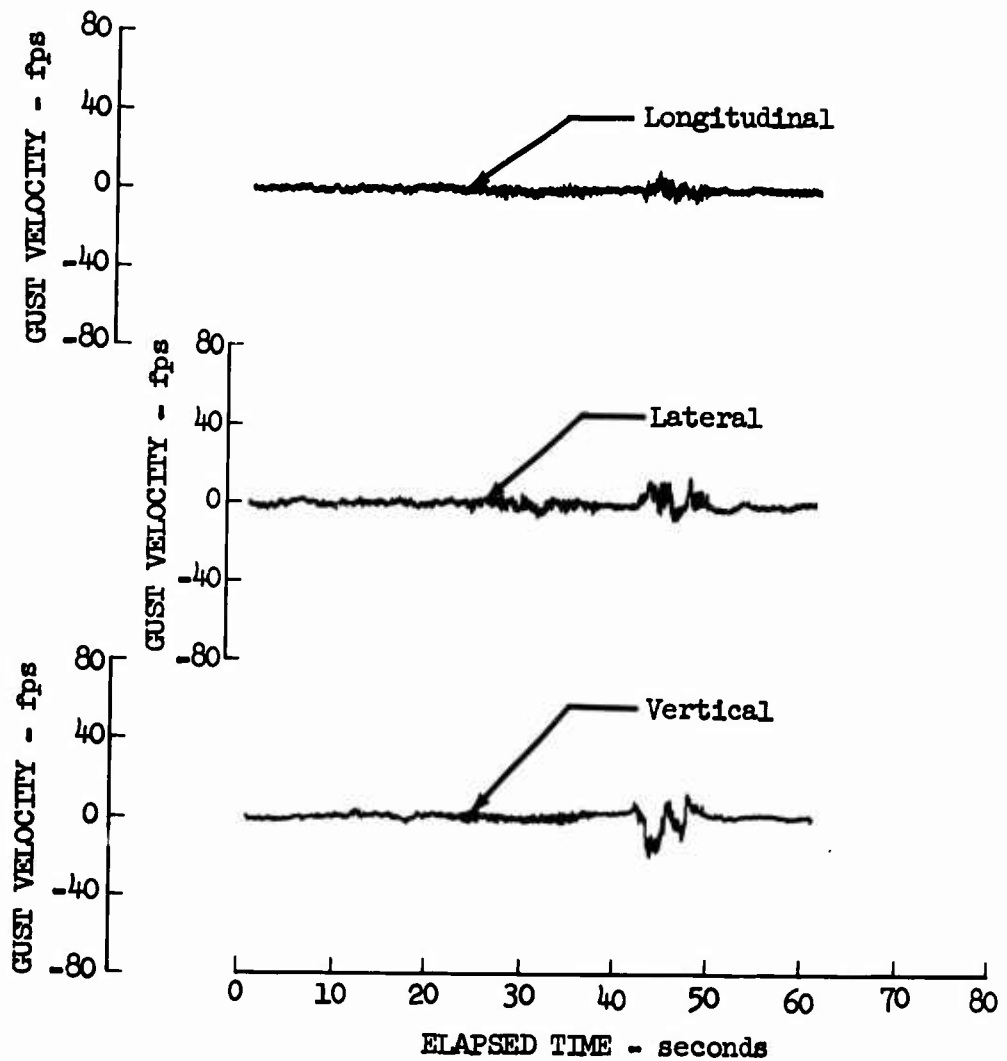


Figure 43.15 Gust Velocity Time Histories - Test 0284,
Sample No. 25

Location on Racetrack - Drop Zone Leg
Pass No. 2
Type of C-141 Formation - No. 2

Recorded Data:

$V_T = 205$ knots
 $h = 349^\circ$
 $H_P = 850$ ft.

Pilot's Comments:

1/4 mile behind, 1000 ft. altitude
Heading = 345° , airspeed = 200 knots
Very light turbulence

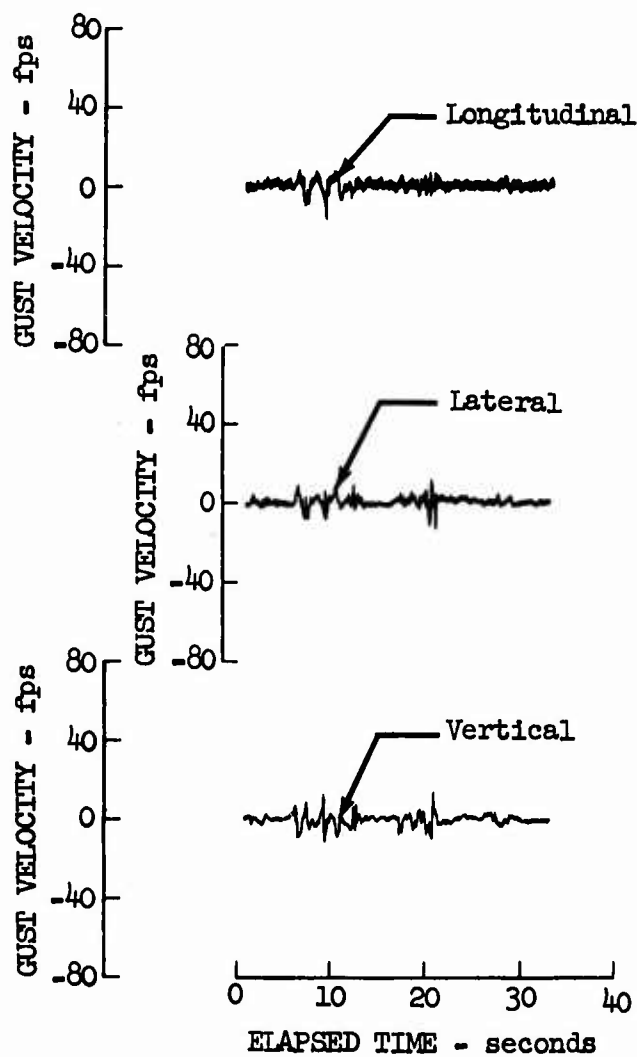


Figure 43.16 Gust Velocity Time Histories - Test 0284,
Sample No. 26

Location on Racetrack - Drop Zone Leg
Pass No. 2
Type of C-141 Formation - No. 2

Recorded Data:

$V_T = 236$ knots

$h = \dots$

$H_P = 1080$ ft.

Pilot's Comments:

1/4 mile behind
Heading = 340° , altitude = 1100 ft.
Airspeed = 236 knots

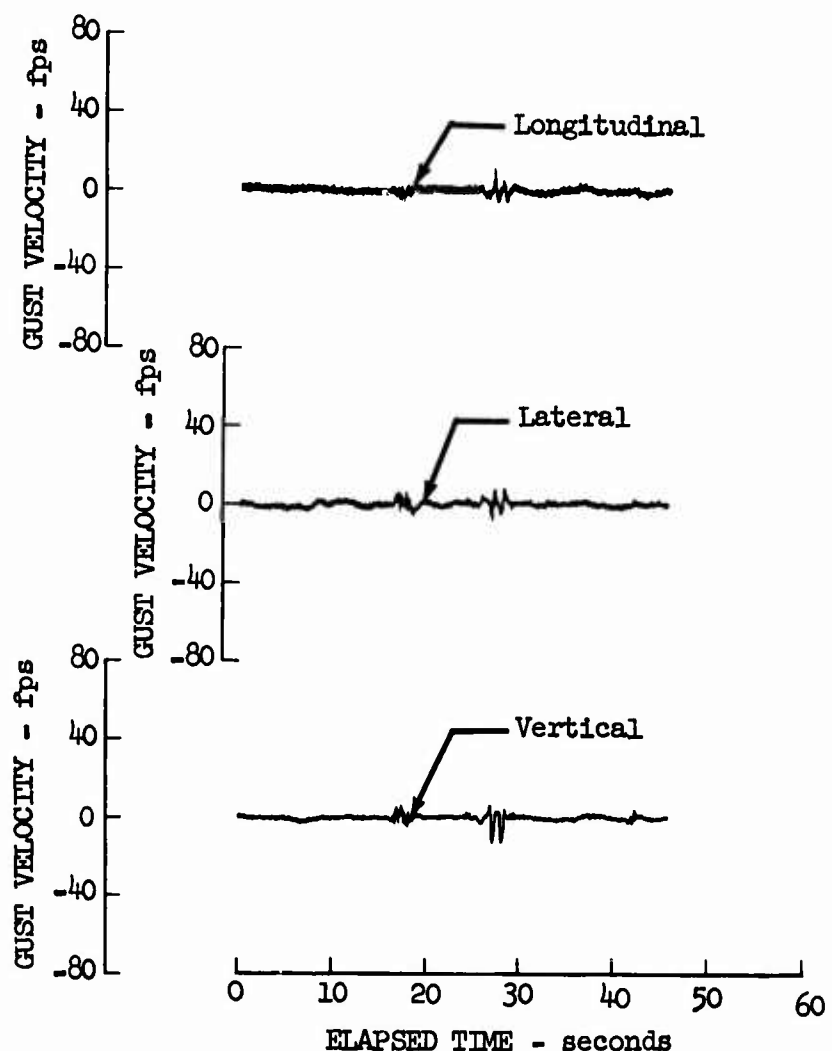


Figure 43.17 Gust Velocity Time Histories - Test 0284,
Sample No. 27

Location on Racetrack - Drop Zone Leg
Pass No. 2
Type of C-141 Formation - No. 2

Recorded Data:

$V_T = 237$ knots

$h = \dots$

$H_P = 1210$ ft.

Pilot's Comments:

Over drop zone
Heading = 85° , altitude = 1200 ft. MSL
Very light turbulence as I pass through wake

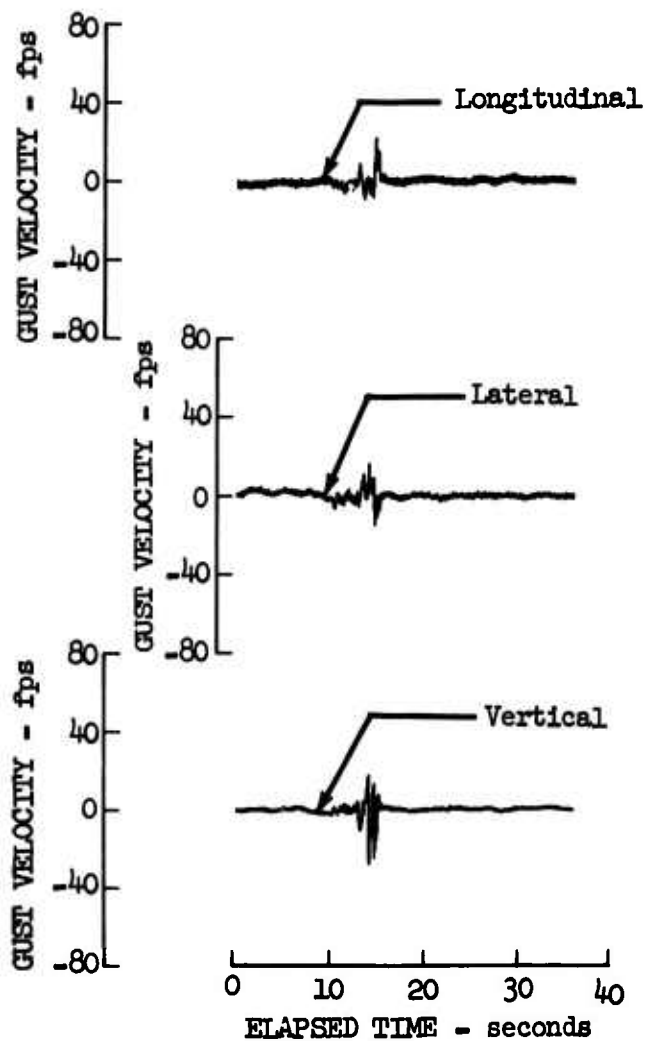


Figure 43.18 Gust Velocity Time Histories - Test 028⁴,
Sample No. 29

Recorded Data:

$V_1 = 298$ knots

$h = 132^{\circ}$

$H_P = 860$ ft.

Location on Racetrack - Enroute Portion

Pass No. 3

Type of C-141 Formation - Modified In-Trail Concept

No Pilot's Comments

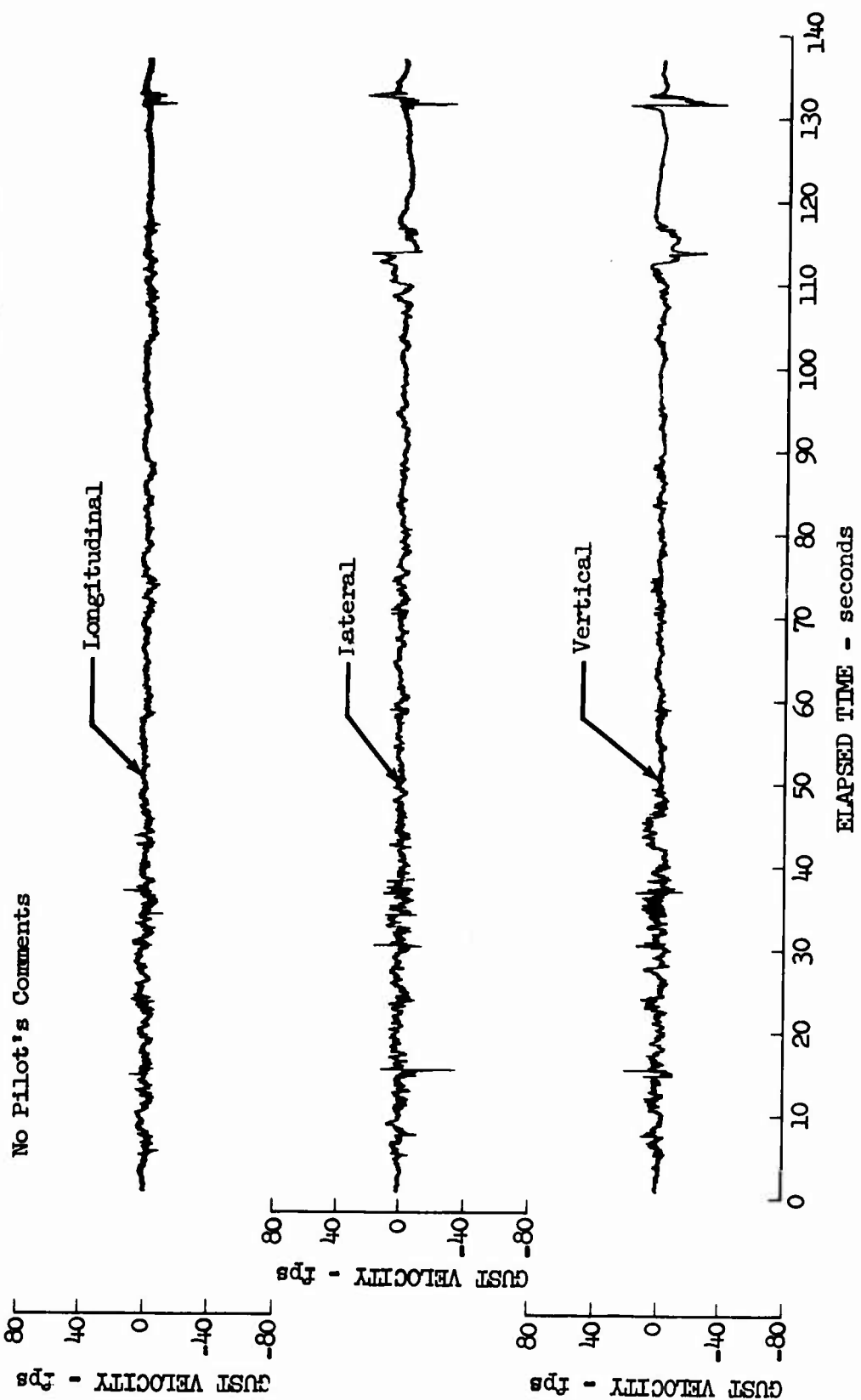


Figure 43.19 Gust Velocity Time Histories - Test 0284,
Sample No. 36

Location on Racetrack - Drop Zone Leg
Pass No. 3
Type of C-141 Formation - No. 2

No Pilot's Comments

Recorded Data:

$V_T = 227$ knots

$h = \dots$

$H_P = 1250$. ft.

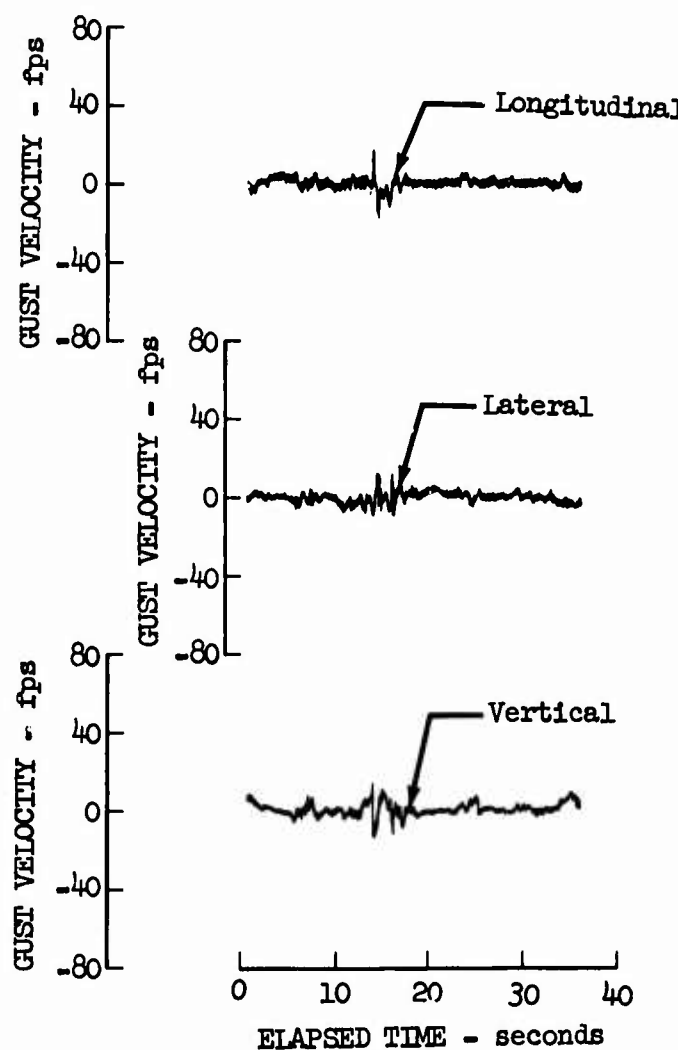


Figure 43.20 Gust Velocity Time Histories - Test 0284,
Sample No. 38

Location on Racetrack - Drop Zone Leg
Pass No. 3
Type of C-141 Formation - No. 2

No Pilot's Comments

Recorded Data:

$V_T = 215$ knots

$h = \dots$

$H_P = 1140$ ft.

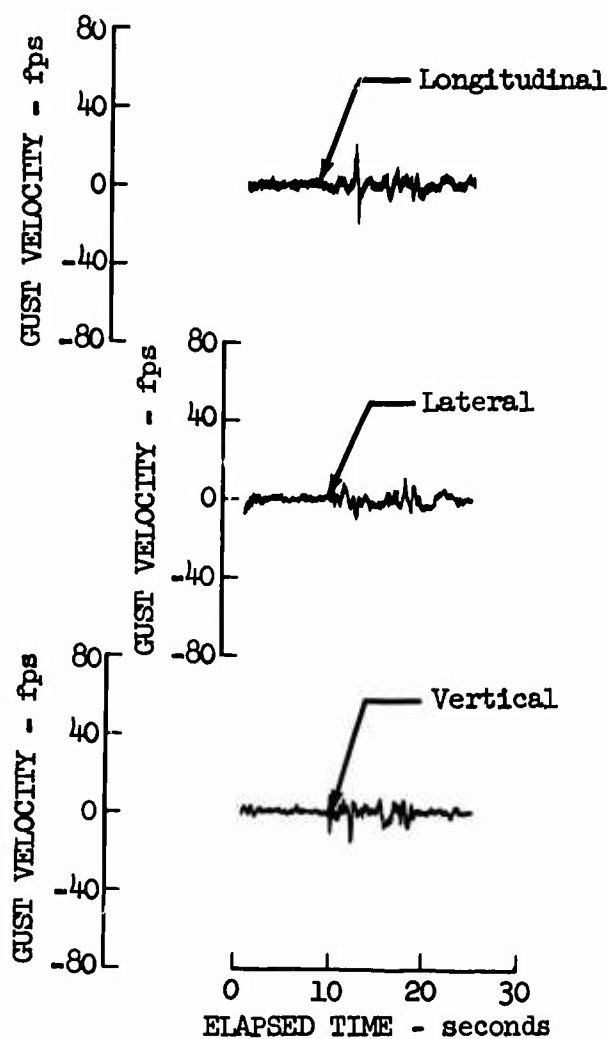


Figure 43.21 Gust Velocity Time Histories - Test 0284,
Sample No. 39

Location on Racetrack - Drop Zone Leg
Pass No. 5
Type of C-141 Formation - No. 3

Recorded Data:

$V_T = 233$ knots

$h = \dots$

$H_P = 590$ ft.

Pilot's Comments:

Airspeed = 230 knots
Altitude = 900 ft.
Heading = 75°

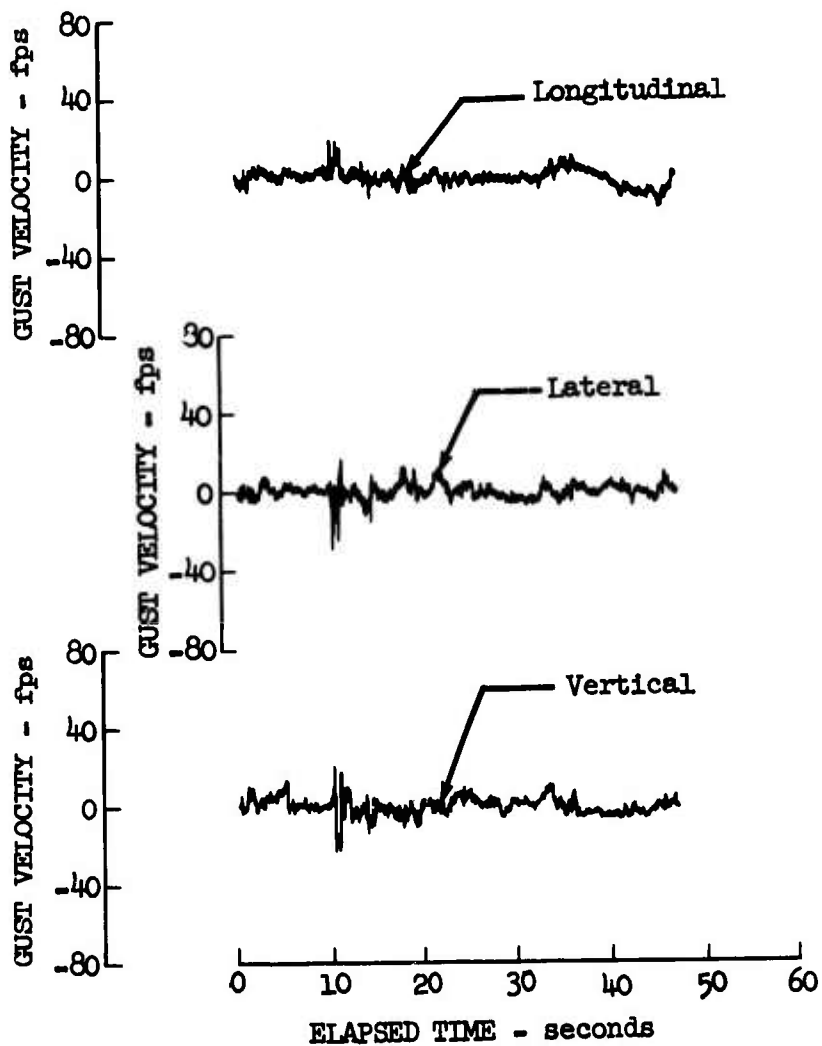


Figure 43.22 Gust Velocity Time Histories - Test 0285,
Sample No. 3

Location on Racetrack - Drop Zone Leg
Pass No. 5
Type of C-141 Formation - No. 3

Recorded Data:

$V_r = 197$ knots
 $h = 3^\circ$
 $H_p = 650$ ft.

Pilot's Comments

1500 ft. behind rear aircraft
Heading = 355° , altitude = 900 ft.
Airspeed = 190 knots
Very light turbulence

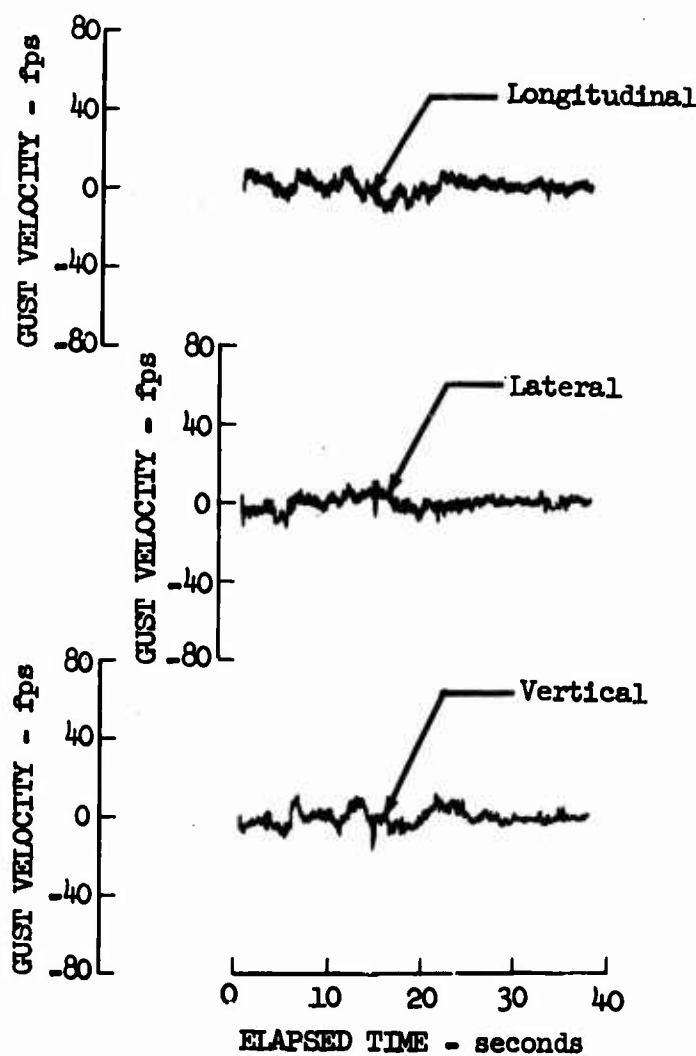


Figure 43.23 Gust Velocity Time Histories - Test 0285,
Sample No. 4

Location on Racetrack - Enroute Portion
Pass No. 6
Type of C-141 Formation - No. 3

Recorded Data:

$V_T = 275$ knots
 $h = 125^\circ$
 $H_P = 940$ ft.

Pilot's Comments

One mile behind rear aircraft, closing slightly
Heading = 130° , altitude - 1100 ft.
Now 1/2 mile behind
Directly in wake of rear aircraft
Slight turbulence

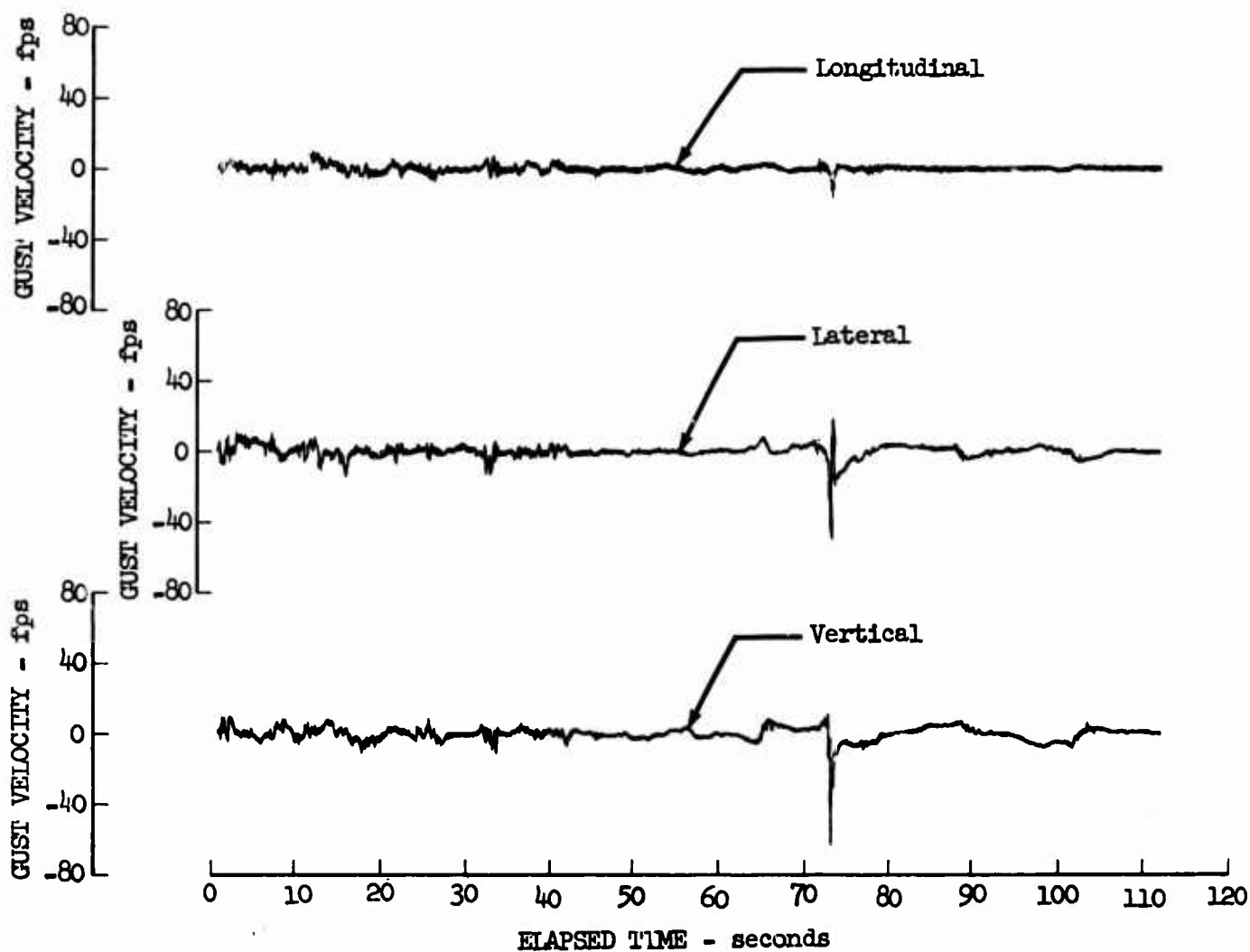


Figure 43.24 Gust Velocity Time Histories - Test 0285,
Sample No. 6

Location on Racetrack - Enroute Portion
Pass No. 6
Type of C-141 Formation - Modified In-Trail Concept

Pilot's Comments:

1/2 mile behind rear aircraft
Heading = 220°, altitude = 1100 ft. MSL
Slight turbulence, slight roll left, descending into wake
Now descending to 500 ft. altitude, 1/4 mile behind
Easing from left to right to go through wake
Very light turbulence

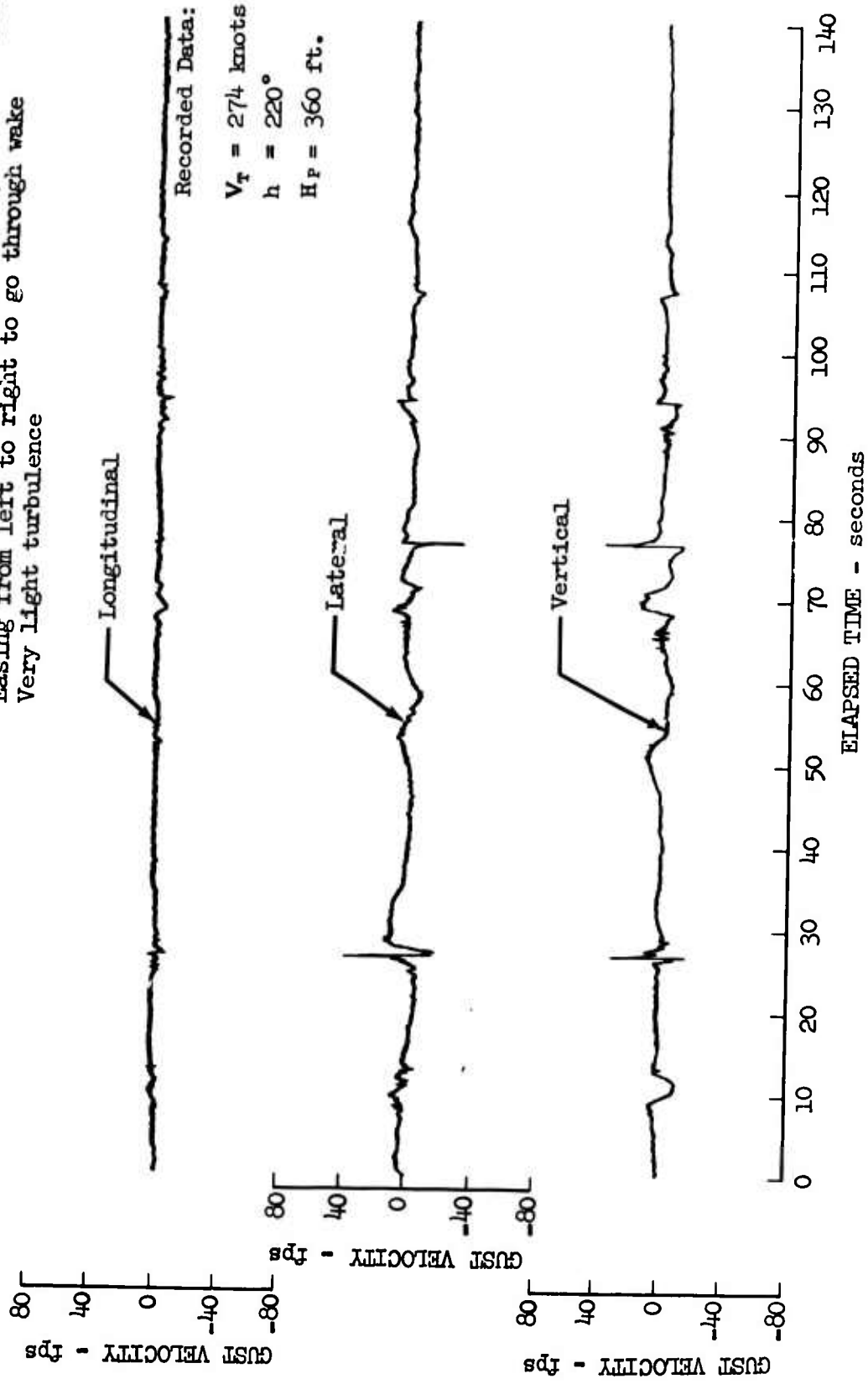


Figure 42.25 Gust Velocity Time Histories - Test 0285,
Sample No. 7

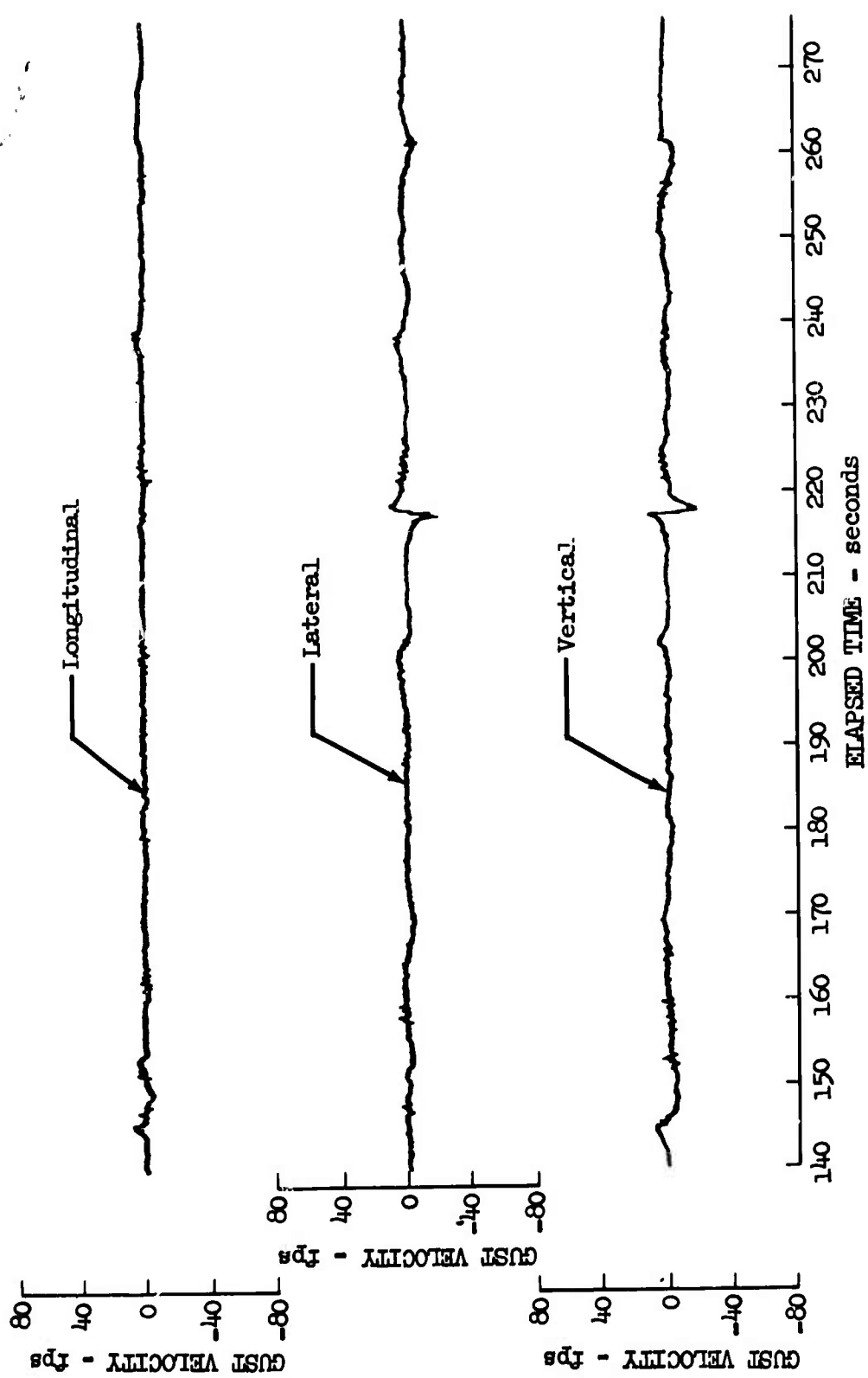


Figure 43.26 Gust Velocity Time Histories - Test 0285,
Sample No. 7 (continued)

Location on Racetrack - Enroute Portion

Pass No. 6

Type of C-141 Formation - Modified In-Trail Concept

Pilot's Comments:

2000 ft. behind and closing

Airspeed = 250 knots, altitude = 500 ft.

1500 ft. behind, very little turbulence

Now 1000 ft. behind, light turbulence, no rolling

Now 800 ft. behind, slightly more turbulence

Slight rolling moment from right wing of C-141

Recorded Data:

$$V_T = 271 \text{ knots}$$

$$h = 230^\circ$$

$$H_P = 350 \text{ ft.}$$

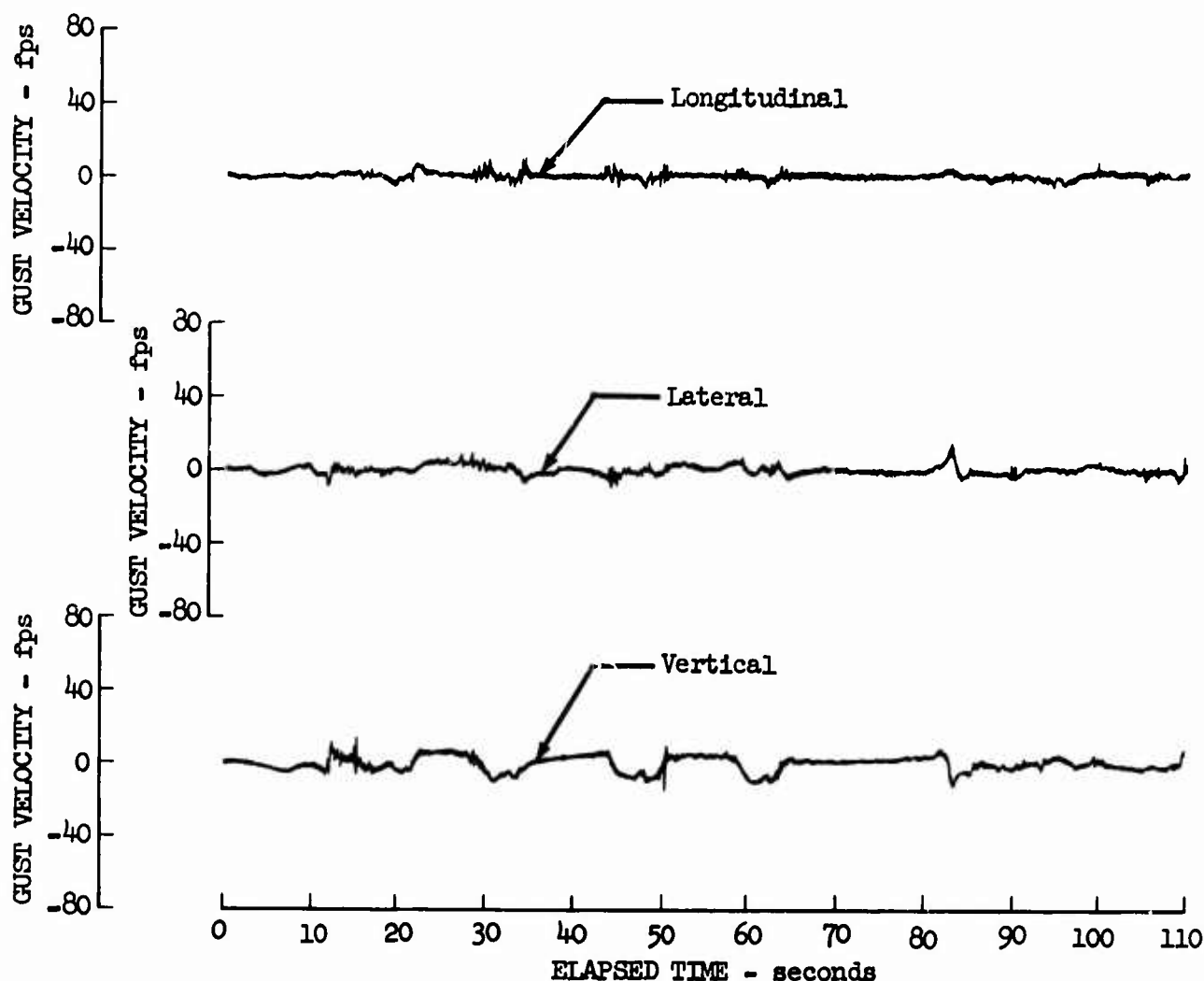


Figure 43.27 Gust Velocity Time Histories - Test 0285,
Sample No. 8

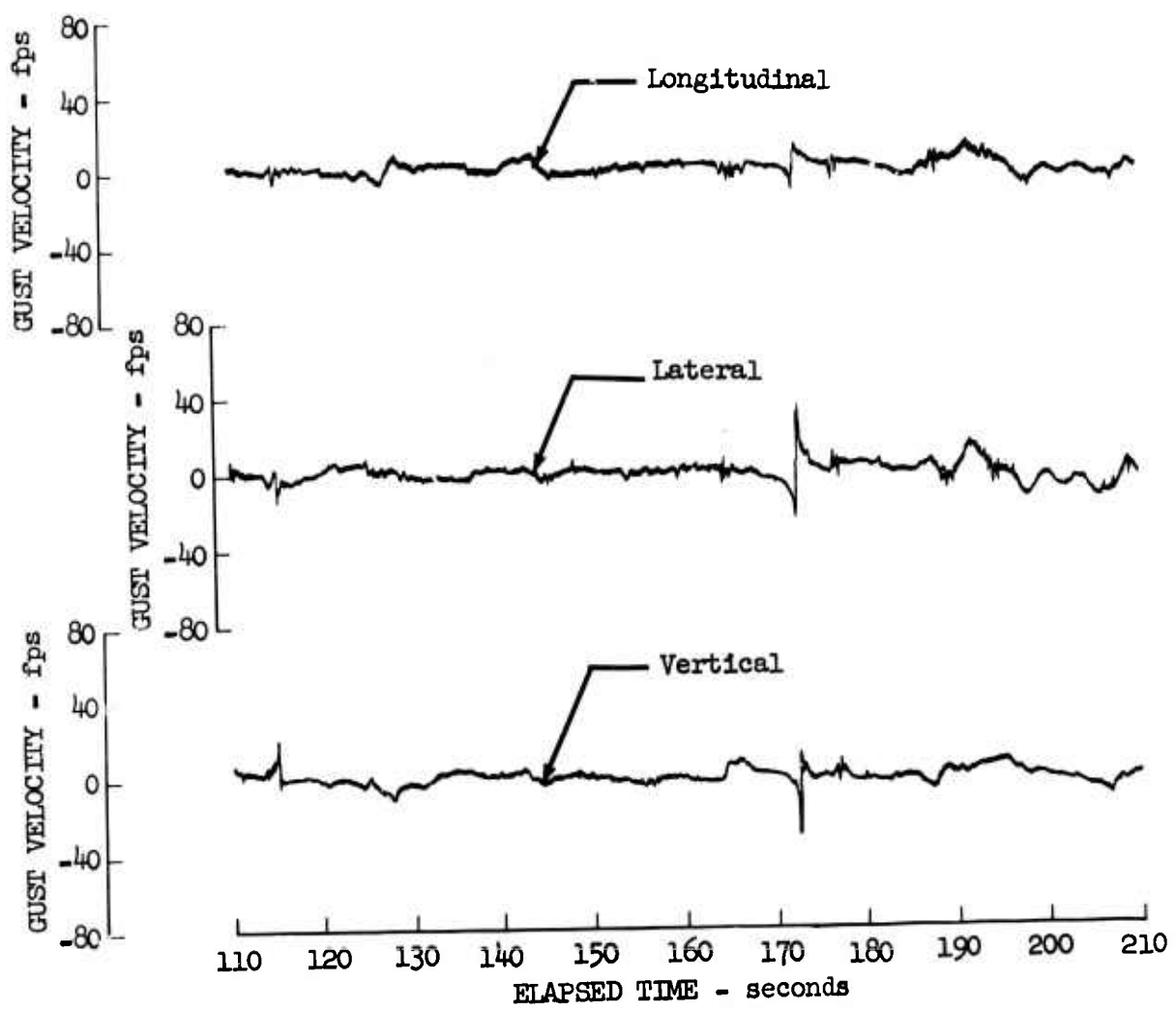


Figure 43.28 Gust Velocity Time Histories - Test 0285,
Sample No. 8 (continued)

Location on Racetrack - Drop Zone Leg

Recorded Data:

Pass No. 6

Type of C-141 Formation - Modified In-Trail Concept

$V_T = 272$ knots

Pilot's Comments:

$h = 8^\circ$

2000 ft. directly behind rear element

$H_P = 310$ ft.

Heading = 360° , altitude = 500 ft., airspeed = 250 knots

In wake of all three aircraft

Now 1000 ft. behind rear aircraft

Airspeed = 290 knots

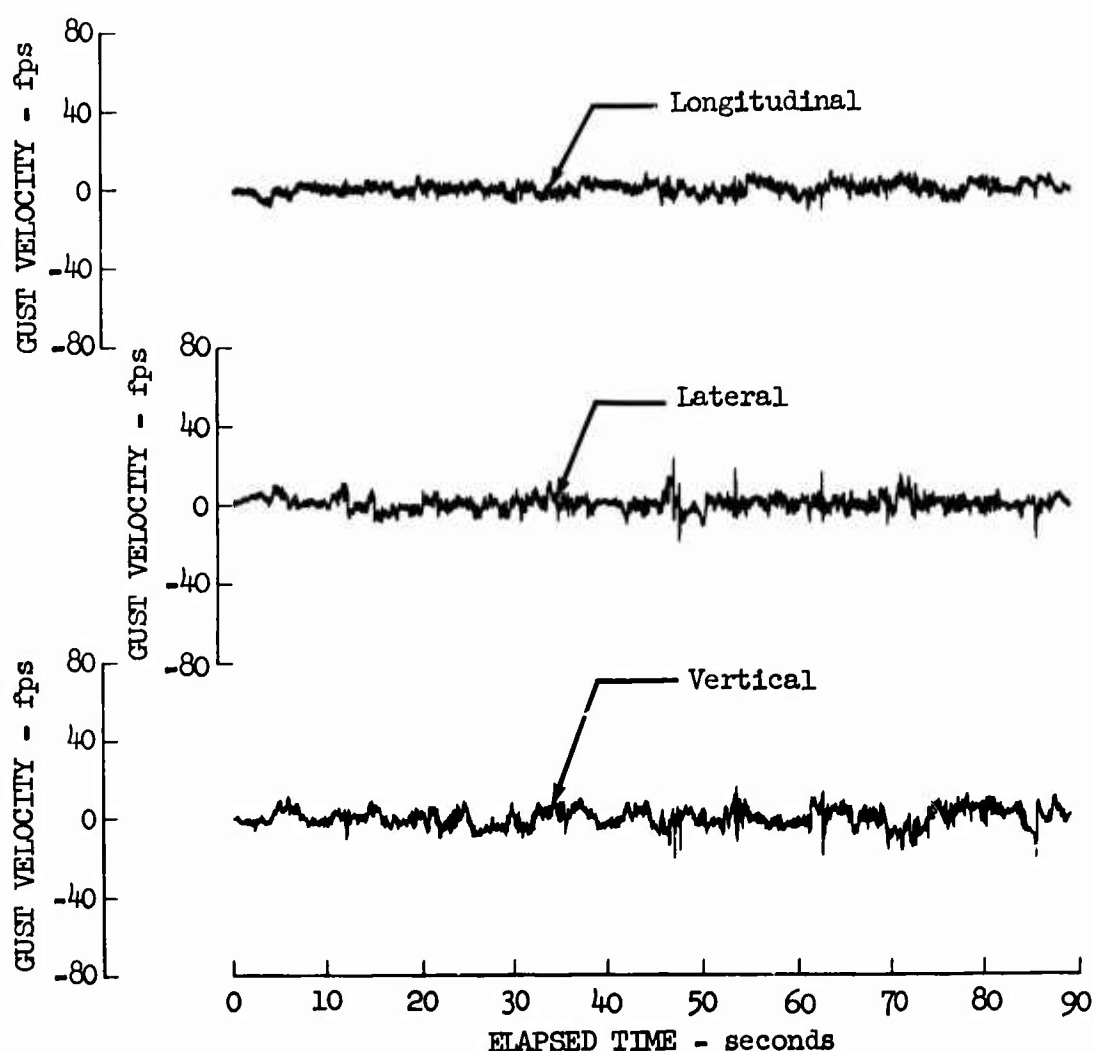


Figure 43.29 Gust Velocity Time Histories - Test 0285,
Sample No. 9

Location on Racetrack - Drop Zone Leg
Pass No. 6

Type of C-141 Formation - Modified In-Trail Concept

Pilot's Comments:

1000 ft. astern, Heading = 40°

Altitude = 500 ft., airspeed = 260 knots

Now working up and down, side to side 500 ft. behind

Very light turbulence

Recorded Data:

$$V_T = 270 \text{ knots}$$

$$h = 19^\circ$$

$$H_P = 400 \text{ ft.}$$

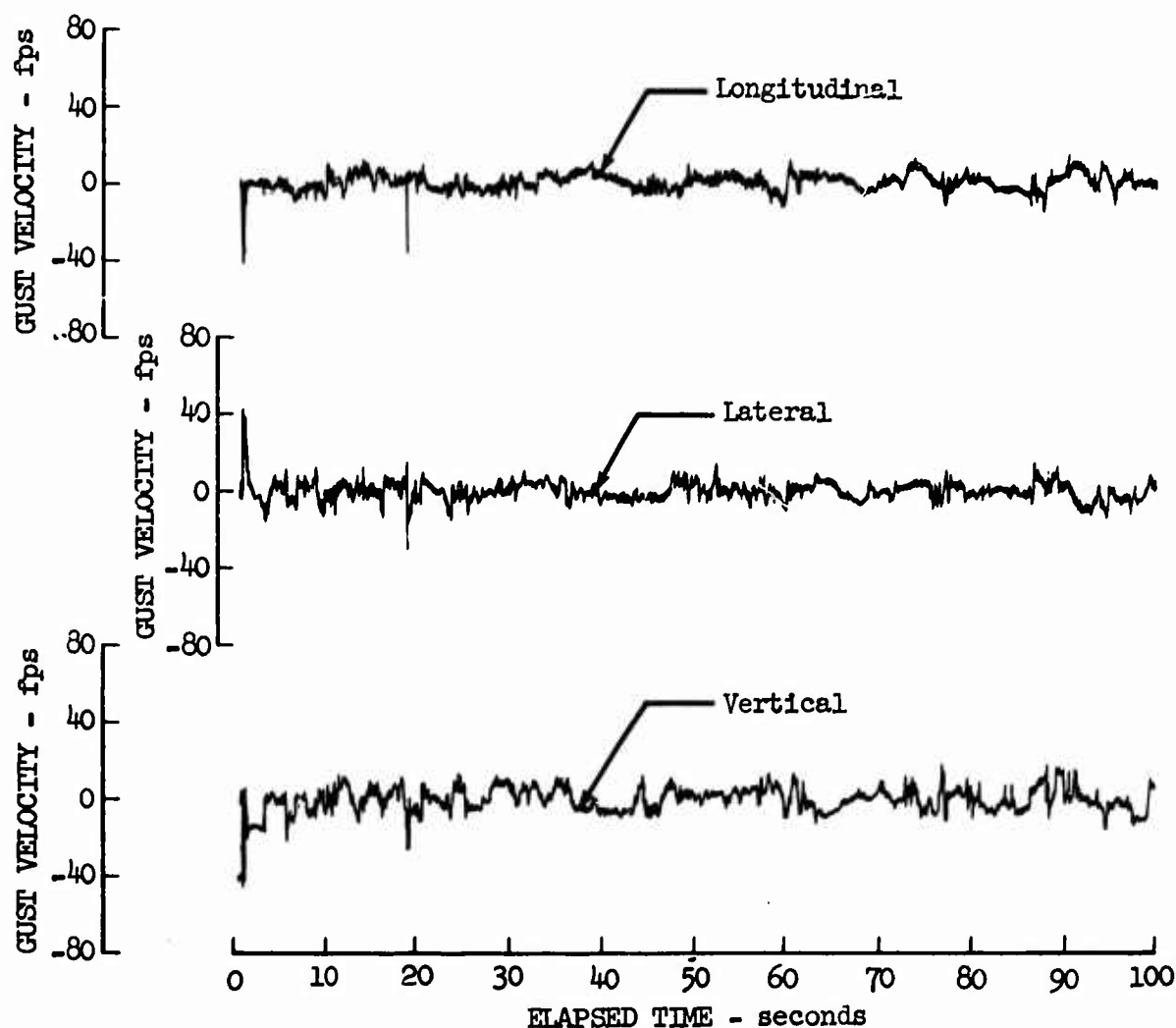


Figure 43.30 Gust Velocity Time Histories - Test 0285,
Sample No. 10

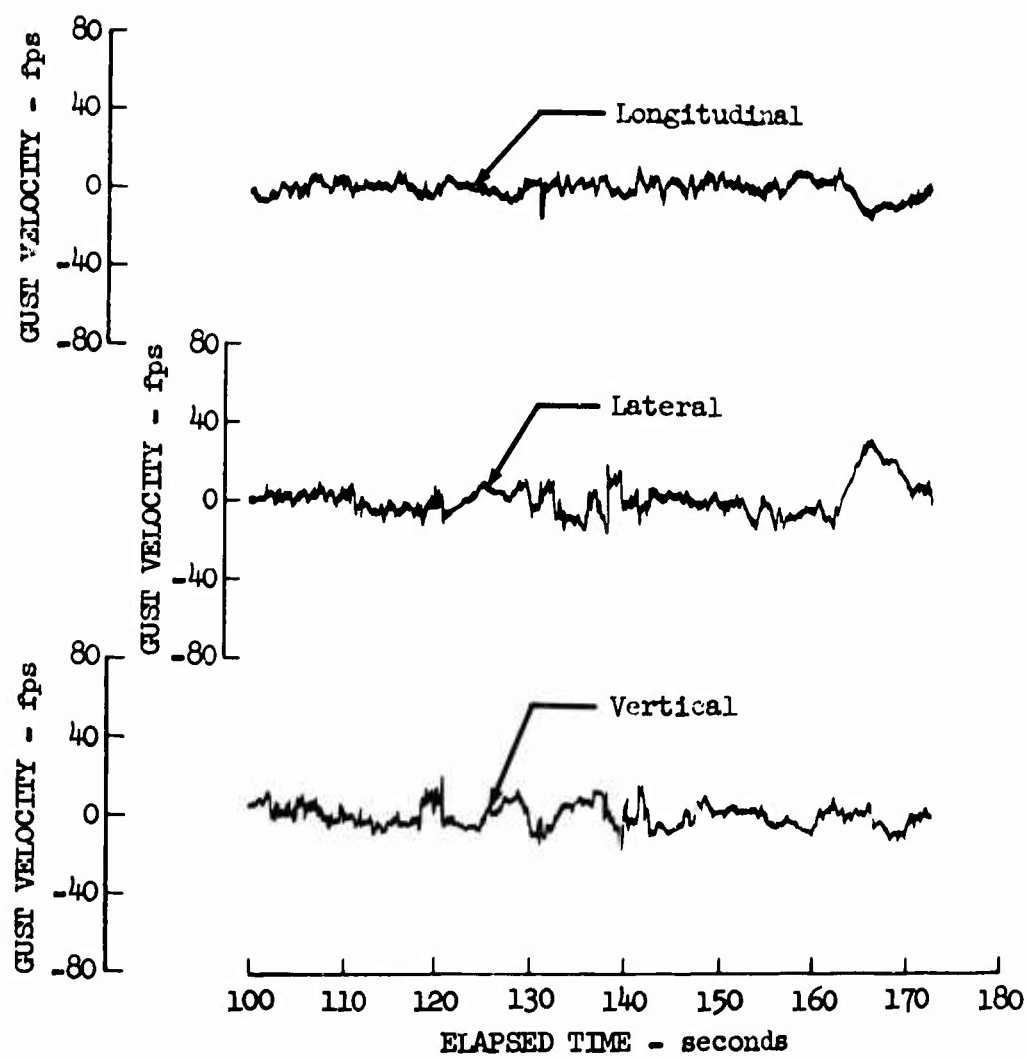


Figure 43.31 Gust Velocity Time Histories - Test 0285,
Sample No. 10 (continued)

Location on Racetrack - Drop Zone Leg
Pass No. 6
Type of C-141 Formation - No. 4

Pilot's Comments:

Heading = 355°, airspeed = 200 knots
Working left to right across whole formation
Altitude = 900 ft., very light turbulence

Recorded Data:

V_T = 210 knots
 h = 345°
 H_P = 750 ft.

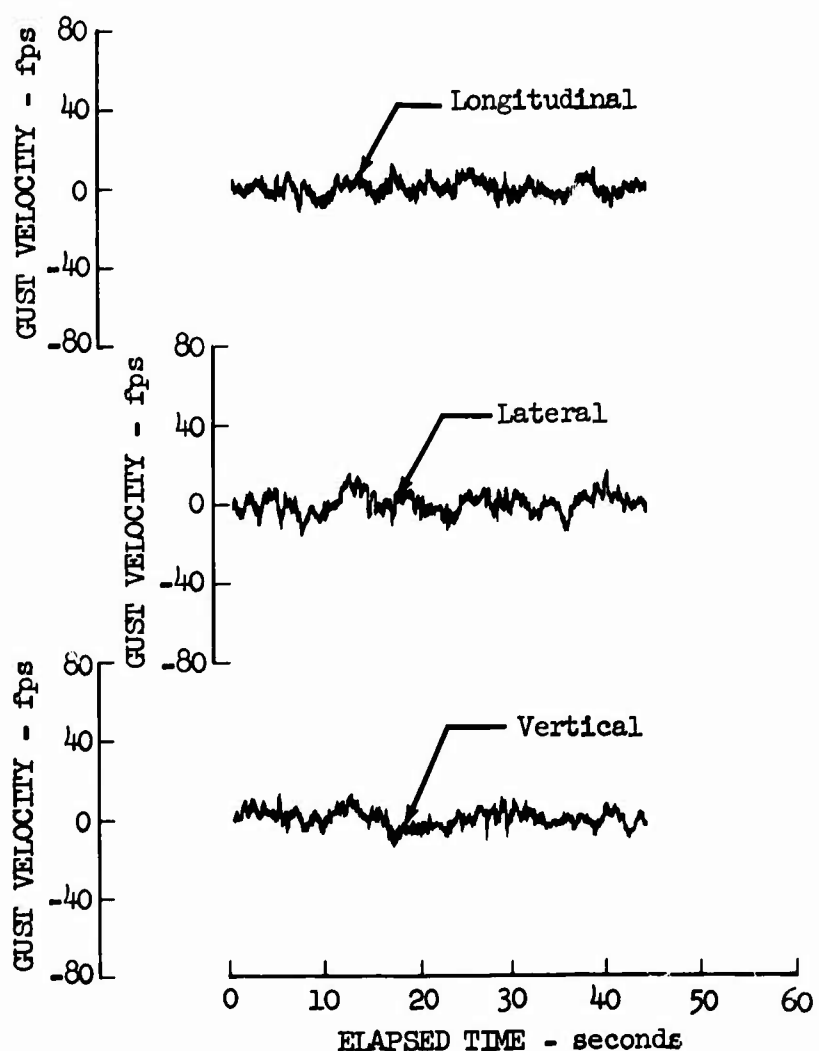


Figure 43.32 Gust Velocity Time Histories - Test 0285,
Sample No. 11

Location on Racetrack - Drop Zone Leg
Pass No. 6
Type of C-141 Formation - No. 1

Recorded Data:
 $V_T = 240$ knots
 $h = \dots$
 $H_P = 730$ ft.

Pilot's Comments:

Proceeding diagonally across formation
Heading = 70°
Crossing at 500 ft. behind rear aircraft, light jolt
Very light turbulence behind rest of formation

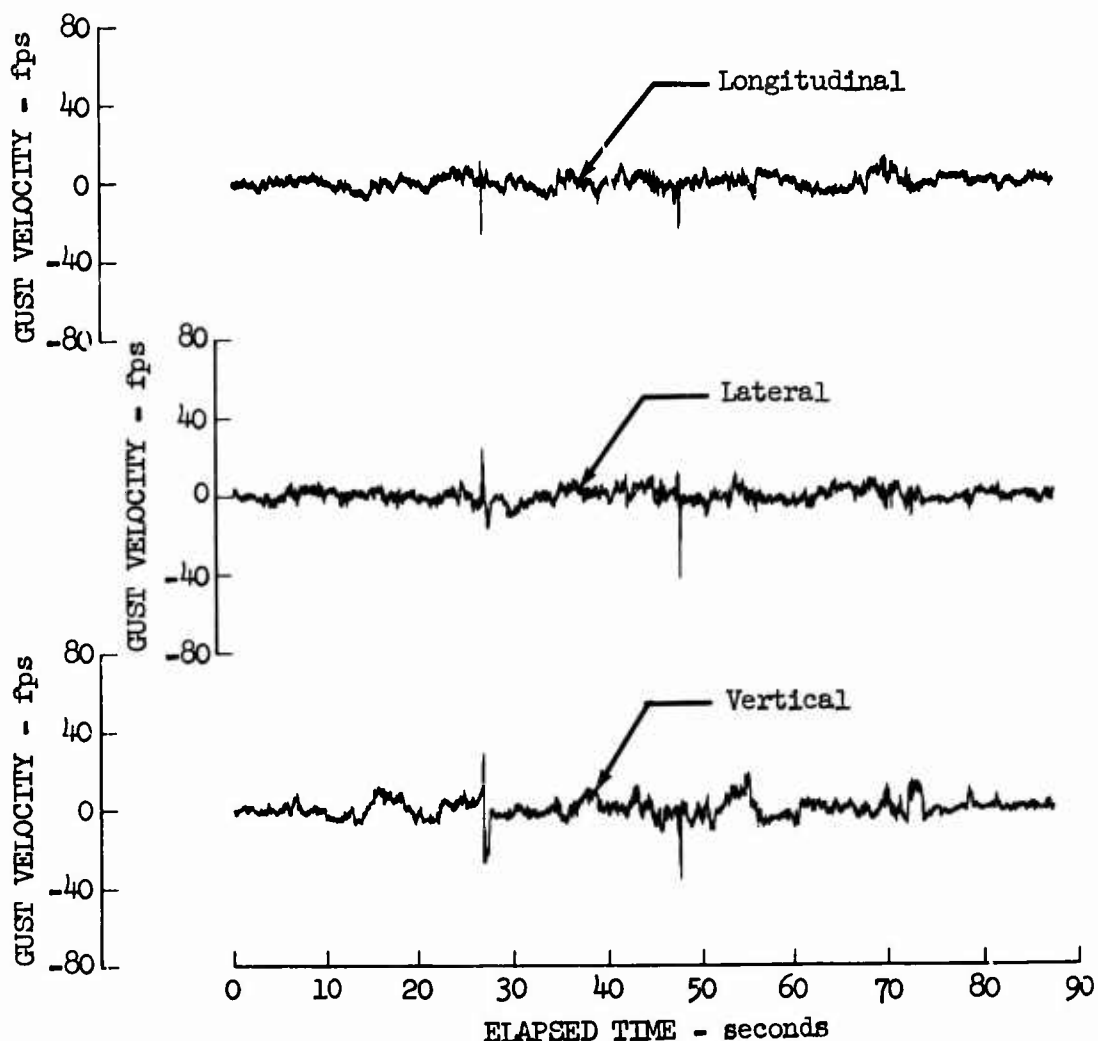


Figure 43.33 Gust Velocity Time Histories - Test 0285,
Sample No. 12

Location on Racetrack - Enroute Portion
Pass No. 7
Type of C-141 Formation - No. 4

Recorded Data:

$$V_T = 306 \text{ knots}$$

$$h = 119^\circ$$

$$H_P = 990 \text{ ft.}$$

Pilot's Comments:

One mile behind and closing
Heading = 120° , altitude = 1300 ft.
Airspeed = 310 knots
1/4 mile behind, directly behind lead aircraft
Slight rolling moment at 1/2 mile behind
Now crossing 500 ft. behind rear aircraft
Slight turbulence

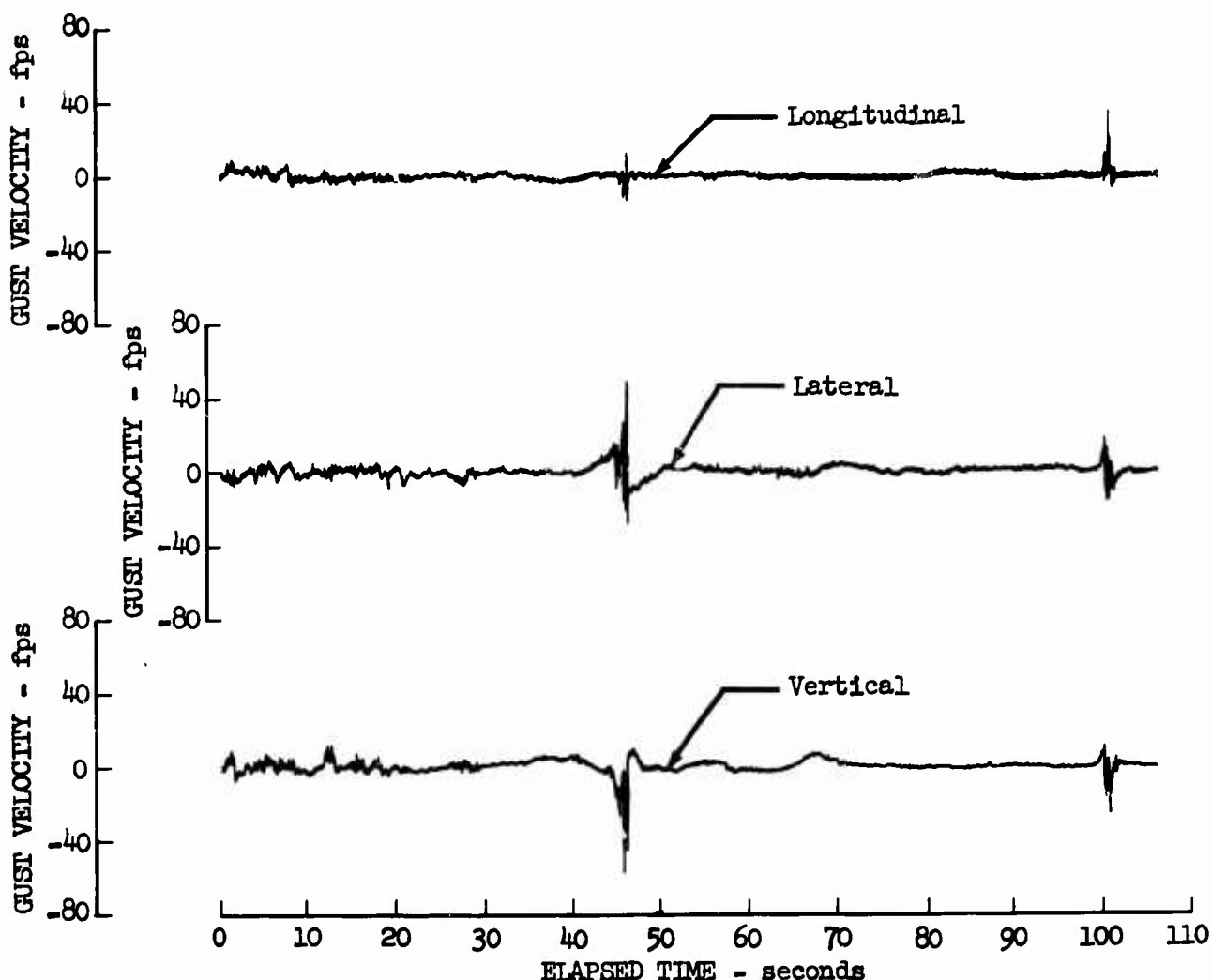


Figure 43.34 Gust Velocity Time Histories - Test 0285,
Sample No. 17

Location on Racetrack - Enroute Portion

Pass No. 7

Type of C-141 Formation - Modified In-Trail Concept

Pilot's Comments:

Working up and down through the wake
 Airspeed = 300 knots, altitude = 500 ft.
 500 ft. behind rear aircraft
 Light turbulence, steady chop, no rolling moment
 Sliding across rear element at 600 ft. altitude
 700 ft. behind rear aircraft, very light turbulence
 Slight rolling moment
 500 ft. behind

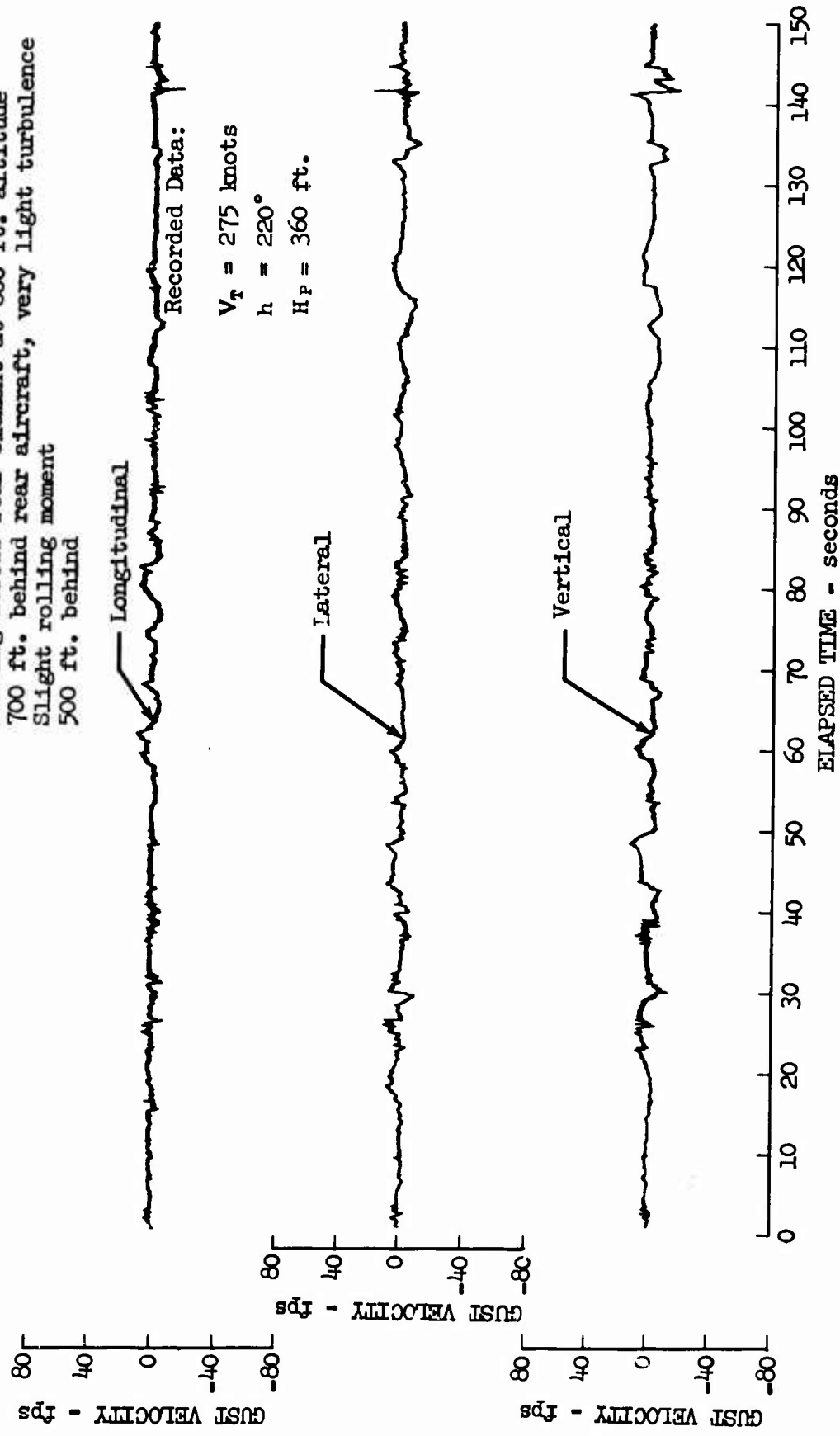


Figure 43.35 Gust Velocity Time Histories - Test 0285,
 Sample No. 18

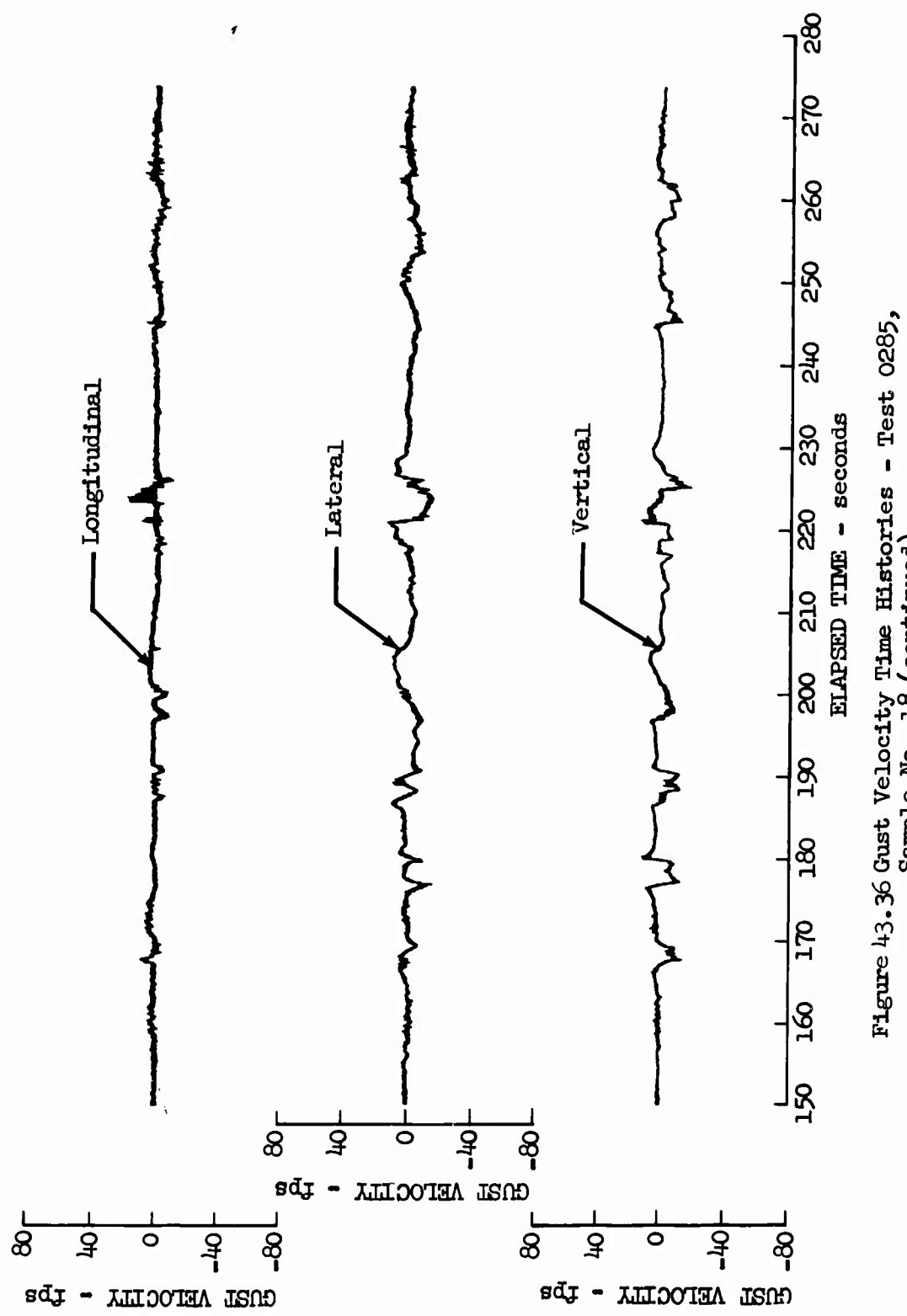


Figure 43.36 Gust Velocity Time Histories - Test 0285,
Sample No. 18 (continued)

Location on Racetrack - Enroute Portion
Pass No. 7

Type of C-141 Formation - Modified In-Trail Concept
Pilot's Comments

500 ft. behind rear aircraft in parallel course
Now easing from left to right across formation
Airspeed = 240 knots, altitude = 580 ft.
Very light turbulence, slight rolling moment

Recorded Data:

V_T = 271 knots

h = 220°

H_P = 370 ft.

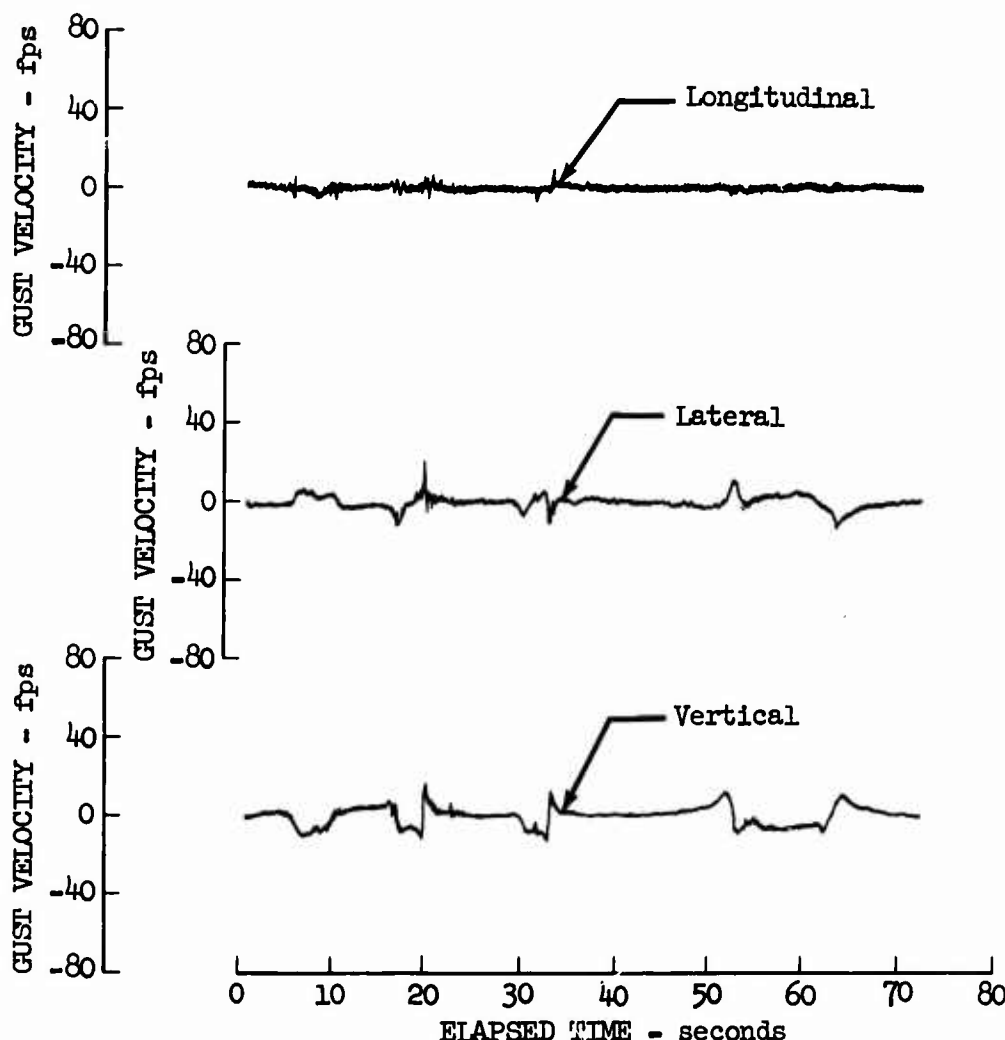


Figure 43.37 Gust Velocity Time Histories - Test 0285,
Sample No. 19

Location on Racetrack - Enroute Portion
Pass No. 7
Type of C-141 Formation - Modified In-Trail Concept

Pilot's Comments:

Crossing back across the rear element
Crossing 500 ft. behind rear aircraft
Very light turbulence

Recorded Data:

$V_T = 256$ knots
 $h = \dots$
 $H_P = 350$ ft.

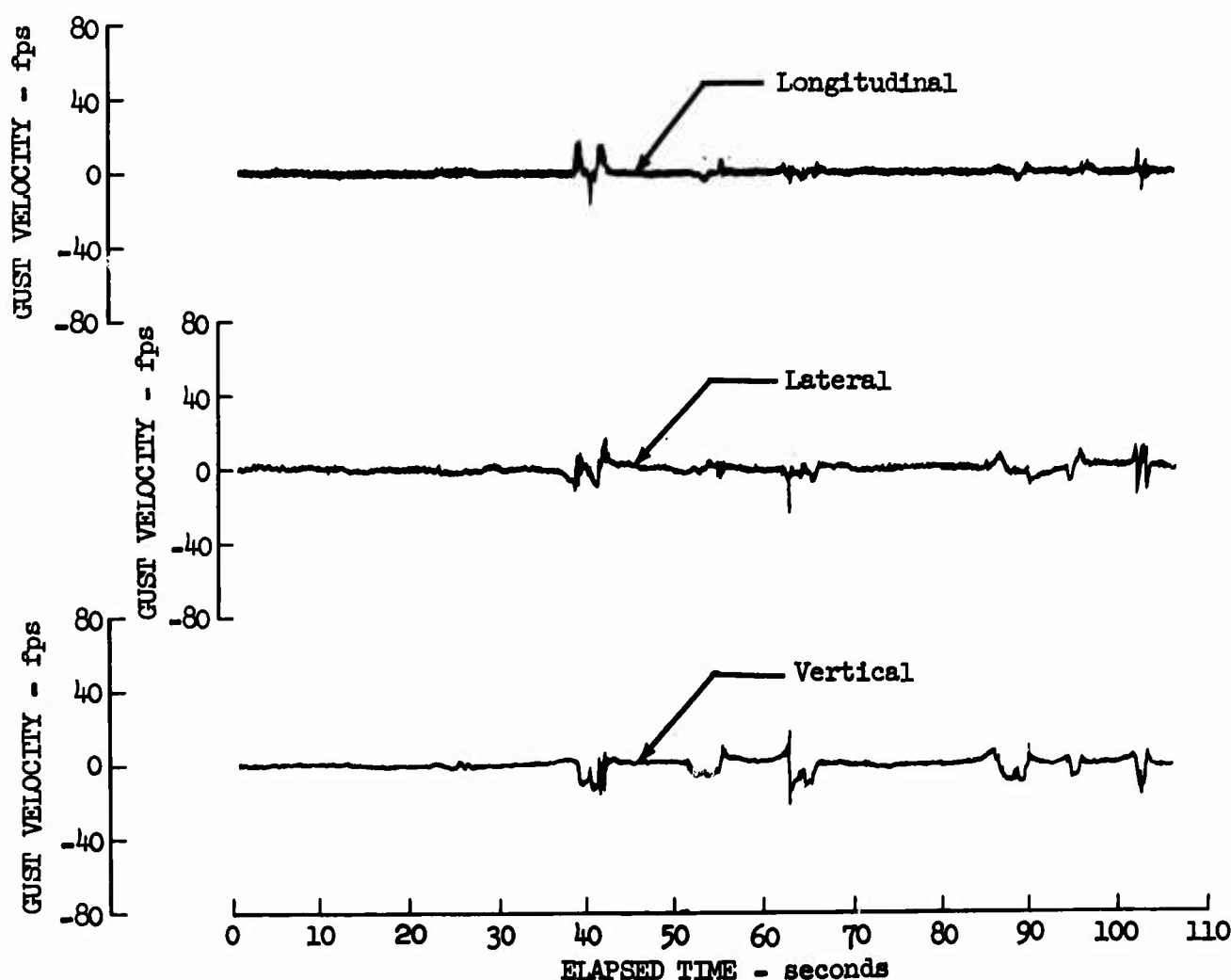


Figure 43.38 Gust Velocity Time Histories - Test 0285,
Sample No. 20

Location on Racetrack - Enroute Portion
Pass No. 7
Type of C-141 Formation - Modified In-Trail Concept

Pilot's Comments:

Closing on the rear element, 2000 ft. behind
Heading = 310° , altitude = 500 ft.
Closing to 1000 ft. behind
Crossing through wakes of all three aircraft
500 ft. behind rear aircraft

Recorded Data:

$V_T = 288$ knots
 $h = 306^\circ$
 $H_P = 320$ ft.

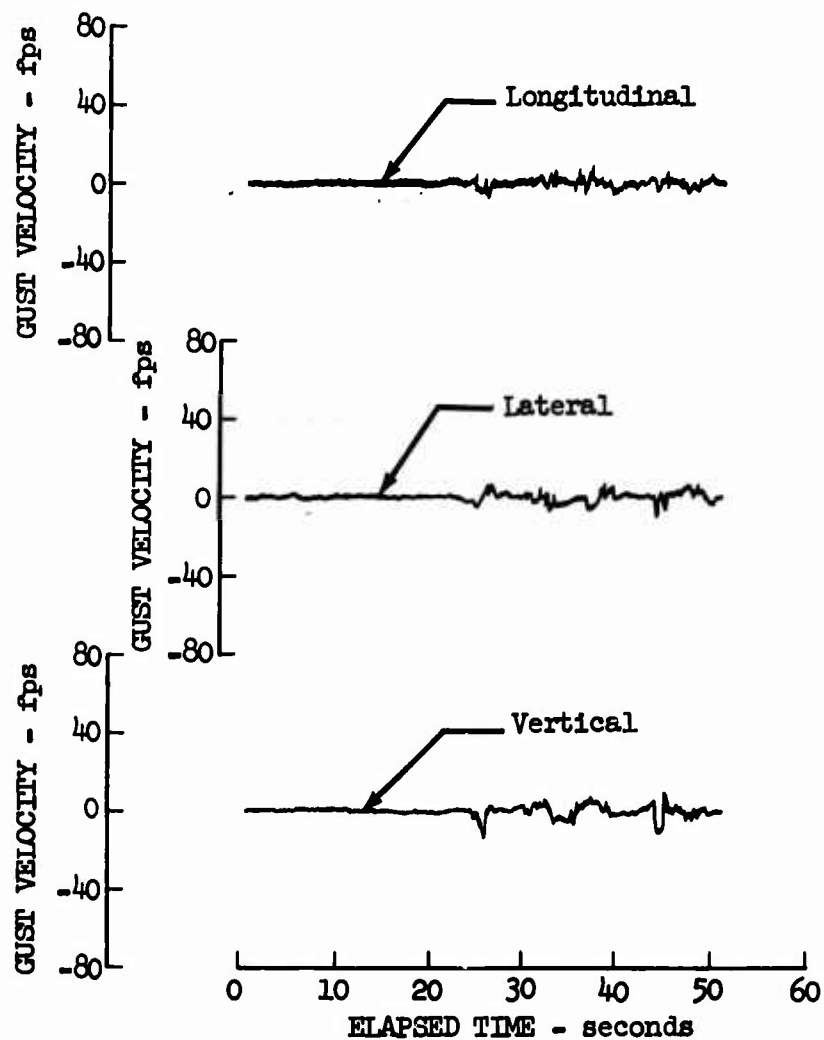


Figure 43.39 Gust Velocity Time Histories - Test 0285,
Sample No. 21

Location in Racetrack - Drop Zone Leg
 Pass No. 7
 Type of C-141 Formation - Modified In-Trail Concept

Recorded Data:

$V_T = 280$ knots
 $h = 43^\circ$
 $H.P. = 340$ ft.

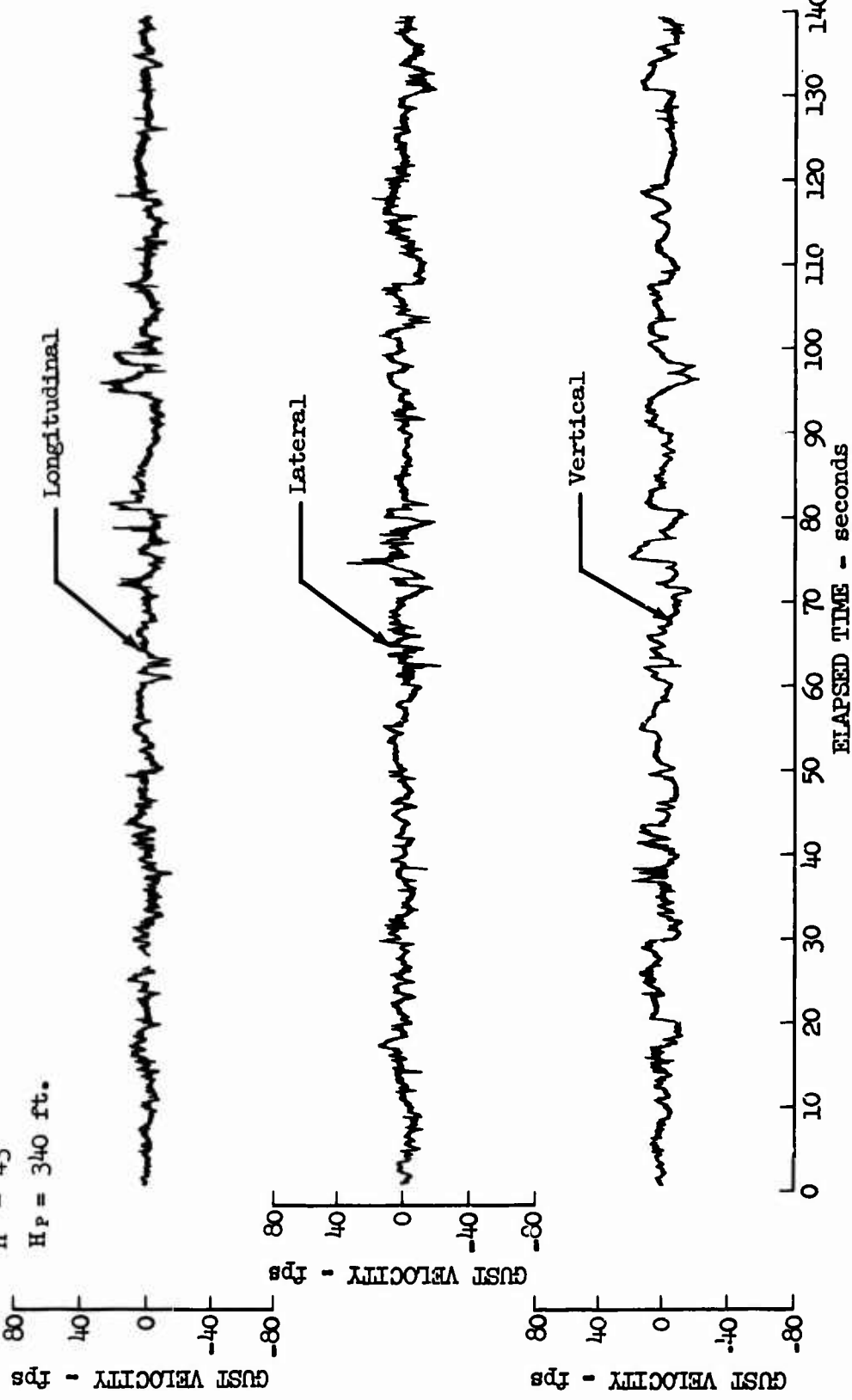


Figure 43.40 Gust Velocity Time Histories - Test 0285,
 Sample No. 22

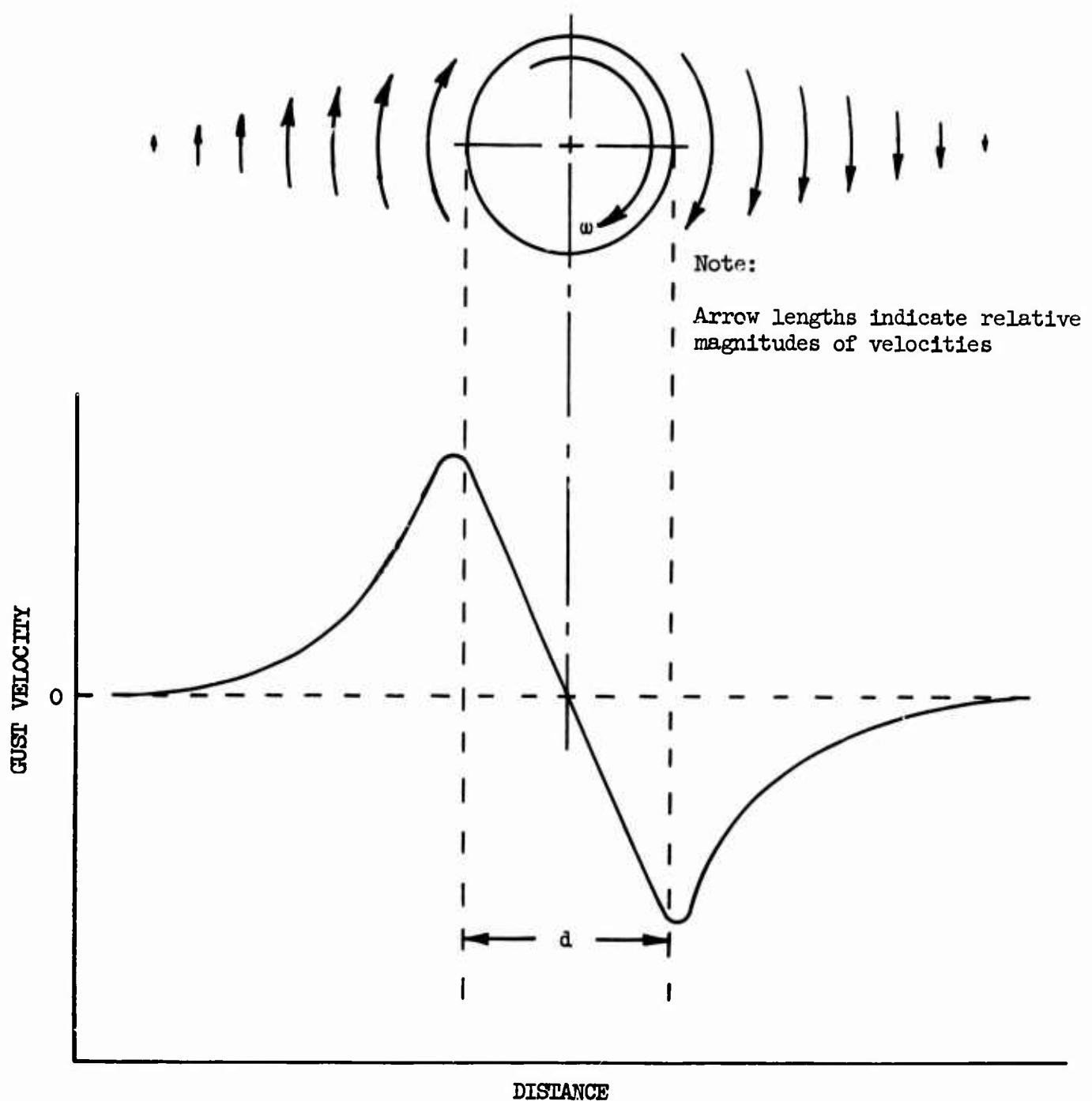


Figure 43.41 Fluid Velocity Distribution Within the Effects of Theoretical Vortex Flow

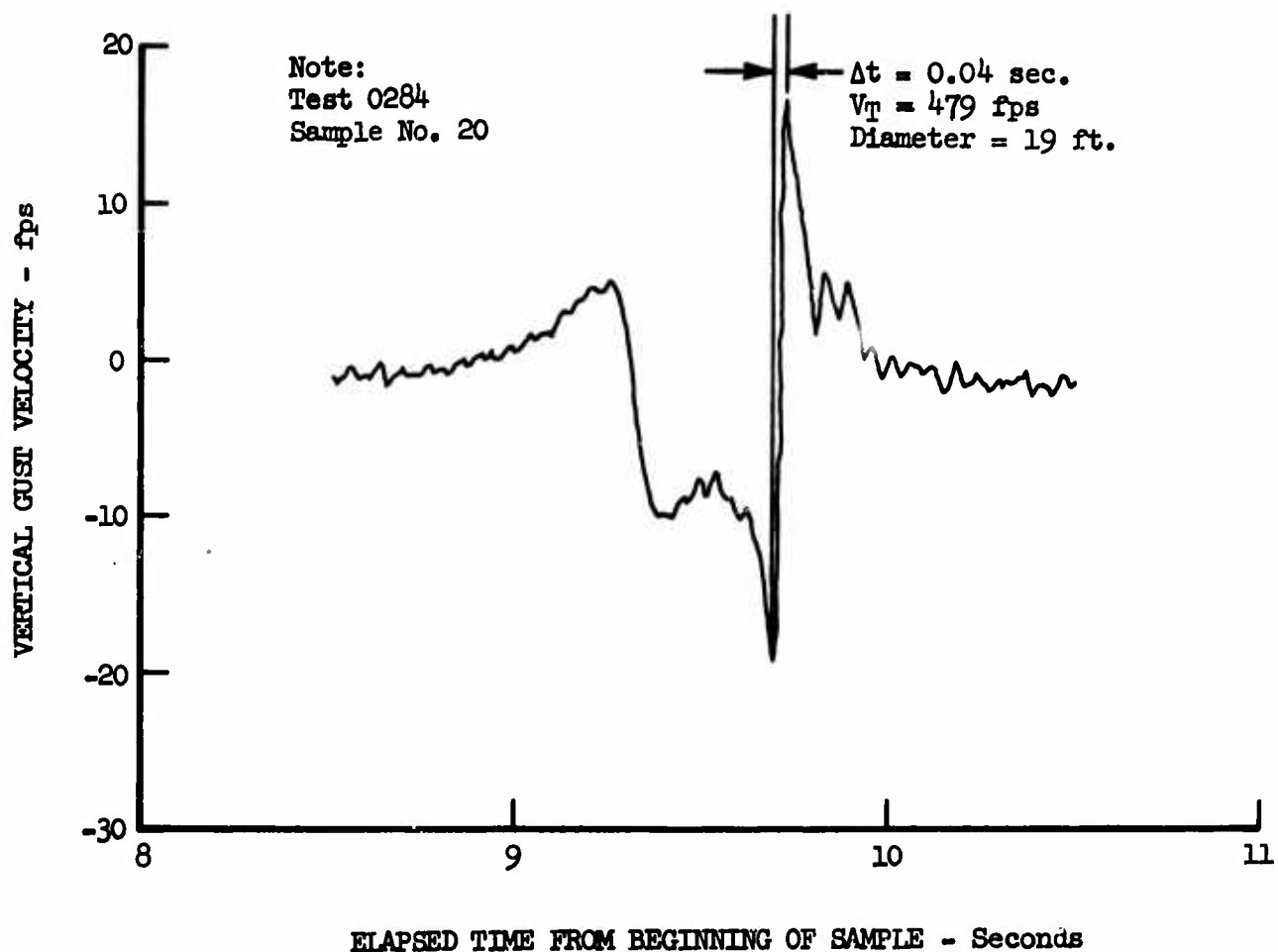


Figure 43.42 Gust Velocity Time History - Wake Turbulence
Vortex Size and Shape Investigation

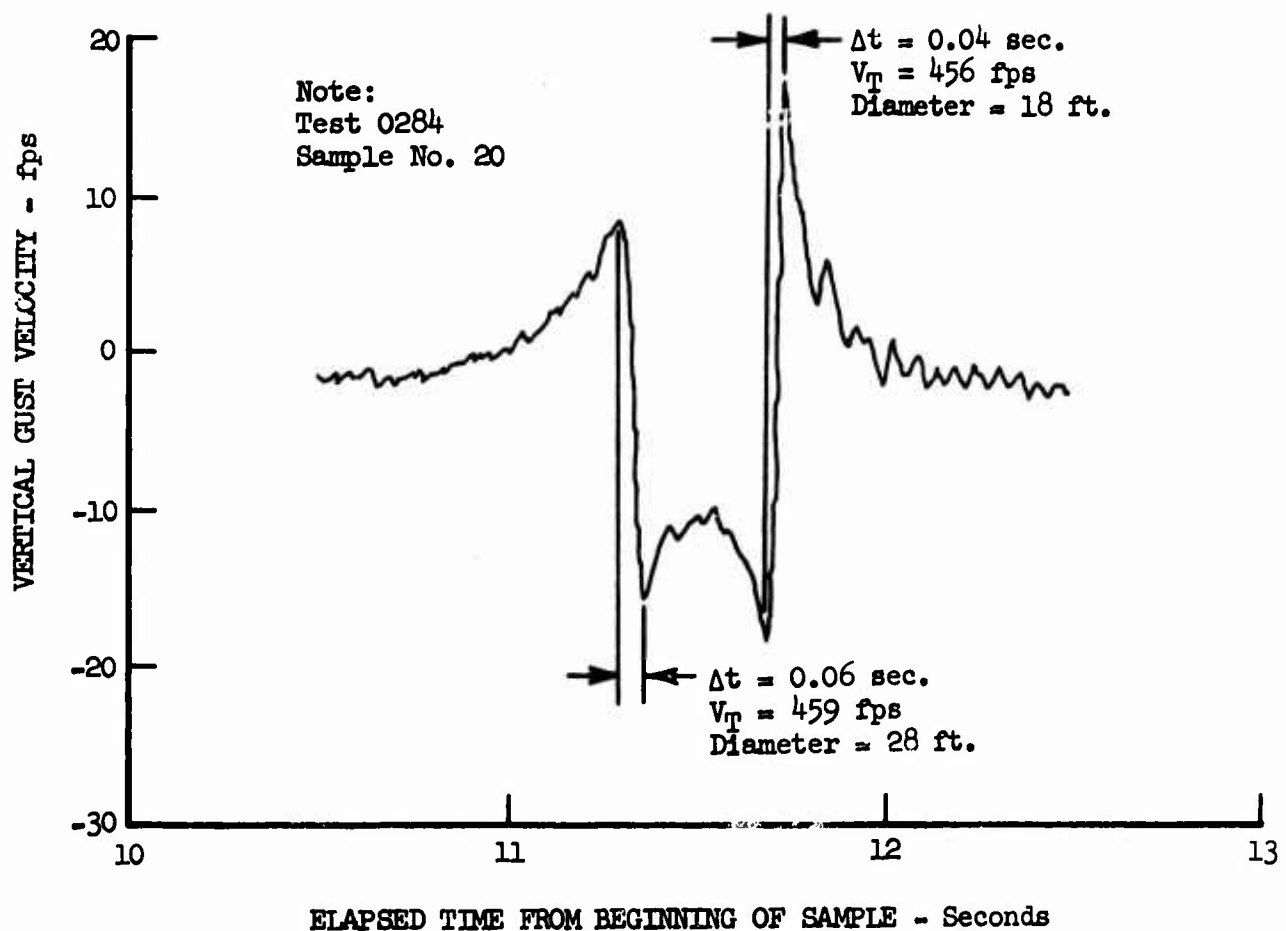


Figure 43.43 Gust Velocity Time History - Wake Turbulence
Vortex Size and Shape Investigation

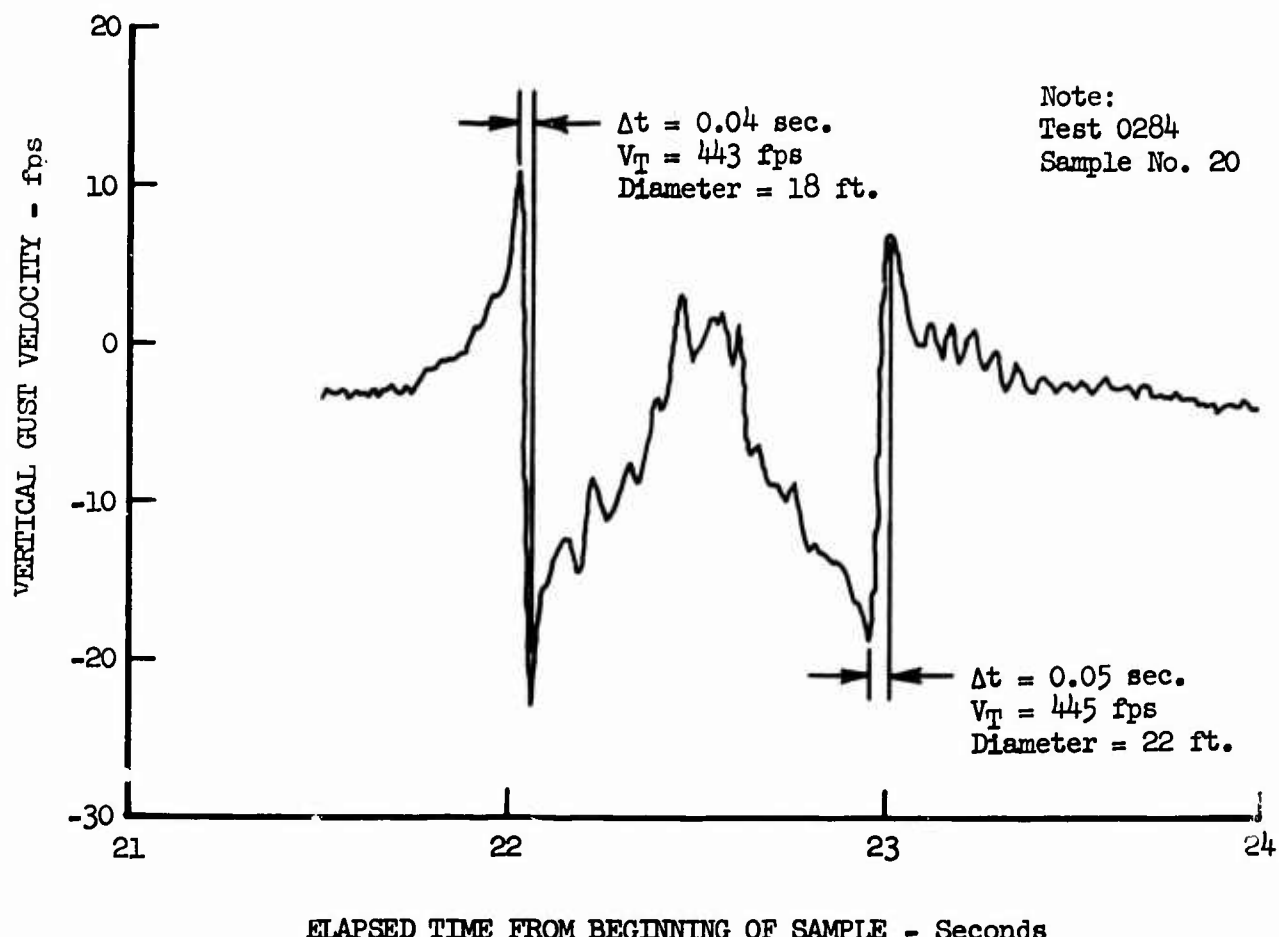


Figure 43.44 Gust Velocity Time History - Wake Turbulence
Vortex Size and Shape Investigation

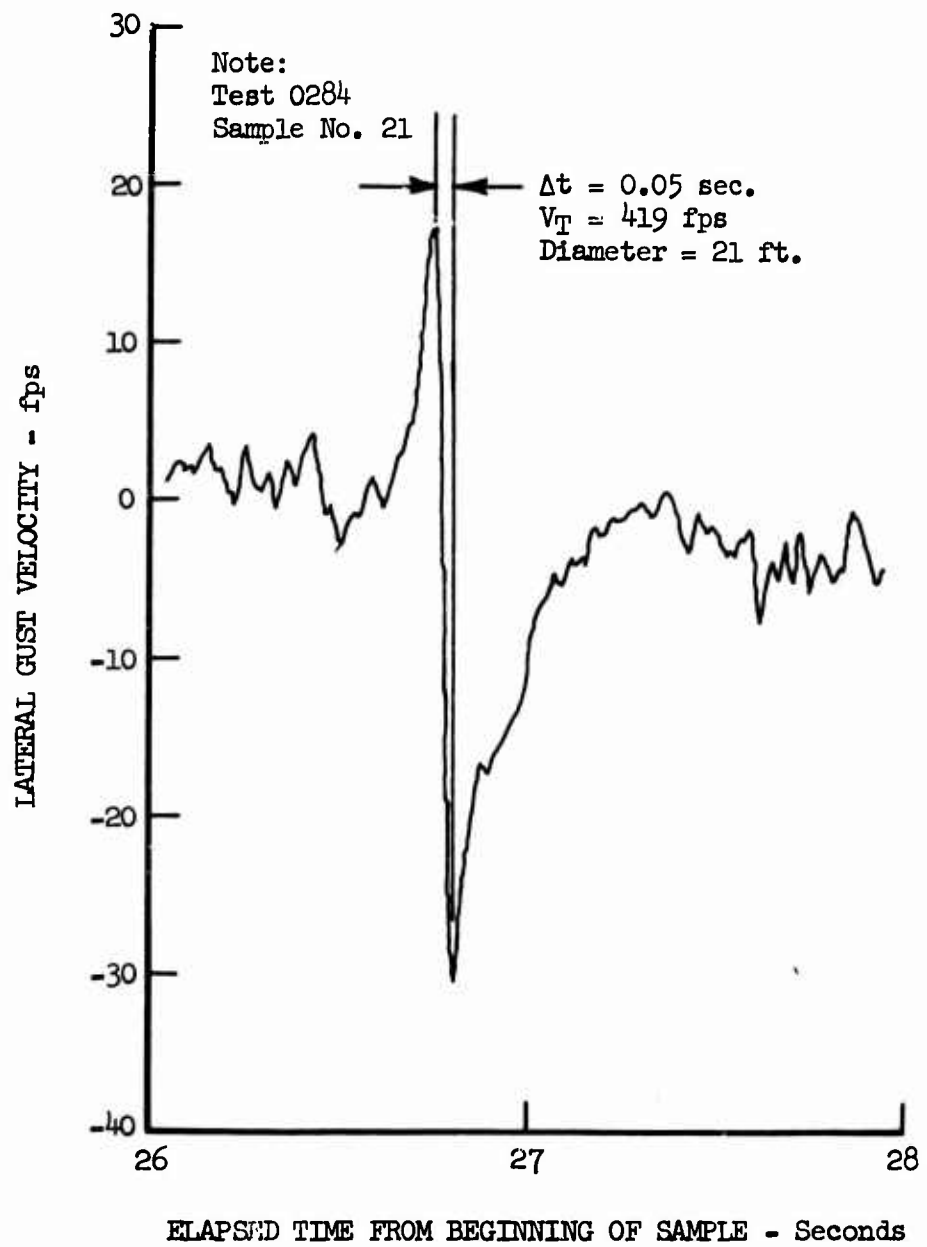


Figure 43.45 Gust Velocity Time History - Wake Turbulence
Vortex Size and Shape Investigation

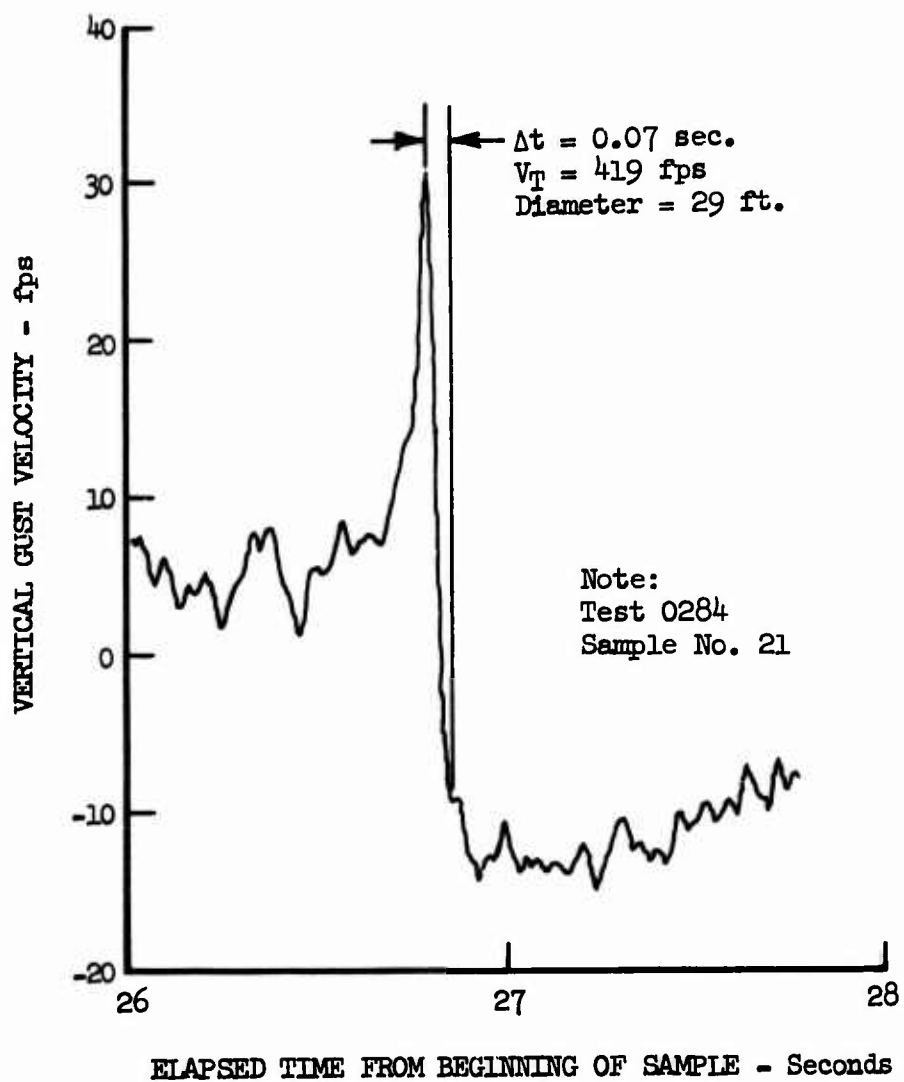


Figure 43.46 Gust Velocity Time History - Wake Turbulence Vortex Size and Shape Investigation

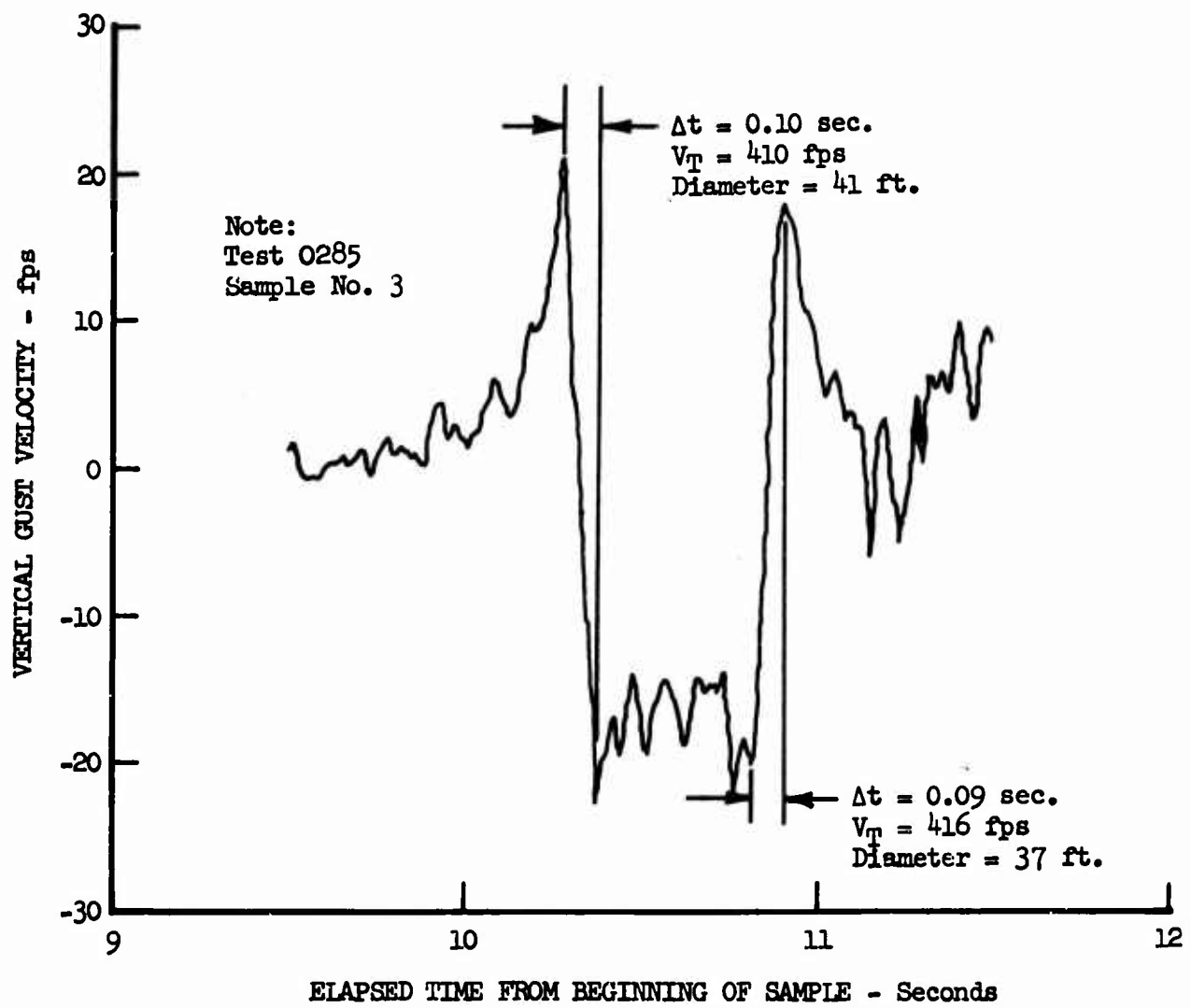


Figure 43.47 Gust Velocity Time History - Wake Turbulence
Vortex Size and Shape Investigation

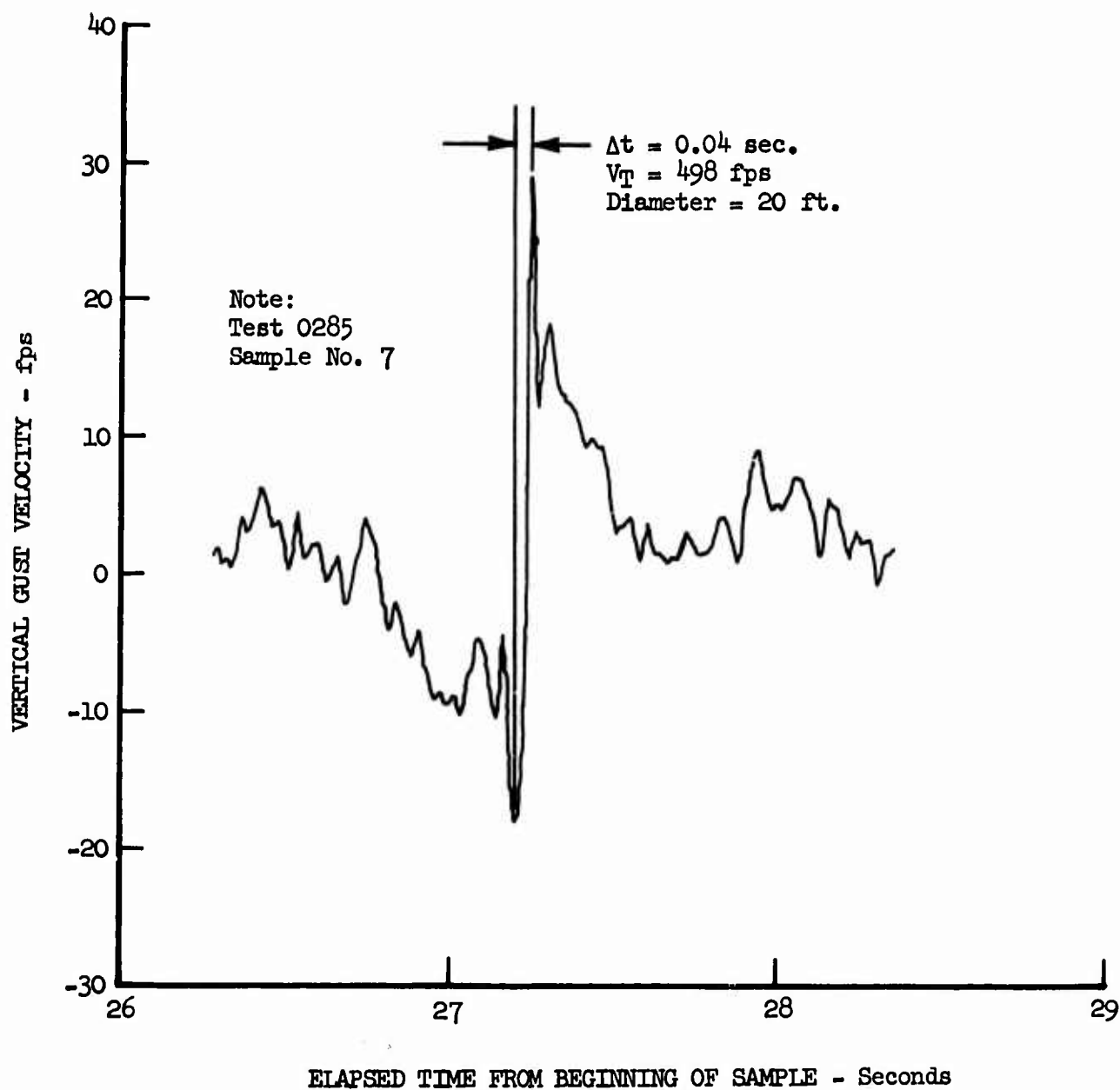


Figure 43.48 Gust Velocity Time History - Wake Turbulence Vortex Size and Shape Investigation

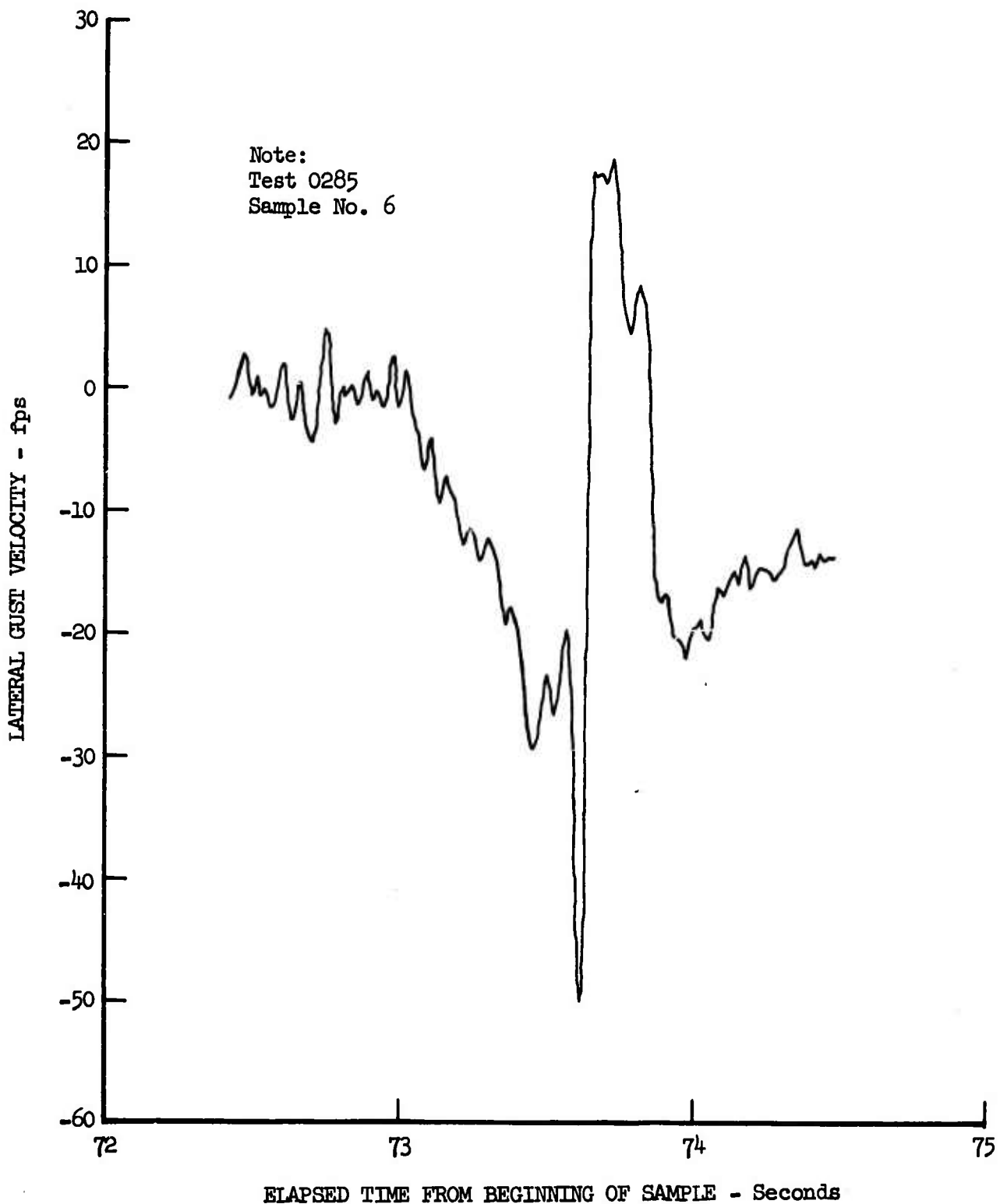


Figure 43.49 Gust Velocity Time History - Wake Turbulence
Vortex Size and Shape Investigation

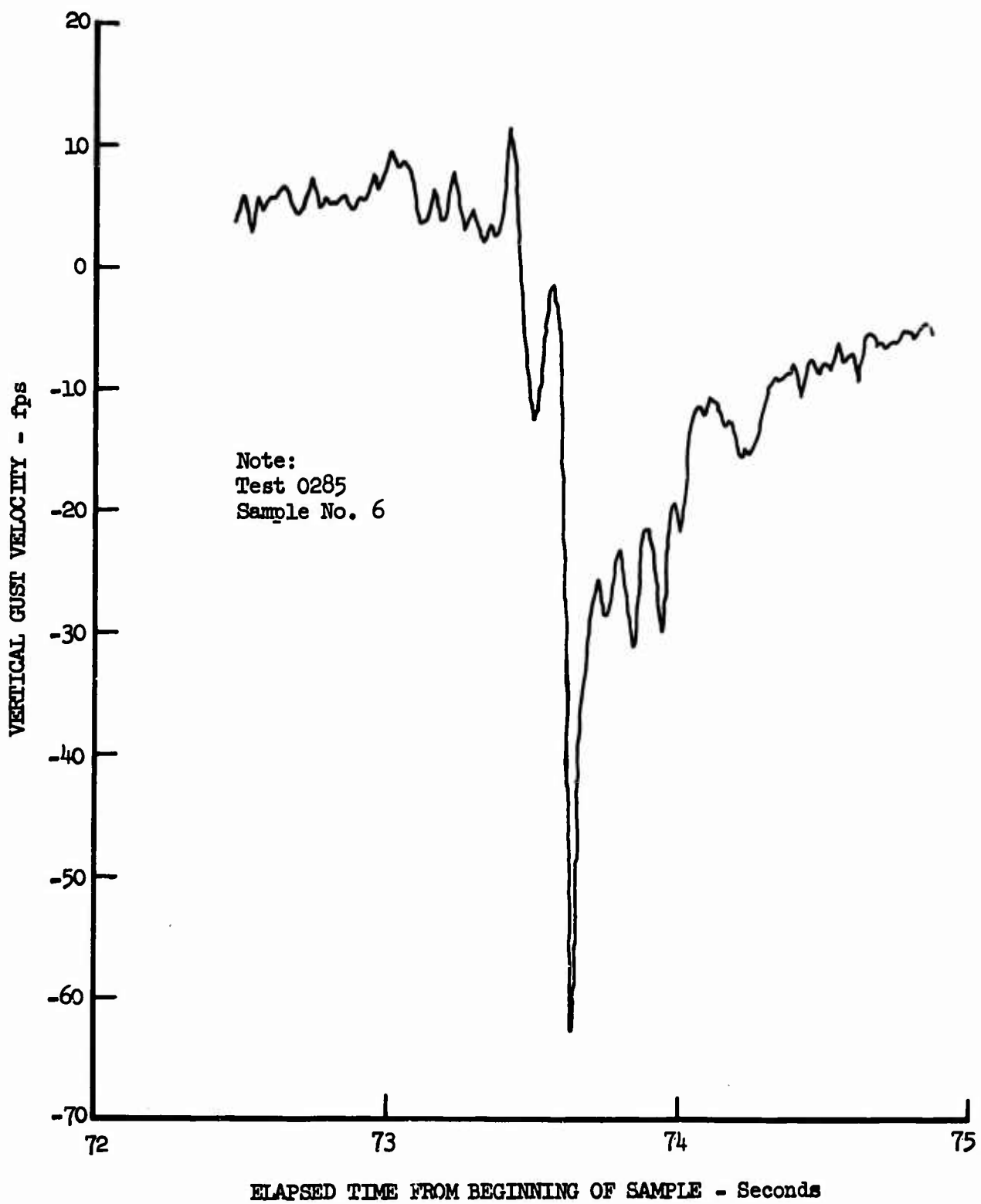


Figure 43.50 Gust Velocity Time History - Wake Turbulence
Vortex Size and Shape Investigation

SECTION IX

COMPARISON OF LO-LOCAT PHASES I AND II WITH PHASE III DATA

44. GUST VELOCITY RMS VALUES

The gust velocity rms values recorded during Phase III were compared to those recorded during Phases I and II of the LO-LOCAT Program. The comparison was made with respect to three characteristics: magnitude, variation with geophysical category, and cumulative probability distribution shape.

The Phase III rms values are significantly greater than those recorded during Phases I and II due to the following:

- Longer wavelength turbulence was recorded during Phase III.
- The Phase III and Phases I and II data were obtained during somewhat different geophysical conditions.

As discussed in other sections, the T-33 airplane utilized during Phase III was flown approximately twice as fast as were the C-131 aircraft during Phases I and II. Since the frequency response range of the instrumentation was the same in both cases, the wavelengths recorded during Phase III were approximately twice those recorded during Phases I and II. These longer wavelengths are in the high power portion of the turbulence spectra and thus increase rms values.

The per cent of total data recorded during contour flight over the various types of terrain are shown in Table 44.1.

TABLE 44.1

PERCENTAGE OF GUST VELOCITY DATA OBTAINED DURING CONTOUR FLIGHT OVER VARIOUS TERRAINS

Type of Terrain	Percentage of Total	
	Phases I and II	Phase III
High Mountain	7.5	48.5
Low Mountain	24.0	17.0
Desert	7.5	6.5
Plains	59.0	20.5
Water	2.0	4.5

The gust velocity rms values for all phases of the program were found to be greater over the rougher terrains. Since a much greater percentage of the data were recorded during contour flight over the rough terrain during Phase III, it would be expected that these rms values would be larger than those recorded during Phases I and II. Not only is the percentage of high

mountain data recorded during Phase III much greater, but most of these data were recorded at Peterson where the gust velocity values are larger than those recorded over the high mountain terrain at Edwards. Table 44.2 shows this comparison.

TABLE 44.2

COMPARISON OF PHASE III HIGH MOUNTAIN DATA BY LOCATION

Location	Number of Samples	σ_{t_u} (fps)	σ_{t_v} (fps)	σ_{t_w} (fps)
Edwards	195	3.14	3.38	3.27
Peterson	658	5.10	5.65	4.77

All of the high mountain data obtained under contour flight conditions during Phases I and II were recorded at the Edwards location. The airplane located at Peterson during the first two phases was not flown contour over those high mountain legs due to safety-of-flight reasons. Therefore, the high mountain data obtained at Peterson were not considered when comparing Phases I and II with Phase III.

The Phases I and II data were adjusted by assuming the same percentage of data were obtained as shown for Phase III in Table 44.1. In addition, the percentage of data referred to as high mountain in Table 44.1 was broken down to reflect the number of samples recorded at Edwards and Peterson as shown in Table 44.2. Thus, of the total number of samples recorded during Phase III, 11.1 per cent were recorded over high mountains at Edwards and 37.4 per cent over high mountains at Peterson. It was assumed that, had data been obtained under contour flight conditions over the high mountain legs at Peterson during Phases I and II, the same ratio between those data and the high mountain data recorded at Edwards would have existed as is shown for the Phase III data in Table 44.2. The results of these adjustments on the mean values are shown in Table 44.3.

TABLE 44.3

COMPARISON OF GUST VELOCITY RMS VALUES - ALL DATA

Component	Phase III $\sigma_t \sim$ fps	Phases I and II	
		$\sigma_t \sim$ fps	Adjusted $\sigma_t \sim$ fps
Longitudinal	3.60	2.55	3.31
Lateral	3.85	2.79	3.63
Vertical	3.39	2.60	3.38

This does not completely make the data from all phases equivalent. Another factor which must be considered is the season of the year during which these data were obtained. During Phases I and II, data were obtained during all four seasons of the year at each location. The data recorded during Phase III were primarily recorded during only one season of the year at each of the locations except Peterson. It was shown that wind speed varies with season (See Reference I.2). It was also shown that, especially over the rougher terrain, turbulence intensity and wind speed are related (See Section 14).

There are many other factors which were different, to some degree, between the different phases. Although the geographic locations remained the same, the legs for the Phases I and II testing were extended in length, or replaced with other ones, for the Phase III testing. Meteorological conditions were probably slightly different during one phase versus the others. However, the aircraft were flown at approximately the same absolute altitudes, during the same times of day, at the same geographic locations, and within approximately the same types of atmospheric stability conditions. Comparisons of the gust velocity rms values obtained during the various LO-LOCAT program phases required the consideration of the terrain type and season of the year, with respect to location. Therefore, cumulative probabilities of gust velocity rms values for Phases I and II are compared with those of Phase III for the same data categories.

Comparison cumulative probability plots are shown in Figures 44.1 through 44.4. A list of gust velocity rms mean values corresponding to the data presented in each of the figures is shown in Table 44.4.

TABLE 44.4

COMPARISON OF GUST VELOCITY RMS MEAN VALUES

Geophysical Category		Phases I and II			Phase III		
Terrain	Season and Location	σ_{t_v} (fps)	σ_{t_v} (fps)	σ_{t_v} (fps)	σ_{t_u} (fps)	σ_{t_u} (fps)	σ_{t_u} (fps)
High Mountain	Fall, Edwards	2.93	3.17	3.00	3.14	3.38	3.27
*Low Mountain	Fall, Edwards + Spring, Griffiss	3.14	3.47	3.24	3.16	3.17	2.89
**Low Mountain	Fall, Edwards + Spring, Griffiss	3.14	3.47	3.24	3.43	3.49	3.17
Desert	Fall, Edwards	1.64	1.90	1.91	1.80	1.86	1.78
Plains	Summer, McConnell + Winter, Peterson + Spring, Peterson + Spring, Griffiss	2.41	2.73	2.46	2.80	2.80	2.53

* Unadjusted Values

** Phase III data adjusted

Two sets of values are given for the low mountain data in Table 44.4 and in Figure 44.2. The reason for this can be understood by looking at the percentages in Table 44.5 of the above category combinations that were recorded at each location. This table includes only the low mountain and plains data, since these are the only data involving more than one location. The percentages are shown in Table 44.5.

TABLE 44.5

RELATIVE AMOUNT OF DATA FROM VARIOUS LOCATIONS

Terrain	Location	Season	Percentage	
			Phases I and II	Phase III
Low Mountain	Edwards	Fall	50	72
	Griffiss	Spring	50	28
Plains	McConnell	Summer	54	65
	Peterson	Winter Spring	33	23
	Griffiss	Spring	13	12

The percentages are similar between phases for the plains data, but not for the low mountain data. This difference for the low mountain data would not be important if these data showed approximately the same magnitude regardless of the location. However, the rms values recorded at Griffiss over low mountains were significantly larger than those recorded over the low mountains at Edwards. Table 44.6 shows the comparison for all phases.

TABLE 44.6

COMPARISON OF GUST VELOCITY RMS VALUES OVER LOW MOUNTAIN TERRAIN

Season and Location	Phases I and II			Phase III		
	σ_{t_s} (fps)	σ_{t_v} (fps)	σ_{t_w} (fps)	σ_{t_s} (fps)	σ_{t_v} (fps)	σ_{t_w} (fps)
Fall, Edwards	2.52	2.83	2.71	2.81	2.75	2.53
Spring, Griffiss	3.76	4.10	3.76	4.05	4.23	3.81

Because of this difference, the Phase III low mountain data were adjusted in Table 44.4 to correspond to the Phases I and II data in terms of the percentages shown in Table 44.5. The mean Phase III values shown in Table 44.6 were weighted as if each accounted for 50 per cent of the low mountain data, as was the case for the corresponding Phases I and II data. The adjusted curves in Figure 44.2 were drawn by moving the unadjusted curves along the abscissa a distance equivalent to the differences between the adjusted and unadjusted values in Table 44.4.

Comparison of cumulative probability distribution curves for the three components of rms gust velocity shows a closer agreement for the Phase III data than for Phases I and II. The reason for this is the same as for the peak count distribution and is discussed in Section 8.

The comparison of these data from all phases indicates that, for corresponding geophysical conditions, the Phase III gust velocity rms values are slightly larger (0.1 to 0.3 fps) than those recorded during Phases I and II. This is probably due to the longer wavelength turbulence recorded during Phase III.

The variations of the rms values with changes in geophysical category show the same trends for all phases. All phases showed increased rms values for data recorded over the rougher terrains. Also, greater rms values were recorded at the lower altitude and during the more unstable atmospheric conditions. Figures 44.5 through 44.7 show the variations of the mean rms values for Phase III and for Phases I and II with variations in type of terrain, altitude, and stability. These mean values were not adjusted for season and location differences as previously discussed. These figures show how the mean values are affected by changes in terrain, altitude, and stability; not how actual magnitudes vary between phases. Further variations of the gust velocity rms values with the various geophysical category combinations are shown in Section 13 for Phase III and in Reference I.2 for Phases I and II.

The shapes of the gust velocity rms cumulative probability distributions from the different phases were compared. This comparison included all contour flown data recorded during the respective phases regardless of geophysical category. Since it was shown that the Phases I and II and the Phase III rms data did not agree in magnitude unless adjusted to be equivalent with respect to geophysical conditions, the distributions were plotted versus a standardized variable t , where t was computed as follows:

$$t = \frac{\text{Gust Velocity rms} - \mu}{\sigma_s} \quad (44.1)$$

This permitted the removal of the effects of turbulence intensity, as represented by the mean (μ) and the dispersion of the distribution (σ_s), so that the data could be compared on the basis of distribution form only.

The rms values not calculated because of low intensity turbulence (reference Section 13) were accounted for in the calculation of μ and σ_s by estimating the distribution of these values within the gust velocity rms bands below 1.5 fps. These estimations were made by extrapolating the cumulative probability curves to zero (Figures 44.8 through 44.10). The number of samples within each of the lower bands was determined. The mean value of the samples within each of these lower three bands (0.0 to 0.5, 0.5 to 1.0, and 1.0 to 1.5 fps) was assumed to be the mid-point value of each respective band. The estimated values are shown in Table 44.7. It should be noted that, within this section, all of the mean values which involve Phase III low intensity turbulence samples (See Table 13.1) were corrected in this manner. The above correction is not applicable to Phases I and II since low intensity turbulence samples were not removed from those data.

TABLE 44.7
ESTIMATED DISTRIBUTION OF GUST VELOCITY RMS VALUES

Band ~ fps	Estimated Percentage of Total			Estimated Mean Value ~ fps		
	σ_{t_u}	σ_{t_v}	σ_{t_w}	σ_{t_u}	σ_{t_v}	σ_{t_w}
0.0 - 0.5	2.0	2.0	2.5	0.25	0.25	0.25
0.5 - 1.0	4.2	4.0	5.0	0.75	0.75	0.75
1.0 - 1.5	6.3	5.8	7.7	1.25	1.25	1.25

The dispersions of the distributions were corrected by noting that:

$$\sigma_{\sigma_1} = \left[\frac{1}{N_1} \sum_{i=1}^{N_1} (\sigma_{t_{1i}} - \mu_1)^2 \right]^{1/2} \quad (44.2)$$

and

$$\sigma_{\sigma_2} = \left[\frac{1}{N_2} \sum_{i=1}^{N_2} (\sigma_{t_{2i}} - \mu_2)^2 \right]^{1/2} \quad (44.3)$$

where the subscript 1 represented the set of estimated rms values and the subscript 2 represented the set of calculated rms values. The dispersion of the distribution (σ_{σ_c}) for the combination of both sets of data is:

$$\sigma_{\sigma_c} = \left\{ \frac{1}{N_1 + N_2} \left[\sum_{i=1}^{N_1} \sigma_{t_{1i}}^2 + \sum_{i=1}^{N_2} \sigma_{t_{2i}}^2 \right] - \left[\frac{N_1 \mu_1 + N_2 \mu_2}{N_1 + N_2} \right]^2 \right\}^{1/2} \quad (44.4)$$

The values of the standardized variable, t , were calculated after these corrections were made. These values are shown in Figures 44.11 through 44.13.

The data from Phases I and II and from Phase III were represented by mathematical expressions consisting of the sums of two normal distributions (See Equation 13.4 and Reference I.2). The distribution shapes are somewhat different for the various phases. This is due to the difference in geophysical categories for which the data were obtained and the fact that the gust velocities were measured over different frequency ranges during the two programs.

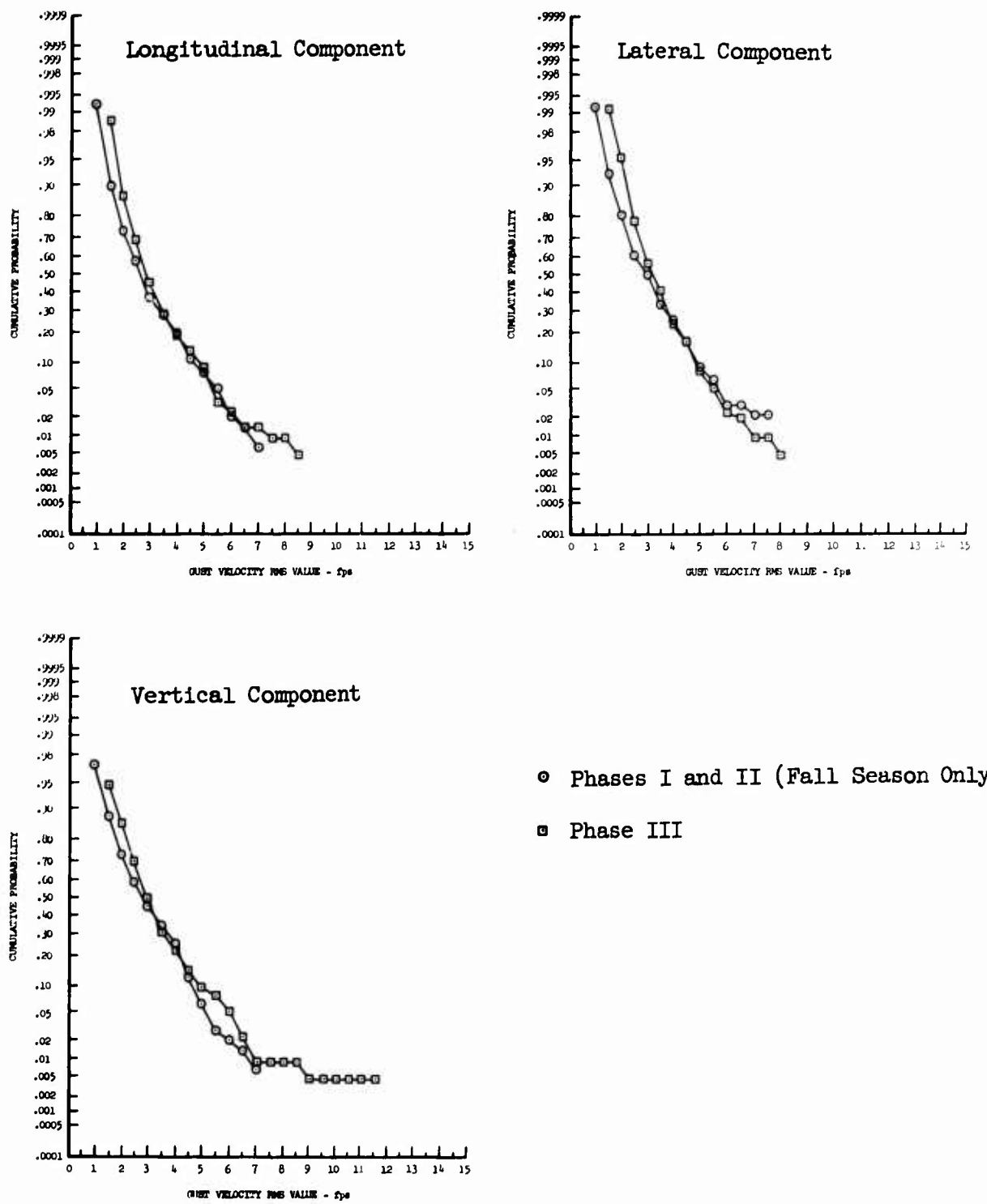


Figure 44.1 Comparison of Gust Velocity RMS Values from Phases I and II with Those from Phase III for Data Recorded Over High Mountains at Edwards

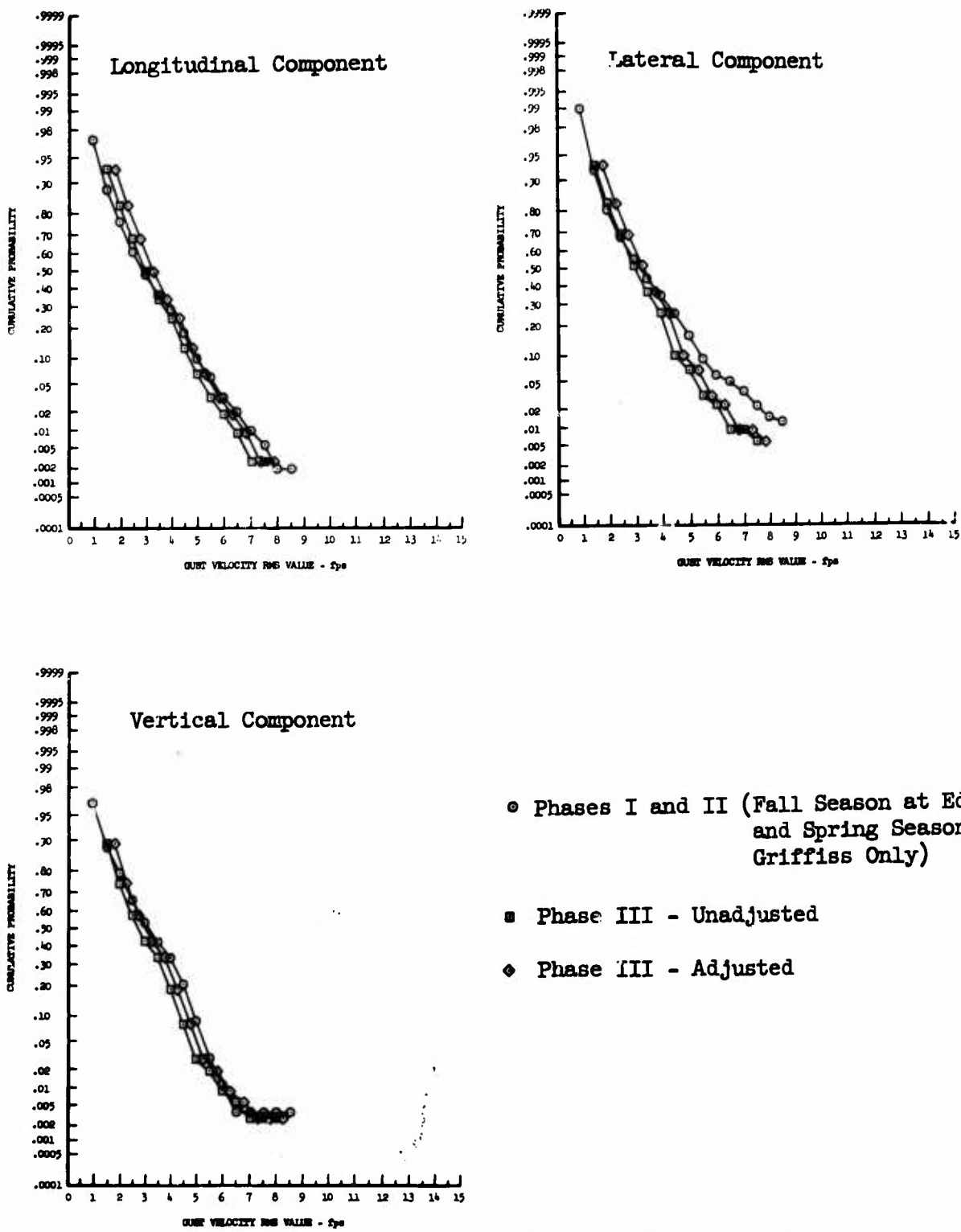


Figure 44.2 Comparison of Gust Velocity RMS Values from Phases I and II with Those from Phase III for Data Recorded Over Low Mountains at Edwards and Griffiss

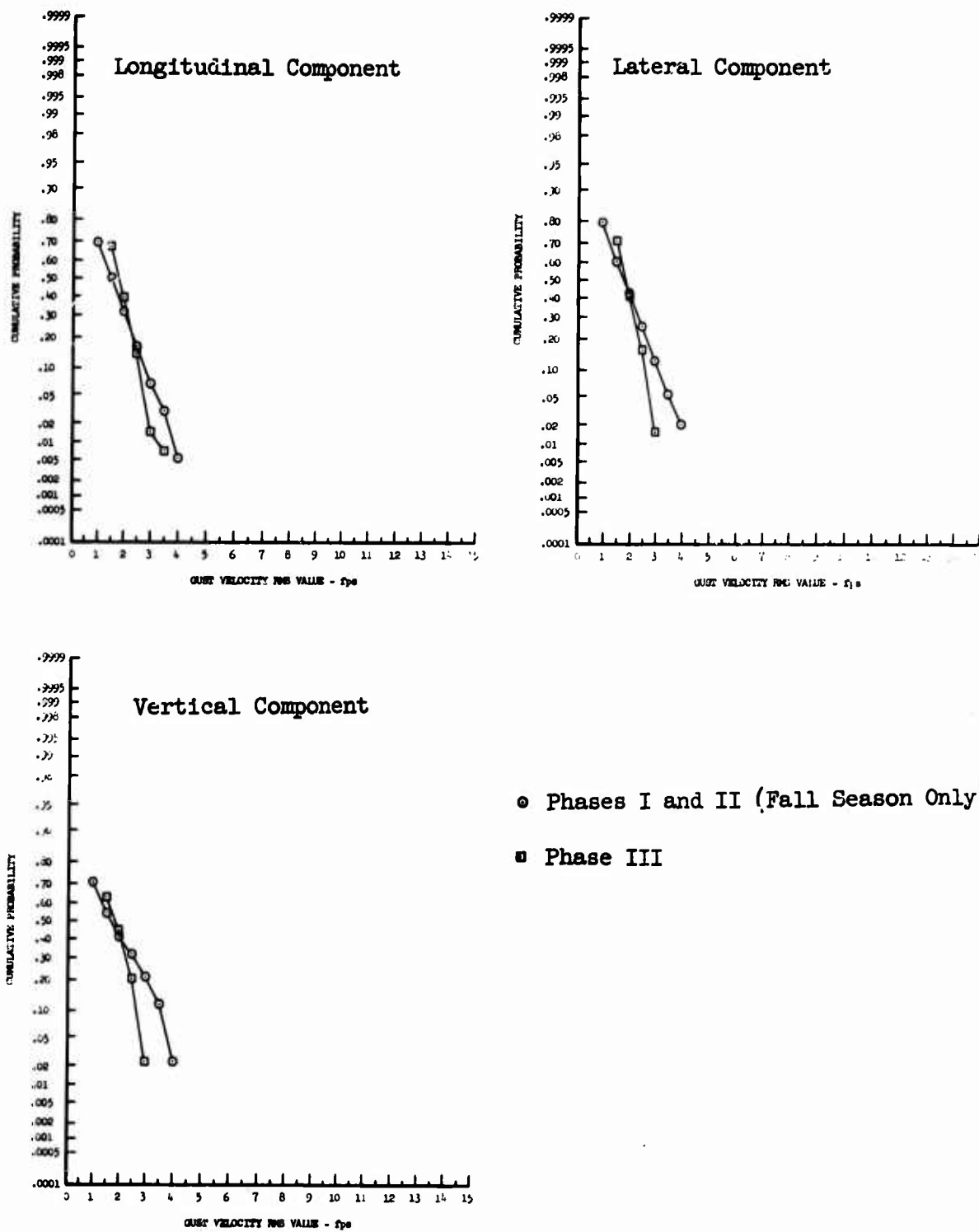


Figure 44.3 Comparison of Gust Velocity RMS Values from Phase I and II with Those from Phase III for Data Recorded Over Desert at Edwards

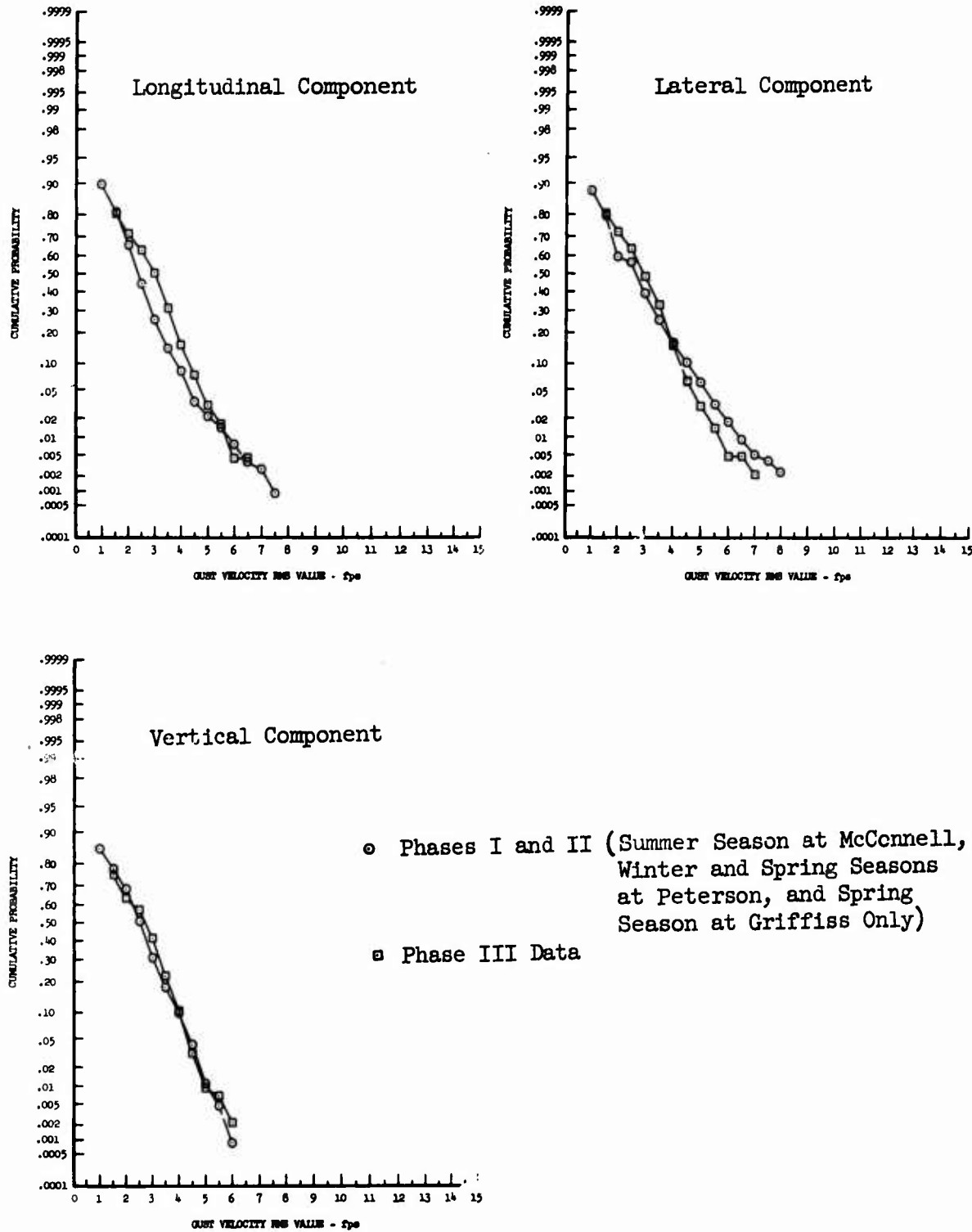


Figure 44.4 Comparison of Gust Velocity RMS Values from Phases I and II with Those from Phase III for Data Recorded Over Plains at McConnell, Peterson, and Griffiss

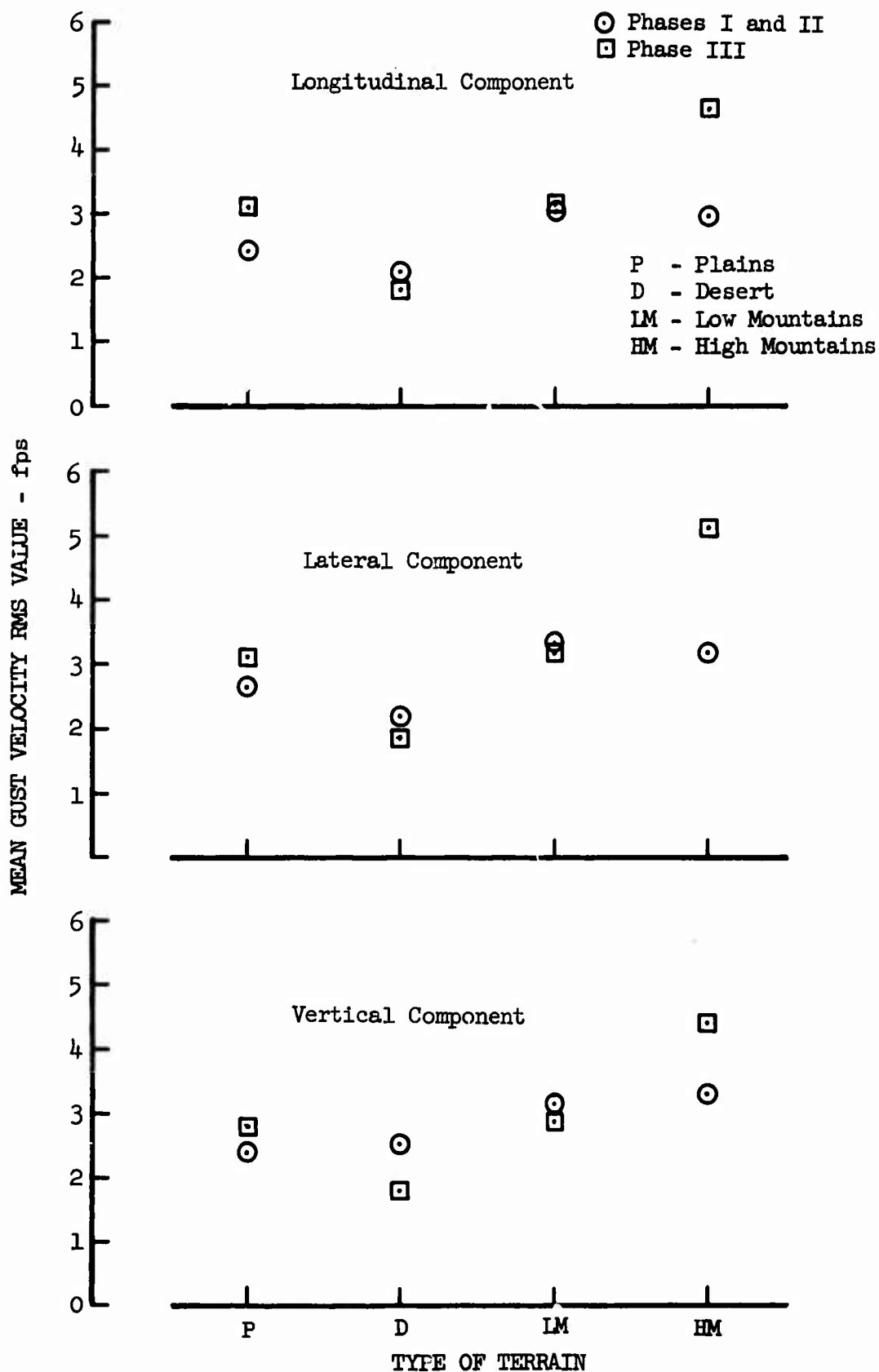


Figure 44.5 Comparison of Phases I and II and Phase III Mean Gust Velocity RMS Values as a Function of Terrain

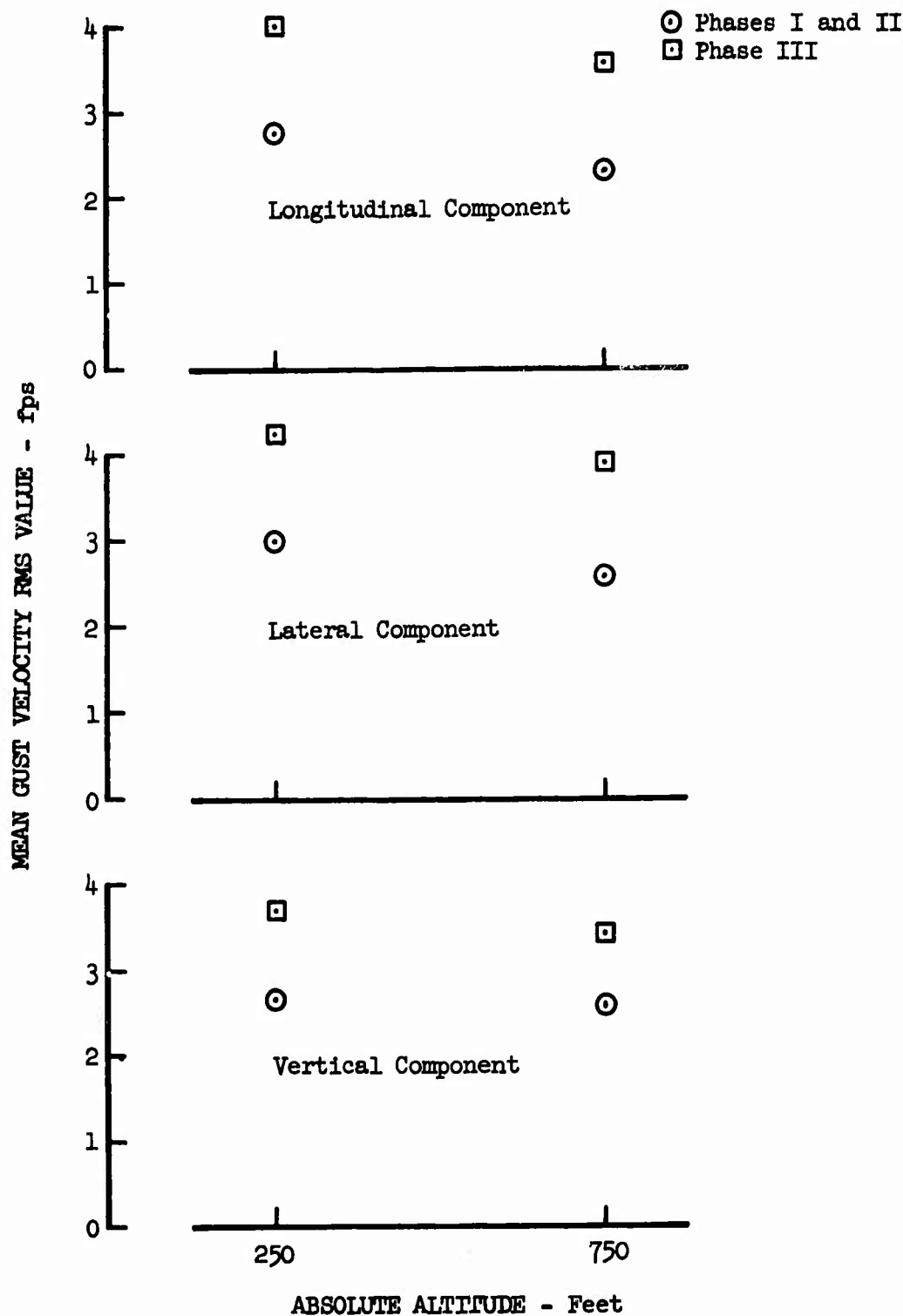


Figure 44.6 Comparison of Phases I and II and Phase III Mean Gust Velocity RMS Values as a Function of Absolute Altitude

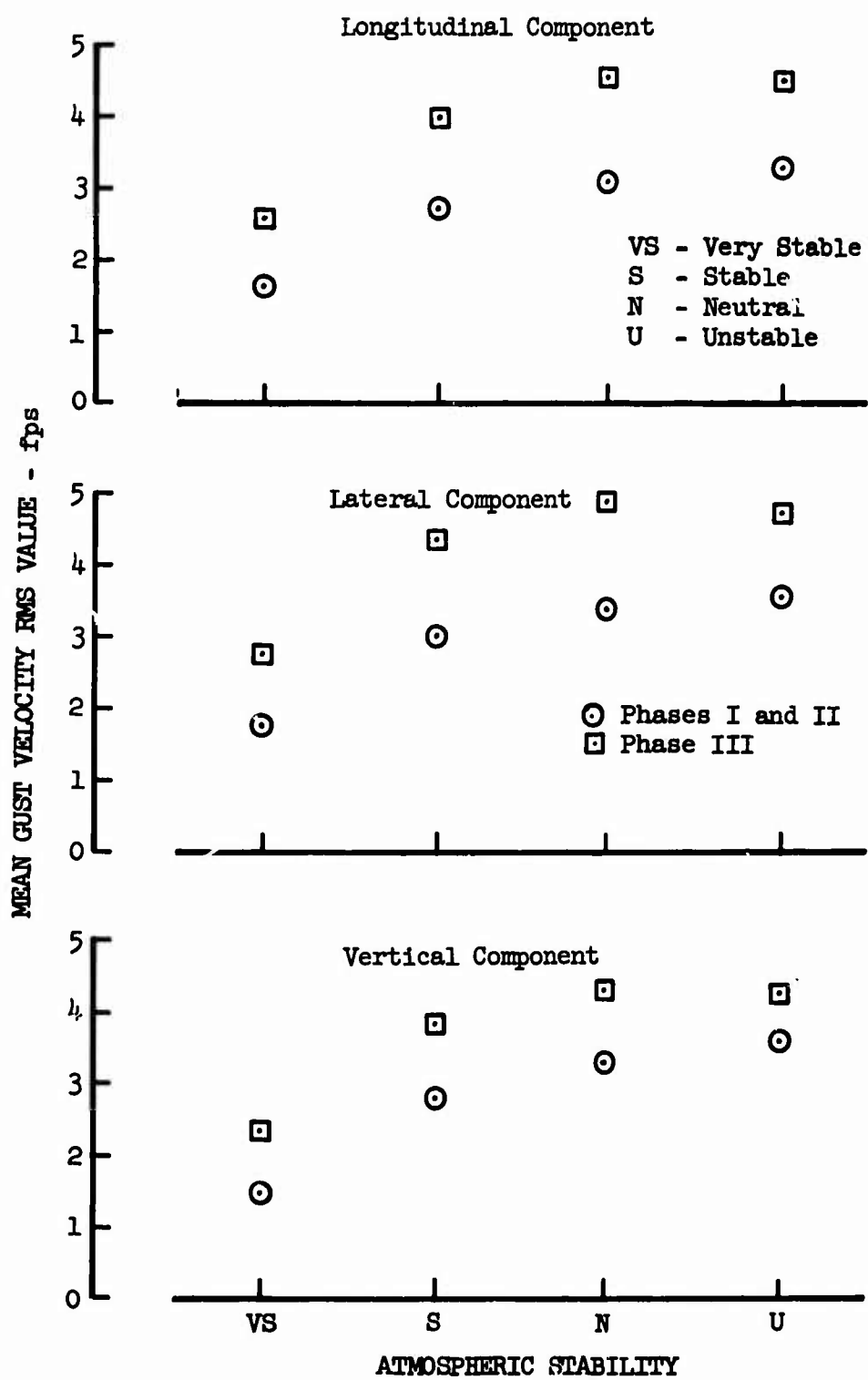


Figure 44.7 Comparison of Phases I and II and Phase III Mean Gust Velocity RMS Values as a Function of Atmospheric Stability

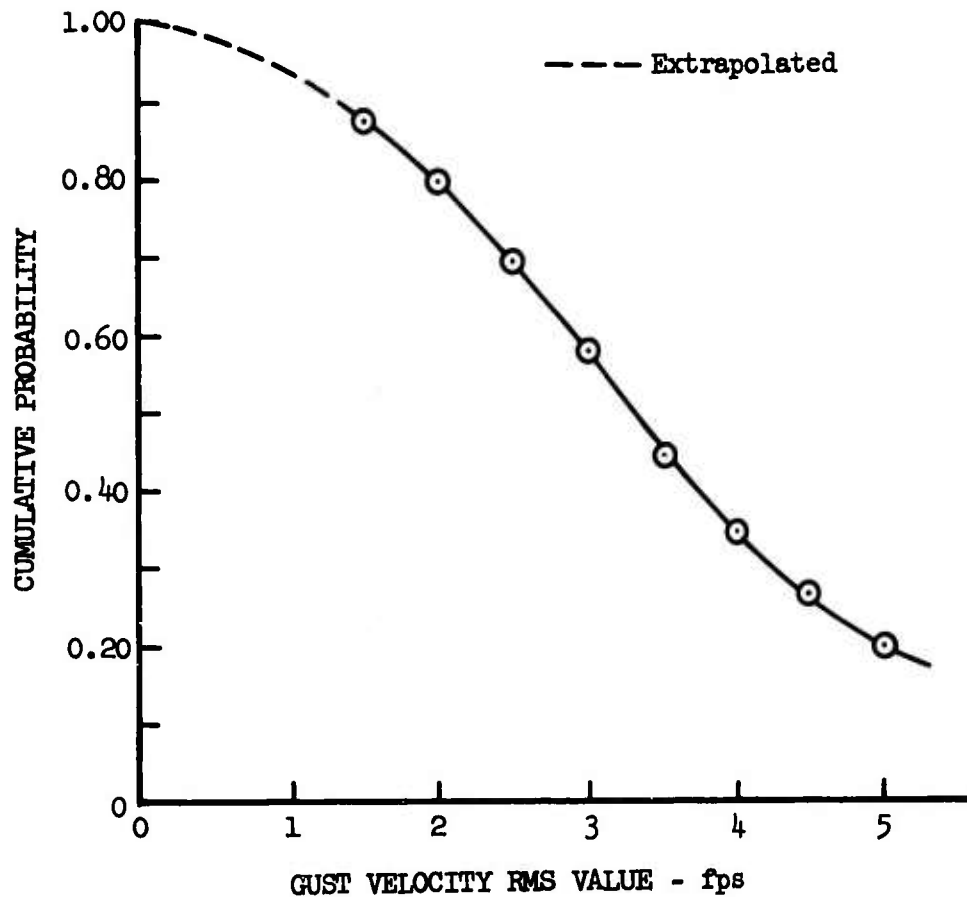


Figure 44.8 Extrapolated Longitudinal Gust Velocity RMS Cumulative Probability

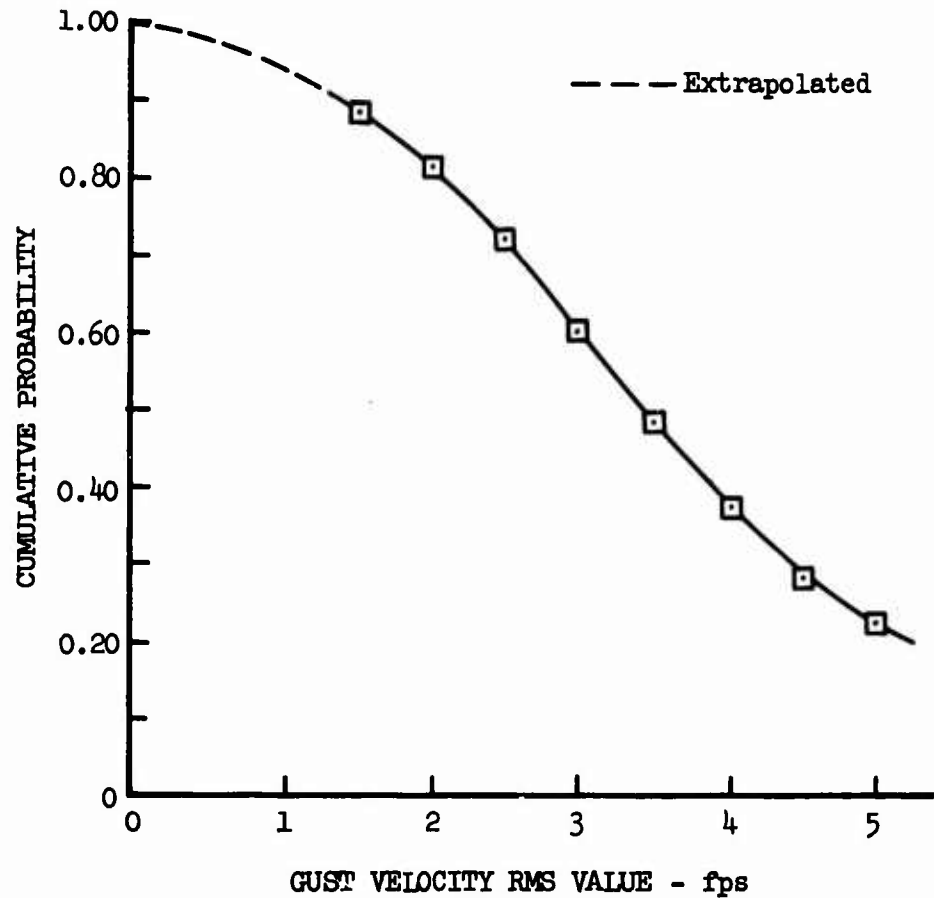


Figure 44.9 Extrapolated Lateral Gust Velocity RMS Cumulative Probability

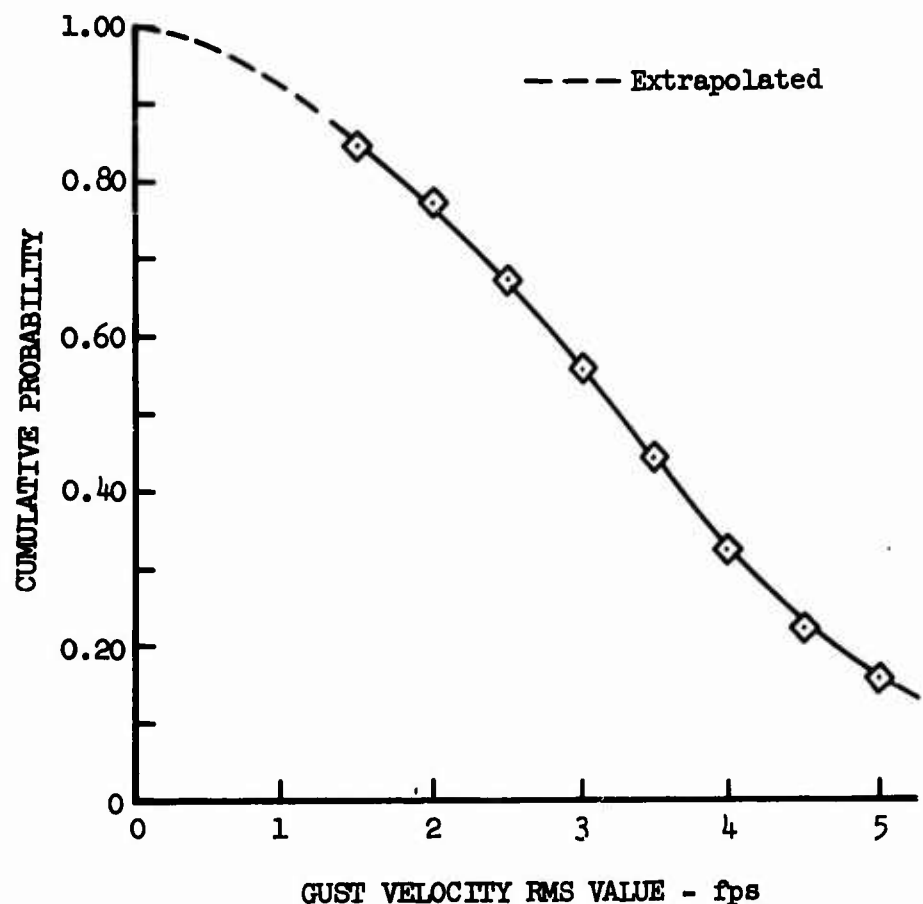


Figure 44.10 Extrapolated Vertical Gust Velocity RMS Cumulative Probability

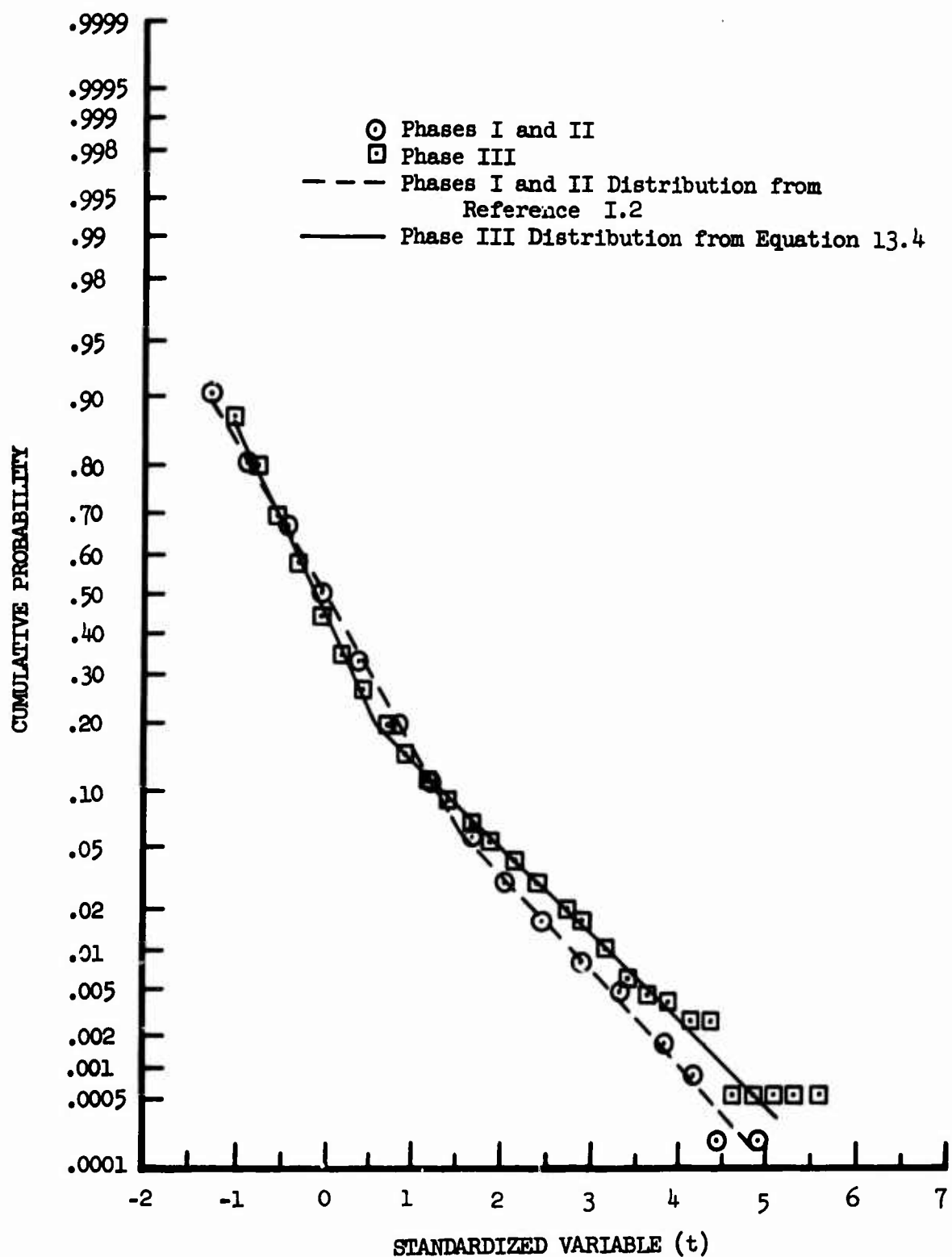


Figure 44.11 Comparison of Standardized Longitudinal Gust Velocity RMS Cumulative Probability Distribution from Phases I and II with that from Phase III

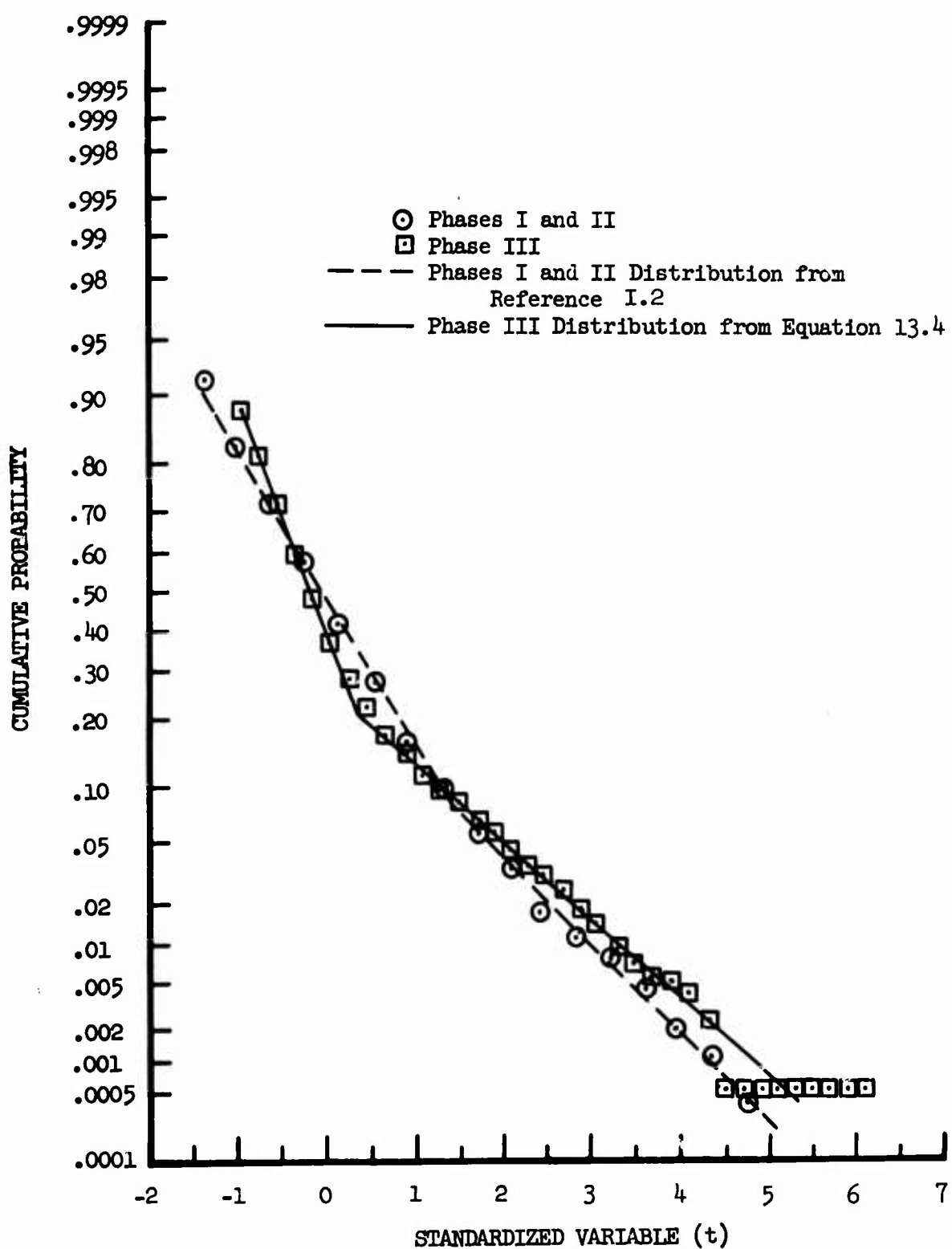


Figure 44.12 Comparison of Standardized Lateral Gust Velocity RMS Cumulative Probability Distribution from Phases I and II with that from Phase III

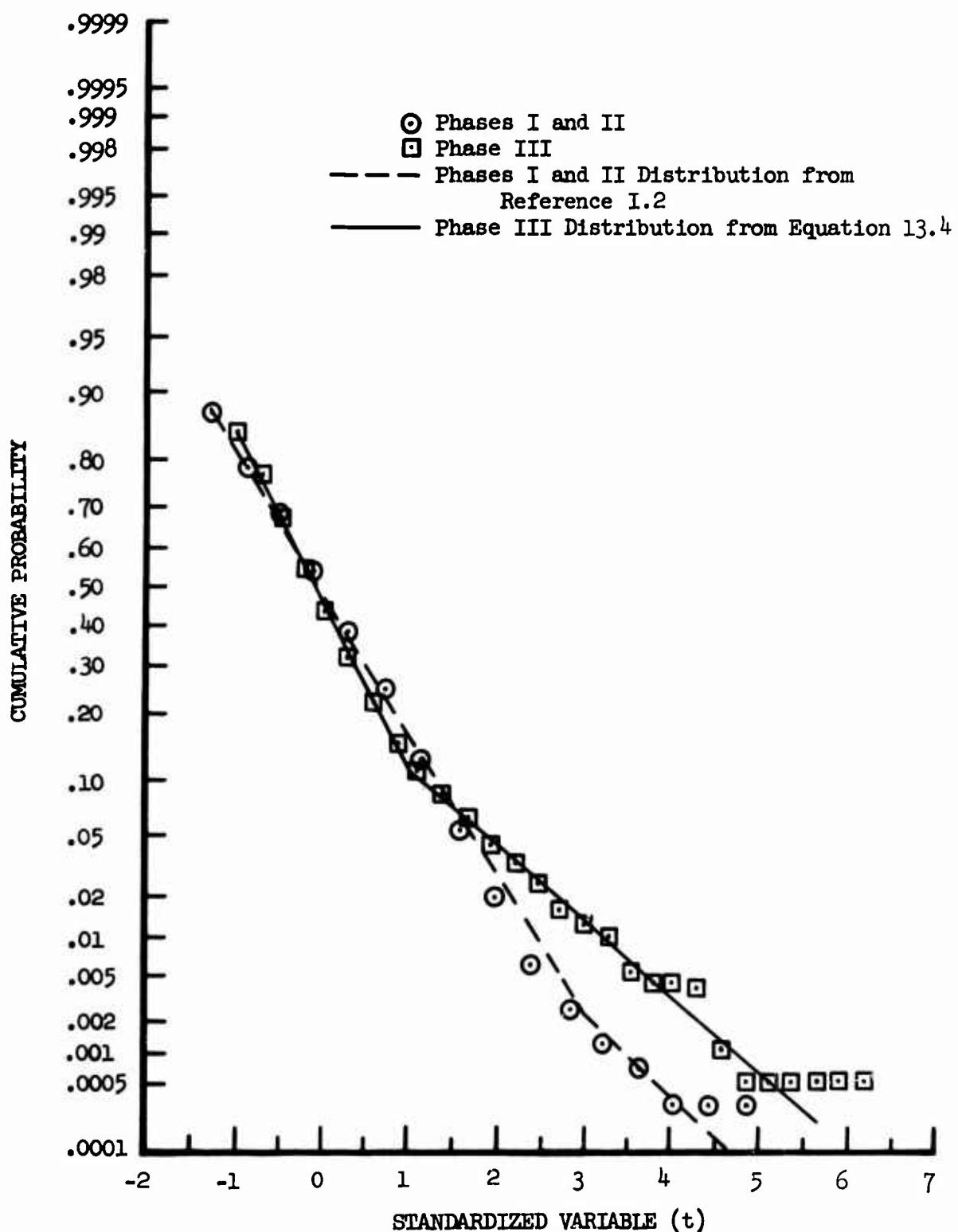


Figure 44.13 Comparison of Standardized Vertical Gust Velocity RMS Cumulative Probability Distribution from Phases I and II with that from Phase III

45. PEAK COUNT

Peak count data obtained during Phase III could not be combined with those data from Phases I and II, (Reference I.2), to obtain overall LO-LOCAT statistics. This was because of the difference of the measured turbulence wavelengths between the phases. Considering the filtering techniques used in data processing, the C-131 aircraft flying at 330 feet per second during Phases I and II were capable of obtaining turbulence data at wavelengths ranging from 33 to 7980 feet. The T-33, flying at 630 feet per second was capable of recording turbulence data at wavelengths ranging from 63 to 15,100 feet. Thus, the wavelength spectrum was not the same for the different phases and the high frequency of occurrence per mile of the 33 to 63-foot wavelengths measured during Phases I and II were not measured during Phase III.

The relationship of peak count data to the various geophysical phenomena is similar to that shown for the rms values in Section 44. Therefore, a direct comparison between Phases I and II and Phase III, accounting for difference in the percentages of data obtained under the various geophysical conditions was not accomplished for the peak count data. Data from both Phases I and II and Phase III are shown in this section. Variations of the peak count distributions with geophysical conditions for Phases I and II are compared with corresponding ones for Phase III.

Figures 45.1 through 45.3 show the terrain effects on peak count cumulative distributions for Phases I and II and for Phase III. Comparison of the different phases shows the Phase III data to have nearly the same distributions for the same type terrain (except for high mountain) as for Phases I and II. The high mountain data obtained during Phases I and II did not include any samples from the Peterson route. During Phase III, the most severe turbulence encountered was over the Peterson high mountains. The reason for the distribution curve being higher for Phase III than for Phases I and II is therefore due primarily to the effects of the Peterson high mountain data. The relationship between the distribution curves for the different types of terrain is very similar for both programs.

Figures 45.4 through 45.6 show the altitude effects on the peak count distributions for Phases I and II and for Phase III. Comparison of the different phases shows that the Phase III distribution curves are higher than those of Phases I and II. The probability of exceeding a given gust velocity is greater at 250 feet than at 750 feet above the terrain in all cases except at the very highest gust velocities. The Phase III curves are higher than for Phases I and II due to the effects of the Peterson high mountain samples at both altitudes.

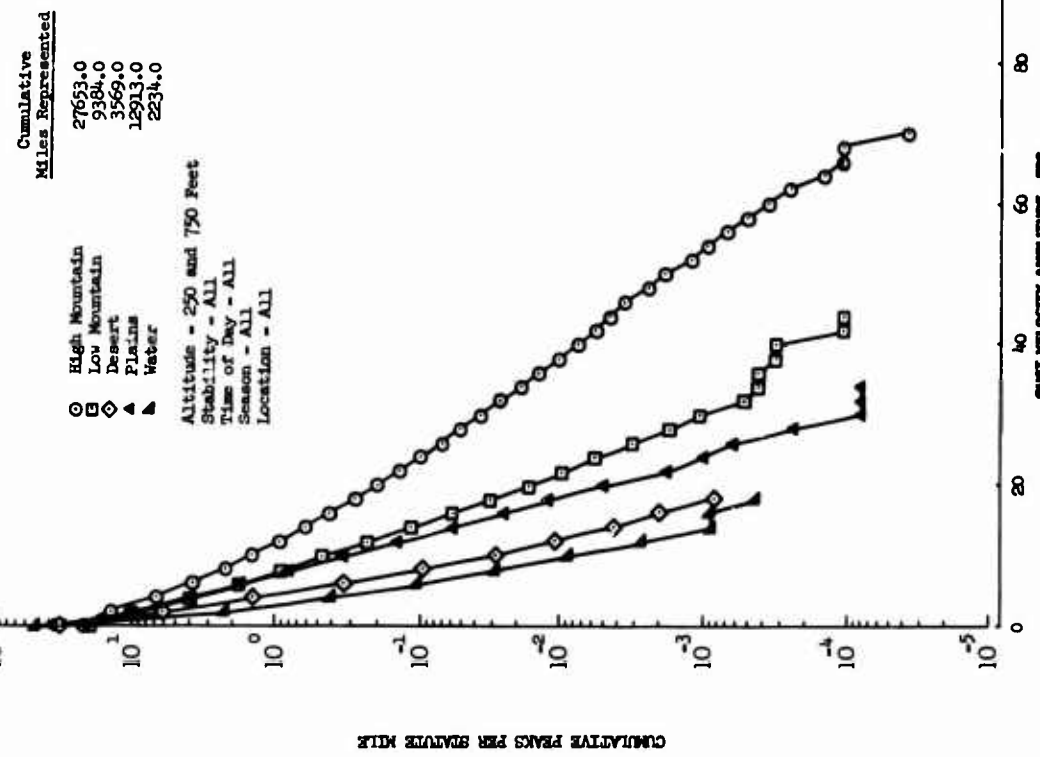
Figures 45.7 through 45.9 show the effects of atmospheric stability on the peak count distributions for Phases I and II and for Phase III. Here again, comparison of the different phases shows the Phase III data to have the highest distribution curves. The distribution curves for all stabilities were higher for Phase III due to the effects of the Peterson high mountain samples. The relationship between distribution curves for different atmospheric stabilities is very similar for both programs.

Figures 45.10 through 45.12 show the effects of time of day on the peak count distributions for Phases I and II and for Phase III. As has been the case for previous comparisons, Phase III distributions are always higher. Very little variation with time of day is shown for any phase.

It can be concluded from these comparisons that the gust velocity data obtained during LO-LOCAT Phase III shows a higher frequency of occurrence of the larger gust velocities than those obtained during Phases I and II primarily due to the effects of the Peterson high mountain data. The relationship between the peak count distribution curves for different geophysical conditions is similar for Phases I and II and Phase III.

A discussion of the relationship between the distribution curves for the three components of gust velocity is given in Section 8. This discussion shows the distribution curves to be in closer agreement, except those categories containing high mountain data, for Phase III than for Phases I and II.

Phase III



Phases I and II

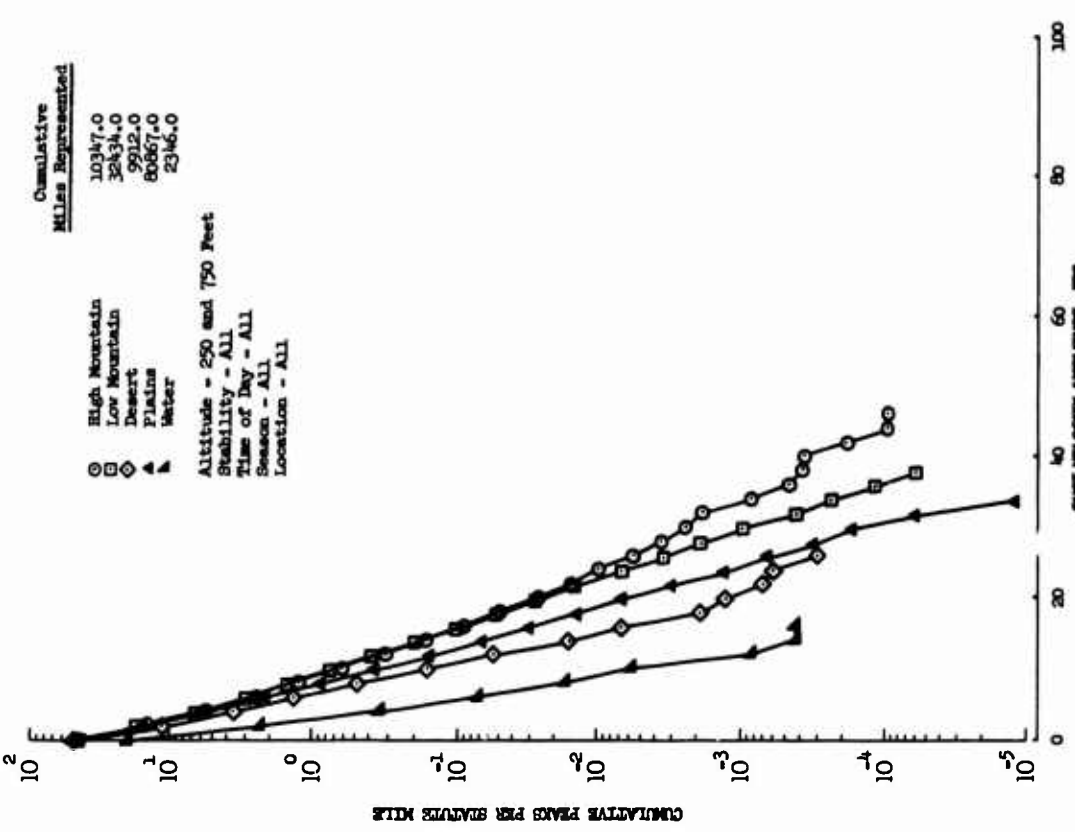
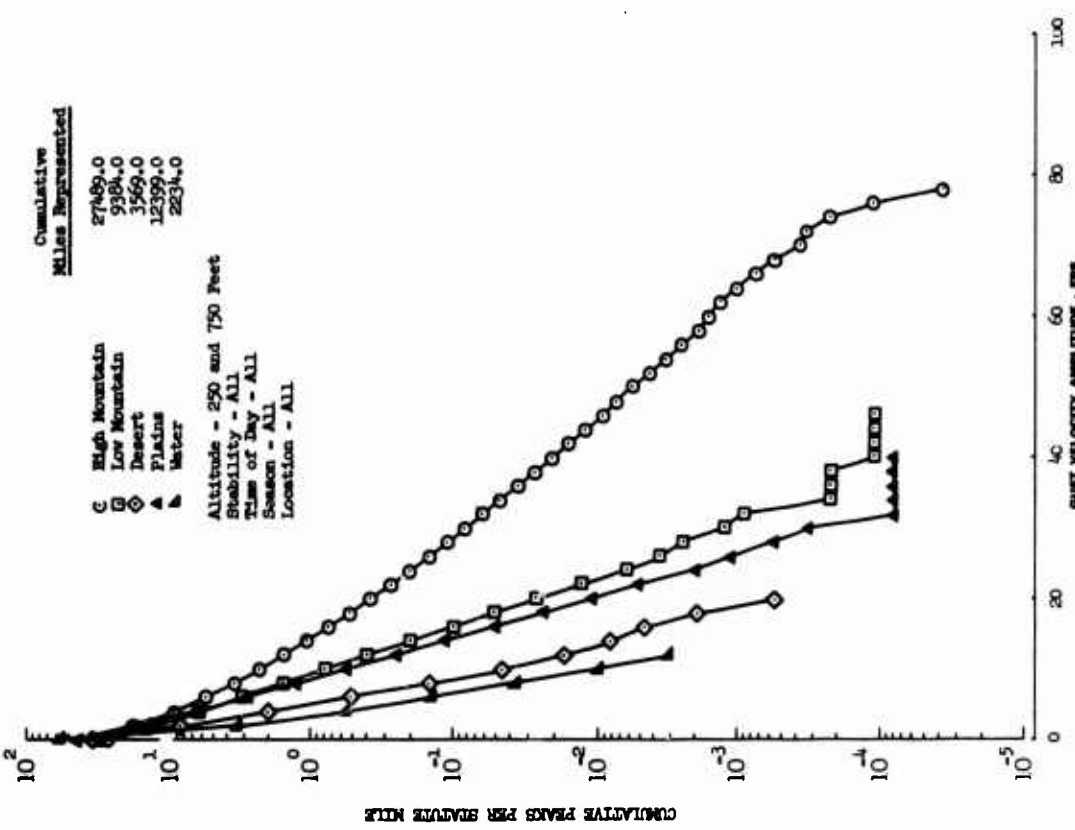


Figure 45.1 Terrain Effects on Longitudinal Gust Velocity Peaks
LO-LOCAT Phases I and II and Phase III

Phase III



Phases I and II

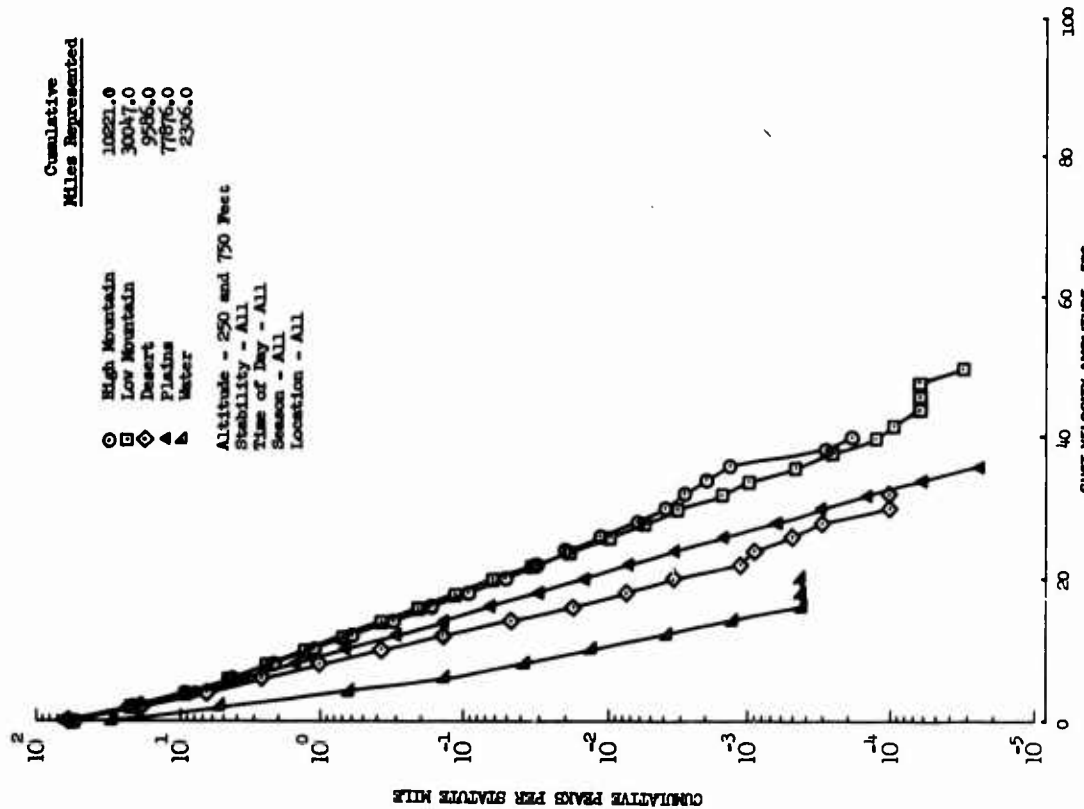


Figure 45.2 Terrain Effects on Lateral Gust Velocity Peaks
LO-LOCAT Phases I and II and Phase III

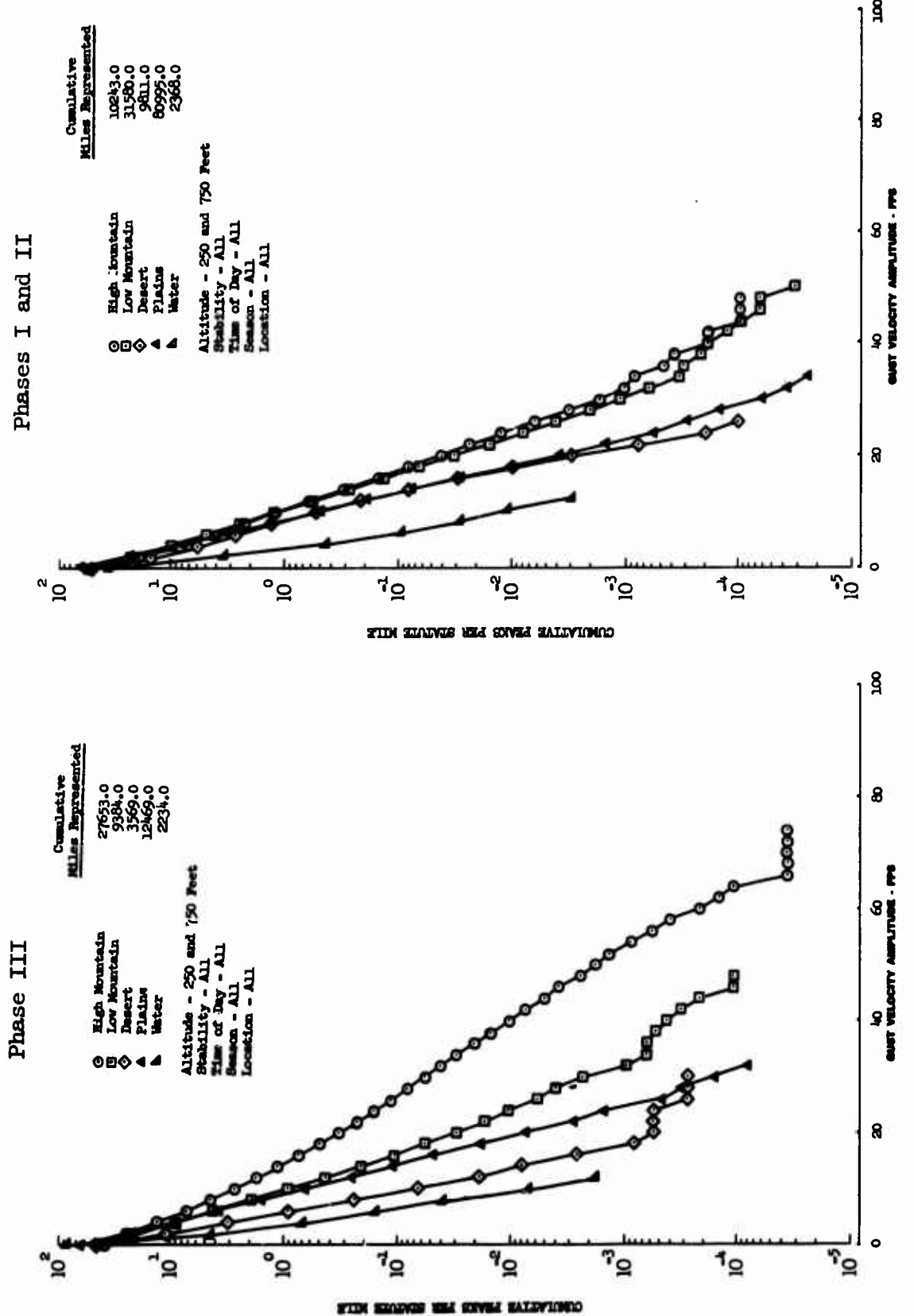


Figure 45.3 Terrain Effects on Vertical Gust Velocity Peaks
LO-LOCAT Phases I and II and Phase III

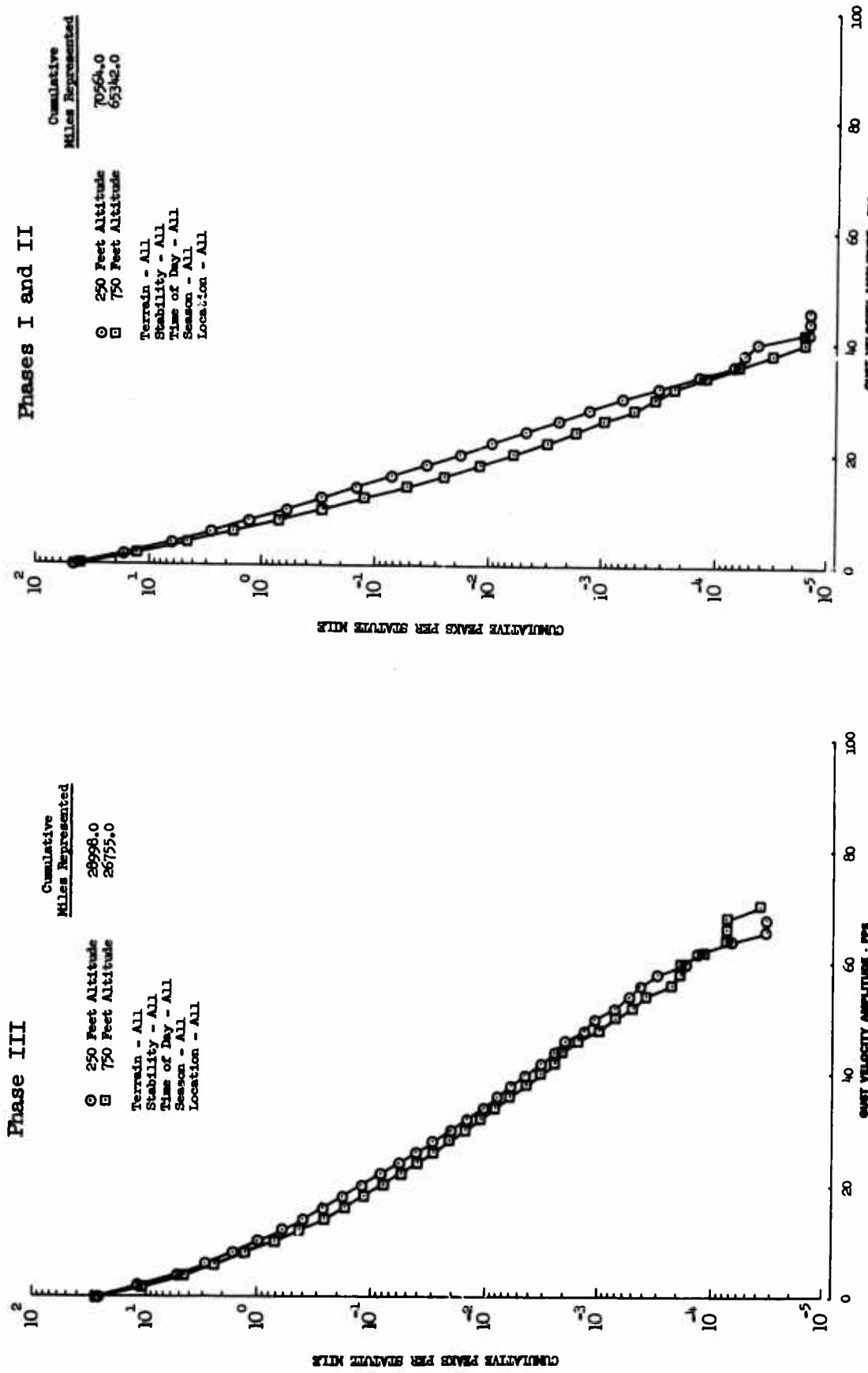


Figure 45.4 Altitude Effects on Longitudinal Gust Velocity Peaks
LO-LOCAT Phases I and II

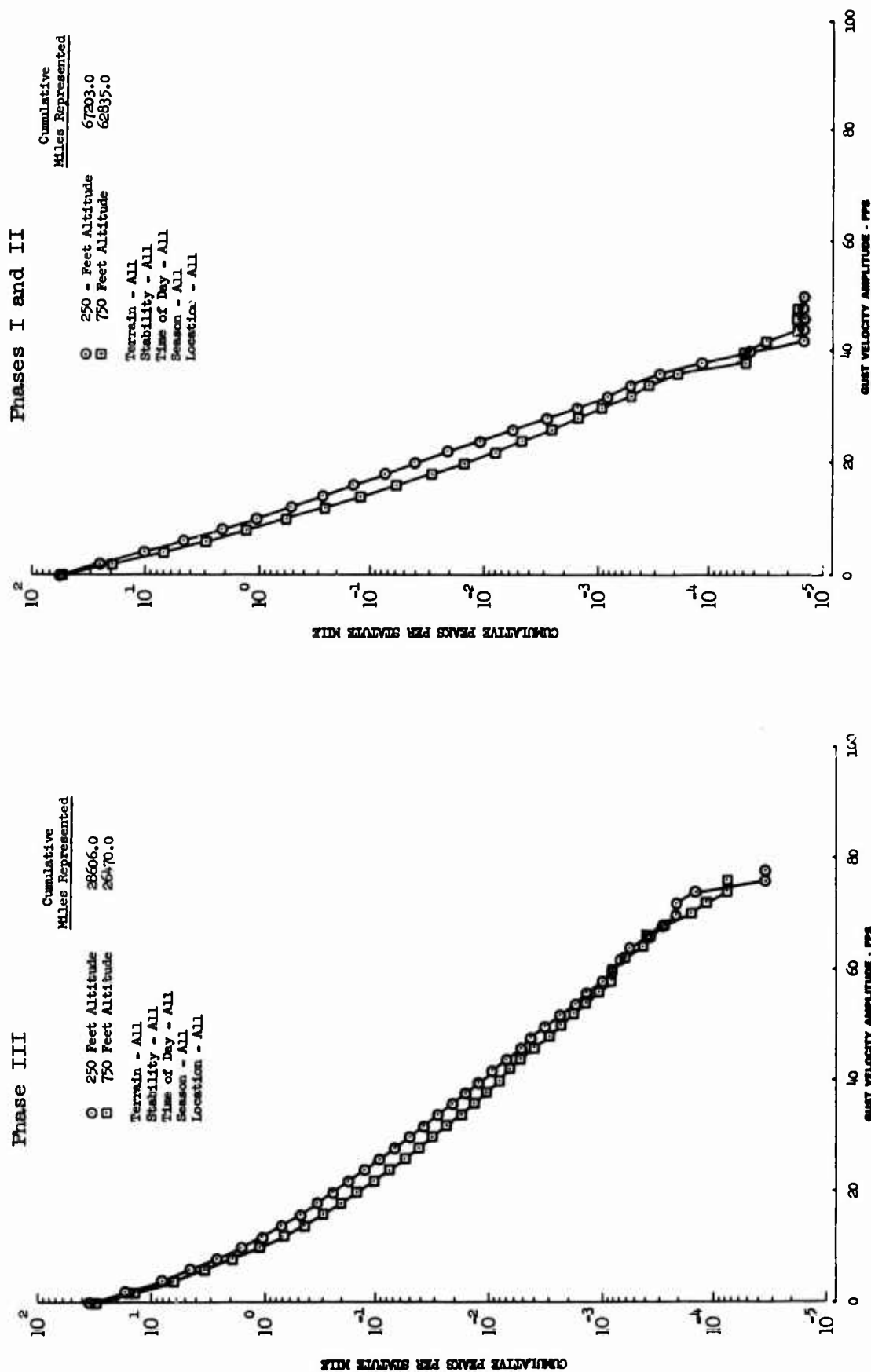


Figure 45.5 Altitude Effects on Lateral Gust Velocity Peaks
IO-LOCAT Phases I and II

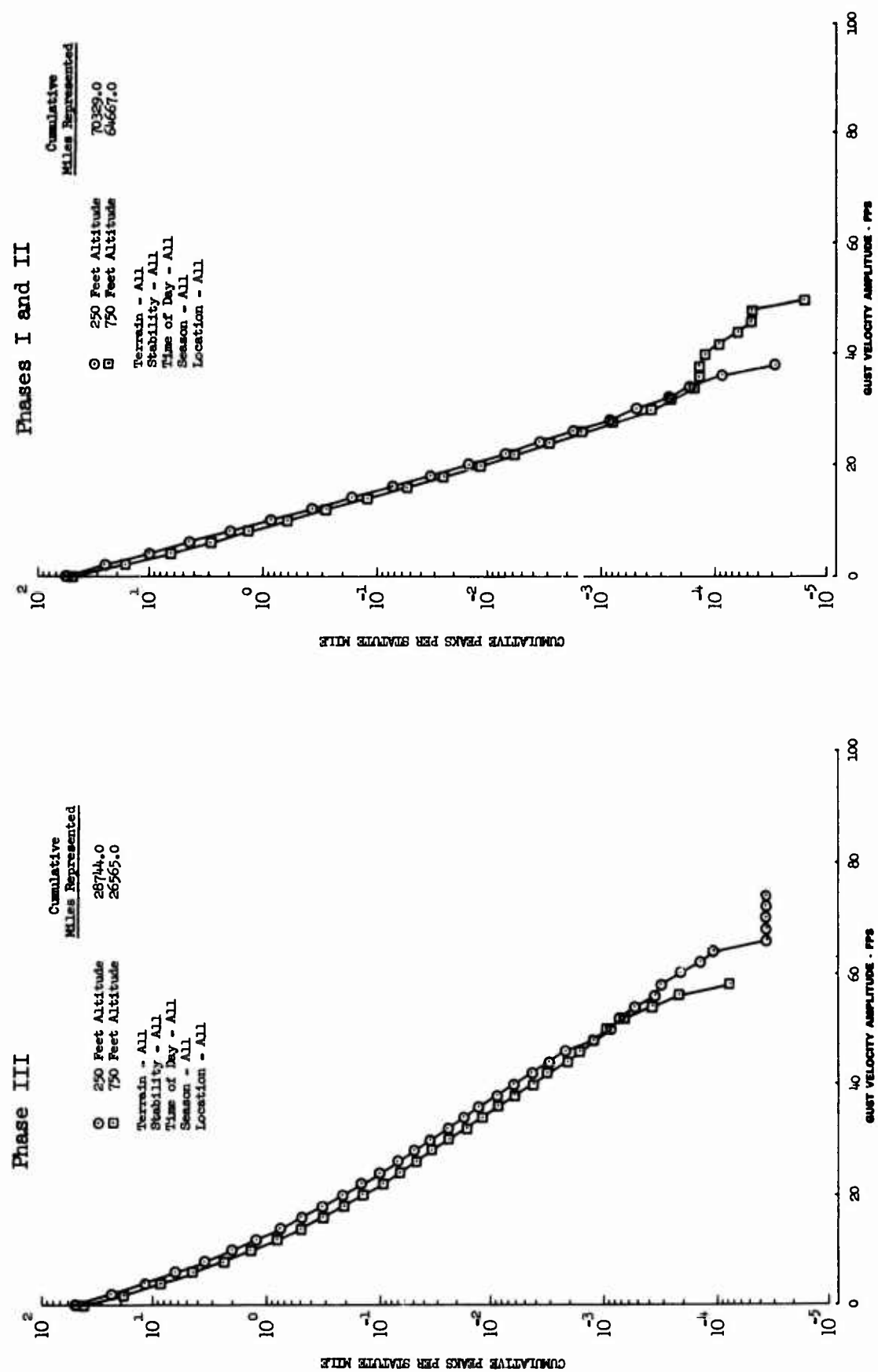


Figure 45.6 Altitude Effects on Vertical Gust Velocity Peaks
LO-LOCAT Phases I and II

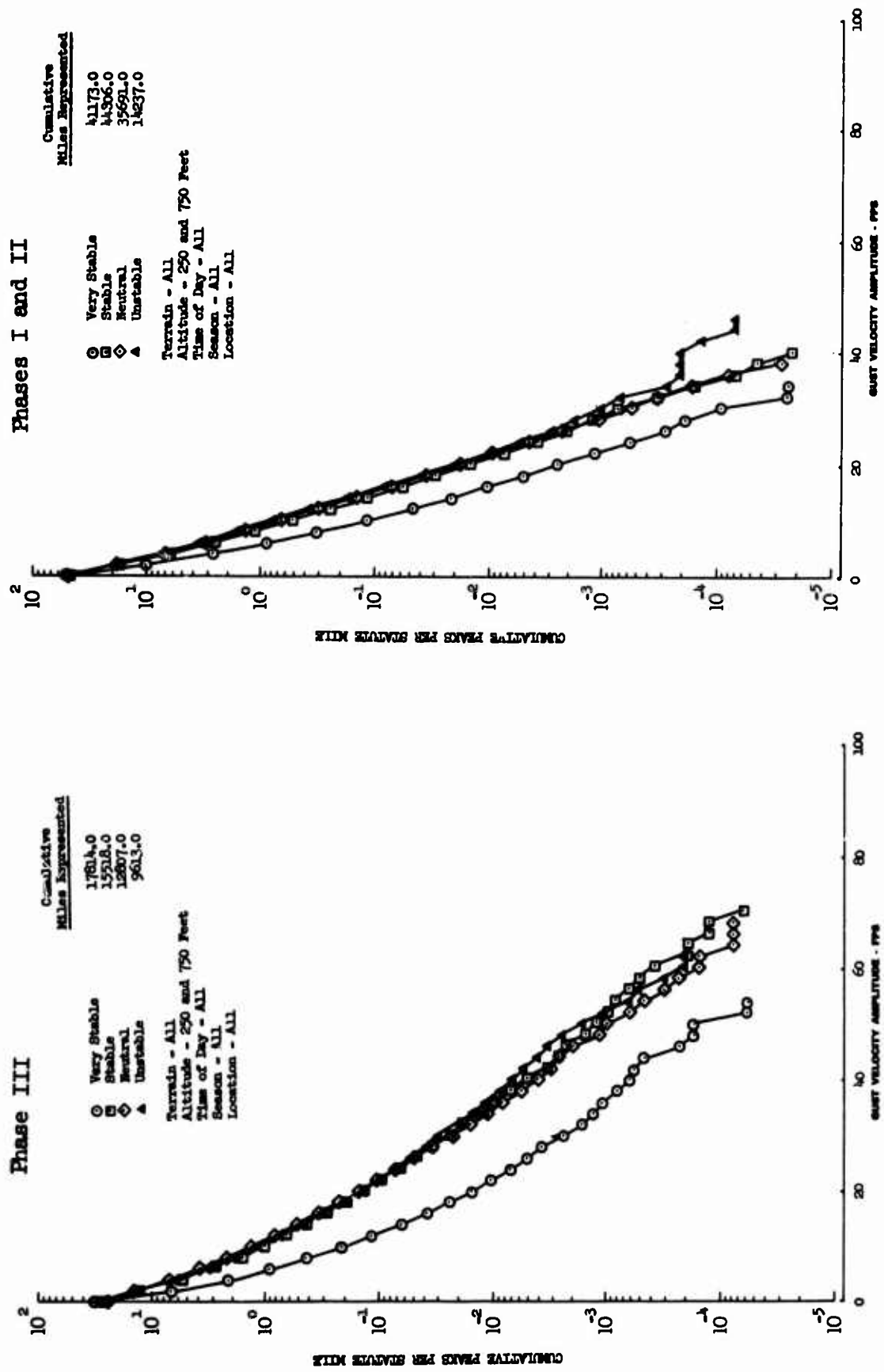


Figure 45.7 Stability Effects on Longitudinal Gust Velocity Peaks
LO-LOCAT Phases I and II

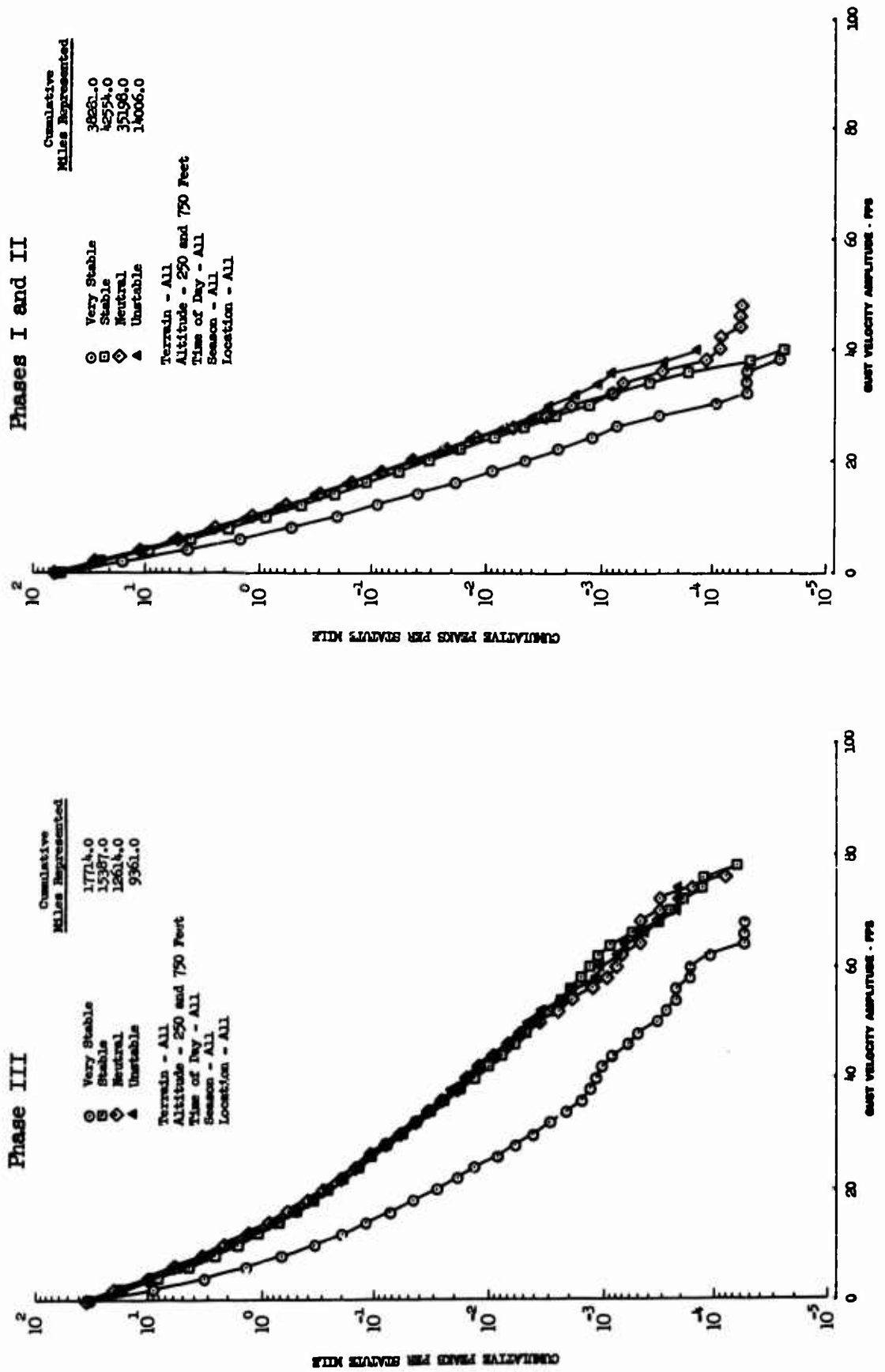


Figure 45.8 Stability Effects on Lateral Gust Velocity Peaks
LO-LOCAT Phases I and II

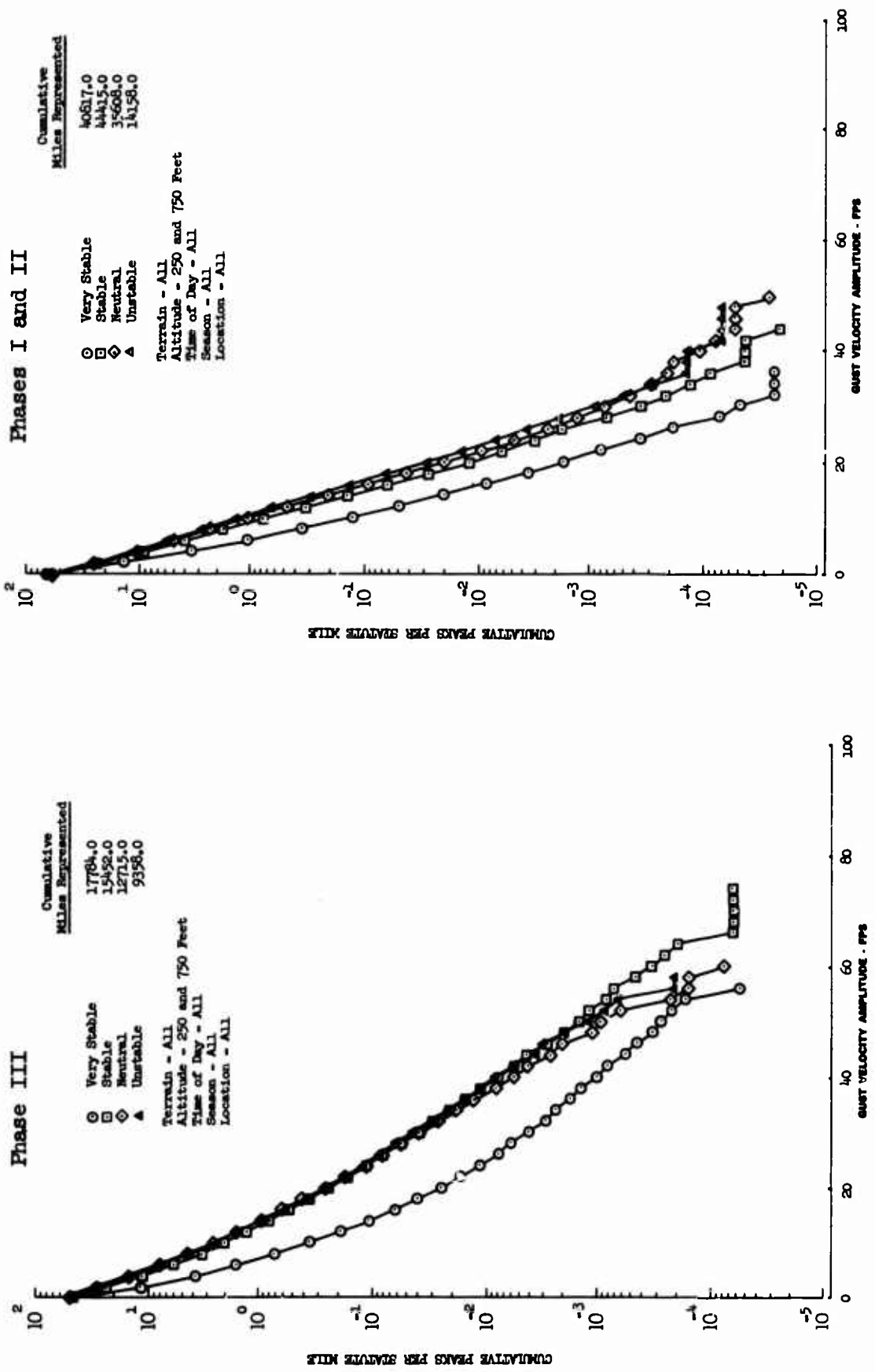


Figure 45.9 Stability Effects on Vertical Gust Velocity Peaks
LO-LOCAN Phases I and II

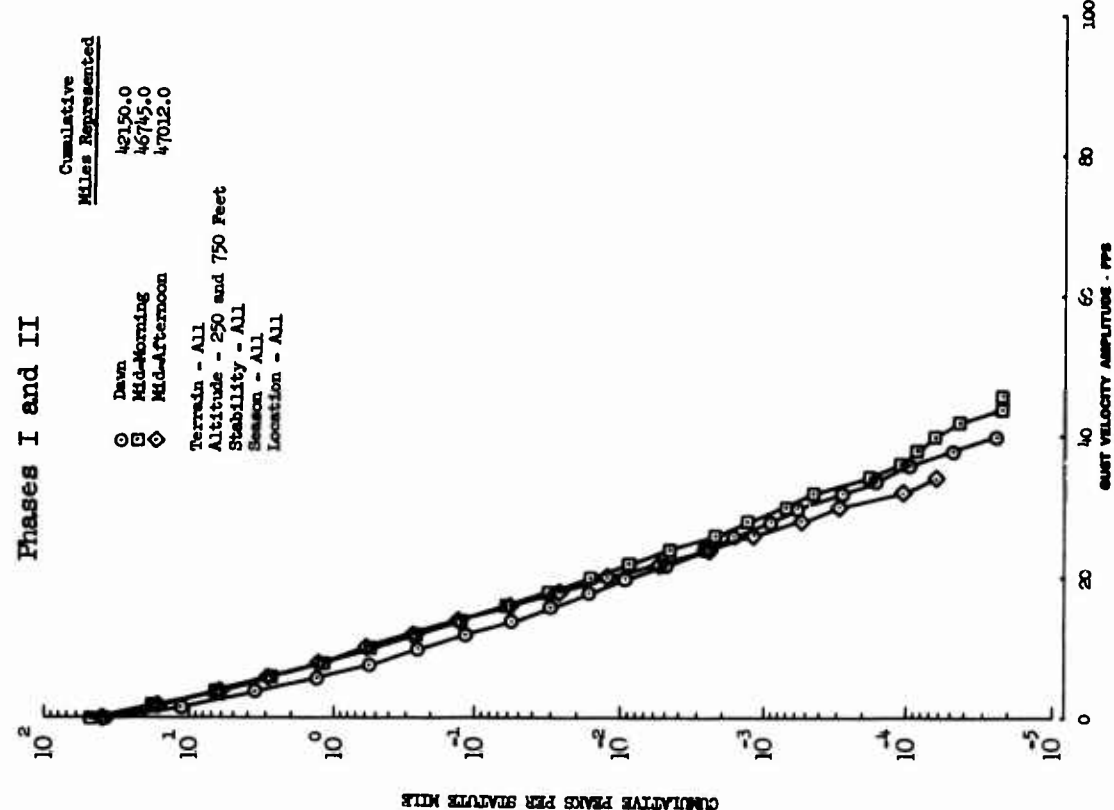
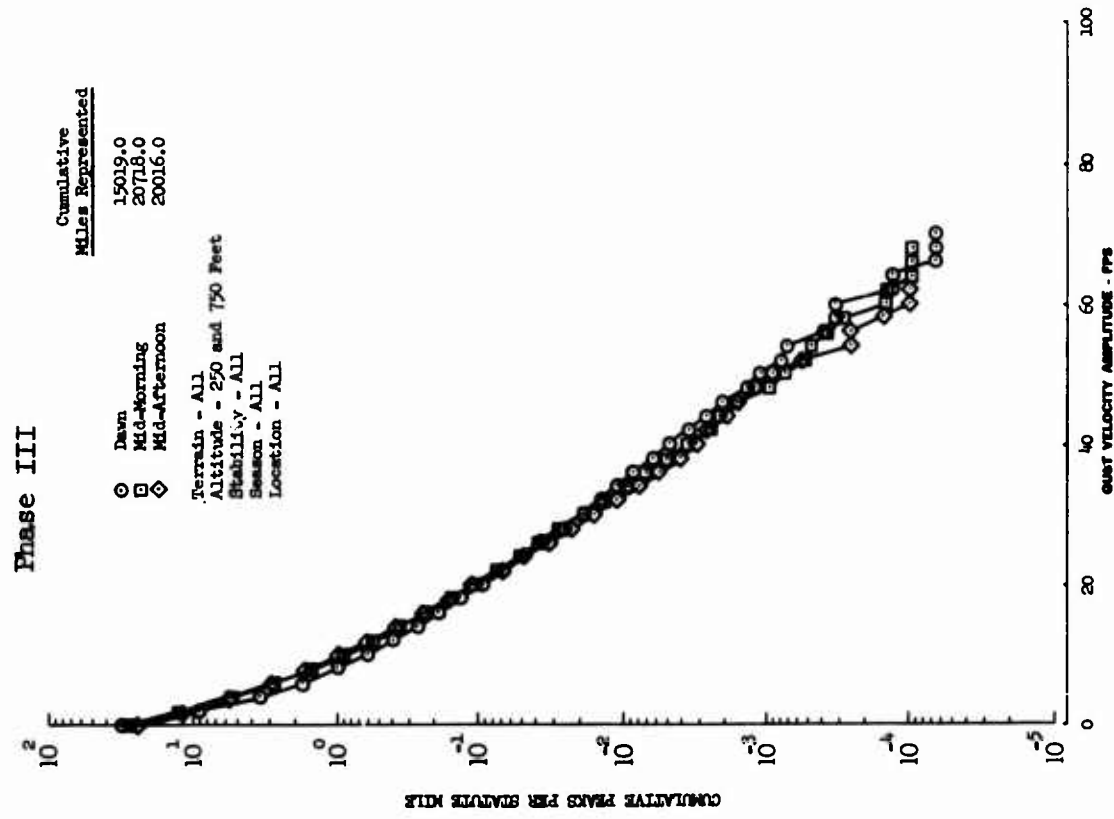


Figure 45.10 Time of Day Effects on Longitudinal Gust Velocity Peaks
LO-LOCAT Phases I and II

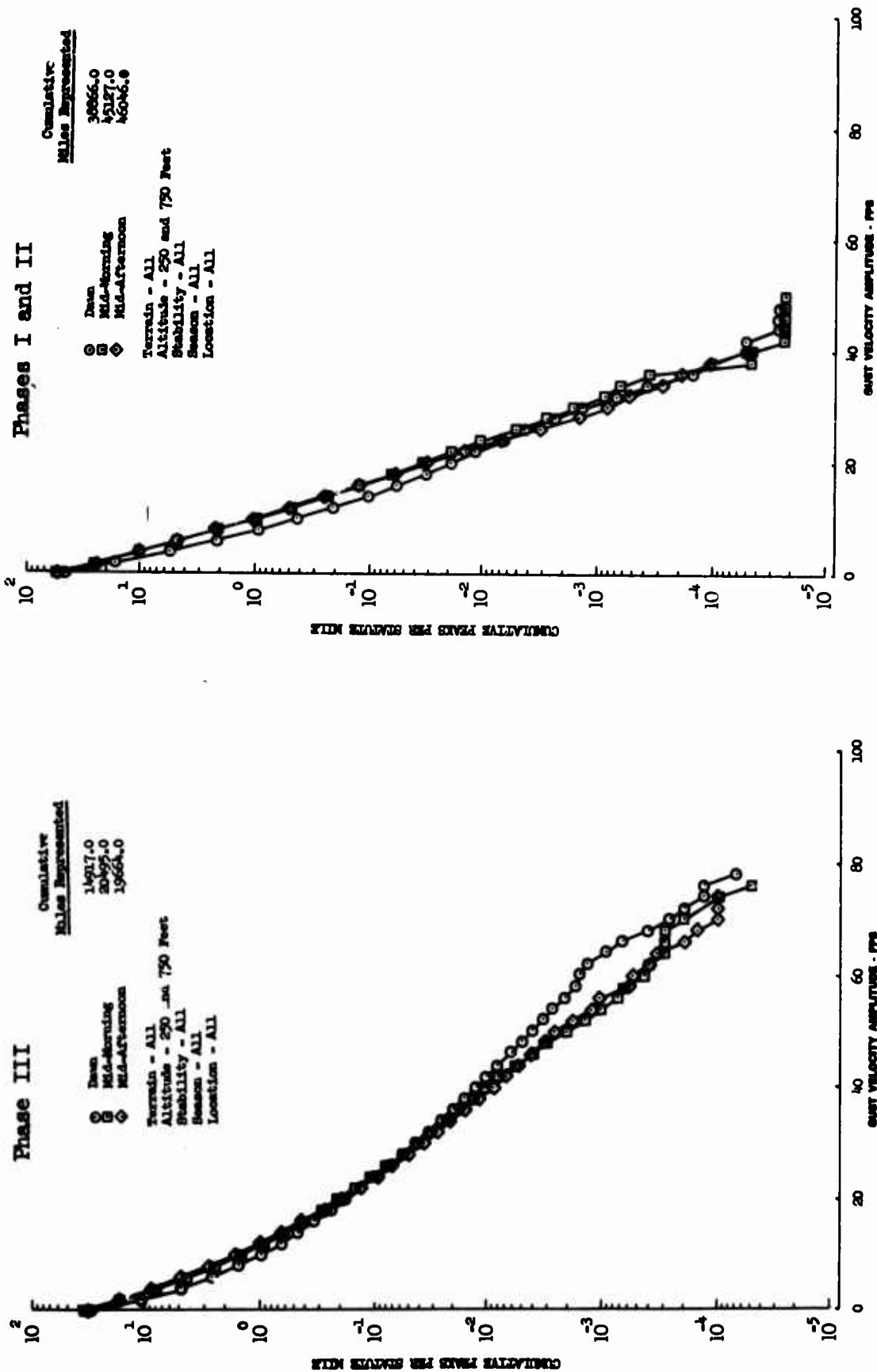


Figure 45.11 Time of Day Effects on Lateral Gust Velocity Peaks
LO-LOCAT Phases I and II

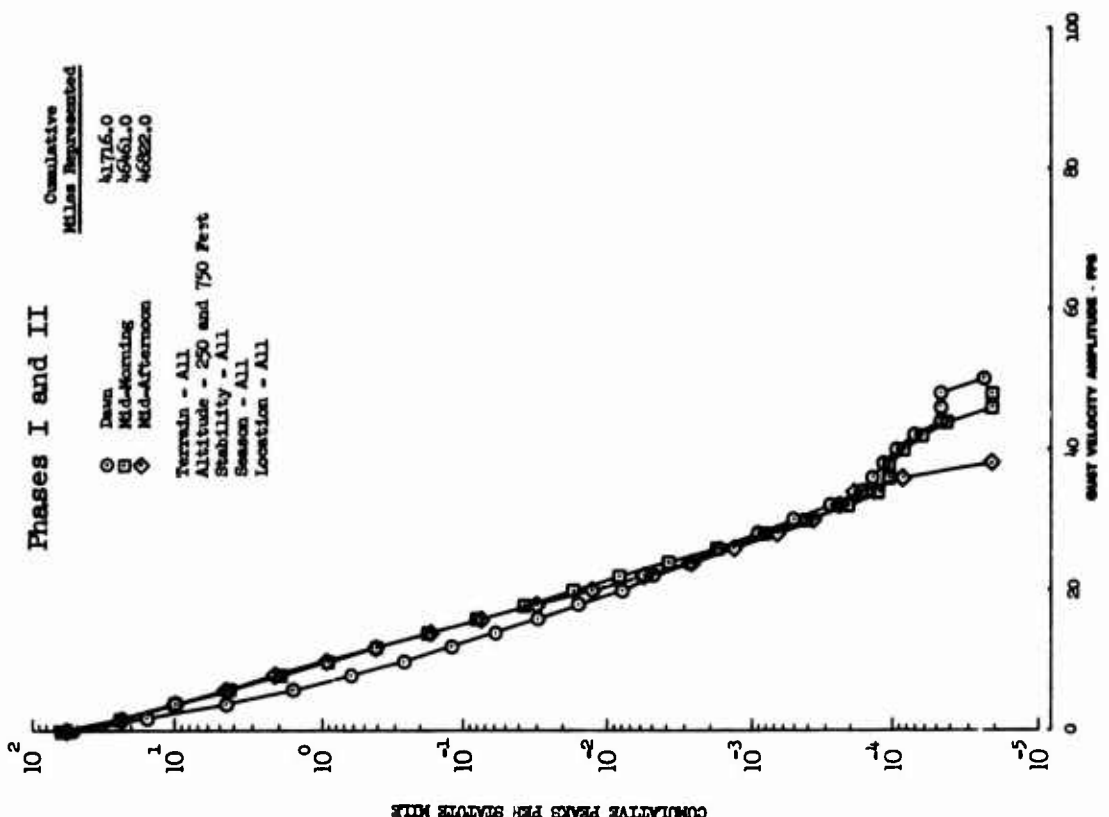
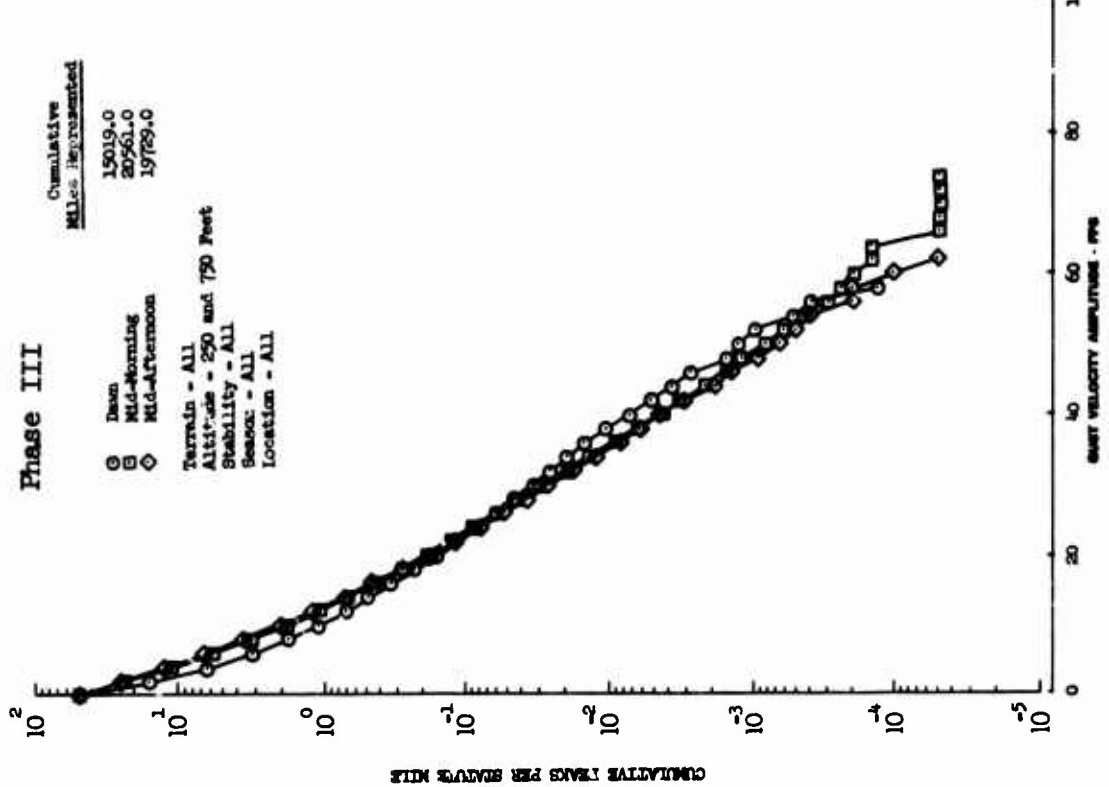


Figure 4F.12 Time of Day Effects on Vertical Gust Velocity Peaks
LO-LOCAT Phases I and III

46. POWER SPECTRA

The normalized spectra based on Phases I and II and Phase III data, along with normalized von Karman spectra, are compared in Figures 46.1 through 46.3. The Phases I and II data define the spectra to higher values of kL and the Phase III data describe the spectra to lower values.

The longitudinal gust spectra are in agreement for the different phases and agree well with the von Karman spectrum. The Phase III lateral and vertical spectra are slightly different from those obtained during Phases I and II. These differences consist of a dip in both lateral and vertical gust spectra in the kL range from 0.1 to 0.4 kL and a predominance of values higher than for Phases I and II and for the von Karman mathematical expressions at kL values less than 0.1. However, as explained in Section 23, these irregularities appear to be caused by the influence of airplane motion. The Phase III spectra, therefore, were defined at the low kL values using the relatively low turbulence samples. These data are presented in Figures 23.5 and 23.10 and are compared to Phases I and II and the von Karman mathematical expressions in Figures 46.2 and 46.3. Assuming that the airplane motion effects (see Section 23) were caused by high levels of turbulence and that the vertical gust spectra obtained at 250 feet involve less isotropy and more airplane motion than the spectra obtained at 750 feet, low turbulence level vertical gust data obtained at 750 feet were used to define the vertical spectrum shape at low frequencies. These data are also presented in Figure 46.3. The low turbulence level vertical gust data in Figure 46.3 agree well with Phases I and II and agree well with the lateral spectra in Figure 46.2. There are, however, a number of points just below Phases I and II data at $kL > 0.10$. This is probably an indication of a small amount of airplane motion being contained in the 750-foot data.

The final turbulence spectra model determined from Phases I, II, and III data is shown and compared to von Karman spectra in Figure 46.4. The final model is based on Phases I and II data at high kL values and Phase III at the low kL values with emphasis placed on the low turbulence level data. The final model is in good agreement with the von Karman model except for lateral and vertical spectra at the very low values. At $kL \leq 0.1$, the lateral and vertical spectra are slightly higher than the von Karman model.

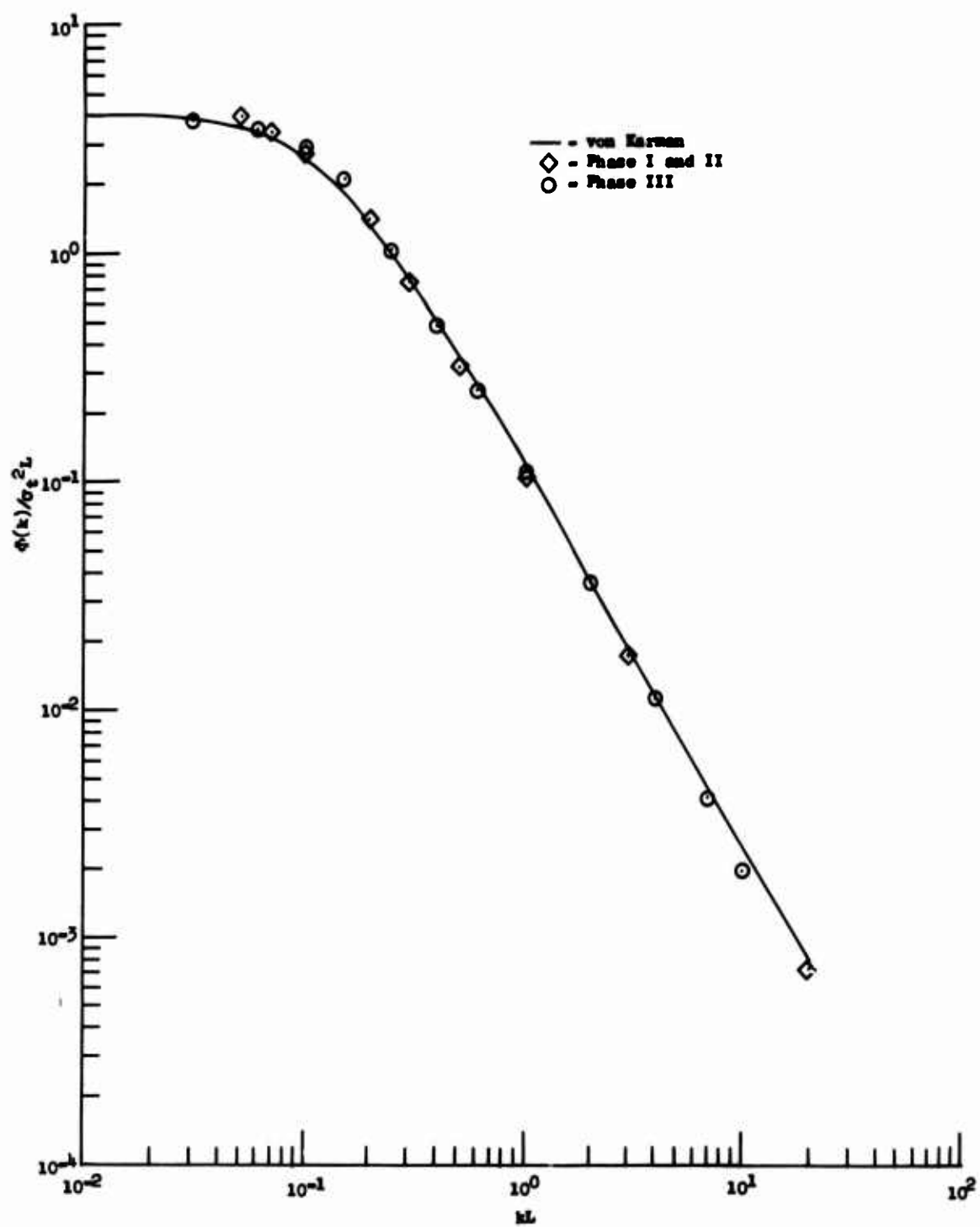


Figure 46.1 Longitudinal Gust Velocity Power Spectra Comparison

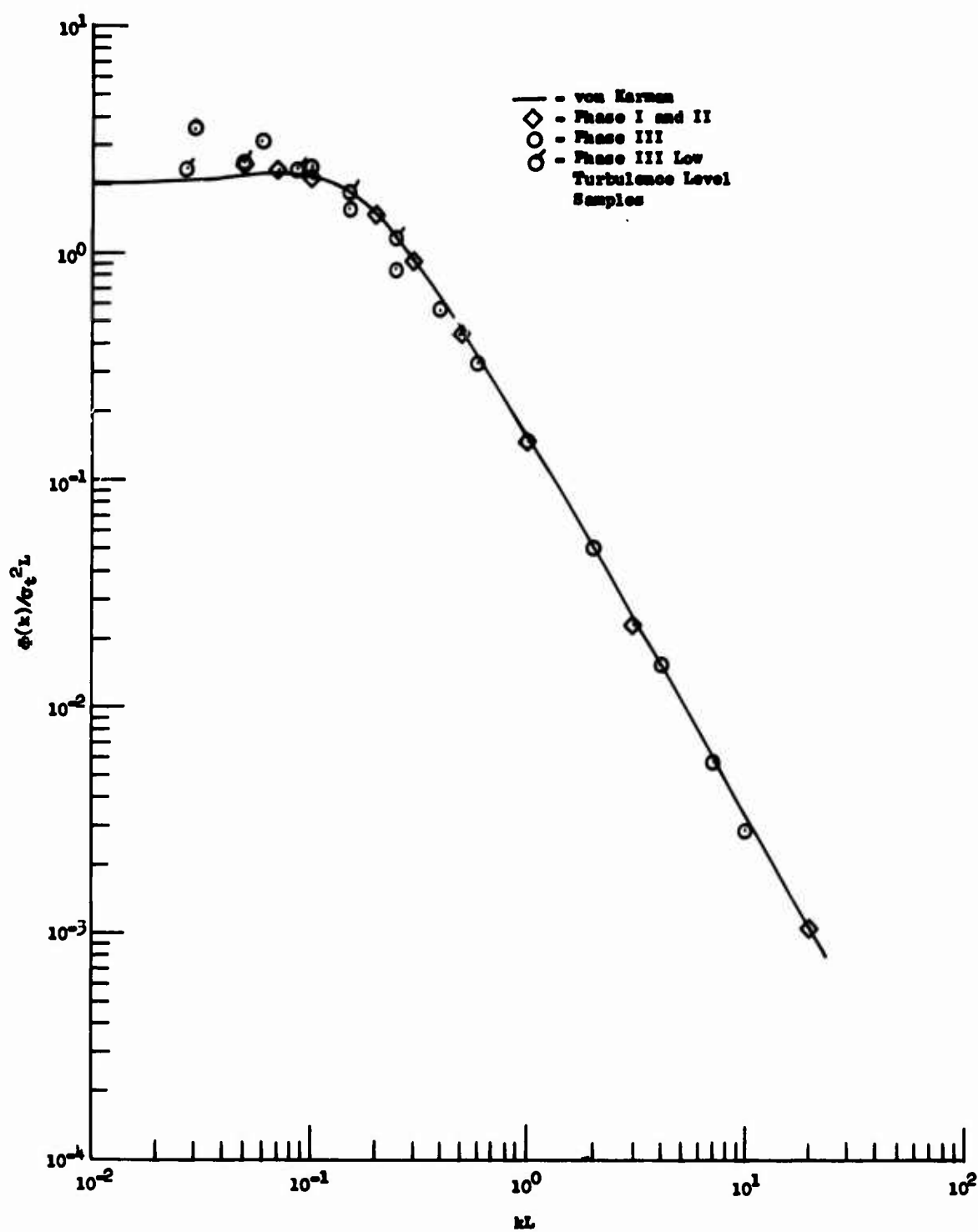


Figure 46.2 Lateral Gust Velocity Power Spectra Comparison

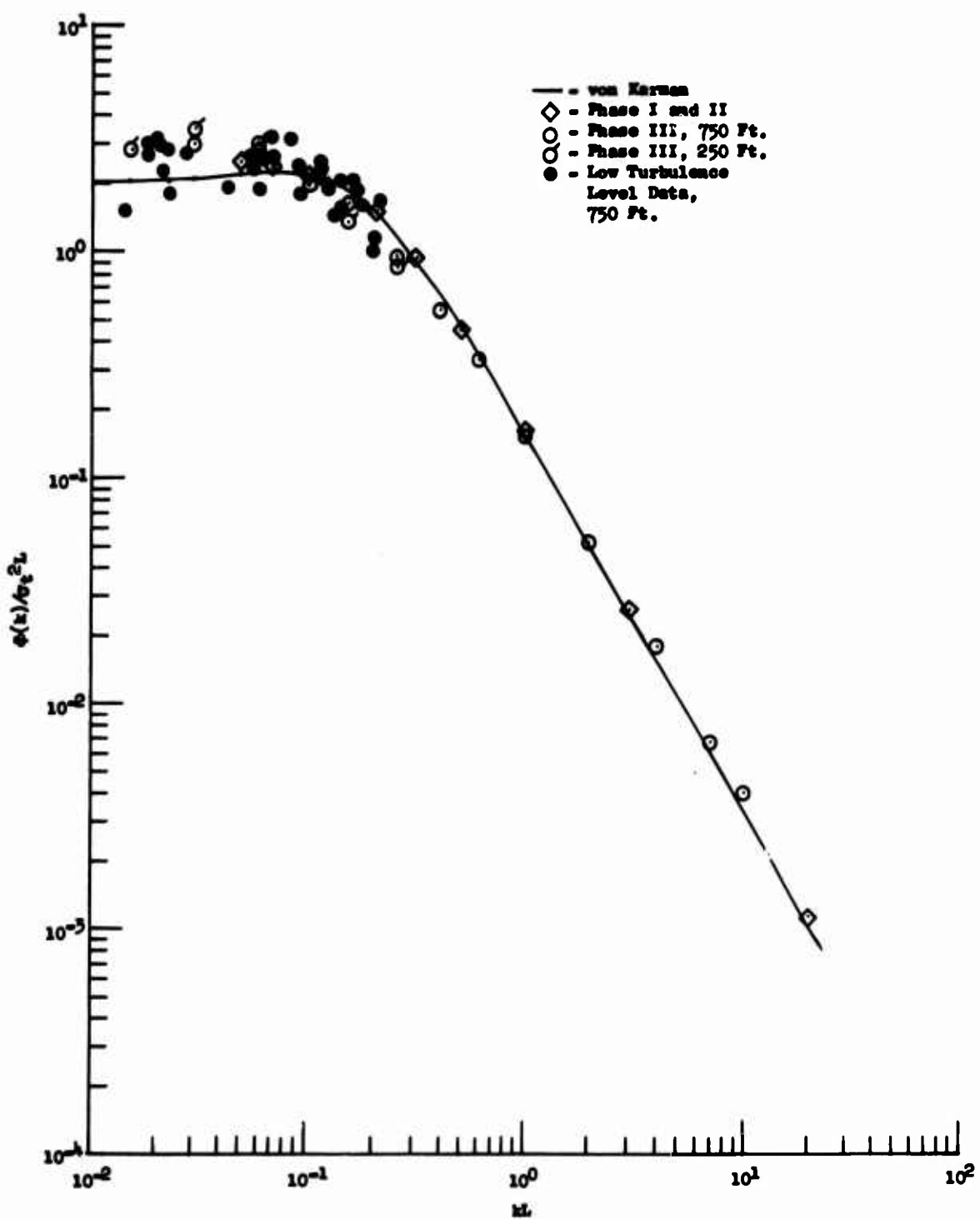


Figure 46.3 Vertical Gust Velocity Power Spectra Comparison

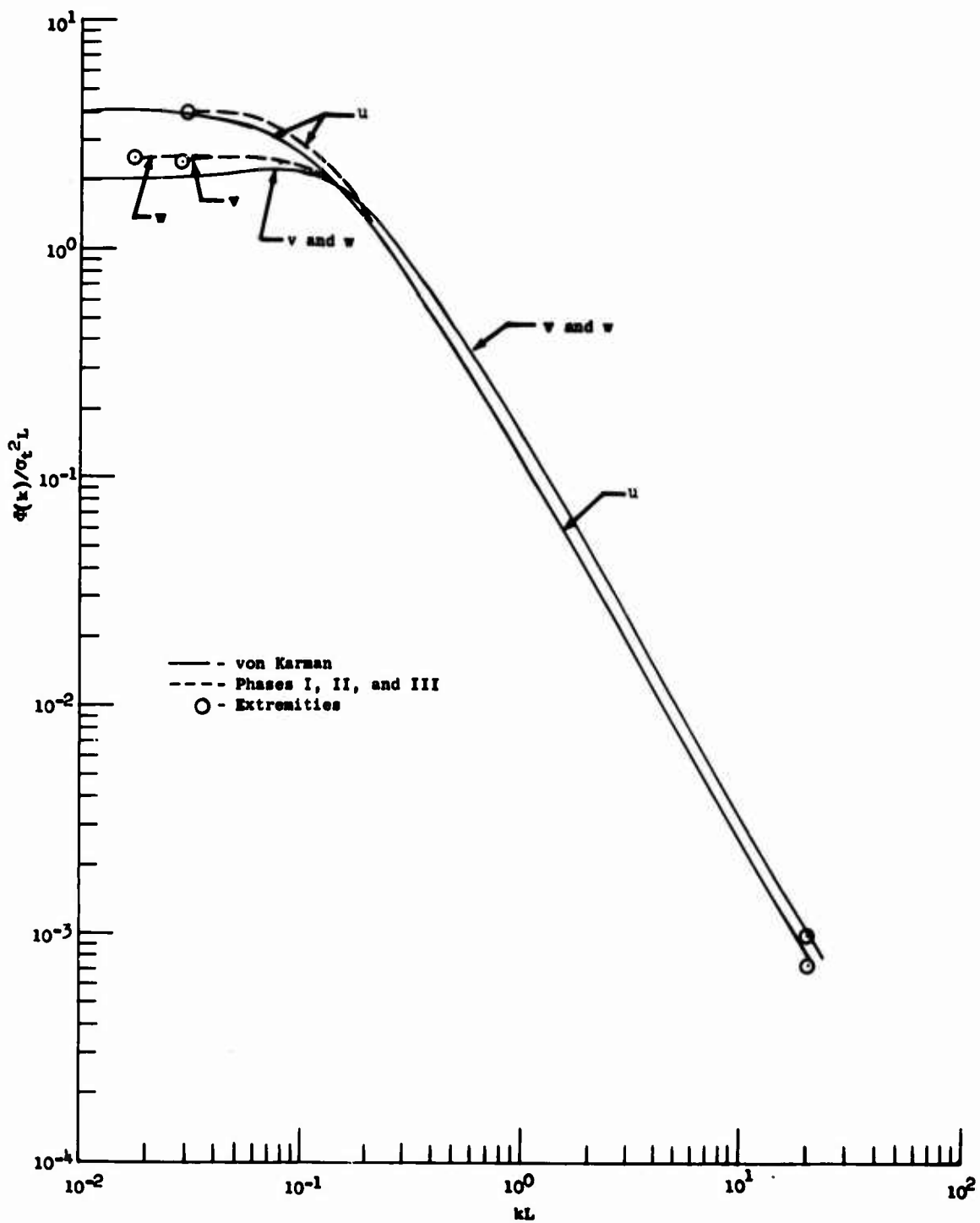


Figure 46.4 Phase I, II, and III Turbulence Spectra Model

47. SCALE LENGTH

The von Karman expressions gave a good representation of the experimentally determined spectra (see Section 28 and Reference I.2). Therefore, the von Karman scale lengths were statistically analyzed and compared for all phases of the LO-LOCAT Program.

The scale length equations 30.4 and 30.5 show that if k_2 and k_3 are constants then scale lengths are a function of $(\sigma_t/\sigma_T)^3$. The average σ_t and σ_T values of the turbulence samples used in the scale length analysis are tabulated in Table 47.1 for both Phases I, II, and Phase III. Also included in this table are the average scale lengths calculated for the different phases.

TABLE 47.1

AVERAGE SCALE LENGTHS AND STANDARD DEVIATIONS FOR
PHASES I AND II AND PHASE III

Parameter	Phases I and II	Phase III
$\bar{\sigma}_{t_u}$ (fps)	2.92	4.32
$\bar{\sigma}_{T_u}$ (fps)	1.54	1.80
\bar{L}_{K_u} (ft.)	387	715
$\bar{\sigma}_{t_v}$ (fps)	3.20	4.77
$\bar{\sigma}_{T_v}$ (fps)	1.93	2.44
\bar{L}_{K_v} (ft.)	409	598
$\bar{\sigma}_{t_w}$ (fps)	3.04	4.18
$\bar{\sigma}_{T_w}$ (fps)	1.91	2.37
\bar{L}_{K_w} (ft.)	367	450

The average σ_t values presented in Table 47.1 were determined from only those turbulence samples used for spectra analysis. Therefore, the σ_t values of Table 47.1 are significantly larger than those tabulated in Table 44.3 which are average values obtained from all Phase II turbulence samples. This is the result of deleting from the spectra analysis those turbulence samples exhibiting low signal to noise ratios and those samples showing non-homogeneity and consequently low σ_t values.

The Phase III average values of σ_t and σ_r presented in Table 47.1 are greater than those of Phases I and II. This is because no turbulence samples were recorded during Phases I and II that were comparable to the high intensity turbulence samples obtained over the high mountain legs of the Peterson route during Phase III.

Table 47.1 does not contain comparable data obtained under similar circumstances during Phases I and II and Phase III. This comparison was made for the data obtained over high mountain legs of the Edwards route during the Fall season. Average values of σ_t , σ_r , and scale lengths are tabulated in Table 47.2 for both Phases I and II and Phase III. Also shown in this table is the average speed for each set of turbulence samples.

TABLE 47.2

AVERAGE SCALE LENGTHS AND STANDARD DEVIATIONS
EDWARDS HIGH MOUNTAIN TERRAIN, FALL SEASON
PHASES I AND II AND PHASE III

Parameter	Phases I and II	Phase III
$\bar{\sigma}_{t_u}$ (fps)	3.02	3.33
$\bar{\sigma}_{T_u}$ (fps)	1.58	1.35
\bar{L}_{K_u} (ft.)	426	743
$\bar{\sigma}_{t_v}$ (fps)	3.30	3.44
$\bar{\sigma}_{T_v}$ (fps)	2.05	1.70
\bar{L}_{K_v} (ft.)	414	654
$\bar{\sigma}_{t_w}$ (fps)	3.12	3.50
$\bar{\sigma}_{T_w}$ (fps)	2.00	1.85
\bar{L}_{K_w} (ft.)	384	561
\bar{V} (fps)	333	604

The values tabulated in Table 47.2 show that, for comparable categories, $\bar{\sigma}_t$ is larger for Phase III than for Phases I and II and that $\bar{\sigma}_T$ is larger for Phases I and II than for Phase III. The cumulative probabilities of σ_t and σ_T , presented in Figure 47.1, show this trend.

The Phase III $\bar{\sigma}_T$ values would be expected to be less than the Phases I and II $\bar{\sigma}_T$ values. The turbulence encountered during Phases I and II for the samples used in this particular analysis was assumed to be of the same intensity as that encountered during the comparable samples of Phase III. The theoretical ratio of $\bar{\sigma}_{T_{III}} / \bar{\sigma}_{T_I}$ was computed from Equations 25.1 and 25.2 using the average speeds tabulated in Table 47.2 and was found to be equal to approximately 0.93. The actual ratio of the $\bar{\sigma}_{T_{III}}$ to the $\bar{\sigma}_{T_I}$ values in Table 47.2 are, in all cases, less than this theoretical value.

The Phase III $\bar{\sigma}_t$ values were expected to be slightly greater than those of Phases I and II even though the turbulence encountered during the two phases was assumed to be of equal intensity. This was because the increased speed of the Phase III aircraft over that of the Phases I and II aircraft permitted the inclusion of longer wavelength turbulence in the statistical analysis of the Phase III turbulence samples.

Since the Phase III $\bar{\sigma}_T$ was somewhat less than the theoretical value and the Phase III $\bar{\sigma}_t$ was slightly greater than that of Phases I and II, the end result for a given set of comparable circumstances was that scale lengths computed from Phase III inputs were larger than those of Phases I and II. Comparison of the Phase III scale lengths with those of Phases I and II in Table 47.2 illustrates this fact. Cumulative probability plots of the scale lengths for the data shown in Table 47.2 are presented in Figure 47.2.

The difference in scale lengths between the phases is attributed to the large effect of the ratio σ_t / σ_T . Since this ratio is a cubic function in the scale length equations (Equations 30.4 and 30.5), small variations in either σ_t or σ_T have a significant effect on the calculated scale length values. The scale lengths would be expected to be larger for the Phase III than for the Phases I and II data since, due to the increased speed, longer wavelengths were measured. The scale lengths calculated from the vertical component would be expected to be less than those calculated from the longitudinal component due to the effects of the compressed longer wavelength vertical eddies near the ground.

Cumulative probabilities of scale lengths for other comparative categories of Phase III and Phases I and II are shown in Figures 47.3 and 47.4. Figure 47.3 shows those scale lengths calculated from data obtained over the plains legs of the McConnell route during the Summer and Figure 47.4 shows those obtained from the plains legs of Peterson route during the Winter and Spring.

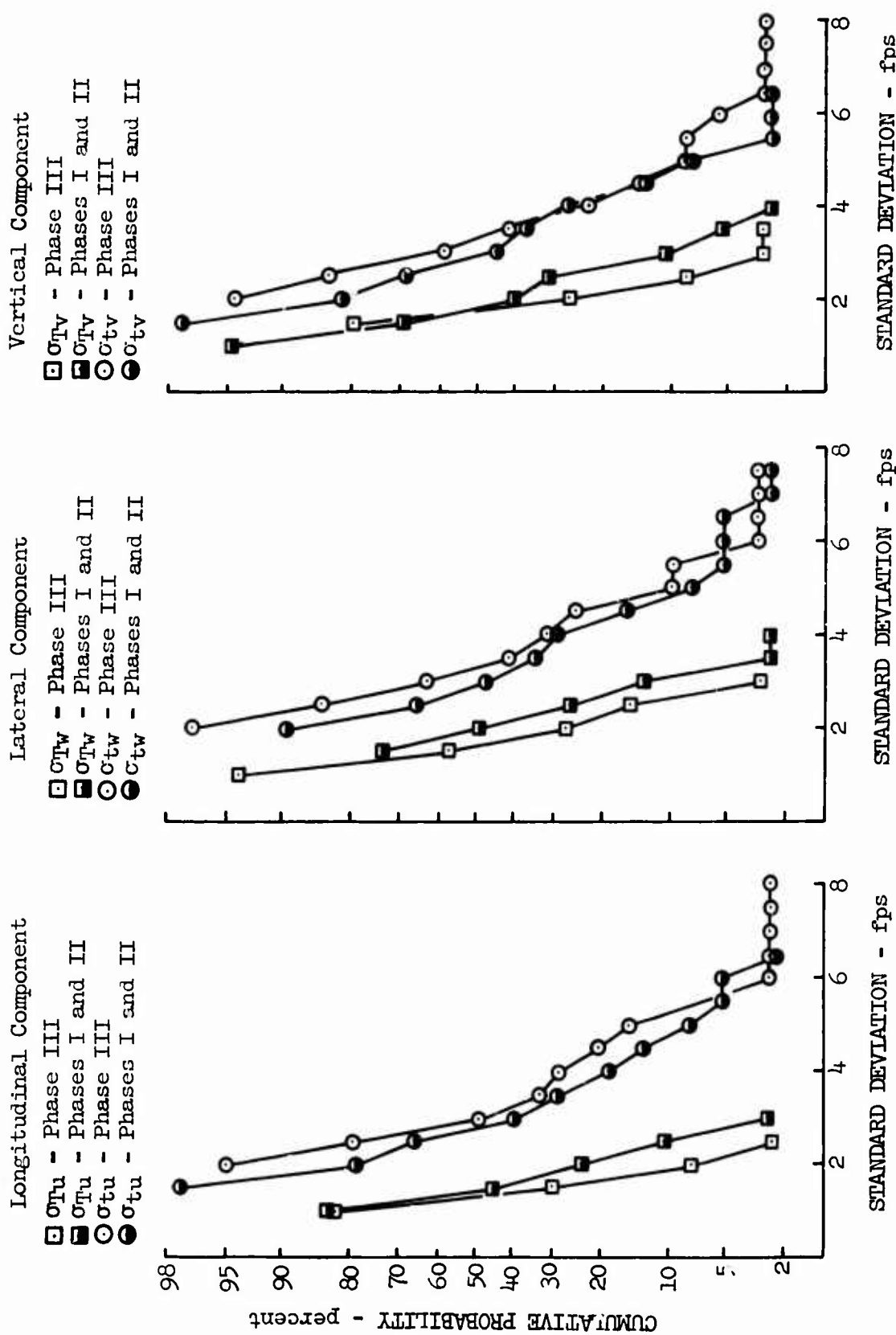


Figure 47.1 Comparison of σ_t and σ_T as Determined from Phases I and II and Phase III - Edwards, High Mountains, Fall

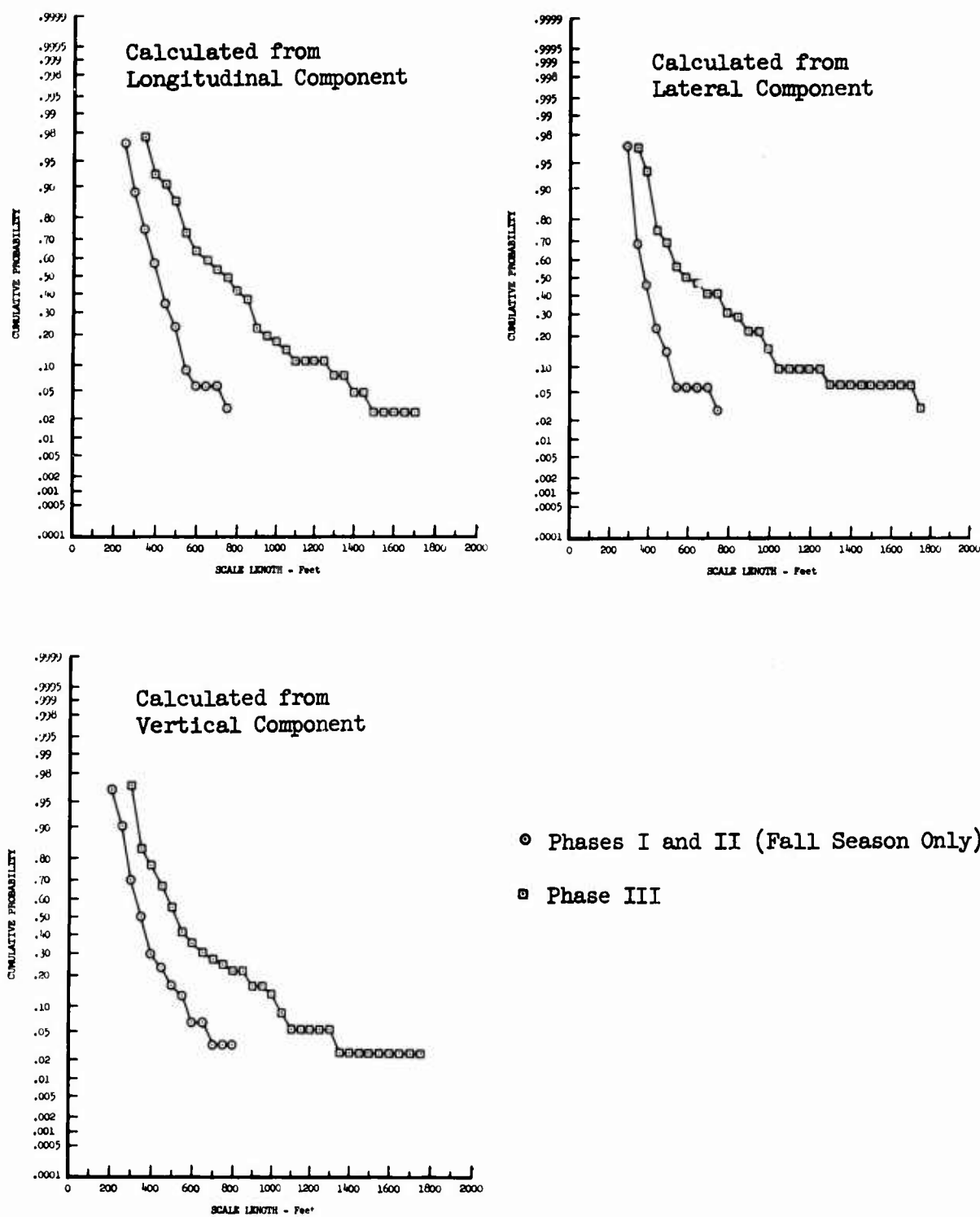


Figure 47.2 Comparison of Longitudinal Scale Length Cumulative Probabilities from Phases I and II with Those from Phase III for Data Obtained Over High Mountains at Edwards

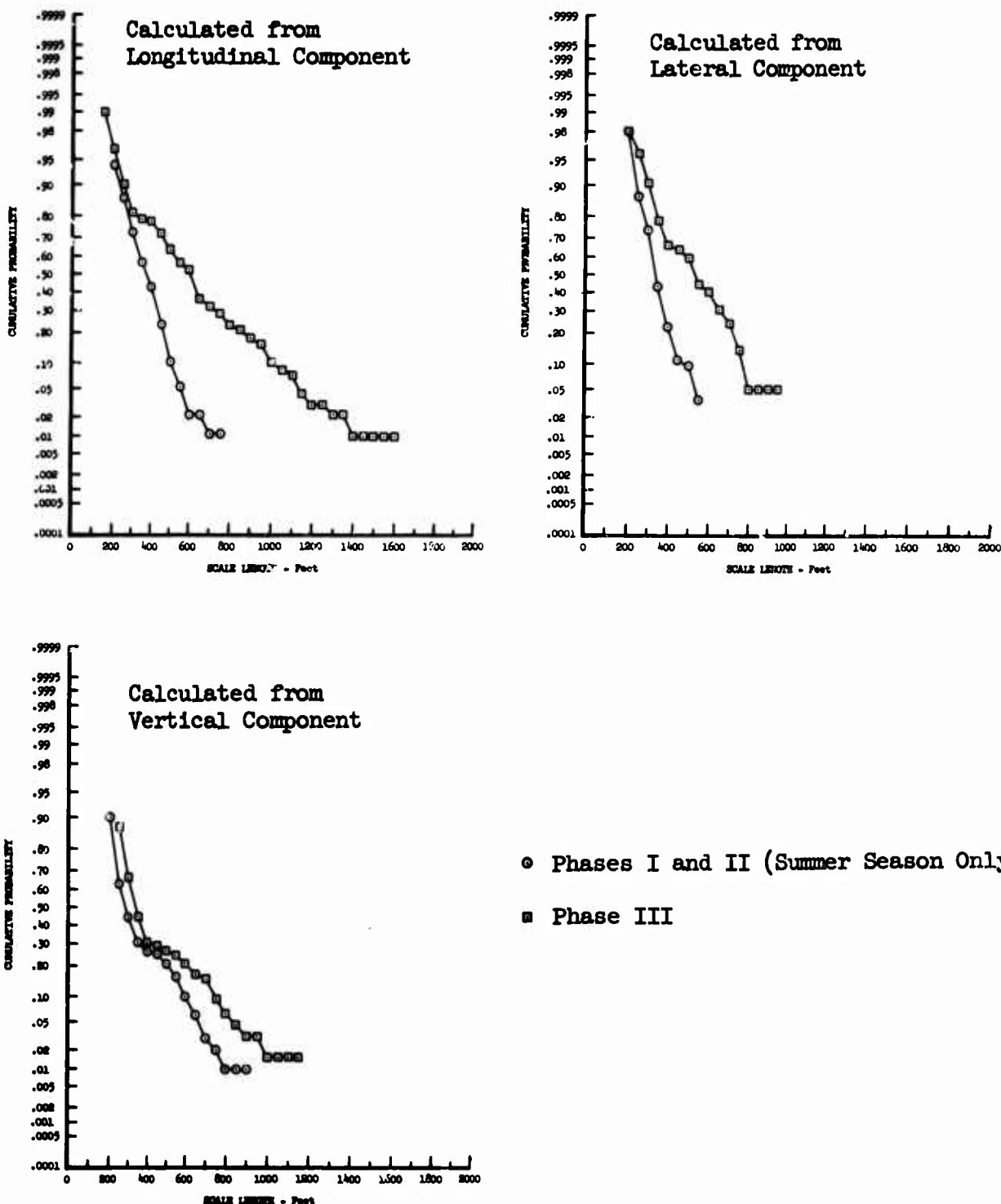


Figure 47.3 Comparison of Longitudinal Scale Length Cumulative Probabilities from Phases I and II with Those from Phase III for Data Obtained Over Plains at McConnell

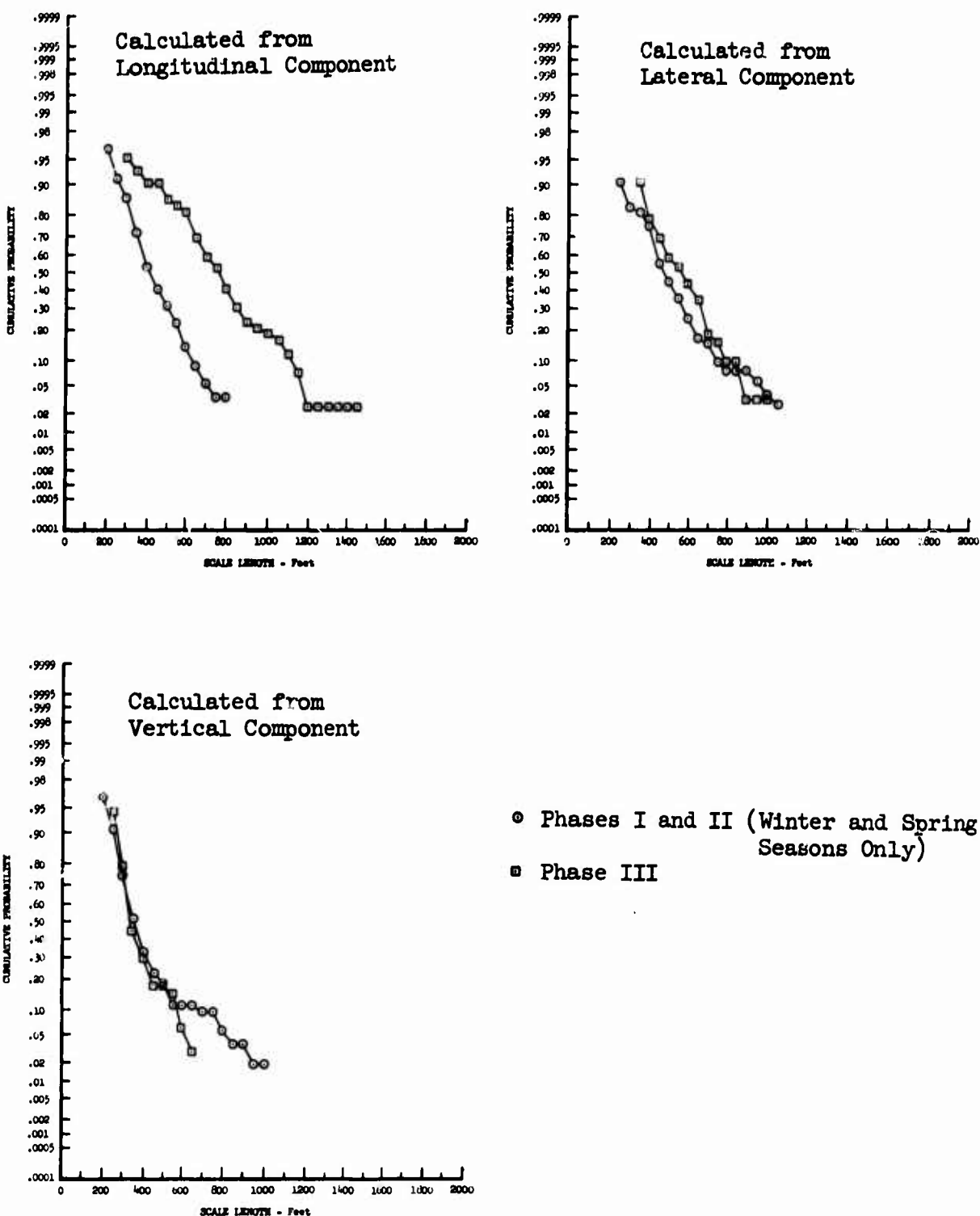


Figure 47.4 Comparison of Longitudinal Scale Length Cumulative Probabilities from Phases I and II with Those from Phase III for Data Obtained Over Plains at Peterson

48. RELATIONSHIPS BETWEEN TURBULENCE AND METEOROLOGICAL DATA

Multiple Regression Analysis

The independent variables utilized in the multiple regression program are listed in Appendix V. The Phases I and II data having gust velocity rms values below 2.40 fps were not utilized in the regression models. Values of rms below this magnitude showed poor correlation with the forecast data. Since the Phase III data sample was smaller than that of Phases I and II, it was not desirable to reduce it further by eliminating data. Instead, percentage errors were obtained for the gust velocity rms above and below an arbitrary value. Overall error was also determined. The arbitrary value was varied with the type of terrain and was chosen so as to include a statistically significant sample of the higher gusts. The regression models are presented in such a way that they can be truncated if so desired. The variables enter the regression equation in decreasing order of significance as measured by the F-ratio criterion. Each independent variable is labeled according to its step entry. Thus X₁ enters in step one; X₂ enters in step two, etc. A complete regression equation is shown for each entry step, utilizing the variables that have entered up to that point. For the Phases I and II models, the wind speed occurs most often in the regression equations, followed closely by the sine of the solar elevation. The Phase III equations, on the other hand, show a completely different pattern. In these equations, the difference between the ground temperature and the temperature 1000 feet above the flight level occurs most often, followed by the lapse rate, wind speed, and absolute altitude.

LATERAL RMS GUST VELOCITY
PHASES I & II REGRESSION MODEL

TERRAIN TYPE: High Mountains

NUMBER OF FLIGHT LEGS: 176

Entry Step	Independent Variable Entering	F-Level At Entry	Coefficient of Simple Linear Correlation	Mean
1	$W^8 \times 1000 \Delta T_{a,z}$	14.363	.2451	5.0784×10^1
2	$T_g \times W_D$	8.402	.4514	3.5034×10^3
3	$H^{2.2}$	8.956	-.1550	1.1258×10^6

Entry Step	Percent Error	Coefficient of Multiple Correlation	Normalized Standard Error of Coefficients	Equation
1	18.530	.5166	X1 .26386	$\sigma_v = 3.3537 + 5.8422 \times 10^{-3} X_1$
2	17.869	.5487	X1 .21563 X2 .34498	$\sigma_v = 3.2165 + 7.4686 \times 10^{-3} X_1 + 7.9486 \times 10^{-5} X_2$
3	17.148	.5797	X1 .19108 X2 .12631 X3 .33416	$\sigma_v = 3.4804 + 7.8530 \times 10^{-3} X_1 + 7.9777 \times 10^{-5} X_2 - 2.5368 \times 10^{-7} X_3$

VERTICAL RMS GUST VELOCITY
PHASES I & II REGRESSION MODEL

TERRAIN TYPE: High Mountains NUMBER OF FLIGHT LEGS: 243

Entry Step	Independent Variable Entering	F-Level At Entry	Coefficient of Simple Linear Correlation	Mean
1	$W^{.25} \times S_{SE}^{-.8}$	117.219	0.5720	2.8269

Entry Step	Percent Error	Coefficient of Multiple Correlation	Normalized Standard Error of Coefficients	Equation
1	13.751	.5720	X1 .09236	$\sigma_v = 2.0490 + .66321X1$

LATERAL RMS GUST VELOCITY
PHASES I & II REGRESSION MODEL

TERRAIN TYPE: Low Mountains

NUMBER OF FLIGHT LEGS: 244

Entry Step	Independent Variable Entering	F-Level At Entry	Coefficient of Simple Linear Correlation	Mean
1	'W·9 arc tan(1000ΔT _g /3.3)	35.069	.3558	1.4292 × 10 ⁻¹
2	DOY × H ²	11.979	-.1587	5.6723 × 10 ⁻⁷

Entry Step	Percent Error	Coefficient of Multiple Correlation	Normalized Standard Error of Coefficients	Equation
1	22.601	0.3558	X1 0.16887	$\sigma_v = 3.2827 + 4.3107 \times 10^{-2} X_1$
2	21.958	0.4098	X1 0.15552 X2 0.28892	$\sigma_v = 3.4893 + 4.5119 \times 10^{-2} X_1 - 4.400 \times 10^{-9} X_2^2$

VERTICAL RMS GUST VELOCITY
PHASES I & II REGRESSION MODEL

TERRAIN TYPE: Low Mountains

NUMBER OF FLIGHT LEGS: 267

Entry Step	Independent Variable Entering	F-Level At Entry	Coefficient of Simple Linear Correlation	Mean
1	S_{SE}^2	52.426	0.3218	0.32182
2	v_g	12.269	0.2549	2.3606×10^1

Entry Step	Percent Error	Coefficient of Multiple Correlation	Normalized Standard Error of Coefficients	Equation
1	16.641	.4064	X1 .13811	$\sigma_v = 3.2370 + 1.5832 X_1$
2	16.002	.4497	X1 .14836 X2 .28549	$\sigma_u = 2.9428 + 1.4621 X_1 + 1.1111 \times 10^{-2} X_2$

LATERAL RMS GUST VELOCITY
PHASES I & II REGRESSION MODEL

TERRAIN TYPE: Desert

NUMBER OF FLIGHT LEGS: 152

Entry Step	Independent Variable Entering	F-Level At Entry	Coefficient of Simple Linear Correlation	Mean
1	$(S_{SE})^2$	36.707	.3594	.44067
2	W	18.192	.6190	1.9799×10^{-1}

Entry Step	Percent Error	Coefficient of Multiple Correlation	Normalized Standard Error of Coefficients	Equation
1	11.116	0.7292	X1 0.16505	$\sigma_v = 2.0521 + 1.1189 X_1$
2	10.509	0.7629	X1 0.11955 X2 0.07924	$\sigma_v = 1.7843 + 1.4819 X_1 + 3.1382 \times 10^{-2} X_2$

VERTICAL RMS GUST VELOCITY
PHASES I & II REGRESSION MODEL

TERRAIN TYPE: Desert

NUMBER OF FLIGHT LEGS: 198

Entry Step	Independent Variable Entering	F-Level At Entry	Coefficient of Simple Linear Correlation	Mean
1	S_{SE}^2	115.275	.6085	.46323

300

Entry Step	Percent Error	Coefficient of Multiple Correlation	Normalized Standard Error of Coefficients	Equation
1	10.301	.6085	X1 .09314	$\sigma_v = 2.6506 + 1.9709 X1$

LATERAL RMS GUST VELOCITY
PHASES I & II REGRESSION MODEL

TERRAIN TYPE: Plains

NUMBER OF FLIGHT LEGS: 152

Entry Step	Independent Variable Entering	F-Level At Entry	Coefficient of Simple Linear Correlation	Mean
1	$w^{3/2}$	49.928	0.4997	1.5110×10^2

301

Entry Step	Percent Error	Coefficient of Multiple Correlation	Normalized Standard Error of Coefficients	Equation
1	17.716	0.4997	X1 0.14152	$\sigma_v = 2.7785 + 3.8143 \times 10^{-3} X1$

VERTICAL RMS GUST VELOCITY
PHASES I & II REGRESSION MODEL

TERRAIN TYPE: Plains NUMBER OF FLIGHT LEGS: 202

Entry Step	Independent Variable Entering	F-Level At Entry	Coefficient of Simple Linear Correlation	Mean
1	$S_{SE}^{2.2}$	9.406	.2119	.34301

Entry Step	Percent Error	Coefficient of Multiple Correlation	Normalized Standard Error of Coefficients	Equation
1	14.661	0.2119	X1 0.32606	$\sigma_v = 2.9440 + .64646 X1$

LATERAL RMS GUST VELOCITY
PHASE III REGRESSION MODEL

TERRAIN TYPE: High Mountains (Peterson)

NUMBER OF FLIGHT LEGS: 480

Entry Step	Independent Variable Entering	F-Level At Entry	Coefficient of Simple Linear Correlation	Mean
1	$\Delta T_{a,z}$	51.959	0.4134	3.7450
2	$\Delta W_{D,z}$	31.146	0.2608	-6.5213×10^{-2}

303

Entry Step	Percent Error $\sigma < 4.5 \text{ fps}$	Overall $\sigma > 4.5 \text{ fps}$	Coefficient of Multiple Correlation	Normalized Standard Error of Coefficients	Equation
1	62.731	38.508	0.3131	X1 0.13873	$\sigma_v = 4.6955 + 0.22375 X_1$
2	59.553	37.371	0.3916	X1 0.13733 X2 0.17918	$\sigma_v = 4.9664 + 0.21929 X_1 + 3.9932 X_2$

VERTICAL RMS GUST VELOCITY
PHASE III REGRESSION MODEL

TERRAIN TYPE: High Mountains (Peterson)

NUMBER OF FLIGHT LEGS: 494

Entry Step	Independent Variable Entering	F-Level At Entry	Coefficient of Simple Linear Correlation	Mean
1	ΔT_{a_s}	95.047	0.4024	3.7361
2	ΔW_{Dz}	40.326	0.2592	-6.5131 $\times 10^{-2}$
3	λ	16.608	-0.2761	1.0996 $\times 10^{-3}$
4	W	20.911	0.1717	1.4168 $\times 10^1$

3C4

Entry Step	Percent Error Overall $\sigma \geq 4.5$ fips	Coefficient of Multiple Correlation	Normalized Standard Error of Coefficients	Equation	
1	36.669	27.099	16.722	0.4024	$\sigma_v = 3.9655 + 1.9868 \times 10^2 X_1$
2	34.821	25.928	16.285	0.4749	$\sigma_v = 4.1636 + 1.9649 \times 10^2 X_1 + 2.9163 X_2$
3	35.686	26.259	16.036	0.5009	$\sigma_v = 6.2829 + 1.8427 \times 10^2 X_1 + 2.4430 X_2 - 1.9139 \times 10^{-3} X_3$
4	34.746	25.735	15.964	0.5307	$\sigma_v = 6.1485 + 1.7642 \times 10^2 X_1 + 2.3741 X_2 - 2.2515 \times 10^{-3} X_3 + 3.7440 \times 10^{-2} X_4$

LATERAL RMS GUST VELOCITY
PHASE III REGRESSION MODEL

TERRAIN TYPE: High Mountains (Edwards)

NUMBER OF FLIGHT LEGS: 120

Entry Step	Independent Variable Entering	F-Level At Entry	Coefficient of Simple Linear Correlation	Mean
1	$\Delta W_z \times \arctan \frac{1000\Delta T_{Ez}}{3.4}$	22.663	0.4014	-1.8353 $\times 10^{-3}$
2	$W^{.8} \times \Delta W_z^{.75}$	8.7620	0.2598	0.39400
3	$H \times \Delta T_E$	6.7602	0.1808	9.3942 $\times 10^1$
4	$S_{sr} \times \arctan \Delta T_E$	2.9710	0.0549	6.3698 $\times 10^{-2}$

Entry Step	Percent Error Overall	Percent Error 24.5 fps	Coefficient of Multiple Correlation	Normalized Standard Error of Coefficients	Equation
1	24.817	25.507	0.4014	X1 0.21006	$\sigma_v = 3.1963 + 6.1095 X_1$
2	24.034	23.447	0.4686	X1 0.20943 X2 0.33783	$\sigma_v = 2.8757 + 5.9419 X_1 + 0.81285 X_2$
3	23.581	27.273	0.5124	X1 0.19949 X2 0.32306 X3 0.38461	$\sigma_v = 2.7691 + 6.0974 X_1 + 0.83008 X_2 + 1.0652 \times 10^{-3} X_3$
4	23.493	26.657	0.5302	X1 0.20201 X2 0.32474 X3 0.34378 X4 0.58016	$\sigma_v = 2.8102 + 5.9802 X_1 + 0.81910 X_2 + 2.0789 \times 10^{-3} X_3 - 2.0752 X_4$

VERTICAL RMS GUST VELOCITY
PHASE III REGRESSION MODEL

TERRAIN TYPE: High Mountains (Edwards)

NUMBER OF FLIGHT LEGS: 144

Entry Step	Independent Variable Entering	F-Level At Entry	Coefficient of Simple Linear Correlation	Mean
1	$H \times \text{arc tan } \frac{1000 \Delta T_{a_z}}{3.4}$	37.285	0.4560	-6.1132 $\times 10^1$
2	$H \times \Delta T_H^{-2}$	25.129	0.3189	6.5905 $\times 10^1$
3	W_s^{-2}	8.675	0.2062	1.5523 $\times 10^2$
4	$\Delta W_H \times (T_G - T_{A_4})$	7.099	0.3323	4.0199 $\times 10^1$

Entry Step	Percent Error Overall $\sigma_{24.5}$ fpm	Coefficient of Multiple Correlation	Normalized Standard Error of Coefficients	Equation
1	29.805	30.969	36.606	X1 0.16377
2	28.260	28.462	29.645	X1 0.14529 X2 0.19948
3	26.960	27.190	28.536	X1 0.14372 X2 0.19142 X3 0.33953
4	25.816	26.001	27.085	X1 0.17375 X2 0.19061 X3 0.33308 X4 0.37531

LATERAL RMS GUST VELOCITY
PHASE III REGRESSION MODEL

TERRAIN TYPE: Low Mountains NUMBER OF FLIGHT LEGS: 156

Entry Step	Independent Variable Entering	F-Level At Entry	Coefficient of Simple Linear Correlation	Mean
1	$(T_g - T_{A_4})^2 W^{.30}$	62.892	0.5385	3.8784×10^4
2	$(700mb - 850mb)^2 W_6 T_{D3}$	50.378	-0.4296	-7.3355×10^5
3	$(T_{D4} - T_{D2})(T_g - T_{A_4})^2 W^{.80}$	13.651	0.2747	-1.9932×10^5
4	$H^{.60} \lambda^2$	13.152	-0.2746	4.2431×10^7

Entry Step	Percent Error $\sigma < 4.0$ fps Overall $\sigma \geq 4.0$ fps	Coefficient of Multiple Correlation	Normalized Standard Error of Coefficients	Equation
1	25.366	25.264	.5385	$X_1 .12610$ $\sigma_v = 2.0554 + 1.8130 \times 10^{-5} X_1$
2	22.287	21.853	.6825	$X_1 .11141$ $X_2 .14083$ $\sigma_v = 1.7829 + 1.7859 \times 10^{-5} X_1$ $- 3.8580 \times 10^{-7} X_2$
3	21.438	20.787	.7141	$X_1 .10410$ $X_2 .16323$ $X_3 .27065$ $\sigma_v = 1.8924 + 1.8429 \times 10^{-5} X_1$ $- 3.3215 \times 10^{-7} X_2$ $+ 4.6298 \times 10^{-7} X_3$
4	20.195	19.634	.7410	$X_1 .10179$ $X_2 .17267$ $X_3 .25514$ $X_4 .27574$ $\sigma_v = 2.4118 - 1.8152 \times 10^{-5} X_1$ $- 3.0520 \times 10^{-7} X_2$ $+ 4.7272 \times 10^{-7} X_3$ $- 1.1475 \times 10^{-8} X_4$

VERTICAL RMS GUST VELOCITY
PHASE III REGRESSION MODEL

TERAIN TYPE: Low Mountains NUMBER OF FLIGHT LEGS: 186

Entry Step	Independent Variable Entering	F-Level At Entry	Coefficient of Simple Linear Correlation	Mean
1	$\arctan^3 \frac{1000\Delta T_{ss}}{3}$	69.894	0.5247	-0.25152
2	$T_{D3} \times W_6$	12.257	-0.3159	-1.3268×10^2
3	CC	9.897	-0.1086	3.9839
4	λ^2	8.719	-0.2213	1.0238×10^6

Entry Step	Percent Error $\sigma_{<24.0 \text{ fpm}}$ Overall	Percent Error $\sigma_{\geq 24.0 \text{ fpm}}$	Coefficient of Multiple Correlation	Normalized Standard Error of Coefficients	Equation
1	33.341	33.959	40.098	X1 0.11961	$\sigma_w = 2.5990 + 0.37123 X_1$
2	31.164	31.957	39.784	X1 0.12960 X2 0.28563	$\sigma_w = 2.4122 + 0.33946 X_1$ - 1.3481 $\times 10^{-3} X_2$
3	30.740	31.341	37.315	X1 0.12323 X2 0.25510 X3 0.31787	$\sigma_w = 2.6131 + 0.34991 X_1$ - 1.4838 $\times 10^{-3} X_2$ - 5.4297 $\times 10^{-2} X_3$
4	28.996	29.598	35.589	X1 0.12076 X2 0.28868 X3 0.30579 X4 0.33867	$\sigma_w = 3.3540 + 0.34973 X_1$ - 1.3018 $\times 10^{-3} X_2$ - 5.5293 $\times 10^{-2} X_3$ - 6.9630 $\times 10^{-7} X_4$

LATERAL RMS GUST VELOCITY
PHASE III REGRESSION MODEL

TERAIN TYPE: Desert

NUMBER OF FLIGHT LEGS: 82

Entry Step	Independent Variable Entering	F-Level At Entry	Coefficient of Simple Linear Correlation	Mean
1	$(T_s - T_{A7}) \arctan^2(T_g - T_{A4})$	34.880	0.55109	9.9670×10^{-1}
2	$(T_s - T_{A7}) \lambda^2 \log_e H$	13.372	0.31130	2.3472×10^{-8}
3	$\Delta W_{NEW} \log_e W$	16.931	-0.2751	-1.5021×10^{-1}
4	$(T_{A2} - T_{A3})(T_g - T_{A4}) \log_e TOD$	7.870	0.3237	4.4050×10^{-1}

Entry Step	Percent Error Overall	Percent Error $\sigma < 2.5$ fpm	Coefficient of Multiple Correlation	Normalized Standard Error of Coefficients	Equation
1	20.158	20.789	.5510	X1 .16932	$\sigma_v = 8.5583 \times 10^{-2} + 1.8268 \times 10^{-2} X1$
2	18.962	19.100	.6360	X1 .15657 X2 .27346	$\sigma_v = 8.5583 \times 10^{-2} + 1.8268 \times 10^{-2} X1$ $\sigma_v = 1.6300 + 3.5969 \times 10^{-2} X2$ $- 7.8434 \times 10^{-9} X2$
3	17.482	17.358	.7146	X1 .13692 X2 .23587 X3 .24303	$\sigma_v = 8.4475 \times 10^{-2} + 3.7638 \times 10^{-2} X1$ $- 8.3092 \times 10^{-9} X2$ $- 1.4290 \times 10^{-1} X3$
4	16.428	16.108	.7457	X1 .14074 X2 .21228 X3 .20534 X4 .35646	$\sigma_v = .39665 + 3.5514 \times 10^{-2} X1$ $- 8.9081 \times 10^{-9} X2$ $- 1.6781 \times 10^{-1} X3$ $+ 8.2705 \times 10^{-4} X4$

VERTICAL RMS GUST VELOCITY

TERRAIN TYPE: Desert **NUMBER OF FLIGHT LEGS:** 83

Entry Step	Independent Variable Entering	F-Level At Entry	Coefficient of Simple Linear Correlation	Mean
1	$(T_G - T_{A_4}) \log_e \text{TOD}$	105.715	0.7522	1.5359×10^2
2	$\lambda^2 \log_e H$	27.384	-0.3957	5.7001×10^6
3	$\Delta W_{HEW} \log_e H$	14.240	-0.0849	-0.29491
4	$(T_{D_5})^4$	8.125	-0.1817	4.7246×10^4

310

NUMBER OF FLIGHT LEGS: 83

Entry Step	Percent Error			Normalized Coefficient of Multiple Correlation	Standard Error of Coefficients	Equation
	$\sigma < 2.5$ fps	Overall $\sigma \geq 2.5$ fps	$\sigma < 2.5$ fps			
1	27.898	25.561	17.127	0.7525	X1 0.097259	$\sigma_w = -0.35105 + 1.4080 x 10^{-2} X_1$
2	26.440	23.381	12.336	0.8227	X1 0.088120 X2 0.19110	$\sigma_w = 2.2491 + 1.3546 x 10^{-2} X_1$ - 4.4179 x $10^{-7} X_2$
3	22.651	20.212	11.404	0.8522*	X1 0.079060 X2 0.15711 X3 0.26300	$\sigma_w = 2.2865 + 1.4115 x 10^{-2} X_1$ - 4.6642 x $10^{-7} X_2$ - 5.3415 x $10^{-2} X_3$
4	21.627	19.246	10.650	0.8672	X1 0.076733 X2 0.15711 X3 0.26299 X4 0.35082	$\sigma_w = 2.4783 + 1.3649 x 10^{-2} X_1$ - 4.7923 x $10^{-7} X_2$ - 5.1605 x $10^{-2} X_3$ - 1.9641 x $10^{-6} X_4$

LATERAL RMS GUST VELOCITY
PHASE III REGRESSION MODEL

TERRAIN TYPE: Plains

NUMBER OF FLIGHT LEGS: 174

Entry Step	Independent Variable Entering	F-Level At Entry	Coefficient of Simple Linear Correlation	Mean
1	$(T_S - T_{A4})^2 (T_{A1} - T_{A3})$	264.261	0.7783	3.1047×10^3
2	$(T_G - T_{A4}) \arctan W_S$	20.658	0.7321	7.4589×10^3
3	$(T_{D5})^2 WA_u$	22.159	-0.3045	1.0280×10^4
4	$W^{.8} (T_G - T_{A4})^2$	27.668	0.5954	6.5753×10^4

311

Entry Step	Percent Error Overall	Percent Error $\sigma < 4.0$ fps	Coefficient of Multiple Correlation	Normalized Standard Error of Coefficients	Equation
1	20.445	20.371	19.687	0.7783	$\sigma_v = 2.3232 + 1.6276 \times 10^{-4} X_1$
2	18.376	18.583	20.493	0.8051	$\sigma_v = 1.5468 + 1.1032 \times 10^{-4} X_1 + 1.2591 \times 10^{-4} X_2$
3	17.041	17.239	19.070	0.8299	$\sigma_v = 1.5324 + 8.5094 \times 10^{-5} X_1 + 1.6237 \times 10^{-4} X_2 - 1.7433 \times 10^{-5} X_3$
4	16.486	16.472	16.344	0.8559	$\sigma_v = 1.1864 + 5.2629 \times 10^{-5} X_1 + 1.5235 \times 10^{-4} X_2 - 2.2953 \times 10^{-5} X_3 + 8.7948 \times 10^{-6} X_4$

VERTICAL RMS GUST VELOCITY
PHASE III REGRESSION MODEL

TERRAIN TYPE: Plains

NUMBER OF FLIGHT LEGS: 123

Entry Step	Independent Variable Entering	F-Level At Entry	Coefficient of Simple Linear Correlation	Mean
1	$(T_g - T_{A_4})^2 \arctan^2 W_s$	324.839	0.8539	1.1198×10^4
2	$W_{A_4} (T_{D_5})^2$	26.199	-0.3724	1.1251×10^4
3	$W_s \arctan \frac{1000 \Delta T_{A_4}}{3.4}$	11.467	0.7002	7.3234
4	$(T_s - T_{A_4})(T_g - T_{A_4})^2$	9.130	0.8413	2.9069×10^5

312

Entry Step	Percent Error Overall	Coefficient of Multiple Correlation	Normalized Standard Error of Coefficients	Equation
1	20.817	20.408	X1 0.055484	$\sigma_v = -0.29191 + 2.4983 \times 10^{-4} X1$
2	17.130	16.987	X1 0.053917 X2 0.19537	$\sigma_v = 0.16878 + 2.3787 \times 10^{-4} X1$ - $1.8852 \times 10^{-5} X2$
3	16.479	16.422	X1 0.079728 X2 0.21838 X3 0.29531	$\sigma_v = 0.27980 + 2.0247 \times 10^{-4} X1$ - $1.6487 \times 10^{-5} X2$ + $2.8254 \times 10^{-2} X3$
4	15.646	15.540	X1 0.53221 X2 0.25461 X3 0.23278 X4 0.33095	$\sigma_v = 0.42789 + 8.1022 \times 10^{-5} X1$ - $1.4045 \times 10^{-5} X2$ + $3.6697 \times 10^{-2} X3$ + $3.8619 \times 10^{-6} X4$

SECTION X

COMPARISON OF LO-LOCAT DATA (PHASES I, II, AND III) WITH OTHER LOW ALTITUDE TURBULENCE DATA

Peak count, power spectra, and von Karman scale lengths obtained during LO-LOCAT Phases I, II, and III were compared to data from seven other turbulence programs (References X.1 through X.7). A short description of each of these turbulence programs is given in Section 50. A similar but less extensive comparison was made during Phases I and II and reported in Reference I.2. Only those data for which the gust velocity power spectra conformed to Kolmogorov's theory were used in making these comparisons. Data that exhibited anomalies associated with excessive gust velocity drift were not used in this analysis.

According to Kolmogorov's theory, the gust velocity power spectrum in the inertial subrange should decrease as a $-5/3$ logarithmic function with increasing frequency. LO-LOCAT Phases I, II, and III data showed very good agreement with this theory. The premise was established, therefore, that gust velocities from these other programs whose spectra did not show a definite $-5/3$ slope could not be a true representative of homogeneous turbulence. Excessive gust velocity drift was assumed to be present whenever the spectra deviated significantly on the higher power density side of a $-5/3$ line drawn through the inertial subrange.

This careful selection was necessary because of the different approaches used in removing the high amplitude, low frequency drift normally encountered in gust velocity calculations. This drift was shown (Appendix III) to be caused by small amounts of drift in the individually recorded parameters coupled with the mathematical operations involved, especially integration. The magnitude of the drift as well as the manner in which it was handled varied considerably from program to program.

49. PEAK COUNT

The peak count data obtained during LO-LOCAT Phases I, II, and III were compared with those obtained during other low altitude turbulence programs. The data available from the other programs were in different forms. The peak count data, when available by class interval, were evaluated by the extrapolation technique previously discussed in Section III. The curve used for this extrapolation was the optimum curve developed for LO-LOCAT Phase III.

The extrapolation technique provided an estimate of the characteristic frequencies associated with each program. It should be noted, however, that the characteristic frequencies vary with the low-pass filter used and with the speed of the airplane.

No attempt was made to categorize the data obtained from the various programs. The selected data were combined for each program and are presented as one curve for each component of gust velocity. Longitudinal gust

velocity data from most of the programs were not believed to be satisfactory for analysis.

The Reference X.6 (B-66) data were not peak counted into bands of equal width. Also, these data were not folded about the mean nor had the mean been set equal to zero. Therefore, for comparison purposes, these data were converted to a form compatible with the data from the other programs.

Figures 49.1 through 49.3 show comparisons of the peak count distributions of those data selected for analyses from the various programs. Table 49.1 shows pertinent information concerning the various test programs.

The information contained in Table 49.1 should be taken into consideration when comparing the peak count distribution curves shown in Figures 49.1 through 49.3. The reason the distribution curve for Reference X.2 data is considerably higher than the others is due to several factors. Among the more important factors are: very low terrain clearance, very rough terrain, contour flight, and short turbulence samples (one minute or less) selected when the turbulence was the most intense. The high speeds flown during this program also made it possible to measure the longer wavelength high amplitude gusts.

The next curve in relative magnitude represents the LO-LOCAT Phase III data. This curve is lower than the one just discussed due to the effects of combining all types of terrain. Also, the LO-LOCAT data were obtained at higher terrain clearances and at lower airspeeds.

The next lower curve is that data from Reference X.5. This curve is actually higher than that for the Phase III data up to gust velocities of 20 to 30 fps, depending upon the component of gust velocity. These samples were obtained over the mountains at relatively high speeds. These data were not obtained while contour flying, therefore, many of the higher magnitude gusts were not encountered.

The curve for the Reference X.6 data is probably lower than the preceding one because of the somewhat lower airspeed, the combination of mountains and plains samples, and the combination of 200 and 1000 foot altitudes which were not contour flown.

The LO-LOCAT Phases I and II data were obtained at the lowest speed of any of the programs discussed here. These data represent the largest number of turbulence samples. The curve is lower than the preceding one because only a very small percentage of the samples were obtained over high mountains and no samples were obtained over the Colorado Rocky Mountains where the larger gusts were measured during Reference X.2 and LO-LOCAT Phase III.

The distribution curves for Reference X.1 and Reference X.4 are very similar since both sets of data were gathered during non-contour flight over the plains.

The average characteristic frequencies obtained for each of these programs are shown in Figures 49.1 through 49.3. The characteristic frequency varies with the speed of the airplane when the same filtering is used during data processing. This is illustrated in Figure 49.4 where a curve has been fitted through all data points associated with the same filter. The Reference X.1, Reference X.2, and Reference X.6 data were not filtered in the same manner as the data from the other programs. The Reference X.2 values fell on the curve fitted through the other data points, but the Reference X.1 and Reference X.6 values did not.

Even though Reference X.1 and Reference X.4 data were obtained under very similar conditions, there is a large difference in the characteristic frequencies obtained for these two programs due to the different manners in which the data were filtered (Figure 49.4).

TABLE 49.1

PERTINENT INFORMATION FOR LOW ALTITUDE
TURBULENCE PROGRAMS

Test Program	Airspeed (fps)	Terrain Classification	Terrain Clearance
Ref. X.1 (F-106)	495 to 620	Plains	1000 ft. - Constant Pressure Altitude
Ref. X.2 (F-106)	651 to 748	High Mountains	100 to 200 ft. - Contour
Ref. X.4 (B-52E)	495 and 620	Plains	500 and 1000 ft. - Constant Pressure Altitude
Ref. X.5 (B-52H)	630 to 700	High and Low Mountains	500 feet - Constant Pressure Altitude
Ref. X.6 (B-66)	608	Mountains and Plains	200 and 1000 ft. - Constant Pressure Altitude
LO-LOCAT Phases I and II (C-131)	330	High and Low Mountains, Plains, Desert and Water	250 and 750 ft. - Contour
LO-LOCAT Phase III (T-33)	630		

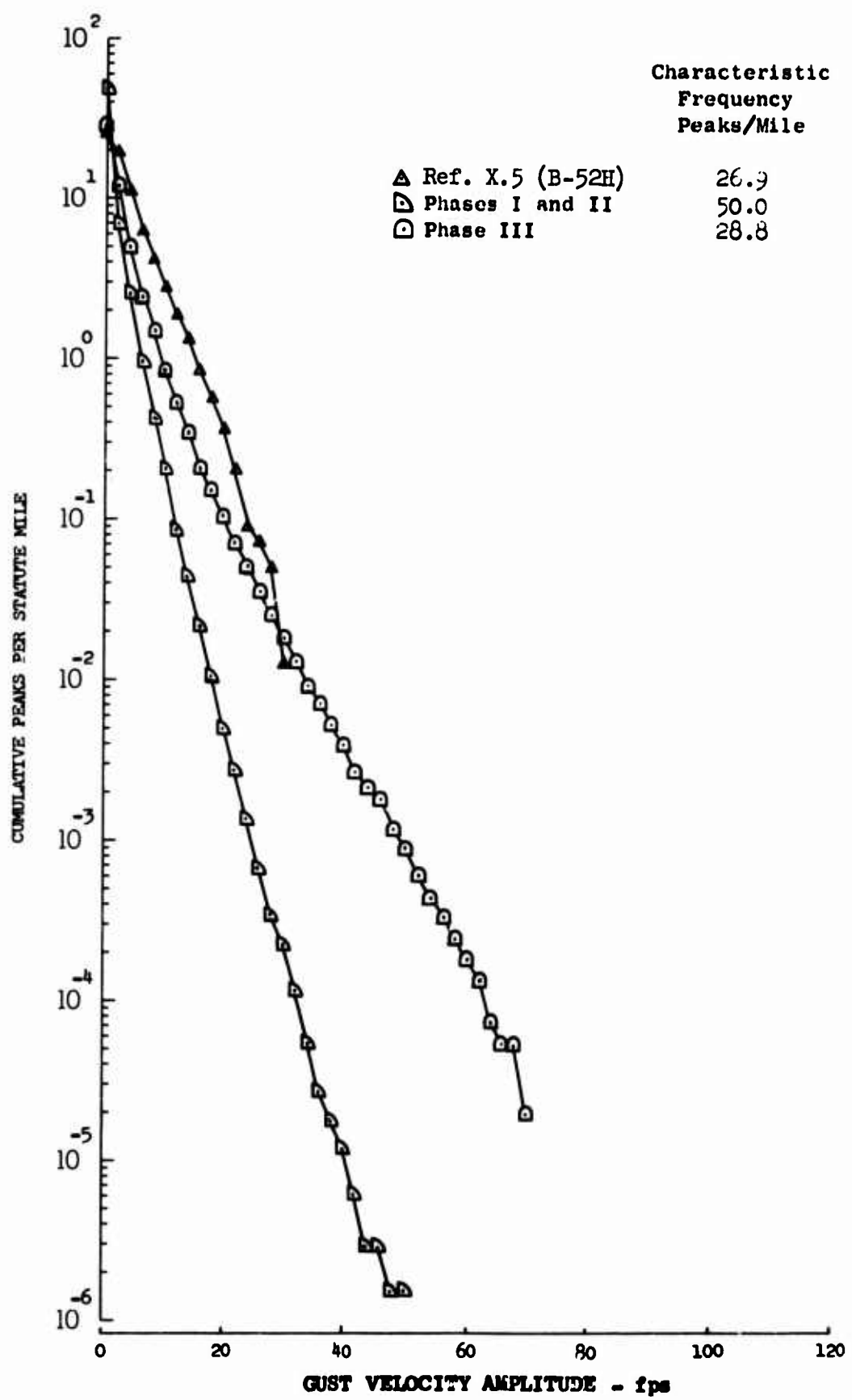


Figure 49.1 Comparison of Longitudinal Gust Velocity Distributions for Different Test Programs

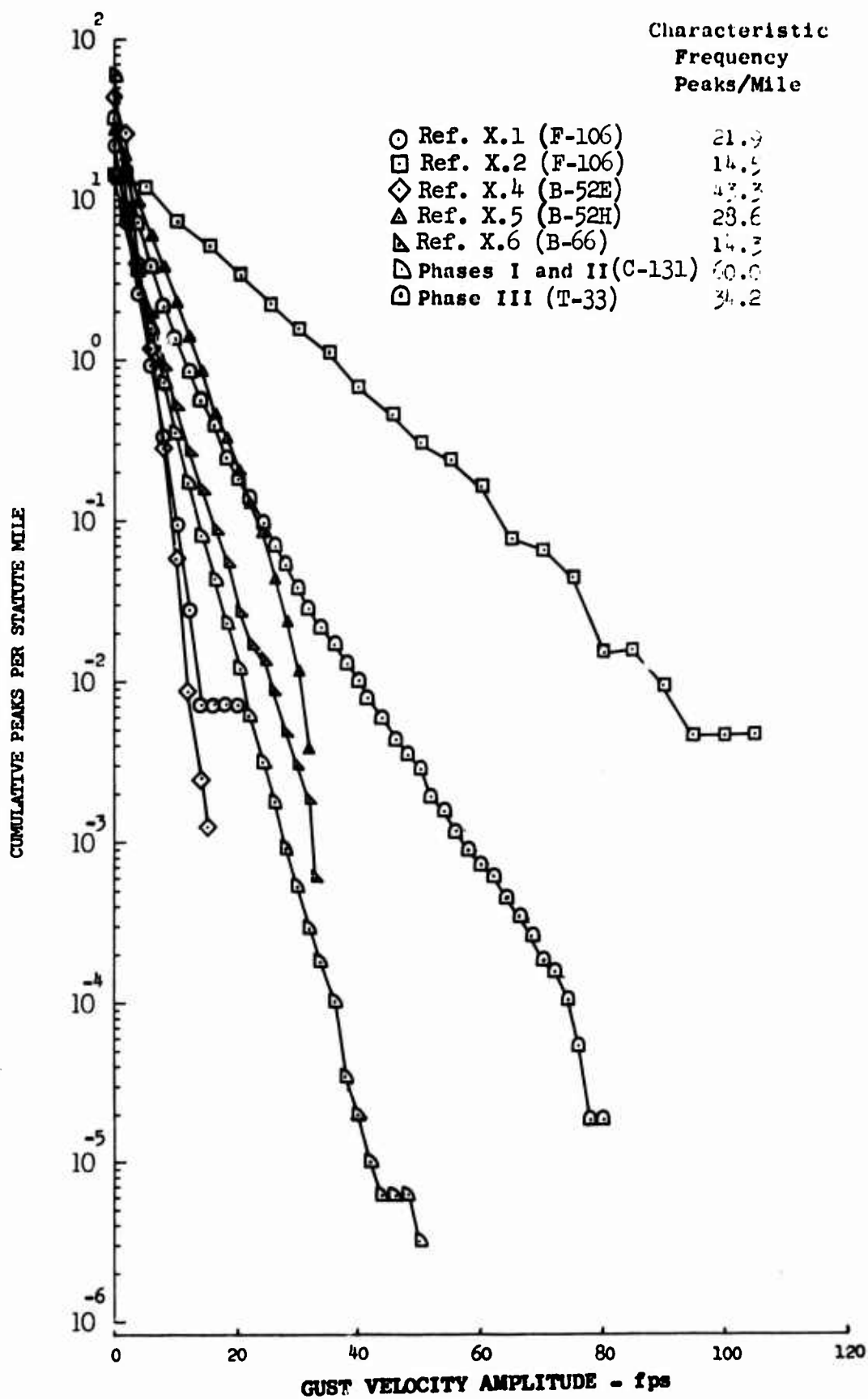


Figure 49.2 Comparison of Lateral Gust Velocity Distributions for Different Test Programs

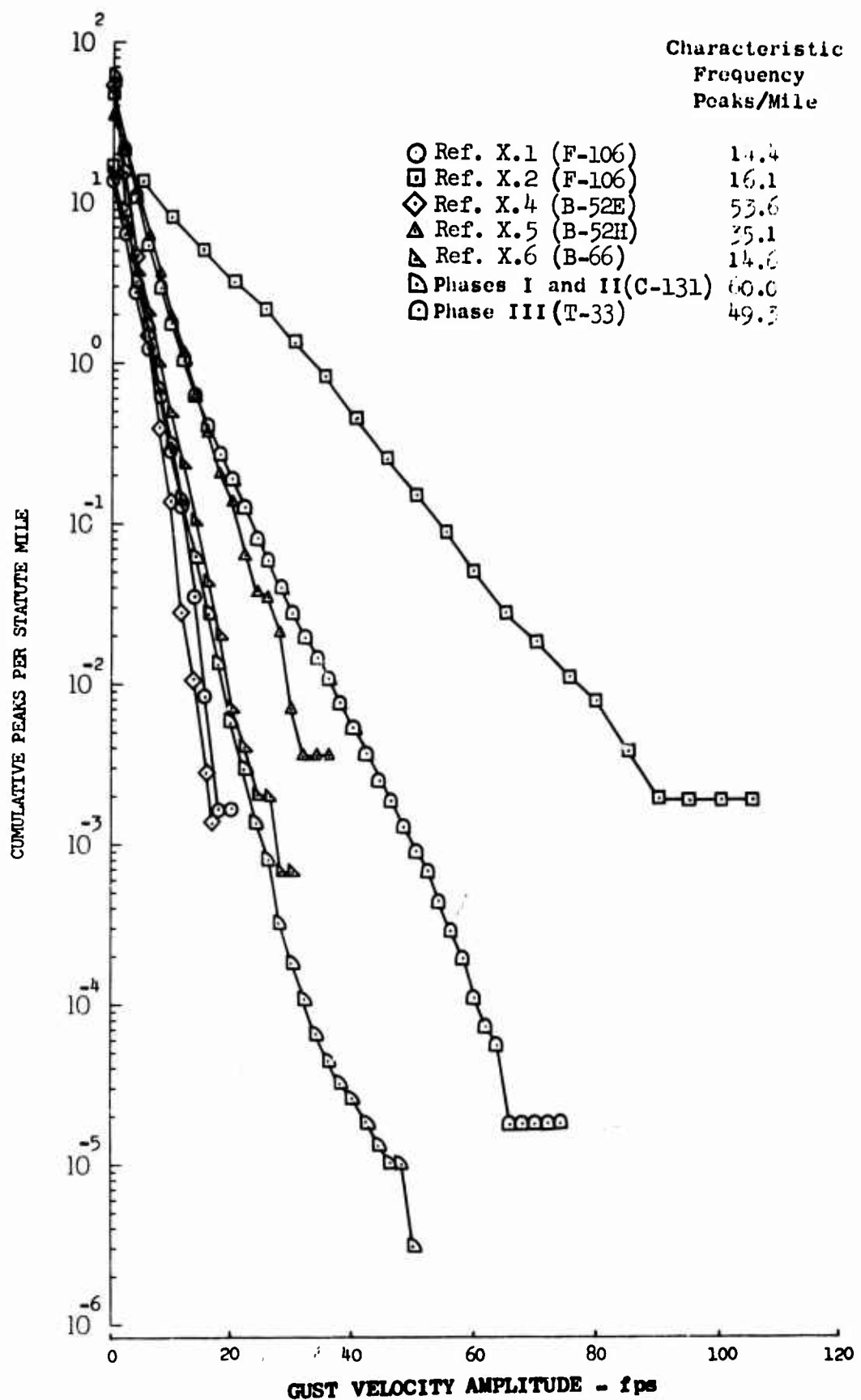


Figure 49.3 Comparison of Vertical Gust Velocity Distributions for Different Test Programs

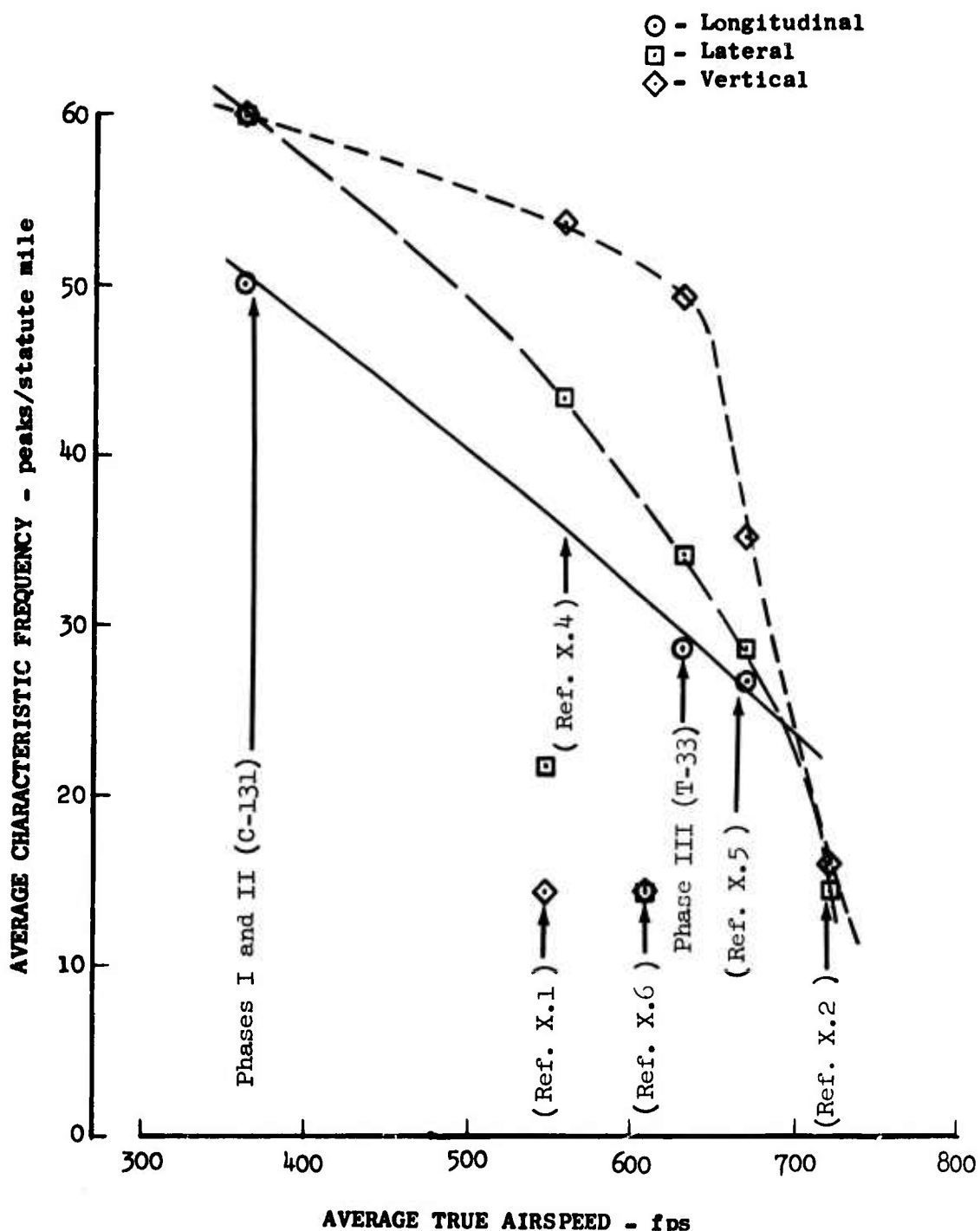


Figure 49.4 Variation of Characteristic Frequency with True Airspeed

50. POWER SPECTRA COMPARISON

The power spectra selected from the Reference X.1 through X.7 programs were converted to normalized spectra by dividing the ordinate (power density) by the $\sigma_t^2 L$ product and multiplying the abscissa k (spatial frequency) by the scale length L . Prior to normalizing in this manner all data from the various programs were converted such that the power density and frequency scales were in the units of $(\text{fps})^2/\text{cpf}$ and cpf , respectively. Since the von Karman mathematical expressions have been shown to be a good representation of LO-LOCAT spectra during Phases I and II (Reference I.2) and Phase III (see Section 28), the spectra comparisons contained in this section were accomplished using the von Karman spectra as the standard.

Reference X.1 (F-106) Spectra

The purpose of the Reference X.1 program was to determine the structural response of the B-52 airplane to the low-level gust environment. The gust data were obtained using an instrumented F-106 airplane which was flown in close wing-tip formation with a B-52 airplane during low-level flight. The F-106 airplane was instrumented, maintained, and flown by Air Force personnel.

The low frequency drift was filtered by segmenting the data sample into 15-second intervals and calculating the best linear fit (least-square line) for the first interval of data and the arithmetic mean of each succeeding interval. A correction curve was determined using the least-squares line to the mid-point of the first interval and connecting this with the mean at the mid-point of each succeeding interval. The last straight line segment was extrapolated to adjust the data during the last part of the last segment. The correction curve was subtracted from the data containing the drift. The result was a gust velocity time function with a mean approximately equal to zero.

Vertical and lateral gust velocity were calculated for twenty 5-minute data samples obtained during the Reference X.1 testing. Those samples selected for analysis are shown in Table 50.1. The standard deviations listed were obtained by:

$$\sigma = \left[\int_a^b \Phi(f) df \right]^{1/2} \quad (50.1)$$

where: $\Phi(f)$ = PSD of the applicable function

a = zero cps

b = 7 cps

TABLE 50.1
REFERENCE X.1 (F-106) TURBULENCE DATA

Test No.	Sample No.	σ (fps)		L_k (feet)	
		v	w	v	w
45-2	11-1	2.7	3.1	660	530
	11-2	2.5	3.7	350	825
	12-1	3.0	2.8	825	900
	12-2	-	3.4	-	940
	13-1	3.4	4.1	660	970
	13-2	-	3.1	-	975
	14-1	-	3.7	-	1600
	15-1	-	3.8	-	1100
	15-2	2.8	3.7	530	900
45-9	45-1	2.8	-	650	-
	45-2	3.1	4.1	800	1500
	47-1	4.0	-	750	-
	48-1	3.7	-	620	-
	49-1	4.0	4.7	825	1500
	49-2	3.7	4.5	1100	1500
	50-1	3.1	4.0	620	1200
	50-2	3.0	3.5	820	1200

Also included in Table 50.1 is an estimation of the scale of turbulence, L . The scale length was estimated by determining the normalized power density value at 0.01 cpf of a line having a -5/3 logarithmic slope and providing a good fit to the spectra normalized by σ_t^2 in the inertial subrange. This power density value was then used to enter a plot of $[\Phi(k)/\sigma_t^2]$ at 0.01 cpf versus L for the von Karman mathematical expressions.

The average longitudinal scale lengths for these data as calculated from both the lateral and vertical components are 715 and 1136 feet, respectively. This is slightly higher than those scale lengths obtained from LO-LOCAT Phase III, however, these data were obtained at 1000 feet absolute altitude and the method of filtering prevented complete removal of the low frequency drift.

Figures 50.1 and 50.2 contain composite plots of the lateral and vertical spectra normalized by $\sigma_t^2 L$. The average of these data for given values of kL are compared to the von Karman spectra in Figure 50.3. This comparison shows that some of the vertical spectra values are above the von Karman line, indicating that there is more drift in vertical gust velocity than in lateral. This effect is also seen in the scale lengths. On the average, vertical scale length is 400 feet greater than lateral. Since $L = f(\sigma_t/\sigma_v)^3$, any low frequency drift which affects σ_t and does not proportionately affect σ_v will cause L to be too high.

Reference X.2 (F-106) Spectra

The purpose of the Reference X.2 program was to investigate the intensity of low altitude clear air turbulence over mountainous terrain, specifically in the Sangre de Cristo Mountains. An F-106 fighter aircraft equipped with a gust boom and a NBFM recording system was used as the test vehicle. This was the same airplane and instrumentation used during Reference X.1 and was instrumented, maintained, and flown by Air Force personnel during this program. A total of 100 turbulence samples, which varied from approximately 45 to 60 seconds in length, were reduced to power spectra form. The turbulence data were recorded while contour flying at approximately 350 knots indicated airspeed at terrain clearances from 200 feet to just above mountain peak elevation. The pressure altitude was generally about 12,000 feet.

Gust velocities obtained from this program contained a low frequency component which appeared to increase in frequency as the magnitude and frequency of the turbulence increased. A computer program was not available to digitally filter the data; therefore, because of scheduling requirements, a correction curve consisting of straight line segments was established by manually estimating the drift during each sample. The low frequency component was removed by subtracting values of the correction curve from the calculated gust velocity data. A portion of these data were re-processed and re-evaluated (see Section XI) to determine if the results would be significantly changed if improved data processing techniques were used. It was concluded that this data in general was changed very little.

Lateral gust velocity data from 24 samples and vertical gust velocity data from 67 samples were selected for analysis. Time series standard deviations and turbulence scale lengths for the selected samples are presented in Table 50.2.

The standard deviations in Table 50.2 were calculated in the same manner that LO-LOCAT values were calculated. The scale lengths were determined in the manner described above for Reference X.1. The average standard deviations for lateral and vertical gust velocities are 15.6 fps and 13.7 fps, respectively. The average longitudinal scale lengths are 1456 feet and 827 feet as calculated from the lateral and vertical components, respectively.

Composite plots of lateral and vertical gust velocity spectra, normalized by $\sigma_t^2 L$, are presented in Figure 50.4 and 50.5. The mean of these data are compared to von Karman normalized spectra in Figure 50.6. The comparisons of these data with the von Karman spectra would have been better if the data had been corrected to 22 cps filters as discussed in Section XI.

TABLE 50.2
REFERENCE X.2 (F-106) TURBULENCE DATA

Test No.	Sample No.	σ_t (fps)		L_K (feet)	
		v	w	v	w
2-7	10	-	10.1	-	440
	11	12.5	9.4	1250	440
2-8	14	-	9.4	-	900
2-21	7	10.1	8.5	1050	580
	28	-	11.9	-	975
	29	14.4	-	1900	-
2-23	25	-	12.2	-	975
2-34	12	-	12.4	-	900
2-35	20	-	14.2	-	800
	21	-	11.8	-	1150
	23	-	14.7	-	975
2-36	15	-	13.9	-	660
	20	-	13.2	-	440
	21	-	11.9	-	530
	24	15.1	12.4	1800	875
2-39	6	-	14.7	-	620
	7	-	12.4	-	740
	8	26.0	-	1650	-
	9	-	15.9	-	1500
	13	-	17.1	-	600
	15	-	18.1	-	1020
	18	-	17.7	-	600
	19	-	19.3	-	980
	20	15.5	13.5	1750	940
	21	11.7	9.2	1350	620
	22	11.5	11.4	1050	360
	23	-	13.0	-	590
	24	-	10.2	-	1200

TABLE 50.2 (CONTINUED)

REFERENCE X.2 (F-106) TURBULENCE DATA

Test No.	Sample No.	σ_t (fps)		L_K (feet)	
		v	w	v	w
2-40	10	17.9	14.1	1600	875
	18	-	14.4	-	1050
	20	16.3	12.9	1700	900
	21	-	21.4	-	1400
	29	15.4	-	1750	-
2-41	6	-	11.7	-	1350
	10	-	13.3	-	1000
	11	-	14.8	-	900
	12	-	12.8	-	1020
	13	-	14.1	-	620
	14	-	14.1	-	980
	16	-	15.3	-	790
	18	-	12.7	-	600
	19	-	17.4	-	1600
	23	-	12.8	-	940
	23-1	-	12.8	-	870
	7	-	11.2	-	1130
2-42	10	-	15.7	-	940
	18	18.9	-	1250	-
	19	-	14.8	-	1250
	28	-	16.5	-	1150
	28-1	-	16.8	-	825
2-45	27	-	14.4	-	1400
2-46	16	-	11.5	-	760
	18	-	11.8	-	1050
	21	-	11.7	-	600
2-49	13	-	19.4	-	760
	14	-	12.7	-	820
	15	-	15.6	-	980
	26	13.4	8.7	1400	260
2-55	41	11.6	-	2100	-
2-56	27	-	12.3	-	900
2-57	6	10.1	8.6	900	470
	16	21.2	17.2	800	420

TABLE 50.2 (CONTINUED)

REFERENCE X.2 (F-106) TURBULENCE DATA

Test No.	Sample No.	σ_t (fps)		L_x (feet)	
		v	w	v	w
2-58	10	-	13.8	-	825
	14	-	13.4	-	430
	21	13.7	-	1400	-
	25	17.2	-	1750	-
2-59	11	13.1	11.3	1300	740
	12	17.8	14.6	1200	430
	12-1	-	21.3	-	1050
	13	22.6	15.8	2200	680
	31	14.2	14.7	1200	850
2-60	14	14.8	12.3	1100	675
	23	19.2	11.9	1500	260
	28	-	13.7	-	470

Reference X.3 (T-38) Spectra

The purpose of this program was to determine the dynamic response characteristics of the T-38 airplane to atmospheric turbulence. The program consisted of seventeen flights conducted in the vicinity of Edwards AFB, California, from April through August 1961. The atmospheric turbulence data were obtained using a Norair designed boom. This boom, installed on the nose of the airplane was 26 inches long and incorporated a Giannini Controls Corporation differential pressure type angle-of-attack and sideslip sensor. The gust velocity time histories obtained during this program also contained low frequency, long period trends upon which the gust data were superimposed. A high pass, moving average type numerical filter having a period of 2.25 seconds was employed to remove the low frequency trends. The original gust velocity time series was passed through this filter to capture all frequency components below approximately 0.4 cps. The resulting low frequency time series was subtracted from the original time functions to yield smoothed or filtered data.

Nine samples of lateral gust spectra and three samples of vertical gust spectra were available from which five lateral samples and the three vertical samples were selected for this comparison. The gust velocity standard deviations and scale lengths for the samples selected are presented in Table 50.3. The standard deviation values were calculated as the square root of the area under the spectrum from 0.5 to 25 cps. The scale lengths were estimated in the same manner as described previously.

TABLE 50.3
REFERENCE X.3 (T-38) TURBULENCE DATA

Test No.	Sample No.	σ (fps)		L_k (feet)	
		v	w	v	w
196-11	6	-	2.51	-	400
196-14	4	-	2.42	-	400
228-13	2	-	1.92	-	400
228-16	8	-	2.28	-	400
230-11	7	-	2.54	-	300
253-12	6	2.36	-	300	-
253-15	4	2.14	-	600	-
253-19	2	2.02	-	600	-

The normalized spectra obtained from these data are shown in Figures 50.7 and 50.8. The average of these spectra is compared to von Karman spectra in Figure 50.9. There is not sufficient data involved in the average to warrant definite conclusions, however, certain observations are worth noting: (1) the vertical spectra and scale length more closely resemble those obtained for the LO-LOCAT Program than does the lateral data, and (2) drift still remains in the data. Evidence that drift remains in the data can be seen by reviewing the modulus squared of the filter function explained in Reference X.3. Here it can be seen that the filter used reacts as a damped oscillatory signal and does not completely attenuate the data below 0.5 cps.

References X.4 (B-52E) and X.5 (B-52H) Spectra

The Reference X.4 and X.5 data are discussed together because of the similarity of the test beds, instrumentation, gust velocity calculations, filtering, and results. Included in the objectives of these two programs was the determination of the turbulence environment and the response of the B-52 airplanes to that turbulence. The test beds consisted of a B-52E and a B-52H airplane. The instrumentation, gust velocity calculations and filtering were all very similar to those used during the LO-LOCAT Program, and are discussed elsewhere in this report.

A total of 38 samples from these two programs were selected for comparison to LO-LOCAT data. The time series standard deviations and estimated scale lengths are presented in Tables 50.4 and 50.5.

TABLE 50.4
REFERENCE X.4 (B-52E) TURBULENCE DATA

Test No.	Sample No.	σ_t (fps)		L_K (feet)	
		v	w	v	w
51-10	1	2.32	2.55	450	320
	2	2.62	2.47	500	290
	4	2.18	2.50	340	320
	21	2.66	3.29	450	510
	22	2.61	2.86	470	450
51-11	15	2.02	1.98	310	160
	16	2.53	-	260	-
	17	2.50	1.70	260	120
	19	2.70	2.04	640	140
	20	-	2.83	-	400
	21	3.04	2.43	600	200
	22	3.53	3.45	580	470
	23	2.01	2.10	480	450
	24	2.01	1.92	825	390
	25	-	1.89	-	500
	26	1.80	2.31	700	925
	27	2.41	2.19	1320	620
	28	2.03	1.80	270	140
	29	2.36	2.05	700	265
51-16	23	2.25	-	520	-
	24	-	1.66	-	825
	25	1.80	1.52	290	140
	28	2.33	-	410	-
	29	2.08	-	240	-
	30	2.69	2.46	530	350
51-17	18	2.19	2.79	360	800
	19	2.09	2.17	975	580
	20	2.02	2.05	640	380

TABLE 50.5
REFERENCE X.5 (B-52H) TURBULENCE DATA

Test No.	Sample No.	σ_t (fps)		L_k (feet)	
		v	w	v	w
13-1	27	4.26	3.51	600	320
13-2	9	6.35	5.57	360	270
	14	7.56	4.82	1050	270
13-5	10	7.23	6.05	1220	530
	12	5.23	4.77	400	290
13-6	17	4.05	-	670	-
13-9	10	-	3.11	-	330
	14	4.10	3.73	680	440
	16	3.24	3.81	530	825
13-10	17	4.38	2.68	600	160

The average longitudinal scale lengths for the B-52E data is 525 feet and 406 feet as computed from the lateral and vertical gust velocities, respectively. The scale lengths for the B-52H data are 679 feet and 382 feet for the lateral and vertical components, respectively. These are in good agreement with the LO-LOCAT Phase III average scale lengths.

Composite plots of the spectra for these data are presented in Figures 50.10 through 50.13. Plots representing the average of the composite spectra are presented in Figures 50.14 and 50.15. These data agree well with the von Karman spectra except at kL values $\leq 10^{-1}$ where the observed data are high.

Reference X.6 (B-66) Spectra

The primary objective of this program was to perform a study of low altitude turbulence. Longitudinal, lateral, and vertical gust velocities were recorded under a variety of meteorological and geophysical conditions similar to the LO-LOCAT Program. The data from this program were digitally filtered. The choice of filter, however, varied from sample to sample, since the data were filtered until the area under the spectrum was equal to the variance of the time series. A detailed description of this filter is presented in Reference X.6.

Scale lengths were calculated for 42 data samples. These scale lengths were obtained using both an area procedure based on the autocorrelation function and a least squares procedure. The values based on the two different methods were in good agreement. The scale lengths varied from 153 to 1327 feet and averaged approximately 630 feet.

Some difficulty was experienced in selecting good samples for comparative purposes and for the calculation of von Karman scale lengths because a definite -5/3 logarithmic slope could not be defined. It was deduced that the problem was caused by an abundance of high frequency noise. Generally, only samples in which this noise was minimal were selected. In the calculation of scale lengths, the noise was ignored since it was not a factor except to the degree that the standard deviation used for normalizing was affected.

Lateral gust velocity data from 58 samples and vertical gust velocity data from 50 samples were selected for analysis. The standard deviations and estimated scale lengths are presented in Tables 50.6 through 50.8.

The data in Tables 50.6 through 50.8 were obtained when the airplane was flying at 360 KIAS. The Group A data (Table 50.6) were obtained over farmlands at constant pressure altitude equal to 1000 feet above the highest terrain. The Group B (Table 50.7) and Group C (Table 50.8) data are for rough terrain, high and low mountains combined, and were obtained at constant pressure altitudes equal to 200 feet and 1000 feet above the highest terrain, respectively.

TABLE 50.6

REFERENCE X.6 (B-66) TURBULENCE DATA - GROUP A

Farmlands - 1000 Feet

Reference X.6 Identification No.	σ_t (fps)		L_k (feet)	
	v	w	v	w
G55E63521	-	3.72	-	1350
G55E63522	3.01	3.46	800	970
G61K62521	-	2.33	-	900
G61K62522	-	3.10	-	600
G65K71521	3.05	2.81	700	900
G65K71522	2.98	2.67	560	550
G73S61521	2.84	3.28	510	825
G83W61521	1.85	-	800	-
G83W71521	2.24	2.21	450	480
G86W61521	2.98	-	700	-
G86W71521	3.69	3.84	820	1250
G87W61521	3.20	-	770	-
G87W71521	3.33	-	600	-
G89W71521	3.11	3.26	860	1100
G91S61521	3.36	-	670	-
G92S61521	3.32	3.32	580	600
G101K62521	4.95	4.76	1050	1050
G101K62522	5.51	4.94	1300	1100
G103K71521	-	4.05	-	1200
G111S61521	2.92	4.44	550	1250
G114S61521	3.94	4.31	970	1100
Average			746	945

TABLE 50.7
REFERENCE X.6 (B-66) TURBULENCE DATA - GROUP B
High and Low Mountain - 200 Feet

Reference X.6 Identification No.	σ_t (fps)		L_k (feet)	
	v	w	v	w
G34K22121	-	5.16	-	550
G34K22122	-	5.29	-	700
G37K22121	4.75	-	1050	-
G54E11121	3.85	3.38	1450	825
G54E11122	3.39	3.92	800	700
G57E23121	-	4.65	-	950
G57E23122	-	5.39	-	850
G62K22121	3.26	2.40	1325	800
G63K11121	2.97	3.15	410	380
G63K11122	3.18	3.23	450	470
G69S21122	3.59	-	1350	-
G83W11121	4.20	3.56	750	470
G85W11121	-	3.11	-	400
G87W11121	-	3.60	-	500
G88W11121	4.30	-	650	-
G91S11121	-	3.84	-	500
G92S11121	4.22	4.37	600	470
G92S21121	4.38	-	825	-
G94S11121	5.10	-	800	-
G94S21121	5.53	4.99	850	650
G100K22121	5.39	-	1050	-
G100K23122	5.56	-	1200	-
G104K11121	8.10	-	1400	-
G110S11121	3.98	-	580	-
G111S11121	3.58	-	600	-
G111S21121	3.08	-	650	-
Average			884	614

TABLE 50.8
REFERENCE X.6 (B-66) TURBULENCE DATA - GROUP C
High and Low Mountain - 1000 Feet

Reference X.6 Identification No.	σ_t (fps)		L_k (feet)	
	V	W	V	W
G54E11521	-	3.69	-	1300
G54E11522	-	2.93	-	850
G57E23521	-	6.65	-	1750
G57E23522	-	5.18	-	600
G62K22521	1.90	1.47	970	390
G62K22522	2.60	2.25	1800	900
G63K11521	2.68	2.57	1250	530
G63K11522	3.25	2.86	775	580
G73S11521	2.09	-	1030	-
G73S11522	1.91	-	1130	-
G73S21521	2.11	-	1350	-
G83W11521	3.06	3.33	450	610
G86W11521	3.97	3.84	700	700
G87W11521	-	3.92	-	970
G89W11521	2.76	3.42	500	970
G92S11521	3.87	4.71	800	1750
G92S21521	2.65	-	820	-
G100K22521	5.24	3.80	1400	740
G100K22522	4.41	3.78	1200	680
G100K23521	5.24	-	1450	-
G100K23522	5.56	-	1400	-
G104K11521	5.59	6.30	950	1700
G104K11522	6.28	-	1400	-
G111S11521	2.93	3.72	530	1350
G113S81521	3.30	-	660	-
G114S11521	3.94	3.61	1000	970
G114S21521	4.31	4.48	1200	1650
Average			1035	999

The average scale length for each group is listed in each table. Certain similarities can be seen between these data and the LO-LOCAT data. Both sets of vertical scale length data are smaller at the lower than at the higher altitudes, and both the vertical and lateral scale lengths obtained over rough terrain are larger than those obtained over smooth terrain for the comparative 1000-foot altitude.

Normalized spectra are not presented for Reference X.6 because the data were not readily convertible to normalized spectra due to the reduced size of available spectra plots and high frequency noise. The method for obtaining the estimated scale lengths was also rendered less accurate than for the other data due to the above problems.

Reference X.7 (B-58) Spectra

The purpose of this program was to compute data which could be used to evaluate gust criterion for strength design. Investigations were conducted in an attempt to deduce values for the scale of turbulence from the gust velocity data measured during the B-58 and RB-57F flight test programs.

Only one sample of gust velocity spectra, Figure 50.16, was presented in Reference X.7. These data were recorded with an instrumented B-58 airplane flying at 900 fps at an absolute altitude of 1200 feet. No spectra of turbulence recorded by the B-57 airplane were presented.

The B-58 spectrum was analyzed in Reference X.7, for various combinations of prewhitening, post darkening, and filtering weights. The turbulence scale lengths presented varied from 47100 feet to 2815 feet depending on the combination of techniques used. The most satisfactory data were obtained using a 0.015 Gamma filter with no prewhitening. The scale length published, however, was higher than that estimated by the method used to evaluate scale lengths from other programs. The scale length for the most satisfactory data was 2815 feet compared to an estimated value of 2250 feet. The spectrum has a -5/3 logarithmic slope except at the high frequencies where the presence of noise is evident.

It was concluded in Reference X.7 that the scales of turbulence seem to increase with increasing speed. This same tendency has been noted during LO-LOCAT.

Based on the assumptions made in selecting the power spectra to be used in this analysis, it is concluded that the spectra of turbulence at low altitudes from various independent research programs are consistent, and their shape can be approximated by the von Karman mathematical expressions with scale lengths generally less than 1000 feet.

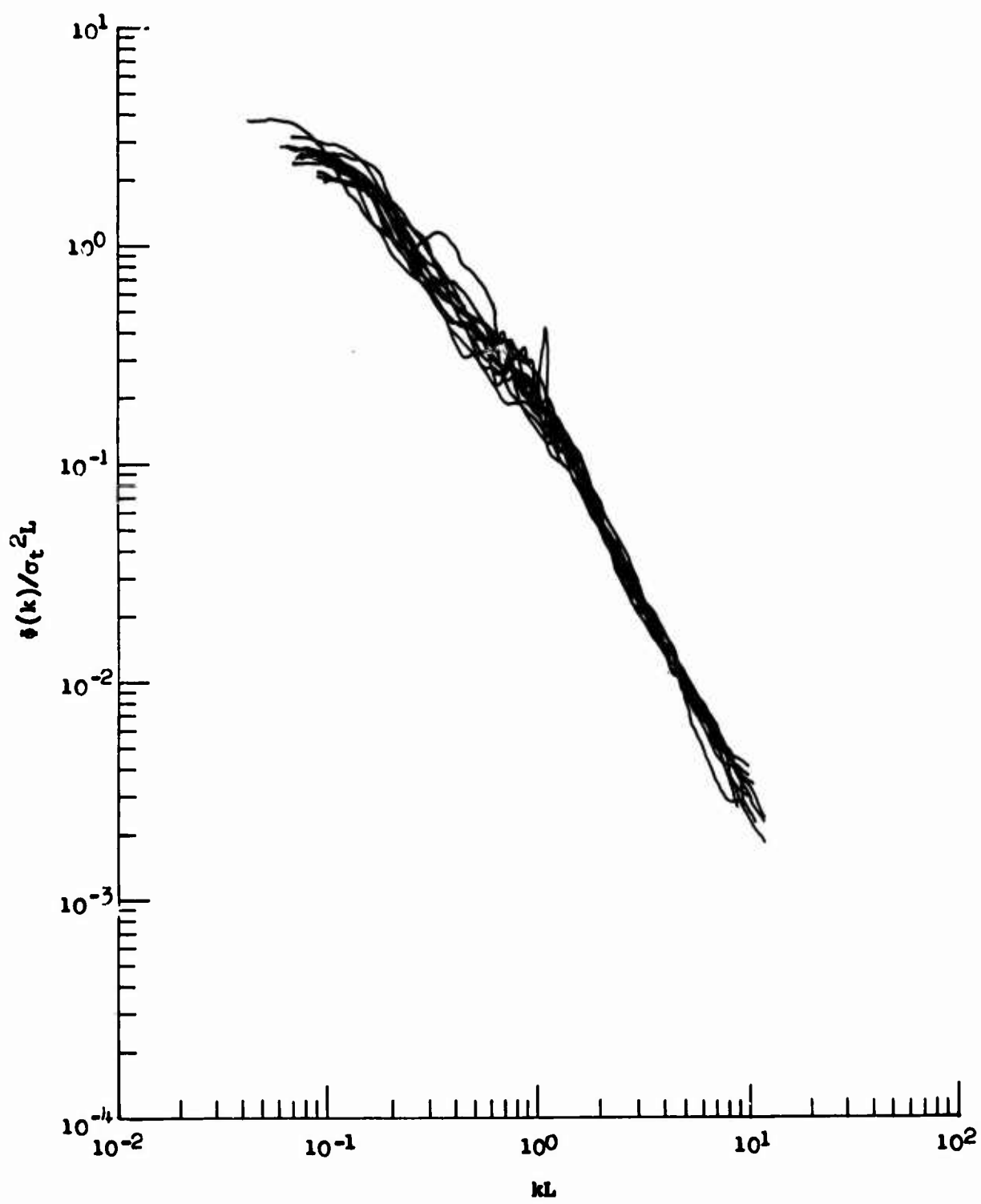


Figure 50.1 Reference X.1 (F-106) Lateral Gust Velocity Normalized Spectra

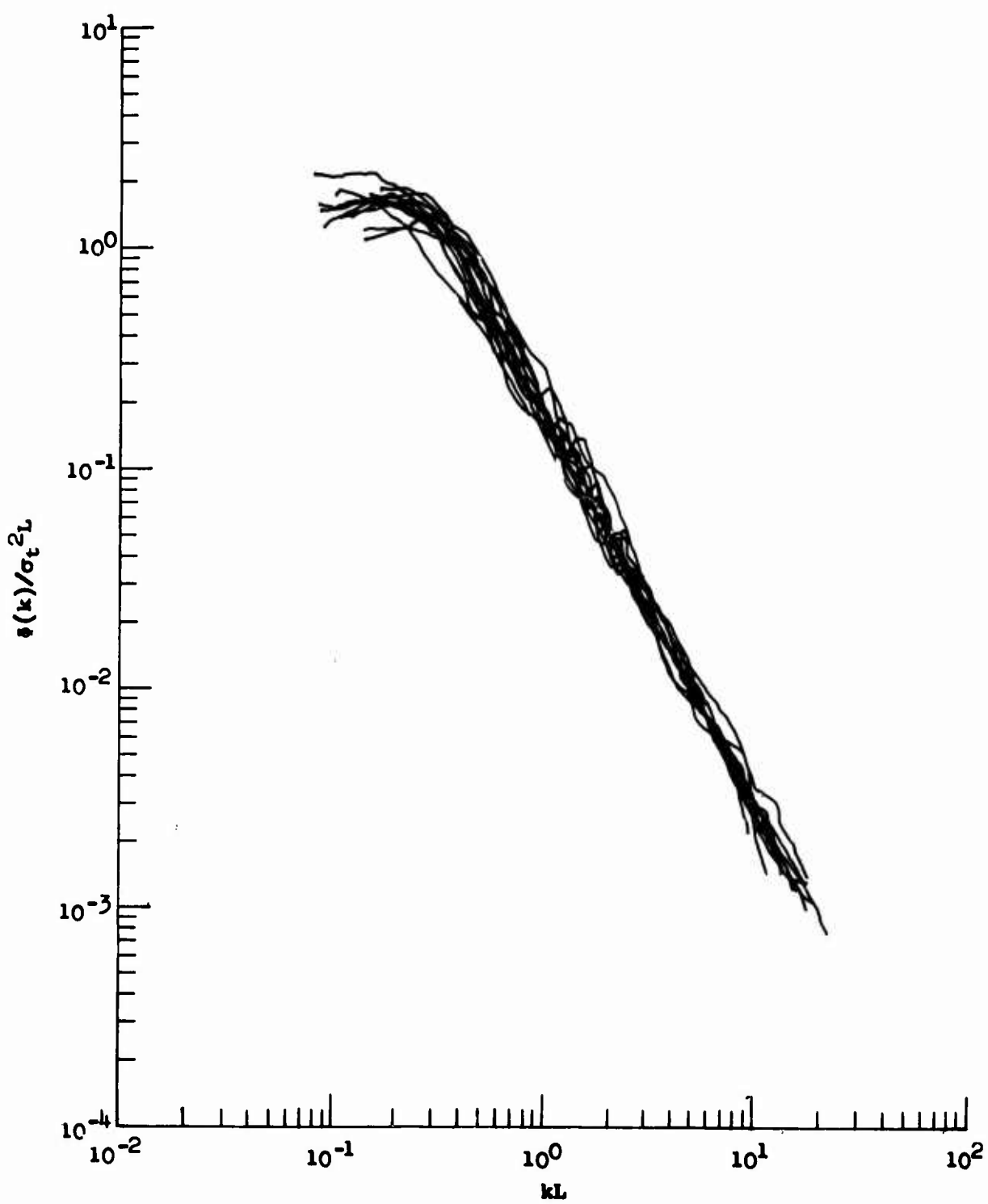


Figure 50.2 Reference X.1 (F-106) Vertical Gust Velocity Normalized Spectra

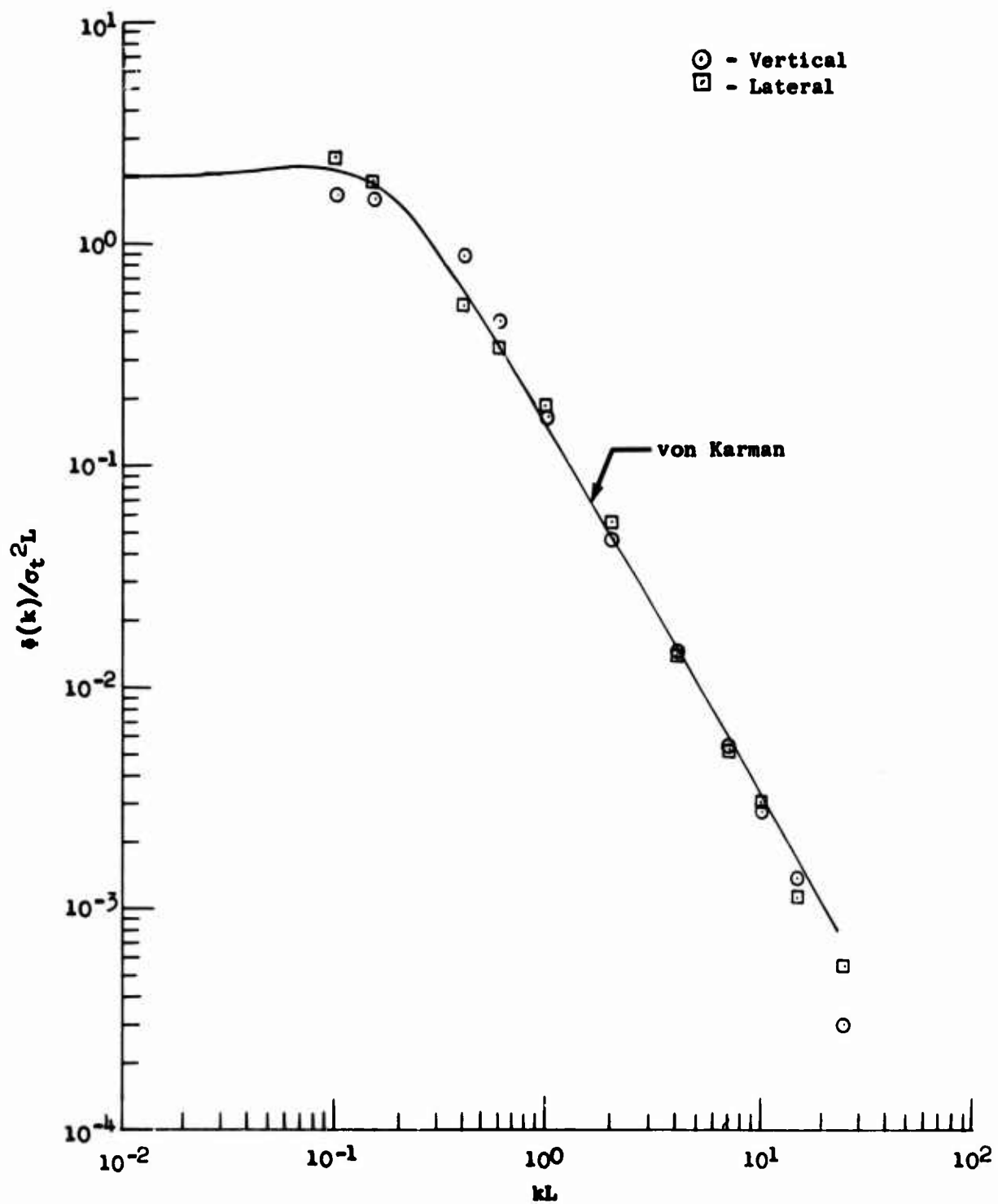


Figure 50.3 Reference X.1 (F-106) and von Karman Spectra Comparison

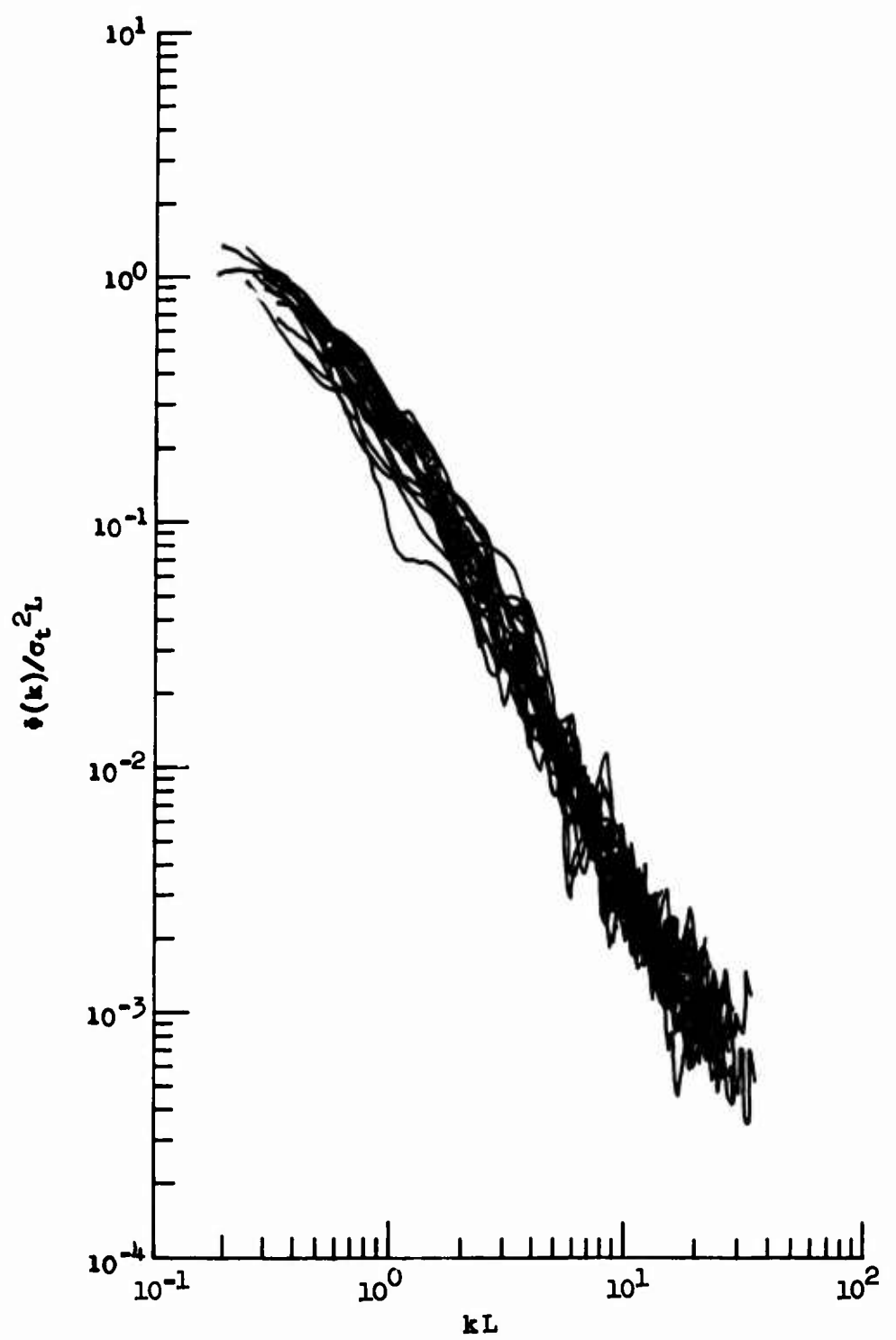


Figure 50.4 Reference X.2 (F-106) Lateral Gust Velocity Normalized Spectra

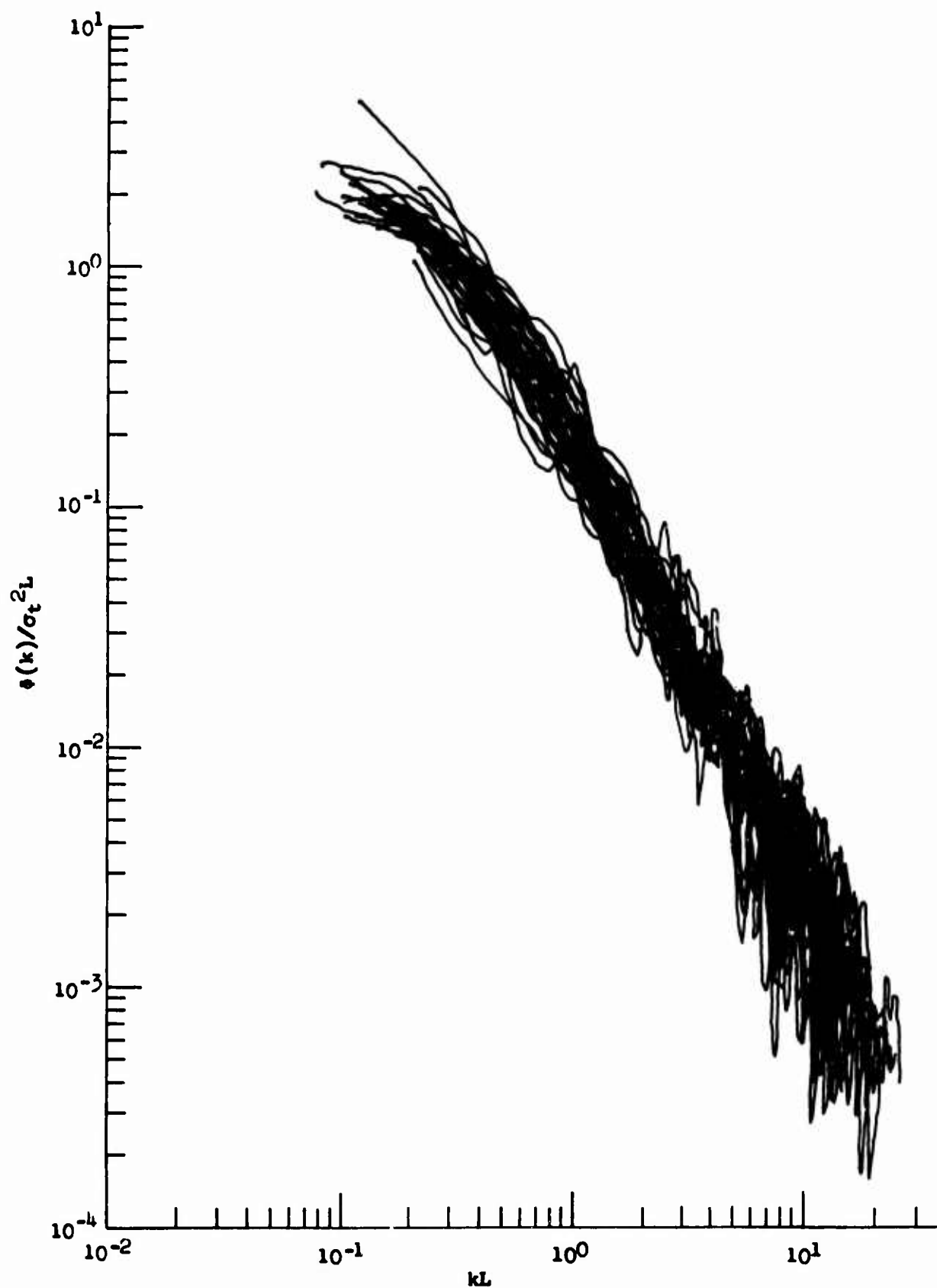


Figure 50.5 Reference X.2 (F-106) Vertical Gust Velocity Normalized Spectra

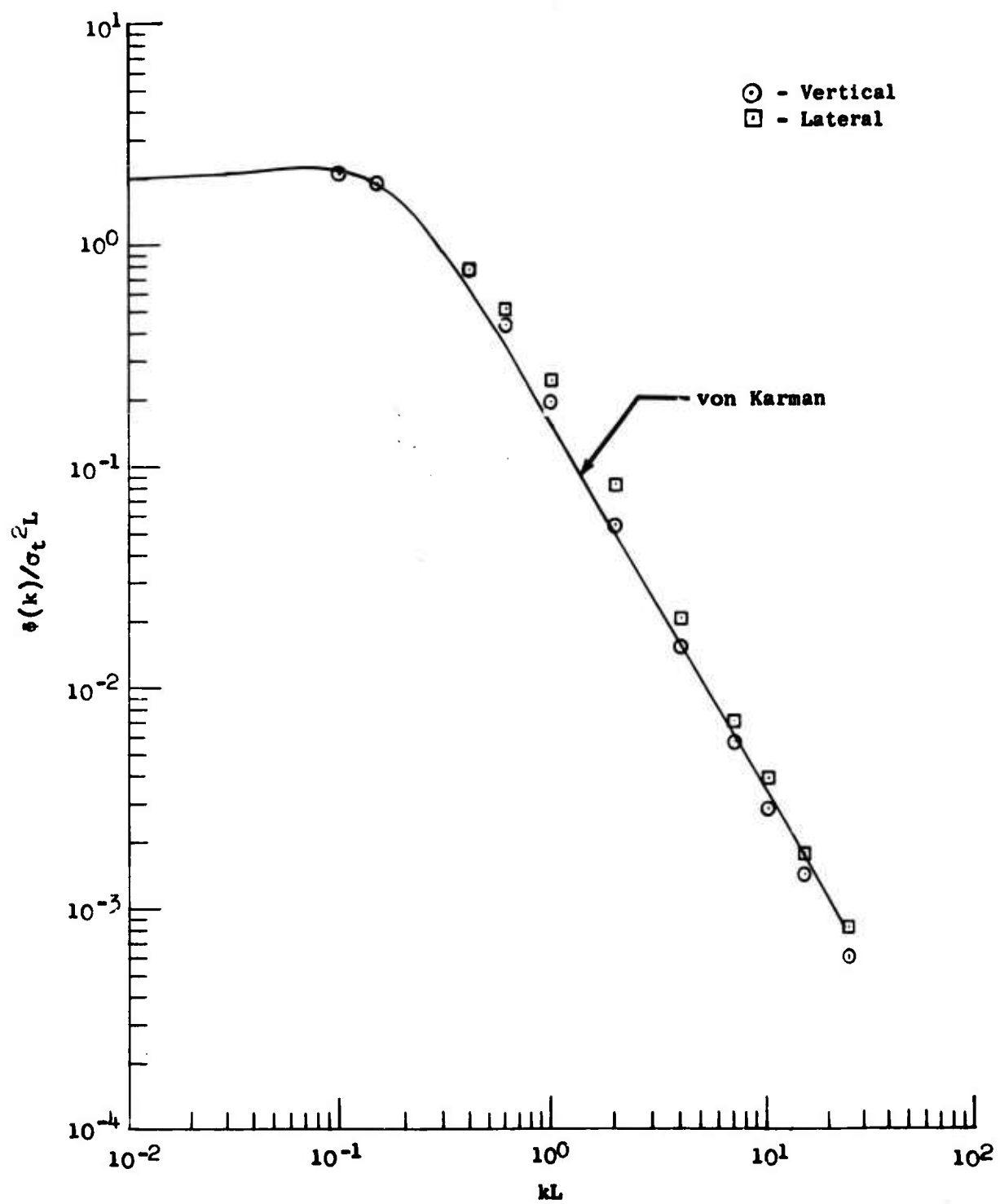


Figure 50.6 Reference X.2 (F-106) and von Karman Spectra Comparison

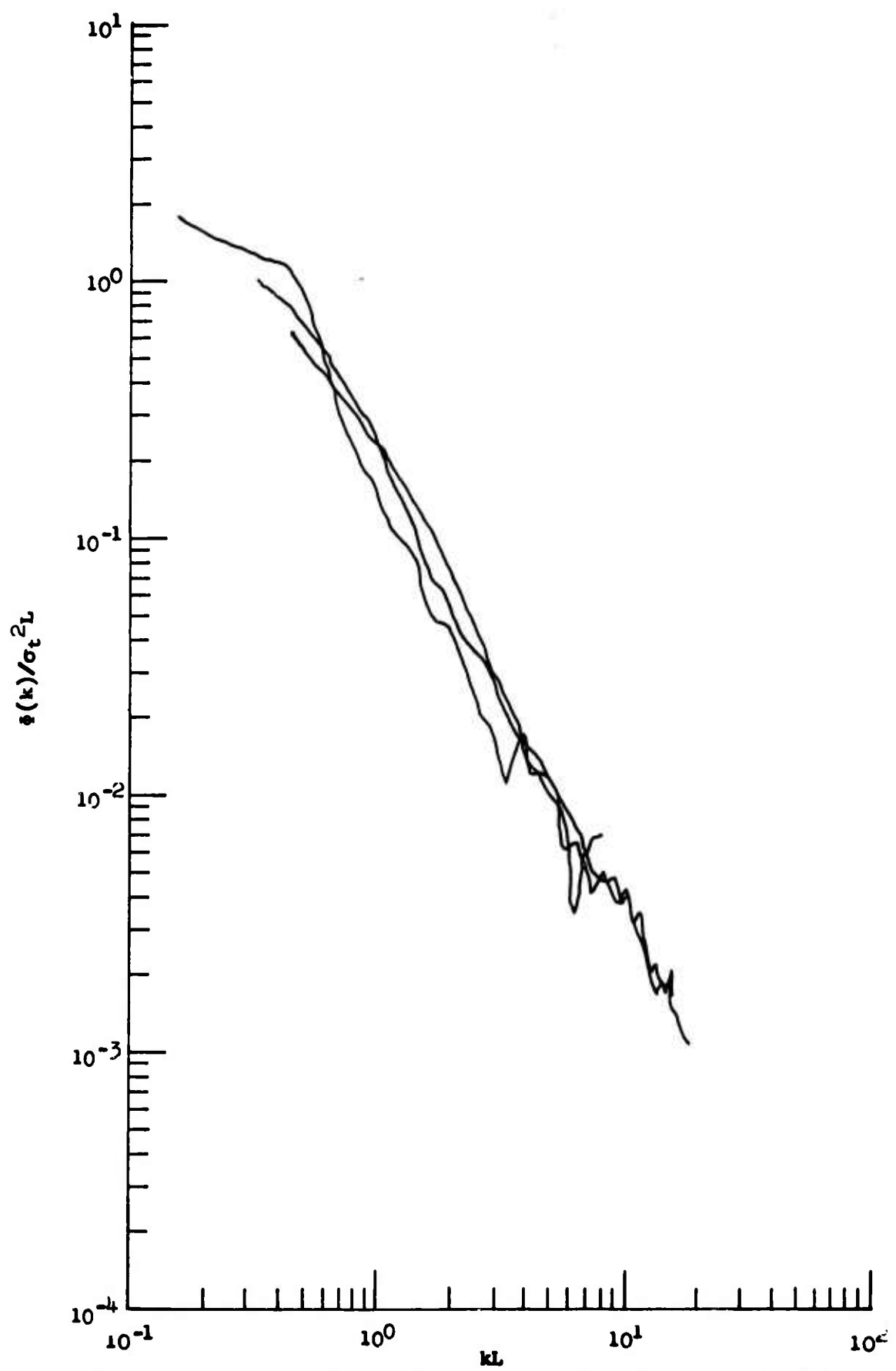


Figure 50.7 Reference X.3 (T-38) Lateral Gust Velocity Normalized Spectra

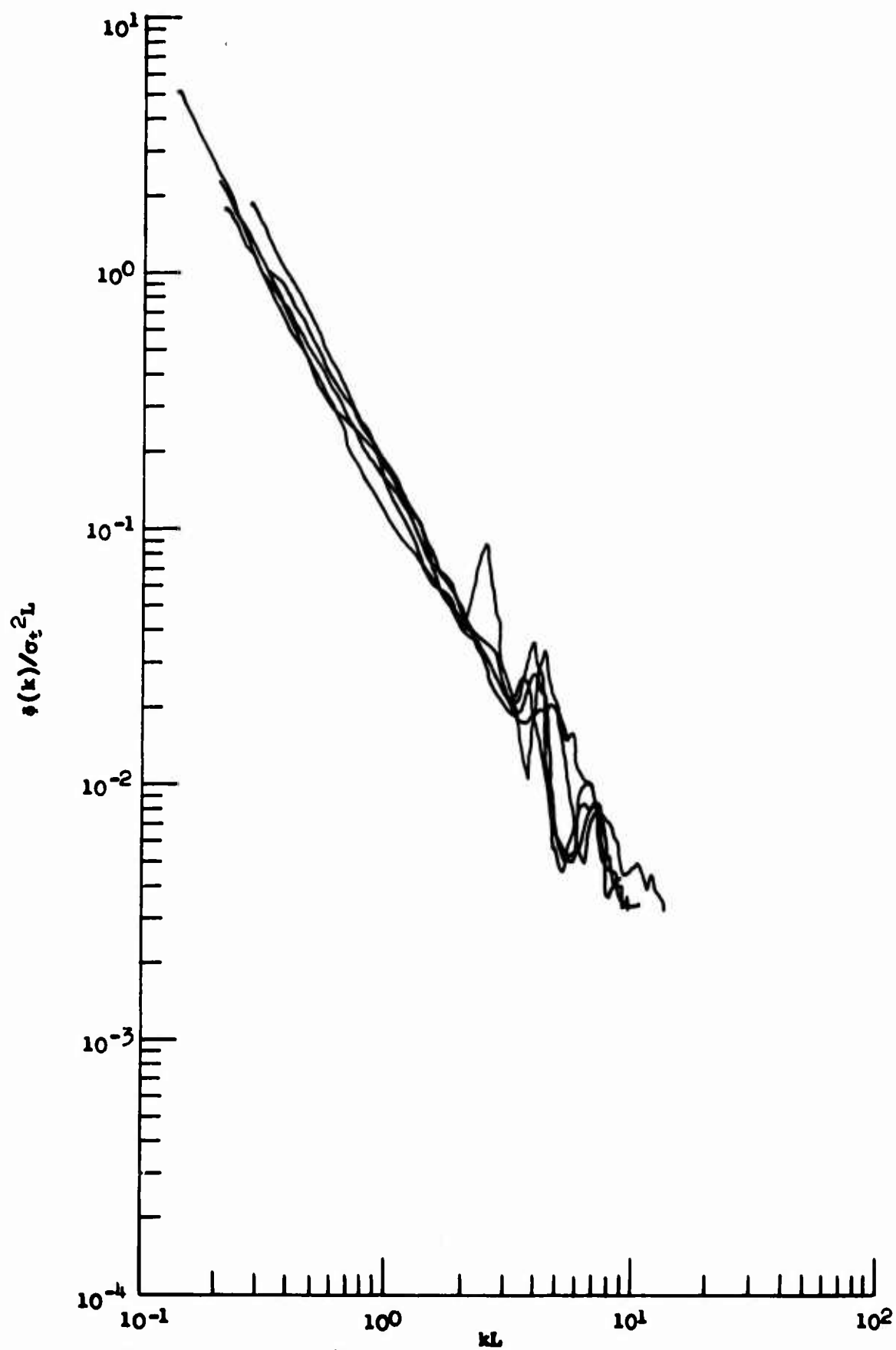


Figure 50.8 Reference X.3 (T-38) Vertical Gust Velocity Normalized Spectra

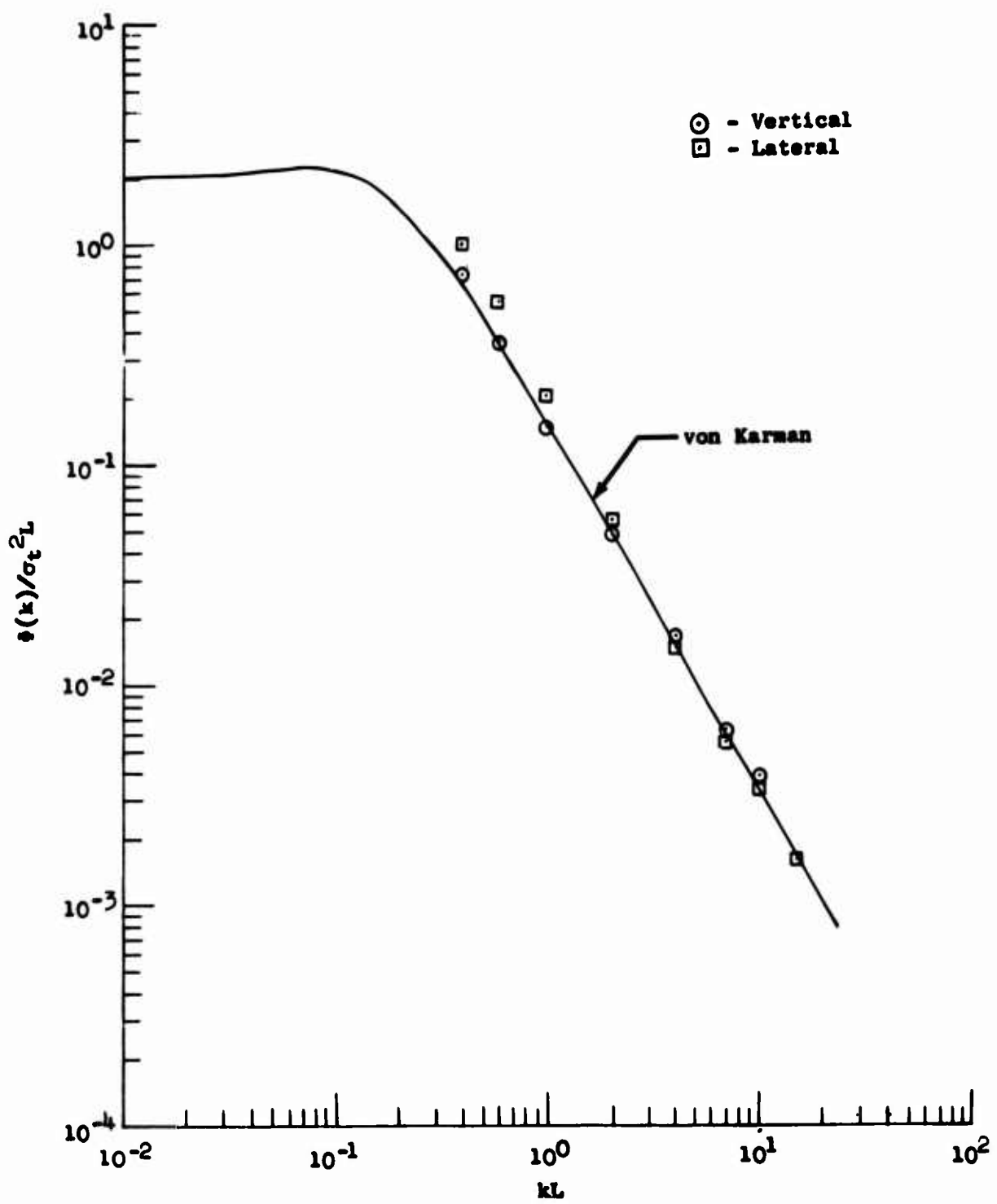


Figure 50.9 Reference X.3 (T-38) and von Karman Spectra Comparison

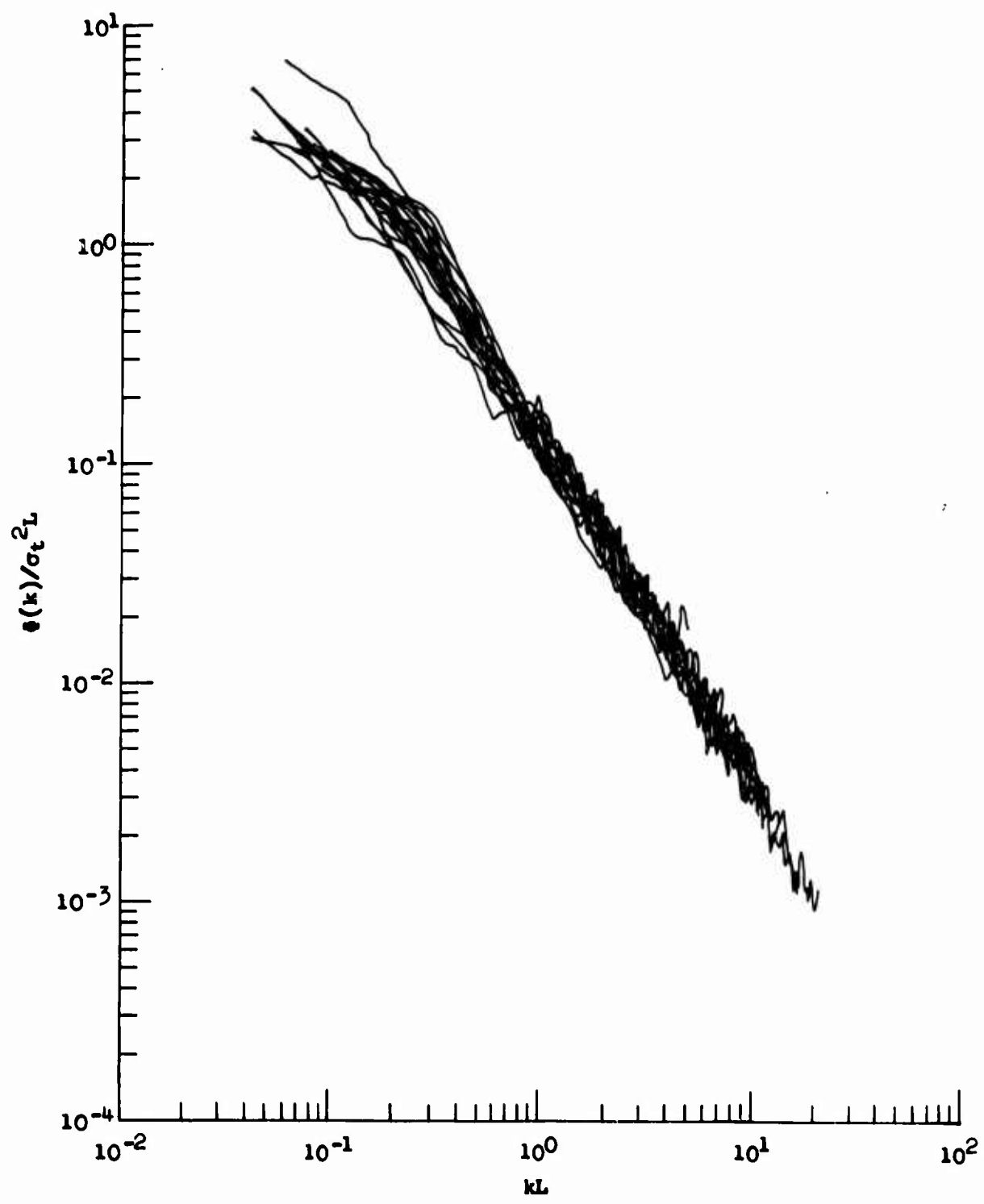


Figure 50.10 Reference X.4 (B-52E) Lateral Gust Velocity Normalized Spectra

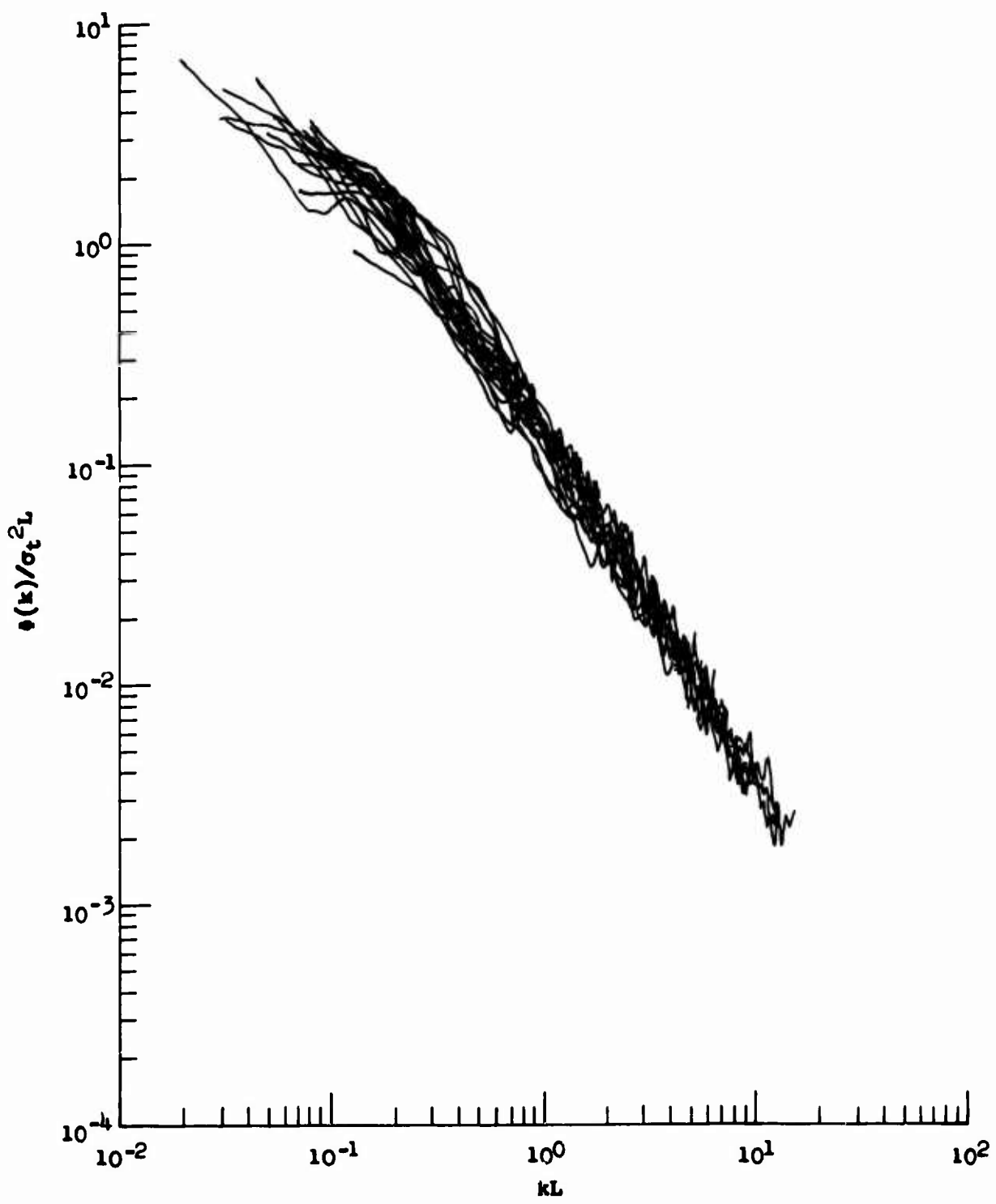


Figure 50.11 Reference X.4 (B-52E) Vertical Gust Velocity Normalized Spectra

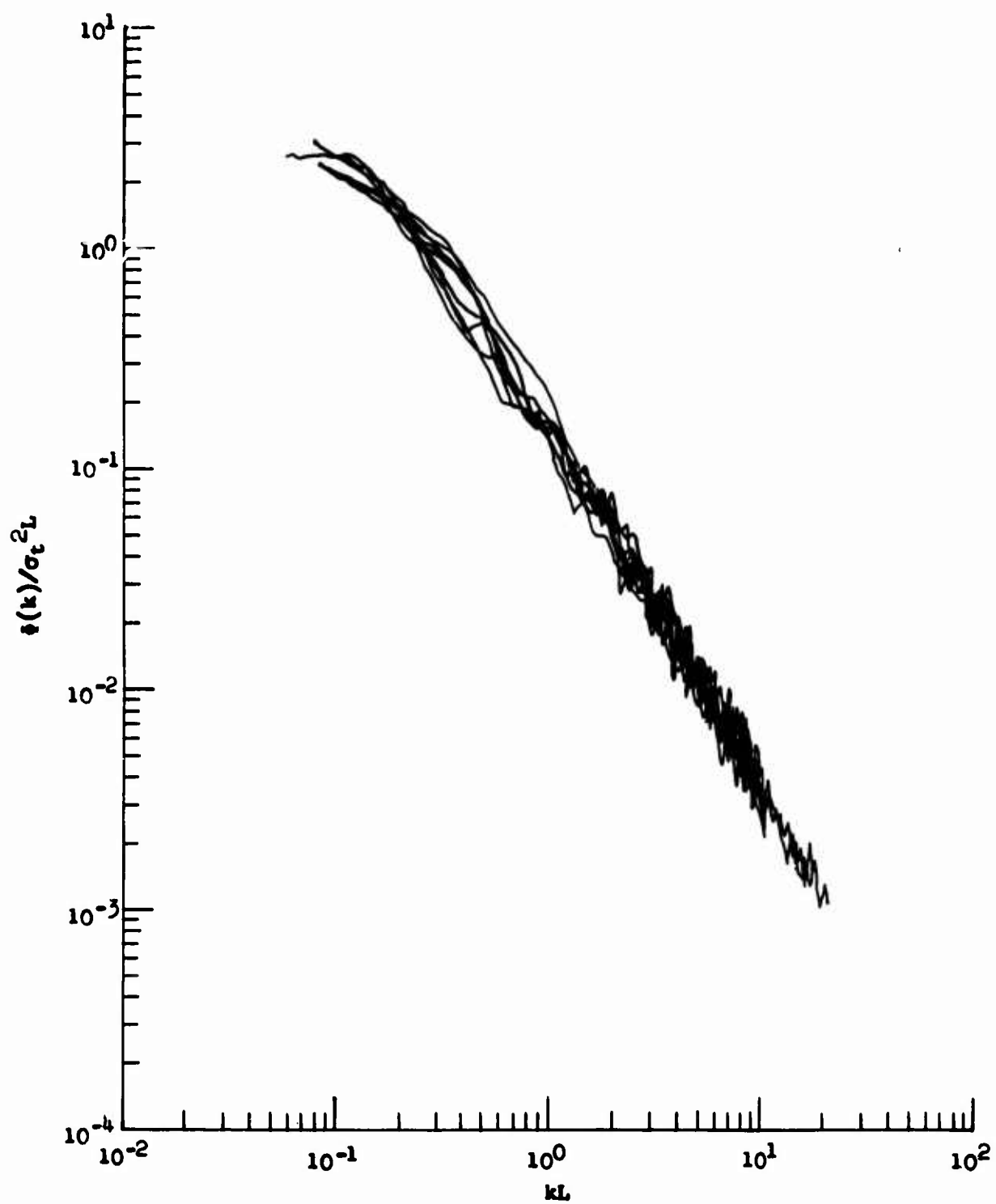


Figure 50.12 Reference X.5 (B-52H) Lateral Gust Velocity Normalized Spectra

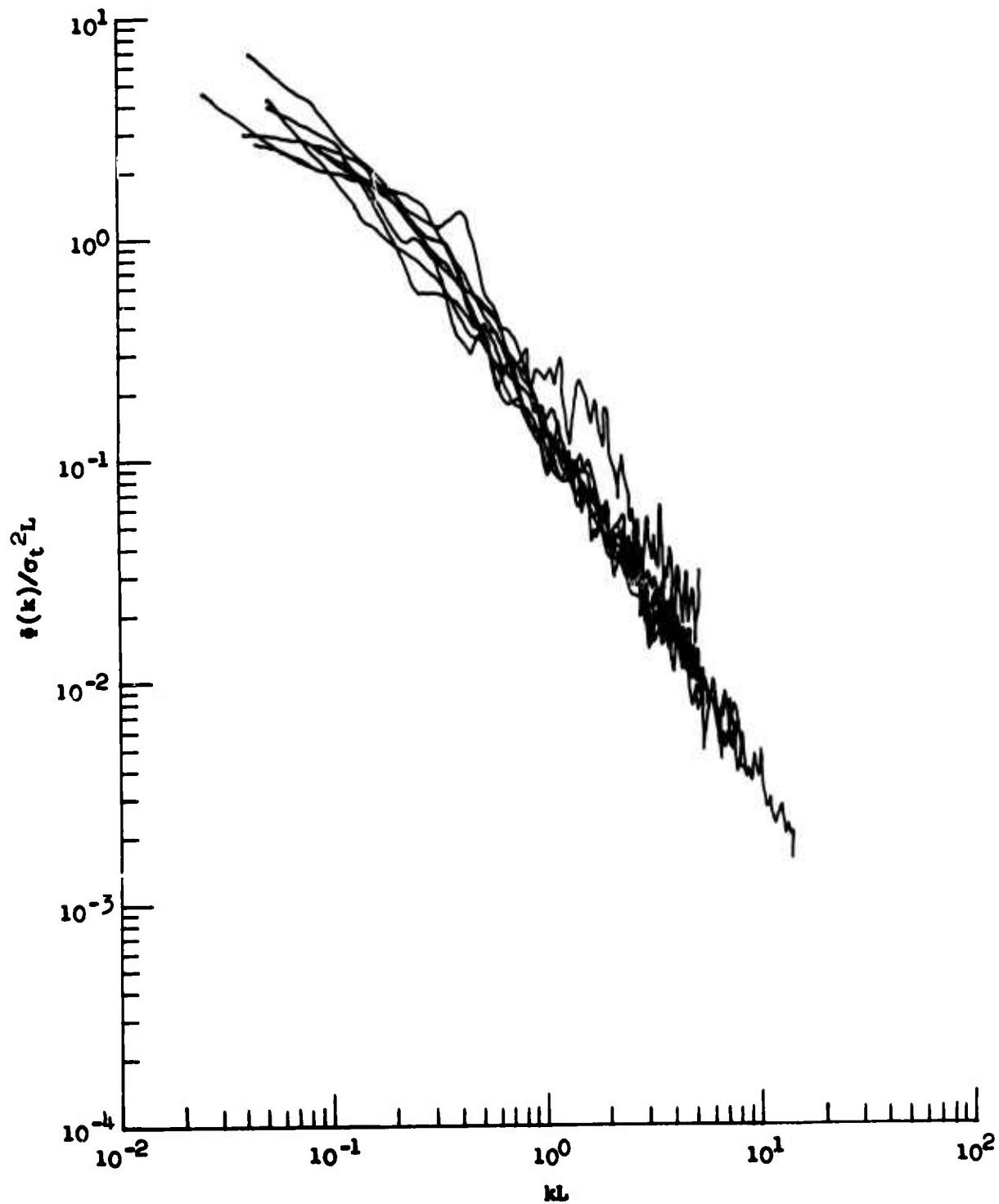


Figure 50.13 Reference X.5 (B-52H) Vertical Gust Velocity Normalized Spectra

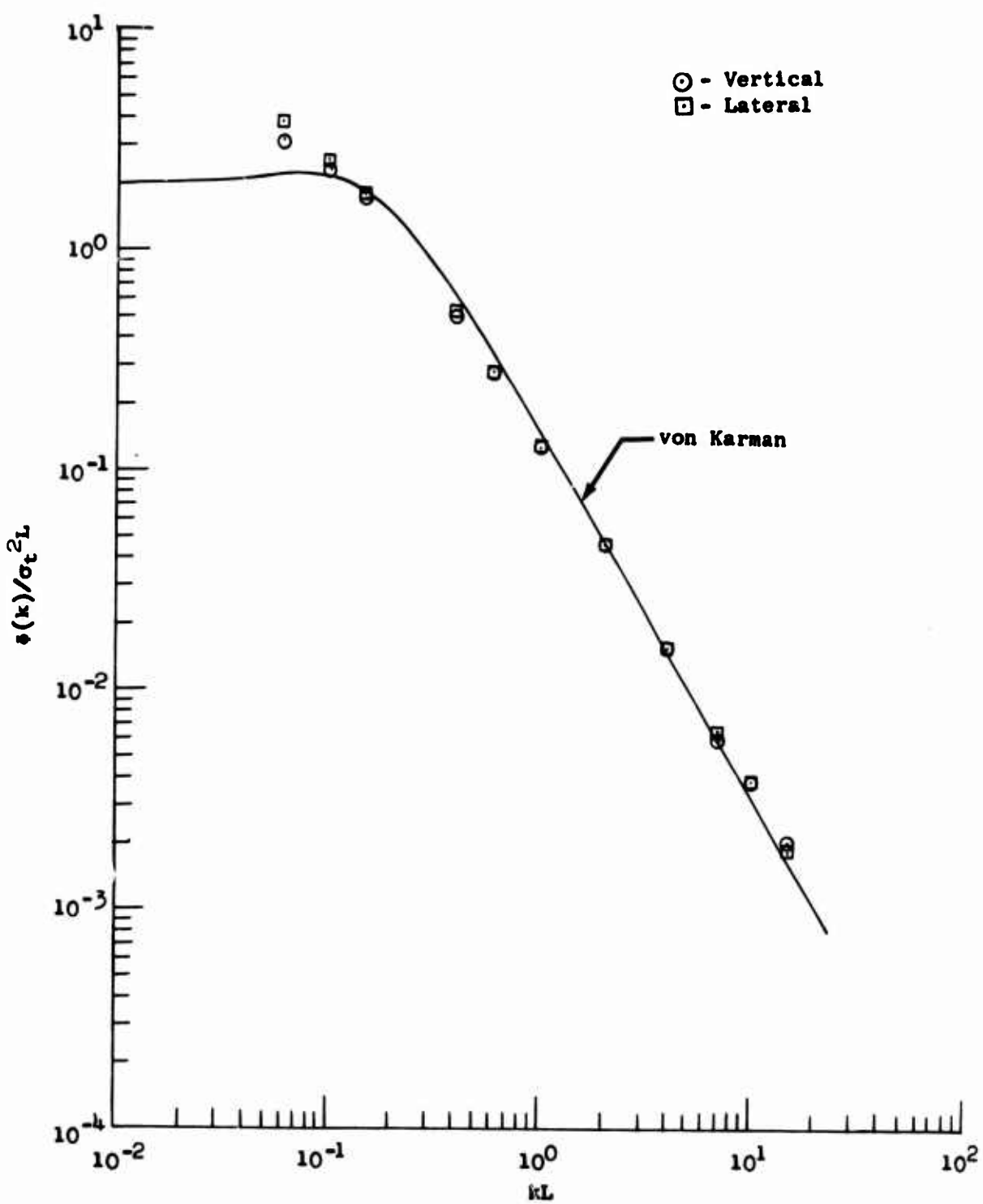


Figure 50.14 Reference X.4 (B-52E) and von Karman Spectra Comparison

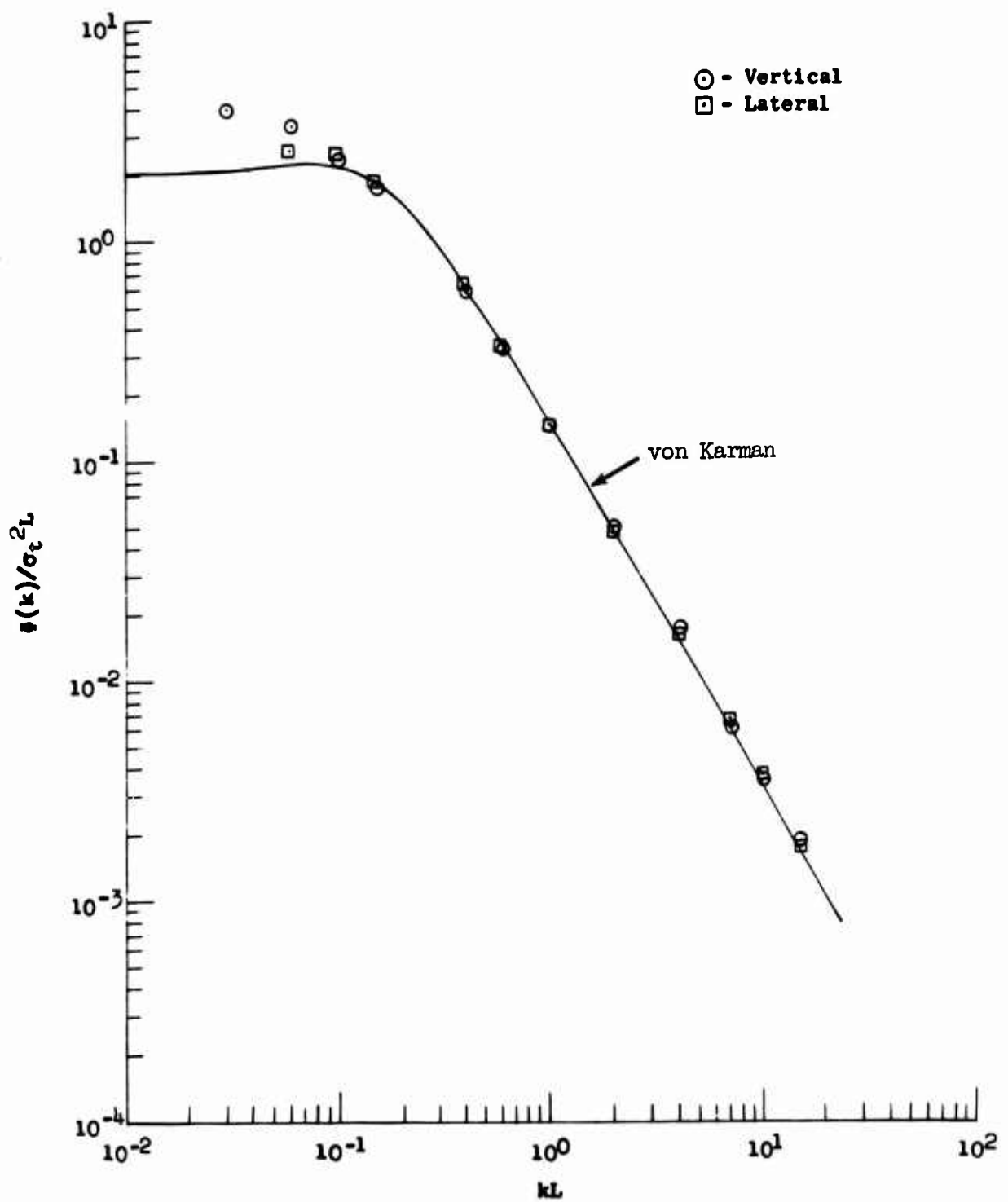


Figure 50.15 Reference X.5 (B-52H) and von Karman Spectra Comparison

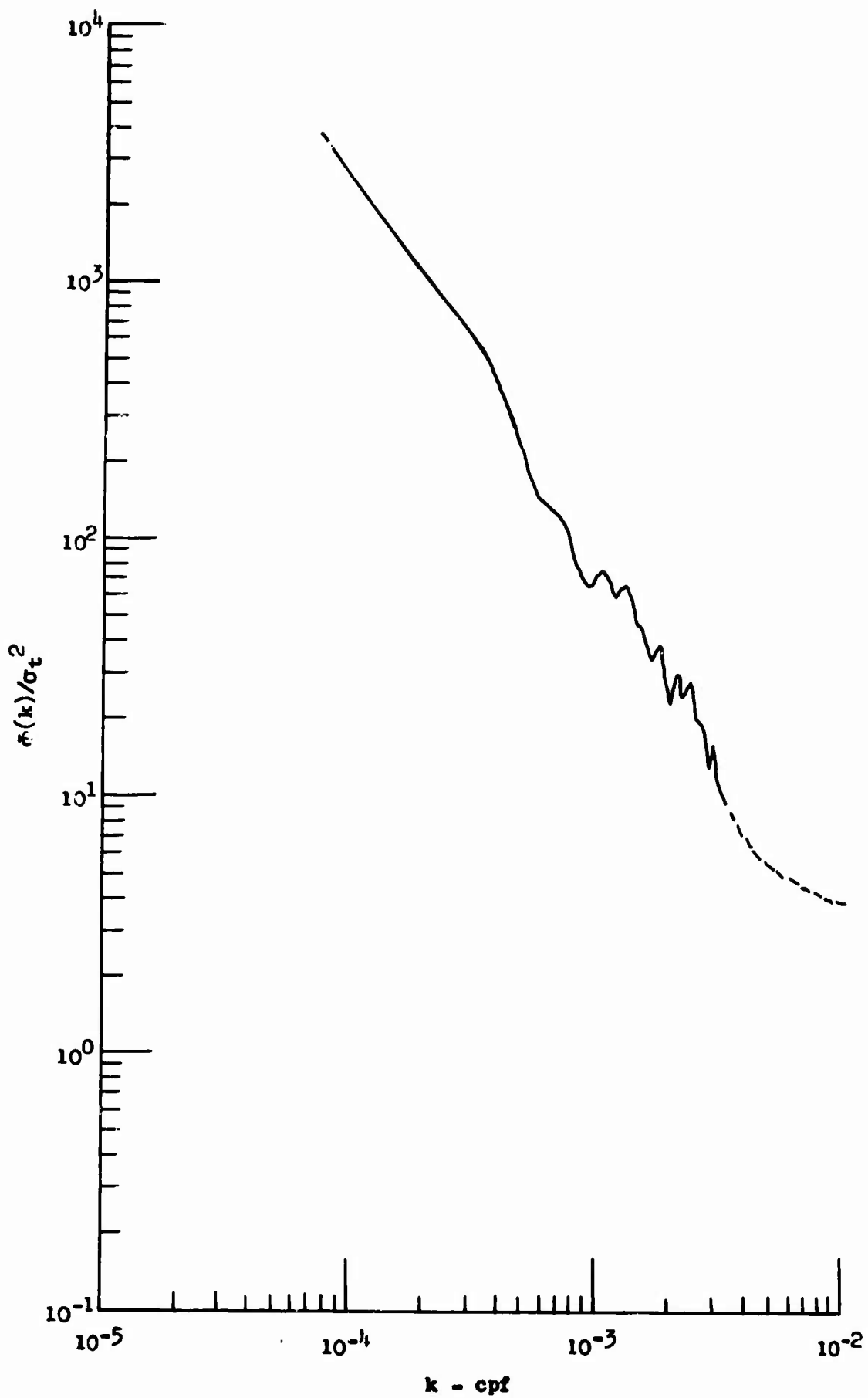


Figure 50.16 Reference X.7 (B-58) Gust Velocity Power Spectrum with $\gamma = .015$ (No Prewhitenning)

SECTION XI
ADDITIONAL RESEARCH

Analyses of the LO-LOCAT data showed that the statistics of measured atmospheric turbulence are significantly influenced by the resolution of long wavelengths. Low frequency instrumentation drift affects computed gust velocities and hence their power spectral densities. This is due to magnification of low frequency errors by the integrations that are required in the probe motion terms in the computation of gust velocities. The purpose of this additional research was to determine whether or not longer wavelengths could be better resolved by using modified data processing techniques. Gust accelerations and wind velocities were calculated and analyzed to determine if the long wavelengths could be better resolved. The computation of gust acceleration rather than velocity eliminates the necessity for integrating, with respect to time, the acceleration measurements which magnifies drift errors. It was theorized that direct conversion of gust acceleration spectra to gust velocity spectra in the frequency domain could result in less error at the low frequencies due to the drift. The spectra of the longitudinal and lateral components of wind velocity were calculated at frequencies one decade lower than those for gust velocity. The computation of wind velocities were at such low frequencies that the airplane motion terms could not be included in the computations.

Thirty turbulence samples were selected for this additional research. These samples were chosen based on the availability of the gust velocity power spectra, the degree of homogeneity, and the geophysical conditions under which they were measured. They are shown in Table XI.1. Geophysical conditions associated with the samples vary only in time of day and season. They were all recorded at 750 feet above high mountains of the Peterson route when the atmosphere was classified as being stable.

Many improvements in data processing techniques were developed during the course of the LO-LOCAT program. Extreme gust data obtained during the High Intensity Gust Investigation (Reference X.2) and processed in 1964 did not have the benefit of these improved techniques since they were developed later. The Reference X.2 data have provided the basis for the specification of turbulence criteria for design of aircraft to operate in the terrain following mode. A portion of the High Intensity Gust Program data was re-evaluated therefore, to determine if the results from this program would be significantly changed if the data were reprocessed using the improved data processing techniques.

Twenty-five of the High Intensity Gust Program turbulence samples were chosen for re-evaluation. They are shown in Table XI.2. The samples were chosen based on the magnitude of the gusts and readability of the magnetic tapes on which the data had been recorded.

TABLE XI.1
LO-LOCAT PHASE III SAMPLES SELECTED FOR
ADDITIONAL RESEARCH

Category	Test No.	Sample Number	Leg No.	Max. Ampl. - fps		
				u	v	w
122213	221	3	1	20	20	22
	221	15	5	22	28	26
	227	3	1	14	18	20
	227	9	3	28	24	34
	239	3	1	20	30	28
	243	9	3	12	12	14
	248	12	6	34	32	26
	258	12	4	12	16	16
	258	18	6	14	14	16
122243	153	3	1	18	18	14
	155	3	1	34	34	38
	155	22	7	40	54	42
	163	9	3	18	24	20
	163	21	7	30	40	34
	178	12	4	10	10	14
	178	18	6	12	14	14
	192	18	6	40	40	30
	200	12	4	10	10	12
	209	3	1	18	20	24
	209	15	5	38	50	34
	209	21	7	26	30	24
	122313	222	6	20	28	20
122143	234	3	4	24	22	26
	244	6	2	12	18	18
	249	3	3	26	26	28
	253	3	1	14	16	16
	253	18	7	18	12	14
	259	3	1	24	18	24
	159	15	7	38	38	38
	162	18	6	34	48	44

TABLE XI.2
 HIGH INTENSITY GUST (F-106) SAMPLES
SELECTED FOR ADDITIONAL RESEARCH

Test No.	Sample Number	Max. Amplitude - fps		
		u	v	w
2-39	7	30	45	45
	8	50	105	75
	9	40	75	50
	10	40	70	60
	12	35	65	40
	13	45	85	50
	15	50	120	50
	18	35	85	75
	19	50	90	65
2-41	10-1	25	50	45
	10-2	35	75	70
	11	35	95	55
	12	40	65	35
	13	30	75	55
	14	35	85	65
	16	50	95	45
	18	35	70	50
	19	35	105	70
	21	40	110	60
	23-1	45	75	45
2-59	11	30	45	40
	12-1	30	60	40
	12-2	65	170	85
	13	45	75	55
	20	50	90	65

51. GUST ACCELERATION INVESTIGATION

The three-component velocities sensed by a gust probe, relative to the probe are the aggregate of true gust velocities and velocities of the probe, both with respect to the earth. Basically, determination of true gust velocities involves subtraction of the probe velocities from the probe sensed relative velocities.

Relative velocities are sensed as impact pressures. However, probe motion velocities, measured relative to the earth, are sensed in terms of accelerations which are then integrated in the time domain to obtain probe velocities with respect to the earth. When the accelerations are integrated with respect to time, any quasi-bias errors appear as trends (drift). This causes the probe velocities at low frequencies to be less accurate than the relative velocities. Drift is known to exist at extremely low frequencies. The actual motion data at these frequencies is small, and when accelerations are integrated in the time domain the drifts tend to mask the motion information.

The gust acceleration technique was devised to improve the resolution of calculated gust velocities at very low frequencies. Calculations are performed in terms of gust accelerations rather than gust velocities. The gust acceleration spectra are then integrated in the frequency domain to obtain the gust velocity spectra.

Drift effects are removed from directly calculated gust velocities by high-pass filtering. Gust accelerations too must be high-pass filtered prior to conversion to gust velocity; however, the advantage of the gust acceleration technique is that the relative amplitudes of unfiltered accelerations at low frequencies are far less than the relative amplitudes of unfiltered gust velocities, and therefore, less filtering is required.

Gust Acceleration Equations

Equations 51.1 are derived by differentiating gust velocity equations. The assumption of small angles was made to reduce the number of terms. It was made after differentiation.

$$\begin{aligned}\dot{u} &= V [(\dot{\alpha} - \dot{\theta})(\theta - \alpha) - (\dot{\beta} + \dot{\psi})(\psi + \beta)] + \dot{v} + g(n_x + \dot{\psi}n_y + \theta n_z) \\ \dot{v} &= V(\phi\dot{\alpha} + \alpha\dot{\phi} - \dot{\psi} - \dot{\beta}) - \dot{v}(\psi + \beta) + g(n_x\psi + n_y + \phi n_z) \\ \dot{w} &= V(\phi\dot{\beta} + \beta\dot{\phi} - \dot{\theta} + \dot{\alpha}) - \dot{v}(\theta - \alpha) + g(n_x\theta - n_y\phi + n_z - 1)\end{aligned}\quad (51.1)$$

If the small angle assumption is made prior to differentiation all the terms involving V except $V\dot{\psi}$, $V\dot{\beta}$, $V\dot{\theta}$, and $V\dot{\alpha}$ disappear.

The effects of small angle assumptions were analyzed. Gust velocities for Test 221, Turbulence Samples 3 and 15, were calculated with and without small angle assumptions. As shown in Figures 51.1 and 51.2 for Sample 3, only slight differences were noted.

Gust accelerations for Test 178, Turbulence Sample 12, were calculated using equations 51.1 and also using equations where small angle assumptions had

been made prior to differentiation. Spectra of these data were computed at the maximum resolution ($\Delta f = 0.0037$ cps) possible. The spectra were compared and found to be essentially equal. Table 51.1 shows standard deviations (σ) of these data over the frequency range of zero to 0.1036 cps. Equations 51.1 are, therefore, adequate for evaluation of the gust acceleration technique.

TABLE 51.1

COMPARISON OF GUST ACCELERATION STANDARD DEVIATIONS - fps²

Component	Gust Acceleration σ (0 to 0.1036 cps)	
	Small Angles Assumed After Differentiation	Small Angles Assumed Before Differentiation
u	0.858	0.944
v	0.528	0.524
w	0.733	0.584

Differentiation

Equations 51.1 require the differentials of α , β , θ , ϕ , ψ , and V. An analysis was performed to determine how these variables could best be arrived at. Newton's Forward and Backward Interpolation Formulae (Reference 51.1) solved for the first derivative were used in the analysis. Gust velocity time series were differentiated using various numbers of differences in the equations. Erratic results were obtained when more than one difference was used. Inspection of the differences showed that errors were being magnified for differences greater than first differences. It was determined, therefore, that differentiation should be accomplished using:

$$\begin{aligned} \left(\frac{dy}{dx} \right)_n &= \frac{1}{\Delta x} (y_{n+1} - y_n) & n = 0 \\ \left(\frac{dy}{dx} \right)_n &= \frac{1}{\Delta x} (y_n - y_{n-1}) & n = 1, 2, 3, \dots, n \end{aligned} \quad (51.2)$$

As a further check on the differentiation, the second moment of the area of the gust velocity spectrum, σ_1 , was calculated for Turbulence Sample 22, Test 155, using Equation 51.3.

$$\sigma_1 = \left[\int_0^k k^2 \Phi(k) dk \right]^{1/2} \quad (51.3)$$

The standard deviation of the time derivative of a function is related to σ_1 over the same frequency interval as shown in Equation 51.4.

$$\sigma_1 2 \pi V = \sigma_{\partial u / \partial t} \quad (51.4)$$

The standard deviation was computed directly from the time history of the time derivative of gust velocity using Equation 51.5.

$$\sigma_{\partial u / \partial t} = \left[\sum_{n=1}^{2700} \frac{(x_n - \bar{x}_n)^2}{n} \right]^{1/2} \quad (51.5)$$

The standard deviation of the time derivative was also computed from the area of the gust acceleration spectra as shown in Equation 51.6.

$$\sigma_{\partial u / \partial t} = \left[\int_0^f \Phi_A(f) df \right]^{1/2} \quad (51.6)$$

Comparisons of $\sigma_{\partial u / \partial t}$ computed from Equations 51.4 through 51.6 are shown in Table 51.2. The fact that these standard deviation values all agreed well indicated that the differentiation and gust acceleration spectra were being correctly computed, and that errors were not being introduced at either low or high frequencies.

TABLE 51.2

COMPARISONS OF GUST ACCELERATION STANDARD DEVIATIONS - fps²

Component	Frequency Range cps	$\sigma_{\partial u / \partial t}$ Equation 51.4	$\sigma_{\partial u / \partial t}$ Equation 51.5	$\sigma_{\partial u / \partial t}$ Equation 51.6
u	0-50	139.2	121.8	121.8
u	0-25	93.6	---	90.4
v	0-10	71.4	---	69.4
u	0-10	50.3	---	50.2
w	0-10	70.6	---	71

Attitude Versus Rate Measurements

Truncated (0-0.1036 cps) standard deviations were calculated for gust accelerations which had been obtained from Test 178, Sample 12, using differentiated

attitude gyro data for $\dot{\theta}$, $\dot{\phi}$, and $\dot{\psi}$. These were compared to corresponding values from gust accelerations using rate gyro data. Only slight differences were noted, the largest of which was for the vertical component as shown in Table 51.3. Therefore, rate gyro measurements were used for the rate of change of attitude variables in Equations 51.1. (It should be noted that the data in Table 51.3 should not be compared directly with data shown in Table 51.1 because different processing techniques were employed for that data. For example, true airspeed had been high pass filtered at 0.04 cps in connection with another investigation.)

TABLE 51.3

EFFECTS OF RATE MEASUREMENTS IN GUST ACCELERATION CALCULATIONS

Component	σ (0-0.1036 cps) Using Rate Measurements	σ (0-0.1036 cps) Using Differentiated Attitude Measurements
u	0.705 fps ²	0.675 fps ²
v	0.541 fps ²	0.521 fps ²
w	0.480 fps ²	0.716 fps ²

Variable Mean Values

The variables n_x , n_y , and n_z in Equations 51.1 are made to have mean values as near to zero as possible by computing the mean of each measurement then subtracting it from each time series sample of the measurement. The same is accomplished for rate gyro measurements. This is done to minimize low frequency errors.

In the evaluation of rate variables in Equations 51.1, means had not been subtracted from the differentiated attitude measurements. These means were small (Table 51.4) however, their effect was evaluated. Also, it was considered possible that the subtraction of the mean of differentiated airspeed might have some effect on results.

TABLE 51.4

MEAN VALUES

Differentiated Measurement	Mean
$\frac{d\theta}{dt}$	0.00088871 deg/sec.
$\frac{d\phi}{dt}$	-0.0045623 deg/sec.
$\frac{d\psi}{dt}$	-0.0045623 deg/sec.
$\frac{dv}{dt}$	0.21883 ft/sec. ²

The gust accelerations were recalculated using differentiated attitudes and airspeed from which the means had been subtracted. Little difference was noted as shown in Table 51.5.

TABLE 51.5

EFFECTS OF DIFFERENTIATED AIRSPEED AND ALTITUDE MEANS

Component	σ (0-0.1036 cps) Without Means Subtracted	σ (0-0.1036 cps) With Means Subtracted
u	0.675 fps^2	0.667 fps^2
v	0.521 fps^2	0.529 fps^2
w	0.716 fps^2	0.715 fps^2

Integration of the Gust Acceleration Spectrum

If a time series is infinite in length, and has a zero mean, it and its derivative may be expressed by:

$$x(t) = \sum_{n=0}^{\infty} (a_n \cos \omega_n t + b_n \sin \omega_n t)$$

$$\dot{x}(t) = \sum_{n=0}^{\infty} (-a_n \omega_n \sin \omega_n t + b_n \omega_n \cos \omega_n t)$$
(51.7)

These time series have an infinite number of power spectrum values given by:

$$\Phi_x(\omega_n) = T (a_n^2 + b_n^2)$$

$$n = 0, 1, 2, \dots \infty$$

$$\Phi_{\dot{x}}(\omega_n) = T \omega_n^2 (a_n^2 + b_n^2)$$
(51.8)

and are simply related by Equation 51.9.

$$\Phi_x(\omega_n) = \frac{1}{\omega_n^2} \Phi_{\dot{x}}(\omega_n)$$
(51.9)

The gust acceleration technique was devised to use Equation 51.9 for converting gust acceleration spectrum values to gust velocity spectrum values. In this technique acceleration spectrum estimates are converted to velocity spectrum estimates at the fine resolution (maximum resolution possible, $\Delta f = 1/T$). The procedure from this point on is equivalent to that used for gust velocity data. The fine resolution estimates are averaged over frequency intervals to

give the desired final resolution and then "hanned" to obtain the smoothed spectrum estimates. Gust velocity standard deviations calculated from the areas of the computed gust velocity spectra are used to represent the gust velocity time series standard deviations.

The errors involved in using Equation 51.9 for finite turbulence samples were evaluated. Spectra of the three components of gust velocity for Test 155, Turbulence Sample 22, were computed. The same gust velocity time series were differentiated. Gust velocity spectra were calculated from the differentiated gust velocities using the technique established for gust accelerations. The directly computed velocity spectra and those obtained using the ω_n^2 transformation were compared. These comparisons are shown in Figure 51.3.

For further evaluation of the accuracy of the computations, the standard deviations calculated from the areas of computed gust velocity spectra were compared with the standard deviations calculated from the gust velocity time series. These comparisons are shown in Table 51.6.

TABLE 51.6

COMPARISONS OF GUST VELOCITY STANDARD DEVIATIONS - fps

Component	From Gust Velocity Time Series	From Gust Acceleration Spectra
v	10.3	10.4
w	6.6	6.8
u	7.6	7.8

High-Pass Filtering of Gust Accelerations

Some degree of high-pass filtering is required to remove the drift in gust acceleration data. This can be seen from the comparisons given in Table 51.7 and Figure 51.4.

TABLE 51.7

COMPARISON OF STANDARD DEVIATIONS AND SCALE LENGTHS
CALCULATED FROM FILTERED AND UNFILTERED GUST
ACCELERATION DATA (TEST 159, SAMPLE 15)

Component	Unfiltered		Filtered	
	σ_t - fps	L - Ft.	σ_t - fps	L - Ft.
u	26.6	38,647	6.2	453
v	23.3	20,944	8.2	834
w	18.2	7,294	6.3	331

One set of spectra in Figure 51.4 are from directly computed gust velocities which were filtered in the time domain below 0.046 cps. The other set are

from gust accelerations which were converted to gust velocities without high-pass filtering. Drift in the unfiltered data is obvious. Slopes of the spectra between the first and second estimates are approximately $-14/3$, nearly three times steeper than those for the inertial subrange. Scale lengths and standard deviations are extremely high.

As discussed in Appendix III, data end extensions are required to give the desired sample length after high-pass filtering. For gust velocity data the method of folding and inverting the required number of samples about the first and last data samples was found to be the most accurate. Unfiltered gust velocity time functions are basically ramp functions due to large drifts encountered when acceleration measurements are integrated. Simply folding out the ends to allow filtering yields a function similar to a back-to-back sawtooth. This results in the introduction of erroneous low frequencies. Folding and inverting, on the other hand, maintains the ramp trend and therefore gives more realistic results.

Unfiltered gust acceleration time functions do not have the ramp function characteristic. Folding and inverting them introduces low frequencies since they do not necessarily start and stop at the same magnitude. More realistic results were obtained in this case when only the ends were folded out. PSD's of filtered and unfiltered gust accelerations are compared in Figure 51.5. One striking thing about comparisons of gust acceleration and gust velocity spectra (e.g., Figures 51.4 and 51.5) is how small variations of gust acceleration at low frequency cause dramatic changes in gust velocity.

Next, the feasibility of filtering in the frequency domain was investigated. This technique appeared attractive for the gust acceleration data since:

- Spectrum estimates were available at high resolution, a necessity for accurate transformation.
- End extensions are not required as in the time domain filtering approach.
- Frequency filtering is computationally expedient. The filter transform can be combined with the transform for converting from acceleration to velocity. This virtually eliminates one computer run (for time filtering). The result was a sizeable savings in both flow time and computer usage.

Turbulence Sample 15 from Test 159 was chosen for the analysis of filtering effects. The gust acceleration data had been obtained during a standard production computer run. No attempts had been made to introduce the special techniques (airspeed mean removal, differentiation of attitude measurements, etc.) previously investigated. A mixture of attitude and rate gyro measurements had been used in the calculations, i.e.,

$$\theta, \phi, \int \dot{\psi} dt, \dot{\theta}, \dot{\phi}, \dot{\psi}$$

where dots indicate rate gyro measurements.

Filtering in the frequency domain was accomplished as follows:

$$\Phi_v(f) = \frac{\Phi_A(f)}{(2\pi f)^2} G(f)^2 \quad (51.10)$$

where:

$\Phi_v(f)$ = Filtered gust velocity estimates

$\Phi_A(f)$ = Unfiltered gust acceleration estimates

$G(f)$ = Filter gain factor

The gust acceleration data were subjected to time domain filtering. This filtering was the same as used for LO-LOCAT gust velocity data (attenuation below 0.046 cps) except end extensions were folded rather than folded and inverted. Figure 51.6 illustrates the results obtained. Good agreement is shown between frequency and time filtered data except for the first point. Here the frequency filtered gust acceleration more closely agrees with the spectrum computed directly from the gust velocity.

Therefore, the 30 turbulence samples in Table XI.1 were processed as follows:

- Calculate gust accelerations using Equations 51.1.
- Use the attitude data previously used in gust velocity calculations for θ , ϕ , and ψ and rate gyro measurements for $\dot{\theta}$, $\dot{\phi}$, and $\dot{\psi}$.
- Filter in the frequency domain.

Accuracy of Gust Velocity Spectra Computed from Gust Accelerations

Gust accelerations were calculated for the 30 turbulence samples using the 0.046 filter. These spectra were converted to gust velocity spectra. Average, normalized gust velocity spectra were calculated. Spectra obtained from the gust acceleration are compared to those obtained directly from gust velocities in Figures 51.7 through 51.9. Von Karman spectra are also shown for comparison.

Essentially the same results were obtained by the two methods for longitudinal and vertical spectra. Lateral spectrum values obtained from the gust acceleration appear to agree with the von Karman spectrum slightly better than those from the gust velocity. Also the dip in the spectrum from .01 to .04 KL appear to be reduced somewhat.

Gust velocity standard deviations were calculated based on the square root of the areas under the gust velocity spectra which had been obtained from the gust accelerations. Limits of the integration were from zero to fifty cps. These were compared to directly computed gust velocity time series standard deviations. Distributions of the differences obtained are shown in Figure 51.10. The standard deviations from the gust acceleration technique were slightly less in the case of longitudinal gust velocity and slightly greater for vertical and lateral.

Turbulence scale lengths were calculated from the gust velocity spectra obtained by the gust acceleration technique. They were calculated based on the von Karman mathematical expressions. Distributions of differences between these scale lengths and those computed originally are shown in Figure 51.11. Scale lengths from the gust acceleration technique were slightly larger for the longitudinal and vertical components. As in the case of gust velocity standard deviations, the largest scale length differences were noted for the lateral component.

As shown by Equation 51.4 the standard deviation of gust acceleration is directly related to σ_1 calculated from gust velocity. The gust accelerations calculated were evaluated by making this comparison. Both the gust acceleration σ and the gust velocity σ_1 were based on the frequency range from zero to ten cps. The gust velocity time series had been high-pass filtered; however, high-pass filtering was not accomplished for the determination of gust acceleration standard deviations. As mentioned previously, the gust acceleration power density is very low at low frequencies and therefore, high-pass filtering had negligible effect on the value of the gust acceleration standard deviation.

Distributions of gust acceleration σ and gust velocity σ_1 values, adjusted to the same units, are compared in Figure 51.12. Close agreement between the two distributions is shown.

Accuracy of Gust Velocity Spectra From Gust Accelerations with Less High-Pass Filtering

The possibility of altering the filter transfer function to provide less filtering of the gust accelerations while maintaining valid gust velocities was investigated.

Maximum resolution gust velocity estimates were obtained from Test 178, Sample 12, gust accelerations computed using differentiated attitude measurements. The characteristic of these data is illustrated in Figure 51.13. In the case of gust acceleration, practically all the drift is concentrated in the first five maximum resolution spectrum estimates. It appeared that there should be little difference between directly computed gust velocity spectra filtered out to the twelfth estimate and gust velocity spectra obtained from gust acceleration filtered out to the sixth estimate.

The filter gain factor shown in Figure 51.14 was used. This placed the frequency below which attenuation occurred at 0.026 cps which is approximately one-half of that previously used. Ten samples were rerun with this modified filter. Four of these samples were also run without filtering. Effectiveness of the 0.026 filter compared to the 0.046 filter is indicated in Table 51.8. The amount each filter reduced the unfiltered standard deviation is given.

TABLE 51.8
 COMPARISON OF GUST VELOCITY STANDARD DEVIATIONS
 WITH TWO DIFFERENT HI-PASS FILTERS

Test	Sample	Component	Reduction in Standard Deviation Percent	
			0.046 Filter	0.026 Filter
159	15	u	76.3	75.6
		v	64.8	61.3
		w	64.8	63.8
178	12	u	52.0	48.0
		v	44.2	44.2
		w	27.8	25.0
221	3	u	45.1	42.2
		v	37.7	34.8
		w	65.2	60.0
221	15	u	58.2	55.4
		v	31.4	29.1
		w	18.2	13.6

The 0.046 filter reduced the standard deviations an average of 48.8 percent while the 0.026 filter reduced them an average of 46.1 percent.

It would appear, based on the samples analyzed, that the 0.026 frequency domain filter was essentially as effective as the 0.046 frequency domain filter in removing drift.

Average spectra were computed for the 10 turbulence samples that had been filtered with the 0.026 filter. Average spectra were also computed for the same 10 samples filtered with the 0.046 filter. The spectra are compared in Figures 51.15 through 51.17. As indicated by the plots and Table 51.9, the 0.026 filter yielded slightly higher turbulence scale lengths. This is to be expected since the range of frequencies involved was extended to larger wavelengths.

TABLE 51.9
FILTER EFFECT ON SCALE LENGTH

Component	Average Scale Length - Feet	
	0.046 Filter	0.026 Filter
u	823	1100
v	769	929
w	616	762

The question naturally arises that if filtering below 0.026 works so well for the gust acceleration technique, what would be its effect on directly computed gust velocities? Gust velocities calculated for Sample 12 of Test 178 were subjected to high-pass filtering both in the time and frequency domains. The frequency domain filter had the gain function shown in Figure 51.14, with attenuation below 0.026 cps. The time domain filter consisted of the Ormsby gain function shifted to attenuate below 0.023 cps.

The frequency domain filter gave obviously erroneous results as shown in Figure 51.18. This was expected since previous analysis (Figures 2.15 through 2.17, Reference I.2) had shown that the large excursions in unfiltered gust velocities distort spectra calculations throughout the frequency range. Since frequency domain filter operates on the estimates themselves, these errors are reduced only at low frequencies.

The time domain filter removes the large excursions prior to spectrum calculations. Spectra of gust velocity time series filtered in the time domain below 0.023 are compared in Figure 51.18 to gust acceleration spectra converted to gust velocity estimates and filtered below 0.026 in the frequency domain. Higher estimates at the low frequencies and higher standard deviations and scale lengths for the time domain filtered data are attributed to the shallower slope of this filter.

Determining the Distribution of the Gust Velocity Level Crossings by Using Gust Acceleration Data

As discussed previously, the shape of the gust velocity spectra, scale lengths, and standard deviations can be satisfactorily determined from gust acceleration data. The airplane designer is also interested in the level crossing distributions of gust velocities. These too, it was found, can be determined from gust acceleration data.

The probability of the gust velocity being equal to or greater than a given level, α , is given by:

$$P_g = N_{\alpha g} / N_{Lg} \quad (51.11)$$

Where $N_{\alpha g}$ is the number of times the gust velocity crosses a given level with a positive slope and N_{Lg} is the total number of times the gust velocity crosses the zero level.

Likewise, the probability of the gust acceleration being equal to or greater than a given level is:

$$P_a = N_{\alpha a} / N_{La} \quad (51.12)$$

By dividing Equation (51.11) by Equation (51.12), one obtains:

$$P_g = P_a \left(\frac{N_{\alpha g}}{N_{\alpha a}} \right) \frac{N_{La}}{N_{Lg}} \quad (51.13)$$

P_a can be determined directly from the gust acceleration data. Example plots of this parameter versus the standardized variable, t , are shown in Figure 51.19, where:

$$t = y / \sigma_y \quad (51.14)$$

where y = the amplitude level and σ_y is the standard deviation.

The amplitude levels of gust accelerations were calculated at rather arbitrarily selected levels of 100 fps². Also shown on these plots for comparisons are P_g versus its respective standardized variable. Gust velocity level crossings were determined at 2 fps intervals, as discussed elsewhere in this document.

N_{Lg} in Equation 51.13 can be derived from Rice's equation:

$$N_{Lg} = \frac{1}{\pi} \frac{\sigma_{ta}}{\sigma_{tg}} \text{ (sample length in seconds)} \quad (51.15)$$

The maximum gust velocity may be estimated as shown in Equation 51.16.

$$\text{Max. Gust} = 5 \sigma_{tg} \quad (51.16)$$

For a normal distribution, the percent probability that an observed value differs from its mean by more than 5σ is 5.73×10^{-5} , Reference 8.4. A plot of σ_{tg} versus the maximum gust recorded for the 30 turbulence samples studied is shown in Figure 51.20. As observed, Equation 51.16 fits the experimental data very well.

The ratio N_{ag}/N_{aa} in Equation 51.13 may be determined by interpolation of the curves shown in Figure 51.21. The plots of $\frac{N_{ag} N_{La}}{N_{aa} N_{Lg}}$ versus $t_{aa}^2 - t_{tg}^2$ were

calculated from samples for which the number of levels of acceleration was at least eight. The curves are apparently functions of scale length (spectrum shape). The interpolation was accomplished as follows:

- The scale length and σ_g was determined for the sample.
- The gust velocity standardized variable, t_g , was then calculated for each 2 fps interval of gust velocity.
- Values of $\frac{N_{ag} N_{La}}{N_{aa} N_{Lg}}$ were obtained from the curves in Figure 51.21 and cross plotted versus scale length on semilog paper.
- The value of $\frac{N_{ag} N_{La}}{N_{aa} N_{Lg}}$ was determined from the cross plot at the appropriate scale length.
- N_{ag} was then calculated by multiplying the quantity $\frac{N_{ag} N_{La}}{N_{aa} N_{Lg}}$ by $\frac{N_{Lg} N_{aa}}{N_{La}}$.

The probabilities of the gust velocities being equal to or greater than given magnitudes were computed from the level crossings. The probabilities obtained from gust accelerations and those obtained directly from the gust velocity time functions are compared in Figure 51.22.

The probabilities compared reasonably well for all three components for the particular turbulence sample selected. Some of the samples, especially those which have a small number of levels, (i.e., smaller standard deviations) probably would not have compared as well. However, it is believed that if these calculations had been performed for all 30 turbulence samples combined, then the gust velocity probability distributions for the entire 30 samples obtained from acceleration data would have agreed reasonably well with those obtained from gust velocity data.

It should be noted that the relationships defined in the curves of Figure 51.21 could be better established. For example, the number of levels of accelerations would have more closely agreed with the number of levels of gust velocities if acceleration level intervals of 80 fps² instead of 100 fps² had been selected. Also, more samples should have been used to establish the relationships; however, time did not allow for a more detailed analysis to be accomplished. In order for gust acceleration data to be used to determine gust velocity distributions, relationships similar to those shown in Figure 51.21 would have to be known for all possible categories. It is possible that more general, all inclusive, sets of relationships could be established. For example, the ordinate and abscissa for the data shown in Figures 51.21 were arrived at by dividing Rice's equation for gust velocity level crossings by his equation for gust acceleration level crossings which results in:

$$\frac{N_{ag} N_{La}}{N_{Lg} N_{aa}} = e^{1/2(t_a^2 - t_g^2)} \quad (51.17)$$

If the probability density functions of level crossings are used, the appropriate relationship is:

$$\frac{\alpha_g F_g \sigma_g^2}{\alpha_a F_a \sigma_a^2} = e^{1/2(t_a^2 - t_g^2)} \quad (51.18)$$

where:

F_g = The probability density function of the gust velocity level crossings, and

F_a = The probability density function of the gust acceleration level crossings.

F_g would be determined in a manner similar to that described for determining N_{ag} . Once F_g is established, N_{ag} would be determined either by:

$$N_{\alpha g} = N_{Lg} \int_0^{\alpha_{max}} F_g d\alpha \quad (51.19)$$

or from Equations 51.17 and 51.18 as follows:

$$N_{\alpha g} = \frac{\alpha_a F_g \sigma_g^2}{\alpha_g F_a \sigma_a^2} \frac{N_{Lg} N_{\alpha a}}{N_{La}} \quad (51.20)$$

This approach may result in a more satisfactory general solution because the effect of band levels of gust acceleration and velocity are included.

However, it was not the purpose of this discussion to define the exact relationships necessary for determining gust velocity distributions from gust acceleration measurements for all possible conditions, but it was the intent to show that the method was feasible.

Comparison of Primary Peak, Level Crossing, and Amplitude Count Statistics

Gust acceleration level crossing, amplitude counts, and primary peak statistics for the 30 samples of Table XI.1 are compared in Figure 51.23. The probability distributions for the three components of each of the three types of data are essentially the same varying with the standard deviation of the data. The standard deviations are given in Table 51.10. It can be seen that the level crossing and cumulative primary peak probability distributions agree very closely. The cumulative amplitude count probability distributions are slightly lower than the other two.

TABLE 51.10

PRIMARY PEAK, AMPLITUDE, AND LEVEL CROSSING STANDARD DEVIATIONS FOR CATEGORY 122000

Component	Gust Acceleration Standard Deviations - fps^2		
	Primary Peaks	Amplitude Counts (Time Series)	Level Crossings
u	124	99	108
v	132	100	132
w	140	107	144

Normalized level crossing probability density functions are shown in Figure 51.24. Not only are they the same for each gust acceleration component, gust acceleration and velocity functions are in good agreement especially at high values of t. This is possibly due to the fact that pooling of the turbulence samples by band causes the overall distribution to approach a limit distribution.

The gust velocity statistics used for comparison were calculated from the combination of all the LO-LOCAT Phase III data obtained at 750 feet above high mountains in stable air. This involved 147 turbulence samples, 117 more than

that for the gust acceleration statistics. The scope of this study did not allow segregation of the 30 gust velocity samples which correspond directly to the 30 gust acceleration samples analyzed. The procedure required would have involved a complete rerun of the 30 gust velocity samples. It appears however, that had this been done, the statistics would have been essentially the same.

The implication is that it may be possible to obtain gust velocity time series statistics directly from gust acceleration statistics if at least 30 samples are pooled for the calculations. Assuming that gust velocity and acceleration values have the same normalized density function, gust velocity probabilities would be determined by integrating the acceleration function and unnormalizing using the gust velocity standard deviation.

This procedure would be valid without question if gust velocity amplitude samples were normally distributed. Any stochastic process, such as the derivative of a function, derived by linear operations from a normal process, is itself a normal process. This fact is proved in Reference 51.2. Unfortunately the velocity and acceleration distributions deviate from the normal as shown in Figure 51.25. The data shown in this figure are compared to Rice's equation for level crossings which was derived assuming that a function and its derivative are characterized by normally distributed amplitudes.

The dashed curves of Figure 51.24 were developed based on Rice's equation for individual turbulence samples. Their equation (51.21) describes the distribution resulting from pooling, by band, a number of level crossing distributions, each of which is from a function with normally distributed amplitudes.

$$f(\alpha) = \frac{\alpha}{N_0} \left[\sum_{i=1}^n \frac{N_{0_i}}{\sigma_i^2} e^{-\frac{\alpha^2}{2\sigma_i^2}} \right] \quad (51.21)$$

where:

$$N_0 = \sum_{i=1}^n N_{0_i}$$

Values of σ_i and N_{0_i} for the thirty samples in question were used in Equation 51.21 to establish the dashed curves. They were normalized by the overall level-crossing standard deviation.

The gust acceleration level crossing normalized probability density data of Figure 51.24 were fit with the solid curve having Equation 51.22.

$$\sigma_L f(\alpha) = 1.42 e^{-1.45 t} + 0.0121 e^{-0.672 t} \quad (51.22)$$

Equation 51.22 yields the cumulative probability function of Equation 51.23.

$$\begin{aligned}
 P(\alpha) &= \int_{\alpha}^{\infty} f(\alpha) d\alpha \\
 &= 0.982 e^{-1.45t} + 0.018 e^{-0.672t}
 \end{aligned} \tag{51.23}$$

This function is compared in Figure 51.26 to cumulative probabilities computed from actual gust velocity level crossing counts. Good agreement of Equation 51.23 with the data tends to substantiate the notion that pooled gust acceleration data possess a reproductive property such that gust velocity and acceleration distributions are closely related.

Test 221, Sample 3
— Small Angles Assumed
--- Small Angles Not Assumed

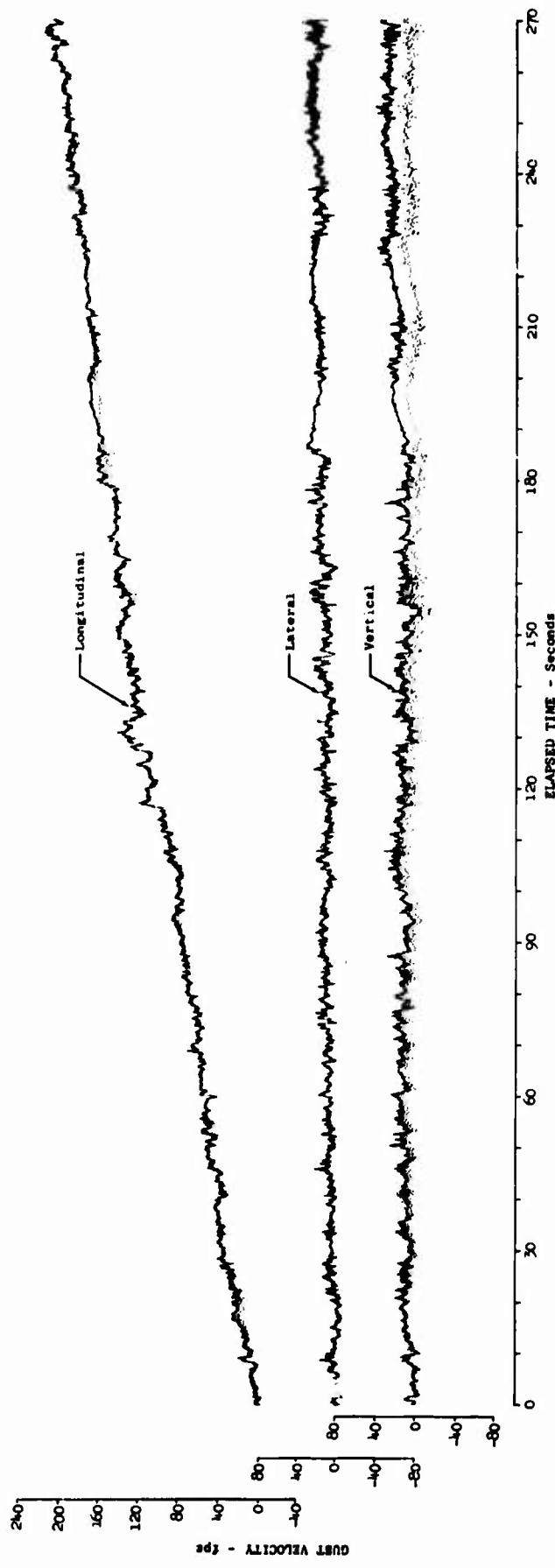


Figure 51.1 Effect of Small Angle Assumption on Gust Velocity Time Series

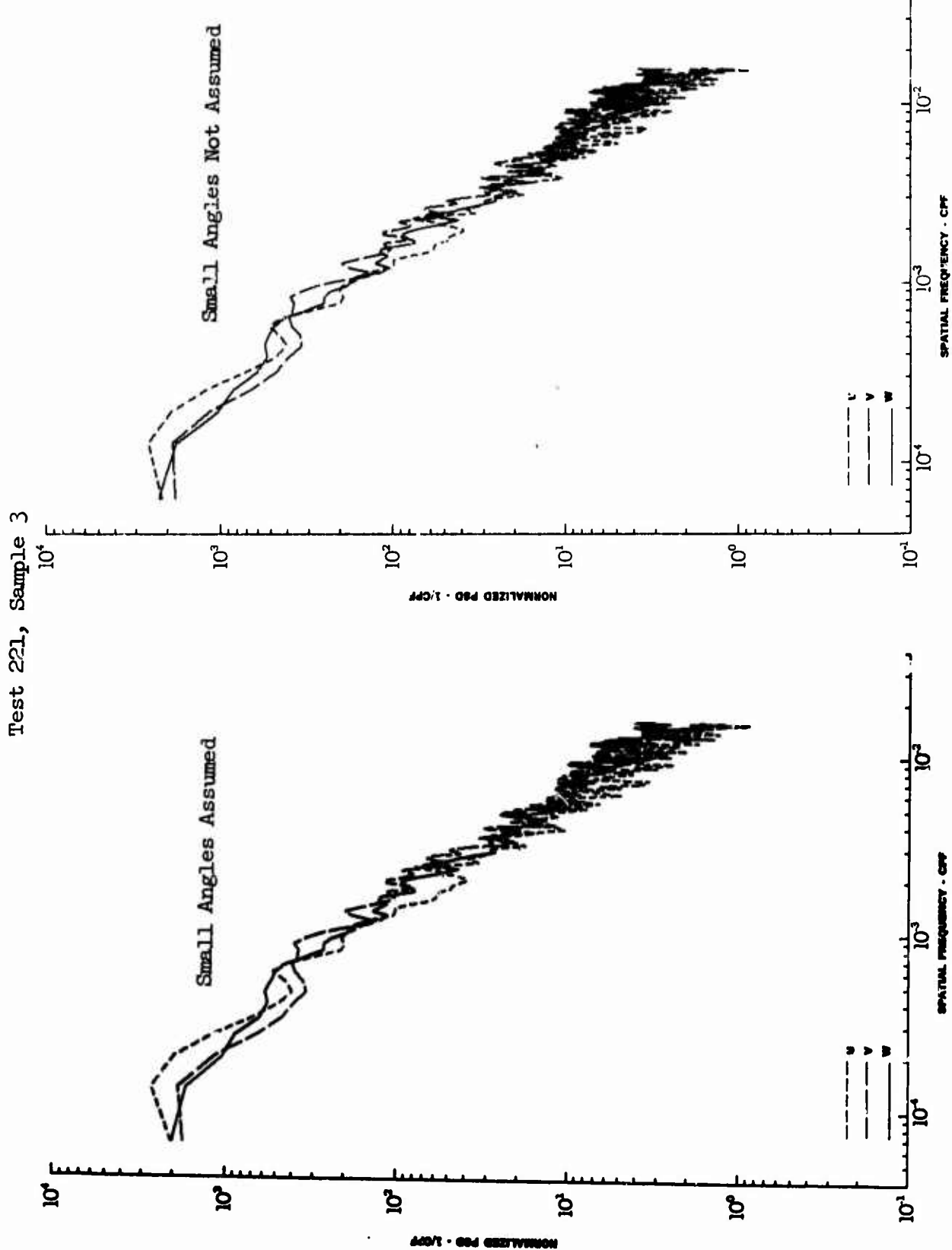


Figure 51.2 Effect of Small Angle Assumption on Gust Velocity Spectra

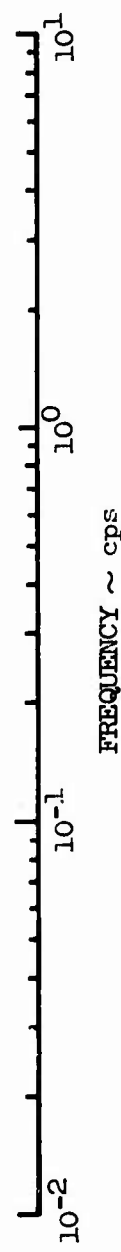
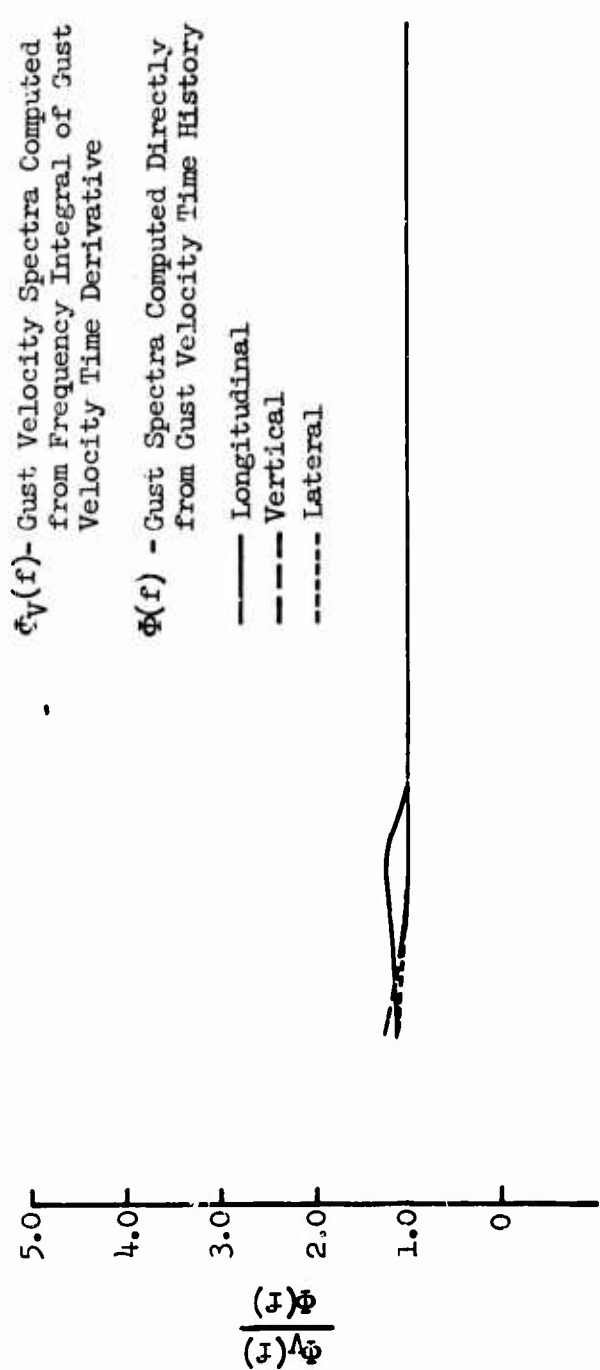


Figure 51.3 Comparisons of Gust Spectra

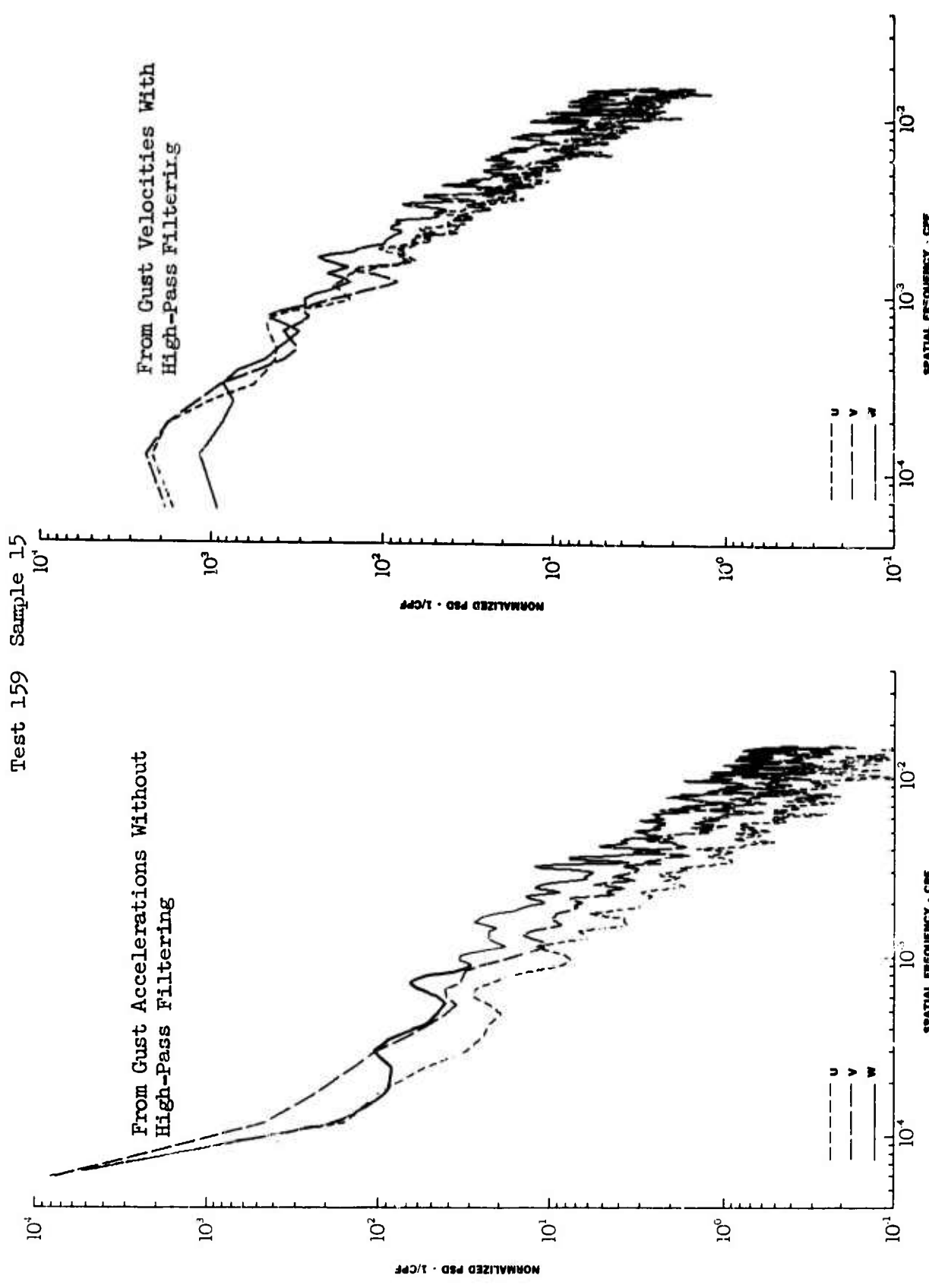


Figure 51.4 Drift in Gust Velocities Obtained from Gust Accelerations Without High-Pass Filtering

Test 159 Sample 15

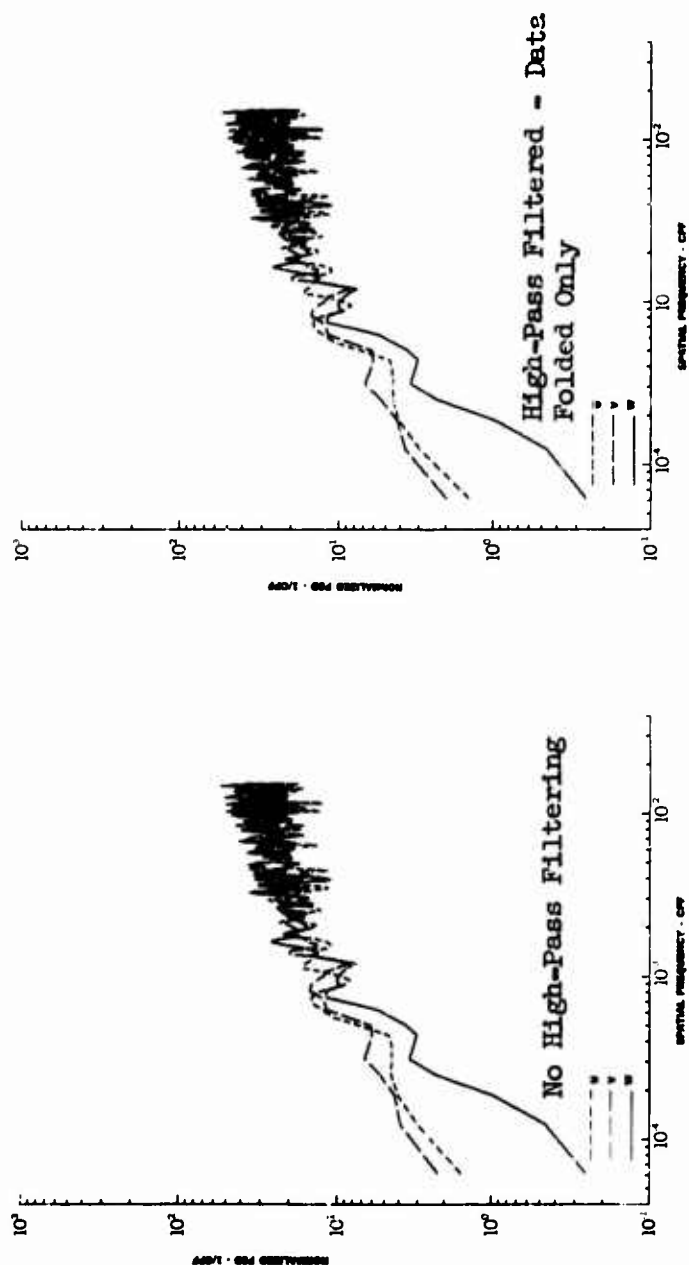


Figure 51.5 Effects of Data Extension on Gust Acceleration Spectra

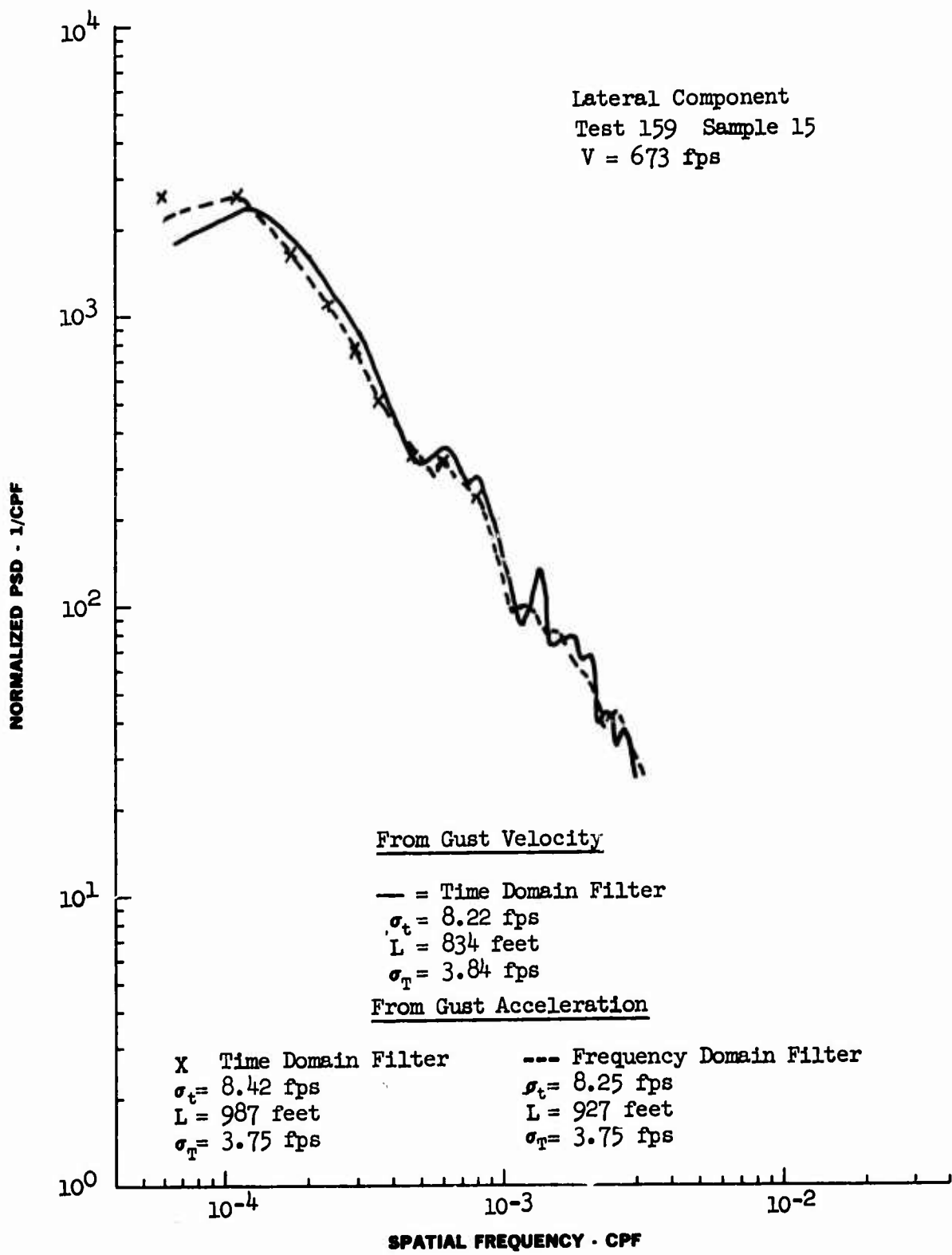


Figure 51.6 Comparison of Gust Velocity Spectra
Obtained Using 0.046 cps Time and
Frequency Domain Filters

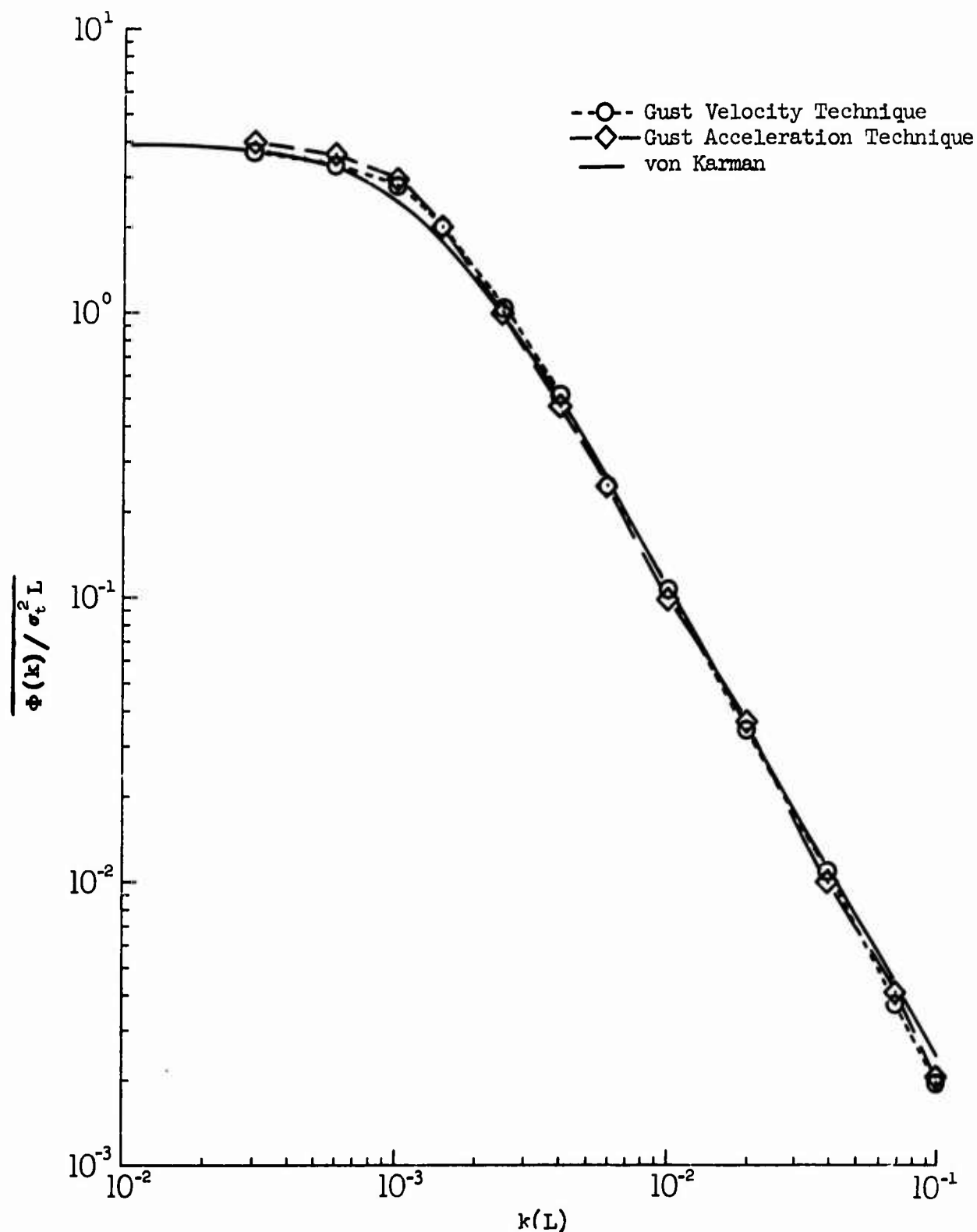


Figure 51.7 Average of Thirty Longitudinal Spectra

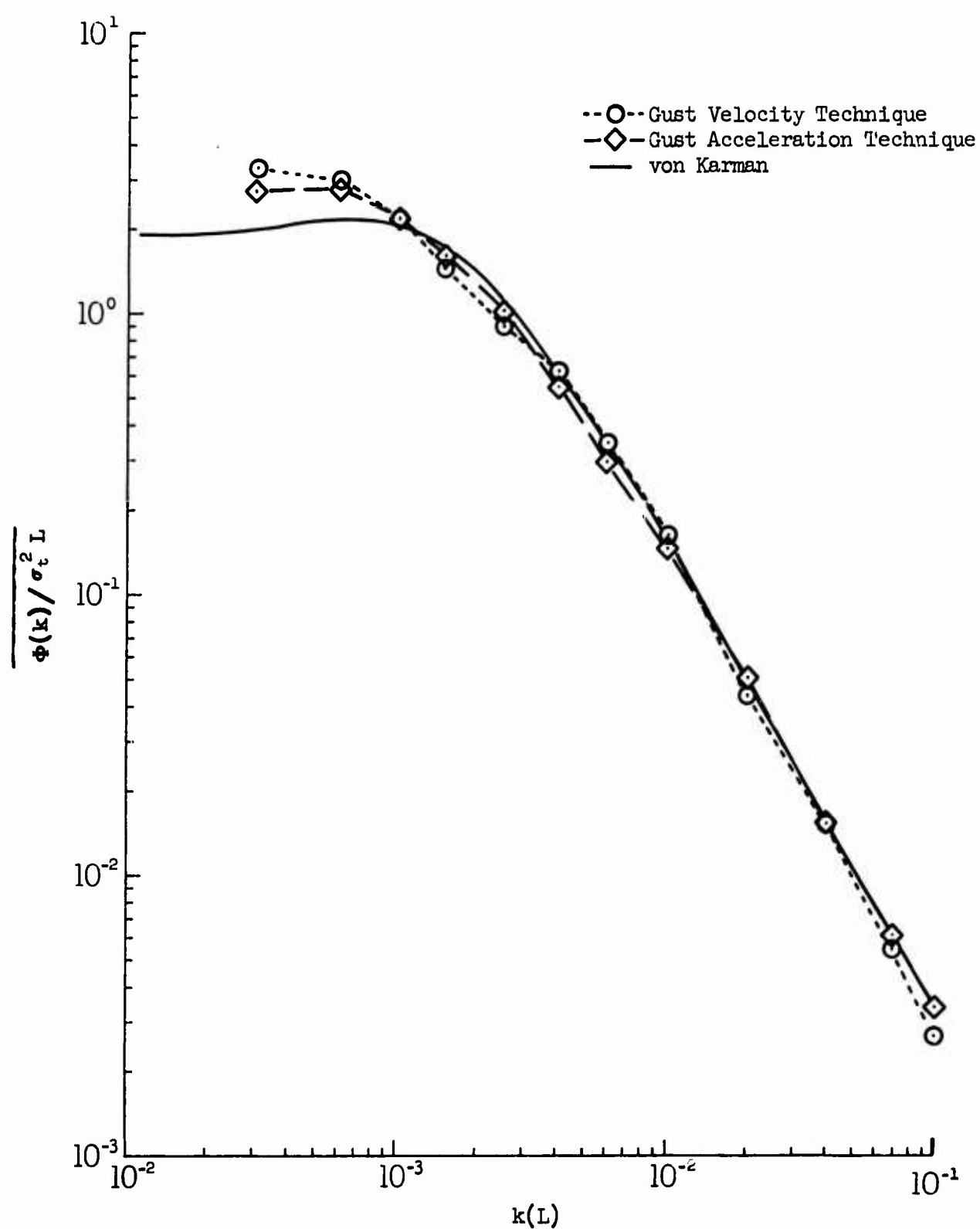


Figure 51.8 Average of Thirty Lateral Spectra

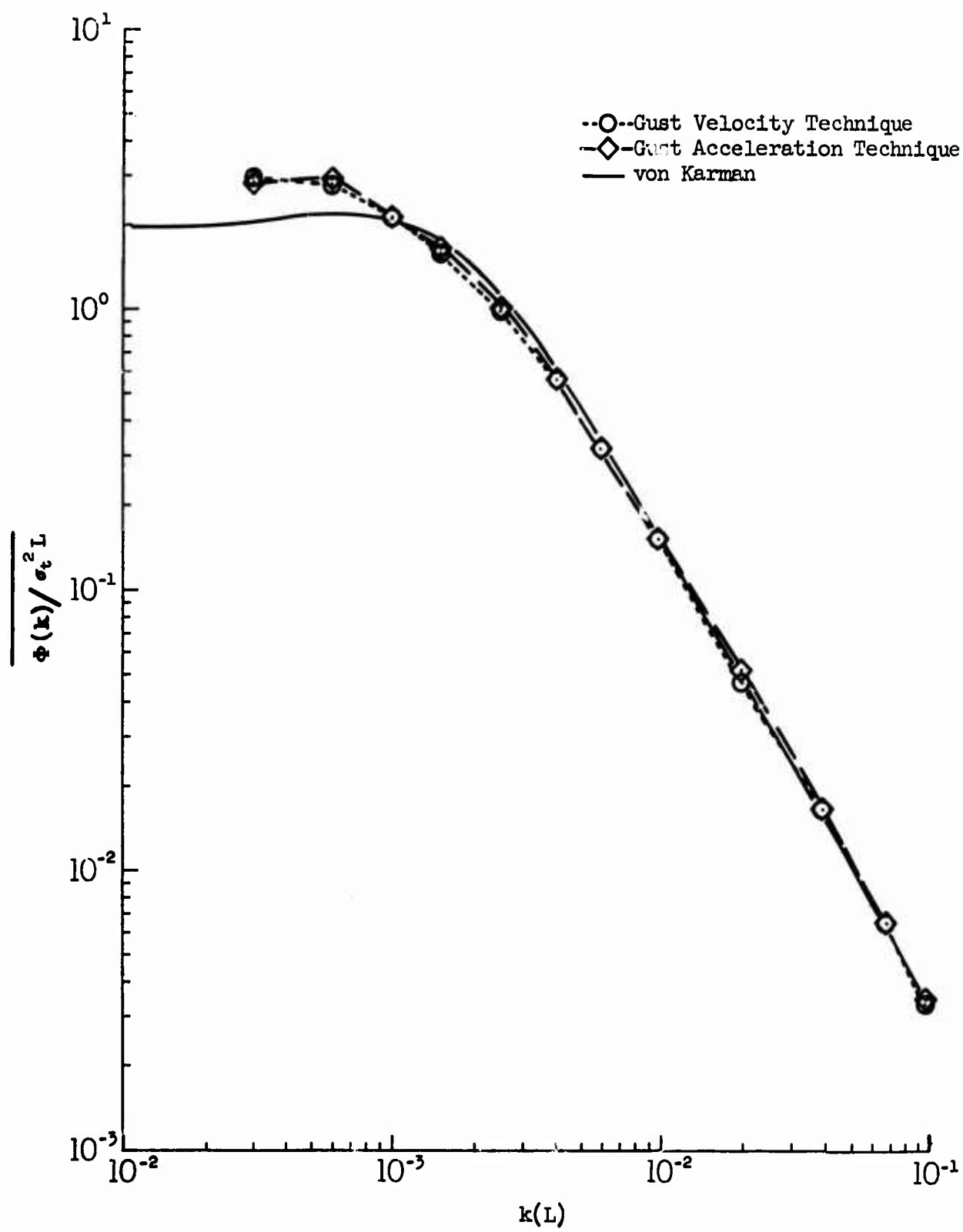
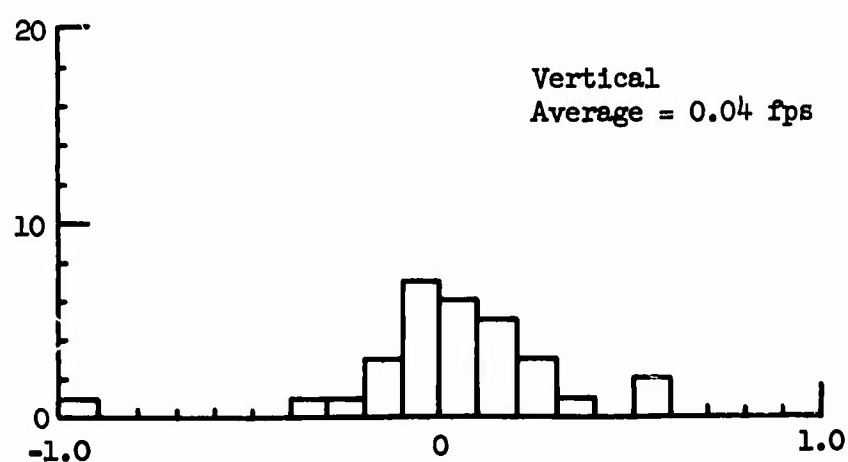
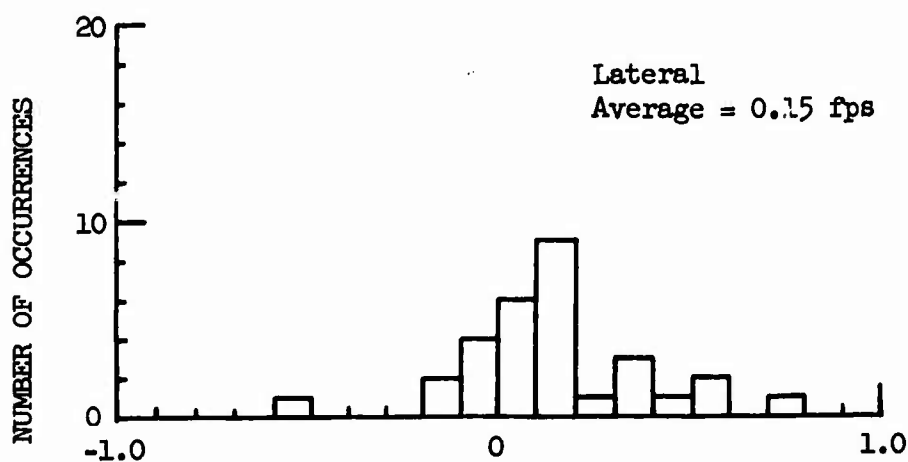
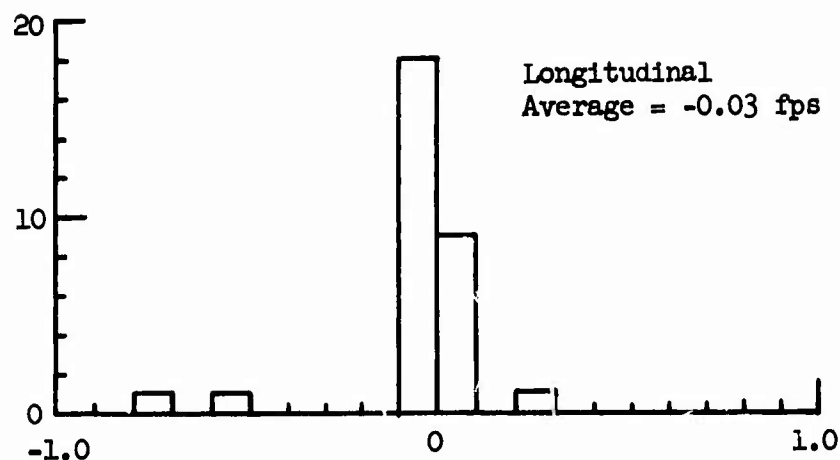
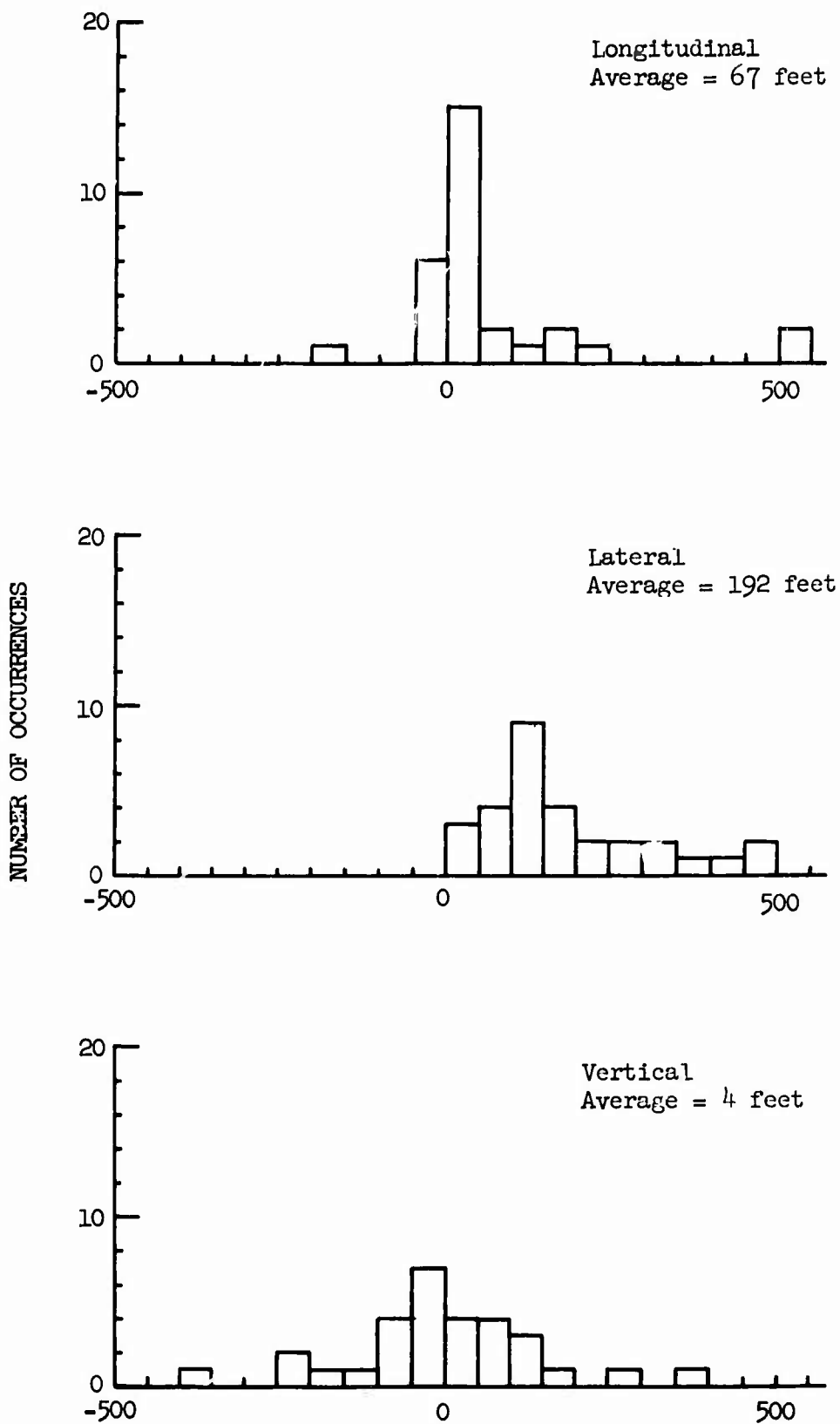


Figure 51.9 Average of Thirty Vertical Spectra



σ FROM GUST ACCELERATION TECHNIQUE - σ FROM GUST VELOCITY TECHNIQUE - fps

Figure 51.10 Comparison of Gust Velocity Standard Deviations Obtained from the Gust Velocity and Acceleration Techniques



L FROM GUST ACCELERATION TECHNIQUE - L FROM GUST VELOCITY TECHNIQUE - feet

Figure 51.11 Comparison of Turbulence Scale Lengths
Obtained from the Gust Velocity and
Acceleration Techniques

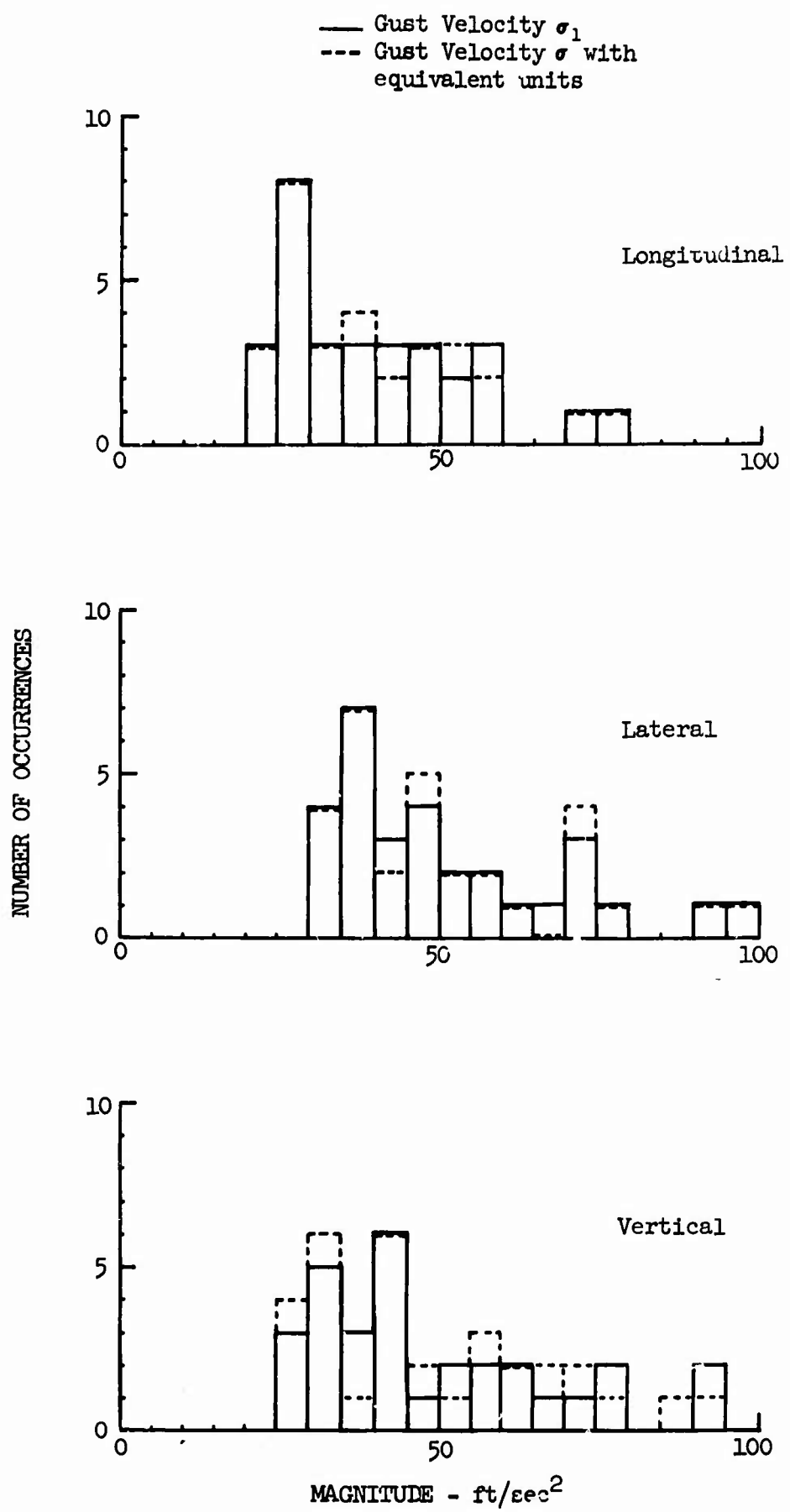


Figure 51.12 Comparison of Gust Velocity σ_1 and Gust Acceleration σ

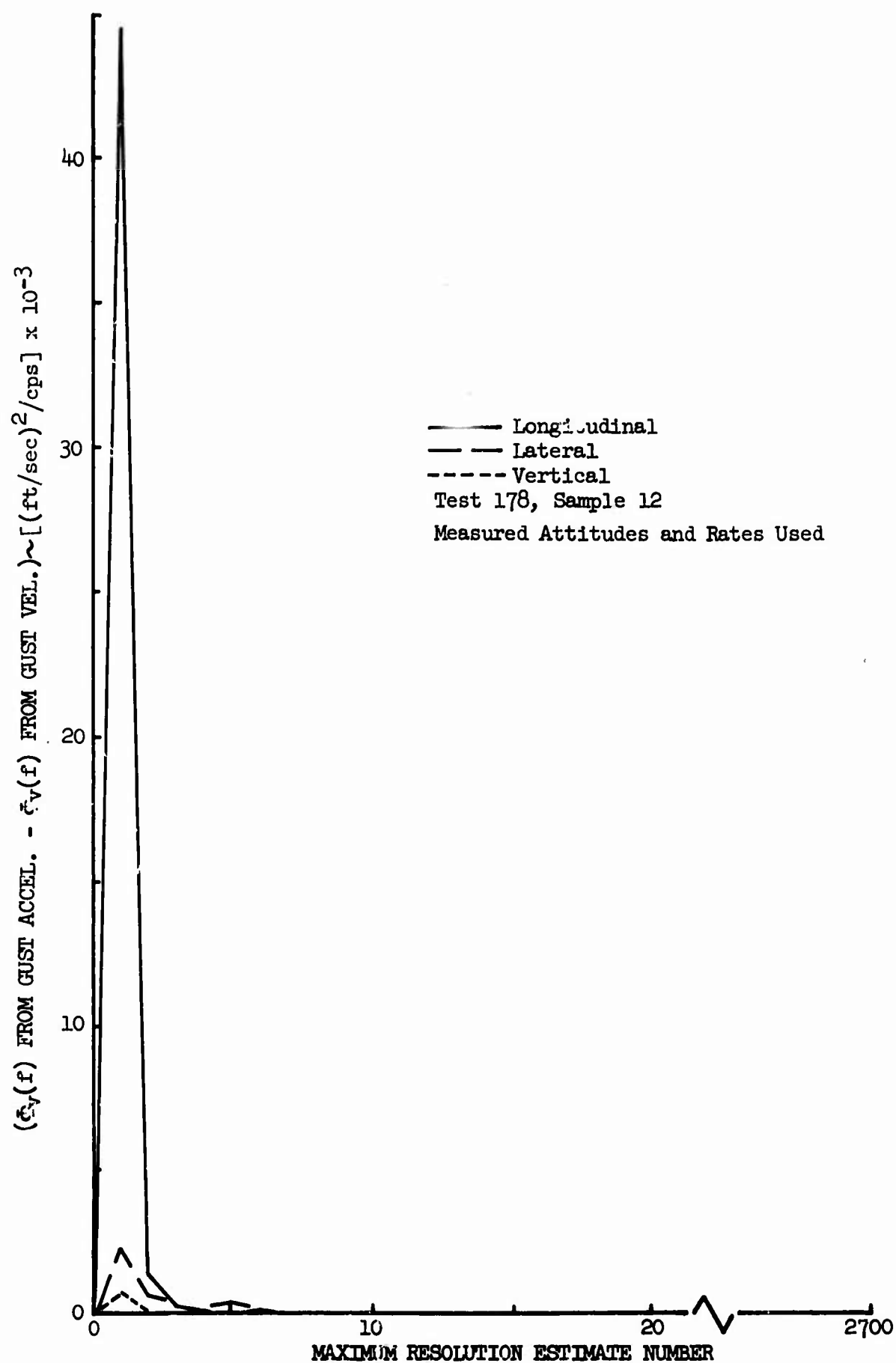


Figure 51.13 Difference Between Gust Velocity Spectrum Estimates from Unfiltered Gust Acceleration and Filtered Gust Velocity

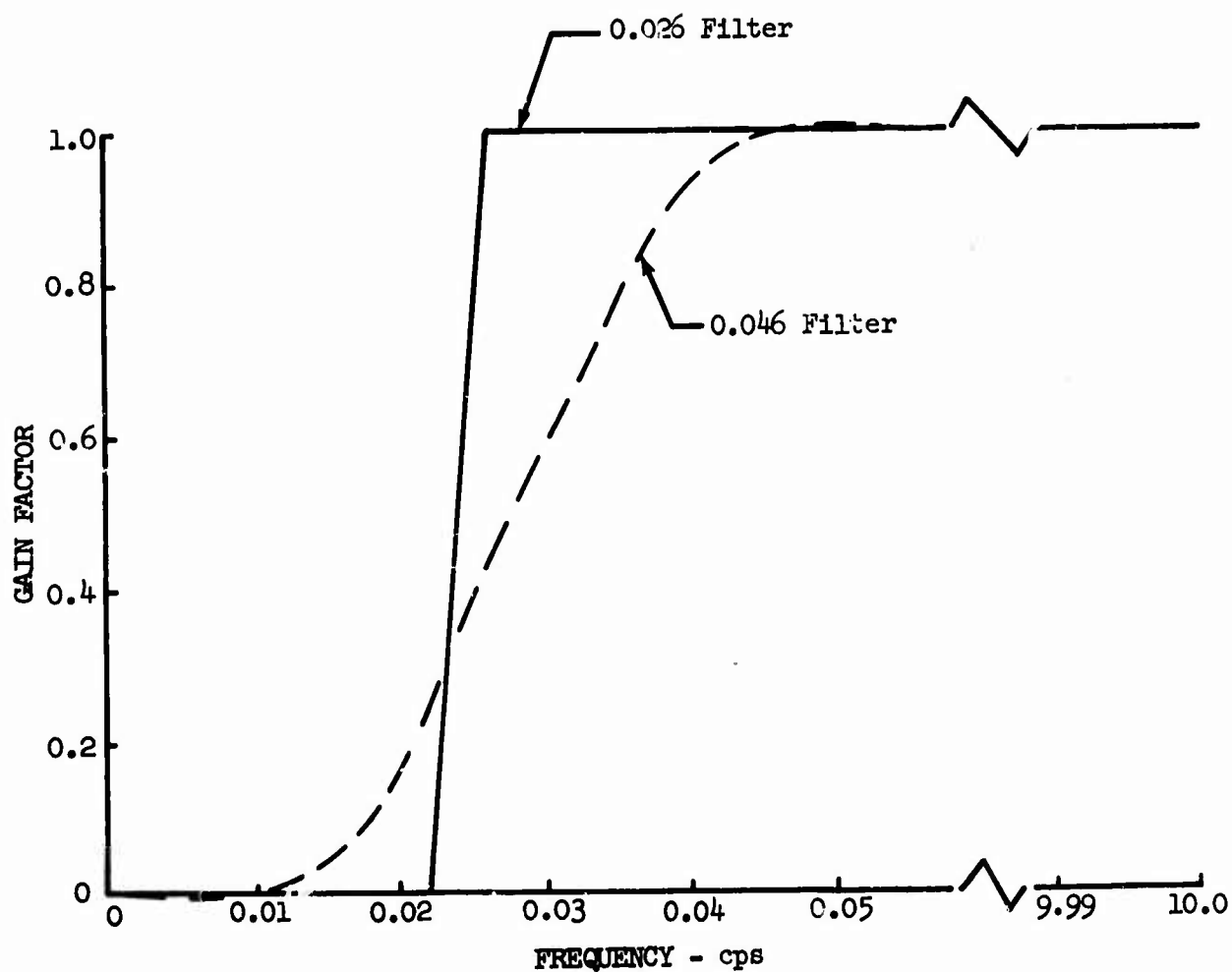


Figure 51.14 Modified High-Pass Filter Transfer Function

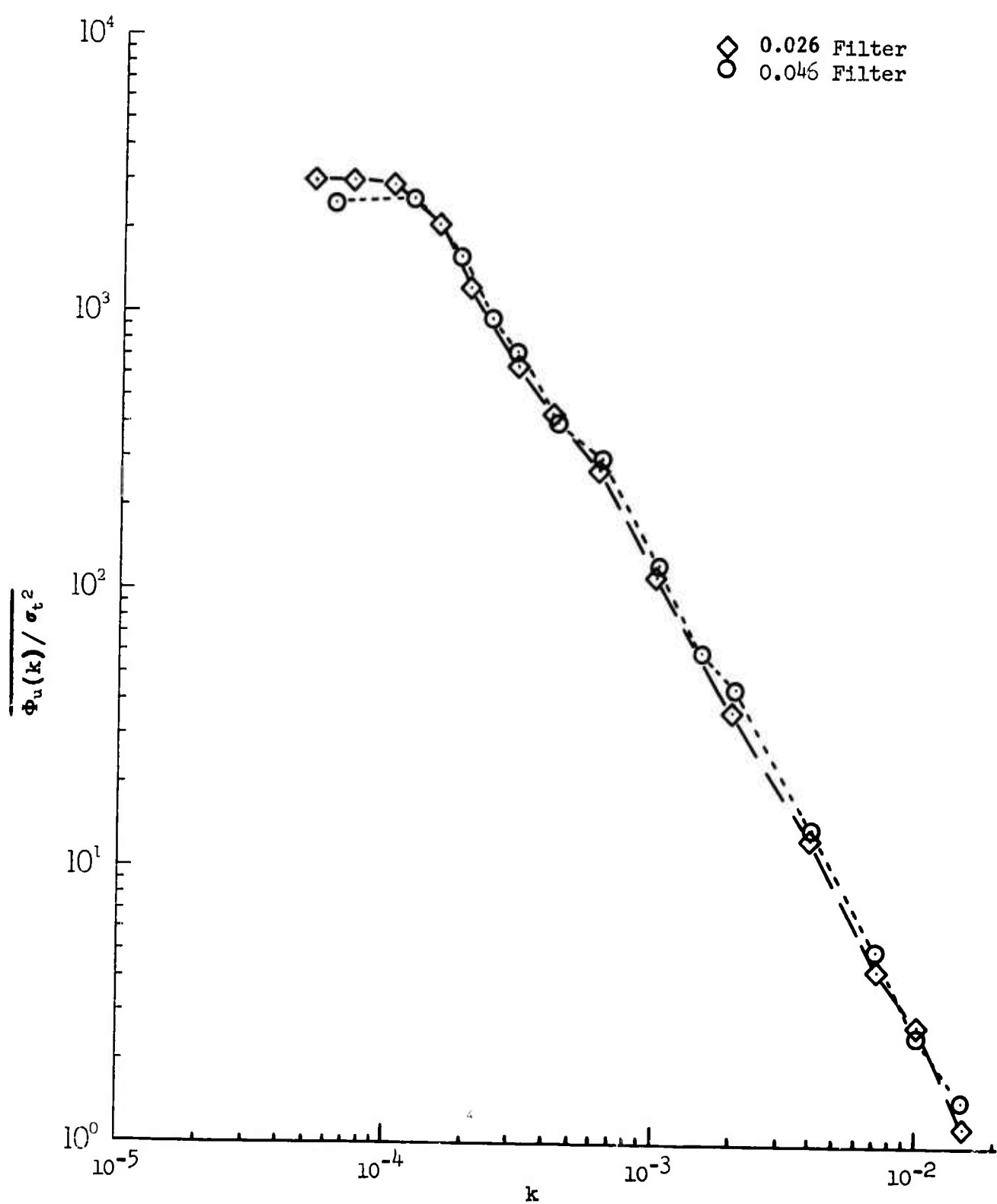


Figure 51.15 Average of Ten Longitudinal Spectra

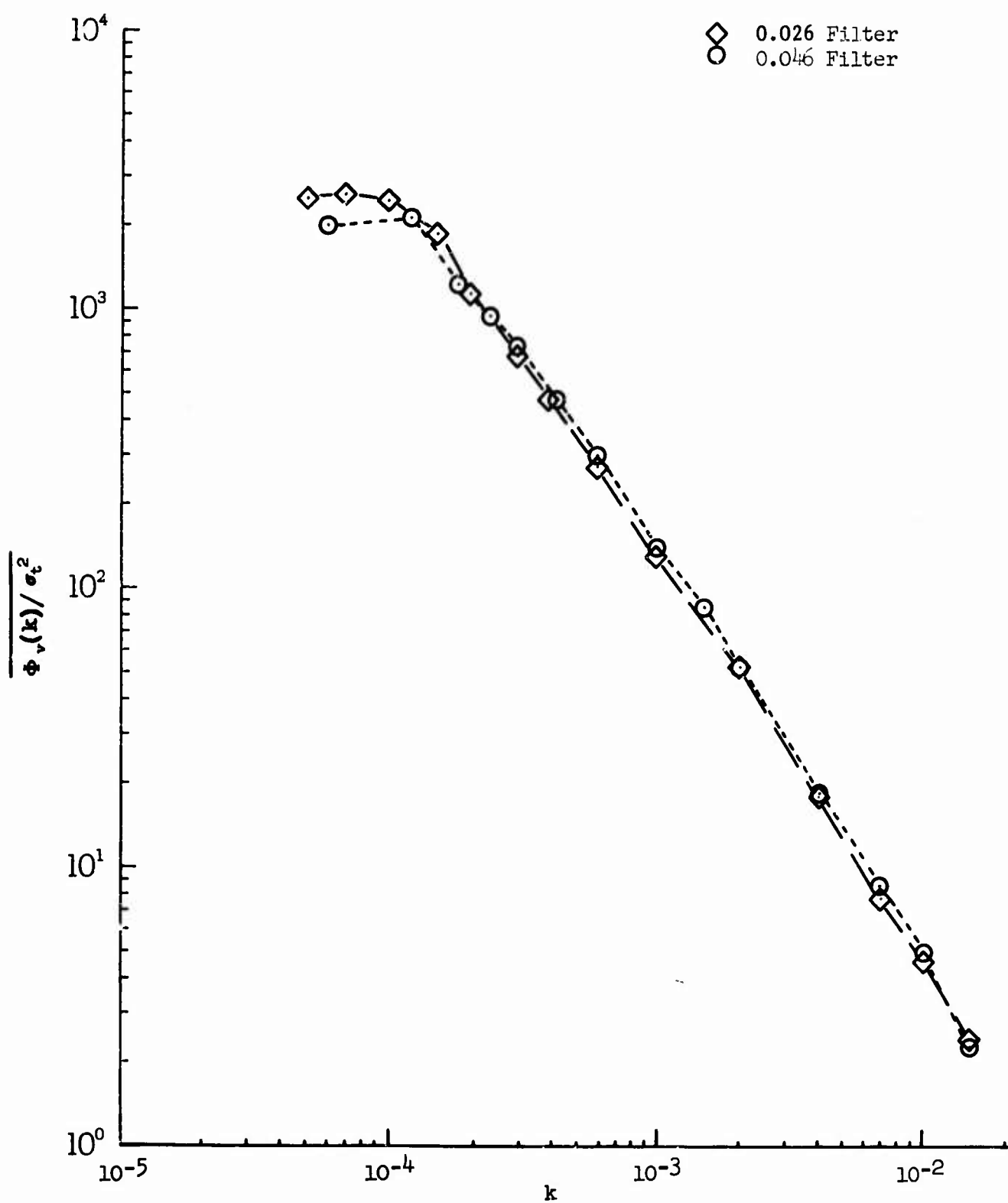


Figure 51.16 Average of Ten Lateral Spectra

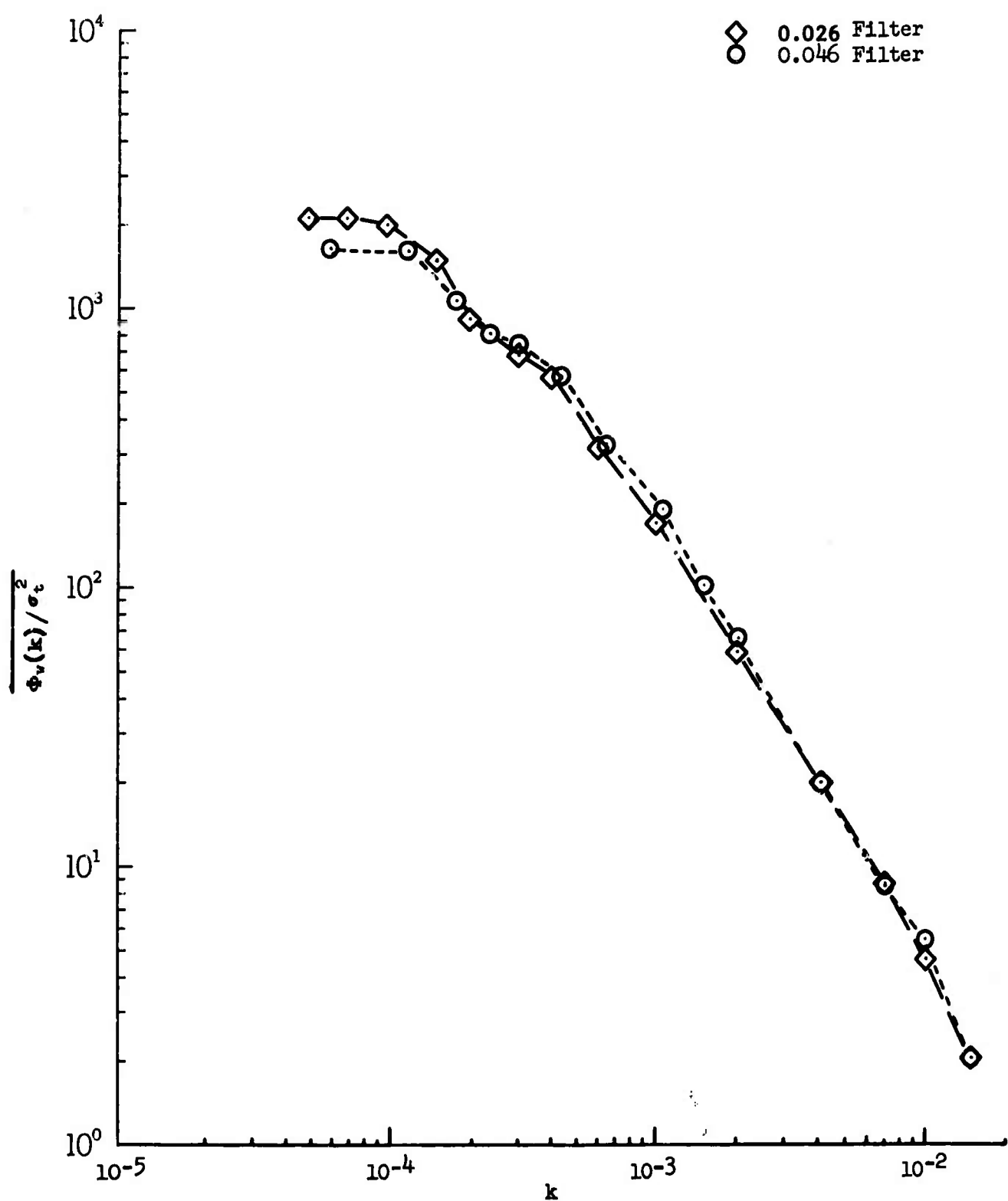


Figure 51.17 Average of Ten Vertical Spectra

Test 178 Sample 12

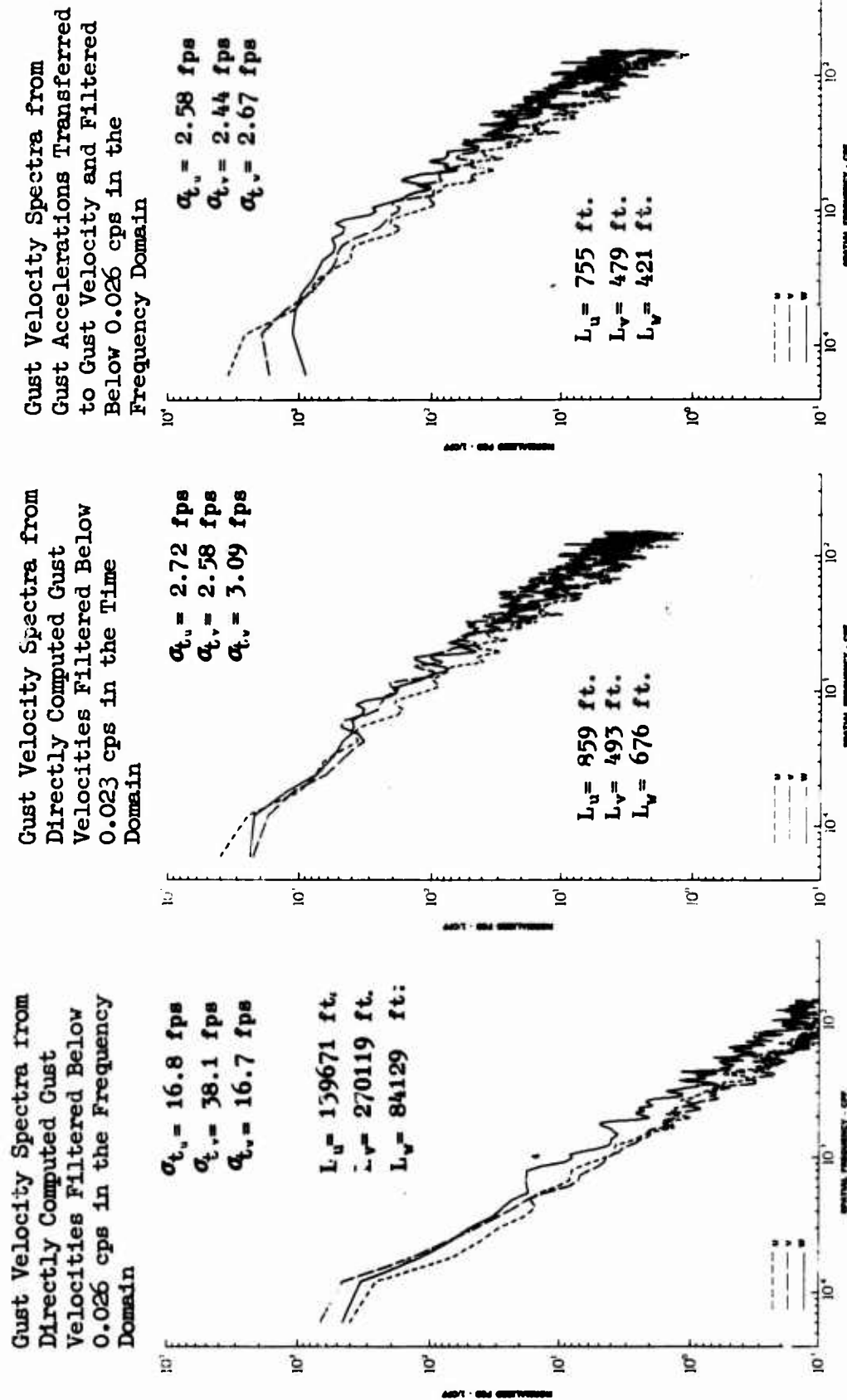


Figure 51.18 Comparison of Spectra Obtained Using 0.026 cps Frequency and 0.023 cps Time Domain Filters

Test 159 Sample 1b Level Crossings

○ Gust Acceleration
◇ Gust Velocity

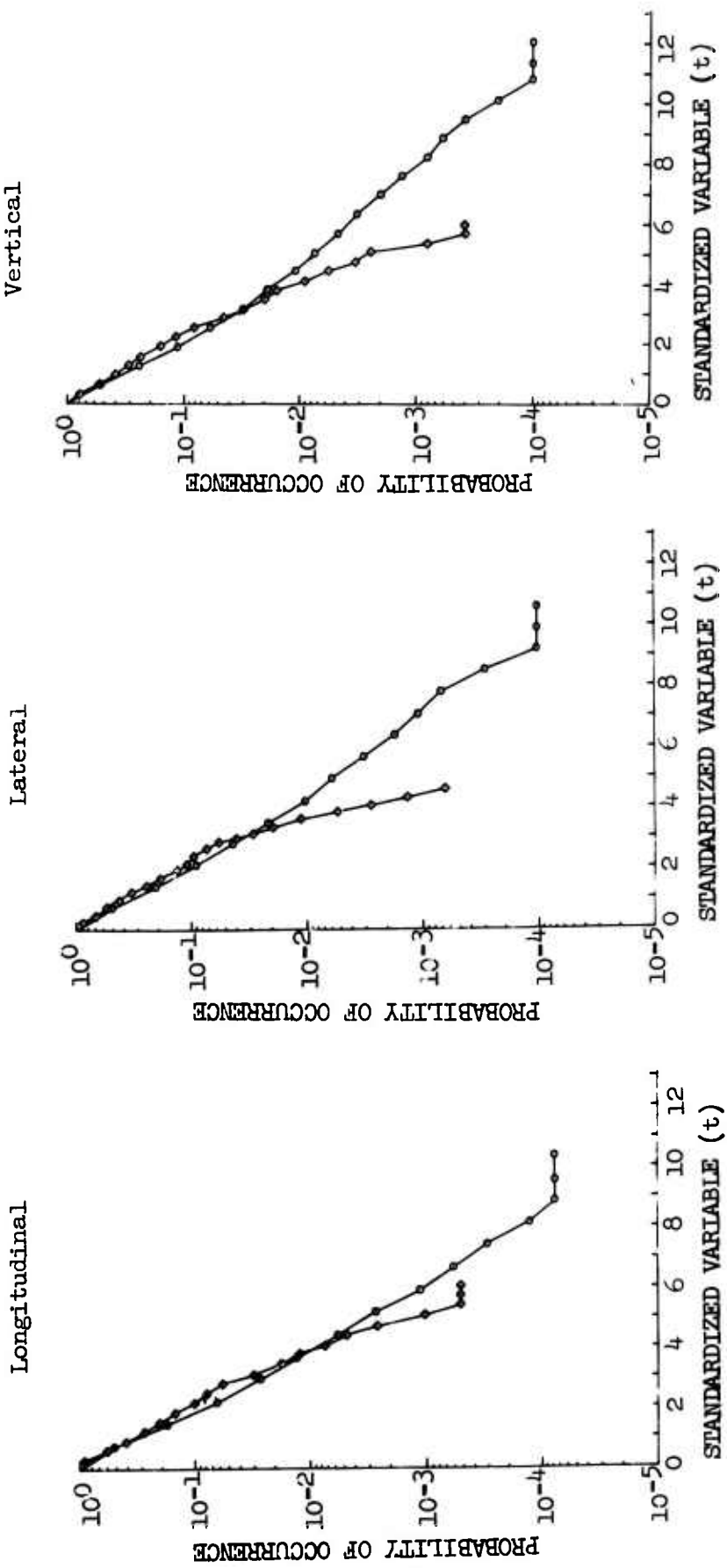


Figure 51.19 Gust Velocity and Gust Acceleration Probability Distributions

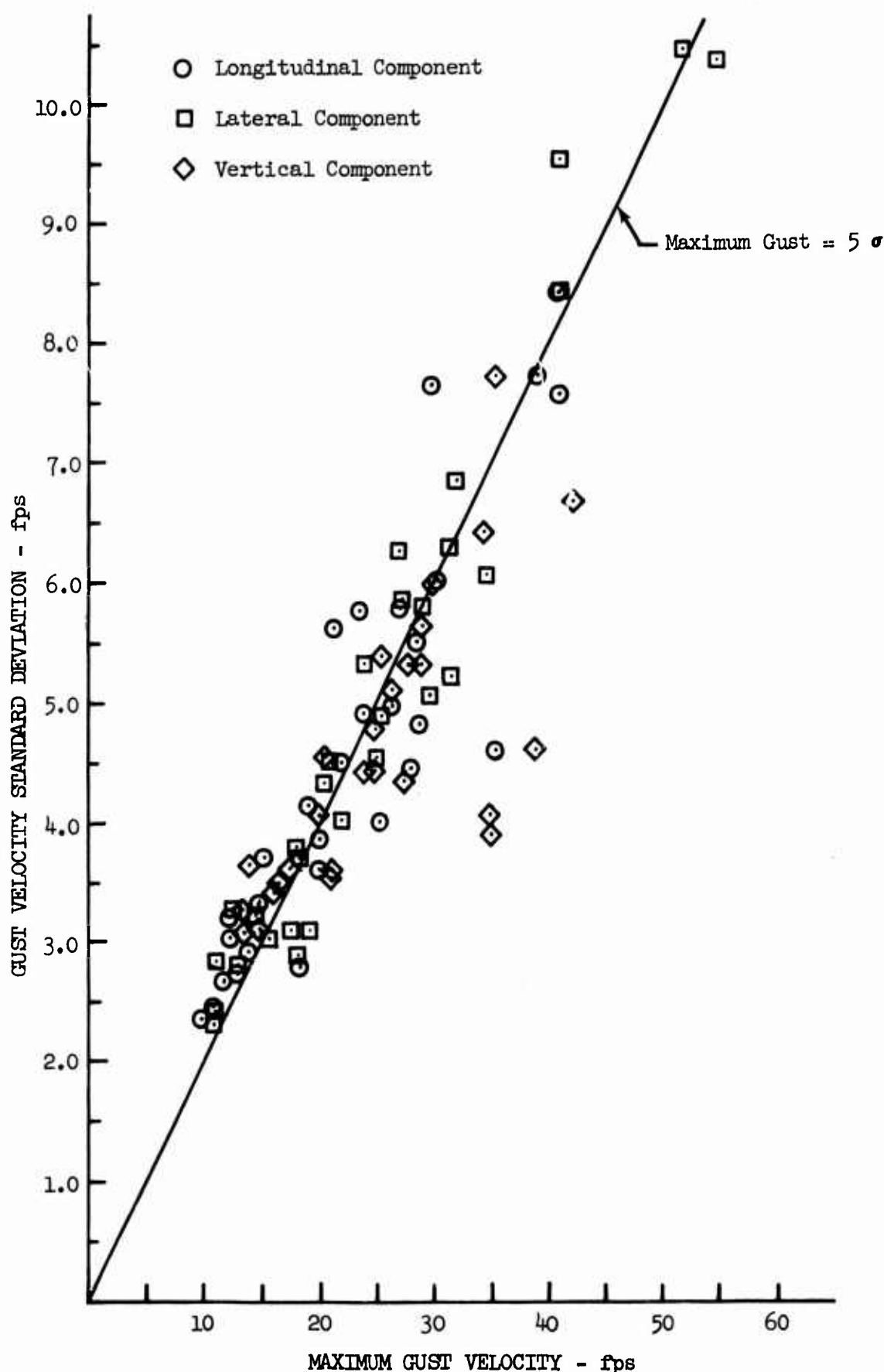


Figure 51.20 Gust Velocity Standard Deviations versus Maximum Gust Encountered

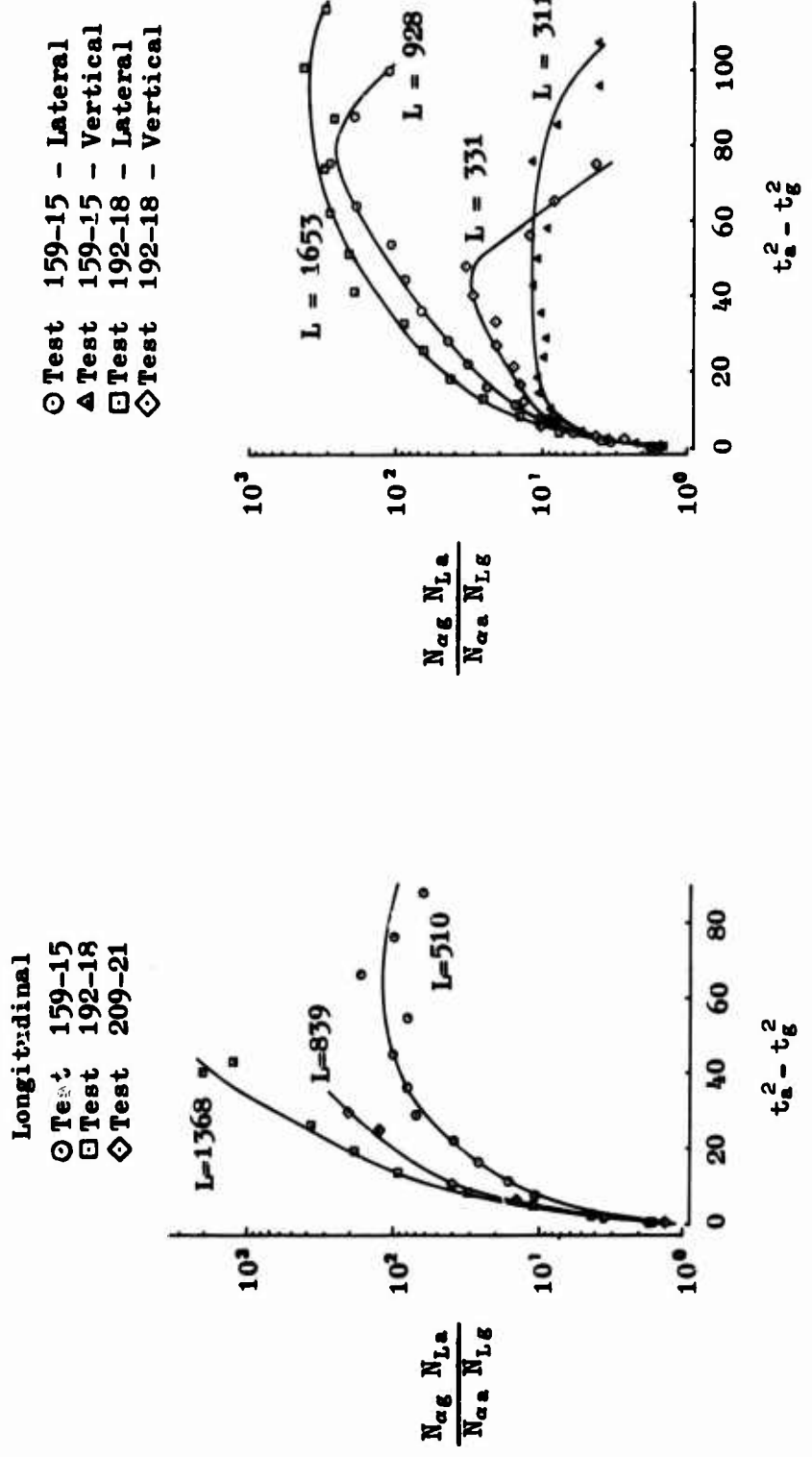


Figure 51.21 Normalized Gust Velocity/Gust Acceleration Level Crossings

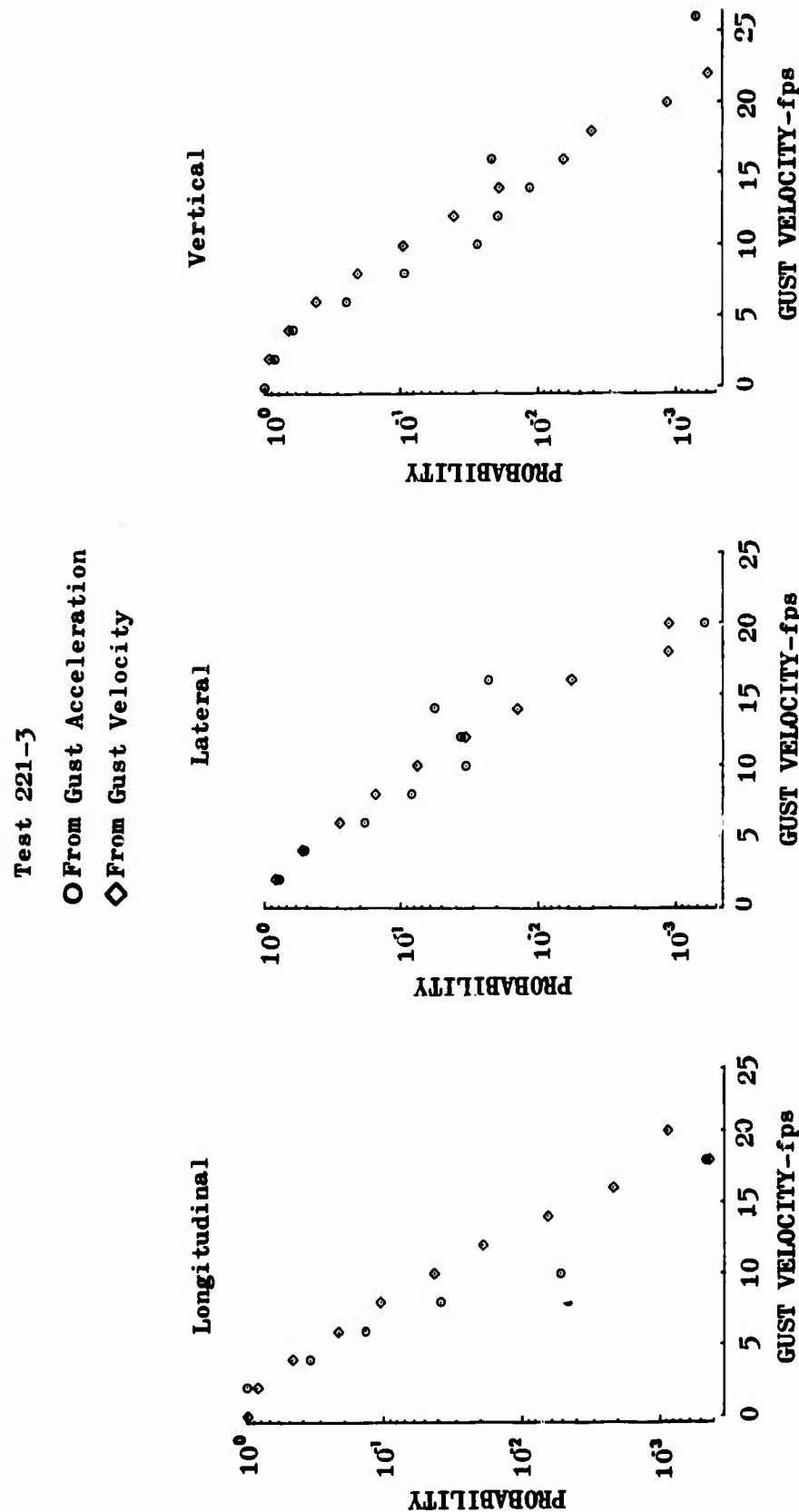


Figure 51.22 Comparisons of Gust Velocity Level
 Crossing Cumulative Probability Distributions

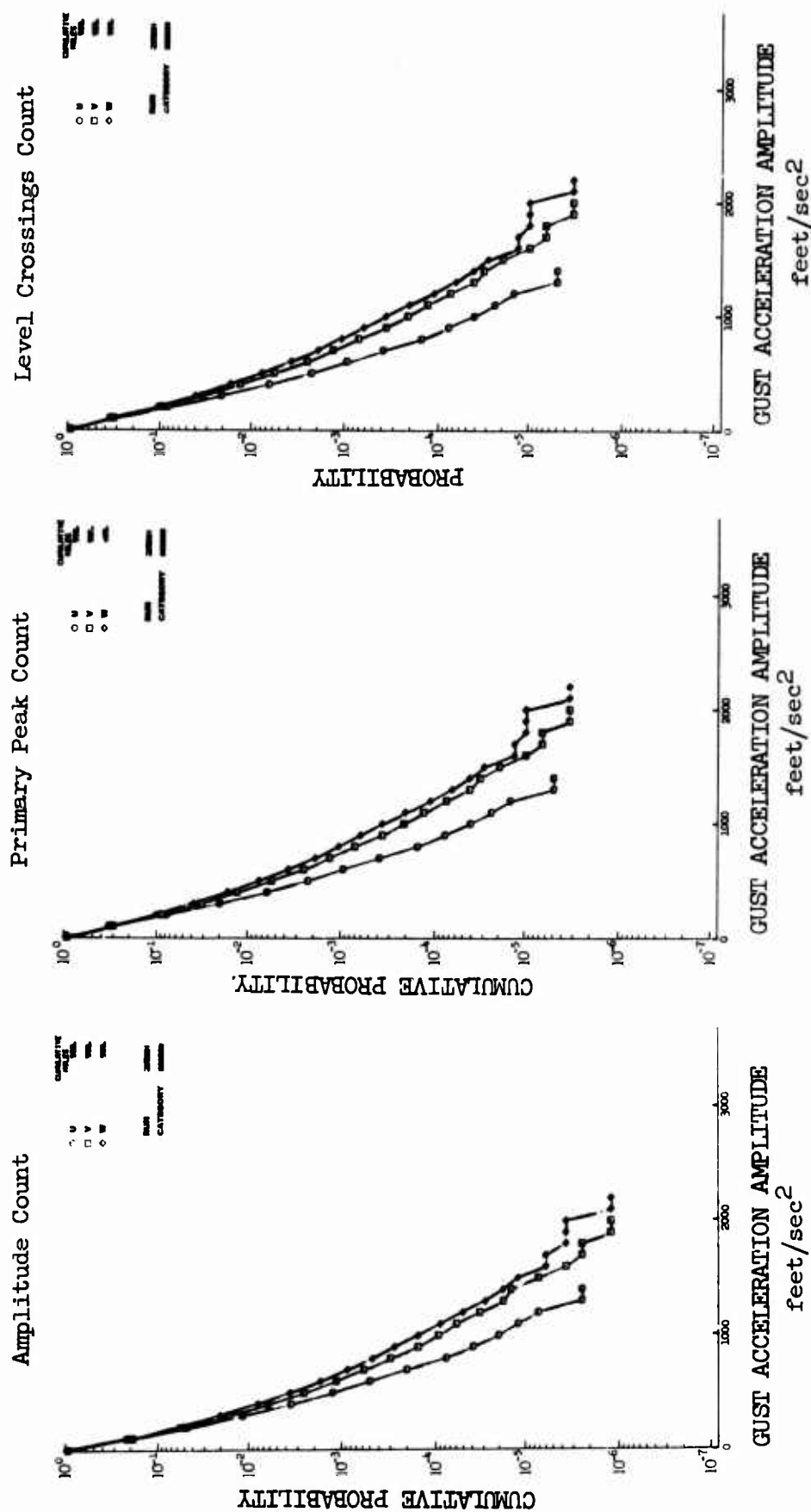


Figure 51.23 Gust Acceleration Probability Distributions for Thirty Combined Samples

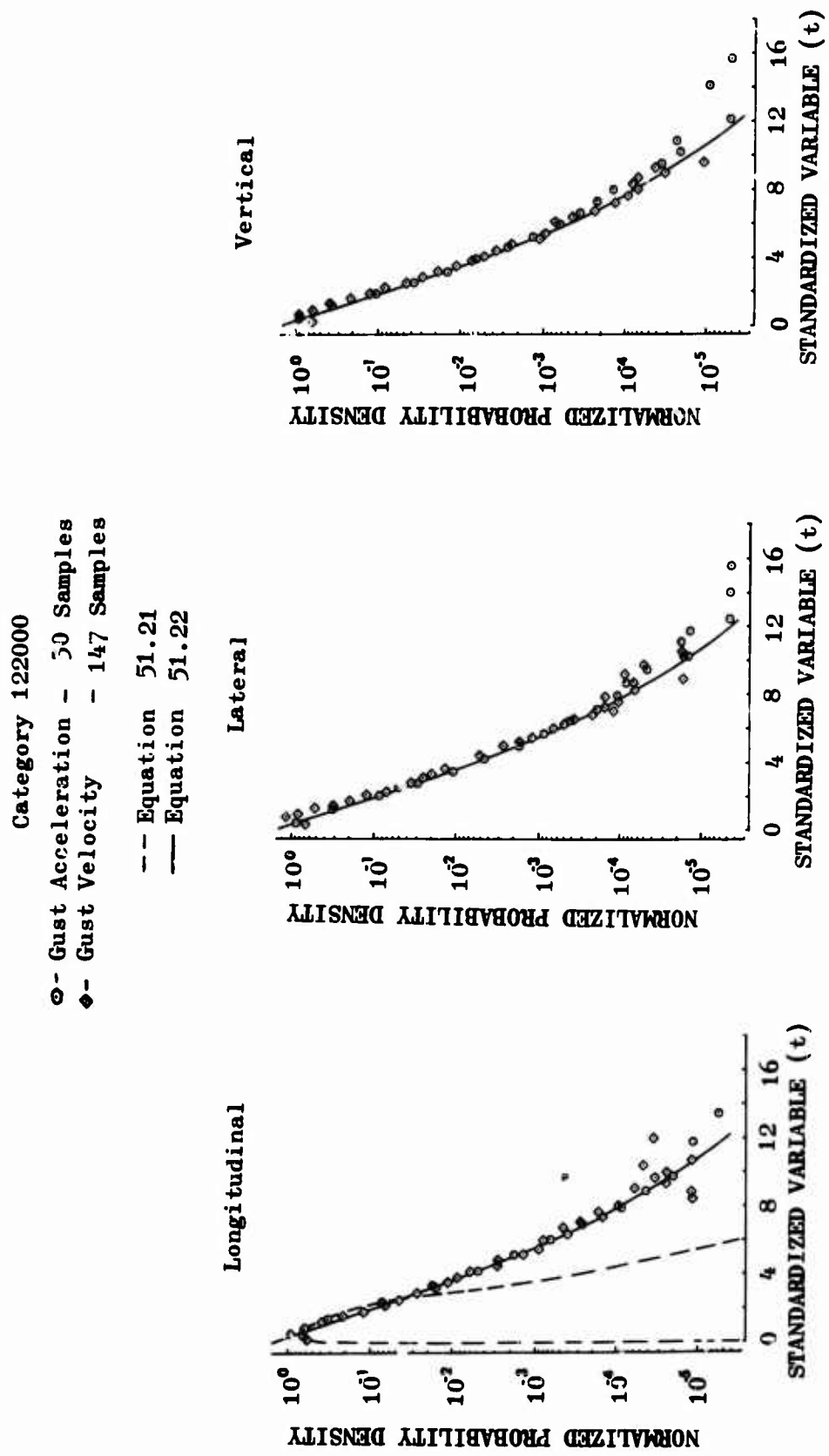


Figure 51.24 Comparison of Gust Velocity and Acceleration Level Crossing Probability Density Functions

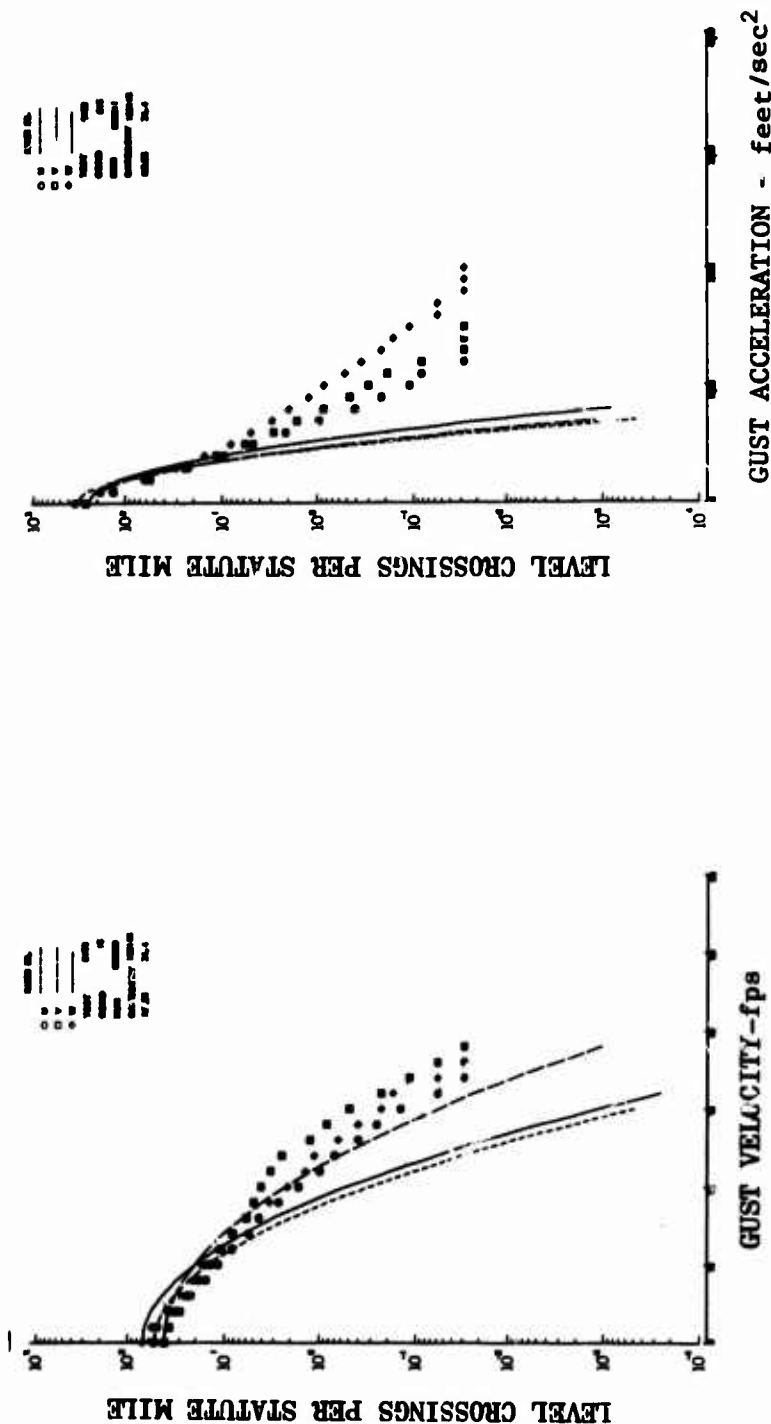


Figure 51.25 Gust Velocity and Gust Acceleration Level Crossing Distributions Compared to Rice's Equation

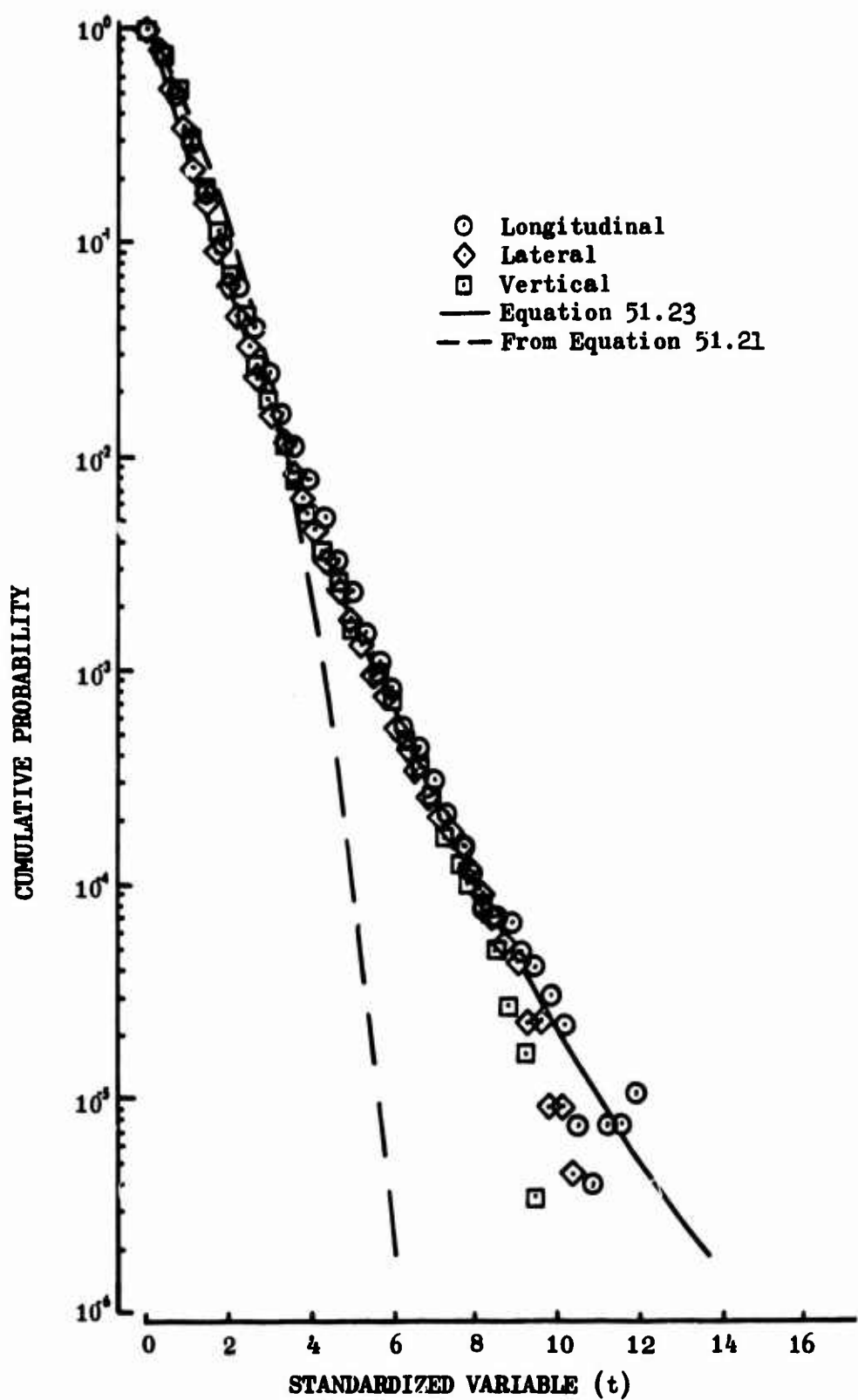


Figure 51.26 Actual Gust Velocity Level Crossing Probabilities Compared to Equations from Gust Acceleration Data

52. WIND SPECTRA

Values of wind velocity were computed at 100 samples per second for each turbulence sample. The north-south and east-west components were calculated as shown by Equations V.16 through V.20 in Appendix V. Longitudinal and lateral wind components referenced to the initial airplane heading (to be consistent with the calculation of gust velocities) were then computed as follows:

Quadrant I:

$$W_u = W_{N_1} \cos h_0 + W_{E_1} \cos (90 - h_0)$$

$$W_v = W_{N_1} \sin h_0 - W_{E_1} \sin (90 - h_0)$$

Quadrant II:

$$W_u = W_{N_{II}} \cos (360 - h_0) - W_{E_{II}} \cos (h_0 - 270)$$

$$W_v = -W_{N_{II}} \sin (360 - h_0) - W_{E_{II}} \sin (h_0 - 270)$$
(52.1)

Quadrant III:

$$W_u = W_{N_{III}} \cos (h_0 - 180) - W_{E_{III}} \cos (270 - h_0)$$

$$W_v = W_{E_{III}} \sin (270 - h_0) - W_{N_{III}} \sin (h_0 - 180)$$

Quadrant IV:

$$W_u = W_{E_{IV}} \cos (h_0 - 90) - W_{N_{IV}} \cos (180 - h_0)$$

$$W_v = W_{N_{IV}} \sin (180 - h_0) + W_{E_{IV}} \sin (h_0 - 90)$$

The 30 data samples chosen for analyses were the same as those chosen for the gust acceleration investigation (Section 51). These samples are tabulated in Table XII and were chosen based on the availability of the gust velocity power spectra, the degree of homogeneity, and the geophysical conditions under which the samples were measured. All of the samples were recorded at 750 feet above the terrain over high mountains at the Peterson route when the atmosphere was classified as being stable.

Low-pass digital filtering was performed to prevent aliasing. The data were then sampled at 10 cps which gave a Nyquist frequency of 5 cps, and high-pass filtering was performed to remove long-period trends and frequencies below .004 cps.

The wind velocity time series were numerically filtered as shown in Equation 52.2.

$$x_i^* = \sum_{n=-N}^{N} h_n (x_{i+n}) \quad (52.2)$$

where x_{i+n} are the input samples and x_i^* the output samples. The Ormsby filter weight function, at discrete equi-spaced intervals, Δt , is given by:

$$h_n = \frac{\cos 2\pi n \Delta t f_c - \cos 2\pi n \Delta t (f_c + \Delta f)}{2\Delta f \Delta t (\pi n)^2} \quad (52.3)$$

Where h_n are the $2N+1$ filter weights for $n = 0, \pm 1, \pm 2, \dots, \pm N$, f_c is the cutoff frequency and $f_c + \Delta f$ is the termination frequency. The gain factor of the low-pass filter is shown in Figure 52.1. High-pass filtering was accomplished in two passes to conserve computer effort. The gain factor for the first pass is shown in Figure 52.2. The gain factor for the second pass is shown in Figure 52.3. Even though the end result was to be high-pass filtering, the filtering was accomplished as low-pass. The resultant data was then subtracted from the original data leaving high-pass filtered data. Amplitudes at frequencies from approximately .004 cps to 1.0 cps were essentially unattenuated.

As discussed in Appendix III, when data are filtered, N values are lost from the beginning and end of the time series because of the required non-circular sums of the lagged products required by Equation 52.2. The scheme used to extend the data so that the output time history length equalled the input time history length was to fold and invert the first and last 2550 data values about the first and last data points, respectively.

The effects of filtering are shown in Figure 52.4 where time histories of filtered wind velocities are compared with unfiltered wind velocities. It is apparent from this figure that both linear trends and frequencies lower than .004 cps were removed from the data. The linear trend illustrated in this case is defined as a straight line which connects the end points of the unfiltered data.

It is also apparent from Figure 52.4 that there is a striking difference in the characteristics of the lateral wind velocity time function compared with the longitudinal. The lateral component contains higher amplitudes at frequencies of approximately .25 cps (the airplane's Dutch roll mode) and the longitudinal component contains higher amplitudes at much higher frequencies. This occurred because longitudinal wind velocity is more sensitive to the higher frequency fluctuations in V_T , and lateral wind velocity is more sensitive to airplane motion which occurs predominately at a frequency of approximately .25 cps.

This can be ascertained from a study of the wind velocity equations referenced to initial airplane heading and written as functions of true airspeed, ground speed, heading, and drift angle, as follows:

$$\begin{aligned} W_u &= -V_T \cos(h - h_0) + G_s \cos(h - h_0 + \delta) \\ W_v &= -V_T \sin(h - h_0) + G_s \sin(h - h_0 + \delta) \end{aligned} \quad (52.4)$$

Airplane motion in Equations 52.4 is primarily manifested by variations in the $(h + \delta)$ quantity. Equations 52.4 show that longitudinal wind velocity is more of a function of V_T and less of a function of the quantity $(h + \delta)$ than is the lateral component. No attempt was made to account for airplane motion effects in the calculations of wind velocities. Attempts to account for motion effects in the time domain would have been unwise since it has previously been shown that there is a significant amount of drift at frequencies much below 0.04 cps in those parameters in the gust velocity equations which correct for airplane motion.

Power spectral densities of wind velocities for the 30 turbulence samples are shown in Figures 52.5 through 52.34. These data have been normalized by their respective time series variances. Only the frequency range from approximately .004 to .125 cps is shown in these figures, since this range is considered to be the most valid due to band-pass filtering and airplane motion effects.

The wind spectra show indications of isotropy for the longitudinal and lateral directions. The longitudinal spectra are usually higher than the lateral at the lower frequencies, and it is generally lower than lateral at the higher frequencies. This is best shown by comparing the average normalized lateral and longitudinal wind spectra plotted in Figures 52.35 and 52.36. Scale lengths of the average normalized spectra appear to be on the order of 6000 feet for both longitudinal and lateral. Also shown in Figures 52.35 and 52.36 are plots of the von Karman longitudinal and lateral spectra for a scale length of 6000 feet. The agreements of the average wind velocity spectra with the von Karman expressions are fairly good.

There was less deviation in the longitudinal spectra from the average than there was in lateral. The average percent deviation of the first point on the spectra from the first point on the average spectrum was 44.8 for longitudinal and 53.4 for lateral. The larger variations in the lateral spectra are no doubt due to its greater sensitivity to airplane motion, as discussed previously.

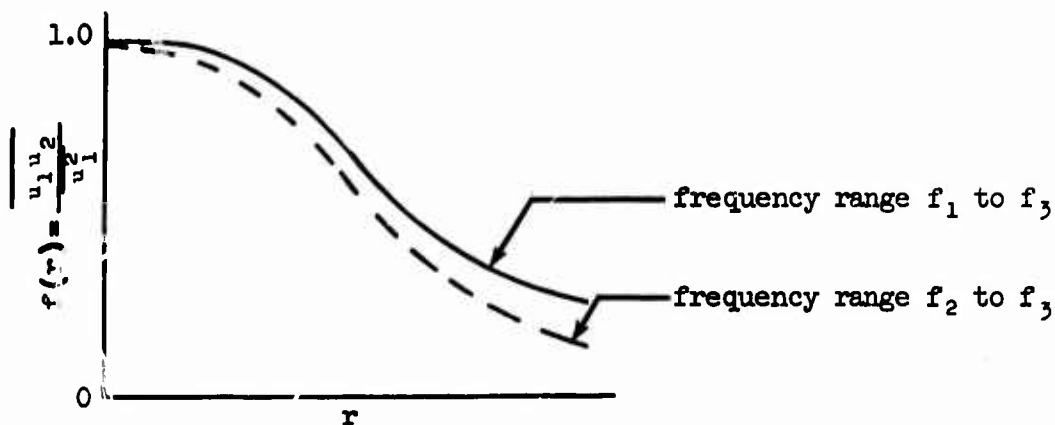
Turbulence power spectra plots are shown in Appendix IX for those samples corresponding by test and leg number to the wind velocity spectra plots presented in Figures 52.5 through 52.34. Comparisons of the wind spectra with the respective gust velocity spectra reveal that wider point-to-point variations occurred in wind spectra than in the gust velocity spectra. One reason for this is because the degrees of freedom for the wind velocity spectra are reduced by a factor of ten since:

$$\text{Degrees of Freedom} = \frac{4V \text{ (Sample length in seconds)}}{\text{maximum wavelength in feet}} \quad (52.5)$$

Sample lengths for both wind and gust velocity time series are the same while the maximum wavelengths involved differ by a factor of ten.

The wind spectra differ from the respective turbulence spectra throughout the frequency range. This can be seen in Figures 52.35 and 52.36 where the average normalized wind spectra are compared with the average normalized turbulence spectra and the respective von Karman expressions. Different spectra (scale lengths) are to be expected even when homogeneous, isotropic turbulence is measured over different frequency ranges. The fact that this difference will be apparent at all frequencies can be visualized as follows:

1. Consider the longitudinal correlation curves shown in the sketch where the data were obtained with instrumentation which could adequately measure turbulence over the frequency range from f_1 to f_3 .



2. Then if that same turbulence is measured with a system which could only measure turbulence over a range from f_2 to f_3 , where $f_2 > f_1$, then for a random process the longitudinal correlation, $f(r)$, would be reduced at a given correlation distance, r , as shown in the sketch.
3. Since the integral scale lengths are defined by:

$$L_u = \int_0^{\infty} f(r) dr, \quad (52.6)$$

then $L_u (f_2 \text{ to } f_3)$ will be less than $L_u (f_1 \text{ to } f_3)$.

4. The relation between the longitudinal velocity spectrum, $\Phi_u(k)$, and the longitudinal velocity correlation $f(r)$ is given (Ref. 21.1) by the Fourier Cosine transformation of $f(r)$:

$$\frac{\Phi_u(k)}{\sigma_u^2} = 4 \int_0^{\infty} dr f(r) \cos(2\pi k \frac{r}{V}) \quad (52.7)$$

It is apparent from Equation 52.6 that the spectra for the two correlation curves will differ since $f(r) [f_1 \text{ to } f_3] \neq f(r) [f_2 \text{ to } f_3]$.

Since the correlation curves are different, then the level crossing distributions, the standard deviations, spectra shapes, and other statistical parameters defining the turbulence environment must also be different. One significance of this is that the turbulence parameters to be considered for airplane design will vary depending on the turbulence wave-lengths to which the airplane will respond.

During LO-LOCAT Phases I and II the correlations of longitudinal and lateral surface winds at Wichita, Kansas, with those measured by the U.S. Weather Bureau for locations at considerable distances from Wichita, were calculated and plotted in a manner similar to the above sketch (Figure 4.79, Ref. I.2). Integration of that curve yielded scale lengths on the order of 322 miles.

This is further proof that different scale lengths are to be expected whenever the frequency interval over which the turbulence is measured is changed. Comparisons of von Karman scale lengths from various phases of the program are shown in Table 52.1.

TABLE 52.1
AVERAGE SCALE LENGTHS CALCULATED DURING THE LO-LOCAT PROGRAM

Measurement*	Average Scale Length - Feet		
	Longitudinal	Lateral	Vertical
Phases I and II Surface Wind Correlations	1,690,000	1,690,000	---
Phase III Wind Velocity Spectra	6000	6000	---
Phase III Gust Velocity Spectra	714	632	508
Phase I and II Gust Velocity Spectra	411	465	449

* All average values are for measurements at the 750-foot altitude except for the surface wind correlations.

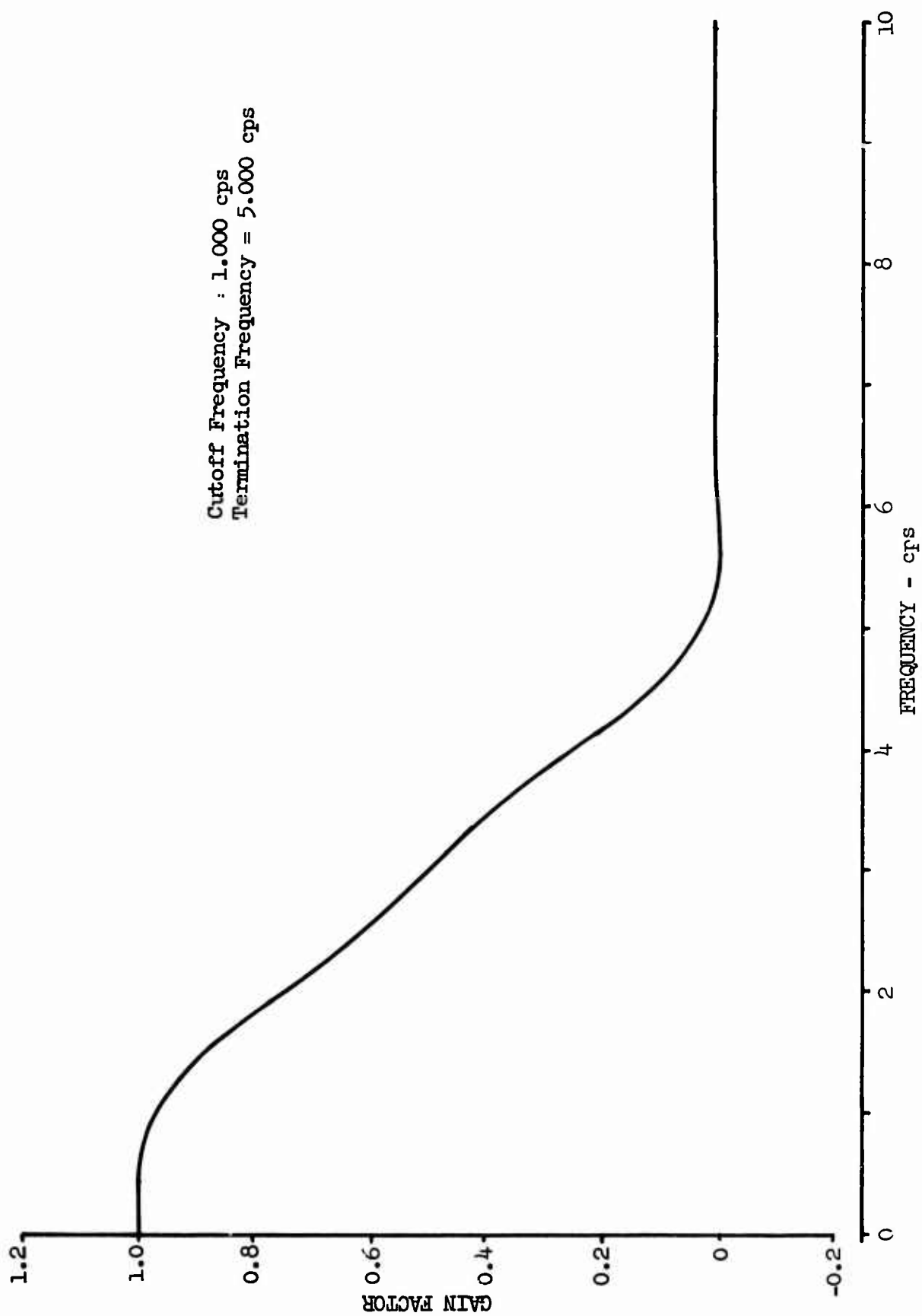


Figure 52.1 Ormsby Low-Pass Digital Filter Used to Filter Winds Data

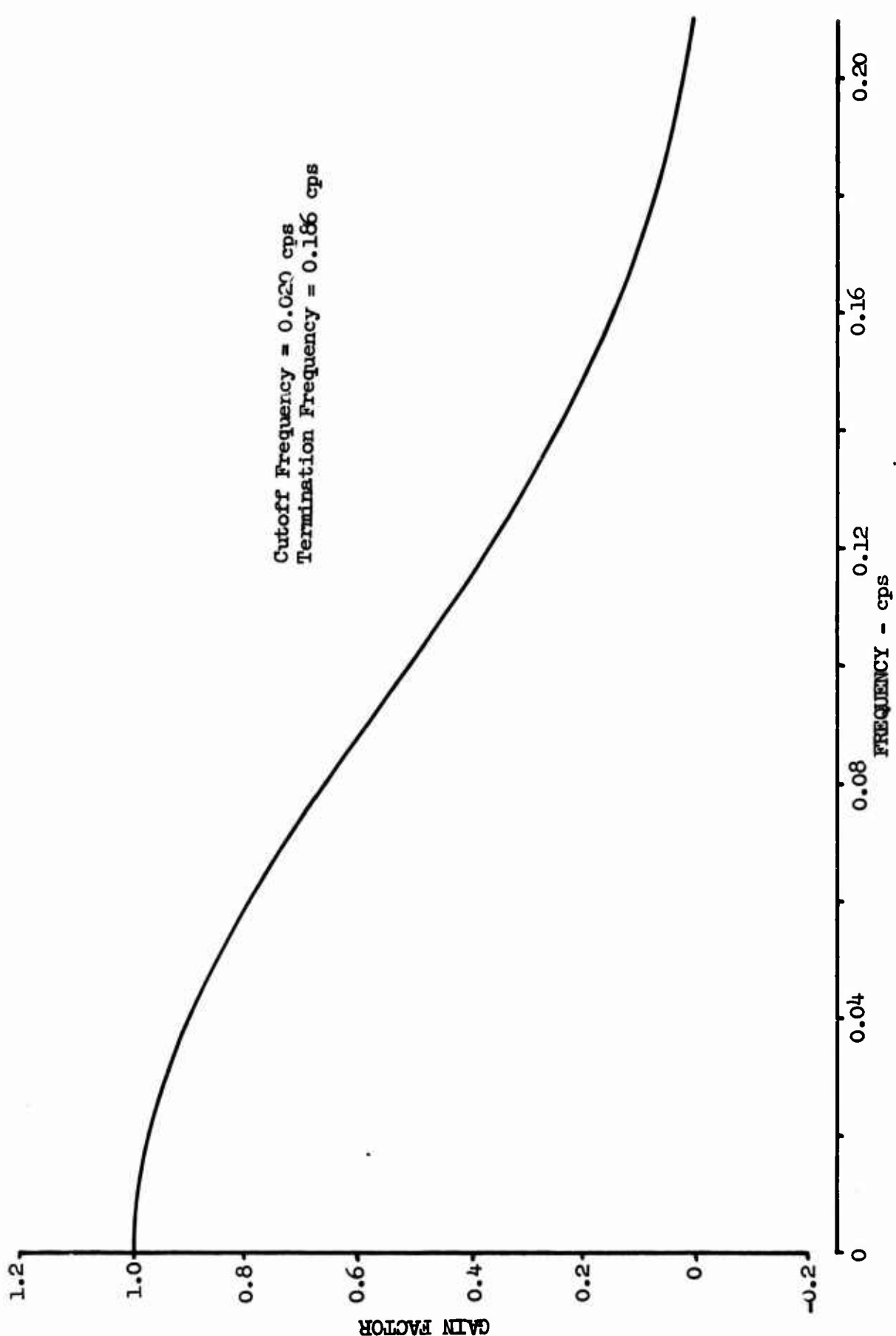


Figure 52.2 Ormsby Low-Pass Digital Filter Used as First Pass in the Two Pass Procedure for High-Pass Filtering Winds Data

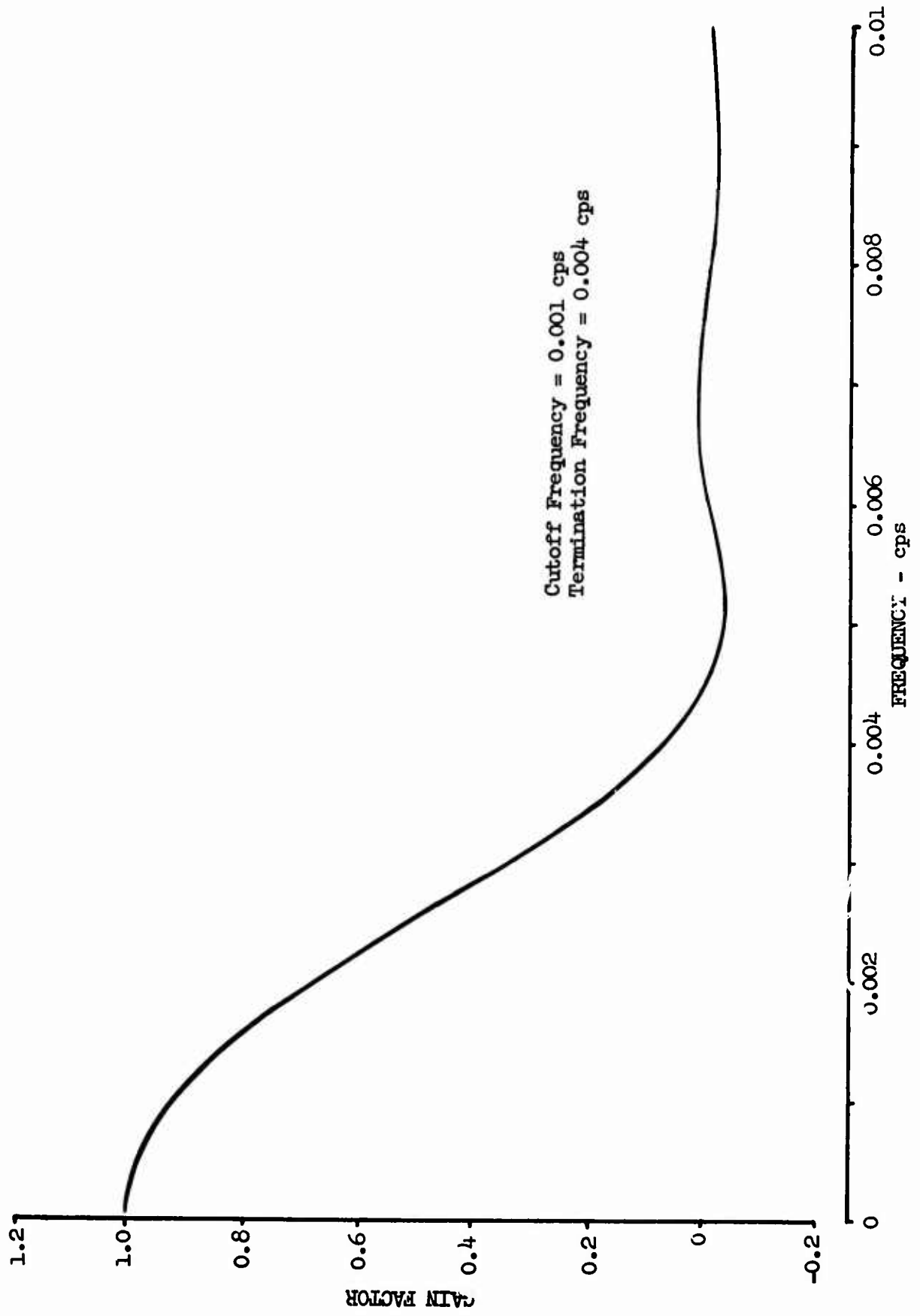


Figure 52.3 Ormsby High-Pass Digital Filter Used as Second Pass in the Two Pass Procedure for High-Pass Filtering Wind Data

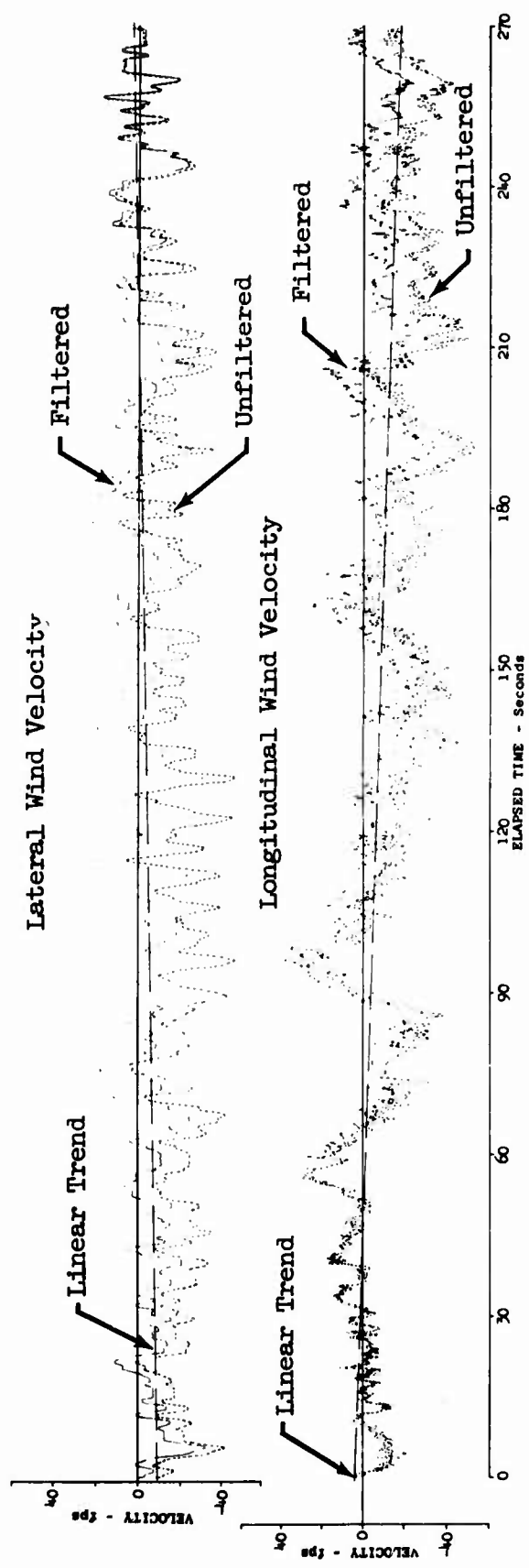


Figure 52.4 Time Histories of Filtered and Unfiltered Wind Velocities

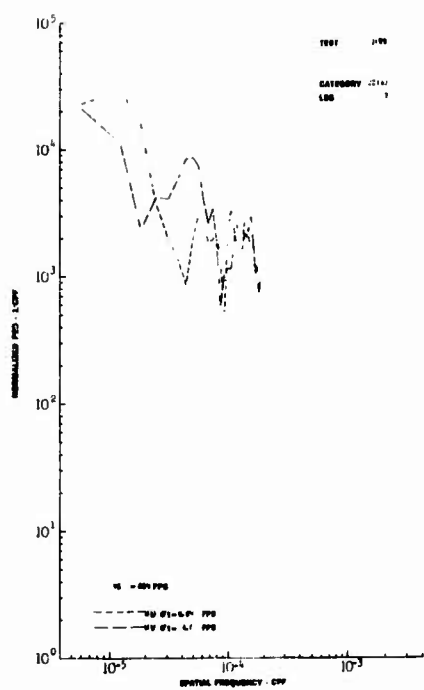


Figure 52.5

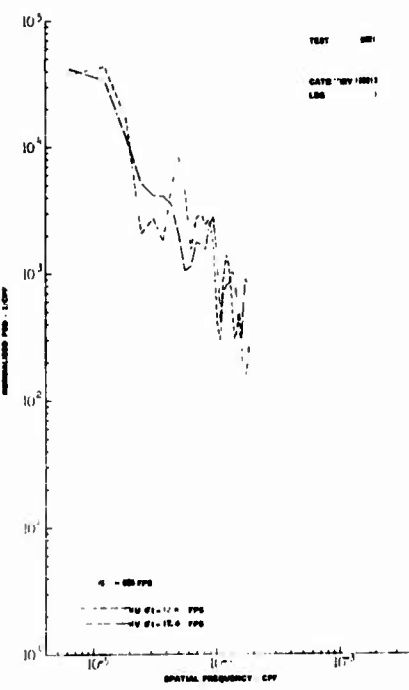


Figure 52.6

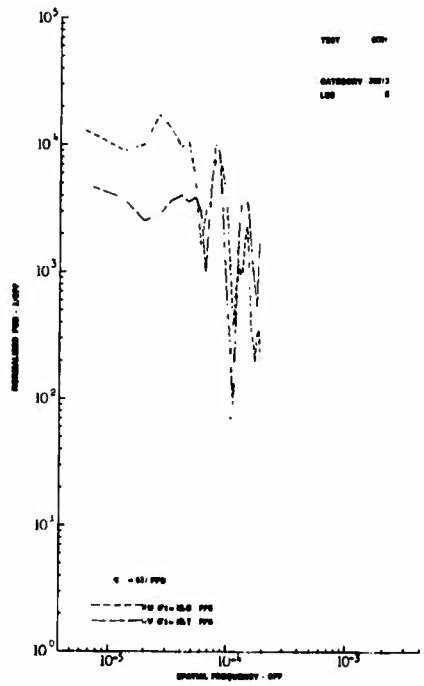


Figure 52.7

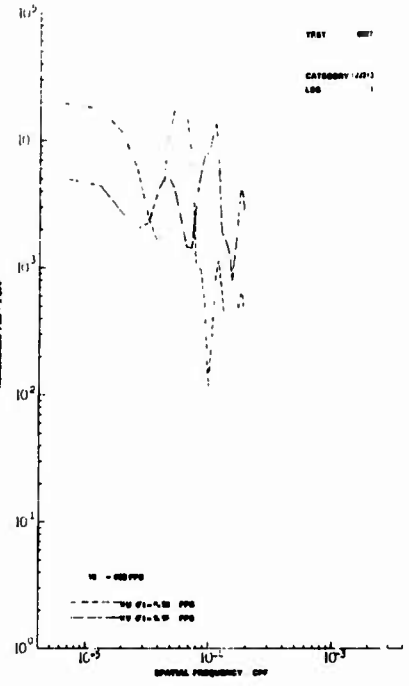


Figure 52.8

Figures 52.5 through 52.8 Wind Velocity Normalized Spectra

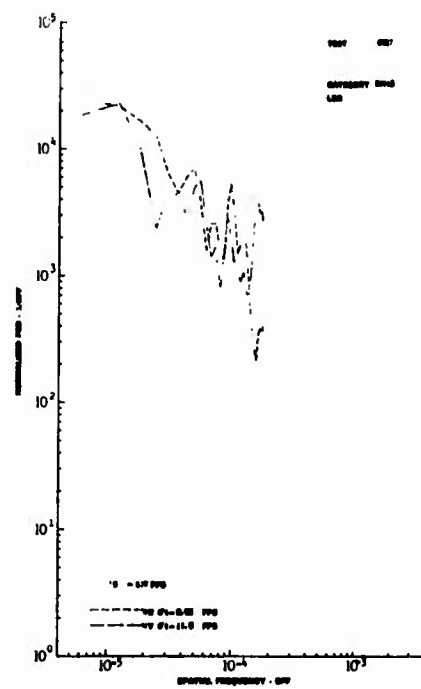


Figure 52.9

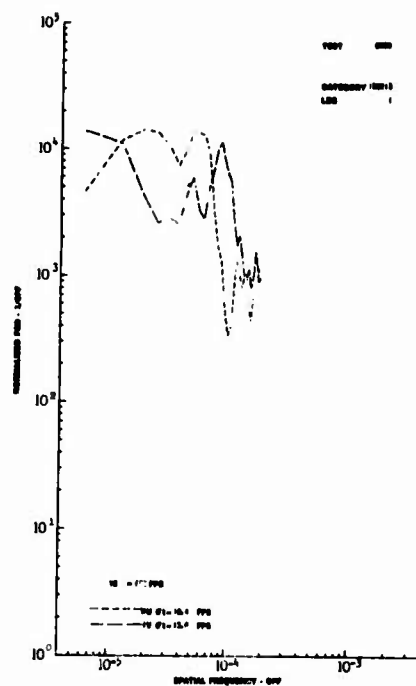


Figure 52.10

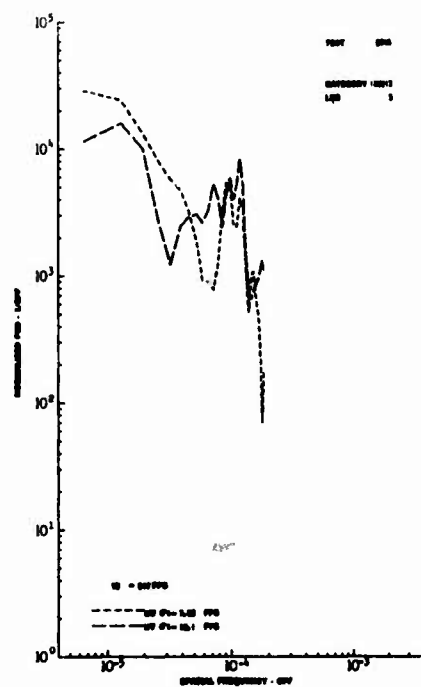


Figure 52.11

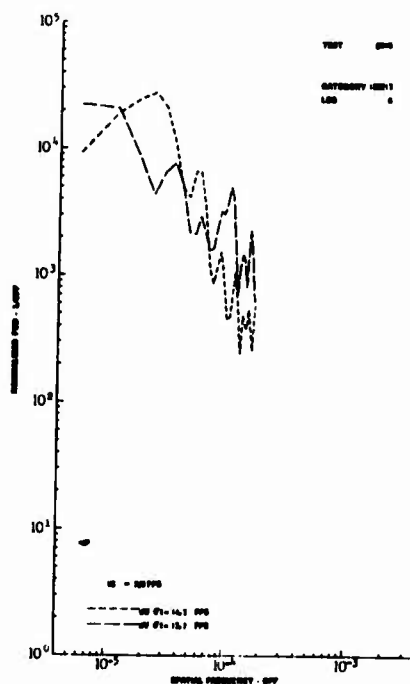


Figure 52.12

Figures 52.9 through 52.12 Wind Velocity Normalized Spectra

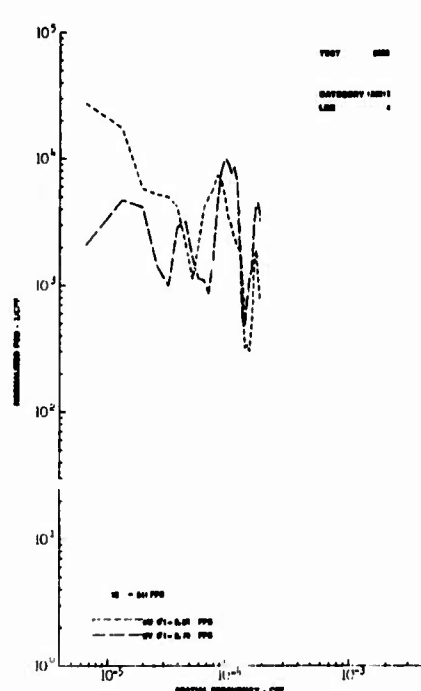


Figure 52.13

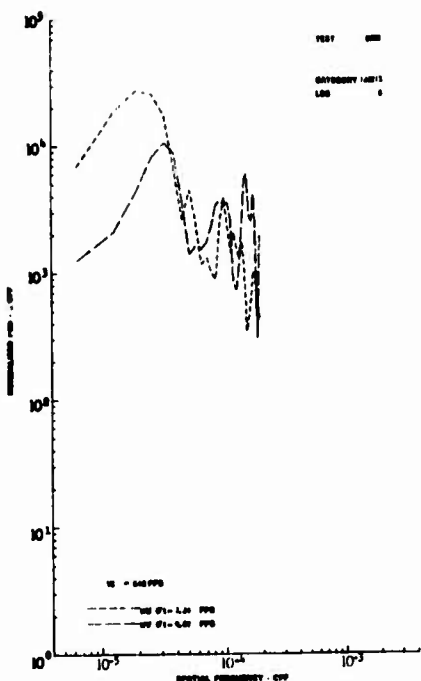


Figure 52.14

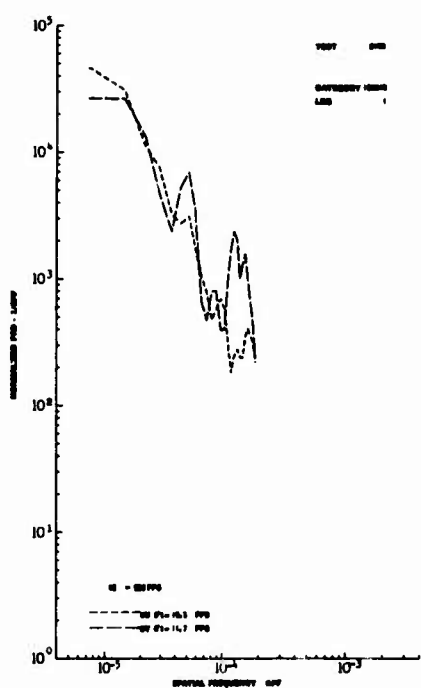


Figure 52.15

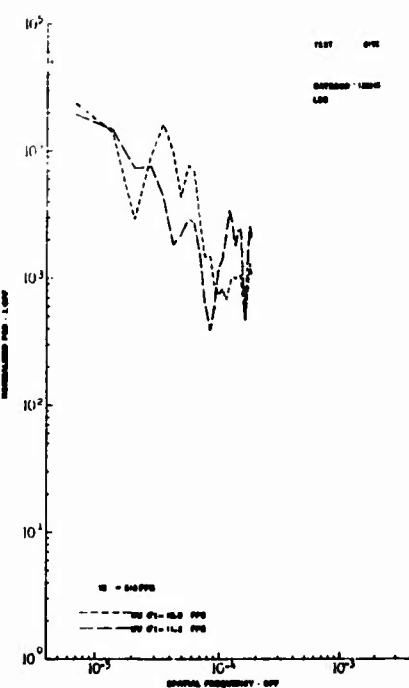


Figure 52.16

Figures 52.13 through 52.16 Wind Velocity Normalized Spectra

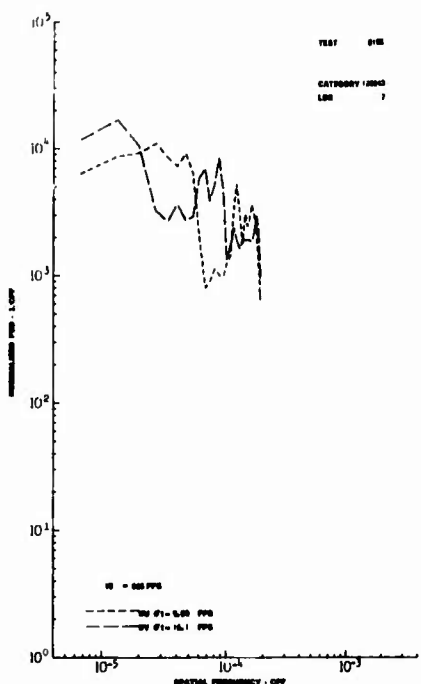


Figure 52.17

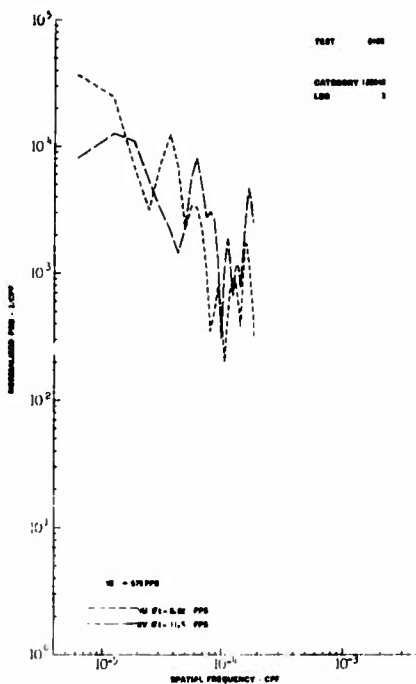


Figure 52.18

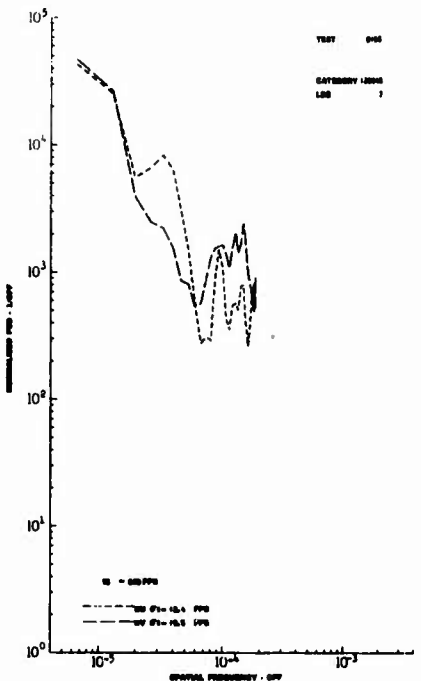


Figure 52.19

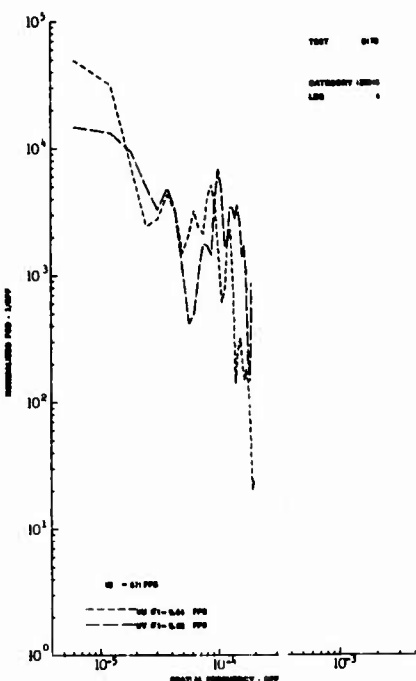


Figure 52.20

Figures 52.17 through 52.20 Wind Velocity Normalized Spectra

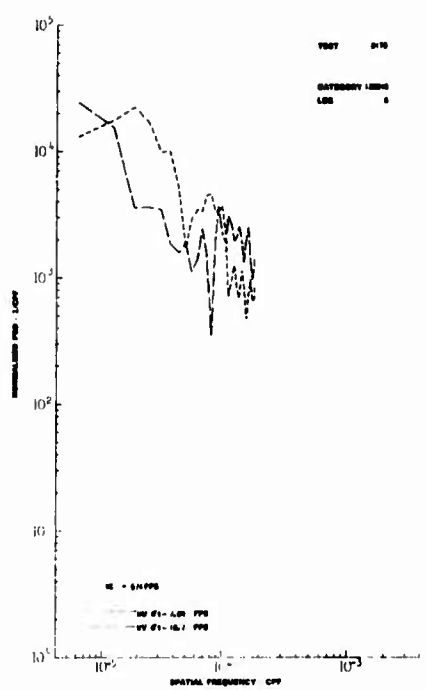


Figure 52.21

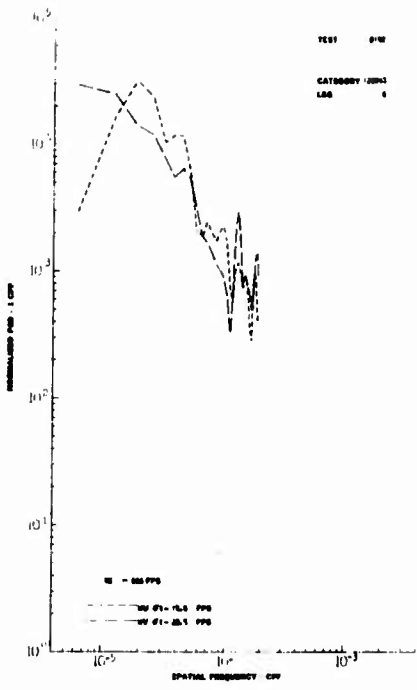


Figure 52.22

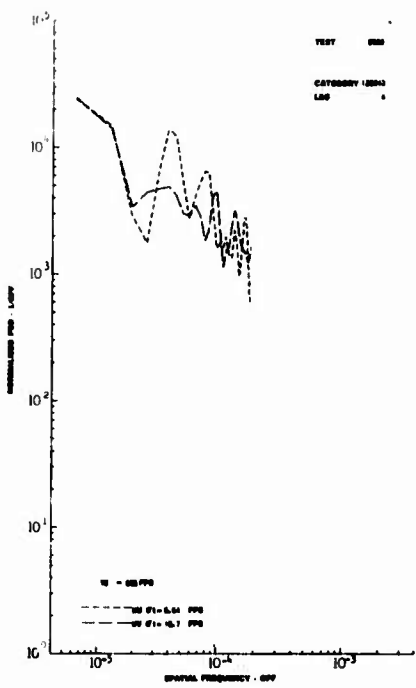


Figure 52.23

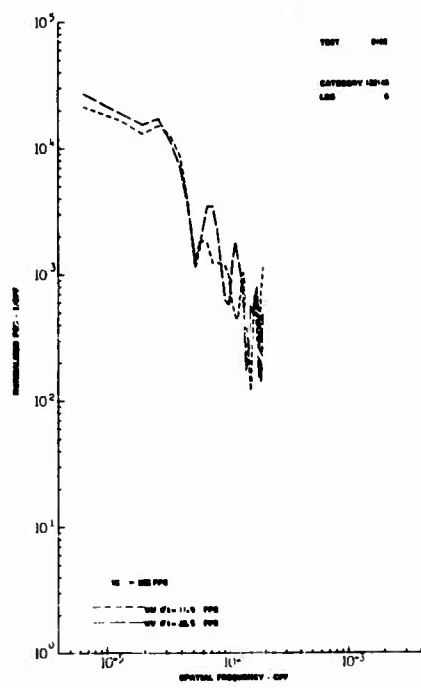


Figure 52.24

Figures 52.21 through 52.24 Wind Velocity Normalized Spectra

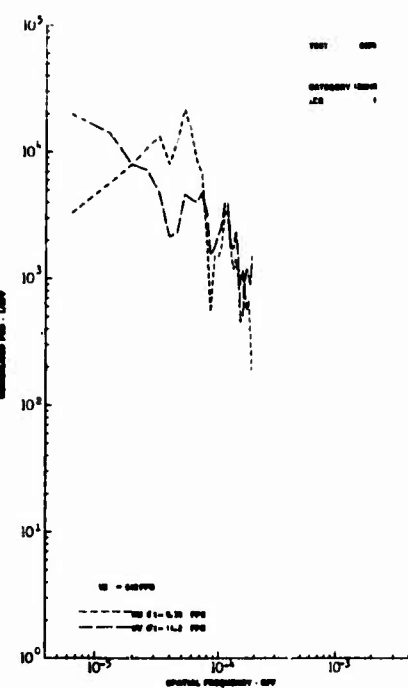


Figure 52.25

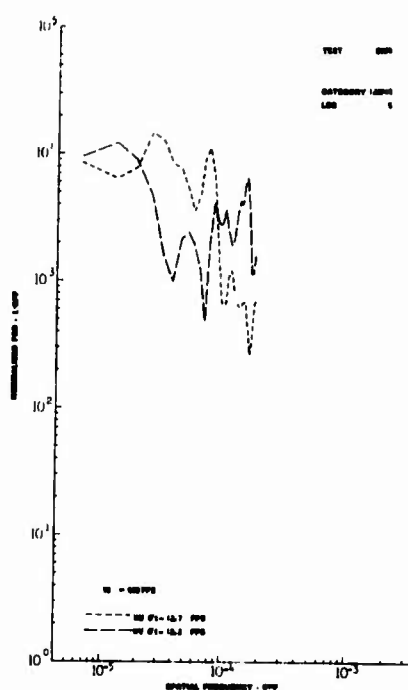


Figure 52.26

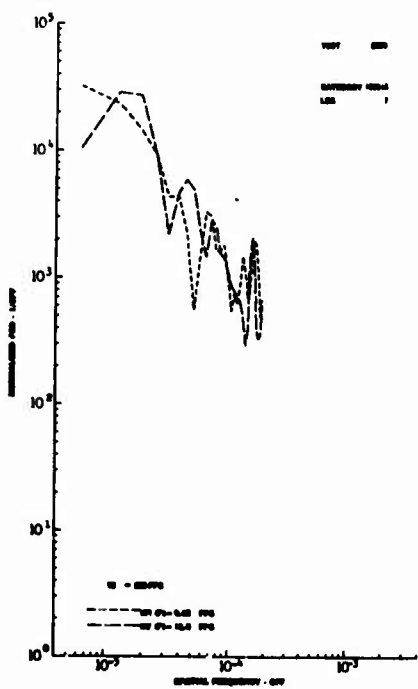


Figure 52.27

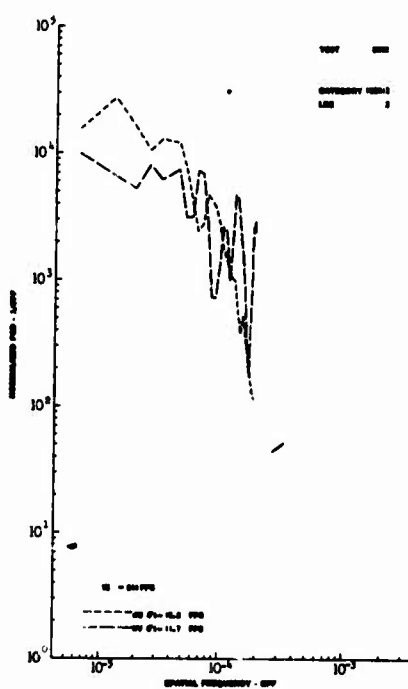


Figure 52.28

Figures 52.25 through 52.28 Wind Velocity Normalized Spectra

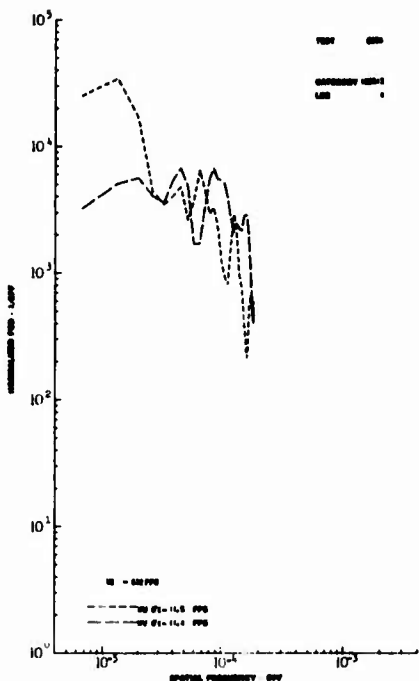


Figure 52.29

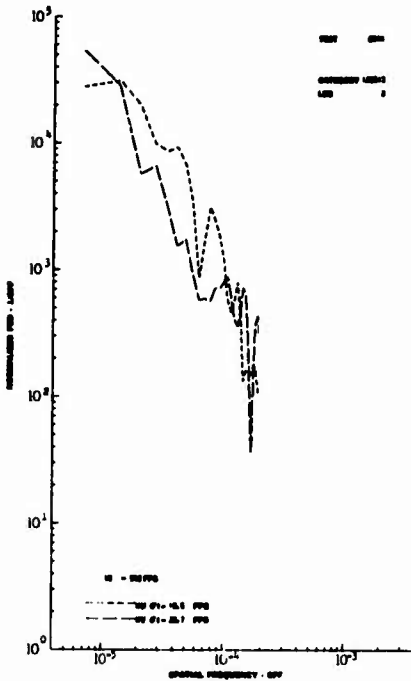


Figure 52.30

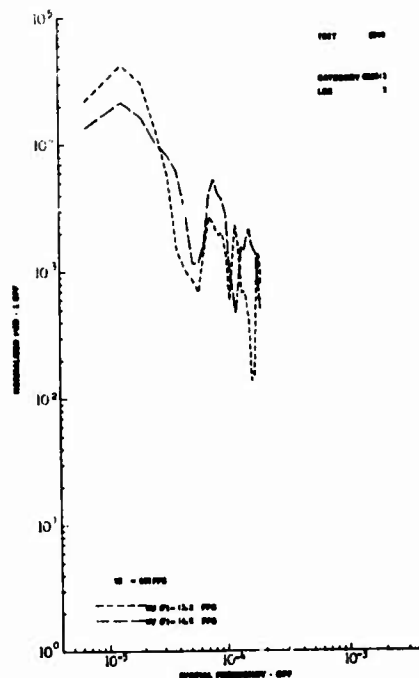


Figure 52.31

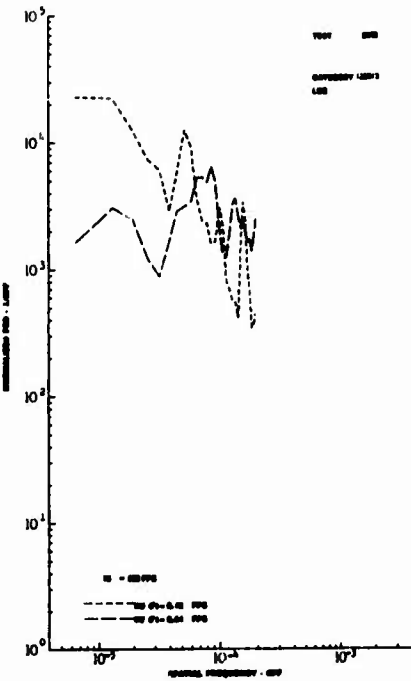


Figure 52.32

Figures 52.29 through 52.32 Wind Velocity Normalized Spectra

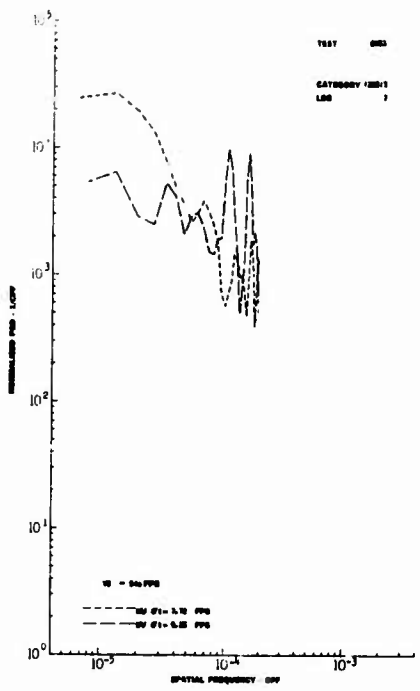


Figure 52.33

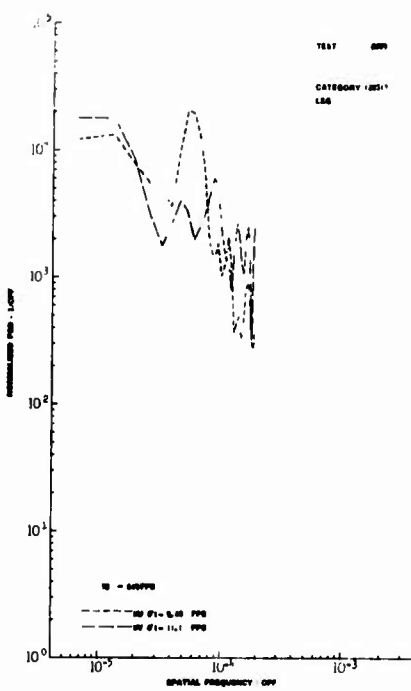


Figure 52.34

Figures 52.33 and 52.34 Wind Velocity Normalized Spectra

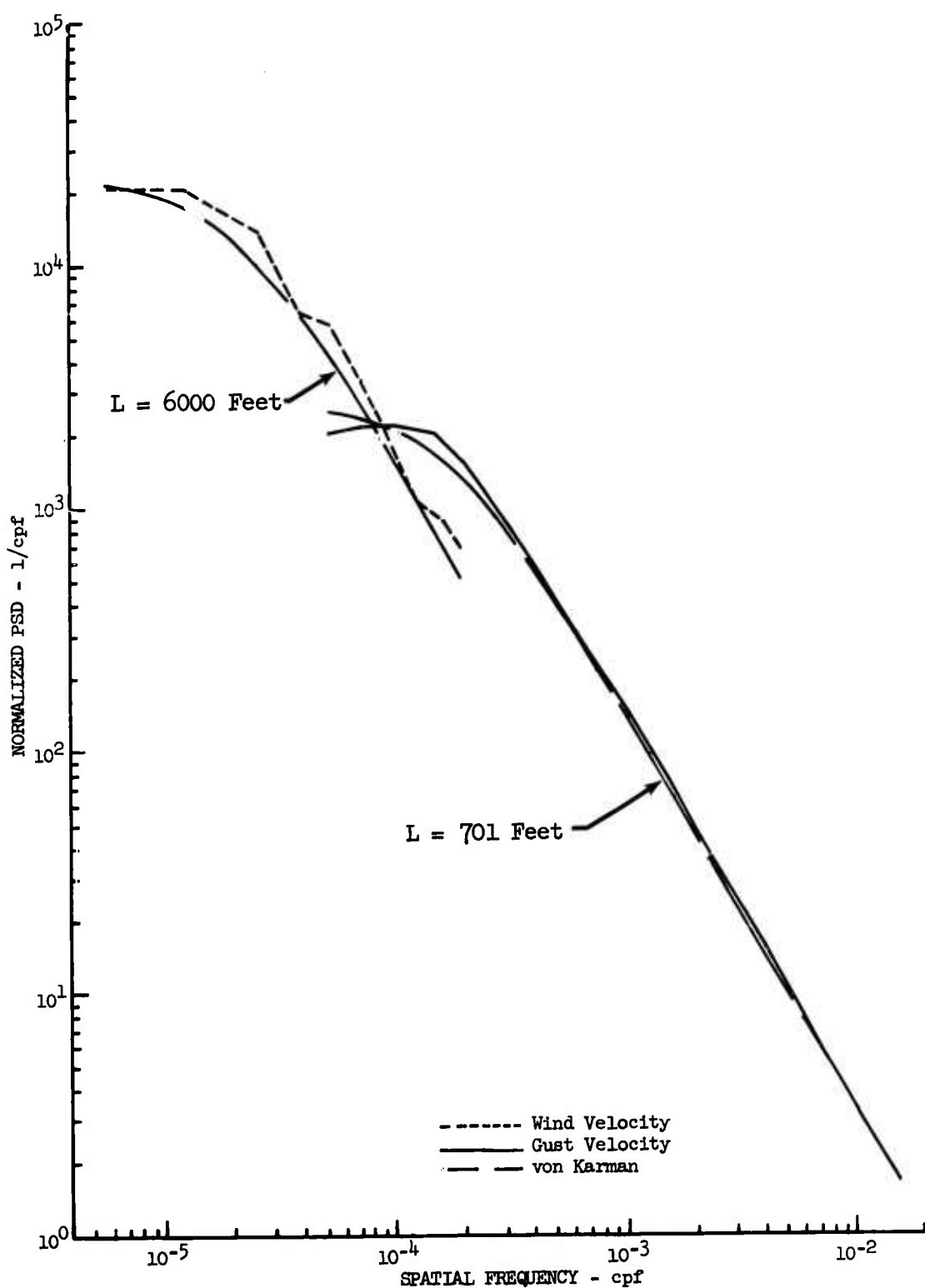


Figure 52.35 Average Longitudinal Wind and Gust Spectra for 30 Selected P^{+a} Samples

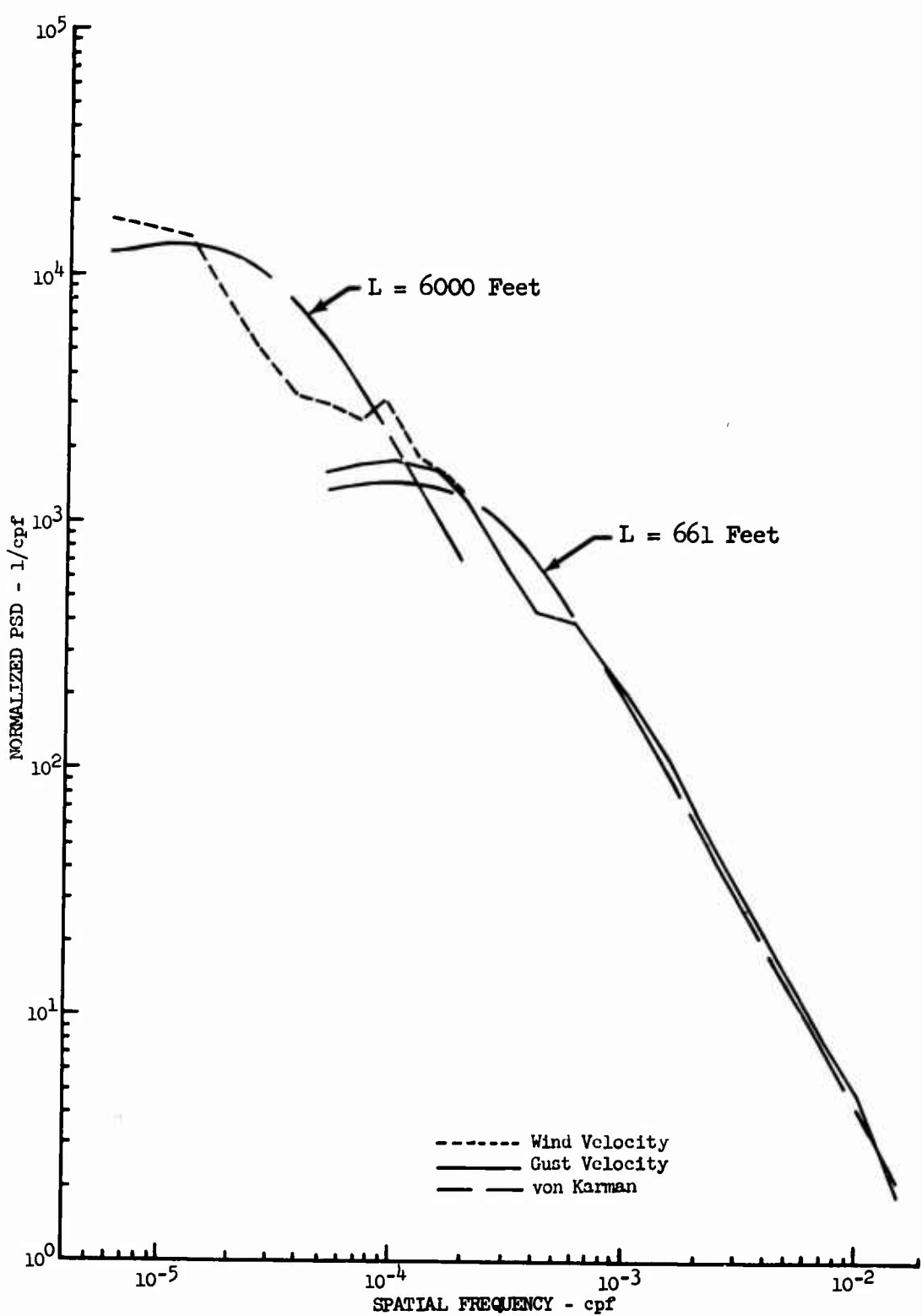


Figure 52.36 Average Lateral Wind and Gust Spectra for 30 Selected Data Samples

53. HIGH INTENSITY GUST PROGRAM RE-EVALUATION

The original High Intensity Gust Program digitized data tapes were processed using the same sequence of computer programs as used for LO-LOCAT Phase III. The major differences in these computer programs over those used originally are as follows:

- Low-pass digital filtering of measured altitudes to minimize noise content.
- Smoothing of the static pressure and outside air temperature measurements using a one second moving average.
- Gust velocity equations that did not involve small angle assumptions.
- Removal of spikes in the data if the differential between adjacent data points (at a sampling rate of 100 samples per second) of the gust velocity components exceeded 30 feet per second.
- High-pass digital filtering to remove low frequency drift from computed gust velocities.

Problem Areas

Some problem areas were encountered during the reprocessing of these data. One area involved the low-pass filters used during recovery of the data from the flight tape. When these data were digitized originally the ground station was equipped with 10 cps low-pass filters. These filters tend to attenuate the data to some extent below 10 cps and they were subsequently replaced with the 22 cps filters. Figure 53.1 shows a comparison of the gain factors of these two filters. Since it was necessary to use the original digitized data tapes for reprocessing, the data were attenuated to some extent below 10 cps. The effect of the 10 cps filters on the data and how it was compensated will be discussed later.

The distance from the airplane center of gravity accelerometers to the gust probe tip was not accounted for in the gust velocity equations (Equation V.12) when the data were reprocessed. The omission of this value resulted in the $\ell\dot{\theta}$ and $\ell\dot{v}$ terms being equal to zero in the vertical and lateral gust velocity calculations, respectively. Longitudinal gust velocity calculations were not affected. In order to determine the effect of this omission, a turbulence sample with considerable airplane motion was reprocessed with the correct value of ℓ included. Figures 53.2 and 53.3 show that there is only a small difference in lateral and vertical power spectra caused by omission of the $\ell\dot{\theta}$ and $\ell\dot{v}$ terms.

An additional check of this problem was accomplished by obtaining the minimum and maximum values of θ and v and calculating corresponding $\ell\dot{\theta}$ and $\ell\dot{v}$ values for each turbulence sample. Table 53.1 shows these extreme values as well as the average of these extremes for all 25 samples. It should be noted that these extreme values of θ and v do not necessarily occur at the

same instant as the extremes in gust velocity. An instantaneous value of gust velocity could however, vary as much as the extreme values shown for a particular sample.

TABLE 53.1

EXTREME VALUES OF \dot{L}_0 AND \dot{L}_V

Test	Sample	\dot{L}_0		\dot{L}_V	
		Minimum ft/sec.	Maximum ft/sec.	Minimum ft/sec.	Maximum ft/sec.
2-39	7	-1.88	4.14	-5.48	3.96
	8	-6.39	8.95	-10.34	7.02
	9	-3.49	4.76	-3.78	3.14
	10	-4.51	4.65	-4.16	5.30
	12	-2.80	4.52	-5.86	4.18
	13	-5.62	7.04	-6.52	5.22
	15	-5.78	7.49	-11.87	9.57
	18	-6.89	8.61	-9.69	5.98
	19	-9.55	9.42	-9.08	6.91
2-41	10-1	-2.20	3.82	-3.85	3.06
	10-2	-4.76	8.59	-6.53	4.31
	11	-5.06	7.21	-5.01	5.50
	12	-3.10	3.82	-5.64	3.80
	13	-5.25	5.17	-8.67	4.66
	14	-3.15	7.40	-4.77	4.50
	16	-4.82	5.56	-5.31	5.31
	18	-3.94	4.24	-9.29	4.85
	19	-4.10	5.81	-9.73	6.29
	21	-3.92	5.72	-6.18	4.87
	23-1	-6.57	6.10	-9.27	6.96
	Average	5.10	5.92	6.81	5.43

Comparison of Gust Velocities

Gust velocities which were computed during re-processing were high-pass filtered using the filter developed for the LO-LOCAT program (Appendix III). The major difference between these samples and those from the LO-LOCAT program is in sample length. The high intensity gust investigation samples that were reprocessed averaged only 66 seconds in length. Figure 53.4 shows a vertical gust velocity time history sample before and after this filter was applied. As shown in Figure 53.4 the high-pass filter removes low frequency drift. When these samples were processed originally they were high-pass filtered using a combination manual and automatic technique.

Straight line segments were manually drawn through the gust velocity time histories. This segmented line was then subtracted by computer from the data to yield high-pass filter data.

The difference between the two high-pass filtering techniques should be most apparent when comparing the maximum and minimum values. This is because the position of the high-pass filtering curve would determine the extreme values of gust velocity. Figures 53.5, 53.6, and 53.7 show comparisons of the original and reprocessed extreme values of the three components of gust velocity. These figures show that the extreme values of gust velocity were increased more often than not by the reprocessing technique.

Figure 53.6 shows one large incremental value of gust velocity which was reduced from approximately -170 to -102 fps by reprocessing. This was the most extreme value calculated originally. Further investigation of this sample (Test 2-59, Sample Number 12-2) revealed that a very high amplitude noise spike in static pressure had occurred at the same instant as the extreme gust. This spike resulted as an increase in the extreme gust velocity during the original processing. The smoothing routine used to smooth static pressure during reprocessing removed the effects of this spike. A special run was made with no smoothing. In this case the effects of the spike were removed by the spike removal routine used during reprocessing. The extreme value was again -102 fps. This example illustrates the value of both the smoothing and spike removal routines used during the LO-LOCAT programs.

Figure 53.8 shows comparisons of original and reprocessed values of rms gust velocities. The lateral and vertical rms values tended to vary in a random fashion due to reprocessing. The longitudinal values tended to be decreased more than they were increased but only by small amounts. The reason for this was probably due to difficulties in manual smoothing of longitudinal gust velocities which were changing greatly due to airplane maneuvers during contour flight over the mountainous terrain. It is concluded that gust velocities were changed very little when the data were reprocessed.

Gust Velocity Amplitude Analysis

The primary peak, amplitude, and level crossing count procedures of amplitude analysis were performed on these samples during reprocessing. These procedures are described in Section III of this report.

Figures 53.9, 53.10, and 53.11 are examples of primary peak, amplitude, and level crossings count distributions respectively for the same turbulence sample. The curves shown on the plot in Figure 53.9 represent those fitted by computer to the data points. These curves are the same as those developed for LO-LOCAT, Phase III data. The form of the equation is discussed in Section 8. The curves shown in Figure 53.11 represent Rice's equation (Equation 10.2).

Figure 53.12 compares the peak count distributions obtained originally for an individual turbulence sample with those obtained during reprocessing. This figure indicates only slight differences in the peak count distribution due to reprocessing. Amplitude and level crossings count were not performed originally so no comparisons could be made.

The peak, amplitude, and level crossings count data obtained for each sample was combined into a single category. Figure 53.13 is a combined peak count distribution for all the reprocessed turbulence samples. The distribution for the longitudinal component falls below the other two components. This is probably due to the low frequency response of the total pressure system caused by the low frequency response of the long pneumatic tubing runs used in the total pressure sensing system of this test airplane (Reference X.1). Figure 53.14 compares the lateral gust velocity peak count distribution for the reprocessed samples with a comparable category from LO-LOCAT Phase III. Figure 53.15 shows a similar comparison for the vertical gust velocity component. Except at the lower amplitudes the High Intensity Gust peaks show a higher rate of occurrence than for LO-LOCAT Phase III. The higher rate of peak occurrences for the High Intensity Gust Investigation at the higher gust velocities is due to the selection and reduction of data only from very turbulence patches of air. The Phase III distribution is higher at low amplitude for two reasons. First, the T-33 airplane flew at slower speeds and as a result measured shorter wavelengths (higher frequencies). Second, many light turbulence samples were included in the pooled Phase III peak count data.

Figures 53.16, 53.17, and 53.18 show the primary peak, amplitude, and level crossings count probability distributions, respectively for all the reprocessed samples combined. Comparison of these three figures shows the level crossings count to have the highest probability distribution curve and amplitude count the lowest with peak count in between. This relationship is consistent with that found for LO-LOCAT data.

Values of characteristic frequency were calculated by three different methods. In the first method, N_0 (in cycles per foot) was obtained from PSD data using Equation 11.1.

In the second method N_p (peaks per mile) was determined by extrapolation of the peak count distribution curve as described in Section 8. In the third method values of N_{OL} (crossings per mile) were obtained using Equation 11.2.

Average values from each of these methods were calculated for the 25 selected samples and are shown in Table 53.2. Also shown in this table are average N_p values for a comparable LO-LOCAT Phase category (Category 110003).

TABLE 53.2
COMPARISON OF CHARACTERISTIC FREQUENCIES

	Longitudinal	Lateral	Vertical
N_0 (occurrences/mile)	15.9	22.1	26.6
N_p (peaks/mile)	5.3	10.5	14.9
N_{OL} (crossings/mile)	11.2	17.2	24.6
N_p (LO-LOCAT Phase III (Peterson - High Mts. - 250 feet)	23.9	31.4	46.2

The average value for the longitudinal component was the smallest and vertical the largest with lateral falling in between for all three computational methods. This relationship is consistent with results obtained for LO-LOCAT Phase III data. As discussed in Section 11 the characteristic frequency obtained is dependent upon the frequency range of the turbulence being investigated. Due to the higher speed of the F-106 airplane and selection of only high intensity turbulence patches for investigation, these characteristic frequencies are smaller than those obtained for Phase III.

The values of characteristic frequency obtained using level crossings data are considerably larger than those from peak count. This is because gust velocity level crossings values correspond to unextrapolated peak count values. The reason for gust velocity peak count extrapolation is explained in Section 8.

The peak count characteristic frequencies were obtained using a curve developed for LO-LOCAT Phase III data to extrapolate the distribution curve to zero amplitude. This curve was an optimum curve for Phase III data but had a tendency to give low values for these data. The High Intensity Gust Investigation N_p values are considered to be somewhat low and as a result caused σ_{pe} values to be high. Reasonable agreement between characteristic frequencies obtained from PSD and level crossings data were obtained.

The average gust velocity standard deviation values obtained from the three different counting techniques are given in Table 53.3. The average time series standard deviation values (σ_t) compare well with the level crossings standard deviation (σ_L). The peak count standard deviation (σ_{pe}) values are larger than for the other two counting techniques. These values are larger because the characteristic frequency values (Table 53.2) used in the calculation of σ_{pe} (Equation 8.5) are smaller than for the other two techniques. The peak count characteristic frequencies were obtained by extrapolating the peak count distribution curve to zero amplitude using a curve developed for LO-LOCAT Phase III. Better agreement between σ_{pe} , and other standard deviation values would have been obtained had sufficient high intensity gust samples been reprocessed to develop a new extrapolation curve for the peak count distributions.

TABLE 53.3
AVERAGE STANDARD DEVIATIONS FOR THE REPROCESSED
HIGH INTENSITY GUST INVESTIGATION SAMPLES

	u	v	w
σ_t	12.43	24.17	16.06
σ_{pe}	16.31	26.33	19.75
σ_L	12.93	25.02	16.91

The chi-square test for statistical normality was performed on each sample reprocessed. The chi-square procedure is described in Section 7. A cumulative probability distribution of the chi-square values from the 25 samples

is shown in Figure 53.19. Levels of significance based on the number of degrees of freedom for these data are shown. This figure indicates that approximately 96 percent of the longitudinal, 92 percent of the vertical, and only 56 percent of the lateral turbulence samples were accepted as normally distributed at the 0.02 level of significance. The lateral gust velocities were probably much less normally distributed than the other two components and the LO-LOCAT data (Figure 7.1) due to their higher magnitude and the shorter sample lengths associated with the High Intensity Gust Investigation Program. The object of this program was the investigation of high intensity gusts. It involved the selection of short time intervals of high intensity gusts, usually in the area of mountain lee waves. If longer time intervals with less lee wave activity had been selected, the three gust velocity components would probably have been more nearly equal in wavelengths and more normally distributed.

Frequency Analysis

Power spectral densities were computed for the 25 turbulence samples selected for reprocessing. These data had been recovered from the flight tape and digitized when the ground station was equipped with 10 cps low-pass analog filters. As previously discussed, these filters attenuated the data to some extent below 10 cps. It was not within the scope of this program to reprocess all samples through the ground station. Therefore, to determine the effect of the 10 cps filters, the spectrum for a turbulence sample which had been processed with them was converted to what it would have been for 22 cps filters using Equation 53.1.

$$\Phi(f)_{22} = \Phi(f)_{10} \left[\frac{G(f)_{22}}{G(f)_{10}} \right]^2 \quad (53.1)$$

Figures 53.20 through 53.22 show the change in gust velocity spectra due to the different filters. As shown by these figures the power spectra is increased at the higher frequencies by using the 22 cps filters. The power spectra originally computed is also shown in these figures so that spectral shapes can be compared. The change in spectral shape between the original and reprocessed data is insignificant except at the lowest frequencies. This difference is attributed to the effects of the improved high-pass filtering performed during reprocessing.

Figures 53.23 through 53.25 show the average spectra normalized by σ_t^2 for the reprocessed samples. These spectra are corrected to represent data obtained using 22 cps filters. The average spectra obtained at 250 feet altitude over the high mountains of the Peterson Field, Colorado, route during LO-LOCAT Phase III are also shown on these plots for comparison purposes. The Phase III spectra has a shallower slope than the reprocessed spectra. The longitudinal spectra had the steepest slope. This was no doubt due to the lowered frequency response caused by the long tubing runs as mentioned previously. However, both the lateral and the vertical spectra appear to have slightly steeper slopes than the LO-LOCAT spectra. This may also be due, in part, to a frequency response problem. The frequency response characteristics of the probe and associated instrumentation used during the High Intensity Gust Investigation was never adequately determined.

Contrary to what would be expected, the LO-LOCAT PSD curves in Figures 53.22 through 53.25 extend to lower spatial frequency than the High Intensity Gust PSD curves. This is due to the method used during calculation of the PSD's. The Δf used for the relatively short High Intensity Gust samples was considerably larger than for much longer LO-LOCAT Phase III samples. This large Δf was used in order to maintain approximately the same statistical confidence as for the Phase III spectra. Statistical confidence is discussed in Section 20. The degrees of freedom and confidence interval for the High Intensity Gust PSD were 52 and ± 38 percent, respectively, compared with 45 and ± 42 percent for Phase III. The Δf used for LO-LOCAT Phase III was 0.0416 cps and for the High Intensity Gust Investigation it varied from 0.149 to .298 depending on sample length. Due to the large Δf values used, the first spectral estimate for the High Intensity Gust samples occurred at a considerably higher spatial frequency than for the LO-LOCAT Phase III samples.

Spectra obtained for the reprocessed samples were compared to the von Karman, Bush-Panofsky, and Lumley-Panofsky mathematical spectra. The expressions for these mathematical spectra are given by Equations 28.1, 28.2, 28.7, and 28.8. Experimental-to-mathematical ratios were computed by dividing the experimental spectra by the mathematical spectra. These ratios were plotted versus spatial frequency. A ratio of 1 indicates perfect agreement between experimental and mathematical spectra. Average experimental to mathematical ratios were computed for the reprocessed samples and are shown in Figures 53.26 and 53.27. The broken lines in these figures represent 10 cps low-pass filtered data. The solid lines represent data corrected to 22 cps filtering. The data corrected to indicate 22 cps filtering shows better agreement with the mathematical expressions than does the 10 cps filtered data. Longitudinal spectra does not show as good agreement with mathematical spectra as do the lateral and vertical components. Again, this is due to the low frequency response of the long pneumatic tubing runs in the total pressure system of the airplane. Figures 53.26 and 53.27 shows that the reprocessed lateral and vertical spectra relationship to mathematical expressions is similar to that shown for LO-LOCAT in Figures 28.1 and 28.3, respectively.

Homogeneity as described in Section 21 was investigated for the reprocessed samples. Figure 53.28 shows the average homogeneity versus spatial frequency for these samples. These samples show good homogeneity, probably due in part to the method of data editing used. Each of these turbulence samples was selected from time history plots using apparent homogeneity as one of the criteria. For this reason computed homogeneity was expected to be good.

The statistical independence of these samples was investigated using the coherency function as described in Section 20. The average lateral to vertical coherency function versus spatial frequency is shown in Figure 53.29. The lateral to longitudinal coherency is not shown due to the known longitudinal frequency response problem. When two parameters have a coherency equal to zero they are completely independent. Inspection of Figure 53.23 indicates that the average statistical independence increases for these samples as spatial frequency increases.

The isotropy of these turbulence samples was also investigated. Isotropy was computed as described in Section 22. Figure 53.29 shows the average vertical to lateral isotropy ratio versus spatial frequency for the 25

selected samples. Longitudinal to lateral isotropy ratios are not shown due to the longitudinal frequency response problem. The isotropy ratios shown in Figures 53.29 indicate more isotropy with increasing spatial frequency. The vertical and lateral components also indicate less isotropy at the lower frequencies when compared with the LO-LOCAT data. This is probably because the airplane was flown at a lower altitude during the High Intensity Gust Investigation, and the longer wavelengths of the vertical component are being more attenuated.

Turbulence Scale Lengths

Scale lengths were computed for the reprocessed samples using the von Karman Equations 30.2 and 30.3. The scale lengths computed included some error due to the use of 10 cps low-pass filters. As discussed previously, these filters tend to attenuate the data at higher frequencies. Both σ_t and σ_T are affected by this filter and both are involved in the computation of scale lengths. Corrected σ_t and σ_T values were computed for a turbulence sample to determine the effects of the 10 cps filter. Scale lengths for this sample were then re-computed using the corrected σ_t and σ_T values. Scale lengths were decreased by the following: longitudinal by 9 percent; lateral by 11 percent; and vertical by 13 percent. The scale lengths for all samples were therefore decreased by these percentages. The average value of these corrected scale lengths are given in Table 53.4. Also shown in this table for comparison purposes are the average values for comparable LO-LOCAT Phase III scale lengths. As shown by this table, considerably larger scale lengths were obtained for the High Intensity Gust Investigation.

The longer scale lengths probably occur because of the steeper slope of the spectra which would attenuate the relative magnitude of σ_T , and also because the airplane was flown at a higher average speed during the High Intensity Gust Investigation (713 fps compared with 648 fps) which would result in longer wavelengths being measured.

TABLE 53.4

COMPARISON OF HIGH INTENSITY GUST INVESTIGATION SCALE LENGTHS WITH THOSE OBTAINED DURING LO-LOCAT PHASE III

	Average Scale Length in Feet		
	L_{ku}	L_{kv}	L_{kw}
LO-LOCAT Phase III High Mountain, 250 Feet	775	636	452
High Intensity Gust Investigation	1432	1335	616

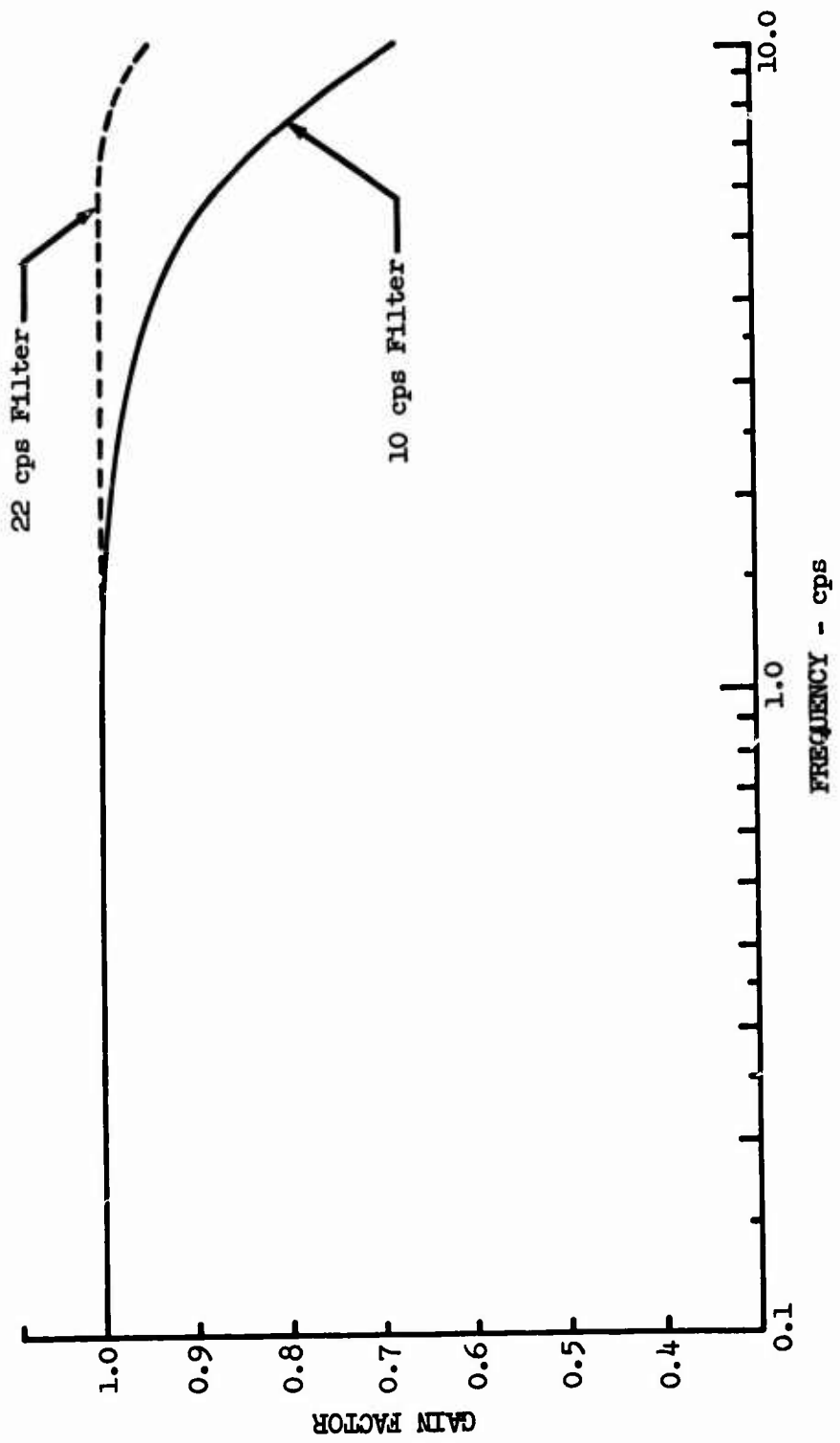


Figure 53.1 Ground Station Low-Pass Analog Filters

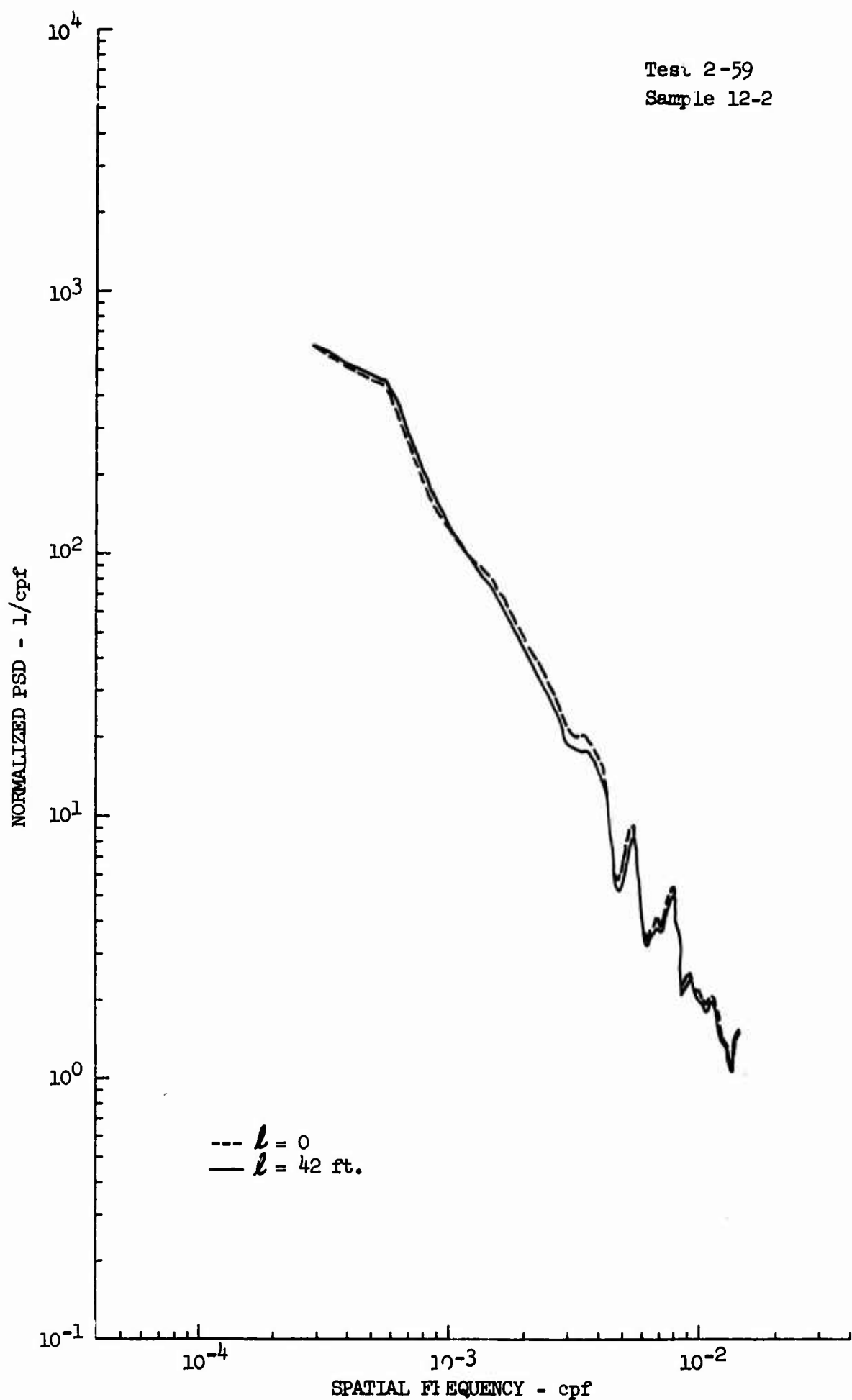


Figure 53.2 Effects of Accelerometer Location Correction on
Lateral Gust Velocity Power Spectral Density

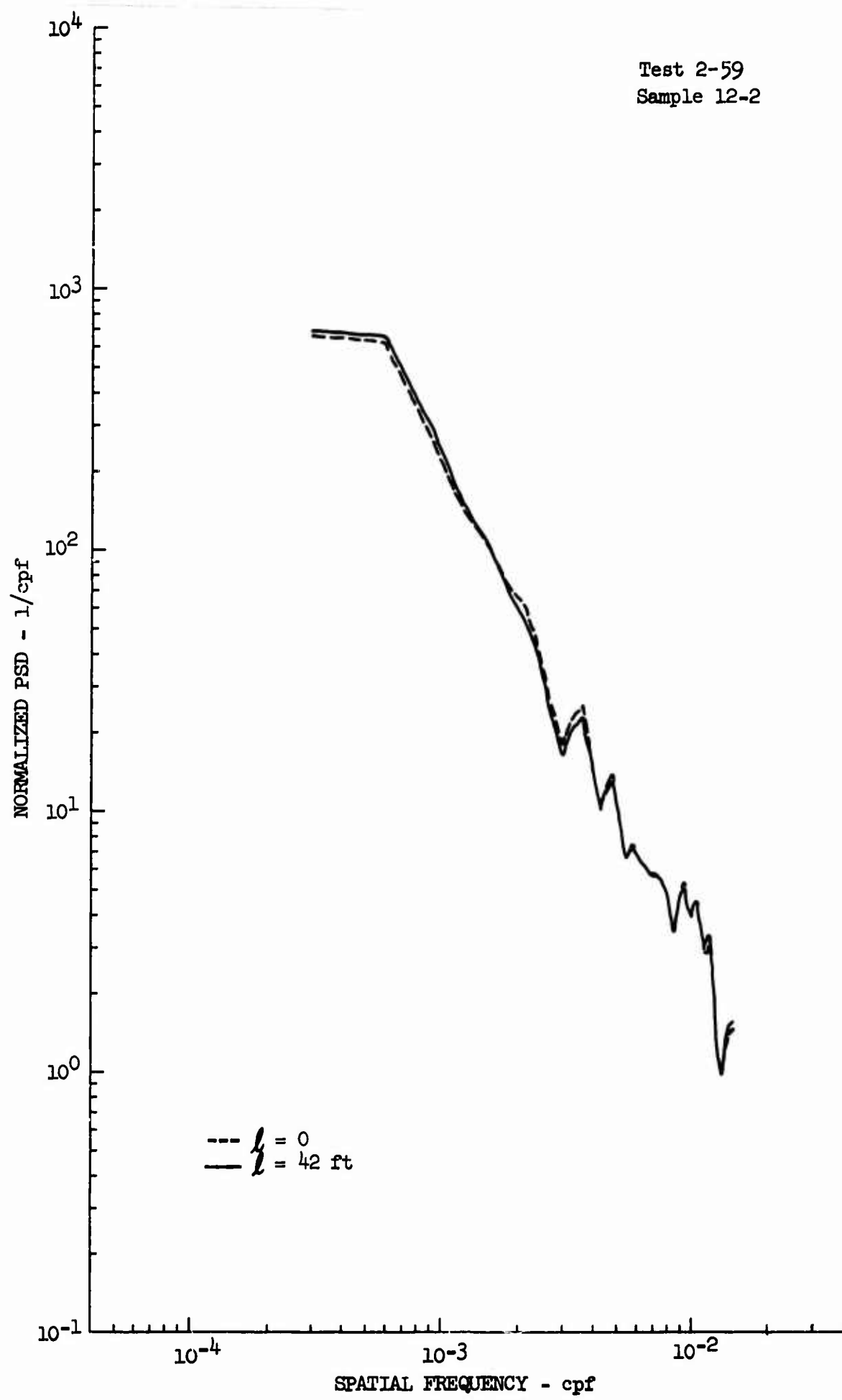


Figure 53.3 Effects of Accelerometer Location Correction on Vertical Gust Velocity Power Spectral Density

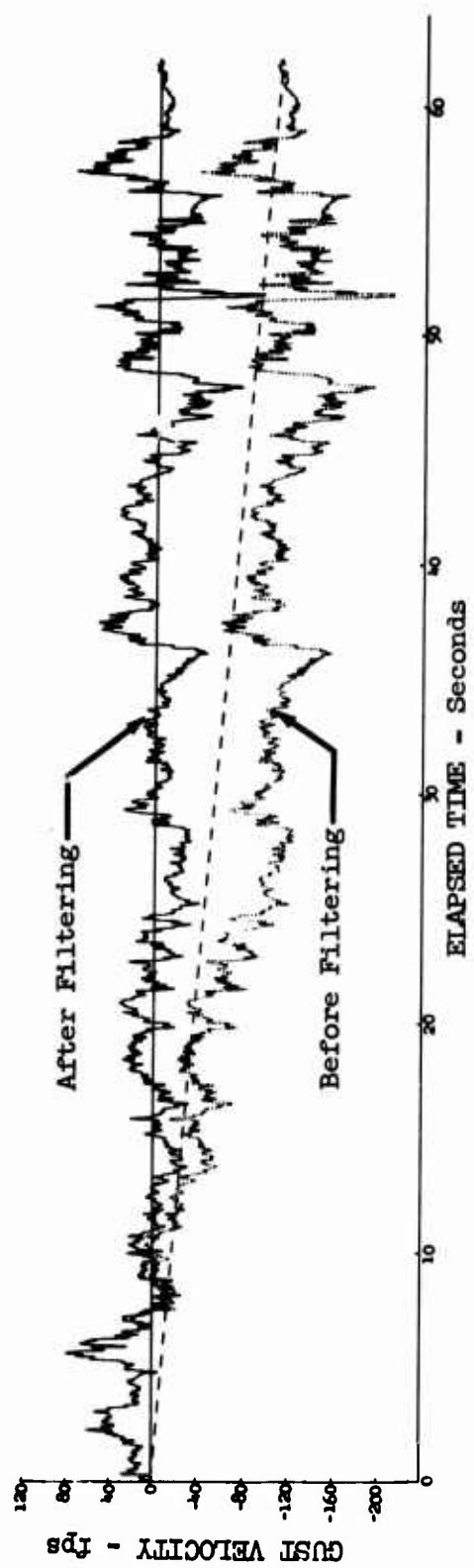


Figure 53.4 Comparison of Vertical Gust Velocity Time History
Before and After High-Pass Filtering

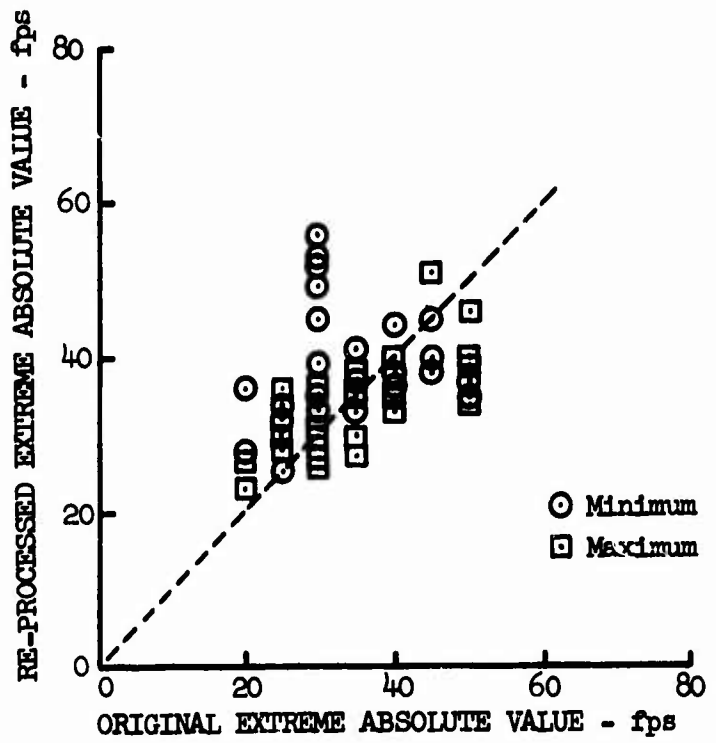


Figure 53.5 Comparison of Original and Re-Processed Extreme Values of Longitudinal Gust Velocity

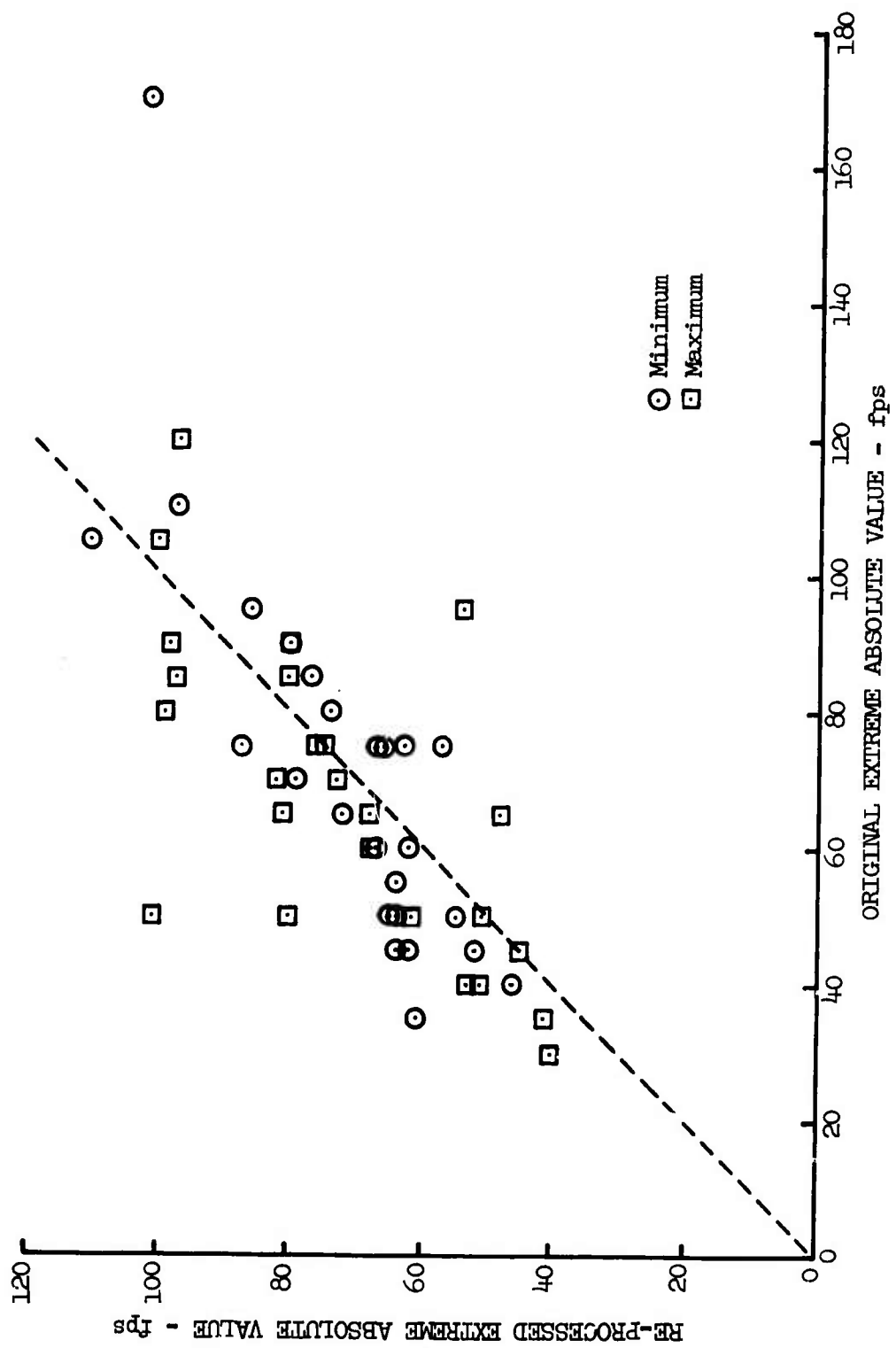


Figure 53.6 Comparison of Original and Re-Processed Extreme Values of Lateral Gust Velocity

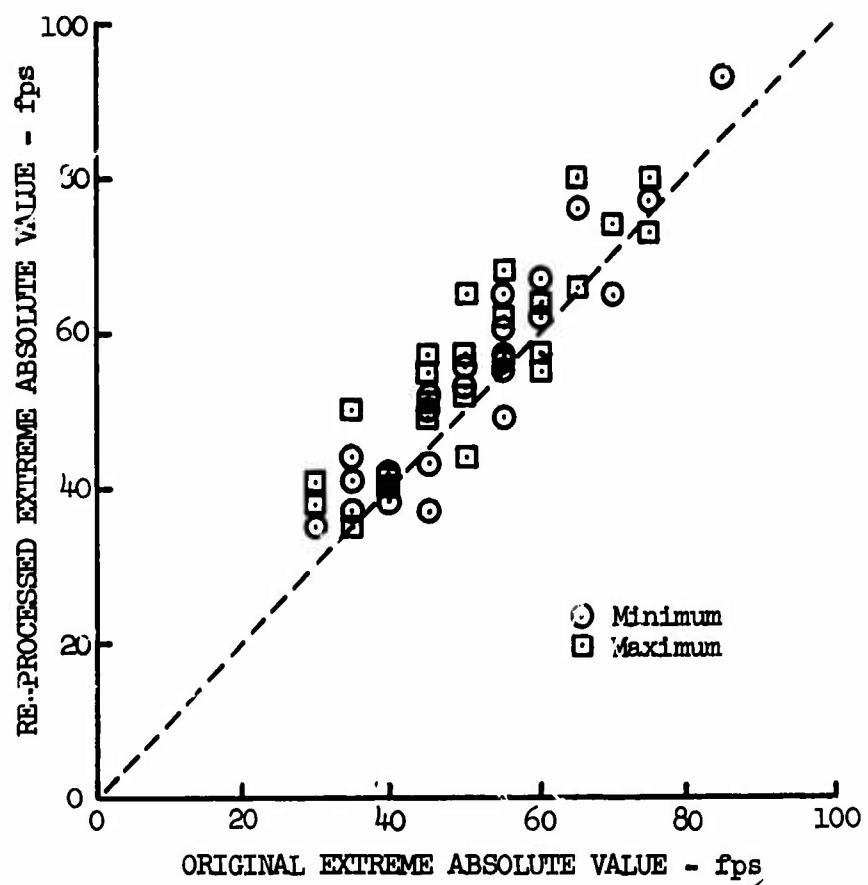


Figure 53.7 Comparison of Original and Re-Processed Extreme Values of Vertical Gust Velocity

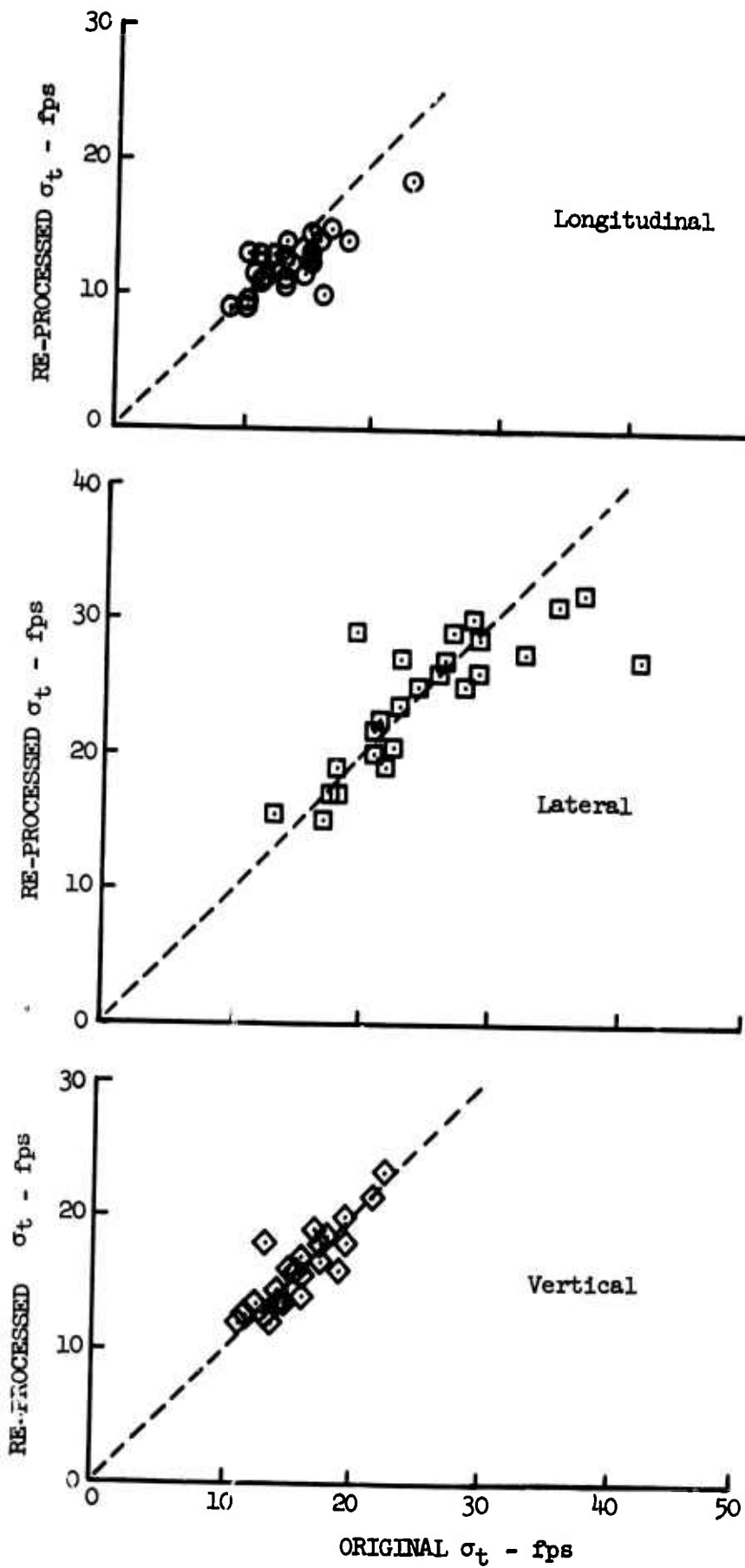


Figure 53.8 Comparison of Original and Re-Processed RMS Gust Velocities

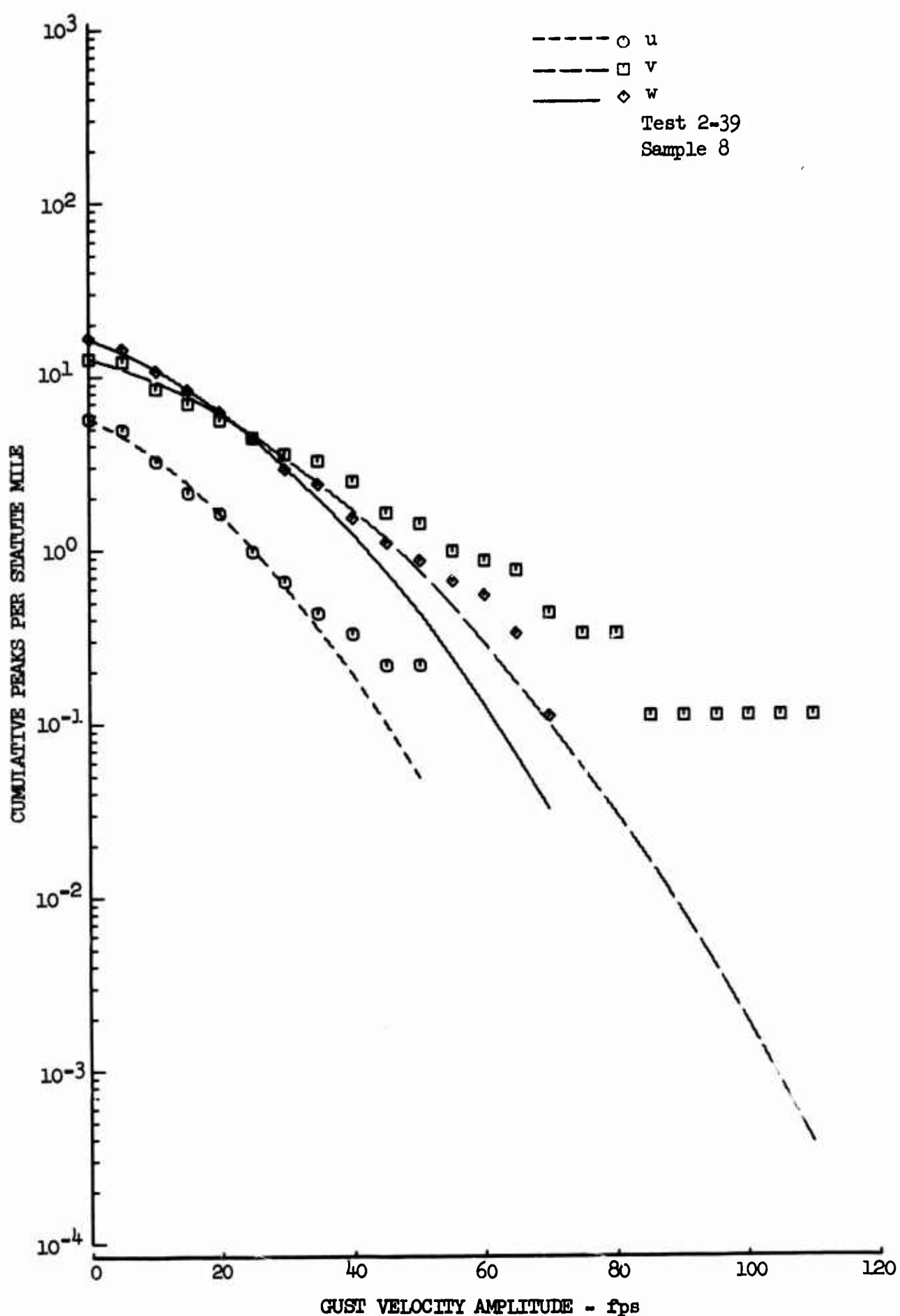


Figure 53.9 Gust Velocity Peak Count Distribution for an Individual Sample

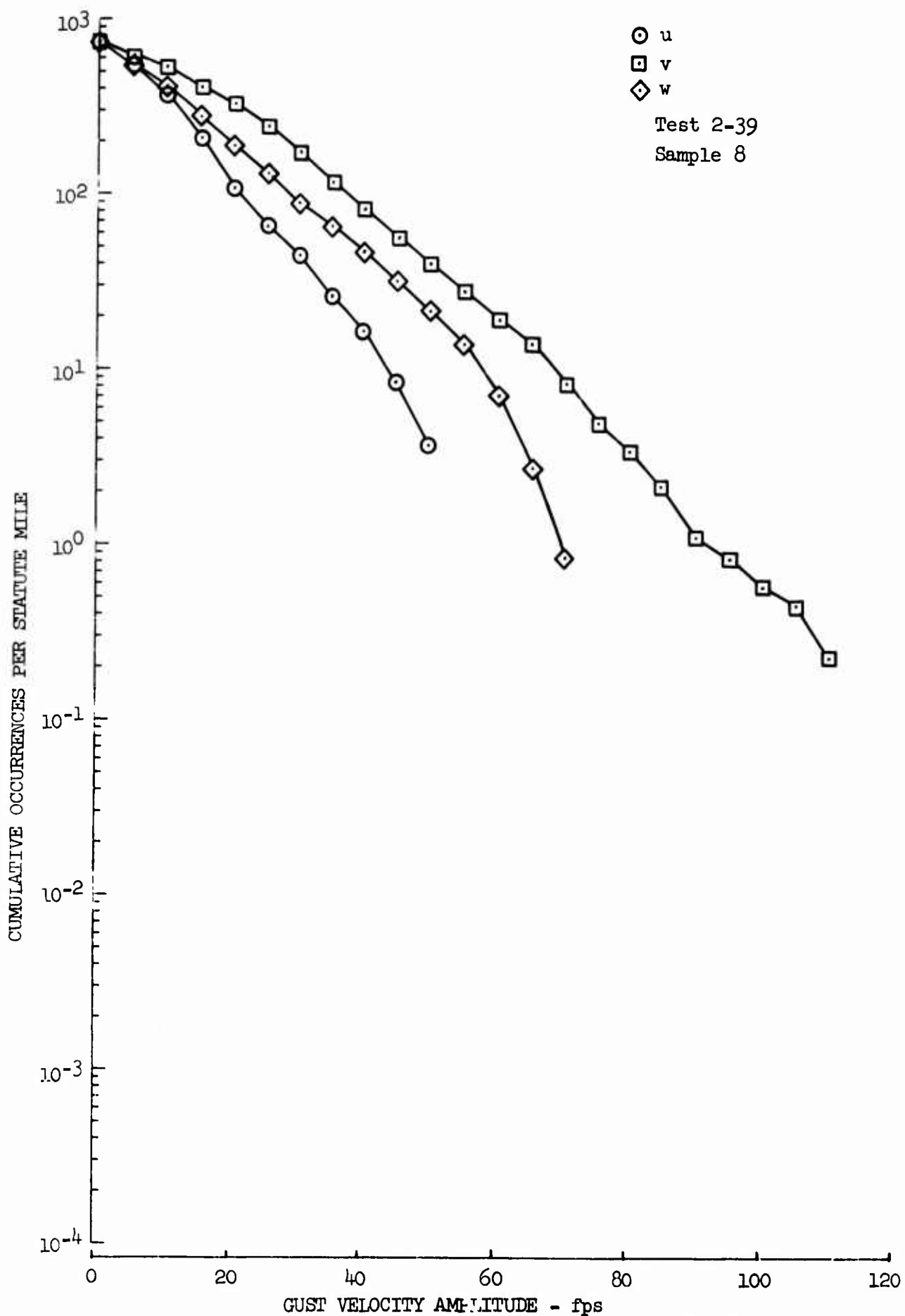


Figure 53.10 Gust Velocity Amplitude Count Distribution
for an Individual Sample

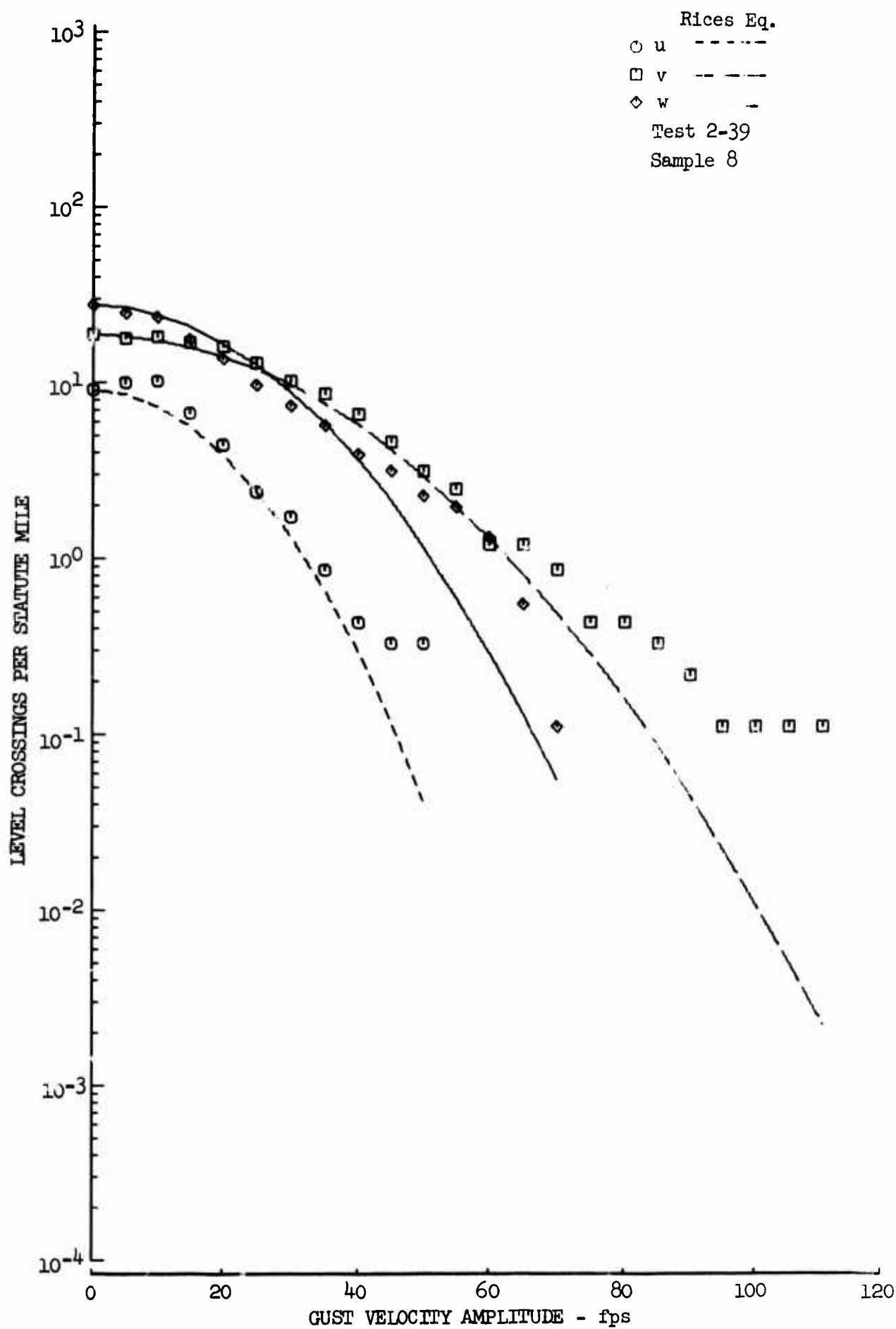


Figure 53.11 Gust Velocity Level Crossing Distribution for an Individual Sample

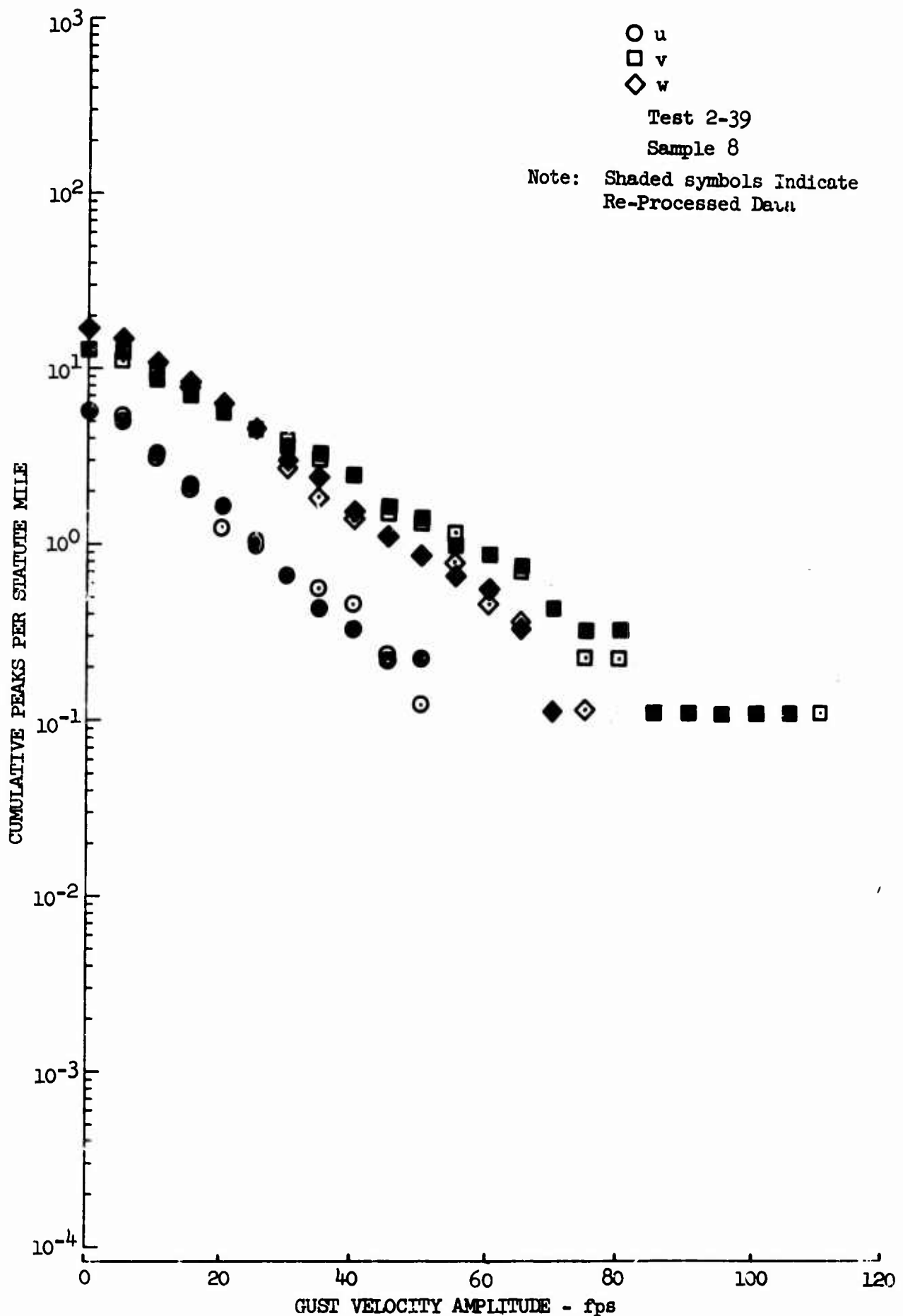


Figure 53.12 Comparison of Original and Re-Processed Peak Count Distributions

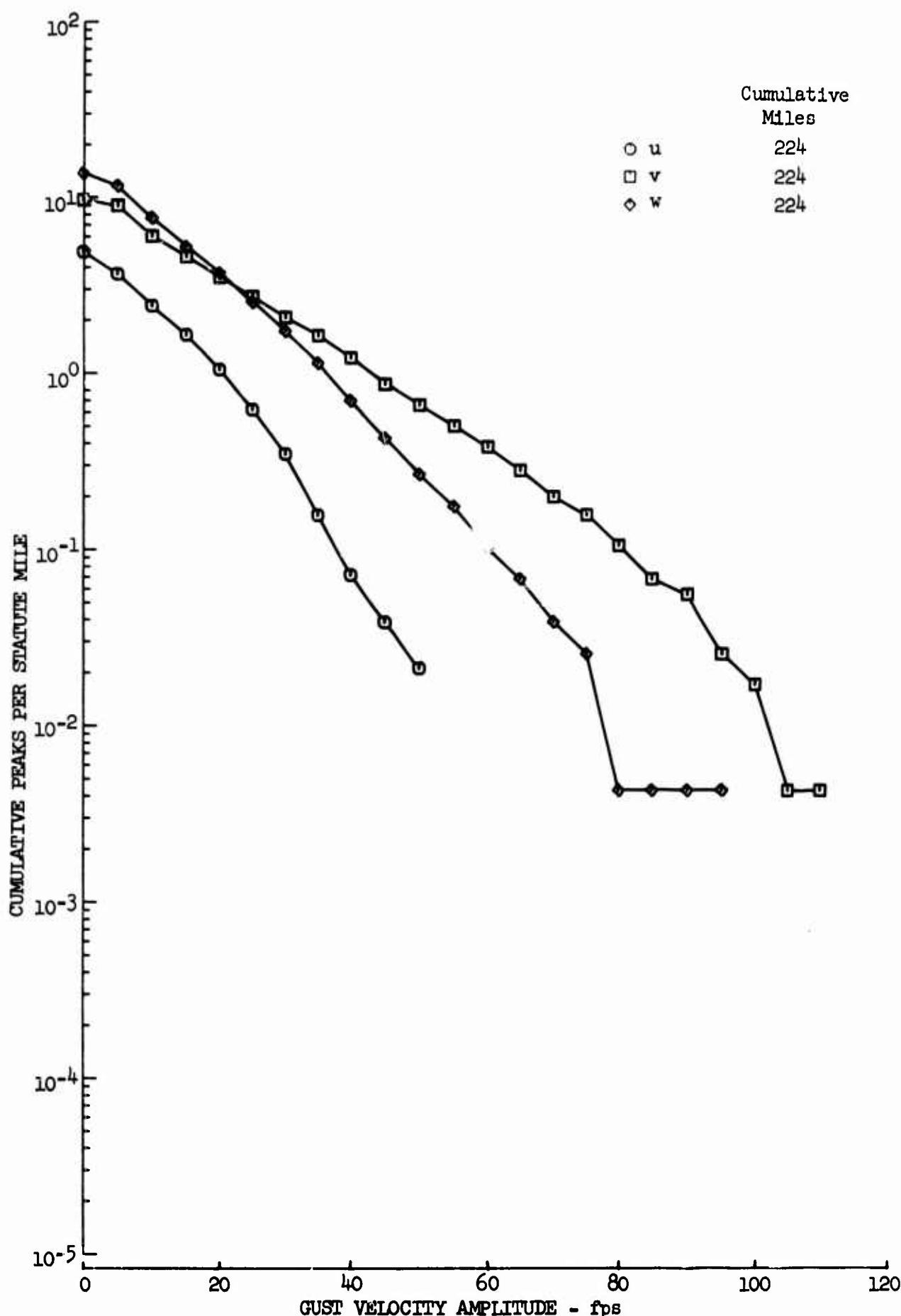


Figure 53.13 Gust Velocity Peak Distribution for Re-Processed High Intensity Gust Samples

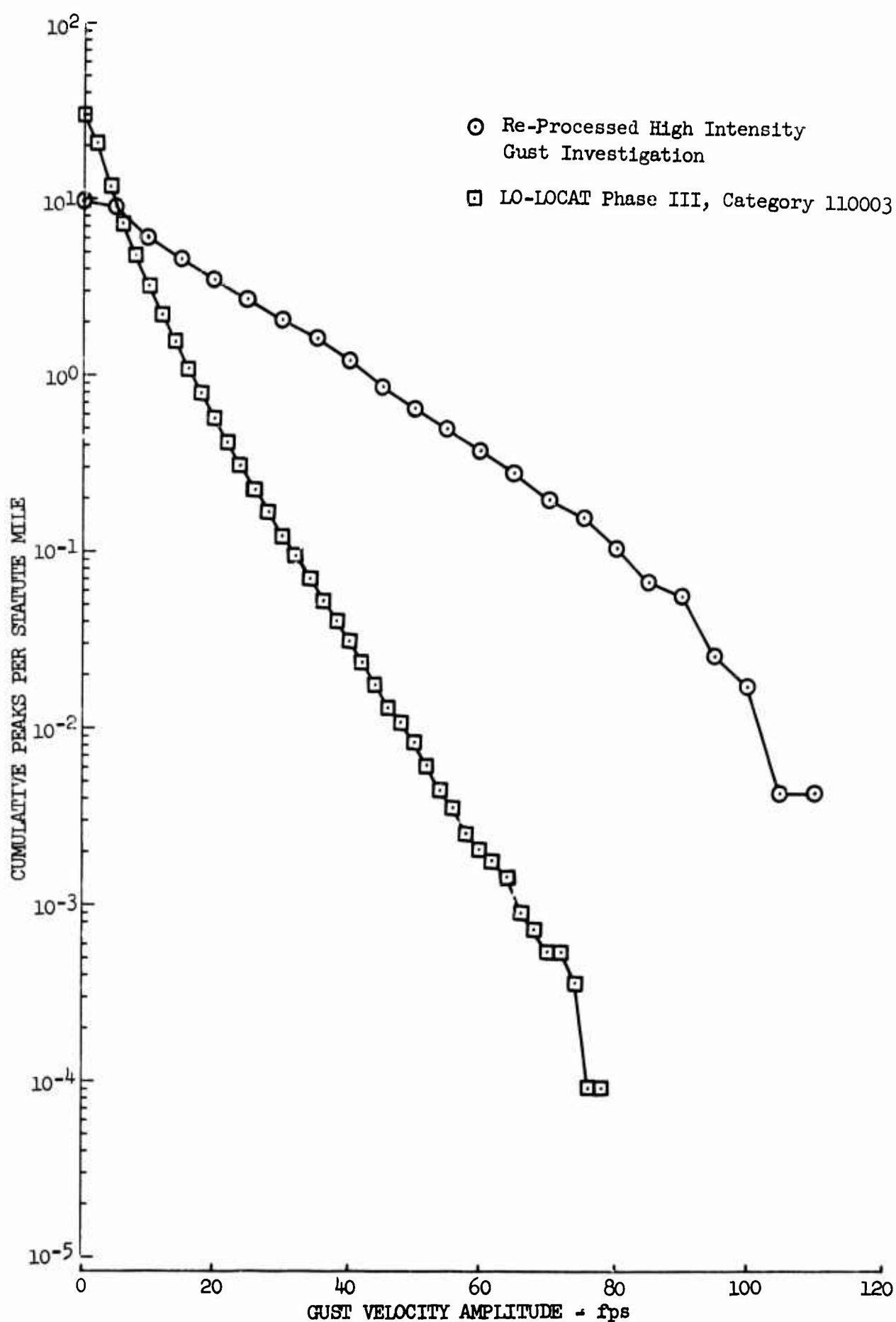


Figure 53.14 Comparison of Lateral Gust Velocity Peak Count From High Intensity Gust Investigation and LO-LOCAT Phase III

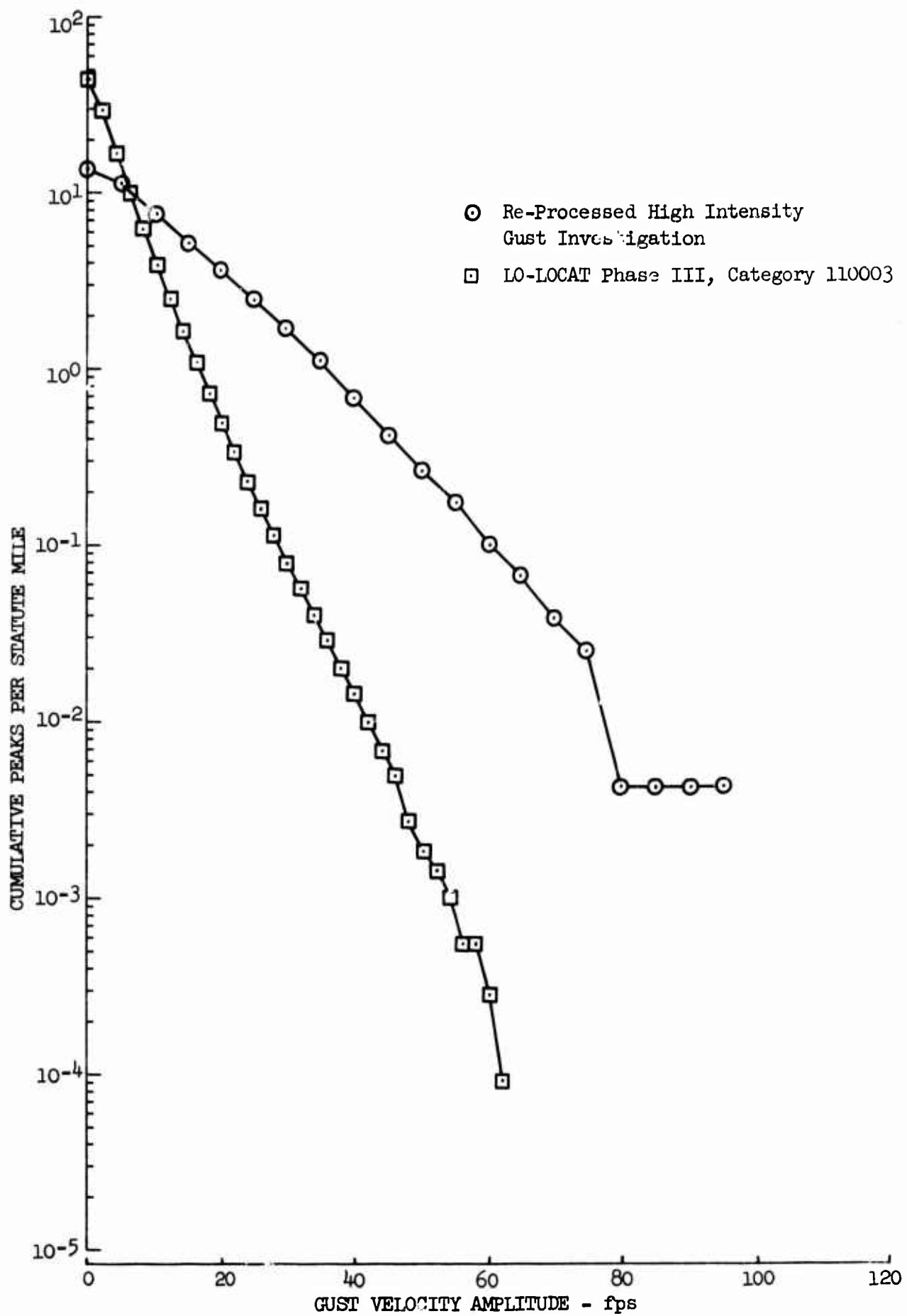


Figure 53.15 Comparison of Vertical Gust Velocity Peak Count From High Intensity Gust Investigation and LO-LOCAT Phase III

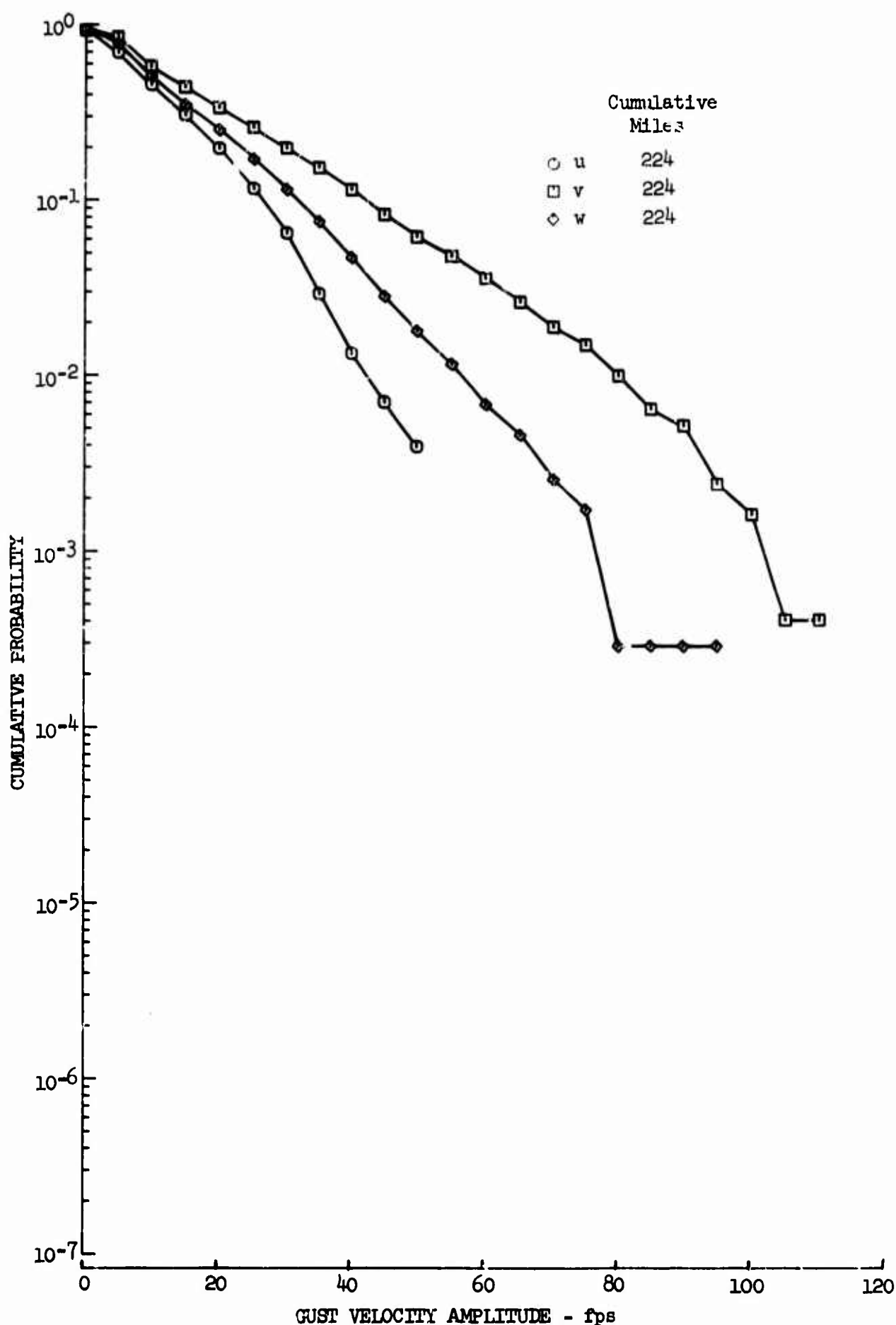


Figure 53.16 Gust Velocity Peak Count Probability Distribution for Re-Processed High Intensity Gust Samples
436

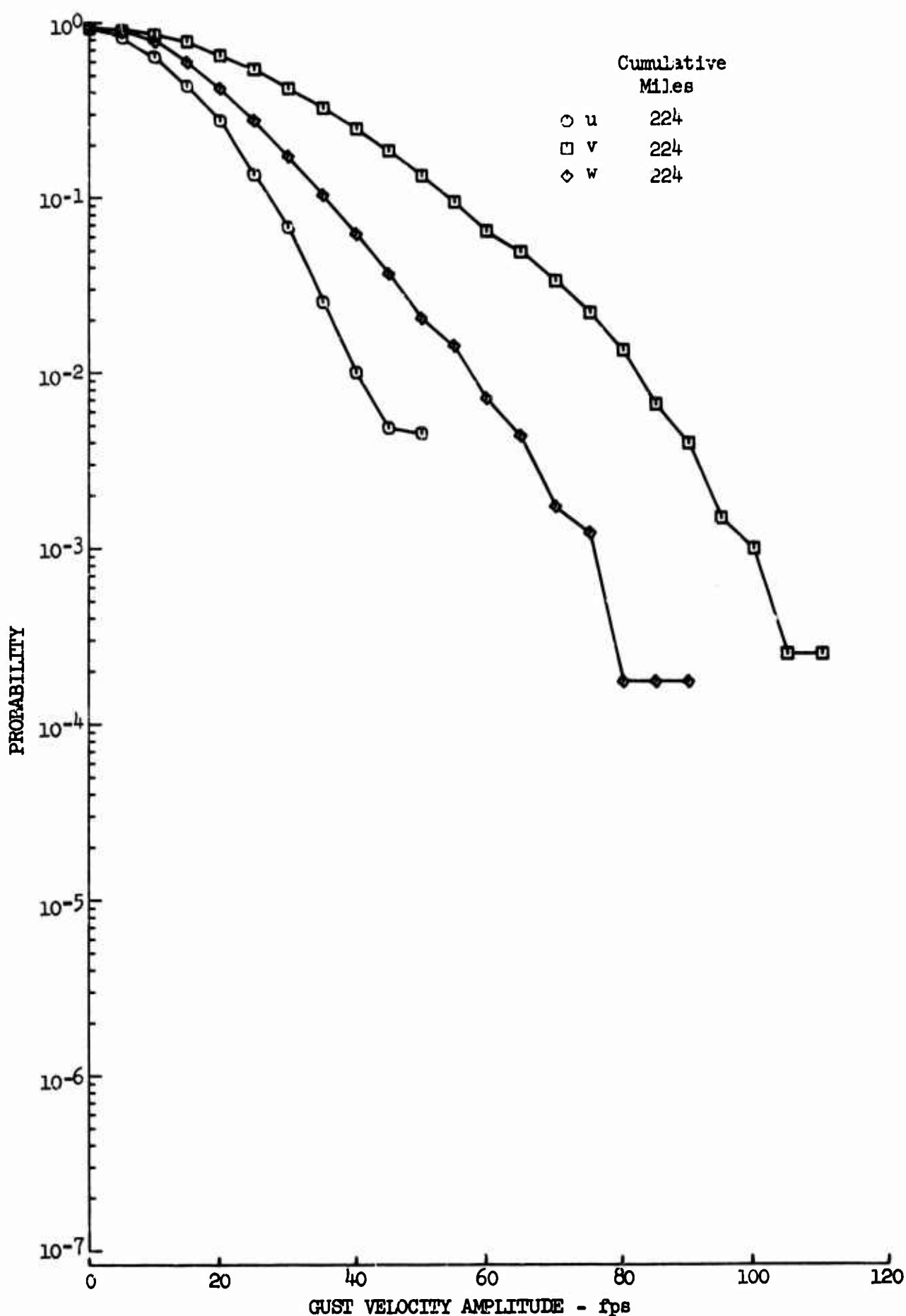


Figure 53.17 Gust Velocity Level Crossing Probability Distribution for Re-Processed High Intensity Gust Samples

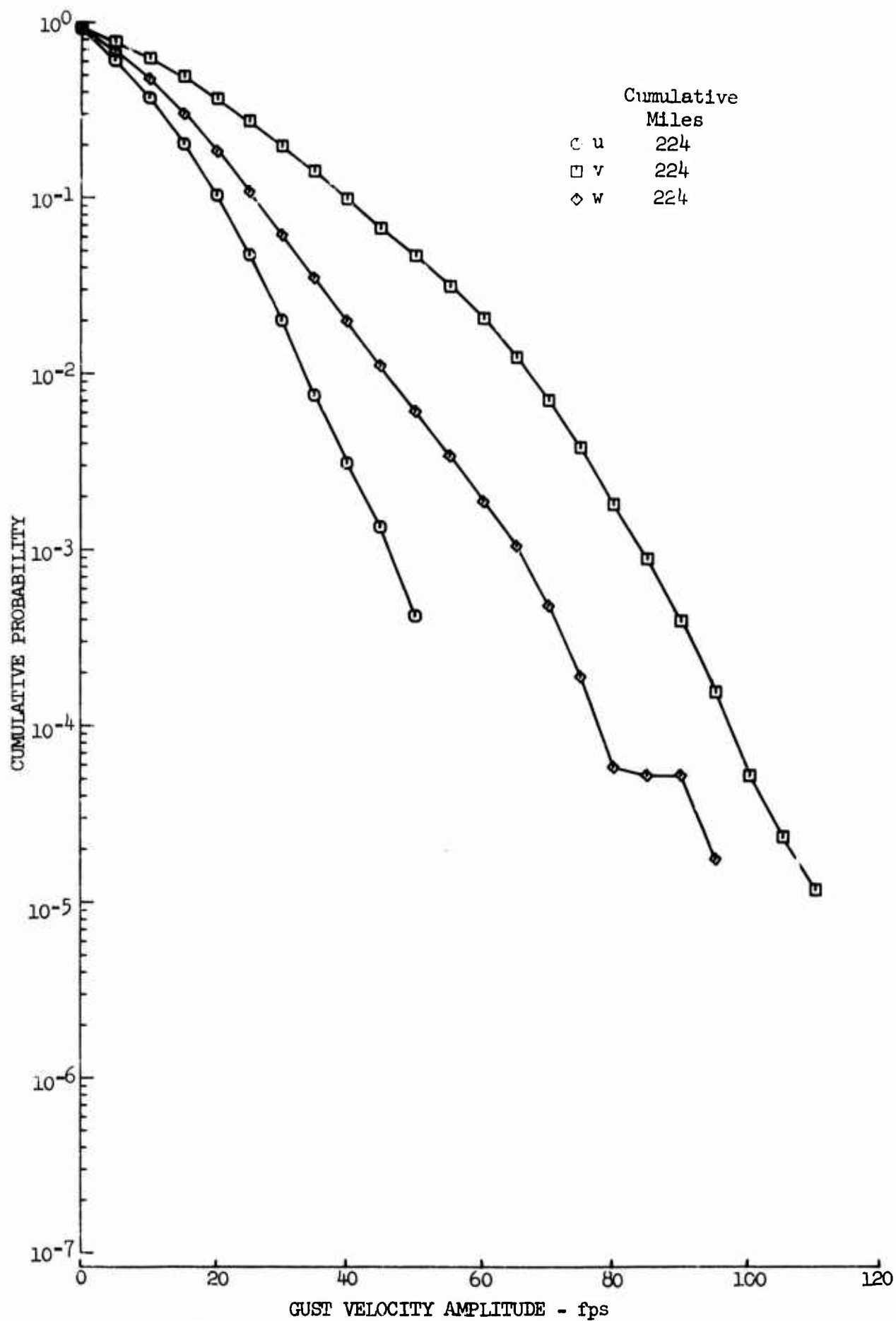


Figure 53.18 Gust Velocity Amplitude Count Probability Distribution for Re-Processed High Intensity Gust Samples

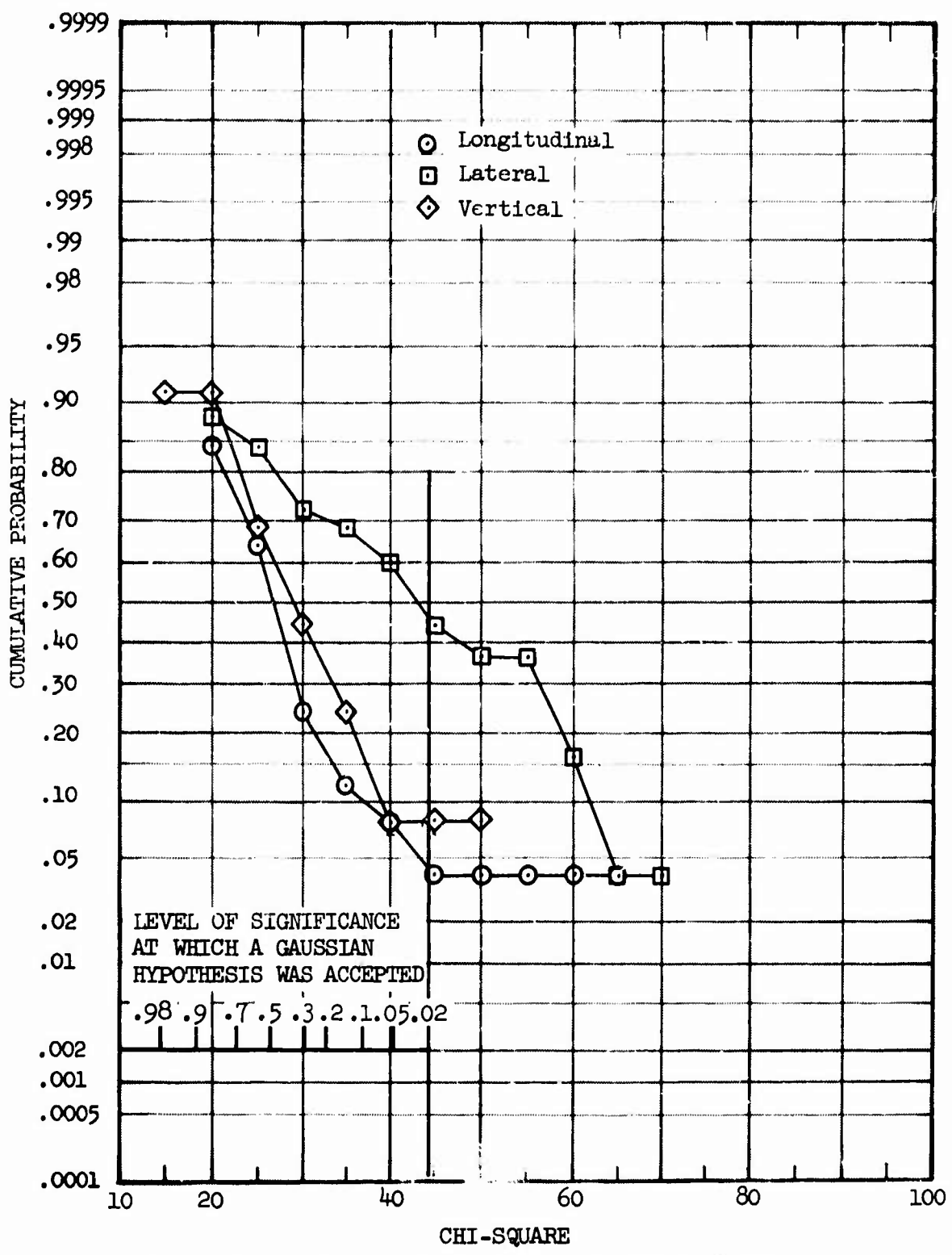


Figure 53.19 Chi-Square Test for Statistical Normality

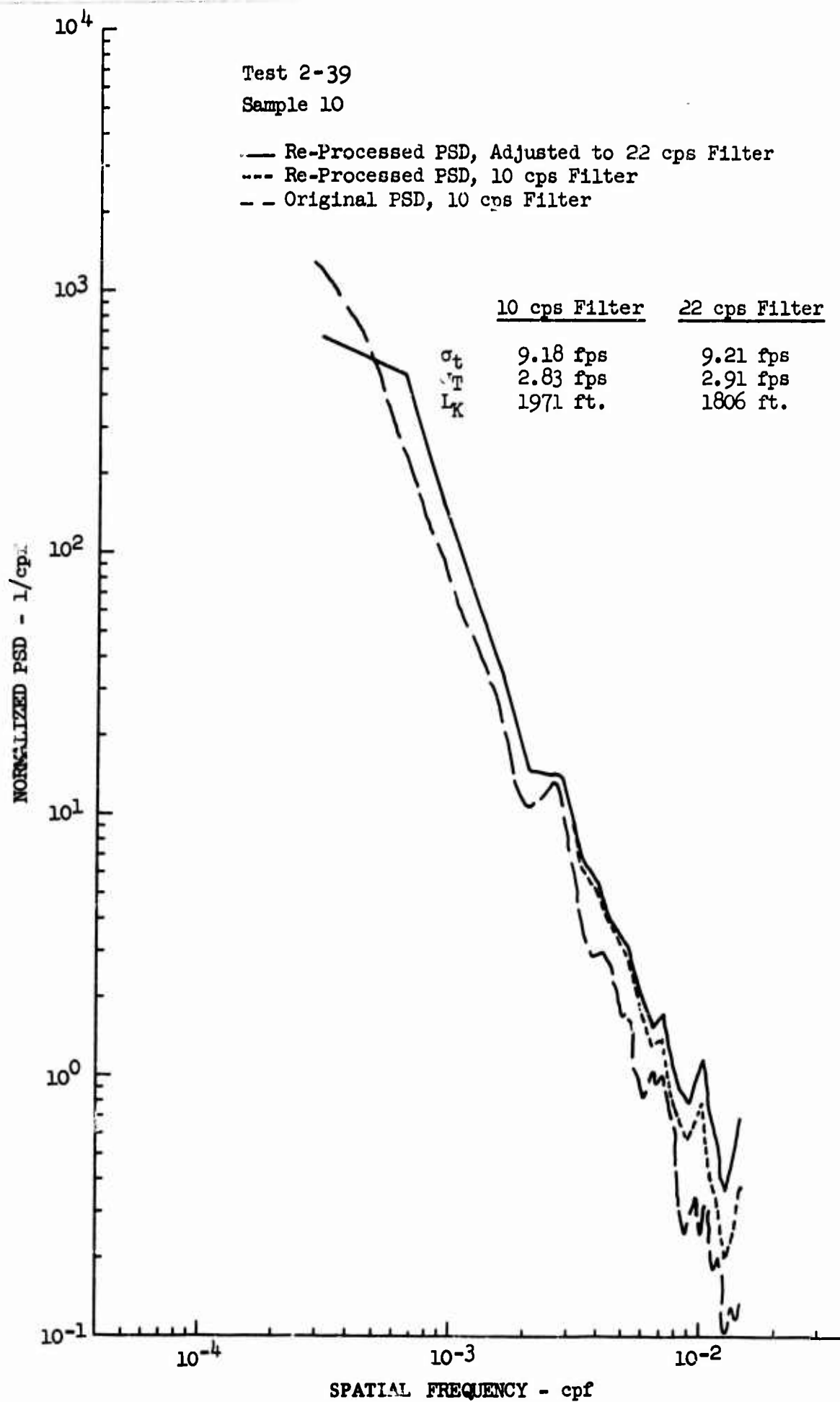


Figure 53.20 Longitudinal Gust Velocity Power Spectra of an Individual Turbulence Sample

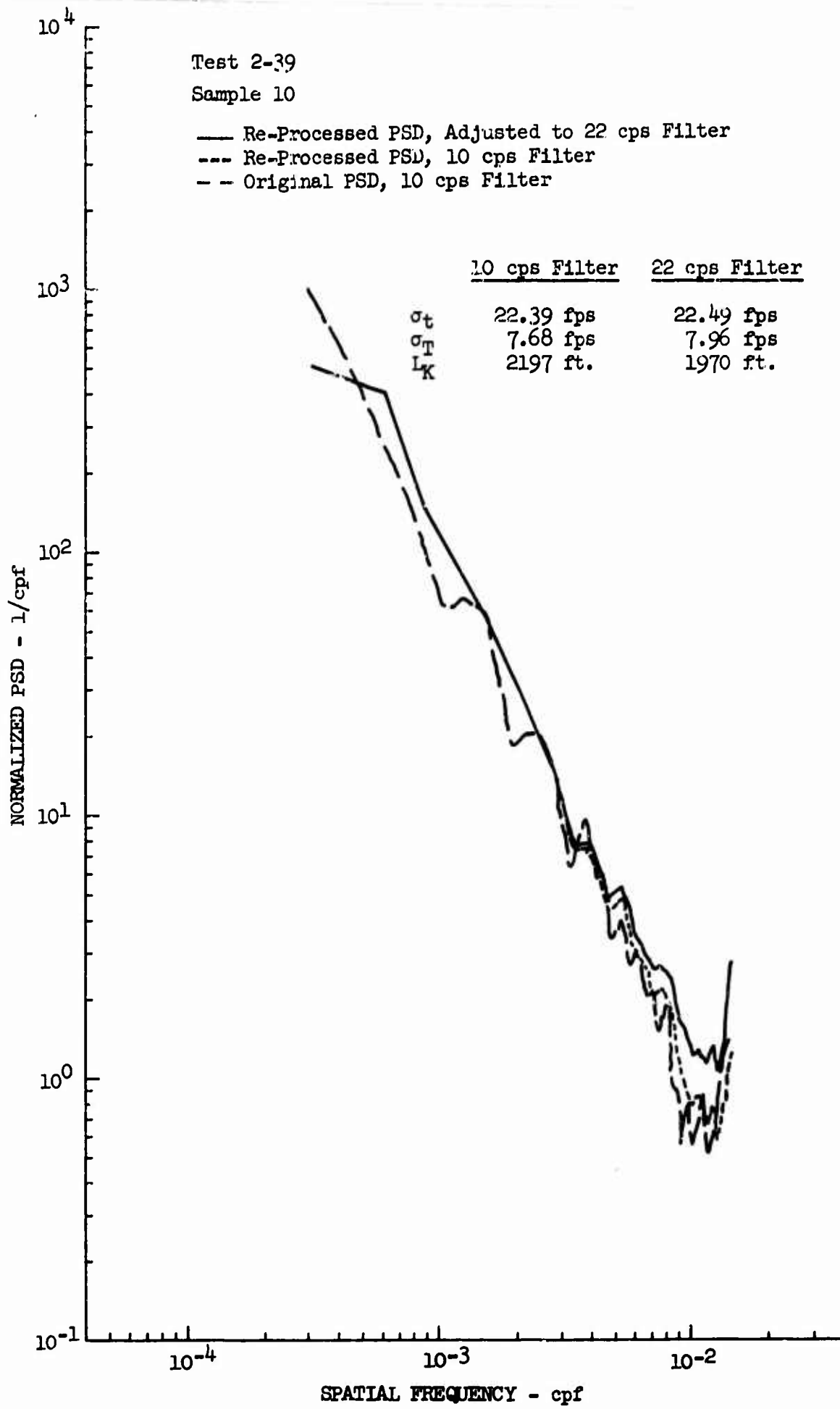


Figure 53.21 Lateral Gust Velocity Power Spectra of an Individual Turbulence Sample

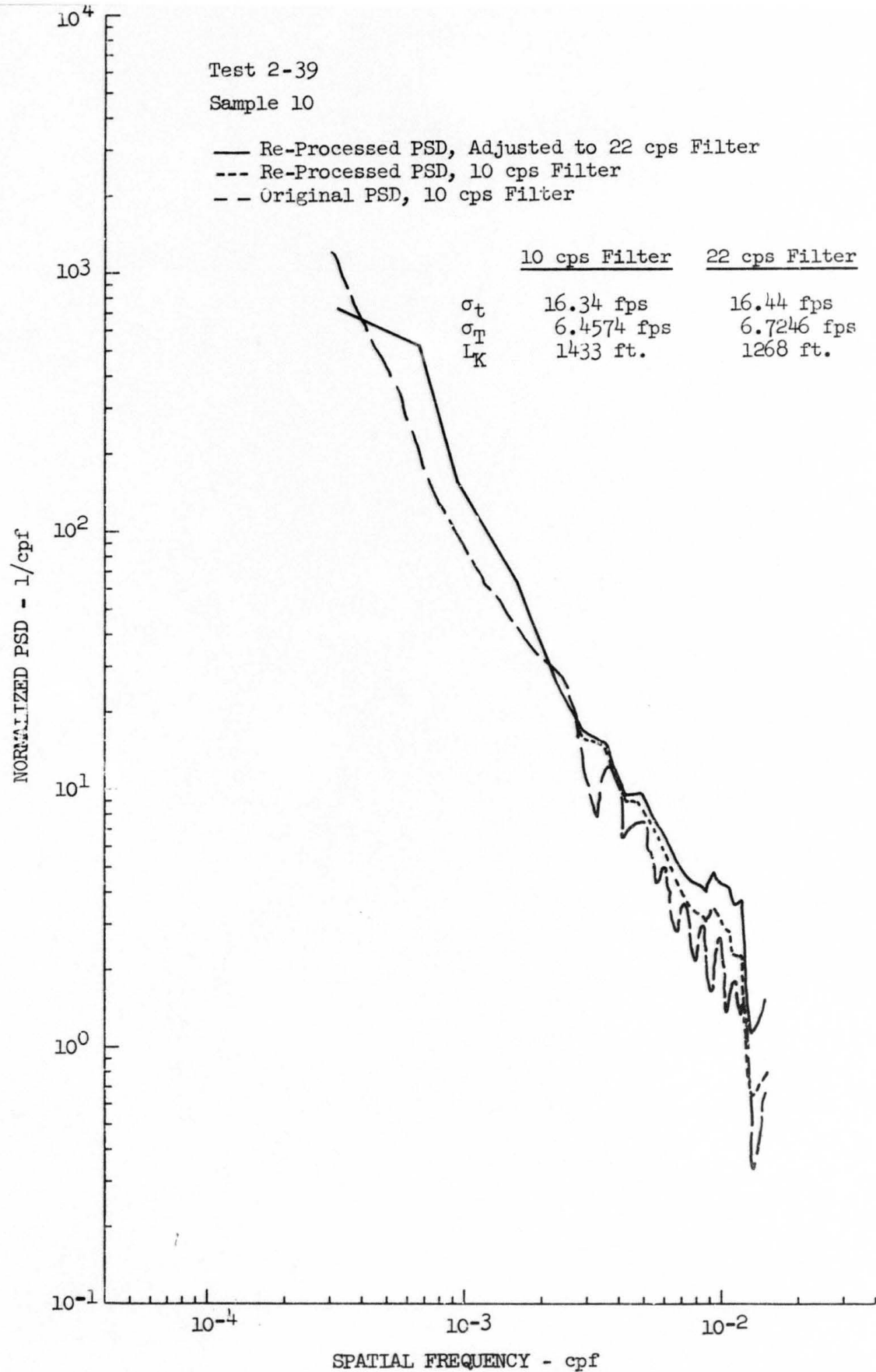


Figure 53.22 Vertical Gust Velocity Power Spectra of an Individual Turbulence Sample

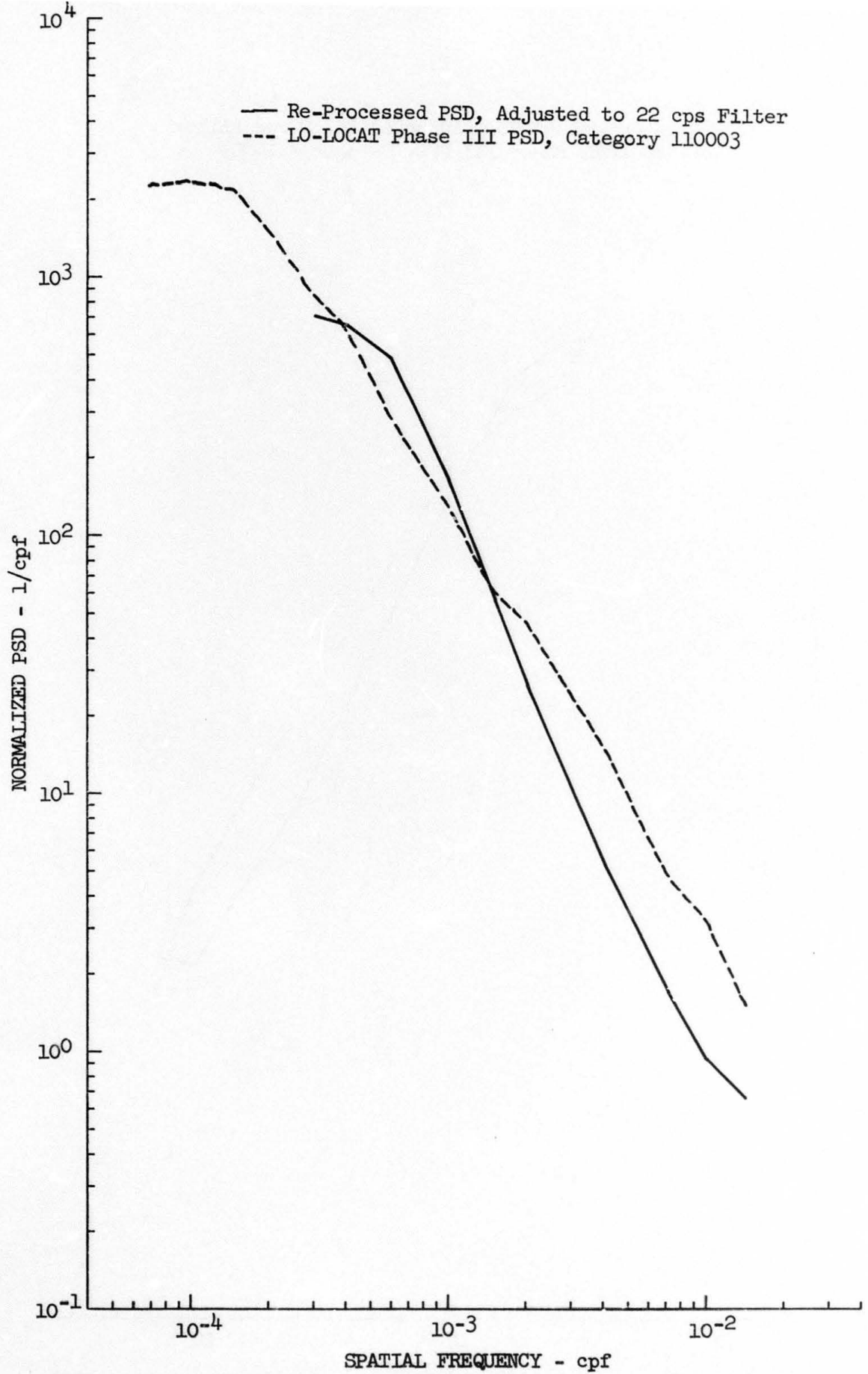


Figure 53.23 Comparison of Average Longitudinal Re-Processed High Intensity Gust Spectra With LO-LOCAT Phase III Spectra
443

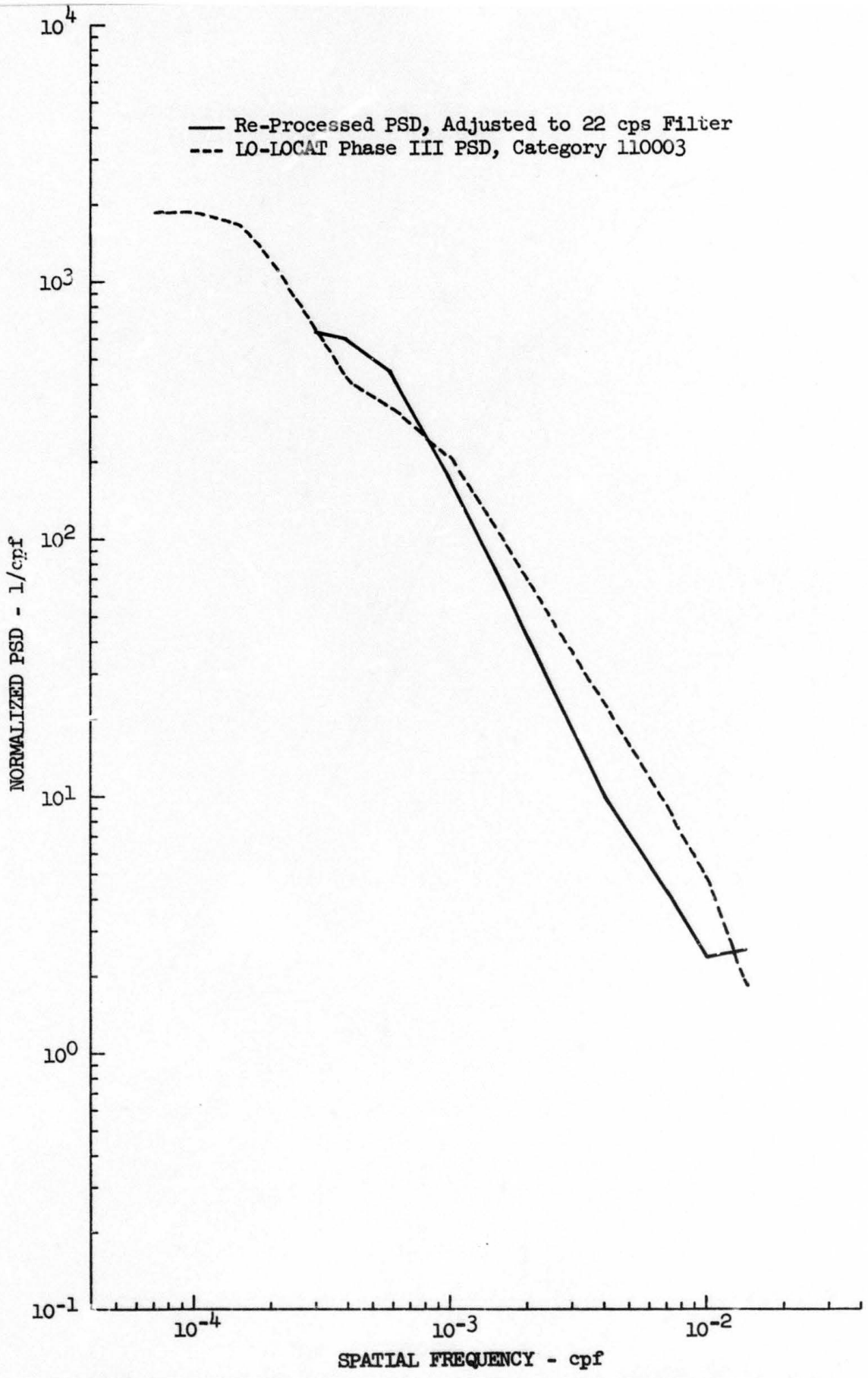


Figure 53.24 Comparison of Average Lateral Re-Processed High Intensity Gust Spectra With LO-LOCAT Phase III Spectra

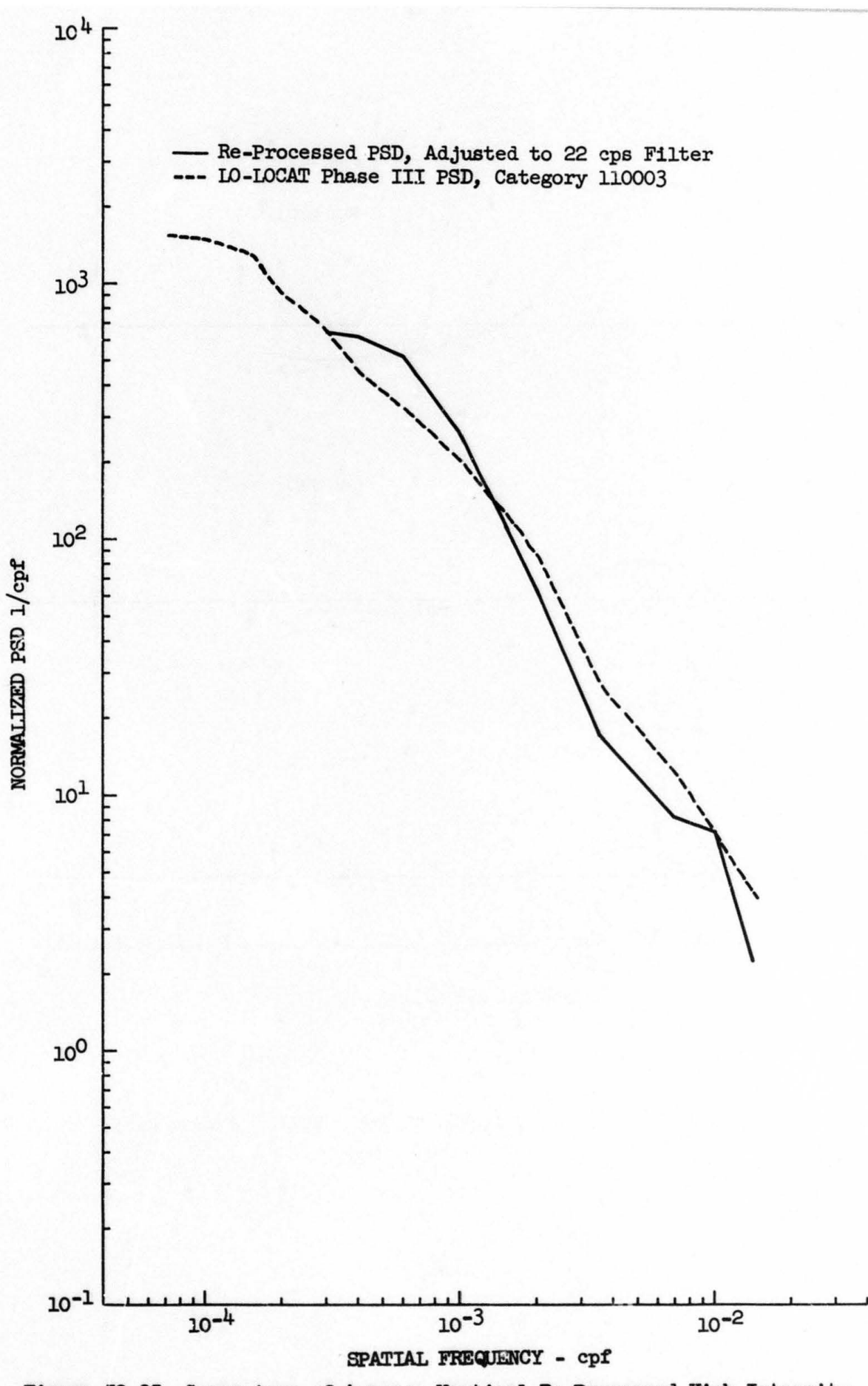


Figure 53.25 Comparison of Average Vertical Re-Processed High Intensity Gust Spectra With LO-LOCAT Phase III Spectra

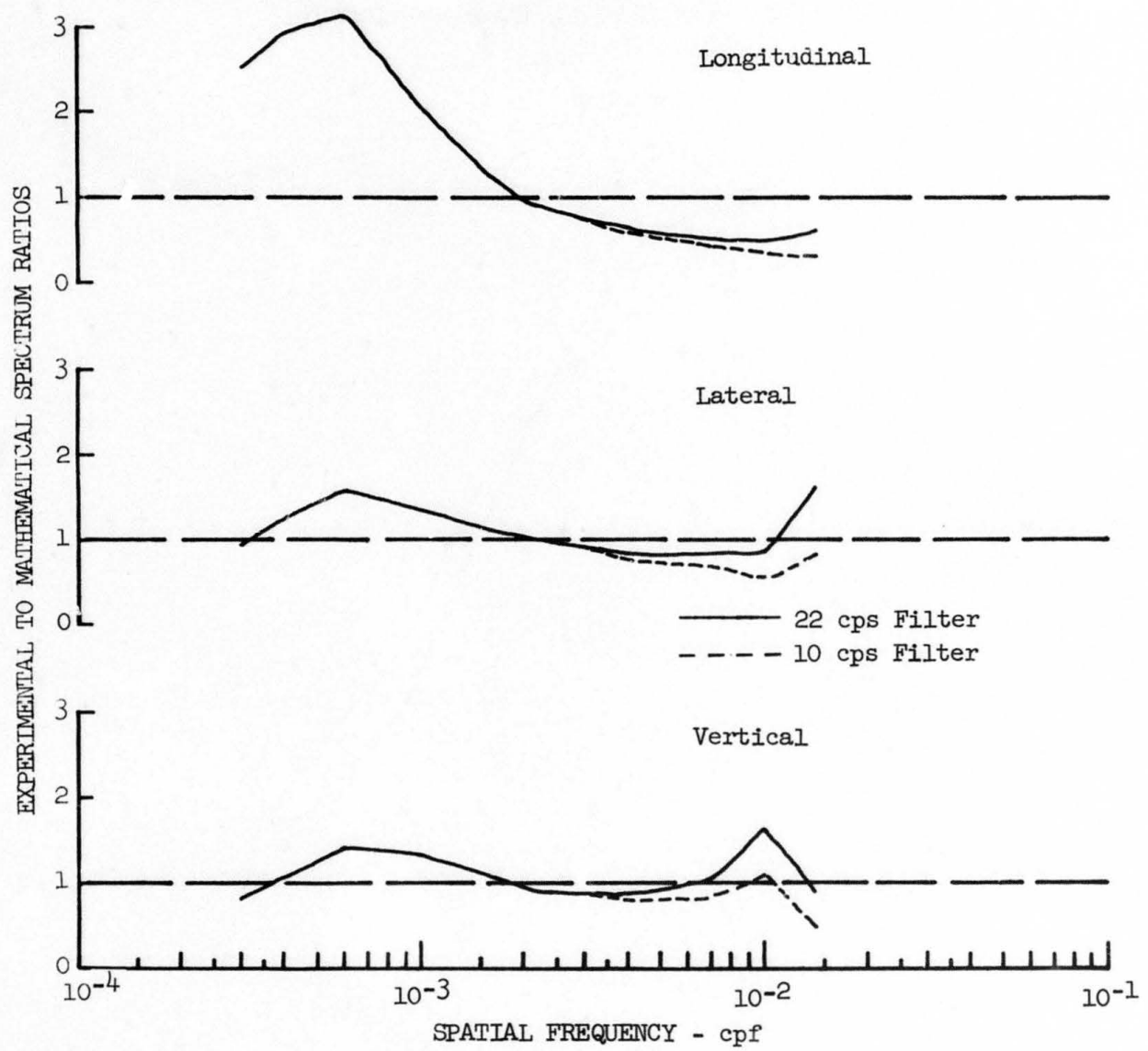


Figure 53.26 Average Experimental to von Karman Spectrum Ratio

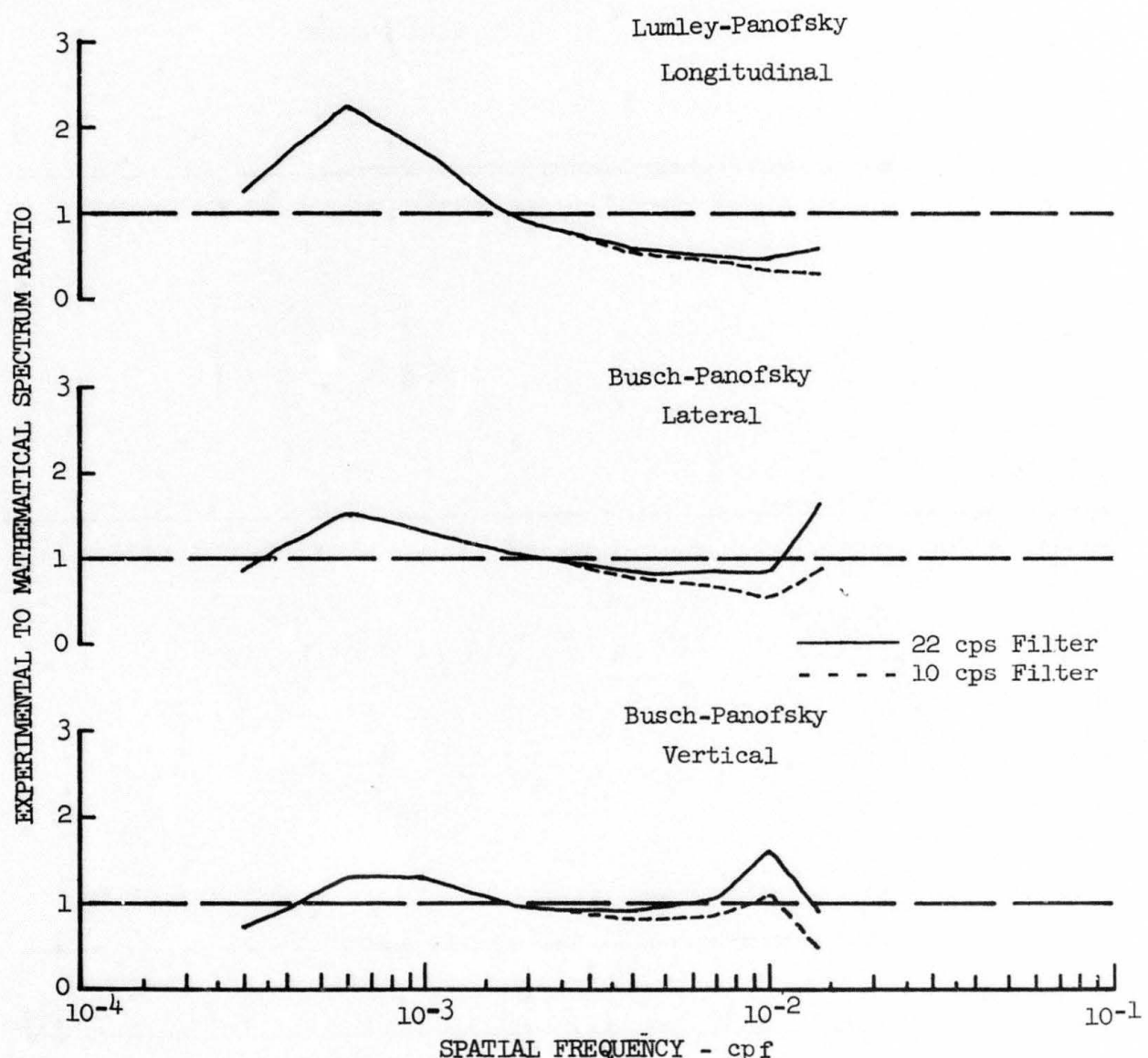


Figure 53.27 Average Experimental to Lumley-Panofsky and Busch-Panofsky Spectrum Ratios

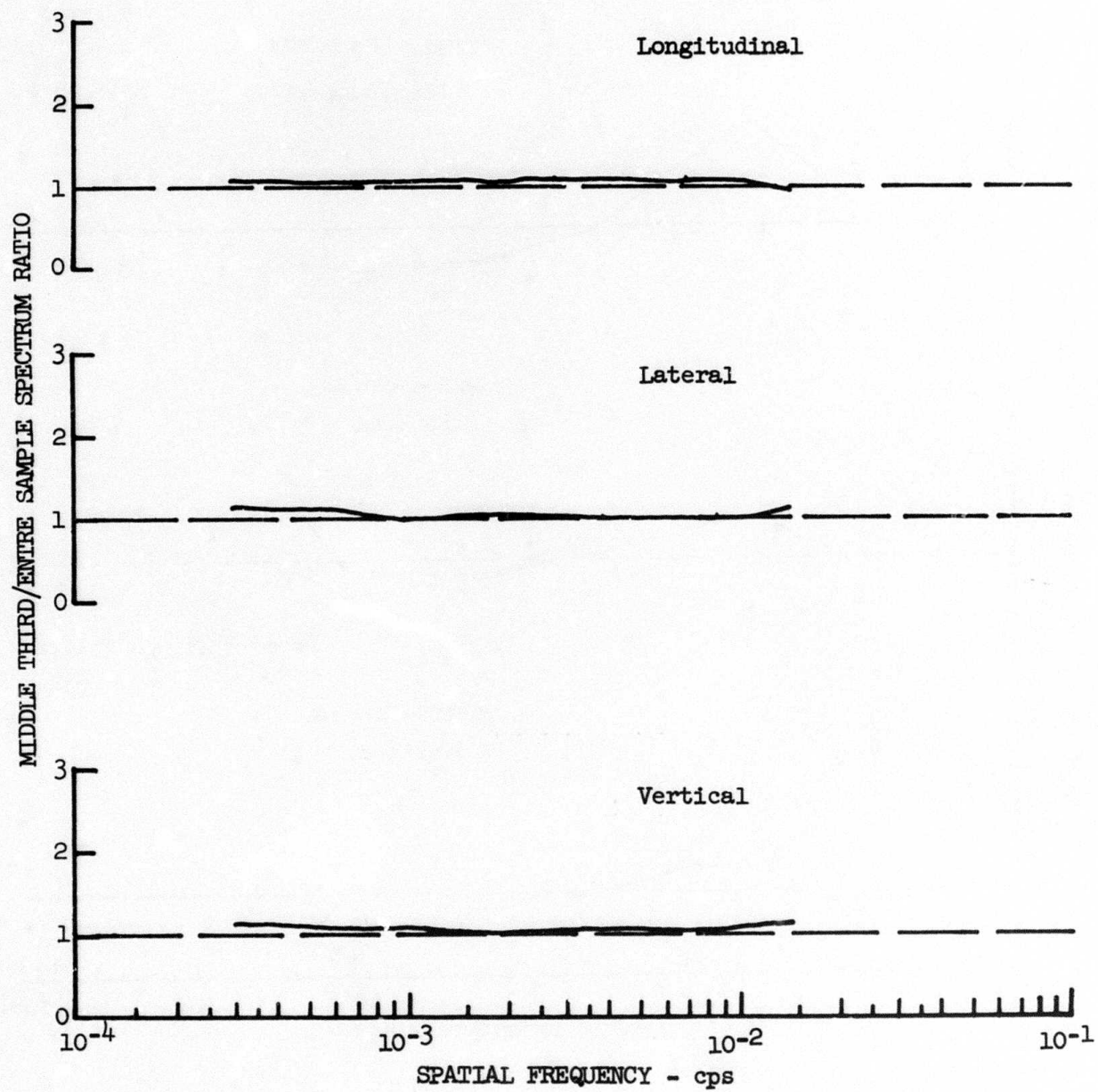


Figure 53.28 Average Homogeneity for Re-Processed High Intensity Gust Data

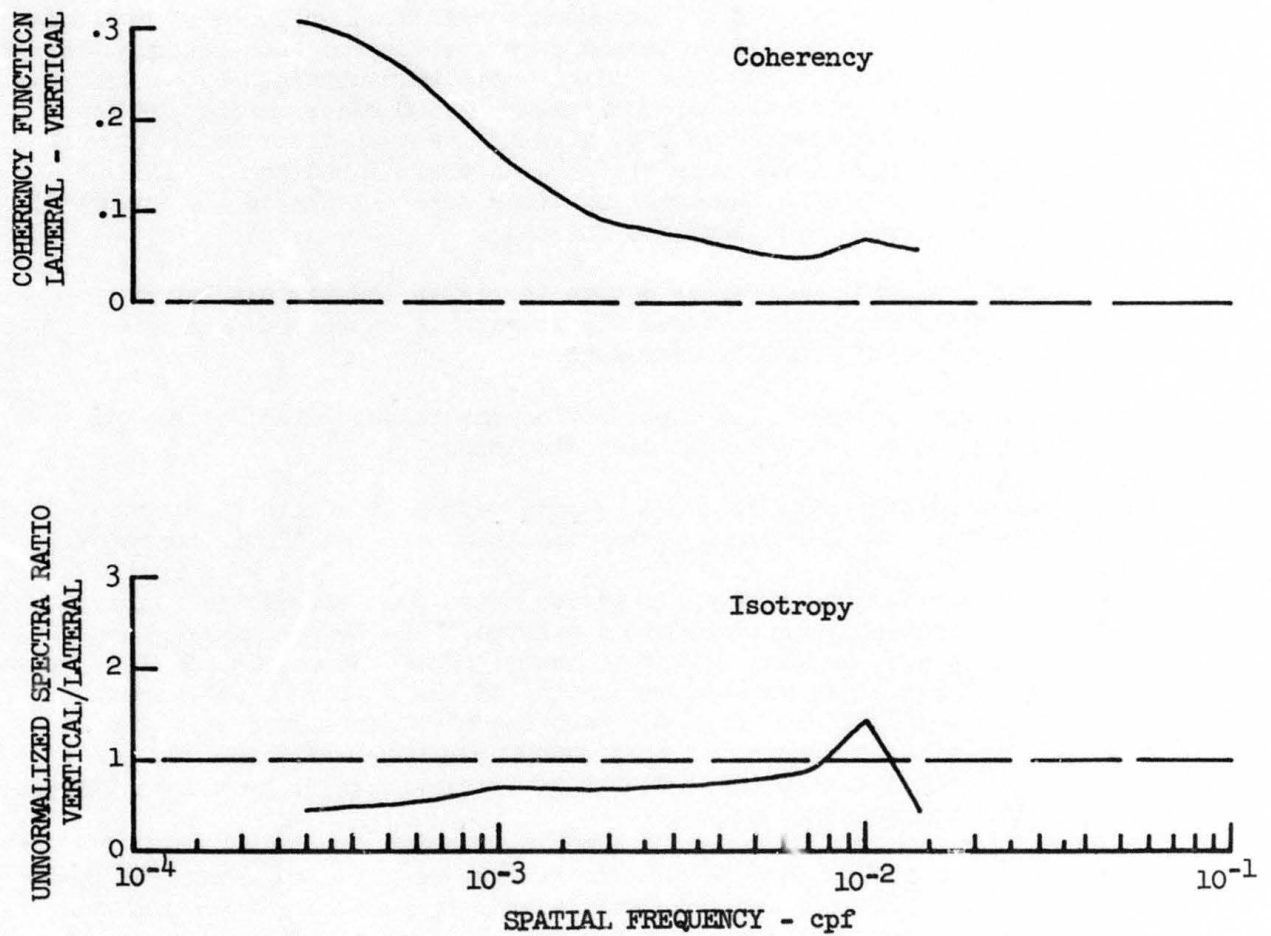


Figure 53.29 Average Coherency and Isotropy Characteristics

SECTION XII

CONCLUSIONS

The LO-LOCAT Phase III Program was based on statistical analyses of approximately 1800 samples of turbulence data and meteorological data recorded at absolute altitudes below 1,000 feet. These data were obtained by an instrumented T-33 aircraft which flew approximately 56,000 miles during 299 low altitude flights. Turbulence was also measured near an instrumented tower, near thunderstorms and in the wake of C-141 aircraft formations. From the numerous variables recorded, hundreds of items were calculated and analyzed. Conclusions drawn from these analyses follow:

- Gust velocity rms values become larger as the terrain becomes rougher, as altitude above the terrain is decreased, and as atmospheric stability decreases.
- The gust velocity rms distribution may be described by the combination of two Gaussian distributions.
- Gust velocity rms values show more correlation with wind speed over the rougher types of terrain than over the smooth terrains.
- The von Karman spectra expressions have good correlation with the experimentally determined spectra. The Dryden expressions do not give as good a representation of the data. In the low frequency, long wavelength portion of the spectrum, an expression suggested by Busch and Panofsky also correlates well with the data. It was noted that experimental spectra tend to be slightly underestimated at the lowest frequencies by the von Karman mathematical expressions.
- Scale lengths increase with increasing terrain roughness and those derived from the vertical and lateral components are greater for the 750 foot altitude than for the 250 foot altitude.
- Drift exists in all computed, unfiltered gust velocities. The drift is not characterized by constant amplitude or frequency, but varies from sample to sample. Drift removal by filtering, therefore, is mandatory for consistent, accurate results in the frequency domain.
- The LO-LOCAT Phase III signal-to-noise ratio is at an acceptable level when $\sigma_t \geq 1.4$ fps. Standard deviations of gust velocity as low as 0.28 fps were obtained from data obtained in smooth air.
- Probable errors in the calculation of LO-LOCAT gust velocities are ± 2 fps with maximum errors of ± 4 fps.
- Normalized LO-LOCAT spectra agree basically with those analyzed from other research programs. The data from one of these programs, The High Intensity Gust Program (Ref. X.2), were reprocessed using the same sequence of computer programs as were used for LO-LOCAT Phase III. Gust velocities were changed very little when these data were reprocessed.

- Approximately 88 per cent of the 4-1/2 minute turbulence samples are normally distributed at 0.02 level of significance based on gust velocity amplitude statistics. However, neither gust velocity nor gust acceleration distributions are normally distributed in the strictest sense and Rice's equation consistently underestimates the distributions.
- An average of 77 per cent of the turbulence samples obtained during Phase III are stationary at 0.02 level of significance.
 - There is an increased probability of larger gust velocity peak values with increasing terrain roughness, decreasing altitude, and decreasing atmospheric stability. Probabilities associated with stable, neutral and unstable conditions are nearly the same.
 - There is little variation in peak count distributions with time of day.
 - Gust velocity time series data obtained during LO-LOCAT Phase III show a higher frequency of occurrence of the larger gust velocities than those obtained during Phases I and II primarily due to the effects of the Peterson high mountain data.
 - The maximum discrete gust velocities encountered are 71.0, 76.9, and 74.5 feet per second for the longitudinal, lateral, and vertical gust velocities, respectively. The maximum value for the vertical component occurred over Leg 3 of the Edwards route while the maximum for the longitudinal and lateral components occurred over Leg 5 of the Peterson route.
 - Favorable agreement exists between the probability distributions of maximum derived equivalent vertical gust velocity and maximum vertical gust velocity.
 - Probability distributions of maximum gust velocity values for the longitudinal and vertical gust velocity components show good agreement. Higher probabilities associated with the lateral component are most likely influenced by the legs which parallel the mountain ridges on the Peterson route.
 - Gust accelerations can be used to calculate the statistics of gust velocities. One advantage of using gust accelerations rather than directly computed gust velocities to obtain these statistics is that less filtering is required because the relative amplitudes of unfiltered accelerations at low frequencies are less than those of unfiltered gust velocities. Another advantage is that filtering may be performed in the frequency domain. This results in a considerable savings in the computer effort required.
 - Good agreement is exhibited between normalized spectra of gust velocities obtained from BREN Tower and the LO-LOCAT research airplane.
 - Power spectra of turbulence near convective clouds exhibits a -5/3 logarithmic slope relationship between power density and frequency.

- Wind speed over rough terrain and lapse rate provide good correlation with turbulence intensity.
- Spectra of longitudinal and lateral wind components show indications of isotropy for the two components. Scale lengths were on the order of 6,000 feet.
- Forecasting of turbulence intensity is most successful when based on vertical wind shear and lapse rate in conjunction with local geographical conditions.
- The highest probability of encountering significant turbulence occurs when Richardson number is in the range of ± 0.2 . The probabilities decrease sharply for given values of gust velocity rms as Richardson number increases.
- Stability ratio is as good an indication of turbulence intensity as Richardson number.

REFERENCES

VOLUME I

- I.1 Neal V. Loving, Clear Air Turbulence (CAT) Measurement for Structural Design Criteria, AIAA Paper No. 65-510, American Institute of Aero-nautics and Astronautics, Easton, Pa., July, 1965.
- I.2 D. E. Gunter, et al., Low Altitude Atmospheric Turbulence LO-LOCAT Phases I and II, ASD-TR-69-12, ASD-AFSC, Wright-Patterson Air Force Base, Ohio, February, 1969.
- 3.1 S. O. Rice, "Mathematical Analysis of Random Noise," Bell System Technical Journal, Vol. 23 (1944), pp 282-332, Vol. 24 (1945), pp 46-156.
- 4.1 Aviation Weather for Pilots and Flight Operations Personnel, AC 006, FAA and DOC, Washington, D.C., 1965.
- 4.2 Richard H. Rhyne and Roy Steiner, Power Spectral Measurement of Atmospheric Turbulence in Severe Storms and Cumulus Clouds, TN D-2469, National Aeronautics and Space Administration, Washington, D.C., October, 1964.
- 4.3 J. T. Lee, "Thunderstorm Turbulence and Radar Echoes, 1964 Data Studies, TN-3-NSSL-24," Papers on Weather Radar, Atmospheric Turbu-lence, Sferics, and Data Processing, U.S. Department Comm., ESSA, August, 1965.
- 5.1 W. J. Dixon and F. J. Massey, Jr., Introduction to Statistical Anal-yisis, McGraw-Hill Book Co., Inc., 1957.
- 5.2 Neal Warner, The Run Test Criteria for Random Data Stationarity, PCOM-2840, United States Army Electronics Command, Fort Monmouth, N.J., 1967.
- 6.1 Julius S. Bendat and Allan G. Piersol, Measurement and Analysis of Random Data, John Wiley and Sons, Inc., New York, 1966.
- 8.1 Franz E. Hohn, Elementary Matrix Algebra, The MacMillan Company, New York, 1965, pp 101-103.
- 8.2 J. F. Price, R. H. Simonsen, Various Methods and Computer Routines for Approximation, Curve Fitting and Interpolation, Mathematical Note No. 249, Mathematics Research Laboratory, Boeing Scientific Research Laboratories, July, 1963, pp 32-54.
- 8.3 Hilbert Schenck, Jr., Theories of Engineering Experimentation, McGraw-Hill Book Company, Inc., New York, 1961, pp 170-180.
- 8.4 R. S. Burrington, C. M. May, Jr., Handbook of Probability and Statis-tics with Tables, Handbook Publishers, Inc., Sandusky, Ohio, 1958.

- 8.5 Harry Press, May T. Meadows, and Ivan Hadlock, A Re-Evaluation of Data on Atmospheric Turbulence and Airplane Gust Loads for Application in Spectral Calculations, NACA Report 1272, Langley Research Center, Langley Air Force Base, Virginia, 1956.
- 8.6 W. H. Austin, Jr., Environmental Conditions to be Considered in the Structural Design of Aircraft Required to Operate at Low Levels, SEG-TR-65-4, Research and Technology Division, Wright-Patterson Air Force Base, Ohio, January 1965.
- 10.1 Julius S. Bendat, Probability Functions for Random Responses: Prediction of Peaks, Fatigue Damage, and Catastrophic Failures, NASA CR-33, April, 1964.
- 10.2 J. Burnham, An Experimental Check on the Theoretical Relationship Between the Spectral Density and the Probability Distribution of Crossings for a Stationary Random Process with Gaussian Distribution, Using Data Obtained in Measurements of Aircraft Response to Turbulent Air, Ministry of Aviation C. P. No. 834, Her Majesty's Stationery Office, London, 1965.
- 12.1 K. R. Monson, et al., Low Altitude Atmospheric Turbulence LO-LOCAT Phase III Interim Report, Aeronautical Systems Division Technical Report, AFFDL-TR-69-63, Wright-Patterson Air Force Base, Ohio, February, 1969.
- 13.1 Francis E. Pritchard, The Turbulence and Terrain Environments Affecting Low-Altitude, High-Speed Flight, FDM No. 393, Cornell Aeronautical Laboratory, Inc., Buffalo, New York, July, 1966.
- 13.2 J. B. Dempster and C. A. Bell, "Summary of Flight Load Environmental Data Taken on B-52 Fleet Aircraft," Journal of Aircraft, Vol. 2, No. 5, September-October, 1965.
- 13.3 C. B. Notess, The Effects of Atmospheric Turbulence Upon Flight at Low Altitude and High Speed, FDM No. 325, Cornell Aeronautical Laboratory, Buffalo, New York, 31 October 1961.
- 13.4 J. K. Zbrozek, The Relationship Between the Discrete Gust and Power Spectra Presentations of Atmospheric Turbulence, With a Suggested Model of Low-Altitude Turbulence, Aeronautical Research Council (England), R and M No. 3216, 1961.
- 14.1 U. O. Lappe, Design of a Low Altitude Turbulence Model for Estimating Gust Loads on Aircraft, AF DL-TR-64-170, Wright-Patterson Air Force Base, Ohio, March, 1965.
- 18.1 Paul W. Kadlec, Flight Data Analysis of the Relationship Between Atmospheric Temperature Change and Clear Air Turbulence, AD 620 989, Dept. of Commerce, Weather Bureau, June, 1965.
- 18.2 J. L. Lumley and H. A. Panofsky, "The Structure of Atmospheric Turbulence," Interscience Monographs and Texts in Physics and Astronomy, Vol. XII, John Wiley and Sons, 1964.

- 20.1 R. B. Blackman and J. W. Tukey, The Measurement of Power Spectra, Dover Publications, Inc., 1958.
- 21.1 J. O. Hinze, Turbulence, An Introduction to its Mechanism and Theory, McGraw-Hill Book Co., Inc., 1959.
- 22.1 John C. Houbolt, et al., Dynamic Response of Airplanes to Atmospheric Turbulence Including Flight Data on Input and Response, NACA Report TR R-199, Langley Research Center, Langley Station, Va., June, 1964.
- 28.1 T. von Karman, "Progress in the Statistical Theory of Turbulence," Turbulence Classic Papers on Statistical Theory, Edited by S. K. Friedlander and Leonard Topper, Interstate Publishers, Inc., 1961, pp 162-173.
- 28.2 H. L. Dryden, "A Review of the Statistical Theory of Turbulence," Turbulence Classic Papers on Statistical Theory, Edited by S. K. Friedlander and Leonard Topper, Interstate Publishers, Inc., 1961, pp 115-150.
- 28.3 J. Taylor, Manual on Aircraft Loads, AGARDograph 83, Pergamon Press Ltd., New York, N.Y., 1965.
- 28.4 N. E. Busch and H. A. Panofsky, "Recent Spectra of Atmospheric Turbulence," Quarterly Journal of the Royal Meteorological Society, Volume 94, 1968.
- 30.1 Francis E. Prichard, et al., Spectral and Exceedance Probability Models of Atmospheric Turbulence for Use in Aircraft Design and Operation, AFFDL-TR-65-122, Wright-Patterson Air Force Base, Ohio, 1965.
- 30.2 Flying Qualities of Piloted Airplanes, MIL-F-008785A, (MSC Project 345-10), October, 1968.
- 30.3 U. O. Lappe, A Climatological-Wind Turbulence Model for Estimating Low Altitude Gust Loads, AFFDL-TR-67-122, Wright-Patterson Air Force Base, Ohio, January, 1968.
- 31.1 O. G. Sutton, Micrometeorology, McGraw-Hill Book Co., Inc., 1953.
- 31.2 R. J. Taylor, "The Dissipation of Kinetic Energy in the Lowest Layers of the Atmosphere," Quarterly Journal of the Royal Meteorological Society, 78, 179-185, 1952.
- 31.3 Paul B. MacCready, Jr., "Structure of Atmospheric Turbulence," Journal of Meteorology, 10, 434-449, 1953.
- 34.1 F. K. Ball, "Viscous Dissipation in the Atmosphere," Journal of Meteorology, No. 18, pg 553, 1961.

- 39.1 Atnip, F. K., "Turbulence at Low Altitudes, Summary of the Results of Phases I and II," Clear Air Turbulence and Its Detection, Plenum Press, 1969.
- 39.2 Taylor, G. I., "Effect of Variation in Density on the Stability of Superposed Streams of Fluid," Proc. Roy. Soc. A-132, pp 499-523, 1931.
- 39.3 Businger, Joost A., On the Energy Supply of Clear Air Turbulence, Clear Air Turbulence and Its Detection, Plenum Press, 1969.
- 40.1 J. C. Kaimal and D. A. Haugen, "Characteristics of Vertical Velocity Fluctuations Observed on a 430-M Tower," Quart. J. R. Met. Soc., Vol. 93, No. 397, July, 1967.
- 40.2 Panofsky and Prasad, International Journal of Air Water Pollution, Pergamon Press, 1965, Vol. 9, pp 419-430.
- 41.1 J. W. Cooley and J. W. Tukey, "An Algorithm for the Machine Calculation of Complex Fourier Series," Math. of Computation, Vol. 19, pp 297-301, April, 1965.
- 41.2 M. J. Hinich and C. S. Clay, "The Application of the Discrete Fourier Transform in the Estimation of Power Spectra, Coherence, and Bispectra of Geophysical Data," Reviews of Geophysics, Vol. 6, No. 3, pp 347-363, August, 1968.
- 41.3 P. J. Daniell, "Discussion of Symposium on Autocorrelation in Time Series," J. Roy. Statist. Soc. (suppl.), pp 8, 88-90, 1946.
- 41.4 S. Pond, S. D. Smith, P. F. Hamblin, and R. W. Burling, "Spectra of Velocity and Temperature Fluctuations in the Atmospheric Boundary Layer Over the Sea," Journal of the Atmospheric Sciences, Vol. 23, No. 4, pp 376-386, July, 1966.
- 41.5 Climatic Change, Technical Note No. 79, World Meteorological Organization, Commission for Climatology, p 36, 1966.
- 41.6 U. O. Lappe, B. Davidson, and C. B. Notess, Analysis of Atmospheric Turbulence Spectra Obtained from Concurrent Airplane and Tower Measurements, Institute of the Aeronautical Sciences Report No. 59-44, January, 1959.
- 41.7 J. Chandran Kaimal, An Analysis of Sonic Anemometer Measurements from the Cedar Hill Tower, Environmental Research Papers, No. 215, Bedford, Mass. Air Force Cambridge Research Laboratories, August, 1966.
- 43.1 C-141 Aircrew Operational Procedures (Tactical Airlift), Military Airlift Command Manual MM55-141, United States Air Force, 31 July 1968.
- 43.2 Combat Airlift Test 4-69, Final Report, Department of the Air Force.

- X.1 J. Jones, Gust Environment Investigation (WFT 1254) - Formal Summary (using an F-106 airplane), B-52 Flight Test Activities Report, Boeing Document D-13273-361A, The Boeing Co., Wichita, Kansas, May, 1964.
- X.2 J. W. Jones, High Intensity Gust Investigation (WFT 1217 R3), B-52 Flight Test Activities Report, Boeing Document D-13273-333A, The Boeing Co., Wichita, Kansas, October, 1964.
- X.3 A. K. Cross, T-38 Dynamic Response Gust Loads Comparison Between Flight Test and Analytical Results, Northrop Corporation, NORAIR Division, Document NOR-60-306, March, 1964.
- X.4 Test Operations Unit, Dynamic Response and Loads Survey - B-52C through B-52F (WFT 1293), B-52 Flight Test Activities Report, Boeing Document D-13273-362A, The Boeing Co., Wichita, Kansas, July, 1966.
- X.5 Test Operations Unit, High Speed Low Level Investigation - B-52G and H (WFT 1286), B-52 Flight Test Activities Report, Boeing Document D-13273-365A, The Boeing Co., Wichita, Kansas, September, 1966.
- X.6 K. D. Saunders, B-66B Low-Level Gust Study, Wright Air Development Division, Wright-Patterson Air Force Base, Ohio, March, 1961.
- X.7 R. B. Peloubet and R. L. Haller, Application of a Power Spectral Gust Design Procedure to Bomber Aircraft, AFFDL-TR-66-35, Air Force Flight Dynamics Laboratory, Wright-Patterson Air Force Base, Ohio, June, 1966.
- 51.1 Ralph H. Pennington, Introductory Computer Methods and Numerical Analysis, The MacMillan Co., New York, New York.
- 51.2 Emanuel Parzen, Stochastic Processes, Holden-Day, Inc., San Francisco, California.
- 51.1 Ralph H. Pennington, Introductory Computer Methods and Numerical Analysis, The MacMillan Co., New York, New York
- 51.2 Emanuel Parzen, Stochastic Processes, Holden-Day, Inc., San Francisco, California

UNCLASSIFIED
Security Classification

DOCUMENT CONTROL DATA - R&D

(Security classification of title, body of abstract and indexing annotation must be entered when the overall report is classified)

1. ORIGINATING ACTIVITY (Corporate author) The Boeing Company Wichita Division Wichita, Kansas 67210		2a. REPORT SECURITY CLASSIFICATION UNCLASSIFIED
		2b. GROUP
3. REPORT TITLE Low Altitude Atmospheric Turbulence LO-LO CAT PHASE III Volume I, Part II <i>Data Analysis</i>		
4. DESCRIPTIVE NOTES (Type of report and inclusive dates) R&D Final Technical Report - 17 April 1968 to 17 August 1970		
5. AUTHOR(S) (Last name, first name, initial) Jones, J. W.; Mielke, R. H.; Jones, G. W.		
6. REPORT DATE NOVEMBER 1970	7a. TOTAL NO. OF PAGES 457	7b. NO. OF REFS 64
8a. CONTRACT OR GRANT NO. F33615-68-C-1468	9a. ORIGINATOR'S REPORT NUMBER(S)	
b. PROJECT NO. ADP682E	None	
c.	9b. OTHER REPORT NO(S) (Any other numbers that may be assigned this report) AFFDL-TR-70-10 Volume I, Part II	
10. AVAILABILITY/LIMITATION NOTICES This document is subject to special export controls and each transmittal to foreign governments or foreign nationals may be made only with prior approval of the Air Force Flight Dynamics Laboratory (FBE), Wright-Patterson AFB, Ohio 45433		
11. SUPPLEMENTARY NOTES <i>See</i>	12. SPONSORING MILITARY ACTIVITY Air Force Flight Dynamics Laboratory FBE Wright-Patterson AFB, Ohio 45433	
13. ABSTRACT This report presents procedures, analysis methods, and final results pertaining to the LO-LOCAT Phase III program. Approximately 150 hours of low altitude (100 - 1000 feet) turbulence and associated meteorological data were recorded from 16 August 1968 through 30 June 1969. A model of the turbulence environment at low-level is presented in terms of gust velocity primary peaks, level crossings, amplitude samples, rms values, and gust maxima, as well as derived equivalent gusts, turbulence scale lengths, and power spectra. Mathematical expressions for turbulence spectra, scale length, and primary peak statistics are shown. Correlations between atmospheric gust velocities and meteorological and geophysical phenomena are evaluated. It was found that gust velocity magnitude at low altitude is most affected by atmospheric stability and terrain. Gust velocity rms values above 1.5 fps may be approximated by truncated Gaussian distributions. For wavelengths less than 15,000 feet, turbulence spectra are best represented by the von Karman mathematical expressions. The turbulence, sampled for 4-1/2 minute intervals over a distance of approximately 32 miles at absolute altitudes below 1,000 feet, was found to be basically stationary, isotropic, and homogeneous. A high percentage of Phase III data were recorded over high mountains since very little high mountain data were recorded under contour flight conditions at low level during Phases I and II. Phase III data are compared with data from Phases I and II and with data from other low altitude programs.		

(Distribution of this Abstract is Unlimited)

UNCLASSIFIED

Security Classification

14.

KEY WORDS

LINK A		LINK B		LINK C	
ROLE	WT	ROLE	WT	ROLE	WT

LO-LOCAT (Low-Low Altitude Critical Atmospheric Turbulence)
 ALL CAT
 Low Level Turbulence (0-1000 feet)
 Clear Air Turbulence (CAT)
 Gust Velocity Statistics
 Low Level Turbulence Model
 Meteorology (Turbulence)
 Turbulence Forecasting

INSTRUCTIONS

1. ORIGINATING ACTIVITY: Enter the name and address of the contractor, subcontractor, grantees, Department of Defense activity or other organization (*corporate author*) issuing the report.

2a. REPORT SECURITY CLASSIFICATION: Enter the overall security classification of the report. Indicate whether "Restricted Data" is included. Marking is to be in accordance with appropriate security regulations.

2b. GROUP: Automatic downgrading is specified in DoD Directive 5200.10 and Armed Forces Industrial Manual. Enter the group number. Also, when applicable, show that optional markings have been used for Group 3 and Group 4 as authorized.

3. REPORT TITLE: Enter the complete report title in all capital letters. Titles in all cases should be unclassified. If a meaningful title cannot be selected without classification, show title classification in all capitals in parenthesis immediately following the title.

4. DESCRIPTIVE NOTES: If appropriate, enter the type of report, e.g., interim, progress, summary, annual, or final. Give the inclusive dates when a specific reporting period is covered.

5. AUTHOR(S): Enter the name(s) of author(s) as shown on or in the report. Enter last name, first name, middle initial. If military, show rank and branch of service. The name of the principal author is an absolute minimum requirement.

6. REPORT DATE: Enter the date of the report as day, month, year, or month, year. If more than one date appears on the report, use date of publication.

7a. TOTAL NUMBER OF PAGES: The total page count should follow normal pagination procedures, i.e., enter the number of pages containing information.

7b. NUMBER OF REFERENCES: Enter the total number of references cited in the report.

8a. CONTRACT OR GRANT NUMBER: If appropriate, enter the applicable number of the contract or grant under which the report was written.

8b, 8c, & 8d. PROJECT NUMBER: Enter the appropriate military department identification, such as project number, subproject number, system numbers, task number, etc.

9a. ORIGINATOR'S REPORT NUMBER(S): Enter the official report number by which the document will be identified and controlled by the originating activity. This number must be unique to this report.

9b. OTHER REPORT NUMBER(S): If the report has been assigned any other report numbers (*either by the originator or by the sponsor*), also enter this number(s).

10. AVAILABILITY/LIMITATION NOTICES: Enter any limitations on further dissemination of the report, other than those

imposed by security classification, using standard statements such as:

- (1) "Qualified requesters may obtain copies of this report from DDC."
- (2) "Foreign announcement and dissemination of this report by DDC is not authorized."
- (3) "U. S. Government agencies may obtain copies of this report directly from DDC. Other qualified DDC users shall request through _____."
- (4) "U. S. military agencies may obtain copies of this report directly from DDC. Other qualified users shall request through _____."
- (5) "All distribution of this report is controlled. Qualified DDC users shall request through _____."

If the report has been furnished to the Office of Technical Services, Department of Commerce, for sale to the public, indicate this fact and enter the price, if known.

11. SUPPLEMENTARY NOTES: Use for additional explanatory notes.

12. SPONSORING MILITARY ACTIVITY: Enter the name of the departmental project office or laboratory sponsoring (*paying for*) the research and development. Include address.

13. ABSTRACT: Enter an abstract giving a brief and factual summary of the document indicative of the report, even though it may also appear elsewhere in the body of the technical report. If additional space is required, a continuation sheet shall be attached.

It is highly desirable that the abstract of classified reports be unclassified. Each paragraph of the abstract shall end with an indication of the military security classification of the information in the paragraph, represented as (TS), (S), (C), or (U).

There is no limitation on the length of the abstract. However, the suggested length is from 150 to 225 words.

14. KEY WORDS: Key words are technically meaningful terms or short phrases that characterize a report and may be used as index entries in cataloging the report. Key words must be selected so that no security classification is required. Identifiers, such as equipment model designation, trade name, military project code name, geographic location, may be used as key words but will be followed by an indication of technical context. The assignment of links, rules, and weights is optional.

UNCLASSIFIED

Security Classification